

ANALYSIS OF THE BLACK SEA GAS HYDRATES

A THESIS SUBMITTED TO  
THE GRADUATE SCHOOL OF NATURAL AND APPLIED SCIENCES  
OF  
MIDDLE EAST TECHNICAL UNIVERSITY

BY

ŞÜKRÜ MEREY

IN PARTIAL FULFILLMENT OF THE REQUIREMENTS  
FOR  
THE DEGREE OF DOCTOR OF PHILOSOPHY  
IN  
PETROLEUM AND NATURAL GAS ENGINEERING

MARCH 2017



Approval of the thesis:

**ANALYSIS OF THE BLACK SEA GAS HYDRATES**

submitted by **ŞÜKRÜ MEREY** in partial fulfillment of the requirements for the degree of **Doctor of Philosophy in Petroleum and Natural Gas Engineering Department, Middle East Technical University** by,

Prof. Dr. Gülbin Dural Ünver  
Dean, Graduate School of **Natural and Applied Sciences** \_\_\_\_\_

Prof. Dr. Serhat Akın  
Head of Department, **Petroleum and Natural Gas Engineering** \_\_\_\_\_

Asst. Prof. Dr. Çağlar Sınayuç  
Supervisor, **Petroleum and Natural Gas Engineering Dept., METU** \_\_\_\_\_

**Examining Committee Members:**

Prof. Dr. Mahmut Parlaktuna  
Petroleum and Natural Gas Engineering Dept., METU \_\_\_\_\_

Asst. Prof. Dr. Çağlar Sınayuç  
Petroleum and Natural Gas Engineering Dept., METU \_\_\_\_\_

Prof. Dr. Günay Çifçi  
Institute of Marine Sciences and Technology,  
Dokuz Eylul University \_\_\_\_\_

Prof. Dr. Selma Kadioğlu  
Geophysical Engineering Dept., Ankara University \_\_\_\_\_

Asst. Prof. Dr. İsmail Durgut  
Petroleum and Natural Gas Engineering Dept., METU \_\_\_\_\_

**Date:** 10.03.2017

**I hereby declare that all information in this document has been obtained and presented in accordance with academic rules and ethical conduct. I also declare that, as required by these rules and conduct, I have fully cited and referenced all material and results that are not original to this work.**

Name, Last name: Şükrü Merey

Signature:

## **ABSTRACT**

### **ANALYSIS OF THE BLACK SEA GAS HYDRATES**

Merey, Şükrü

Ph.D., Department of Petroleum and Natural Gas Engineering

Supervisor: Asst.Prof. Dr. Çağlar Sınayuç

March 2017, 376 pages

In this study, it was estimated that 71.8 standard tcm of methane can be available in the Black Sea gas hydrates. However, only 13.6 tcm of this amount was calculated as energy sources.

With HydrateResSim simulator, gas production potentials from a hypothetical Class 1 hydrate in the Black Sea conditions by depressurization and depressurization with wellbore heating were simulated. Wellbore heating might be necessary to avoid hydrate reformation along the wellbore during production. For comparison with the data of Class 1 hydrate simulations, hypothetical Class 3 hydrate simulations by depressurization with and without wellbore heating were conducted by HydrateResSim.

Experimental set-up for gas production from the Black gas hydrates by depressurization was designed according to the results of HydrateResSim. HEP.m code was written with Matlab to predict hydrate properties. This code was integrated with other codes written to calculate gas compositional change (HEPComp.m) during hydrate formation of gas mixtures, the amount of gas and water to obtain target saturations in experimental studies of hydrate in sediments inside high pressure reactors (SM.m and SMmix.m). BSR.m code was written to predict gas composition near the bottom simulating reflectance in marine sediments. These codes were tested

and compared with literature experimental, numerical data, and other software, consistent results were obtained.

The Black Sea sediments were investigated and it was observed that clay content is high and turbidites include fine silty sand and sandy silt. However, there might be thin coarse sand sections that might be good hydrate reservoirs for gas production.

**Keywords:** gas hydrates, methane hydrates, hydrate properties, the Black Sea, depressurization, HydrateResSim, sediments, the Black Sea sediments

## ÖZ

### KARADENİZ GAZ HİDRATLARININ ANALİZ EDİLMESİ

Merey, Şükrü

Doktora, Petrol ve Doğal Gaz Mühendisliği Bölümü

Tez Yöneticisi: Yrd.Doç. Dr. Çağlar Sınayuç

Mart 2017, 376 sayfa

Bu çalışmada Karadeniz gaz hidratlarında 71.8 standart trilyon metre küp metan gazı olabileceği hesaplanmıştır. Ancak bu miktarın sadece 13.6 trilyon metre küpünün enerji kaynağı olarak düşünülebileceği hesaplanmıştır.

HydrateResSim programı ile, Karadeniz şartlarında varsayılan tip 1 hidrat rezervinden, kuyunun ısıtılması veya ısıtılmadan basınç düşürme metodu ile simülasyon çalışmaları yapılmıştır. Üretim süresince kuyu cidarında hidrat oluşumunun engellenmesi için, kuyunun kuyu boyunca ısıtılması gerektiği belirlenmiştir. Tip 1 hidrat simülasyonları ile karşılaştırmak için, Karadeniz şartlarında varsayılan tip 3 hidratı için kuyunun ısıtılması veya ısıtılmadan basınç düşürme metodu ile farklı basınçlarda simülasyon çalışmaları HydrateResSim ile yapılmıştır.

Karadeniz gaz hidratlarından başlıca basınç düşürme metodu ile gaz üretimi için deneysel düzenek HydrateResSim programı simülasyon verileri kullanılarak dizayn edilmiştir. Matlab ile yazılan hidrat özelliklerini tahmin edebilen HEP.m kodu yazılmıştır. Ayrıca bu kod diğer yazılan kodlarla bağdaştırılarak, hidrat oluşumu sırasında gaz kompozisyon değişiminin analiz edilmesi (HEPComp.m) ve deneysel çalışmalarda yüksek basınç hücresi içerisindeki sedimentlerde hidratlarda hedeflenen saturasyonlar için gerekli gaz ve su miktarının hesaplanması (SM.m ve SMmix.m) gibi durumlar için kullanılmaktadır. Denizel sedimentlerindeki BSR yansımalarının

civarındaki hidratlarda gaz karışımının tespit edilmesi için BSR.m kodu yazılmıştır. Bu kodlar literatür deneysel, matematiksel verileri, ve diğer benzer programlar ile test edilmiş ve karşılaştırılmıştır, tutarlı sonuçlar elde edilmiştir.

Karadeniz sedimentleri araştırılmıştır ve yüksek kil oranı olduğu ve ayrıca türbiditlerin küçük tanecikli siltli kum ve kumlu silt içerdiği gözlenmiştir. Fakat, Karadeniz'deki iri tanecikli ince kum tabaklarının gaz üretimi için uygun olan, üretimi kolay hidrat rezervleri içerebilir.

**Anahtar Kelimeler:** gaz hidratlar, metan hidratları, hidrat özellikleri, Karadeniz, basınç düşürme metodu, HydrateResSim, Karadeniz sedimentleri

*To My Wife Ayşe and My Daughter İpek*

## ACKNOWLEDGEMENT

I would like to acknowledge and express my sincere gratitude to my thesis advisor Asst. Prof. Dr. Çağlar Sınayuç for his supervision and support throughout the study. I would also like to thank my thesis committee members for their contributions.

I would like to thank Dr. Atanas Vassilev, Institute of Oceanology, Bulgarian Academy of Sciences, for his helps related to the Black Sea. I also wish to thank Asst. Prof. Dr. Nagasree Garapati, Department of Chemical Engineering, West Virginia University, for her help about numerical simulations in gas hydrates. I appreciate the helps of Murat Öney about geological analysis in the Black Sea. During the evaluation of geophysical data and the Black Sea gas hydrates, I have very good discussions and analysis with Dr. Hilmi Mert Küçük, Dokuz Eylul University SEISLAB. I would like to thank him and SEISLAB, Institute of Marine Sciences and Technology, Dokuz Eylul University for their contributions to this study and gas hydrate studies in Turkey. I would also like to thank Cemal Gülamber, Innosys Innovative Systems, for his helps while designing METU reactor.

It is easy to write thesis, articles or be successful in any projects if you work well and love your job but it is not easy to have good friends who support you in your good and bad days. During my studies at METU, I have gained three very good friends who are like my sister and brothers: Betül Yıldırım, Abbas Abbasov and Murat Akın. I wish to thank them for their supports. Moreover, I wish to thank you İnanç Alptuğ Hıdıroğlu, Gökhan Mamak, Caner Baytar, Emre Ergin, and Yashar Oskoueı for their supports during this study. I also want to thank my coworkers for their support. Finally, I would like to extend my sincere thanks to my wife Ayşe and my family for their patience and supports during the long course of my graduate program.

This study was supported by Faculty Development Program (ÖYP-Batman University) and the Scientific and Technological Research Council of Turkey (TÜBİTAK) under National Scholarship Programme for Ph.D. Students.

## TABLE OF CONTENTS

ABSTRACT .....	v
ÖZ .....	vii
ACKNOWLEDGEMENT .....	x
TABLE OF CONTENTS .....	xi
LIST OF TABLES .....	xiv
LIST OF FIGURES .....	xviii
CHAPTERS	
1. INTRODUCTION .....	1
2. GAS HYDRATES .....	9
2.1 Structural Characteristics of Gas Hydrates .....	10
2.2 The Potential of Gas Hydrates in Nature.....	16
2.3 The Origin of Gas Hydrates in Nature .....	20
2.4 The Types of Gas Hydrate Reservoirs .....	25
2.5 The Gas Production Methods from Gas Hydrate Reservoirs .....	26
2.5.1 Depressurization .....	26
2.5.2 Thermal Stimulation .....	30
2.5.3 Chemical Injection .....	32
2.5.4 CO <sub>2</sub> Injection .....	34
2.6 Field Scale Studies .....	37
3. GAS HYDRATE POTENTIAL OF THE BLACK SEA.....	43
3.1 General Information about the Black Sea .....	43
3.2 Evidences of Gas Hydrate Existence in the Black Sea.....	49
3.3 Gas Hydrate Potential of the Black Sea .....	61
4. DETERMINATION OF GAS HYDRATE PROPERTIES .....	73
4.1 Gas Hydrate Equilibrium Point Determination .....	73
4.2 Gas Hydrate Equilibrium Point Determination with Inhibitors .....	85
4.3 Determination of Cage Occupancy of Gas Molecules in Hydrates.....	86

4.4 Determination of Hydration Number.....	89
4.5 Determination of Molecular Weight and Density of Gas Hydrates .....	90
4.6 Determination of Enthalpy of Hydrate Dissociation .....	90
4.7 Determination of the Geomechanical Properties of Gas Hydrates.....	93
4.8 Determination of Thermal Properties of Gas Hydrates .....	94
4.9 Flash Calculations in Gas Hydrates .....	96
5. GAS HYDRATE PRODUCTION MODELLING .....	99
5.1 Reservoir Scale Simulations.....	101
5.2 Laboratory Scale Simulations.....	104
5.3 HydrateResSim.....	105
5.4 Important Parameters for Hydrate Simulations .....	113
5.4.1 The Parameters of Kinetic Equation .....	113
5.4.2 Permeability and Relative Permeability.....	116
5.4.3 Capillary Pressure .....	123
6. STATEMENT OF THE PROBLEM .....	125
7. RESULTS AND DISCUSSION .....	127
7.1 Initial Methane in-Place in the Black Sea Gas Hydrates .....	127
7.2 Analysis of Gas Production Methods for the Black Sea Gas Hydrates.....	134
7.3 Experimental Set-up Design for the Black Sea Gas Hydrate Studies .....	145
7.3.1 Design of the High Pressure Reactor (METU Reactor) and Other Equipment.....	148
7.4 Depressurization Simulations in Field Cases in the Black Sea .....	181
7.4.1 Class 1 Hydrate Reservoir Simulations .....	181
7.4.2 Class 3 Hydrate Reservoir Simulations .....	200
7.4.3 Gas Production Simulations from Gas Hydrate Reservoirs deposited in Turbidites in the Black Sea .....	212
7.5 A New Gas Hydrate Software (HEP) to Predict Gas Hydrate Properties ....	248
7.6 Prediction of Gas Mixture Composition Change during Hydrate Formation with HEPComp.....	270

7.7 Calculations to Form Target Hydrate, Gas and Water Saturation in the High Pressure Reactor for CH <sub>4</sub> Hydrates .....	276
7.8 Calculations to Form Target Hydrate, Gas and Water Saturation in the High Pressure Reactor for Natural Gas Hydrates.....	283
7.9 Prediction of Natural Gas Hydrate Composition by using BSR data.....	286
7.10 Analysis of the Black Sea Sediments in terms of Gas Hydrate Potential by using the Core Data of Deep Sea Drilling Project (DSDP) Leg 42B program ..	295
8. CONCLUSION .....	319
9. RECOMMENDATION .....	325
REFERENCES.....	327
CURRICULUM VITAE .....	371

## LIST OF TABLES

### TABLES

Table 2-1: Geometry of cages of hydrates (Sloan and Koh, 2008) .....	11
Table 2-2: Ratio of molecular diameters to cavity diameters for gas hydrate formers and a few others (Sloan and Koh, 2008) .....	15
Table 2-3: Gas in Place in Hydrate-Bearing Sands (Adapted from Johnson, 2011) .....	19
Table 3-1: Gas compositions of hydrate samples taken from Bush Hill, Gulf of Mexico (Sassen and MacDonald, 1994).....	57
Table 3-2: Methane potential of the Black Sea hydrates.....	70
Table 3-3: CH <sub>4</sub> potential of the Black Sea hydrates (in sands only) .....	72
Table 4-1: Coefficients for Equation (4-16) systems without H <sub>2</sub> S when T ≤ 32 F ....	79
Table 4-2: Coefficients for Equation (4-17) systems without H <sub>2</sub> S-CO <sub>2</sub> when T > 32 F .....	79
Table 4-3: Coefficients for Equation (4-18) systems without H <sub>2</sub> S .....	80
Table 4-4: Coefficients for Equation (4-19) systems with H <sub>2</sub> S when T ≤ 32 F .....	80
Table 4-5: Coefficients for Equation (4-20) systems with H <sub>2</sub> S when T > 32 F .....	81
Table 4-6: Constants in Equation (4-21) for salts (Østergaard <i>et al.</i> , 2005) .....	85
Table 4-7: Constants in Equation (4-21) for organic inhibitors (Østergaard <i>et al.</i> , 2005).....	86
Table 4-8: Parameters for Equation (4-26) between 260 and 300 K for sI hydrate (Parrish and Prausnitz, 1972) .....	88
Table 4-9: Parameters for Equation (4-26) between 260 and 300 K for sII hydrate (Parrish and Prausnitz, 1972) .....	88
Table 4-10: Hydrate formation enthalpy for three phase conditions of single natural gas components (Kamath, 1984) .....	91
Table 4-11: Properties of CH <sub>4</sub> and THF, their hydrates, and water ice (Adapted from Lee <i>et al.</i> , 2007).....	93
Table 5-1: Reservoir simulators used for hydrate reservoirs (Adapted from Garapati, 2013).....	100

Table 5-2: Primary variables in equilibrium hydrate simulations without inhibitor* (Moridis <i>et al.</i> , 2005) .....	111
Table 5-3: Primary variables in kinetic hydrate simulations without inhibitor* (Moridis <i>et al.</i> , 2005) .....	112
Table 5-4: Hydrate kinetic constants in Equation (5-14).....	116
Table 5-5: Relative permeability at different saturation (Santamarina and Tsouris, 2007) .....	122
Table 5-6: Capillary pressure in hydrate-bearing sediments (Jang and Santamarina, 2014) .....	123
Table 7-1: Parameters calculated for the calculation of the amount of CH <sub>4</sub> in the Black Sea hydrates in this study .....	128
Table 7-2: Parameters obtained from HEP.m for Monte Carlo simulation by @Risk for the evaluation of expansion factor.....	128
Table 7-3: CH <sub>4</sub> potential of the Black Sea hydrates .....	130
Table 7-4: CH <sub>4</sub> potential of the Black Sea hydrates (in sands only).....	132
Table 7-5: Different zones for CO <sub>2</sub> -N <sub>2</sub> injection for the Black Sea hydrates .....	140
Table 7-6: CO <sub>2</sub> -N <sub>2</sub> injection analysis between 76.67 mbsf and 120 mbsf in Figure 7-10 .....	141
Table 7-7: Some criteria for constant pressure depressurization and constant flow rate depressurization methods (Adapted from Moridis <i>et al.</i> , 2008b; Sun <i>et al.</i> , 2015; Myshakin <i>et al.</i> , 2016) .....	144
Table 7-8: High pressure reactors used for gas hydrate studies recently.....	150
Table 7-9: Comparison of HIGUMA and METU reactor.....	153
Table 7-10: The conditions for the simulations of METU reactor.....	155
Table 7-11: Simulation parameters for METU reactor at the Black Sea conditions .....	158
Table 7-12: Kinetic parameters chosen for the kinetic model comparison.....	169
Table 7-13: Maximum gas flow rate, average gas flow rate and maximum water production in the simulations of the high pressure reactor (METU reactor) .....	180
Table 7-14: Properties of the hypothetical Class 1 CH <sub>4</sub> hydrate in the Black Sea	184

Table 7-15: Properties of the Hypothetical Class 3 CH <sub>4</sub> Hydrate in the Black Sea .....	201
Table 7-16: Properties of the hypothetical CH <sub>4</sub> hydrate deposited in turbidites and Class 3 CH <sub>4</sub> hydrate in the Black Sea conditions.....	215
Table 7-17: Properties of CH <sub>4</sub> Hydrates in the Danube Fan of the Black Sea.....	228
Table 7-18: Error Analysis from Figure 7-103 to Figure 7-115 with Minitab 17..	251
Table 7-19: Comparison of enthalpy of hydrate dissociation of gas mixtures.....	268
Table 7-20: Comparison of some hydrate properties determined with HEP and CSMHYD.....	269
Table 7-21: Comparison of some hydrate properties determined with HEP and the experimental study of Kida <i>et al.</i> (2009).....	270
Table 7-22: Composition change of feed gas during hydrate formation with experimental data and software (HEPComp).....	272
Table 7-23: Hydrate properties at the equilibrium conditions in Table 7-22 with HEPComp.....	272
Table 7-24: Feed gas composition in the study of Le Quang <i>et al.</i> (2016).....	275
Table 7-25: Comparison of experimental hydrate composition of feed gas in Table 7-24 and predicted hydrate composition with HEPComp.....	275
Table 7-26: Experimental (Lim <i>et al.</i> , 2017) and predicted compositions of CH <sub>4</sub> /N <sub>2</sub> /CO <sub>2</sub> for gas phase after hydrate formations .....	275
Table 7-27: Some constants used in the studies of Li <i>et al.</i> (2012), Wang <i>et al.</i> (2013b), Li <i>et al.</i> (2014) and Feng <i>et al.</i> (2015).....	278
Table 7-28: Target saturations, pressure and temperature data in the study of Li <i>et al.</i> (2014) .....	279
Table 7-29: The amount of gas and water needed for the target saturations in the study of Li <i>et al.</i> (2014) .....	280
Table 7-30: Experimental Data in the study of Li <i>et al.</i> (2014) during depressurization .....	281
Table 7-31: Calculated saturations during depressurization in Table 7-30.....	281
Table 7-32: Initial conditions for SMMix code analysis.....	285
Table 7-33: Output results of SMmix code .....	285

Table 7-34: The data available for BSRs in the study of Popescu <i>et al.</i> (2006) ....	289
Table 7-35: Scenario 1: Output of BSR.m code for BSRs detected in the study of Popescu <i>et al.</i> (2006).....	290
Table 7-36: Scenario 2: Output of BSR.m code for BSRs detected in the study of Popescu <i>et al.</i> (2006).....	293
Table 7-37: The details of the holes drilled in Leg 42B in the Black Sea (Supko <i>et al.</i> , 1978) .....	298

## LIST OF FIGURES

### FIGURES

Figure 1-1: The distribution of gas hydrates in the world (Koh <i>et al.</i> , 2012) .....	2
Figure 1-2: Timeline chart of gas hydrate field projects in the world (Collett <i>et al.</i> , 2015).....	2
Figure 1-3: Natural gas production of Turkey between 1975 and 2014 (Özgür, 2016) .....	3
Figure 1-4: Turkey's natural gas supply and its domestic production rates between 2004 and 2014 (Adapted from TPAO, 2015).....	3
Figure 1-5: Black Sea relief location map with exclusive economic zones (Wikipedia, 2016).....	4
Figure 2-1: Comparison of guest molecule sizes and cavities occupied as simple hydrates (Giavarini and Hester, 2011) .....	10
Figure 2-2: Three types of gas hydrate structure and their component cavities (Hester and Brewer, 2009) .....	12
Figure 2-3: Three structures of gas hydrates: (a) sI, (b) sII, and (c) sH (Zheng <i>et al.</i> , 2015).....	12
Figure 2-4: Hydrate equilibrium curve of some simple gas hydrates (Q <sub>1</sub> : lower quadruple point; Q <sub>2</sub> : upper quadruple point) (Sloan, 1998).....	16
Figure 2-5: Resource estimation of hydrates (a) Trofimuk <i>et al.</i> , (b) Dobrynin <i>et al.</i> (c) Kvenvolden, (d) MacDonald, (e) Gronitz and Fung, (f) Kvenvolden, (g) Milkov, (h) Klauda and Sandler, (i) Archer <i>et al.</i> , (j) Boswell and Collett , (k) Johnson (Adapted from Chong <i>et al.</i> , 2015) .....	17
Figure 2-6: Gas hydrate stability conditions for a) marine hydrates b) permafrost hydrates (Orange curve: hydrate equilibrium curve, Blue curve: thermal gradient curve) (Beaudoin <i>et al.</i> , 2014).....	20
Figure 2-7: Fate of buried organic matter for biogenic and thermogenic gas hydrates (Beaudoin <i>et al.</i> , 2014) .....	22

Figure 2-8: Solubility of CH <sub>4</sub> in brine for (A) the Mallik test site (permafrost) and (B) the Ulleung Basin (marine field) (w: water, h: hydrate, g: gas) (Spangenberg <i>et al.</i> , 2015) .....	24
Figure 2-9: Types of Gas Hydrate Reservoirs in Nature.....	25
Figure 2-10: Illustration of hydrate dissociation by depressurization, thermal stimulation and chemical injection with HEP.m.....	26
Figure 2-11: Average rates of CH <sub>4</sub> hydrate dissociation calculated by its half-life time after pressure drops to 0.1 MPa at various temperatures (Stern <i>et al.</i> , 2003) .....	28
Figure 2-12: Diagram of CH <sub>4</sub> -CO <sub>2</sub> -H <sub>2</sub> O phase equilibrium (Goel, 2006).....	34
Figure 2-13: Schematic diagram of the guest molecule replacement in the M-cage and the CH <sub>4</sub> re-occupation in the S-cage (Zhao <i>et al.</i> , 2012b) .....	35
Figure 2-14: A) Cross section of the Messoyokha field B) Production behavior at the Messoyokha field (Makogon <i>et al.</i> , 2005) .....	38
Figure 2-15: Gas production rates of different gas hydrate field test projects (Boswell <i>et al.</i> , 2016) .....	39
Figure 2-16: Technology maturity curve of gas hydrates (SBC, 2015).....	41
Figure 3-1: Lithology of the Black Sea (Adapted from Ross <i>et al.</i> , 1974).....	43
Figure 3-2: Bathymetry of the Black Sea (Vassilev, 2006) .....	44
Figure 3-3: Salinity, temperature and O <sub>2</sub> concentration with sea level depth of the Black Sea and typical global ocean (Railsback, 2010) .....	44
Figure 3-4: Temperature, salinity, density and $\sigma_t$ (isopycnal parameter) in the Black Sea at the location with lat. 42.951, long. 39.114 with depth (Stanev <i>et al.</i> , 2014)..	45
Figure 3-5: Figure showing how pore water salinity changes: A) Before gas hydrate formation, B) Just after gas hydrate formation, C) 1000s years after gas hydrate formation (Adapted from Bohrmann and Torres, 2006).....	46
Figure 3-6: Temperature Gradient in the Black Sea (Vassilev, 2006).....	47
Figure 3-7: Profile of a) CH <sub>4</sub> and b) H <sub>2</sub> S concentration profile at Sta.BKS2 in the Black Sea (Adapted from Sozansky, 1997) .....	48
Figure 3-8: Gas seepages in the “Golden Sands” area showing: (a) a small seep producing gas with a flux rate of 0.26–0.62 l/min; (b) two medium strength seeps with 1.0–2.0 l/min; (c) a strong seep with 2.5–3.8 l/min (Dimitrov, 2002).....	49

Figure 3-9: Gas seepages from the Batumi seep area during ROV observations (Pape <i>et al.</i> , 2011).....	50
Figure 3-10: Scheme of distribution of the free CH <sub>4</sub> and CH <sub>4</sub> hydrate in the Black Sea (Adapted from Sozansky, 1997).....	51
Figure 3-11: Gas bubbles and gas hydrate formed inside the funnel at Vodyanitskii mud volcano (~2080 mbsl; Sorokin Trough) in the Black Sea (Adapted from Sahling <i>et al.</i> , 2009).....	51
Figure 3-12: Sea-floor observations, showing bacterial mats and carbonates in CH <sub>4</sub> venting areas, Dnepr paleo-delta, NW Black Sea (Naudts <i>et al.</i> , 2008) .....	53
Figure 3-13: CH <sub>4</sub> seeps in the Dnepr paleo-delta, NW Black Sea, at water depths of 66 to 825 m (Adapted from Naudts <i>et al.</i> , 2006 and Naudts <i>et al.</i> , 2009) .....	54
Figure 3-14: Location of the mud volcanoes gas seeps and gas hydrates in the Black Sea: Triangles in black, mud volcanoes; circles in red, gas seeps; squares in ice blue, gas hydrate; bold dashed lines in black, shelf edge; bold squared lines, boundaries of tectonic units; filled rectangular in red, Dniro palaeo-delta area; I, NW Shelf; II, Kerch-Taman trough; III, Sorokin trough; IV, Tuapse trough; V, Shatsky ridge; VI, Andrusov ridge; VII, Arkhangelsky ridge; VIII, Giresuan basin (Starostenko <i>et al.</i> , 2010).....	55
Figure 3-15: Gas hydrate zones in the Black Sea (Küçük, 2016) .....	55
Figure 3-16: a) Gas hydrates in the Core BS308K in the NW of the Black Sea (Kenyon <i>et al.</i> , 2001) b) Gas hydrates in Core BS-288G in Crimean deep-water margin in the Black Sea (Ivanov <i>et al.</i> , 1998) c) Chips of gas hydrates in the core catcher in the sediment interval 10–35 cm in core GeoB 11913 taken at Vodyanitskii mud volcano in the Black Sea (Sahling <i>et al.</i> , 2009) .....	56
Figure 3-17: A) BSRs detected in the Black Sea B) Analysis of BSRs (Popescu <i>et al.</i> , 2006).....	58
Figure 3-18: Gas hydrate stability zones/BSR number in the cross section (Vassilev, 2006).....	60
Figure 3-19: The hydrate resource pyramid (Zou, 2013).....	62

Figure 3-20: Hydrate saturation $S_h$ distribution in a) Clay Reservoirs b) Silt Reservoir c) Sand Reservoir during gas production with 3.0 MPa depressurization (Huang <i>et al.</i> , 2015) .....	63
Figure 3-21: Relation between absolute permeability and porosity for core samples in Eastern Nankai Trough (Konno <i>et al.</i> , 2015).....	64
Figure 3-22: Mean grain sizes of gas hydrate samples in the Black Sea (Klapp, 2009) .....	65
Figure 3-23: Gas hydrate saturation relation with intrinsic reservoir quality (Boswell and Collett, 2016).....	66
Figure 3-24: Black Sea Sediments (Adapted from Nikishin <i>et al.</i> , 2003) .....	67
Figure 3-25: Ordinary outcrop example of turbidites (alternating layers of fine and coarse sediments) (Swewe, 2016) .....	68
Figure 3-26: Typical gas hydrate bearing sand dominated turbidite layern (top) separated from gas hydrate free mud (bottom) at U1328 (Riedel <i>et al.</i> , 2009) .....	68
Figure 3-27: CH <sub>4</sub> stored in the Black Sea gas hydrates at STP (Klauda and Sandler, 2003) .....	70
Figure 4-1: A) Hydrate equilibrium of CO <sub>2</sub> in silica pores B) Hydrate equilibrium of CH <sub>4</sub> in silica pores (Kang <i>et al.</i> , 2007) .....	83
Figure 4-2: Hydrate configuration in different layered media (water conversion ratio is a) 23.1% b) 16.2%) (Zhang <i>et al.</i> , 2011).....	84
Figure 4-3: a) Thermal conductivities of pure ice, THF hydrate, methane hydrate, propane hydrate, pure water and methane gas in literature b) Composite thermal conductivities in sediments (Sloan and Koh, 2008).....	96
Figure 5-1: a) Cumulative gas production b) Water production (Gaddipati, 2008) .....	101
Figure 5-2: Space discretization and geometry data in the integral finite difference method (Moridis <i>et al.</i> , 2005) .....	109
Figure 5-3: Gas hydrate (GH) occurrences in nature: Thin (A) and thickly veined (B) sediment-displacing GH in fine-grained sediment; (C) pore-filling GH in sand; (D) GH mounds on the sea floor; (E) Disseminated GH in fine-grained sediment; (F) GH in coarse sands (Beaudoin <i>et al.</i> , 2014).....	118

Figure 5-4: Gas hydrate occurrences in sediments (Green color: hydrate, yellow color: sands) (Boswell <i>et al.</i> , 2011).....	119
Figure 7-1: Porosity distribution in the Black Sea sediments (Vassilev, 2006).....	129
Figure 7-2: Temperature distribution in the Black Sea sediments (Vassilev, 2006) .....	129
Figure 7-3: Probability of initial CH <sub>4</sub> amount in the Black Sea hydrates .....	131
Figure 7-4: Sensitivity of parameters in Table 7-1 .....	131
Figure 7-5: Probability of initial CH <sub>4</sub> amount in the Black Sea hydrates (in sands only).....	133
Figure 7-6: Sensitivity of parameters in Table 7-1 (in sands only).....	133
Figure 7-7: Hydrate equilibrium curves for pure CH <sub>4</sub> and CO <sub>2</sub> hydrates, along with phase equilibrium lines of liquid and gaseous CO <sub>2</sub> (Adapted from Goel, 2006)...	134
Figure 7-8: Density versus pressure at 9°C for CO <sub>2</sub> (Calculated with NIST).....	136
Figure 7-9: Density versus pressure at 9°C for 22.5 % CO <sub>2</sub> +77.5 % N <sub>2</sub> (Calculated with WebGasEOS) .....	137
Figure 7-10: Hydrate equilibrium curves of CO <sub>2</sub> , CH <sub>4</sub> and N <sub>2</sub> and their mixture and potential Black Sea temperature and profile .....	139
Figure 7-11: Relationships between the productivity using depressurization method and effective permeability and reservoir temperature (MH-21, 2008) .....	143
Figure 7-12: Schematic of the experimental setup designed in this study for gas hydrate experiments .....	146
Figure 7-13: a) Flow rate (Q <sub>R</sub> ) b) Total gas production (V <sub>R</sub> ) (Kowalsky and Moridis 2007).....	149
Figure 7-14: General view of the high pressure reactor (METU reactor).....	152
Figure 7-15: Schematics describing gas production behavior in METU reactor for A) Simulation set 1 and 2 B) Simulation set 3 and set 4 .....	155
Figure 7-16: Gas hydrate saturation with grids in the half of the high pressure cylindrical reactor A) for simulation set 1 and set 2 B) for simulation set 3 and set 4 .....	159
Figure 7-17: Cumulative gas production in simulation set 1 A) Depressurization stage + Constant pressure stage B) Depressurization stage.....	160

Figure 7-18: Cumulative water production in simulation set 1 A) Depressurization stage + Constant pressure stage B) Depressurization stage .....	161
Figure 7-19: Gas to water production ratio in simulation set 1.....	161
Figure 7-20: Gas production rate in simulation set 1 .....	162
Figure 7-21: Pressure, temperature, hydrate saturation, gas saturation, and aqueous saturation in simulation set 1 of the half of the high pressure reactor at 2.7 MPa.	164
Figure 7-22: Cumulative water production in simulation set 2 A) Depressurization stage + Constant pressure stage B) Depressurization stage .....	165
Figure 7-23: Cumulative water production in simulation set 2 A) Depressurization Stage + Constant pressure stage B) Depressurization stage.....	166
Figure 7-24: Gas to water production ratio in simulation set 2.....	166
Figure 7-25: Gas production rate in simulation set 2 .....	167
Figure 7-26: Pressure, temperature, hydrate saturation, gas saturation, and aqueous saturation in simulation set 2 of the half of the high pressure reactor at 2.7 MPa.	168
Figure 7-27: Equilibrium and kinetic models comparisons in simulation set 1 at the depressurization pressure of 2.7 MPa A) Cumulative gas production B) Cumulative water production.....	170
Figure 7-28: Equilibrium and kinetic models comparisons in simulation set 1 at the depressurization pressure of 3.0 MPa A) Cumulative gas production B) Cumulative water production.....	171
Figure 7-29: Equilibrium and kinetic models comparisons in simulation set 2 at the depressurization pressure of 2.7 MPa A) Cumulative gas production B) Cumulative water production.....	171
Figure 7-30: Equilibrium and kinetic models comparisons in simulation set 2 at the depressurization pressure of 3.0 MPa A) Cumulative gas production B) Cumulative water production.....	172
Figure 7-31: A) Cumulative gas production in simulation set 3 B) Cumulative water production in simulation set 3 .....	173
Figure 7-32: Gas to water production ratio in simulation set 3.....	174
Figure 7-33: Gas production rate in simulation set 3 .....	175

Figure 7-34: Pressure, temperature, hydrate saturation, gas saturation, and aqueous saturation in simulation set 3 of the half of the high pressure reactor at 2.7 MPa .	176
Figure 7-35: A) Cumulative gas production in simulation set 4 B) Cumulative water production in simulation set 4 .....	177
Figure 7-36: Gas to water production ratio in simulation set 4.....	178
Figure 7-37: Gas production rate in simulation set 4 .....	178
Figure 7-38: Pressure, temperature, hydrate saturation, gas saturation, and aqueous saturation in simulation set 4 of the half of the high pressure reactor at 2.7 MPa .	179
Figure 7-39: CH <sub>4</sub> at standard conditions in the Black Sea hydrates (Klauda and Sandler, 2003) .....	182
Figure 7-40: Grid structure of the hypothetical Class 1 hydrate reservoir in the Black Sea conditions.....	185
Figure 7-41: Cumulative gas production from the Class 1 CH <sub>4</sub> hydrate by depressurization at different pressures .....	187
Figure 7-42: Cumulative gas production from the upper hydrate section of the Class 1 CH <sub>4</sub> hydrate by depressurization at different pressures .....	188
Figure 7-43: Cumulative water production from the Class 1 CH <sub>4</sub> hydrate by depressurization at different pressures .....	188
Figure 7-44: Gas to water production ratio of the Class 1 CH <sub>4</sub> hydrate by depressurization at different pressures .....	189
Figure 7-45: Gas production flow rate from the Class 1 CH <sub>4</sub> hydrate by depressurization at different pressures .....	189
Figure 7-46: Hydrate formation along the wellbore during depressurization at 2.0 MPa after 16 days.....	190
Figure 7-47: Changes in pressure, temperature, S <sub>h</sub> , S <sub>g</sub> and S <sub>aq</sub> from initial conditions to 7.3 years production from the Class 1 CH <sub>4</sub> hydrate with depressurization at 3.0 MPa .....	192
Figure 7-48: Cumulative gas production by depressurization with wellbore heating .....	194
Figure 7-49: Cumulative gas production from the upper hydrate section of the Class 1 CH <sub>4</sub> hydrate by depressurization at different pressures with wellbore heating ..	194

Figure 7-50: Gas to water production ratio of depressurization with wellbore heating .....	195
Figure 7-51: Gas production flow rate by depressurization with wellbore heating	195
Figure 7-52: Cumulative water production by depressurization with wellbore heating .....	196
Figure 7-53: Changes in pressure, temperature, $S_h$ , $S_g$ and $S_{aq}$ from initial conditions to 320 days for the Class 1 $CH_4$ hydrate with depressurization at 2.5 MPa with wellbore heating .....	197
Figure 7-54: Ice formation due to fast depressurization at 2.5 MPa with wellbore heating .....	198
Figure 7-55: A) Gas production B) Gas production ratio by depressurization at 2.7 MPa with wellbore heating .....	198
Figure 7-56: Depressurization at 2.7 MPa with wellbore heating at different intrinsic permeabilities .....	200
Figure 7-57: Grid structure of the hypothetical Class 3 reservoir.....	202
Figure 7-58: Cumulative gas production from the Class 3 $CH_4$ hydrate by depressurization at different pressures .....	203
Figure 7-59: Cumulative water production from the Class 3 $CH_4$ hydrate by depressurization at different pressures .....	204
Figure 7-60: Gas to water production ratio of the Class 3 $CH_4$ hydrate by depressurization at different pressures .....	205
Figure 7-61: Gas production flow rate from the Class 3 $CH_4$ hydrate by depressurization at different pressures .....	206
Figure 7-62: Changes in pressure, temperature, $S_h$ , $S_g$ and $S_{aq}$ with depressurization at 3.0 MPa without wellbore heating .....	207
Figure 7-63: Comparison of cumulative gas production from the Class 3 $CH_4$ hydrate by depressurization and depressurization with 50 C wellbore heating .....	209
Figure 7-64: Comparison of cumulative water production from the Class 3 $CH_4$ hydrate by depressurization and depressurization with 50 C wellbore heating .....	209
Figure 7-65: Comparison of gas to water production ratio of the Class 3 $CH_4$ hydrate by depressurization and depressurization with 50 C wellbore heating .....	210

Figure 7-66: Comparison of Cumulative gas production flow rates from the Class 3 CH <sub>4</sub> hydrate by depressurization and depressurization with 50 °C wellbore heating .....	210
Figure 7-67: Gas production from Class 3 hypothetical reservoir by depressurization at 3.0 MPa without and with wellbore heating (50 °C) at different intrinsic permeability .....	211
Figure 7-68: Alternating gas hydrate layers in turbidites (for illustration purpose) .....	213
Figure 7-69: Hydrate saturations and grids in a) Turbidites b) Class 3 reservoir ..	216
Figure 7-70: Cumulative gas production by depressurization in the hypothetical hydrate deposited in turbidites .....	217
Figure 7-71: Cumulative water production by depressurization in the hypothetical hydrate deposited in turbidites .....	217
Figure 7-72: Gas to water production ratio of depressurization in the hypothetical hydrate deposited in turbidites .....	218
Figure 7-73: Gas production rate by depressurization in the hypothetical hydrate deposited in turbidites .....	218
Figure 7-74: Cumulative Gas Production by depressurization in the hypothetical Class 3 reservoir .....	219
Figure 7-75: Cumulative Water Production by depressurization in the hypothetical Class 3 reservoir .....	219
Figure 7-76: Gas to water production ratio of depressurization in the hypothetical Class 3 reservoir .....	220
Figure 7-77: Gas production rate by depressurization in the hypothetical Class 3 reservoir .....	220
Figure 7-78: Changes in pressure, temperature, S <sub>h</sub> , S <sub>g</sub> and S <sub>aq</sub> with depressurization at 4.0 MPa with wellbore heating at 50 °C in turbidite hydrate reservoirs .....	221
Figure 7-79: Changes in pressure, temperature, S <sub>h</sub> , S <sub>g</sub> and S <sub>aq</sub> with depressurization at 6.0 MPa without wellbore heating in Class 3 hydrate reservoir .....	222
Figure 7-80: 3D view of a digital elevation model of the western Black Sea (Konerding, 2009) .....	224

Figure 7-81: a) A seismic section in the Danube Delta (coarse grained sediments are highlighted with purple and light red) (Zander <i>et al.</i> , 2016) b) BSR analysis by BSR.m code in this study for 100 % CH <sub>4</sub> hydrate for the system in Figure 7-81-a .....	225
Figure 7-82: Scheme of gas hydrate sections in the Danube fan in the Black Sea	227
Figure 7-83: Grid structure in the Danube Fan in Figure 7-82 .....	230
Figure 7-84: Cumulative gas production for upper gas hydrate section .....	232
Figure 7-85: Cumulative water production for upper gas hydrate section at different depressurization pressures.....	233
Figure 7-86: Gas to water production ratio of upper gas hydrate section.....	233
Figure 7-87: Gas flow rate for upper gas hydrate section.....	234
Figure 7-88: Pressure, temperature, hydrate saturation ( $S_h$ ), and ice saturation ( $S_i$ ) at 2.0 MPa depressurization for upper gas hydrate section at 420 <sup>th</sup> day of gas production .....	235
Figure 7-89: Pressure, Temperature, hydrate saturation, gas saturation, and aqueous saturation at a) 0-day b) 60 days at 3 MPa depressurization pressure for upper gas hydrate section .....	237
Figure 7-90: Effect of absolute permeability on gas production at 3 MPa depressurization pressure from upper gas hydrate .....	239
Figure 7-91: Effect of absolute permeability on water production at 3 MPa depressurization pressure from upper gas hydrate .....	239
Figure 7-92: Effect of absolute permeability on gas flow rate at 3 MPa depressurization pressure from upper gas hydrate .....	240
Figure 7-93: Cumulative gas production for lower gas hydrate section .....	241
Figure 7-94: Cumulative water production for lower gas hydrate section at different depressurization pressures.....	241
Figure 7-95: Gas to water production ratio of lower gas hydrate section at different depressurization pressures.....	242
Figure 7-96: Gas flow rate for lower gas hydrate section.....	242
Figure 7-97: Pressure, Temperature, hydrate saturation, gas saturation, and aqueous saturation at a) 0-day b) 60 days at 3 MPa depressurization pressure .....	243

Figure 7-98: Effect of absolute permeability on gas production at 3 MPa depressurization pressure from lower gas hydrate .....	245
Figure 7-99: Effect of absolute permeability on gas flow rate at 3 MPa depressurization pressure from lower gas hydrate .....	245
Figure 7-100: Effect of absolute permeability on water production at 3 MPa depressurization pressure from lower gas hydrate .....	246
Figure 7-101: Pressure, gas production rate and water production rate during 6-day depressurization test in Nankai Trough, Japan (Kawamoto, 2014) .....	247
Figure 7-102: Algorithm of HEP code .....	250
Figure 7-103: Comparison of CH <sub>4</sub> hydrate equilibrium curve of HEP, CSMHYD, CSMGem and HydraFLASH with experimental and other software data .....	253
Figure 7-104: Comparison of CH <sub>4</sub> hydrate equilibrium curve of HEP, CSMHYD, CSMGem and HydraFLASH with experimental and other software data at high temperatures .....	255
Figure 7-105: Comparison of enthalpy of CH <sub>4</sub> hydrate of HEP and Kamath (1984)'s equation with experimental data.....	257
Figure 7-106: Comparison of hydrate equilibrium of pure C <sub>2</sub> H <sub>6</sub> , C <sub>3</sub> H <sub>8</sub> , and CO <sub>2</sub> with HEP, CSMHYD, CSMGem and HydraFLASH and experimental data .....	258
Figure 7-107: Comparison of hydrate equilibrium of 93.2 % CH <sub>4</sub> , 4.25% C <sub>2</sub> H <sub>6</sub> , 1.61 % C <sub>3</sub> H <sub>8</sub> , 0.51% CO <sub>2</sub> , 0.43% N <sub>2</sub> with HEP, CSMHYD, CSMGem and HydraFLASH and experimental data.....	259
Figure 7-108: Comparison of hydrate equilibrium of 78 % CH <sub>4</sub> , 2 % C <sub>3</sub> H <sub>8</sub> , 20% CO <sub>2</sub> with HEP, CSMHYD, CSMGem and HydraFLASH and experimental data .....	260
Figure 7-109: Comparison of hydrate equilibrium of 88.36 % CH <sub>4</sub> , 6.82 % C <sub>2</sub> H <sub>6</sub> , 2.54 % C <sub>3</sub> H <sub>8</sub> , 0.38 % i-C <sub>4</sub> H <sub>10</sub> , 0.89 % n-C <sub>4</sub> H <sub>10</sub> , 1.01 % n-C <sub>5</sub> H <sub>12</sub> with HEP, CSMHYD, CSMGem and HydraFLASH and experimental data .....	261
Figure 7-110: Comparison of hydrate equilibrium of gas mixture (87 % CH <sub>4</sub> , 13% CO <sub>2</sub> ) and gas mixture (88.3 % CH <sub>4</sub> , 11.7 % C <sub>3</sub> H <sub>8</sub> ) with HEP, CSMHYD, CSMGem and HydraFLASH and experimental data .....	262
Figure 7-111: CH <sub>4</sub> hydrate equilibrium curve with 10 weight % Methanol with HEP, CSMGem and HydraFLASH and experimental data .....	263

Figure 7-112: CH <sub>4</sub> hydrate equilibrium curve with 10.81 weight % NaCl with HEP, CSMGem and HydraFLASH and experimental data.....	264
Figure 7-113: Comparison of hydrate equilibrium of CH <sub>4</sub> with inhibitors (6.21 % weight NaCl and 10.0 weight % Methanol) with HEP, CSMGem and HydraFLASH and experimental data .....	265
Figure 7-114: Comparison of hydrate equilibrium of 78 % CH <sub>4</sub> , 2 % C <sub>3</sub> H <sub>8</sub> , 20% CO <sub>2</sub> with inhibitors (9.99 % NaCl and 10.01 % Methanol) with HEP and HydraFLASH and experimental data .....	266
Figure 7-115: Comparison of hydrate equilibrium of 84.13 % CH <sub>4</sub> , 4.67 % C <sub>2</sub> H <sub>6</sub> , 2.34 % C <sub>3</sub> H <sub>8</sub> , 0.93 % n-C <sub>4</sub> H <sub>10</sub> , 0.93 % n-C <sub>5</sub> H <sub>12</sub> , 7% N <sub>2</sub> with 10.0 % Methanol with HEP, CSMHYD, CSMGem and HydraFLASH and experimental data.....	267
Figure 7-116: Algorithm of HEPComp code .....	273
Figure 7-117: Algorithm of SM code .....	278
Figure 7-118: Algorithm of SMProd code .....	282
Figure 7-119: Algorithm of SMmix code .....	284
Figure 7-120: Algorithm of BSR.m code.....	287
Figure 7-121: Detail of the multiple BSRs observed by Popescu <i>et al.</i> (2006).....	288
Figure 7-122: BSR analysis by BSR.m code for BSR 1 with CH <sub>4</sub> hydrate.....	289
Figure 7-123: BSR analysis by BSR.m code for BSR 2 with 97.86 % CH <sub>4</sub> , 2.14% H <sub>2</sub> S hydrate .....	291
Figure 7-124: BSR analysis by BSR.m code for BSR 3 with 95.54 % CH <sub>4</sub> , 4.46% H <sub>2</sub> S hydrate .....	291
Figure 7-125: BSR analysis by BSR.m code for BSR 4 with 94.31 % CH <sub>4</sub> , 5.69% H <sub>2</sub> S hydrate .....	292
Figure 7-126: BSR analysis by BSR.m code for BSR 2 with 98.02 % CH <sub>4</sub> , 1.98% C <sub>3</sub> H <sub>8</sub> hydrate.....	293
Figure 7-127: BSR analysis by BSR.m code for BSR 3 with 96.58 % CH <sub>4</sub> , 3.42% C <sub>3</sub> H <sub>8</sub> hydrate.....	294
Figure 7-128: BSR analysis by BSR.m code for BSR 4 with 95.65 % CH <sub>4</sub> , 4.35% C <sub>3</sub> H <sub>8</sub> hydrate.....	294
Figure 7-129: Essential elements for gas hydrate reservoir as an energy source...	295

Figure 7-130: CH <sub>4</sub> hydrate stability zone thickness (Wood and Jung, 2008) .....	296
Figure 7-131: DSDP Legs 1-96, Sites 1-624 (DSDP, 2016).....	297
Figure 7-132: Drilling sites in Leg 42B in the Black Sea (Supko <i>et al.</i> , 1978) .....	298
Figure 7-133: Supply of sedimentary material to the Black Sea on annual basis (Shimkus and Trimonis, 1974).....	299
Figure 7-134: Vertical distribution of total Sulphur and organic carbon content at Hole 379A (Calvert and Batchelor, 1978).....	300
Figure 7-135: a) Core profiles of Cl at Site UBGH2-2_1 b) Estimates of gas hydrate saturation ( $S_h$ ) from Cl concentration at Site UBGH2-2_1, compared with $S_h$ estimates based on well log resistivity data (black line) (Kim <i>et al.</i> , 2013) .....	301
Figure 7-136: Distribution of Cl in a) Sites 379A/B b) Sites 380/380A c) Site 381 (Adapted from Shishkina, 1978) .....	302
Figure 7-137: Core 14 at Site 381 (Site 381, 1978) .....	303
Figure 7-138: Tentative identification of marine and lacustrine horizons at Hole 379A based on the distribution of sulfur in the bulk sediment (left), the chlorinity of the pore water (Calvert and Batchelor, 1978) .....	304
Figure 7-139: Hydrate equilibrium curves and lithostratigraphy at Site 379.....	306
Figure 7-140: Sand layer intercalated in a terrigenous mud sequence (Site 379, 1978) .....	307
Figure 7-141: a) Core 28 (254-263.5 mbsf) of Site 379: Dark greenish gray terrigenous mud with abundant muddy sand to sandy mud layers suggesting turbidites b) Core 43 of Site 379: Dark greenish gray terrigenous mud with numerous silt and sandy mud layers, some indicating turbidite deposits. (Site 379, 1978) .....	308
Figure 7-142: a) Soupy sediments from Hole 381 Core 18 (170 mbsf) b) Mousse-like sediments from Hole 379A Core 11 (100 mbsf) (Site 379, 1978; Site 381, 1978) .....	309
Figure 7-143: Hydrate equilibrium curves and lithostratigraphy at Site 380.....	310
Figure 7-144: a) Core 30 of Site 380 (275.5-285 mbsf): interbedded sandy silt layers deposited by turbidite currents b) Core 32 of Site 380 (294.5-305.0 mbsf) in muds, dark greenish gray, greenish black, color variation attributed to the varying abundance of pyrite with intercalation of sandy silt, deposited by turbidity currents (Site 380, 1978) .....	311

Figure 7-145: Hydrate equilibrium curves and lithostratigraphy at Site 381.....	312
Figure 7-146: a) Core 18 of Site 381 (161.5-171 mbsf) Coarse medium gray terrigenous calcareous silt with abundant mollusc fragments. Lower part of the core is a finer greenish gray terrigenous carbonate mud. Several 5-10 cm voids due to gas expansion b) Core 42 of Site 381 (380-399.5 mbsf): Pebble, sand, mud (Site 381, 1978) .....	313
Figure 7-147: Grain size fractions and clay contents of Sites 379, 380 and 381 (Adapted from Site 379 (1978), Site 380 (1978), Site 381(1978), and Trimonis <i>et al.</i> (1978)).....	314
Figure 7-148: Core 13 of Site 379 (111.5-121 mbsf): Patches of coarser silt to sandy silt occur throughout the core (high gas expansion and voids are due to gas expansion) (Site 379, 1978).....	315
Figure 7-149: Changes in the mechanical (deformative) properties of the deposits from Site 381 and Hole 380A and their reaction with the distillate water downsection (Kuprin <i>et al.</i> , 1978).....	316



## CHAPTER 1

### INTRODUCTION

The consumption of fossil fuels has been increasing sharply in all over the world. However, current conventional oil and gas reserves are not limitless. Advancement of technology has triggered the production of natural gas from unconventional natural gas reservoirs such as gas hydrates, shale gas, tight gas, and coalbed methane reserves. Except gas hydrate reservoirs, huge amount of gas is being currently produced from shale gas, tight gas, and coalbed methane reserves, mainly in the United States of America (Laherrere, 2000; Kok and Merey, 2014; Ma and Holditch, 2016; Max and Johnson, 2016). However, gas production technology from gas hydrate reservoirs are still immature (SBC Energy Institute, 2015; Ma and Holditch, 2016; Max and Johnson, 2016). Therefore, many studies related to seismic, drilling, well completion, coring, geomechanics, geology, geochemistry and production in gas hydrate reservoirs are essential to provide alternative gas production methods for gas hydrates.

Figure 1-1 shows the known and inferred locations of gas hydrate reservoirs in the world. Gas hydrates form at high pressure and low temperature conditions from water (host molecules) and guest molecules. Gas hydrate reservoirs mostly consist of methane ( $\text{CH}_4$ ) but also they include other impurities such as ethane ( $\text{C}_2\text{H}_6$ ), propane ( $\text{C}_3\text{H}_8$ ), hydrogen sulfide ( $\text{H}_2\text{S}$ ) and carbon dioxide ( $\text{CO}_2$ ). 1  $\text{m}^3$  of gas hydrate can release of 160-180  $\text{m}^3$  of natural gas at standard conditions (0 °C and 1 atm) (Sloan, 2003). Koh *et al.* (2012) proposed that even the most conservative estimates place the amount of gas contained within gas hydrate deposits at least 2–10 times larger than the global estimates of conventional natural gas of  $4.4 \times 10^{14}$  standard  $\text{m}^3$ . Therefore, recently, many field-scale pilot projects have been conducting especially in Japan, USA, India, China, Canada, and Korea (Collett *et al.*, 2015).

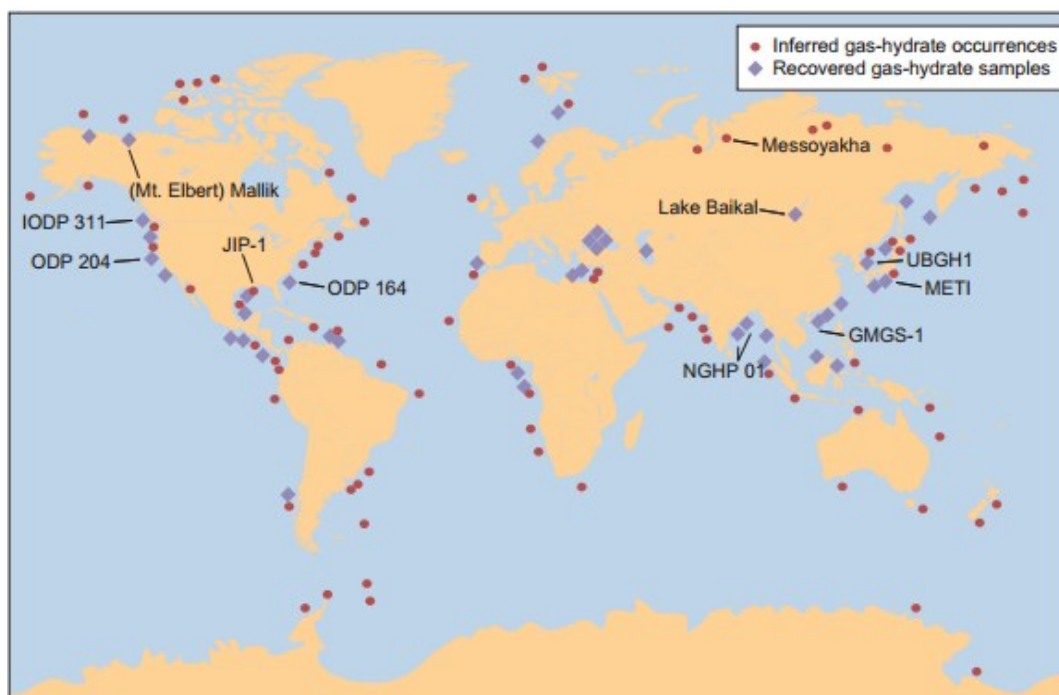


**Figure 1-1:** The distribution of gas hydrates in the world (Koh *et al.*, 2012)

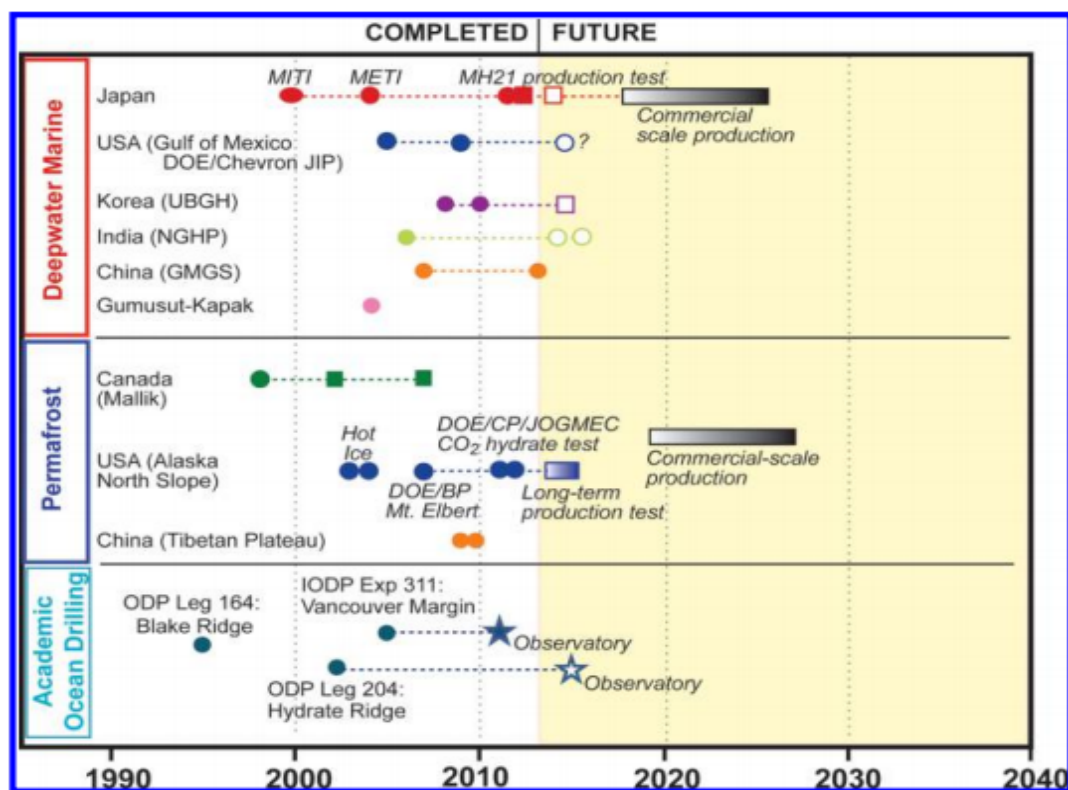


**Figure 1-2:** Timeline chart of gas hydrate field projects in the world (Collett *et al.*, 2015)

Figure 1-2 briefly summarizes the timeline charts for the main gas hydrate projects in the world. Recently, seismic surveys have been conducting in Turkish part of the Black Sea for gas hydrate exploration (Max and Johnson, 2016). As seen in Figure 1-3, Turkey's natural gas production from conventional gas reservoirs has declined sharply. Turkey's natural gas consumption is approximately 49.8 standard billion cubic meters (Bcm) per year (TPAO, 2015). However, domestic natural gas production supplies only approximately 1 % of this amount of gas consumption and rest 99 % of natural gas (Figure 1-4) is imported from Iran, Russia, Nigeria, etc. Potential gas hydrates in the Black Sea might decrease Turkey's natural gas import (Ocakoğlu, 2009).

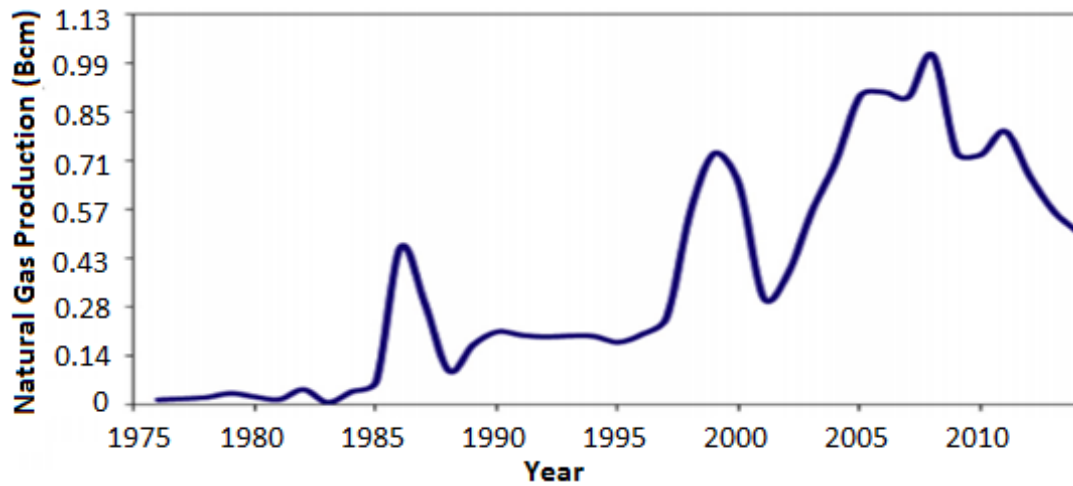


**Figure 1-3:** Natural gas production of Turkey between 1975 and 2014 (Özgür, 2016)

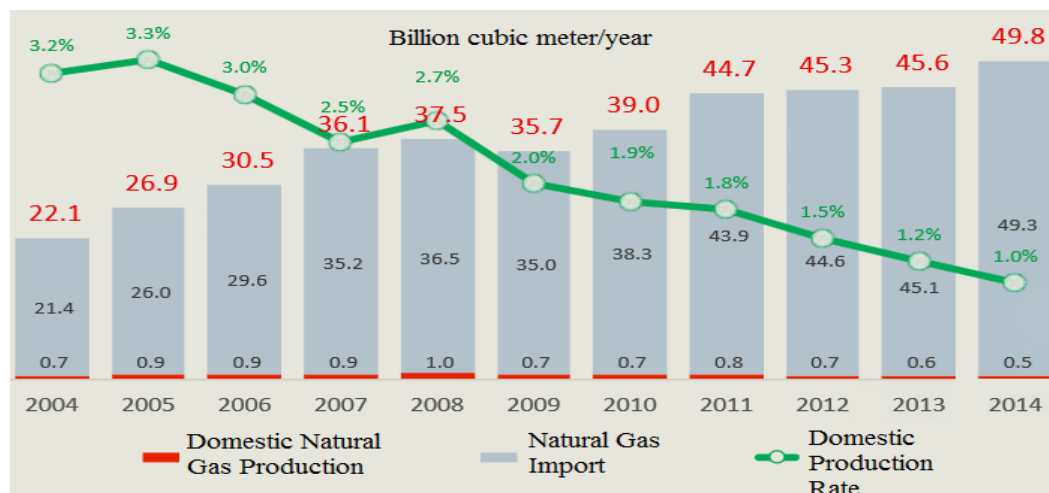


**Figure 1-4:** Turkey's natural gas supply and its domestic production rates between 2004 and 2014 (Adapted from TPAO, 2015)

The Black Sea might have a huge potential of gas hydrates (Vassilev, 2006; Johnson and Max, 2015). Dutta (2012) proposed that the Black Sea might be next the North Sea and emphasized the energy potential of the Black Sea, especially its gas hydrate potential but according to him, the Black Sea is still widely unexplored. As seen from Figure 1-5, Turkey, Bulgaria, Romania, Ukraine, Russia and Georgia have borders to the Black Sea but Turkey's border occupy large portion of the Black Sea. According to the gas in place calculations of Klauda and Sandler (2003), the greatest amount of methane hydrate could exist in the southern Black Sea bordering Turkey. Moreover, bottom simulation reflectance (BSR) lines were detected with a total of 2500 km multichannel seismic, chirp sub-bottom profiler and multi-beam bathymetry data during three different expeditions in 2010 and 2012 along the southwestern margin of the Black Sea (Küçük *et al.*, 2013; Küçük *et al.*, 2015; Küçük *et al.*, 2015b). BSRs are important indicators of gas hydrates (Popescu *et al.*, 2006; Majumdar, 2015; Paganoni *et al.*, 2016).



**Figure 1-5:** Black Sea relief location map with exclusive economic zones (Wikipedia, 2016)

Huge potential of gas hydrates in the Black Sea should be evaluated effectively to decrease Turkey's high amount of natural gas import. Although there are many studies and field projects in many countries such as Japan, Canada, USA, China,

Germany, Korea and India, there are only a few basic laboratory studies (e.g. SEISLAB) related to gas hydrates in Turkey. Seismic studies in the Black Sea targeting the Black Sea gas hydrates have still been conducting in the southwestern region of the Black Sea (Max and Johnson, 2016). As well as geophysical studies in the Black Sea, potential Black Sea gas hydrates should be evaluated from the view of petroleum and natural gas engineering, chemical engineering, geological engineering, environmental engineering and civil engineering.

In the experimental study of Bülbul *et al.* (2014), gas hydrate as bulk was formed inside 600 cm<sup>3</sup> high pressure cell by using methane (CH<sub>4</sub>)-hydrogen sulfide (H<sub>2</sub>S) mixtures at different concentrations. This study was important to understand the effect of H<sub>2</sub>S on the Black Sea gas hydrates because H<sub>2</sub>S is common gas component in the Black Sea. It was observed that H<sub>2</sub>S eases hydrate formation (Bülbul *et al.*, 2014). Ors (2012) conducted CO<sub>2</sub>-CH<sub>4</sub> swapping experiments within CH<sub>4</sub> hydrate formed in sediments inside 600 cm<sup>3</sup> high pressure cell at 4°C. Similarly, Abbasov (2014) conducted CO<sub>2</sub>-CH<sub>4</sub> swapping experiments within 94 % CH<sub>4</sub>, 2 % CO<sub>2</sub>, 3 % C<sub>3</sub>H<sub>8</sub> hydrate formed in sediments inside 600 cm<sup>3</sup> high pressure cell at 4°C. However, although it was claimed that these experiments (Ors, 2012; Abbasov, 2014) were conducted in the Black Sea conditions, they do not reflect the actual Black Sea conditions because the average temperature on the seafloor of the Black Sea is approximately 9 °C (Vassilev, 2006). Therefore, before conducting any experiments related to gas hydrates and gas production such as depressurization, thermal injection, chemical injection or CO<sub>2</sub>-CH<sub>4</sub> swapping, detailed literature survey and analysis are necessary for the Black Sea conditions.

As a result, this study focuses on the following topics:

- i. Analysis of the Black Sea conditions and potential gas hydrate properties in the Black Sea
- ii. The selection of production method(s) for the Black Sea gas hydrates
- iii. High pressure reactor and experimental set-up design for the gas production from the Black Sea gas hydrates

- iv. Gas production modelling studies from the Black Sea gas hydrates at laboratory scale and reservoir scale (for Class 1 hydrate, Class 3 hydrate, hydrate deposited in turbidites and gas hydrate sections in the Danube fan) by using HydrateResSim numerical simulator
- v. HEP.m code to predict gas hydrate properties
- vi. HEPComp.m code to predict gas compositional change during gas hydrate formation
- vii. SM.m and SMmix.m codes to calculate the amount of gas and water needed to reach target saturations for pure CH<sub>4</sub> hydrate and mixed gas hydrates, respectively in the high pressure reactor (METU reactor)
- viii. BSR.m code to predict gas composition at BSR lines
- ix. Characterization of the Black Sea gas hydrates and its sediments

The research results of this PhD thesis are organized in the following chapters:

Chapter 2 is a review of the literature survey on gas hydrates, their chemistry, origin of gas hydrates in nature, types of gas hydrate reservoirs, types of gas production methods from hydrates and hydrate field projects in the world.

Chapter 3 summarizes general information about the Black Sea, evidences showing gas hydrate existence in the Black Sea and properties of the potential Black Sea gas hydrates.

Chapter 4 gives the equations and methods for gas hydrate equilibrium conditions and hydrate properties such as hydration number, hydrate molecular weight, hydrate density, hydrate dissociation enthalpy, geomechanical properties, thermal properties and flash calculations.

Chapter 5 presents the basis of gas production modelling from gas hydrates in reservoir scale and laboratory scale, the main mass and heat balance equations of HydrateResSim numerical simulator, permeability and relative permeability in gas hydrates, and capillary pressure in gas hydrates.

Chapter 6 presents an explicit statement of the problem.

Chapter 7 presents the results and discussions of CH<sub>4</sub> in-place calculations in the Black Sea gas hydrates, the selection of gas production method(s) from gas hydrates in the Black Sea conditions, the experimental set-up design for gas production from the Black Sea gas hydrates, reservoir and laboratory scale simulations in the Black Sea conditions and the verification of HEP.m, HEPComp.m, SM.m, SMmix.m and BSR.m codes. Finally, in the end of Chapter 7, the core data, grain size data, mineral content data, pore geochemistry data of 6 holes drilled in the Black Sea in 1975 with DSDP Leg 42B drilling program were evaluated to characterize the Black Sea sediments and gas hydrates.

Chapter 8 presents the conclusion of this thesis.

Chapter 9 presents the recommendations for future studies.

The results of this PhD thesis were also reported in the following articles and conference papers:

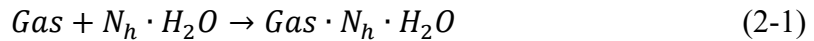
- 1) Merey, S, Sinayuc, C. (2016). Investigation of Gas Hydrate Potential of the Black Sea and Modelling of Gas Production from a Hypothetical Class 1 Methane Hydrate Reservoir in the Black Sea Conditions, *Journal of Natural Gas Science and Engineering* 29 (2016) 66-79.
- 2) Merey, S., Sinayuc, C. (2016). New Software That Predicts Hydrate Properties and Its Use in Gas Hydrate Studies. *Journal of Chemical & Engineering Data*, 61 (5), 1930–1951.
- 3) Merey, S., Sinayuc, C. (2016), Experimental set-up design for gas production from the Black Sea gas hydrate reservoirs, *Journal of Natural Gas Science and Engineering*, 33 (2016) 162-185.
- 4) Merey, S., Sinayuc, C. (2016). Analysis of the Black Sea Gas Hydrates. *World Academy of Science, Engineering and Technology, International Science Index* 116, *International Journal of Chemical, Molecular, Nuclear, Materials and Metallurgical Engineering*, 10(8), 886 - 894.

- 5) Merey, S., Sinayuc, C. (2016). Analysis of the Black Sea sediments by evaluating DSDP Leg 42B drilling data for gas hydrate potential. *Marine and Petroleum Geology*, 78: 151–167.
- 6) Merey, S., Sinayuc, C. (2015). Simulation of Gas Production from Hydrate Reservoirs by using HydrateResSim Numerical Simulator. 20<sup>th</sup> International Petroleum and Natural Gas Congress and Exhibition, May 29, 2015, Ankara, Turkey.
- 7) Merey, S., Sinayuc, C. (2015). Investigation of Gas Hydrate Potential and Modelling of Gas Production from Hydrate Reservoirs in the Black Sea. The 65<sup>th</sup> Canadian Chemical Engineering Conference, October 4-7, 2015, Calgary, Canada.
- 8) Merey, S., Oney, M., Sinayuc, C. (2016). Characterization of the Potential Black Sea Gas Hydrates. Turkish Marine Sciences Conference, May 31-June 3, 2016, Ankara, Turkey.

## CHAPTER 2

### GAS HYDRATES

Gas hydrates are ice-like crystalline structures formed by water and gas molecules at high pressure and low temperature conditions. They are defined as nonstoichiometric compounds, which means that the ratio of the atoms present in the composition is not a simple integer (Carroll, 2009). The chemical formula of a gas hydrate compound is shown in Equation (2-1). Hydration number ( $N_h$ ) determines the chemical formula.  $N_h$  changes according to the type of gas, pressure, temperature, salinity, and pH (Klapp, 2009; Hesse and Schacht, 2011; Ye and Liu, 2013).



Hydrogen bonding and Van der Waals forces are the causes of gas hydrate formation. Water molecules consist of one oxygen and two hydrogen atoms. Hydrogen atoms connect to oxygen with covalent bonds. However, there are unbounded electrons: mainly negative charges on oxygen and positive charges on hydrogen atoms. Due to the electrostatic attraction between the positive charges of hydrogen atoms and the negative charges of oxygen atoms of different water molecules, hydrogen bonding forms between water molecules. Covalent bond is 10 to 20 times stronger than hydrogen bonding. When water and hydrate forming gases or liquid components are together at high pressure and low temperature conditions, water molecules form a cage like structure around gas molecules. This is because of  $105^\circ$  angle between oxygen and hydrogen atoms. Water molecules trapping gas molecules inside the cages are called “host” molecules and gas molecules are defined as “guest” molecules (Carroll, 2009; Zou, 2013; Rajput and Thakur, 2016). Although there are Van der Waals forces between non-polar molecules in a gas hydrate structure, these forces are relatively weak compared to hydrogen bonding. For example, in order to break hydrogen bond, approximately, 5 kcal/mole energy is necessary while only 0.3

kcal/mole energy is essential to break Van der Waals forces. However, the covalent bond between hydrogen and oxygen atoms in water is the strongest bond among these three bonds (102 kcal/mole bond breaking energy) (Sloan and Koh, 2008; Carroll, 2009). Therefore, during the dissociation of gas hydrates, Van der Waals forces between non-polar molecules and hydrogen bonds between different water molecules are broken (Sloan and Koh, 2008; Zou, 2013). Generally, hydrate formation is considered as a “highly reversible chemical reaction” (Hesse and Schacht, 2011; Johnson and Max, 2015; Max and Johnson, 2016).

## 2.1 Structural Characteristics of Gas Hydrates

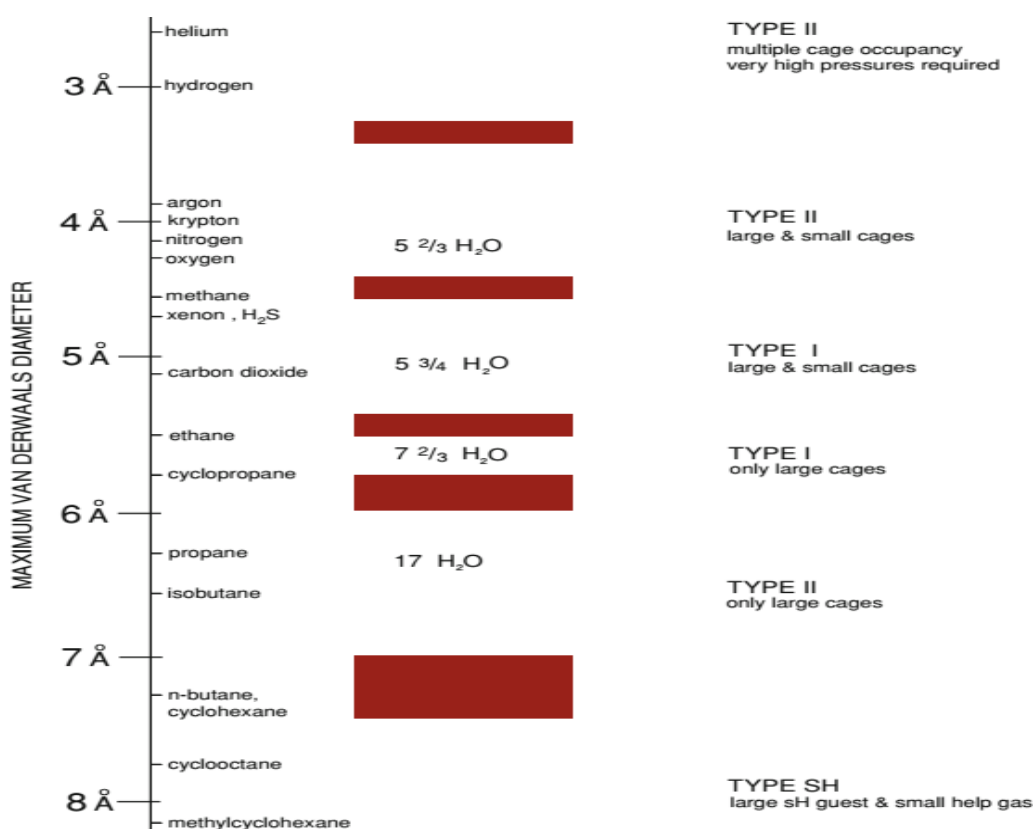


**Figure 2-1:** Comparison of guest molecule sizes and cavities occupied as simple hydrates (Giavarini and Hester, 2011)

It is known that approximately 130 compounds form hydrates (sI, sII, or sH) with water (Sloan and Koh, 2008). Hydrocarbon molecules such as methane (CH<sub>4</sub>), ethane (C<sub>2</sub>H<sub>6</sub>), propane (C<sub>3</sub>H<sub>8</sub>) and i-butane (i-C<sub>4</sub>H<sub>10</sub>) form their own hydrate (simple or pure

hydrate) at high pressure and low temperature conditions when there is enough water in the system. Similarly, carbon dioxide (CO<sub>2</sub>), hydrogen sulfide (H<sub>2</sub>S), nitrogen (N<sub>2</sub>), oxygen (O<sub>2</sub>) and other gases form hydrates at their hydrate equilibrium conditions (Giavarini and Hester, 2011). As seen in Figure 2-1, different components form different types of hydrate structures depending on their molecular sizes.

**Table 2-1:** Geometry of cages of hydrates (Sloan and Koh, 2008)

<b>Crystal structure of gas hydrate</b>	<b><i>sI</i></b>		<b><i>sII</i></b>		<b><i>sH</i></b>		
<i>Cavity</i>	<b>Small</b>	<b>Big</b>	<b>Small</b>	<b>Big</b>	<b>Small</b>	<b>Medium</b>	<b>Big</b>
<i>Description</i>	5 <sup>12</sup>	5 <sup>12</sup> 6 <sup>2</sup>	5 <sup>12</sup>	5 <sup>12</sup> 6 <sup>4</sup>	5 <sup>12</sup>	4 <sup>3</sup> 5 <sup>6</sup> 6 <sup>3</sup>	5 <sup>12</sup> 6 <sup>8</sup>
<i>Number of cavities/unit cell</i>	2	6	16	8	3	2	1
<i>Average cavity radius, (Å)</i>	3.95	4.33	3.91	4.73	3.94	4.04	5.79
<i>Variation in radius, %</i>	3.4	14.4	5.5	1.73	4.0	8.5	15.1
<i>Number of water molecules/cavity</i>	20	24	20	28	20	20	36

There are mainly three types of hydrate structures in nature: Structure I (sI), Structure II (sII) and Structure H (sH) (Sloan, 1998). Figure 2-2 illustrates the shapes of these hydrate structures and the information about their geometry is listed in Table 2-1. Each hydrate structure is composed of different types of cages. These cages are pentagonal dodecahedron (5<sup>12</sup>), tetrakaidecahedron (5<sup>12</sup>6<sup>2</sup>), hexakaidecahedron (5<sup>12</sup>6<sup>4</sup>), irregular dodecahedron (4<sup>3</sup>5<sup>6</sup>6<sup>3</sup>) and icosahedron (5<sup>12</sup>6<sup>8</sup>). For example, pentagonal dodecahedron (n<sup>m</sup>=5<sup>12</sup>) is formed from 12 (m=12) pentagonal (n=5) faces. Hence, n and m numbers are used to define the shape of different cages of hydrates. As seen in Table 2-1, one sI hydrate structure consists of 2 pentagonal dodecahedron cages (small cages: 5<sup>12</sup>) and 6 tetrakaidecahedron cages (large cages: 5<sup>12</sup>6<sup>2</sup>). sII hydrate structure is larger than sI hydrate structure and they are composed of 16 small cages (5<sup>12</sup>) and 8 large cages (hexakaidecahedron: 5<sup>12</sup>6<sup>4</sup>). Finally, sH hydrate consists of 3 small (5<sup>12</sup>), 2 medium (4<sup>3</sup>5<sup>6</sup>6<sup>3</sup>) and 1 large cages (5<sup>12</sup>6<sup>8</sup>) (Sloan, 2003; Zou, 2013). Approximately 46, 136 and 34 water (H<sub>2</sub>O) molecules are essential for sI, sII and sH hydrates respectively (see Figure 2-2).

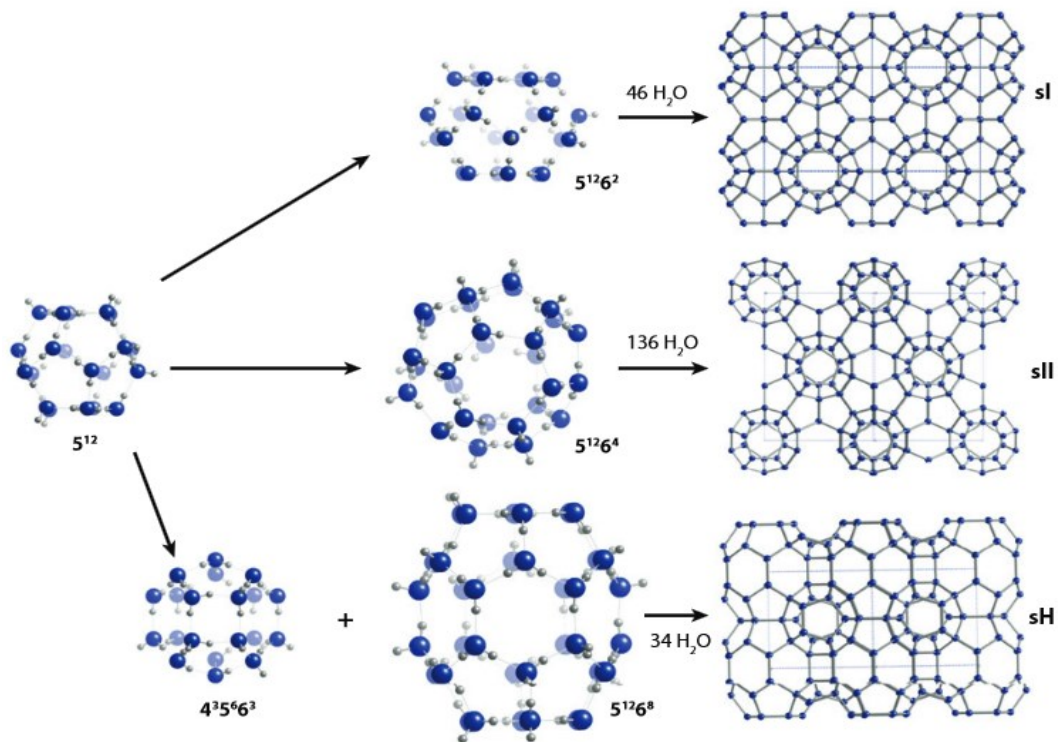


**Figure 2-2:** Three types of gas hydrate structure and their component cavities (Hester and Brewer, 2009)

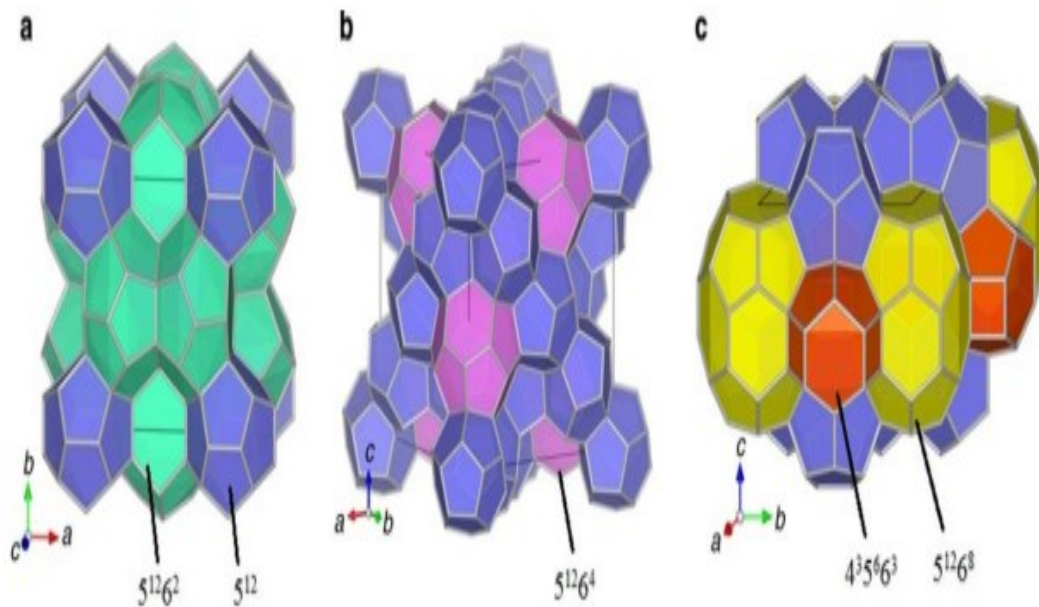


**Figure 2-3:** Three structures of gas hydrates: (a) sI, (b) sII, and (c) sH (Zheng *et al.*, 2015)

Figure 2-3 is very useful to visualize gas hydrate structures (sI, sII and sH) and their geometry.  $5^{12}$ ,  $5^{12}6^2$ ,  $5^{12}6^4$ ,  $4^35^66^3$ ,  $5^{12}6^8$  cages are represented as purple, green, pink, red, and yellow respectively.

Simple (or pure) gas hydrates are defined as gas hydrates formed with only one type of gas. Hence, depending on the molecular diameter of gas, different types of gas hydrates form at high pressure and low temperature and these formed hydrate structure changes with the type of gas. Figure 2-1 shows that simple hydrates of  $\text{CH}_4$ ,  $\text{C}_2\text{H}_6$ ,  $\text{CO}_2$ ,  $\text{H}_2\text{S}$ , and  $\text{Xe}$  are sI type of gas hydrate. Moreover,  $\text{C}_3\text{H}_8$ , i- $\text{C}_4\text{H}_{10}$ ,  $\text{N}_2$  and  $\text{O}_2$  form sII type of gas hydrate. Different from sI and sII hydrates, for the formation of sH hydrates, one help gas such as  $\text{CH}_4$  and other large molecules with diameters greater than those of isobutane (i- $\text{C}_4$ ), such as i- $\text{C}_5$  are necessary. sI and sII hydrates are common in all over the world but sH hydrates are rare and they were only found in a few areas such as the Gulf of Mexico, the Cascadia margin and the Caspian Sea (Hester and Brewer, 2009).

In order to understand the reason of the different types of gas hydrate structures with different gas molecules, Table 2-2 is commonly used. This table shows the values of the molecular diameters ratio to the cavity diameters of some gases. For instance, these ratios for  $\text{CH}_4$  in sI hydrate are 0.744 for small cages and 0.855 for large cages. For  $\text{CH}_4$  in sII hydrate, the ratios are 0.868 for small cages and 0.655 for large cages. In sI hydrate,  $\text{CH}_4$  molecules fill large cages much compared to  $\text{CH}_4$  in sII hydrates. Therefore,  $\text{CH}_4$  molecules form sI hydrate when low temperature and high pressure conditions are satisfied. Differently,  $\text{C}_3\text{H}_8$  molecules form sII hydrate because these molecules are quite large to fit to the cages of sI hydrate. As seen in Table 2-2,  $\text{C}_3\text{H}_8$  molecules only fit into the large cages of sII hydrate. In simple hydrate of  $\text{C}_3\text{H}_8$ , 16 small cages of sII hydrate structure stay empty. Because of empty cages,  $\text{C}_3\text{H}_8$  hydrate is not stable at high temperature conditions. The hydrate equilibrium curves of  $\text{C}_3\text{H}_8$  and other gases are in Figure 2-4. When pressure and temperature values cross above the equilibrium lines, hydrate forms and in the reverse case, hydrates of those gases cannot form. Hence, for the formation of pure  $\text{C}_3\text{H}_8$  hydrate, high pressure values are needed after approximately 278 K (4.85 °C). This is related to unstable hydrate of

$C_3H_8$  due to empty cages. Furthermore, according to Sloan and Koh (2008), if gas molecules fill the cages of hydrate as much as possible, hydrate will be much more stable. Therefore, at least 0.76 ratio of cavity filling is a need for stable gas hydrates (Sloan and Koh, 2008). Large molecules such as  $C_3H_8$  cannot enter into the small cages of sI and sII hydrates. However, the cavity ratio of  $CO_2$  for the small cages of sI hydrate is equal to 1.00 or it might be little more at different hydrate formation conditions. Hence, if  $CO_2$  gas molecules enter into the small cages of sI and sII hydrates, this may cause the distortion of these cages (Donohoue and College, 2000). In order to understand the behavior of gas molecules in the cavities of simple hydrates and hydrates of gas mixtures, Table 2-2 is quite beneficial.

Although in nature,  $CH_4$  hydrates are common in both permafrost and ocean (~99 %) of known gas hydrate reservoirs (Sloan and Koh, 2008; Max and Johnson, 2016), there are also sII gas hydrates formed by natural gas including  $CH_4$ ,  $C_2H_6$ ,  $C_3H_8$  and other impurities (Rogers, 2015). Even the addition of 1 %  $C_3H_8$  into  $CH_4$  gas molecules causes the formation of sII hydrates at the hydrate equilibrium conditions (Zanjani *et al.*, 2011; Rogers, 2015). Moreover, during the transportation of natural gas and its impurities with pipelines, there is a risk of mixed gas hydrate formation in winter seasons. Hence, the investigation of mixed gas hydrates is important. Abbasov (2014) and Küçük *et al.* (2015) conducted the experiments with the gas mixture composed of 95 %  $CH_4$ , 3 %  $C_3H_8$ , and 2 %  $CO_2$  in the sediments. During the hydrate formation, the composition of  $C_3H_8$  in free gas decreased while the percentage of  $CH_4$  increased. In these experiments, sII hydrate formed in the high pressure cell due to  $C_3H_8$  concentration. Mostly large cages of sII hydrate were filled by  $C_3H_8$  gas molecules. Small cages and some of large cages were filled by  $CH_4$  and  $CO_2$  molecules. Contrary to the simple hydrate of  $C_3H_8$ , the small cages of mixed sII hydrate were filled. Therefore, the formed hydrate was very stable. Similar observations for mixed hydrates were obtained in the studies of Schicks (2010) and Schicks and Luzi-Helbing (2013).

**Table 2-2:** Ratio of molecular diameters to cavity diameters for gas hydrate formers and a few others (Sloan and Koh, 2008)

<i>Guest hydrate former</i>		<i>Molecular diameter/cavity diameter for cavity type</i>			
		<i>Structure I</i>		<i>Structure II</i>	
<i>Molecule</i>	<i>Diameter (Å)</i>	$5^{12}$	$5^{12}6^2$	$5^{12}$	$5^{12}6^4$
<i>He</i>	2.28	0.447	0.389	0.454* <sup>β</sup>	0.32* <sup>β</sup>
<i>H<sub>2</sub></i>	2.72	0.533	0.464	0.542* <sup>β</sup>	0.408* <sup>β</sup>
<i>Ne</i>	2.97	0.582	0.507	0.592* <sup>β</sup>	0.446* <sup>β</sup>
<i>Ar</i>	3.8	0.745	0.648	0.757*	0.571*
<i>Kr</i>	4.0	0.784	0.683	0.797*	0.601*
<i>N<sub>2</sub></i>	4.1	0.804	0.700	0.817*	0.616*
<i>O<sub>2</sub></i>	4.2	0.824	0.717	0.837*	0.631*
<i>CH<sub>4</sub></i>	4.36	0.855*	0.744*	0.868	0.655
<i>Xe</i>	4.58	0.898*	0.782*	0.912	0.687
<i>H<sub>2</sub>S</i>	4.58	0.898*	0.782*	0.912	0.687
<i>CO<sub>2</sub></i>	5.12	1.00*	0.834*	1.02	0.769
<i>C<sub>2</sub>H<sub>6</sub></i>	5.5	1.08	0.939*	1.10	0.826
<i>c-C<sub>3</sub>H<sub>6</sub></i>	5.8	1.14	0.990	1.16	0.871*
<i>(CH<sub>2</sub>)<sub>3</sub>O</i>	6.1	1.20	1.04*	1.22	0.916*
<i>C<sub>3</sub>H<sub>8</sub></i>	6.28	1.23	1.07	1.25	0.943*
<i>i-C<sub>4</sub>H<sub>10</sub></i>	6.5	1.27	1.11	1.29	0.976*
<i>n-C<sub>4</sub>H<sub>10</sub></i>	7.1	1.39	1.21	1.41	1.07

\* shows the cavity occupied by the simple hydrate former

<sup>β</sup> shows that the simple hydrate is only formed at very high pressure

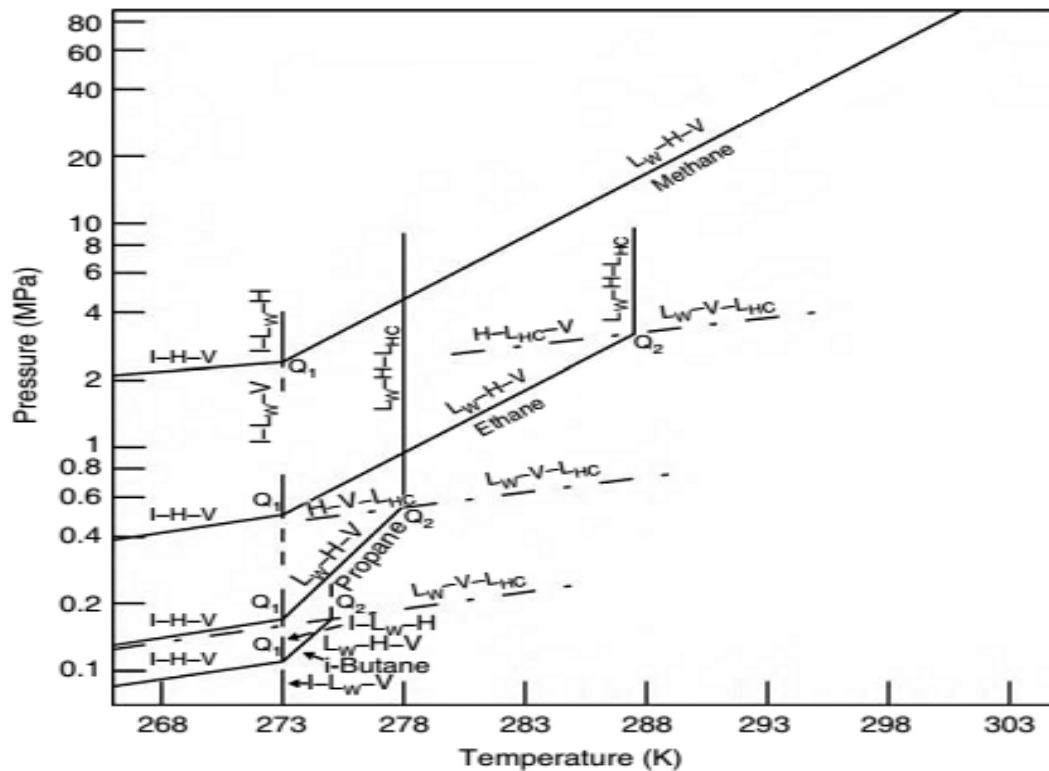


**Figure 2-4:** Hydrate equilibrium curve of some simple gas hydrates (Q<sub>1</sub>: lower quadruple point; Q<sub>2</sub>: upper quadruple point) (Sloan, 1998)

## 2.2 The Potential of Gas Hydrates in Nature

Scientists and engineers make studies about gas hydrates for different purposes. These purposes are mainly as:

- Future potential energy sources in permafrost regions and ocean sediments (Kvenvolden, 2002; Koh *et al.*, 2012; Chong *et al.*, 2015)
- Storage and transportation of natural gas as gas hydrates (Gudmundsson *et al.*, 1995; Hao *et al.*, 2008)
- Gas separation by the formation of gas hydrate (i.e. CH<sub>4</sub> purification) (Zanjani *et al.*, 2011; Eslamimanesh *et al.*, 2012)
- Water desalination of seawater with the formation of gas hydrate (Max *et al.*, 2006; Sangwai *et al.*, 2013)

- Inhibition of gas hydrate during natural gas transportation with pipelines (Hammerschmidt, 1934; Wu et al., 2007; Li *et al.*, 2013))
- Food industry for juice concentration and sugar separation from sugar beet (Li *et al.*, 2016; Kungrani *et al.*, 2016)

The main purpose of this study is to investigate gas hydrate reservoirs in nature especially in the Black Sea as an energy source. Gas hydrate reservoirs are considered as future energy sources because it is found abundantly in both permafrost regions and marine sediments (Abid *et al.*, 2015). With this huge potential of gas hydrates, many scientists focused on the determination of initial gas-in-place in gas hydrate reserves in the world. Figure 2-5 indicates gas hydrate reserve calculations done by different scientists from 1973 to 2014. In these estimations, mainly gas hydrate stability zone (GHSZ) thicknesses were calculated by using sea depth, thermal gradients, pressure gradient, and salinity. Then, CH<sub>4</sub> in place calculations in CH<sub>4</sub> hydrates were done for different ranges of average gas hydrate saturation (Max *et al.*, 2013).

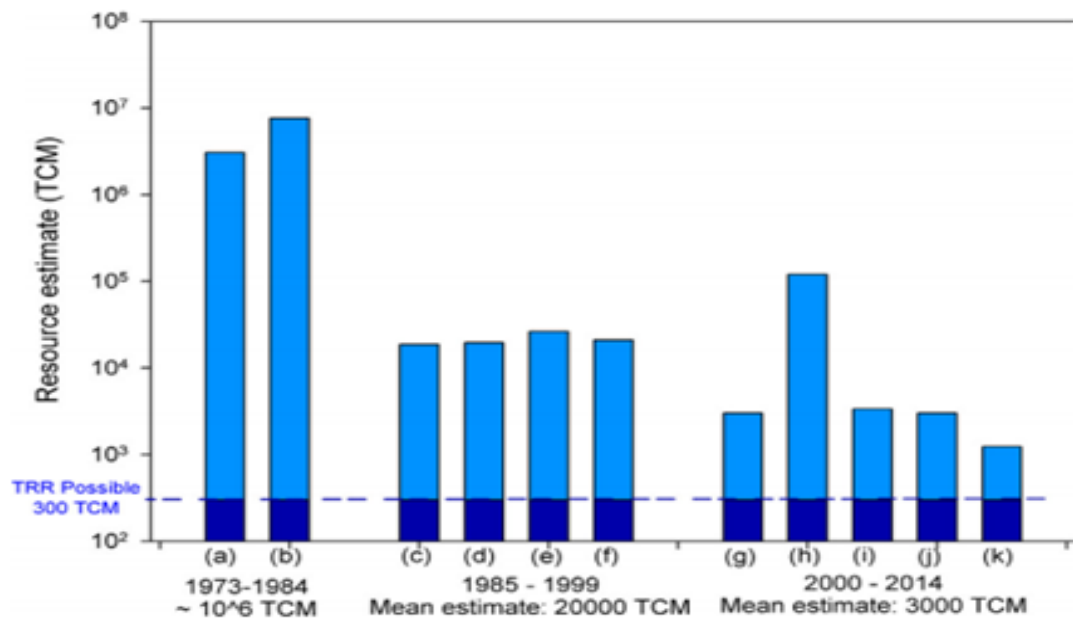


**Figure 2-5:** Resource estimation of hydrates (a) Trofimuk *et al.*, (b) Dobrynin *et al.*, (c) Kvenvolden, (d) MacDonald, (e) Gronitz and Fung, (f) Kvenvolden, (g) Milkov, (h) Klauda and Sandler, (i) Archer *et al.*, (j) Boswell and Collett, (k) Johnson (Adapted from Chong *et al.*, 2015)

According to the studies between 1973 and 1984, there is around 106 standard trillion cubic meters (tcm) of gas (CH<sub>4</sub>) in gas hydrates. However, in these studies, it was assumed that all potential hydrate zones were fully saturated with CH<sub>4</sub> and hydrate formation limiting factors (e.g. sulphur reduction) were not considered. Moreover, in some of these studies, gas hydrate potentials in arctic sands, arctic sands away from infrastructure, marine sands, other marine deposits, massive mounds, and dispersed in shale or filling veins and fractures were calculated. Even though these calculations are important in terms of environmental studies, they are not good references for energy resource studies. This is because only gas hydrates in arctic sands, arctic sands away from infrastructure and marine sands are considered as energy sources (Boswell and Collett, 2006; Boswell and Collet, 2011; Johnson, 2011; Max *et al.*, 2013; Johnson and Max, 2015; Kumar *et al.*, 2016). Recent gas hydrate resource estimation studies were conducted by considering the limiting factors for hydrate formation obtained during the field trials. According to recent studies (Figure 2-5), technically recoverable gas hydrate resource amount in the world is around 3000 tcm.

Johnson (2011) estimated gas in place in gas hydrates deposited in coarse sands. Table 2-3 lists a huge range of gas hydrate resource between 133 tcm and 8891 tcm. It can be concluded that even the most conservative estimates of the total quantity of gas in gas hydrates are much larger than the conventional gas resources (404 tcm) and shale gas (204 tcm–456 tcm) (Chong *et al.*, 2015). The magnitude of this resource can make hydrate reservoirs a substantial future energy resource.

**Table 2-3:** Gas in Place in Hydrate-Bearing Sands (Adapted from Johnson, 2011)

<b>Region (United Nations Designation)</b>	<b>Gas in Place Range (tcm)</b>	<b>Gas in Place Median (tcm)</b>
<i>USA</i>	43-437	199
<i>Canada</i>	15-254	63
<i>Western Europe</i>	1-421	40
<i>Central and Eastern Europe</i>	0-3	0
<i>Former Soviet Union</i>	43-290	108
<i>North Africa</i>	0-52	6
<i>Eastern Africa</i>	1-728	52
<i>Western and Central Africa</i>	2-747	90
<i>Southern Africa</i>	3-747	89
<i>Middle East</i>	1-109	16
<i>China</i>	0-51	5
<i>Other East Asia</i>	0-77	11
<i>India</i>	1-178	26
<i>Other South Asia</i>	1-99	16
<i>Japan</i>	2-13	6
<i>Oceania</i>	1-191	23
<i>Other Pacific Asia</i>	2-735	47
<i>Latin America and the Caribbean</i>	7-901	140
<i>Southern Ocean</i>	4-1280	102
<i>Arctic Ocean</i>	5-1572	187
<b><i>Total</i></b>	<b>133-8891</b>	<b>1226</b>

### 2.3 The Origin of Gas Hydrates in Nature

Gas hydrates in nature are found in permafrost and ocean sediments. Permafrost is defined as “frozen soil”. In these formations, temperature is mostly near or below 0 °C. Hence, these low temperature conditions are optimum for the formation of gas hydrates when high pressure conditions exist. Gas hydrates in permafrosts are common especially on the continental shelves of Alaska, Canada, and Russia (Max *et al.*, 2006; Maslin *et al.*, 2010; Rajput and Thakur, 2016). However, gas hydrates in ocean sediments are much more common compared to gas hydrates in permafrost. Max (2003) and Max and Johnson (2016) proposed that at least 95 % of gas hydrates in nature is in ocean sediments and the rest is found in permafrost.

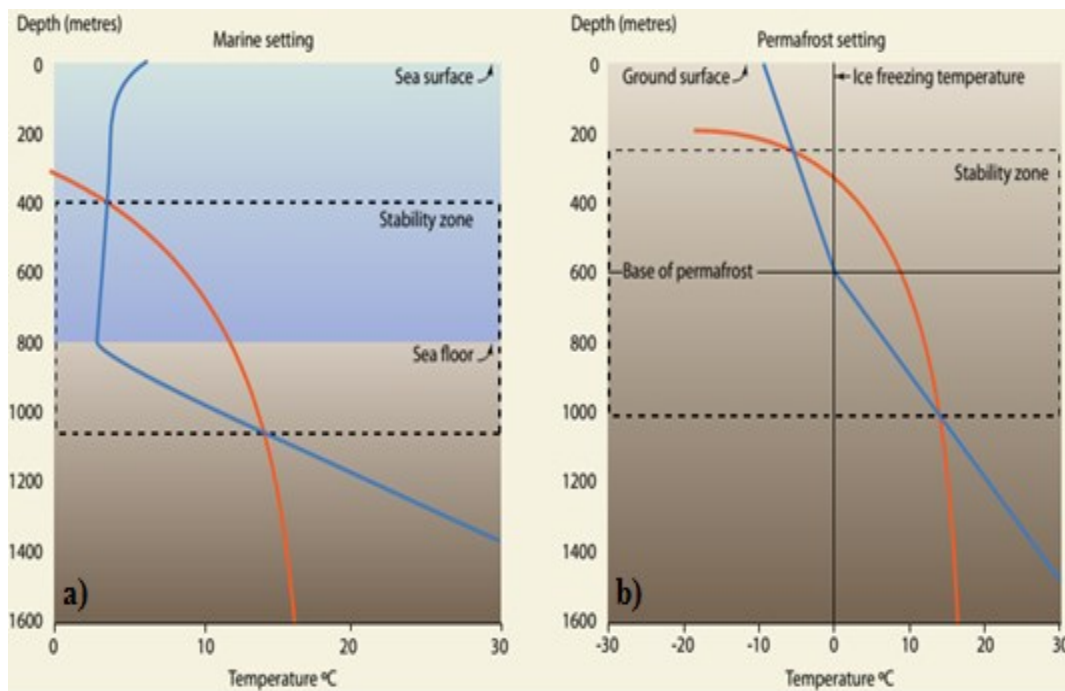
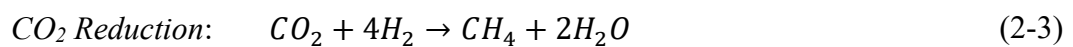
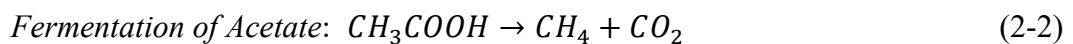


**Figure 2-6:** Gas hydrate stability conditions for a) marine hydrates b) permafrost hydrates (Orange curve: hydrate equilibrium curve, Blue curve: thermal gradient curve) (Beaudoin *et al.*, 2014)

High pressure, low temperature, hydrate-forming gas (guest molecules) and water (host molecules) are the required factors for the formation of gas hydrate. As seen in Figure 2-6, both for marine (ocean) sediments and permafrost, the required conditions

are satisfied below certain depths. If geothermal line (thermal gradient line) is above the phase boundary line, gas hydrate cannot form. Another important point is about the origin of gas to form hydrate. Firstly, it is known that approximately 99 % of gas hydrates in nature is methane (CH<sub>4</sub>) hydrate (sI type of hydrate) (Kvenvolden, 1995; Ruppel, 2011; Max *et al.*, 2013). Conventional oil and gas resources are found in the deeper part of the earth. However, gas hydrates are mostly found in the shallower part of ocean sediments and permafrost regions. For example, in ocean sediments, CH<sub>4</sub> hydrates can be found between 500 m and 3000 m depending on hydrate formation conditions. However, the possibility of CH<sub>4</sub> hydrate in deeper sediments is very low because in deeper parts, temperature is high due to geothermal gradient so very high pressure values are essential for hydrate formation (Johnson and Max, 2015). According to Max and Johnson (2016), target gas hydrate reservoirs for gas production are found between sea floor and 1 km underneath sea floor.

The origin of CH<sub>4</sub> source for CH<sub>4</sub> hydrates is mainly biogenic (Hester and Brewer, 2009). The biogenic CH<sub>4</sub> forms during diagenesis stage in the evolution of organic materials in sediments. These organic materials may include every organism from zooplankton to whales. Then, as seen in Figure 2-7 with the burial of organic materials, oxygen concentration decreases. During the oxidation processes, H<sub>2</sub>O, CO<sub>2</sub>, SO<sub>4</sub> and NH<sub>3</sub> are produced. Then, in anoxic environment, nitrate and sulphate reductions occur. Finally, the last stage of fermentation starts where the methanogens produce CH<sub>4</sub> by acetate fermentation and CO<sub>2</sub> reduction (Equation (2-2) and Equation (2-3) respectively). The generated CH<sub>4</sub> at diagenesis stage is immature and biogenic gas (Hunt, 1995; Giavarini and Hester, 2011; Ma and Holditch, 2016). Then, when generated CH<sub>4</sub> has low temperature and high pressure conditions in the pores of the sediments filled with water, biogenic origin CH<sub>4</sub> hydrate (sI hydrate) forms.



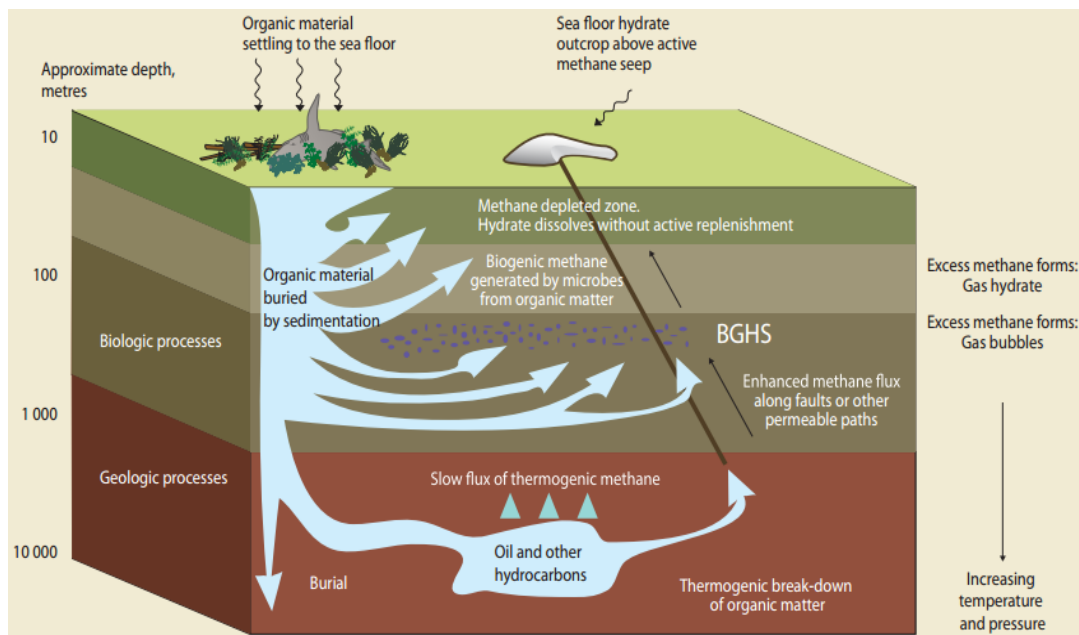


**Figure 2-7:** Fate of buried organic matter for biogenic and thermogenic gas hydrates (Beaudoin *et al.*, 2014)

Gas hydrate formed by thermogenic natural gases are defined as “thermogenic” hydrates. As seen in Figure 2-7, the origin of these thermogenic gases is similar to the origin of conventional oil and gas reservoirs. Gas and/or oil formed at catagenesis and metagenesis stages in source rocks migrate to these conventional oil and gas reservoirs with different mechanism such as diffusion, aqueous solution, micellar solution, separate phase, buoyancy effect, capillary pressure and water flow (Hunt, 1995; Rajput and Thakur, 2016). Similarly, for thermogenic gases formed in the source rock at high temperature conditions migrate with faults and permeable rock through the shallower parts of marine sediments and thermogenic gas hydrate forms when hydrate equilibrium conditions exist. Thermogenic gas hydrates include mostly  $\text{CH}_4$ ,  $\text{C}_2\text{H}_6$ ,  $\text{C}_3\text{H}_8$ ,  $n\text{-C}_4\text{H}_{10}$ ,  $i\text{-C}_4\text{H}_{10}$ ,  $\text{CO}_2$ ,  $\text{H}_2\text{S}$  and other impurities (Rogers, 2015; Ma and Holditch, 2016; Max and Johnson, 2016). If the concentration of  $\text{C}_3\text{H}_8$  is approximately 1 % in gas mixture, the type of thermogenic gas hydrate is structure II (sII) and they form at lower pressure than  $\text{CH}_4$  hydrate at same temperature (Abbasov, 2014; Rogers, 2015; Abbasov *et al.*, 2016). Although thermogenic gas hydrates are not common compared to biogenic  $\text{CH}_4$  hydrates, they have been found in several places worldwide, including the Gulf of Mexico, the Caspian Sea, the Black Sea, the

Sea of Japan and the Marmara Sea (Hester and Brewer, 2009; Bourry *et al.*, 2009). Thermogenic gas hydrates are generally found in deeper ocean sediments because their hydrates are much more stable than biogenic CH<sub>4</sub> hydrates (Hester and Brewer, 2009).

When source gas is released during biogenic or thermogenic stages, especially in marine sediments, gas is dissolved in water due to hydrostatic pressure. Gas dissolved in water reaches to gas or methane hydrate stability zone (GHSZ or MHZ) by convection or advection and gas hydrate forms in these zones if pressure and temperature conditions are appropriate. Therefore, with hydrate formation, dissolved gas percentage in water decreases. As well as gas hydrate formation from gas dissolved in water; hydrates in nature might form from free gas source. When free gas reaches to GHSZ or MHZ where there are water molecules in pores and/or grains by convection, gas hydrate forms at low temperature and high pressure conditions. Compared to gas dissolved in water, in this case, large amount of gas hydrate forms and it causes sudden increases in salt concentration of pore water; this increase is very low for gas hydrates formation from gas dissolved in seawater. However, even there is a large increase in salinity after hydrate formation, with time, salinity decreases due to diffusion (Tohidi *et al.*, 1997; Ginsburg, 1998; Schicks, 2010; Chong *et al.*, 2015; Heeschen *et al.*, 2016). Even though gas hydrate experiments with gas invasion is common, there are only a few experimental studies with gas hydrates formed in sediments from gas dissolved in water (Priegnitz *et al.*, 2013; Priegnitz *et al.*, 2015; Heeschen *et al.*, 2016). Figure 2-8 is quite helpful to understand the movement of source gas dissolved in brine through hydrate reservoirs in permafrost (Figure 2-8-A: Mallik Field, Canada) and marine sediments (Figure 2-8-B: Ullung Basin, Korea). As seen in this figure, CH<sub>4</sub> solubility in brine increases with depth so generally highest hydrate formation rates and hydrate saturations are observed in the bottom of MHZ (Spangenberg *et al.*, 2015). In Figure 2-8-A, if gas dissolved in brine moves through MHZ as liquid along the black dotted line at 0.098 mol/kg solubility and the green dotted line at 0.0114 mol/kg solubility, gas hydrate in MHZ is formed by gas dissolved in water (liquid phase). However, along the dotted black line at 0.0118 mol/kg solubility, the phase of gas dissolved in brine changes from liquid to liquid +

gas phase above 1900 m. Then, it (liquid+gas phase) moves along the dotted-dashed black line in free gas zone (FGZ) until it enters into the base of MHZ (BGHS). Hence, in MHZ, gas hydrate forms from liquid + free gas for this case. Similar observations can be carried out for Figure 2-8-B in Ulleung Basin of Korea. Figure 2-8-B shows high variation in  $\text{CH}_4$  solubility curve because in this region, thermal gradient is higher. These solubility curves are quite important to understand the morphology of gas hydrates in sediments. Therefore, before conducting any gas hydrate experiments, the morphology of gas hydrate reservoir should be known and gas hydrate in sediments in the experimental conditions should be formed according to actual reservoir conditions to mimic real conditions (Spangenberg *et al.*, 2015). It is considered that gas hydrates in marine sediments are likely to be formed from gas dissolved in water but gas hydrates in permafrost are likely to be formed from free gas (Collett *et al.*, 2009; Schindler *et al.*, 2015). Generally, pore-filling gas hydrates occur from gas dissolved in water whereas grain-cementing gas hydrates form from free gas (Schindler *et al.*, 2015).

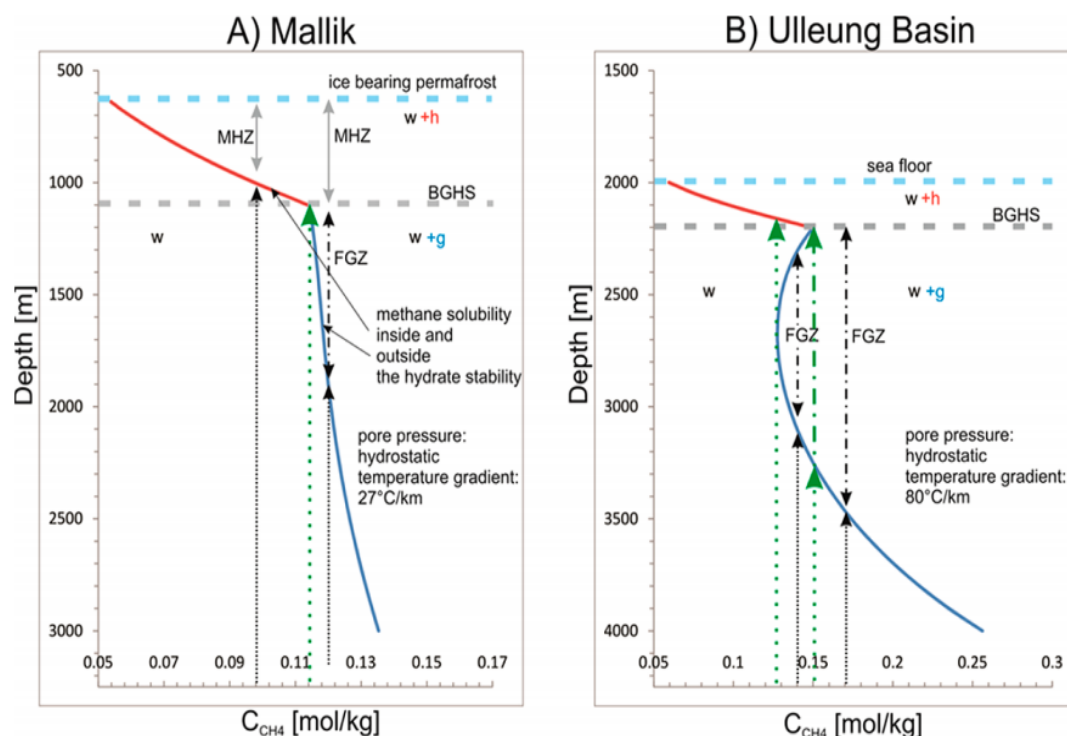


**Figure 2-8:** Solubility of  $\text{CH}_4$  in brine for (A) the Mallik test site (permafrost) and (B) the Ulleung Basin (marine field) (w: water, h: hydrate, g: gas) (Spangenberg *et al.*, 2015)

## 2.4 The Types of Gas Hydrate Reservoirs

Even though gas hydrate reservoirs are considered as potential energy sources for future, currently there is no commercial gas production method. Conventional gas and oil production techniques cannot be directly applied to gas hydrate reservoirs because gas hydrate is in solid form at reservoir conditions. Before discussing production methods in gas hydrate reservoirs, it is important to understand the reservoir types of gas hydrates in nature. Depending on the types of gas hydrate reservoirs, different production scenarios can be developed by using experimental studies, numerical studies and field pilot gas production applications. Gas hydrate reservoirs are mainly divided into four classes. As shown in Figure 2-9, Class 1 hydrate consists of stable hydrate layer and an underlying free gas zone. Class 2 hydrate is composed of stable hydrate layer and an underlying free water zone. Class 3 hydrate only consists of stable hydrate layer bounded by permeable or impermeable shale or clay zones. Although there is another Class 4 hydrates, they are only distributed in sea floor with low hydrate saturation and there are no geologic strata around Class 4 hydrates. Hence, they are not considered as target gas hydrate reservoirs for gas production (Worthington, 2010; Kurihara, 2011; Moridis *et al.*, 2013; Chong *et al.*, 2015). Even though there are many uncertainties related to these reservoirs, Class 4 hydrate is the most common hydrate in nature and then Class 1 hydrates are second most common hydrate reservoir (Worthington, 2010).

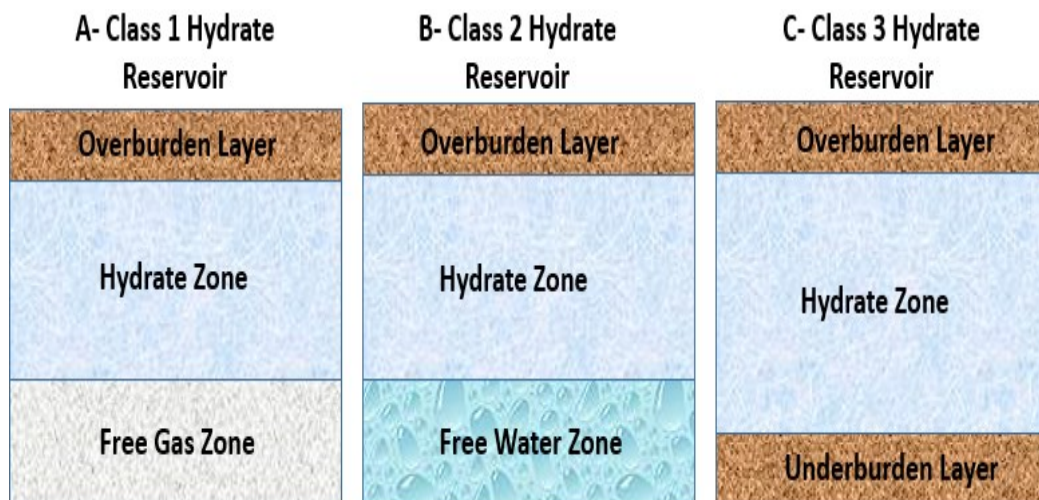


**Figure 2-9:** Types of Gas Hydrate Reservoirs in Nature

## 2.5 The Gas Production Methods from Gas Hydrate Reservoirs

Currently, there are mainly four gas production methods from gas hydrate reservoirs (Kurihara, 2011; Xu and Li, 2015):

- Depressurization
- Thermal Stimulation
- Chemical Injection
- CO<sub>2</sub> Injection or CO<sub>2</sub>/N<sub>2</sub> Injection

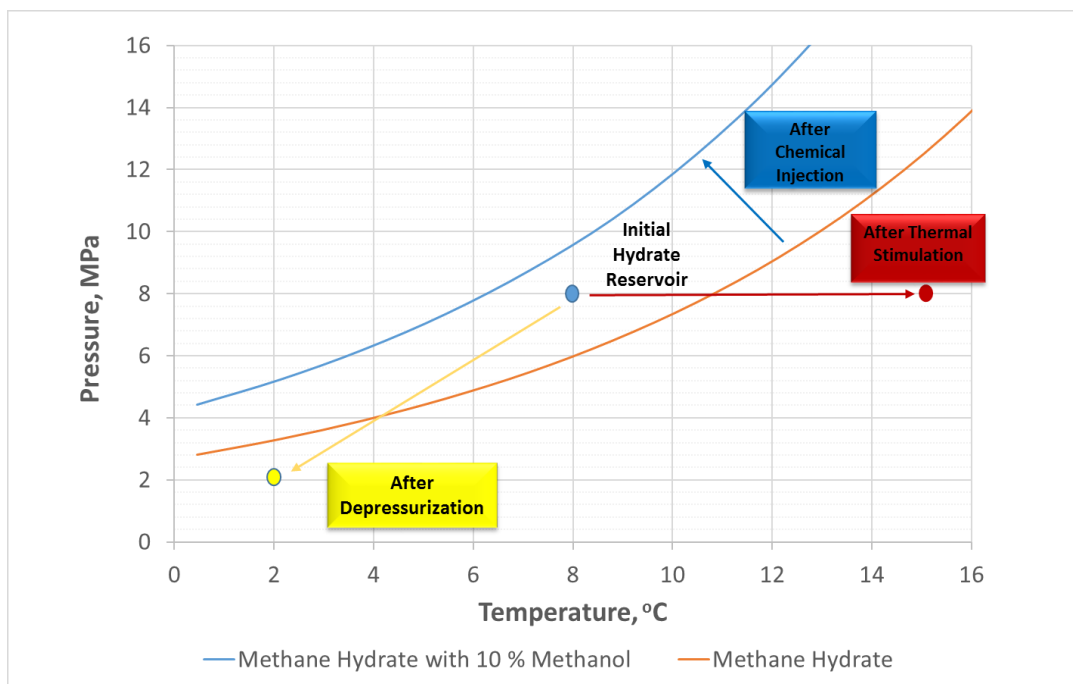


**Figure 2-10:** Illustration of hydrate dissociation by depressurization, thermal stimulation and chemical injection with HEP.m

### 2.5.1 Depressurization

Depressurization is presumed to be the most economically viable production method for gas hydrates because there is no extra heat introduced into the system. This method is applied by decreasing reservoir pressure below hydrate equilibrium pressure, causing hydrate to decompose and release gas and water that will migrate towards wellbore. Although there is no additional heat input cost of depressurization

method, its disadvantages are low gas production rates, high amounts of water production, the risk of hydrate reformation due to fast depressurization, and risk of geomechanical failures (Konno *et al.*, 2010; Chong *et al.*, 2015; Xu and Li, 2015; Huang *et al.*, 2016). Figure 2-10 was prepared to illustrate hydrate dissociation by depressurization, thermal stimulation and chemical injection. This figure was drawn for illustration purposes in this study. During gas production with depressurization method, the temperature of hydrate reservoir is expected to decrease due to Joule-Thomson cooling and endothermic hydrate dissociation (Zhou, 2009; Moridis *et al.*, 2013). For example, during depressurization from 8 MPa to 2 MPa in Figure 2-10, the temperature of hydrate reservoir decreases from 8 °C to 2 °C because hydrate dissociation is endothermic and fast depressurization can cause temperature decrease because of Joule-Thomson cooling effect.

With the decrease of depressurization pressure, gas production rate and cumulative gas production increase (Li *et al.*, 2011; Xiong *et al.*, 2012; Zhao *et al.*, 2015). However, during gas production with depressurization method, there is a risk of hydrate reformation and ice formation in the wellbore and/or in the sediments (Seo and Myshakin, 2011; Zhao *et al.*, 2015). Ice formation and hydrate reformation can plug pores and stop gas production (Seol and Myshakin, 2011). To understand the effects of all these factors on gas production, recently, many laboratory and modelling studies have been conducted. Even though laboratory and modelling studies cannot describe the conditions in real hydrate reservoirs completely, they are useful tools to understand the effects of many parameters on hydrate formation and dissociation. Cheng *et al.* (2015) conducted the depressurization production experiments after forming hydrate in sediments inside a 5 L high pressure reactor. It was observed that during the production with depressurization method, the sensible heat of sediments was consumed. After a certain time, this caused ice formation in the sediments. The latent heat released with ice formation provided additional heat into the system and increased temperature and then gas production. Even there is no ice or hydrate reformation, temperature decrease during production slows the dissociation of gas hydrate (Konno *et al.*, 2014). Similar to Cheng *et al.* (2015)'s study, the latent heat released with ice formation increased gas production from hydrate sediments in the

HIGUMA reactor (1710 L) in the study of Konno *et al.* (2014). They observed that ice formation had a positive impact on gas production and the blockings of pores by ice were not observed in their study. Differently, Konno *et al.* (2012)'s laboratory scale-numerical study and experimental study, pore plugging and permeability reduction by ice formation were found but still gas production rate with ice formation was larger than that without ice. According to these results, ice formation might be considered as advantageous for gas production. Similar positive effects of ice formation in gas production were observed in the experimental and numerical study of Li *et al.* (2015). However, in the study of Yang *et al.* (2012), ice formation slowed the hydrate dissociation rate and decreased the gas production during fast depressurization from hydrate sediments in a cylindrical high pressure reactor (~7 L). Furthermore, Merey and Sinayuc (2015) simulated gas production from hydrate reservoirs at 8 °C and 5.7 MPa by using HydrateResSim simulator and they observed that ice plugs the pores and stops gas production due to fast depressurization. Similar results were obtained in the reservoir scale simulations using Tough-Fx codes such as Tough+Hydrate (Moridis, 2003). Ice might form in a gas hydrate reservoir with gas production because the temperature of the reservoir decreases due to endothermic hydrate dissociation and Joule-Thomson cooling.

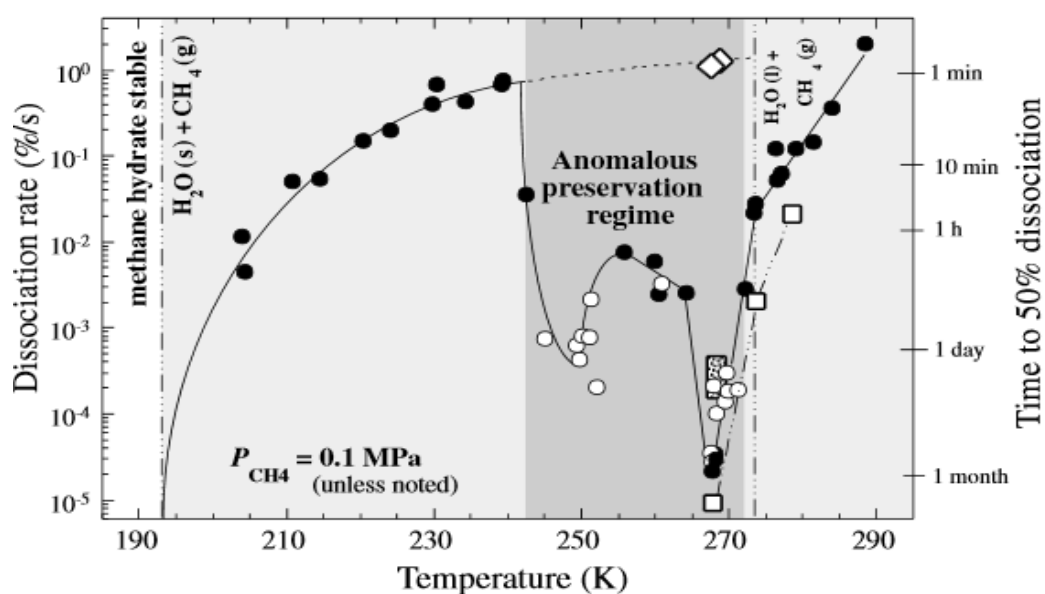


**Figure 2-11:** Average rates of CH<sub>4</sub> hydrate dissociation calculated by its half-life time after pressure drops to 0.1 MPa at various temperatures (Stern *et al.*, 2003)

Although there is an increase in gas production with the formation heat of ice in some studies, there is also a risk of self-preservation as well as pore plugging effect of ice. Self-preservation of gas hydrate is defined as a very slow decomposition of gas hydrates when the external pressure drops below a three-phase equilibrium pressure of the gas-ice hydrate system at sub-zero temperature (below -3 or -2°C) as a result of thin ice film emergence on gas hydrate surface (Chuvilin *et al.*, 2011). The self-preservation phenomena in gas hydrates occurs between 242 K (-31.15°C) and 271 K (-2.15°C) as shown Figure 2-11. This mechanism is very important for natural gas transportation at low pressure conditions as gas hydrates.

In order to produce gas from gas hydrate reservoirs, firstly, water and/or gas in free spaces should be produced and then with the decrease of pressure below hydrate equilibrium pressure, hydrate starts to dissociate. However, if the effective permeability of hydrate reservoir is very low (between 1-10 mD), it is difficult to produce free water and/or gas and to decrease pressure below hydrate equilibrium pressure. Therefore, for depressurization production method, effective permeability (permeability of the sediments containing gas hydrate) should be higher than 10 mD (Konno *et al.*, 2010). According to the simulation study of Huang *et al.* (2016), above 70 % gas hydrate saturation, depressurization is not possible when intrinsic permeability of sediments are higher than 2 Darcy (D). During depressurization, no external heat is applied. However, the boundaries of hydrate zone provide heats through hydrate zone when the temperature of hydrate zone decreases because of Joule-Thomson effect and endothermic nature of hydrate dissociation (Oyama *et al.*, 2009; Konno *et al.*, 2010; Marinakis *et al.*, 2015). Hence, the higher the temperature of hydrate zone and its boundaries, the better depressurization method is.

Depressurization method also causes the high amount of water production because water is released after hydrate dissociation. Mostly it is expected that water produced from gas hydrate reservoirs is fresh water and it might be released to sea floor in marine environment (Max and Johnson, 2016). However, it is better to analyze pore water from core samples to decide on this. Li *et al.* (2014) conducted depressurization experiments in hydrate sediments inside a high pressure reactor (117.8 L). According

to this study, water production rate is very high at low depressurization pressures. Huge amount of water production creates water disposal problems especially in offshore environments (Chong, 2015; Xu and Li, 2015). Another disadvantage of the depressurization method is the risk of geomechanical instability of the sediments during hydrate dissociation. The strength of hydrate reservoir increases with hydrate saturation (Hyodo *et al.*, 2013). Hyodo *et al.* (2014) conducted geomechanical experiments on CH<sub>4</sub> hydrate sediments and investigated the effect of depressurization on CH<sub>4</sub> hydrate geomechanical stability. Although there is not much effect of fast depressurization on the ultimate deformation of hydrate sediments, the initial deformation rate increases with increasing depressurization rate. However, it is obvious that as gas is produced by depressurization from hydrate sediments, the axial strain and volumetric strain increase (Miyazaki *et al.*, 2011; Hyodo *et al.*, 2014). Furthermore, in the simulation studies of Rutqvist and Moridis (2009) and Rutqvist *et al.* (2012), the geomechanical stability of hydrate reservoirs is significantly affected by depressurization if the sediments are structurally weak. Moreover, there is a risk of collapse of casing and environmental problems because of these geomechanical problems.

### **2.5.2 Thermal Stimulation**

As seen in Figure 2-10, by increasing the temperature of gas hydrate reservoirs, the reservoir conditions are shifted the outside of hydrate equilibrium conditions. Below the hydrate equilibrium line, hydrate starts to dissociate after the increase of the temperature. There are several ways to increase temperature such as steam injection, hot water injection, electric heating or microwave heating (Liang *et al.*, 2008; Xu and Li, 2015; Chong *et al.*, 2015). Thermal stimulation is very effective to dissociate hydrate fast. However, the injection of heat into hydrate reservoirs is very expensive. Moreover, injected heat is not only absorbed by hydrate sections, it is also absorbed by sediments without hydrates and equipment such as tubings, boundaries, etc. Therefore, cost estimations and energy efficiency ratio calculations are important for thermal stimulation studies. There are many experimental and numerical studies to understand the effect of thermal stimulation on hydrate dissociation. By using a five-

spot well system in a cubic high pressure reactor (5.8 L), gas was produced from CH<sub>4</sub> hydrate sediments with hot water injection (Wang *et al.*, 2013). It was found that heat conduction is dominant compared to convection during thermal stimulation. Moreover, there is a linear correlation between hot water injection rate and rate of hydrate dissociation. However, Wang *et al.* (2013) proposed that high hot water injection rate decreases the energy efficiency. Similar conclusions were also made in the study of Zhao *et al.* (2012).

Fitzgerald and Castaldi (2013) conducted combustion experiments (heating rates: 20 W and 100 W at different hydrate saturations) on hydrate sediments formed inside a large scale cylindrical high pressure reactor (59.3 L). The results showed that higher energy efficiencies were obtained with higher hydrate saturation at both high and low heating tests. In the study of Kawamura *et al.* (2007), hydrate formed inside the core with 5 cm diameter and 50 cm length. Then, steam was injected at different rates and hydrate in core sample dissociated. Approximately 44 % of total gas in hydrate was produced with steam injection. Microwave heating was investigated by Liang *et al.* (2008). Compared to hot water injection at the similar conditions, gas hydrate dissociated more rapidly with microwave heating.

Recently, there is an attempt to combine gas hydrate production methods. Thermal stimulation and depressurization are combined to produce much gas from hydrate reservoirs. Feng *et al.* (2015) formed CH<sub>4</sub> hydrate in sediments inside the cubic hydrate simulator (5.832 L). They produced gas with dual horizontal pipes (wells) from the reactor during depressurization combined with warm water injection (22 °C). If the temperature of water increases, the energy ratio declines because of heat loss to non-hydrate zones. Similarly, Falser *et al.* (2012) proposed that with additional heat at the same depressurization pressure, gas production from hydrate can be increased 1.8 to 3.6 times in simulations and experiments compared to the only depressurization. Moreover, Feng (2015) and Feng (2015b)'s experiments indicated that depressurization with horizontal wells is much more efficient than the depressurization with vertical wells. Another way to combine depressurization and thermal stimulation is the huff and puff method. The huff and puff method has also

been studied recently in detail. Firstly, hot water or steam is injected. Then, the system is closed for a while in order to allow heat diffusion, which is called soaking period (Li *et al.*, 2012). Li *et al.* (2012) applied this method numerically and experimentally on hydrate sediments inside a 117.8 L cylindrical high pressure reactor. It was concluded that this method can be effective if the intrinsic permeability of hydrate sediments is high. In another study of Minagawa *et al.* (2015), depressurization and electrical heating were combined. They concluded that this method might be an effective method of gas production from hydrate layers.

According to the experimental results, Tang *et al.* (2005) suggested that a higher hydrate saturation and lower injection temperature resulted higher energy ratio during thermal stimulation. Therefore, the choice of effective thermal treatments for appropriate hydrate reservoir is important. Hao *et al.* (2012) concluded that thermal stimulation of hydrate reservoirs might be feasible if the effective thermal treatments are applied. Geomechanical stability is also a problem during thermal stimulation as depressurization. According to Hyodo *et al.* (2009), the strength of gas hydrate reservoirs increases as hydrate saturation increases and temperature decreases. Similarly, in the study of Hyodo *et al.* (2014), it was concluded that CH<sub>4</sub> hydrate sediments failed after thermal recovery because the axial load was higher than the strength of CH<sub>4</sub> hydrate bearing sediments.

### **2.5.3 Chemical Injection**

The aim of chemical injection into gas hydrate reservoirs is to shift hydrate equilibrium line upward and then reservoir conditions will be below hydrate equilibrium line (Figure 2-10). At these conditions, hydrate starts to dissociate. Compared to other production methods such as depressurization and thermal inhibition, this method is not preferred much by scientists because it is very expensive and environmentally harmful (Moridis *et al.*, 2013; Chong, 2015; Max and Johnson, 2016). Methanol, ethylene glycols, calcium chloride and salt are considered as hydrate inhibitors (Sloan and Koh, 2008). They are mainly used to avoid gas hydrate formation in pipelines during natural gas transportation.

Before injecting any chemicals or water through gas hydrate reservoirs, high permeability is essential for injection. Moreover, in marine environments, there is a risk of polluting the environment. In order to understand the injection of chemicals into gas hydrates, several experiments were conducted. Fan *et al.* (2006) injected ethylene glycol (EG) inside synthetic hydrate formed in a small high pressure cell at different concentrations. The results showed that hydrate dissociation rate increased with EG concentration and injection rate of EG. Moreover, hydrate dissociation heat decreased with increasing EG concentration. Similar results were also obtained in the study of Sira *et al.* (1990) for methanol and glycol injection.

Instead of chemical injection only, there is a tendency to combine chemical injection and thermal stimulation production methods. Yuan *et al.* (2013) compared different chemical inhibitors (NaCl, Na<sub>2</sub>SO<sub>4</sub> and EG) with hot water at different temperatures in terms of effective gas production from gas hydrates. Experiments were conducted in a cylindrical high pressure reactor (7 L). As expected, gas production increased with increasing hot water temperature. However, after 313.0 K, this effect decreased. At the same conditions, with the injection of NaCl, the gas production from hydrate sediments is highest compared to Na<sub>2</sub>SO<sub>4</sub> and EG injections. For this reason, many studies related to hot brine injections have been conducted. Chong *et al.* (2015b) conducted many experiments to understand the effect of NaCl on the dissociation kinetics of gas hydrates. NaCl increased the first stage dissociation rate and resulted in a faster recovery of CH<sub>4</sub>. With the increase of the concentration of NaCl, hydrate dissociation increases but this is until certain value because precipitated salt particles plug the pores at higher NaCl concentrations dissolved in hot water. For instance, hot brine injection experiments at different NaCl concentration were conducted by Li *et al.* (2008). At 50 °C, there was almost no difference between gas production values of brine injection at 16 and 24 % NaCl. However, gas production at 16 % NaCl dissolved in 50°C hot water was much higher than gas production at 8 % NaCl dissolved in 50°C hot water.

The determination of hydrate properties of a specific gas hydrate reservoir is quite important because many factors might affect the selected production scenario. In the

study of Li *et al.* (2016b), hot brine injection experiments into CH<sub>4</sub> hydrate formed in sediments inside a large cubic high pressure reactor were conducted in different hydrate saturation, brine concentration, brine injection rate, injected heat, brine temperature, hydrate temperature, and intrinsic permeability (permeability of sediments without gas hydrate). Then, their effects on energy efficiency were conducted. When hydrate reservoir temperature (-1 to 5 °C), intrinsic permeability (100 to 1200 10<sup>-3</sup> mm<sup>2</sup>) and brine concentration (2%~20%) increase; energy efficiency (EE) increases until certain conditions. Injected heat increases from 100 kJ to 1240 kJ (480 kJ for the maximum EE of 6.4), the temperature of injected brine changes from 30 °C to 50 °C (40 °C for the maximum EE of 5.2), the brine injection rate ranges from 10 cm<sup>3</sup>/min to 25 cm<sup>3</sup>/min (20 cm<sup>3</sup>/min for the maximum EE of 5.1), and hydrate saturation changes from 16% to 64% (48% for the maximum EE of 7.2). Therefore, careful analysis is required in such complex reservoirs like gas hydrates.

### 2.5.4 CO<sub>2</sub> Injection

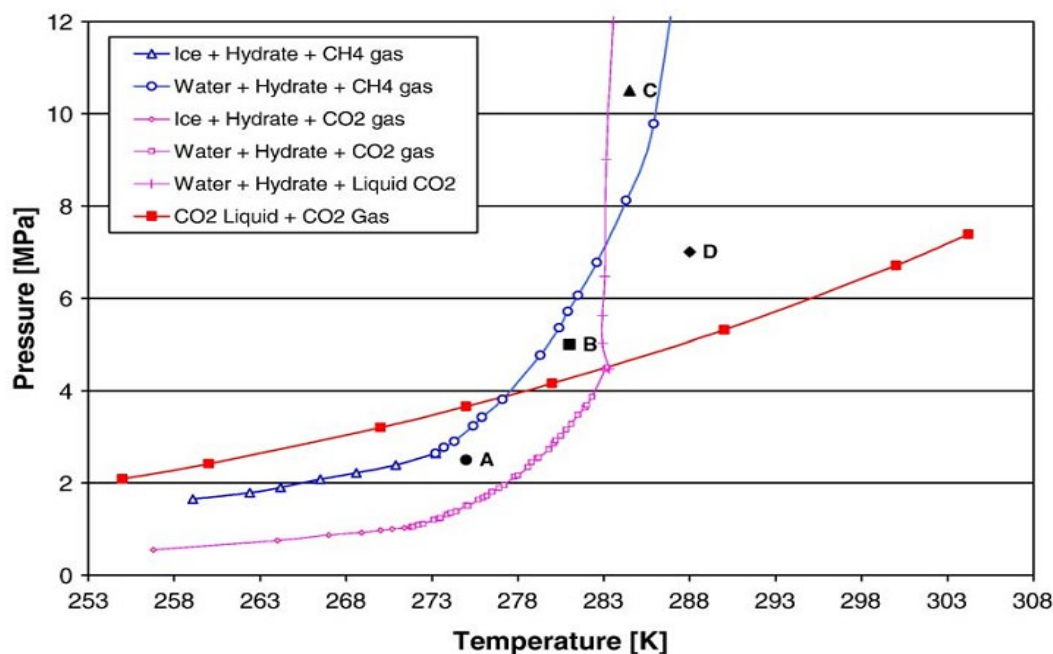


**Figure 2-12:** Diagram of CH<sub>4</sub>-CO<sub>2</sub>-H<sub>2</sub>O phase equilibrium (Goel, 2006)

CO<sub>2</sub> injection is quite different among the production methods of gas hydrate reservoirs. This method was firstly suggested by Ohgaki *et al.* (1996). Basically, the

difference of thermodynamic stability between  $\text{CH}_4$  and  $\text{CO}_2$  causes  $\text{CH}_4$  molecules' leaving the cages of its hydrates and empty cages are filled by  $\text{CO}_2$ . This replacement is called  $\text{CO}_2$ - $\text{CH}_4$  swapping or replacement (Ohgaki *et al.*, 1996; Xu and Li, 2015). This method is advantageous both in terms of  $\text{CH}_4$  production from hydrates and  $\text{CO}_2$  sequestration for environmental purposes (Uchida *et al.*, 2005; Zhao *et al.*, 2012b; Ors and Sinayuc, 2014; Abbasov, 2014; Abbasov *et al.*, 2016). The hydrate equilibrium curves of  $\text{CO}_2$  and  $\text{CH}_4$  in different phases are shown in Figure 2-12. As seen in Figure 2-12, at points A and B,  $\text{CO}_2$  is in hydrate state while  $\text{CH}_4$  is in gaseous state. This means that at certain conditions (temperature below 283 K),  $\text{CO}_2$  hydrate is more stable than  $\text{CH}_4$  hydrate.

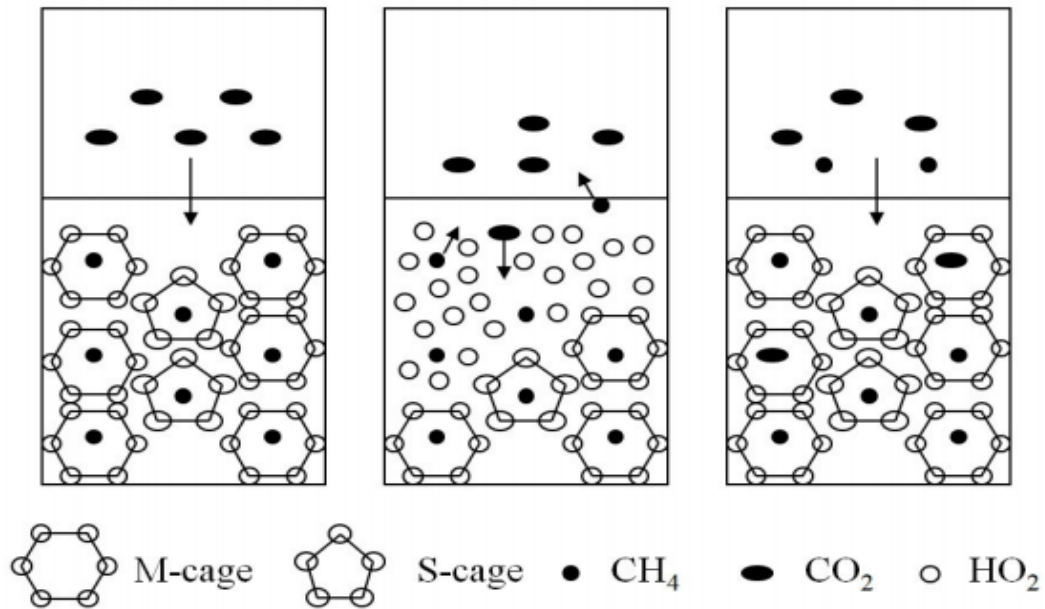


**Figure 2-13:** Schematic diagram of the guest molecule replacement in the M-cage and the  $\text{CH}_4$  re-occupation in the S-cage (Zhao *et al.*, 2012b)

Figure 2-13 is useful to understand the replacement (swapping) mechanism between  $\text{CH}_4$  hydrate and  $\text{CO}_2$ . Basically, when  $\text{CO}_2$  is injected to  $\text{CH}_4$  hydrate, the cages of  $\text{CH}_4$  hydrate are opened because of thermodynamic differences between  $\text{CO}_2$  and  $\text{CH}_4$ . Then,  $\text{CO}_2$  fills mostly large cages (M-cage in Figure 2-13) and  $\text{CH}_4$  is pushed outside of the cages. However, as seen in Table 2-2, the ratio of molecular diameter of  $\text{CO}_2$  to cavity diameter is 1.0 for small cages and 0.834 for large cages. Hence, the

CO<sub>2</sub>-CH<sub>4</sub> swapping is extremely low in small cages and mostly CH<sub>4</sub> molecules stays in the small cages of sI hydrate (Yuan *et al.*, 2012). Then, mostly CH<sub>4</sub> molecules are taken out of large cages and they are produced. Finally, the mixed CO<sub>2</sub>-CH<sub>4</sub> hydrate stays in sediments. According to Geng *et al.* (2009), the mixed CO<sub>2</sub>-CH<sub>4</sub> hydrate formed after the replacement is the most stable hydrate compared to pure CO<sub>2</sub> and pure CH<sub>4</sub> hydrate. This is because the cages are filled perfectly in the mixed CO<sub>2</sub>-CH<sub>4</sub> hydrate. Therefore, even though there is a risk of reservoir subsidence in gas hydrates during depressurization and thermal stimulation, this risk is very low with CH<sub>4</sub>-CO<sub>2</sub> swapping production method and water production is expected to be low. To support this idea, Hyodo *et al.* (2014b) conducted geomechanical experiments on hydrate sediments before and after CO<sub>2</sub>-CH<sub>4</sub> swapping. Their results indicated that newly formed CH<sub>4</sub>-CO<sub>2</sub> mixed hydrate would keep the reservoir mechanically stable. Similar results were also observed in the study of Liu *et al.* (2016).

Recently, many CO<sub>2</sub>-CH<sub>4</sub> hydrate swapping experiments were conducted and the replacements were observed and CH<sub>4</sub> gas was produced at different ratios (Yuan *et al.*, 2012; Ors and Sinayuc, 2014; Chong *et al.*, 2015; Xu *et al.*, 2015). Furthermore, CO<sub>2</sub> replacement with CH<sub>4</sub> was observed in natural gas hydrates (sII hydrate including CH<sub>4</sub> and C<sub>3</sub>H<sub>8</sub>) (Schicks *et al.*, 2011; Abbasov, 2014; Abbasov *et al.*, 2016). Even CO<sub>2</sub>-CH<sub>4</sub> swapping was observed in sH gas hydrate of CH<sub>4</sub> and neohexane up to 88 % CH<sub>4</sub> recovery (Lee *et al.*, 2015). Although CO<sub>2</sub> injection is advantageous, its disadvantages are low replacement rate, pure CO<sub>2</sub> hydrate reformation and low CH<sub>4</sub> recovery (Komatsu *et al.*, 2013; Xu and Li, 2015). Due to generally low permeability of gas hydrate reservoirs, the injection of CO<sub>2</sub> through hydrate reservoirs is a big problem. Especially CO<sub>2</sub> phase easily changes from gaseous state to liquid or supercritical state. Hence, the injection pressure increases easily. This also increases the chance of formation of pure CO<sub>2</sub> hydrate when there is free water in pores. As pure CO<sub>2</sub> hydrate is formed instead of the mixed CO<sub>2</sub>-CH<sub>4</sub> hydrate, the permeability of hydrate reservoir decreases further after the plugging of pores due to newly formed pure CO<sub>2</sub> hydrate. During CO<sub>2</sub>-CH<sub>4</sub> swapping, CO<sub>2</sub> almost only fills the large cages of sI CH<sub>4</sub> hydrate and the small cages mostly consist of CH<sub>4</sub> molecules. Therefore,

even in better replacement mechanism, up to 64 % of CH<sub>4</sub> can be produced from hydrate reservoirs with CO<sub>2</sub> injection (Nago and Nieto, 2011).

In order to increase the effectiveness of CO<sub>2</sub> injection and to avoid the CO<sub>2</sub> injection problem at high pressures, 77 % N<sub>2</sub> and 23 % CO<sub>2</sub> mixture injection to gas hydrates was suggested by University of Bergen and it was proved experimentally and also in Ignik Sikumi field pilot project (Schoderbek *et al.*, 2013; Kvamme, 2015; Kvamme, 2016). During swapping processes in experimental studies, it was observed that large cages of sI hydrate filled by mostly CO<sub>2</sub> and small cages are filled by N<sub>2</sub>. Therefore, gas recovery was increased from 64 % to 85 % by the mixture of CO<sub>2</sub> and N<sub>2</sub> injection. This also avoids the injection problem of CO<sub>2</sub> and reduces the chance of pure CO<sub>2</sub> hydrate formation because N<sub>2</sub> concentration is high. Moreover, N<sub>2</sub> can only form its pure sII hydrate at very large pressure values (i.e. ~11,885 psia at 8°C). It also increases the recovery of CH<sub>4</sub> hydrate by replacing CH<sub>4</sub> in small cages. In another studies of Kang *et al.* (2014) and Ahn *et al.* (2015), air and CO<sub>2</sub> injection was suggested for gas production from hydrate with the replacement mechanism because it is feasible compared to prepare CO<sub>2</sub> and N<sub>2</sub> mixture.

## 2.6 Field Scale Studies

Laboratory and experimental studies are quite important to analyze gas production from gas hydrate reservoirs. However, without any field pilot project or any actual data comparisons between experimental and or numerical modelling, these studies are not enough. In conventional oil and gas reservoirs, the modelling and experimental results are always compared with actual production data and if there are big differences between these data, the reasons are investigated. However, the problem in gas hydrate reservoirs is that there is only one long-term field application: Messoyokha Field (permafrost), Russia. Rest of other gas hydrate field production activities are short-term production tests: mainly Mallik Field (Canada), Nankai Field (Japan) and Ignik Sikumi Field (USA) (Giavarini and Hester, 2011; Nandanwar *et al.*, 2016).

Gas production from Messoyokha gas hydrate field started in 1970. It was the first gas hydrate field discovered in nature. It is a Class 1(G) hydrate reservoir in the Russian permafrost as seen in Figure 2-14-A. Makogon *et al.* (2005) interpreted that pressure increase during gas production was due to hydrate dissociation in 1981 in Figure 2-14-B. It was claimed that the field has a cumulative gas production of  $12.9 \times 10^9 \text{ m}^3$  and  $5.4 \times 10^9 \text{ m}^3$  of this amount was obtained via hydrate decomposition by depressurization method (Makogon *et al.*, 2005). However, in several studies, there are some proposals that gas production in this field was not due to hydrate dissociation and the reliability of this field was questioned (Collett *et al.*, 1998).

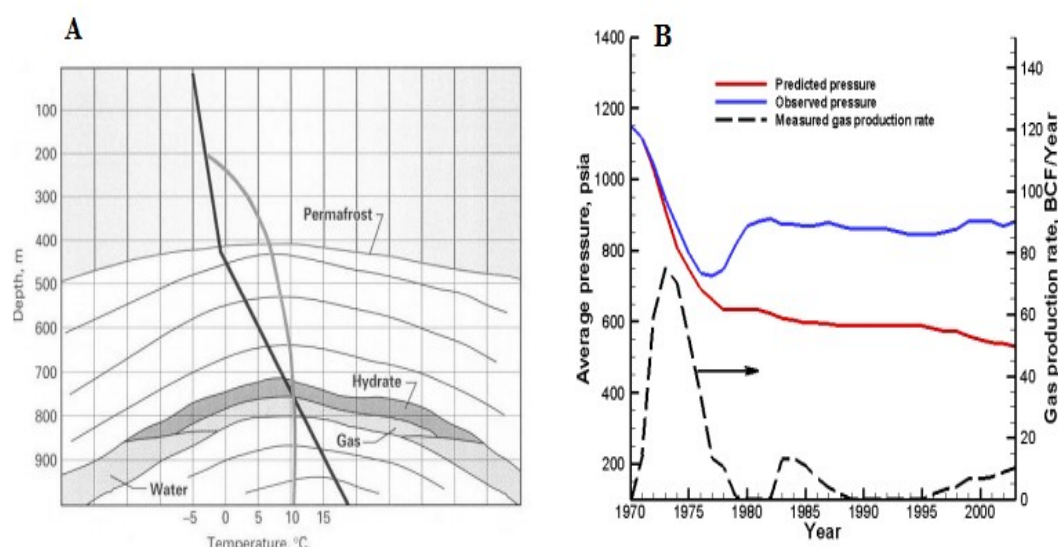


**Figure 2-14:** A) Cross section of the Messoyokha field B) Production behavior at the Messoyokha field (Makogon *et al.*, 2005)

In another permafrost located in the Mackenzie Delta, Canada, the Mallik gas hydrate pilot production tests were conducted in 2002, 2007 and 2008. The type of gas hydrate reservoir is Class 3 and it includes almost 100 %  $\text{CH}_4$  (sI hydrate). In 6 days, continuous gas production with depressurization (at 4.5 MPa) from a 12 m perforated interval was held. Approximately,  $13,000 \text{ m}^3$  of  $\text{CH}_4$  produced with a production rate of  $2000 \text{ m}^3/\text{day}$ . Moreover, in different hydrate zones, thermal injection was tested (Uddin *et al.*, 2014; Chong *et al.*, 2015). Figure 2-15 shows the gas production rates in the depressurization tests conducted in Mallik Field in 2007 and 2008. The aim of field pilot tests in the Mallik field was to enhance the available codes for the

simulation of gas production from gas hydrates such as CMG-Stars, HydrateResSim, Tough + Hydrate, Hydrsim Simulator, and MH-21 HYDRES. Therefore, according to the results of these projects, these codes were improved for the simulations of laboratory scale and reservoir scale natural gas hydrates (Collett *et al.*, 2009; Johnson and Max, 2015).

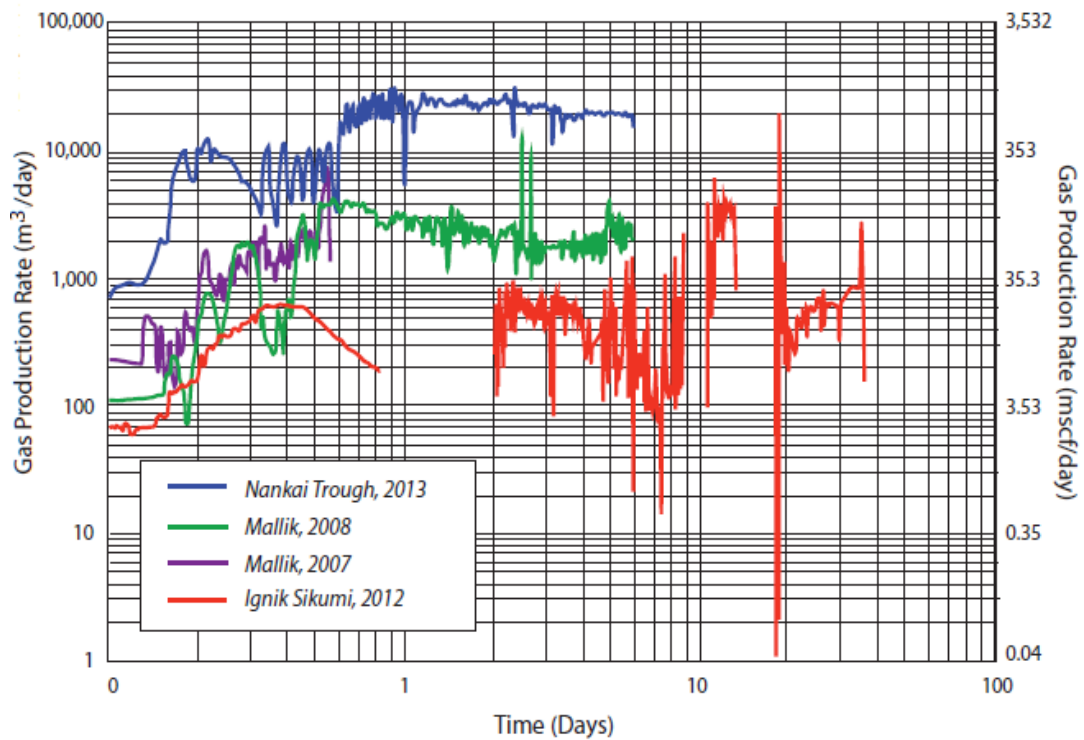


**Figure 2-15:** Gas production rates of different gas hydrate field test projects (Boswell *et al.*, 2016)

Different from the previous pilot projects on gas hydrate reservoirs, CO<sub>2</sub>/N<sub>2</sub> mixture was injected into the Ignik Sikumi field on the Alaska North Slope. It is a permafrost consisting gas hydrates. In the laboratory, the effectiveness of CO<sub>2</sub>/N<sub>2</sub> mixture compared to only CO<sub>2</sub> injection was proved experimentally by University of Bergen (Kvamme, 2015). In 2012, this method was applied to the Ignik Sikumi field by injecting 77.5 % N<sub>2</sub> and 22.5 % CO<sub>2</sub> (167. Mscf of N<sub>2</sub> and 48.6 Mscf of CO<sub>2</sub>) mixture and gas was produced after injection and soaking periods. The similar replacement mechanism as in the experiments were observed in this field pilot project. Approximately 210,000 standard cubic feet (scf) of this gas mixture was injected.

Then, 855 Mscf CH<sub>4</sub> was produced during the total production period including a 6 weeks of flow back of gas. With CH<sub>4</sub>, N<sub>2</sub> and CO<sub>2</sub> were also produced. Approximately 70 % of injected N<sub>2</sub> was produced but only 40 % of CO<sub>2</sub> was recovered. It was considered that the rest of CO<sub>2</sub> stored in the mixed hydrate after the replacement (White and Lee, 2014). Figure 2-15 shows the gas production rates in the CO<sub>2</sub>-CH<sub>4</sub> swapping test conducted in Ignik Sikumi well in 2012. Although in this well, it is considered that CO<sub>2</sub>-CH<sub>4</sub> swapping occurred, it is not proved scientifically (Boswell *et al.*, 2016). Moreover, there are still many studies needed to improve this method (i.e. improved well logging techniques to prove the existence of CH<sub>4</sub>-CO<sub>2</sub> mixed hydrate in the reservoir after the replacement) but depressurization method will remain the primary basis of future gas hydrate field production tests (Boswell *et al.*, 2016).

In the MH-21 (2008)'s project, the gas hydrate deposits were discovered in the Nankai Trough, Japan. Geological and geophysical studies were conducted during this project and then the field production tests were conducted in 2013. This is the first field production test from marine gas hydrates. During 6 day-gas production test with depressurization method (pressure was lowered from 13.5 MPa to 4.5 MPa), 120,000 m<sup>3</sup> of gas (CH<sub>4</sub>) and 1200 m<sup>3</sup> of water were produced. Produced water was fresh water as expected and distilled to the sea (Kawamoto, 2014). Figure 2-15 shows the gas production rates in the depressurization tests conducted in Nankai Trough field in 2013. With gas production, it was observed that sand production increased. Then, production test was stopped in the 6<sup>th</sup> day of the test. In order to understand and test the gas hydrate reservoirs in marine sediments, this project is quite important and unique. Most of gas hydrates in nature exists in marine sediments and this study is the first offshore gas hydrate field production trial. Long-term production tests in this field can provide many clues about the effectiveness of depressurization, and its effect on the geomechanical stability of marine sediments. For this reason, in the Phase 3 of the MH-21 project, it is aimed to produce gas from 2016 to 2018 (MH-21, 2008; Chong *et al.*, 2015). In this project, new production well and monitoring wells have been drilled in 2016 and they are going to start to produce natural gas from methane hydrate reservoir in the spring of 2017 as long as possible (Personal

communication with Dr. Jun Yoneda, 2016). Moreover, in Krishna-Godavari Basin of India, first pilot gas production test is planned during 2017-2018 after the analysis of geophysical data, geological data and the data of drilled 42 gas hydrate wells (Kumar, 2016).

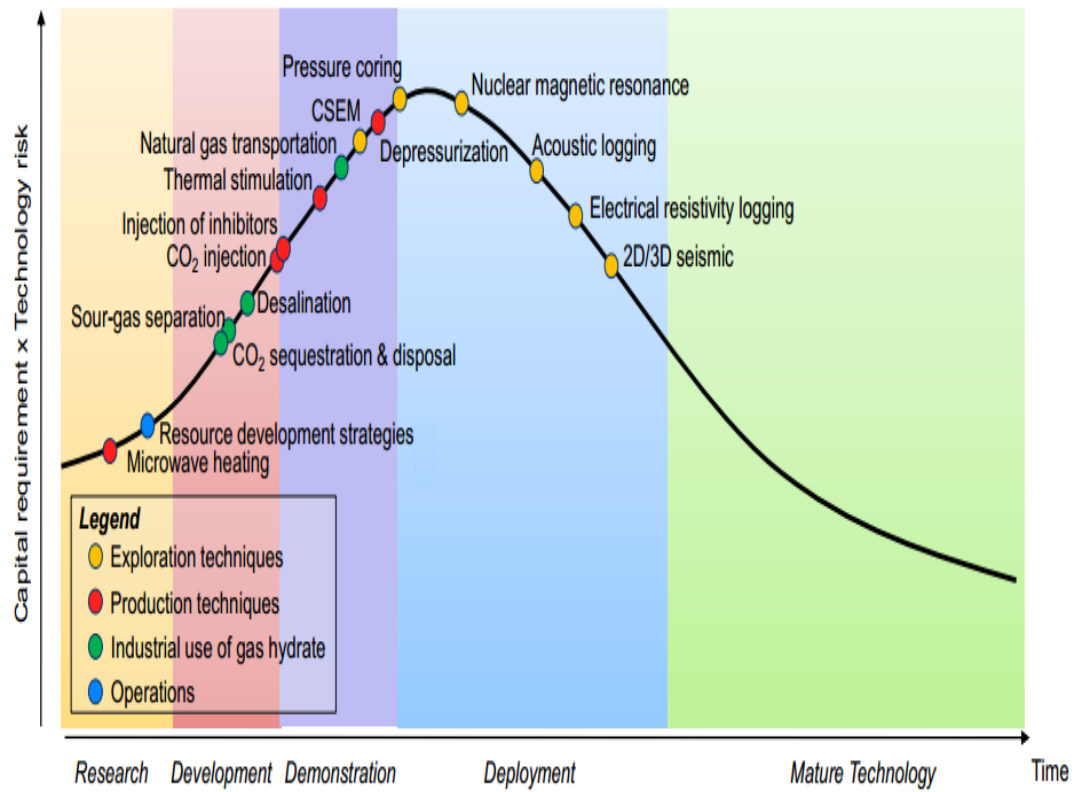


**Figure 2-16:** Technology maturity curve of gas hydrates (SBC, 2015)

As seen in Figure 2-16 and summarized in this chapter, gas production from gas hydrates are still at the early stages of development. The targets of all gas hydrate projects are gas hydrate occurrences in sand reservoirs because of its optimum reservoir properties such high porosity and high permeability (Kumar *et al.*, 2016). SBC Energy Institute (SBC, 2015) prepared Figure 2-16 to show the current stages of gas hydrate technology. As seen in Figure 2-16, exploration techniques such as controlled source electromagnetic method (CSEM), pressure coring, nuclear magnetic resonance, acoustic logging, electrical resistivity logging and 2D/3D seismic are in mostly deployment stage in the maturity curve. However, production

techniques such as depressurization, thermal stimulation, inhibitor injection and CO<sub>2</sub> injection are still below deployment stage. When exploration techniques are at mature technology stage in future, these data gained from exploration studies will be helpful for the development of production techniques in gas hydrates.

## CHAPTER 3

### GAS HYDRATE POTENTIAL OF THE BLACK SEA

#### 3.1 General Information about the Black Sea

The Black Sea is an inland sedimentary basin, located between the latitudes of 41 °to 46 °N and longitudes of 28° to 41.5°E with an area of 423,000 km<sup>2</sup>, a volume of 547,000 km<sup>3</sup> and a maximum depth of 2200 m (Murray, 1991). It has a connection to the Sea of Azov by the Kerch Strait in the north, while it is connected to the Mediterranean Sea with the Bosphorus Strait through the Sea of Marmara in the south. Near the shores of the Black Sea, the depth of sea is shallow but after little far away from the shores, the sea level depth suddenly increases up to 2,212 m as shown in Figure 3-1 and Figure 3-2.

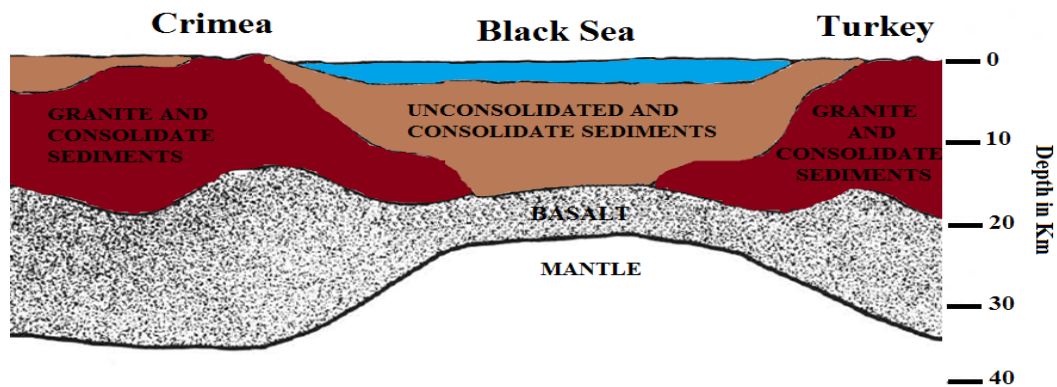


**Figure 3-1:** Lithology of the Black Sea (Adapted from Ross *et al.*, 1974)

As shown in Figure 3-1, the Black Sea is a deep valley, which was filled with unconsolidated and consolidate sediments above basalt and mantle layer. According to Klaucke *et al.* (2005), the sedimentation rate in the Black Sea is high because the Black Sea is almost a closed sea and many rivers transport sediments with time. The thickness of the sediments in the Black Sea is considered up to 19 km (Ross *et al.*, 1974; Nikishin *et al.*, 2003).

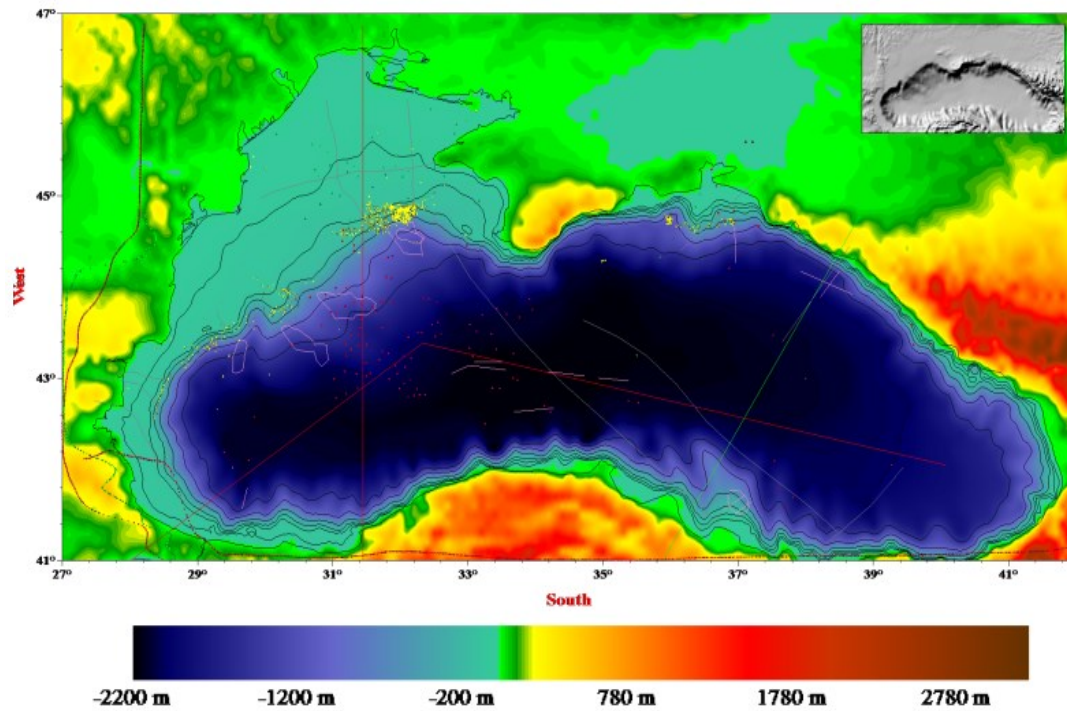


**Figure 3-2:** Bathymetry of the Black Sea (Vassilev, 2006)

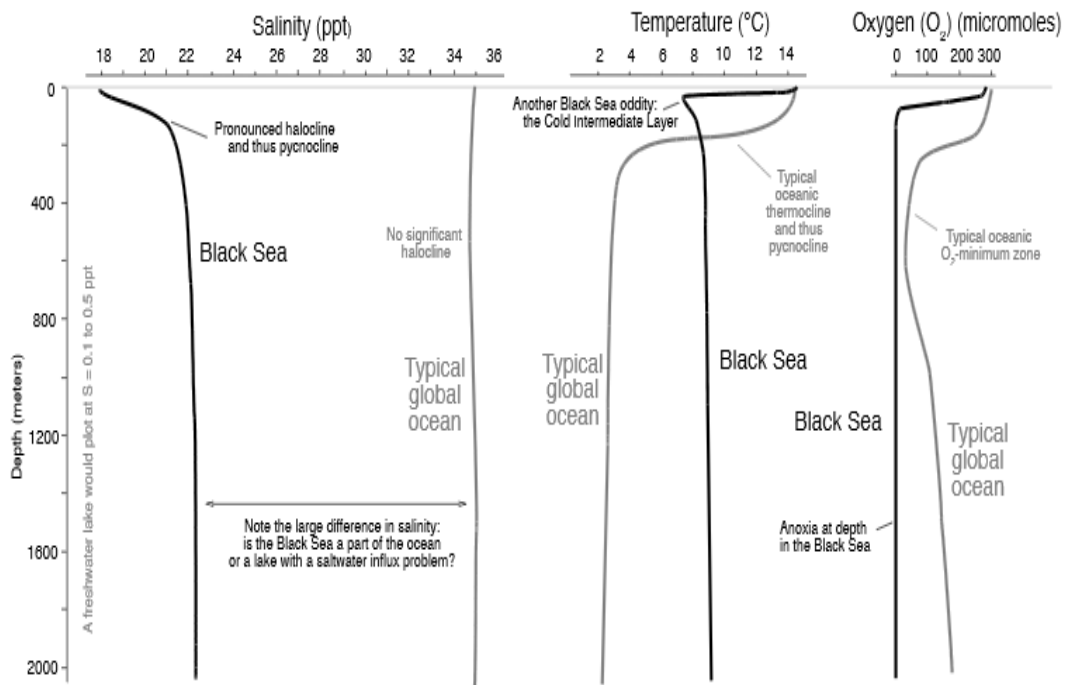


**Figure 3-3:** Salinity, temperature and O<sub>2</sub> concentration with sea level depth of the Black Sea and typical global ocean (Railsback, 2010)

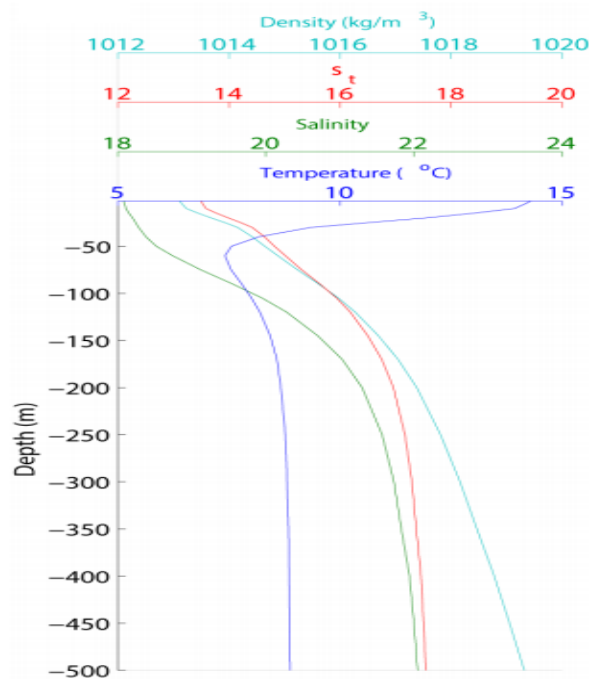


**Figure 3-4:** Temperature, salinity, density and  $s_t$  (isopycnal parameter) in the Black Sea at the location with lat. 42.951, long. 39.114 with depth (Stanev *et al*, 2014)

The Black Sea was a fresh water lake from 22,000 to 9,000 year B.P. After the rise of the sea levels, the warm saline waters of the Mediterranean Sea flowed through the Black Sea via the Bosphorus. Then, the denser saline water sank and less dense water raised to the top and this created halocline. This also formed anoxic water body because halocline creates anoxic environment (Deuser, 1974; Neprochnov and Ross, 1978; Okay, 2008). The salinity, temperature and  $O_2$  concentration values with sea level depth are shown in Figure 3-3 and in this figure, the comparison with typical ocean conditions are made. Seawater salinity changes between 1.75 and 2.23% (17.5-22.3 ppt) (Murray, 1991; Railsback, 2010). The salinity of the Black sea increases from 1.75 % to 2.23 % between sea level and 200 m below sea level. Then, it is almost constant from 200 m below sea level to sea floor (Railsback, 2010). Similar observations were observed in the study of Stanev *et al.* (2014). Moreover, in Figure 3-4, the density of seawater and isopycnal parameter are shown. However, in the study of Shishkina (1978), Hole 379A was drilled in the Black Sea. Sea surface chlorinity and salinity were measured as 1.144 % and 2.02 % respectively. After drilling of Hole 379A, it was observed that chlorinity and salinity decrease with

depth. Chlorinity drops to 0.27 % at 32.4 meters and maintains low salinities to 268 meter depth, fluctuating between 0.18 and 0.33 %. Therefore, salinity and chlorinity in sediments below sea floor might be different from seawater at sea floor. This behavior was interpreted as the freshening of the basins during Neoeuxinian epoch in the Black Sea by Shishkina (1978). Similarly, pore water salinity was measured as very low according to the data obtained from DSDP 42B well in the central Black Sea and it was measured as 0.5 %. This low salinity is due to dominant fresh water stages in the Quaternary deposits, corresponding to phases of isolation of the Black Sea (Popescu *et al.*, 2006). Soloviev and Ginsburg (1994) stated that the water responsible for gas hydrate formation is of a lower salinity than the Black Sea water. Furthermore, the determination of chloride concentration is important to calculate gas hydrate saturation. If hydrate saturation increases, chloride concentration of pore water decreases because pore water freshening occurs due to hydrate formation (Hesse and Schacht, 2011). Hydrate saturations determined by chloride (Cl) concentration (Equation (3-1)) and well log are compared (Wang *et al.*, 2011).

$$S_h = \frac{1}{\rho_h} \left( 1 - \frac{Cl_{pw}}{Cl_{sw}} \right) \quad (3-1)$$

where  $\rho_h$ : density of hydrate, g/cm<sup>3</sup>;  $Cl_{sw}$ : in-situ baseline pore water chlorinity;  $Cl_{pw}$ : Measured chloride concentration in core water samples after gas hydrate dissociation.

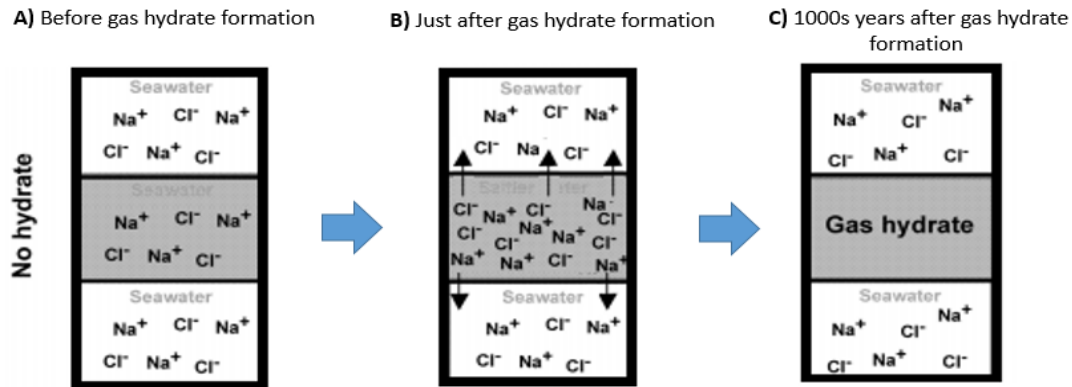


**Figure 3-5:** Figure showing how pore water salinity changes: A) Before gas hydrate formation, B) Just after gas hydrate formation, C) 1000s years after gas hydrate formation (Adapted from Bohrmann and Torres, 2006)

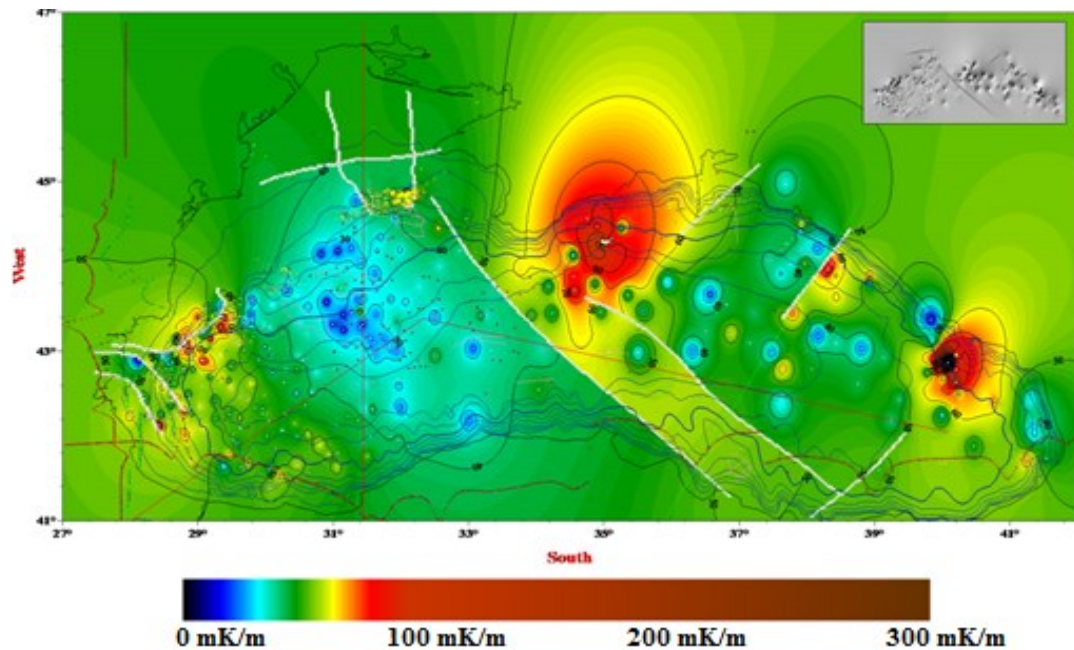


**Figure 3-6:** Temperature Gradient in the Black Sea (Vassilev, 2006)

Pore water Cl anomaly is commonly used while determining gas hydrate sections in sediments and calculating gas hydrate saturations (Hesse and Schacht, 2011). When gas reaches to the sediments filled with water, hydrate starts to form if temperature and pressure conditions are appropriate. Then, Cl concentration of free water increases after gas hydrate formation. If the system is closed, normally in-situ salinity is high after hydrate formation (Meyer and Flemings, 2014). However, with time, high Cl in free water of sediments diffuse away if the system is not closed. Therefore, when pore water of gas hydrate samples is analyzed after dissociation, Cl concentration is quite low compared to Cl gradient of the sediments (Bohrmann and Torres, 2006; Hesse and Schacht, 2011; Thakur and Rajput, 2011). Figure 3-5 describes how water Cl content in pores changes with gas hydrate formation. According Dahlmann and De Lange (2003), another reason of pore water freshening might be due to clay mineral diagenesis instead of gas hydrate formation. Hence, many parameters such as pore water Cl anomaly, well log, and coring should be evaluated together for accurate gas hydrate studies instead of trusting only one data. Different from gas hydrates in deeper sediments, in massive gas hydrates near sea floor in the eastern margin of the Japan Sea, it was observed that Cl concentration is quite higher compared to normal Cl gradient because massive gas hydrates near sea

floor form fast where there is high methane flux (Melgar, 2009; Tomaru *et al.*, 2016). As seen in Figure 3-3 and Figure 3-4, the average temperature of seafloor in the Black Sea is approximately 9°C (Klauda and Sandler, 2003; Railsback, 2010; Stanev *et al.*, 2014). Moreover, Figure 3-6 shows the sediments' temperature gradient below seafloor in the Black Sea. This information is useful for the simulation studies of the potential gas hydrates of the Black Sea.

The Black Sea has large amounts of organic matters carried by rivers and they are stored. Therefore, during the bacterial sulfur reduction of these organic matters, H<sub>2</sub>S evolves and it is stored in the Black Sea as dissolved gas (Deuser, 1974). Similarly, CH<sub>4</sub> concentration dissolved in the sea increases with depth until certain values. The profiles of CH<sub>4</sub> and H<sub>2</sub>S concentrations with depth at Sta.BKS2 in the Black Sea are shown in Figure 3-7.

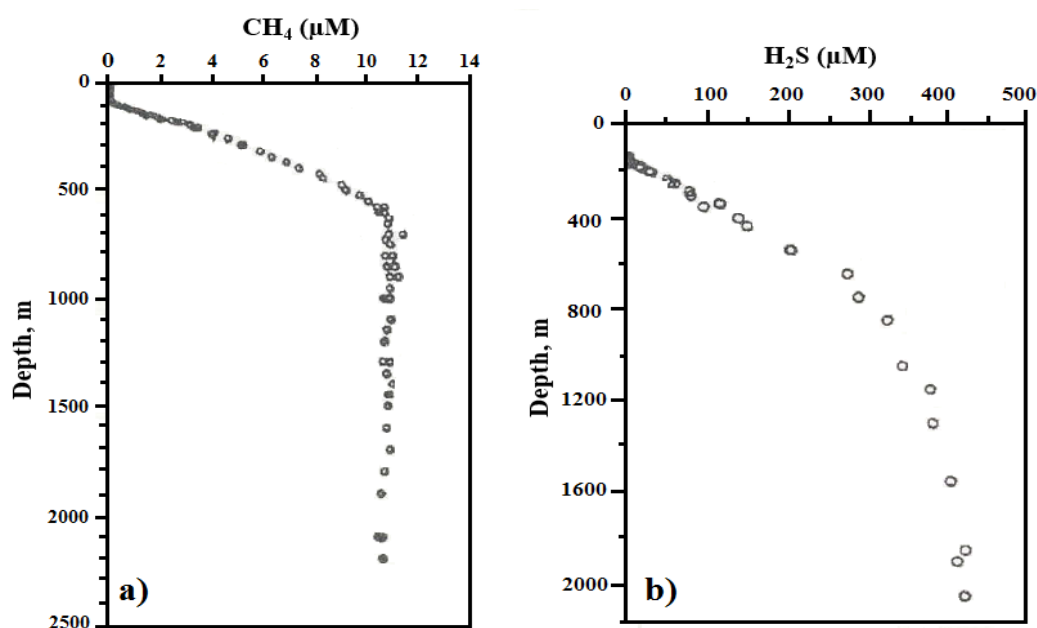


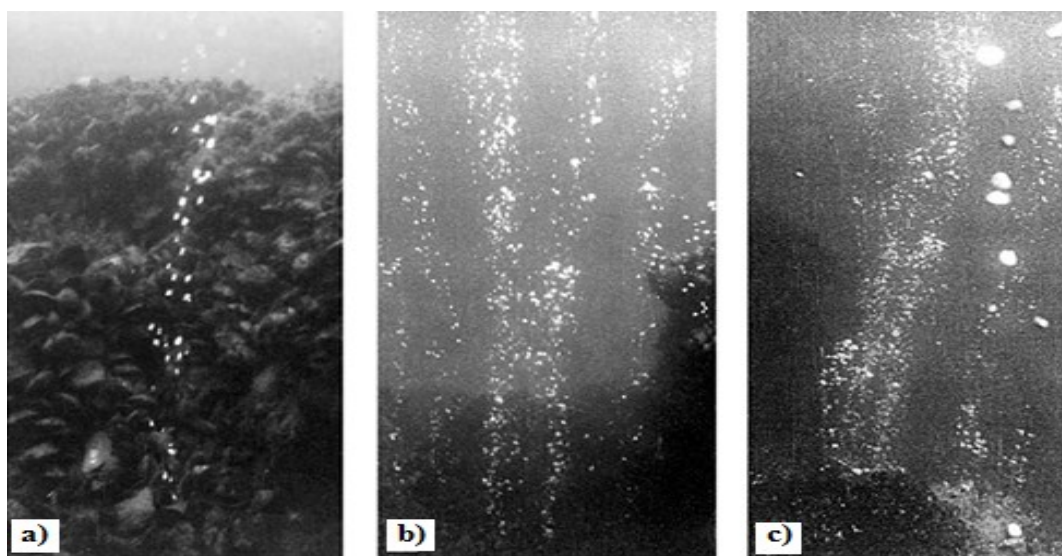
**Figure 3-7:** Profile of a) CH<sub>4</sub> and b) H<sub>2</sub>S concentration profile at Sta.BKS2 in the Black Sea (Adapted from Sozansky, 1997)

With the impact of post-glacial flooding in the Black Sea, the seafloor temperature of the Black Sea increased by 5°C and it was considered that 15-60 % of gas hydrates

in the Black Sea dissociated (Poort *et al.*, 2005). Hence, all of these periods have still been investigated by scientists but it is not in the scope of this study.

### 3.2 Evidences of Gas Hydrate Existence in the Black Sea

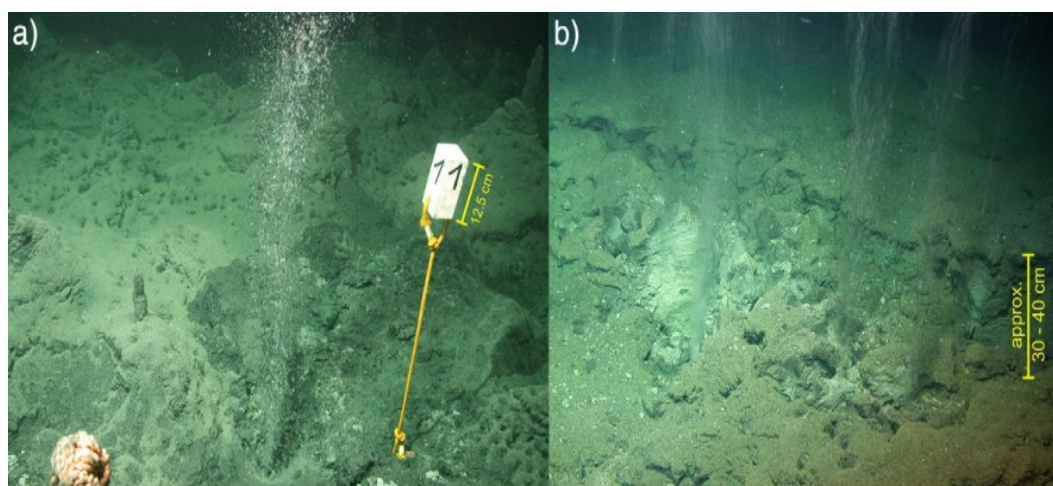
As many places in the world, the Black Sea also has a huge gas hydrate potential and it is also considered as the world's most isolated sea, the largest anoxic water body on the planet and a unique energy-rich sea (Ergun and Cifci, 1999; Overmann and Manske, 2006). Moreover, low pore water salinity in the Black Sea sediments promotes gas hydrate formation (Vasilev, 2015; Haeckel *et al.*, 2015). It abundantly contains gas hydrates and H<sub>2</sub>S as CH<sub>4</sub> and hydrogen source, respectively (Sozansky, 1997). CH<sub>4</sub> seepage is extremely intense on the shelf and on the slope of the Black Sea (Sozansky, 1997; Vassilev and Dimitrov, 2000; Dimitrov, 2002; Heeschen *et al.*, 2011; Xing, 2013; Küçük *et al.*, 2015).



**Figure 3-8:** Gas seepages in the “Golden Sands” area showing: (a) a small seep producing gas with a flux rate of 0.26–0.62 l/min; (b) two medium strength seeps with 1.0–2.0 l/min; (c) a strong seep with 2.5–3.8 l/min (Dimitrov, 2002).

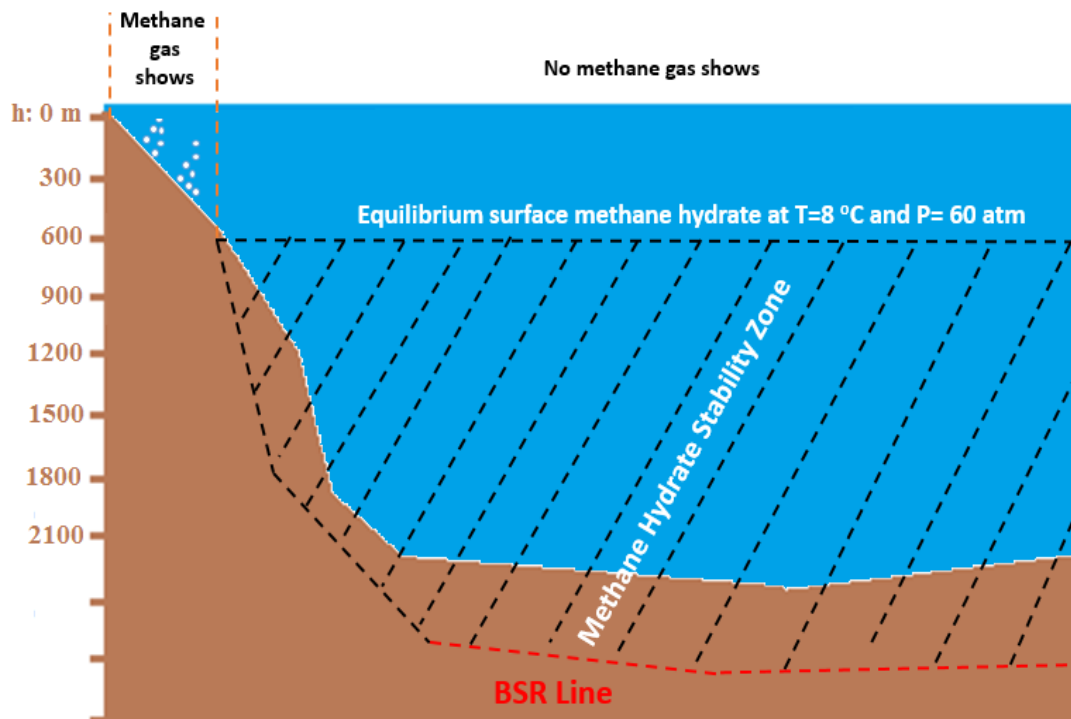
In Figure 3-8 and Figure 3-9, natural gas seepages along the Bulgarian Black Sea coast (Dimitrov, 2002) and Batum region are shown respectively. The gas composition in the Bulgarian Black Sea coast (Figure 3-8) includes 92-96.3 % CH<sub>4</sub>,

0.2 %  $C_2+$ , 0-0.9 %  $CO_2$ , and 0.8-4.4 %  $N_2$ . More than 3000 gas seeps were detected in the Black Sea (Collins *et al.*, 2016). These gas seeps also formed mud volcanoes in the sea floor of the Black Sea (Kenyon *et al.*, 2001).

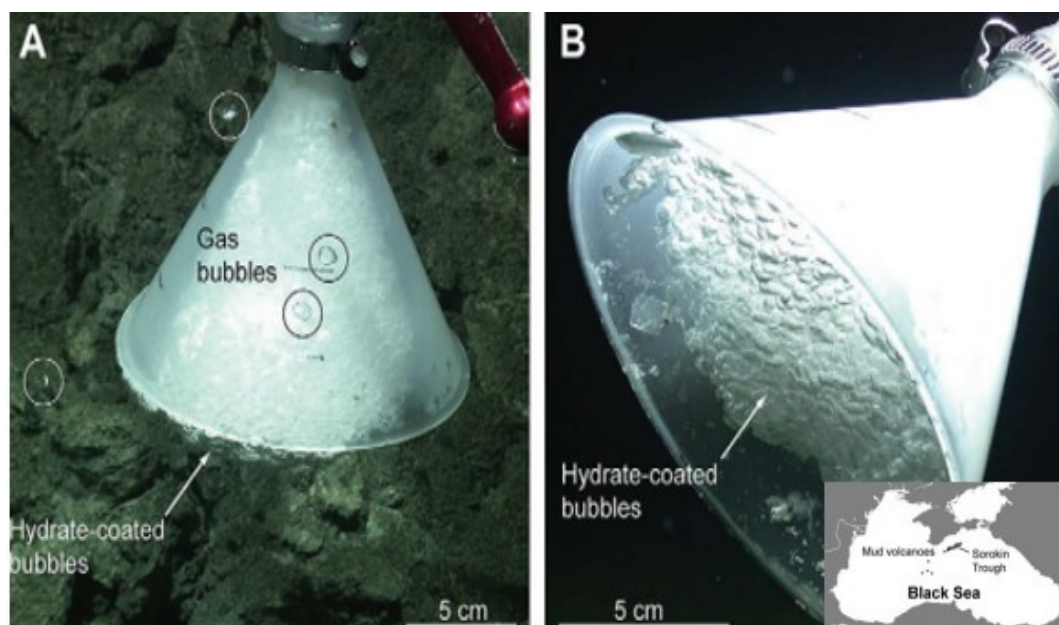


**Figure 3-9:** Gas seepages from the Batumi seep area during ROV observations (Pape *et al.*, 2011)

In the Black Sea, there are many mud volcanoes (mostly due to gas seepages as seen in Figure 3-10) (Ergun and Cifci, 1999). At the Vodyanitskii mud volcano (~2080 mbsf, Sokorin through) in the central north part of the Black Sea, when funnel was put just above gas seepage area, gas hydrate formed inside the funnel because pressure in the funnel is above hydrate equilibrium conditions as shown in Figure 3-11 (Sahling *et al.*, 2009). Miwa *et al.* (2016) categorizes marine gas hydrates as shallow type gas hydrate existence (near sea floor) and deep type gas hydrate existence (in deeper sediments). Gas seepages or gas plumes are considered as an important index of shallow type gas hydrate existence (Miwa *et al.*, 2016). The reason of these gas seepages is that at certain temperature conditions, gas pressure is below hydrate equilibrium curve so hydrate does not form in Figure 3-10. However, in some cases, even in gas hydrate stability zone, hydrate might not form in marine sediments. According to Matsumoto *et al.* (2009), the main reasons of the existence of free gas and free water in gas hydrate stability zones are high salinity effect of residual waters, degassing from ascending fluids, bound water effect and deficiency of free-waters, micro-pore effect of porous media.

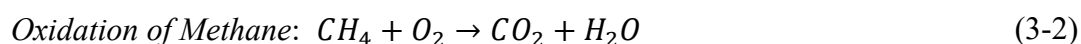


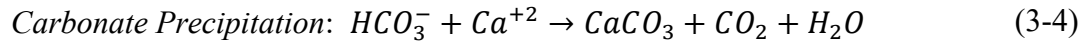
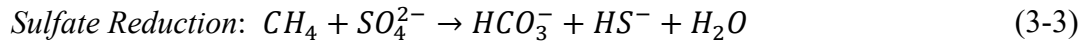
**Figure 3-10:** Scheme of distribution of the free  $\text{CH}_4$  and  $\text{CH}_4$  hydrate in the Black Sea (Adapted from Sozansky, 1997)



**Figure 3-11:** Gas bubbles and gas hydrate formed inside the funnel at Vodyanitskii mud volcano (~2080 mbsl; Sorokin Trough) in the Black Sea (Adapted from Sahling *et al.*, 2009)

Gas seepages were observed in many places of the shallow part of the Black Sea because between sea level (SL) and 580 m below SL, CH<sub>4</sub> hydrate formation conditions are not satisfied. However, CH<sub>4</sub> hydrates can form in the Black Sea at water depths exceeding 580 to 700 meters because the hydrostatic pressure is enough to provide the hydrate equilibrium conditions (Sozansky, 1997; Ivanov *et al.*, 1998; Vassilev and Dimitrov, 2003; Pape *et al.*, 2011). Formation pressure of gas hydrate reservoirs mostly follow hydrostatic pressure with small sediment weight but in conventional reservoir, reservoir pressure is mostly higher than hydrostatic pressure (overpressurized) (Berndt, 2005; Max and Johnson, 2016). Figure 3-10 is very useful to visualize the reason of gas seepages. For example, Naudts *et al.* (2006) observed gas seepages and plumes between 66 and 825 mbsl (meter below sea level) in the Dnepr paleo-delta, northwestern Black Sea as shown in Figure 3-13. However, in this area below 825 mbsl, there is no gas seepage observed because gas hydrate stability zone is below 825 mbsl for this delta. If these seepages are natural and slow, most of gas released is oxidized in seawater or there is sulfate reduction reaction as seen in Equation (3-2) and Equation (3-3) respectively. In gas seepage areas, carbonates are commonly observed because of carbonate precipitation as described in Equation (3-4) (Cremiere *et al.*, 2011). According to Pasyukov *et al.* (2014), the height of gas seeps in the Black Sea varies from 10 to 250 m (mostly 10-50 m) and their diameter changes from 10 to 40 m. Pasyukov *et al.* (2014) proposed that almost all of these gas seeps do not reach to the surface. Kessler *et al.* (2006) also proved that currently released CH<sub>4</sub> is almost balanced by oxidation in the upper water column such that little CH<sub>4</sub> escapes to the atmosphere. Furthermore, in the Macondo well blowout in 2010, all of released CH<sub>4</sub> and 50 % of released oil were dissolved in sea and also consumed by bacterias (McNutt *et al.*, 2012). However, if there are sudden gas releases because of slope failures, etc., it is harmful for environment (Xing, 2013). According to Vassilev and Dimitrov (2003), the area of the Black Sea suitable for gas hydrate formation is evaluated at 288,100 km<sup>2</sup>, representing about 68.5% of the total Black Sea or almost 91% of the deep-water basin.





Oxidation of  $\text{CH}_4$ , sulfate reduction and carbonate precipitation as shown in Equation (3-2), Equation (3-3) and Equation (3-4) are commonly observed in gas seepage areas in marine environment (Max and Johnson, 2016). Figure 3-12 shows precipitated carbonates and bacterial mats (white color) formed by anaerobic oxidation of  $\text{CH}_4$  in  $\text{CH}_4$  venting areas, Dnepr paleo-delta, NW Black Sea (Naudts *et al.*, 2008). Due to anoxic environment inhibiting the development of benthic ecosystems (Collins *et al.*, 2016), oxidation of  $\text{CH}_4$ , carbonate precipitation and sulfate reduction in the Black Sea, Tinivella (2016) proposed that the Black Sea gas hydrates might be good production test sites with minimum risks (mainly environmental risks).

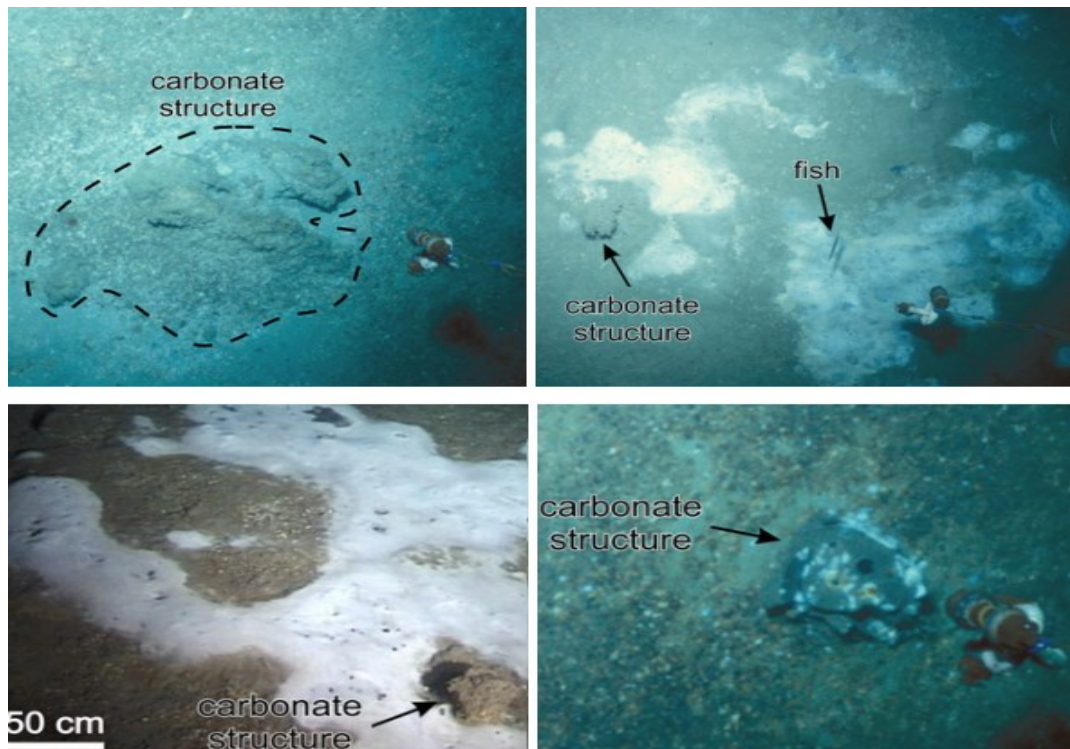


**Figure 3-12:** Sea-floor observations, showing bacterial mats and carbonates in  $\text{CH}_4$  venting areas, Dnepr paleo-delta, NW Black Sea (Naudts *et al.*, 2008)

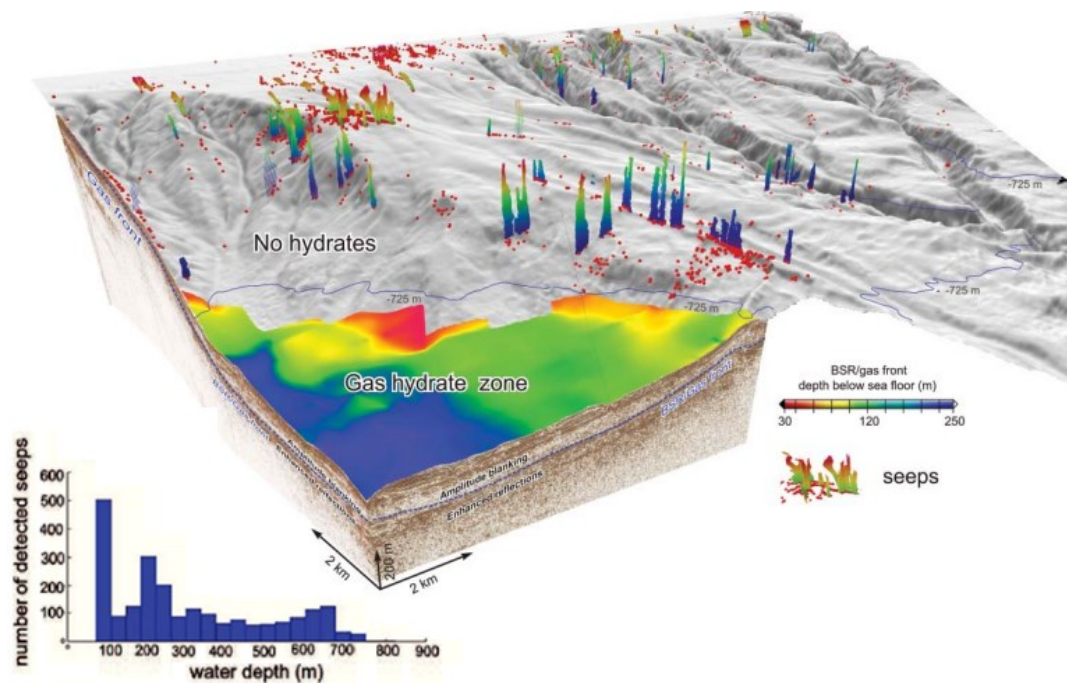


**Figure 3-13:** CH<sub>4</sub> seeps in the Dnepr paleo-delta, NW Black Sea, at water depths of 66 to 825 m (Adapted from Naudts *et al.*, 2006 and Naudts *et al.*, 2009)

In Figure 3-14, the locations of the gas hydrate samples recovered as squares in ice blue color and the potential places in terms of gas hydrate inferred from other seismic studies (i.e. mud volcanoes) in the Black Sea are shown (Starostenko *et al.*, 2010). Moreover, Küçük (2016) prepared Figure 3-15 to show potential gas hydrate places in the Black Sea. Both in Figure 3-14 and Figure 3-15, the gas seepage areas in the Black Sea are shown. These seepages are due to the conditions in those places out of hydrate formation conditions or high gas fluxes cutting GHSZ. First gas hydrate samples from the Black Sea sediments were discovered by Yefremova and Zhizchenko (1974). Moreover, with the TTR-11 cruise of RV Professor Logachev, gas hydrate samples were recovered for the first time in the Northwestern (NW) part of the Black Sea in the area without mud volcanoes and at a water depth of 900 m as shown in Figure 3-16 (Kenyon *et al.*, 2001). As seen in Figure 3-16-a, gas hydrates fill sediments in nodular filling type. Similarly, Ivanov *et al.* (1998) observed gas hydrates as nodules (Figure 3-16-b) in the sediments in Crimean deep-water margin in the Black Sea.

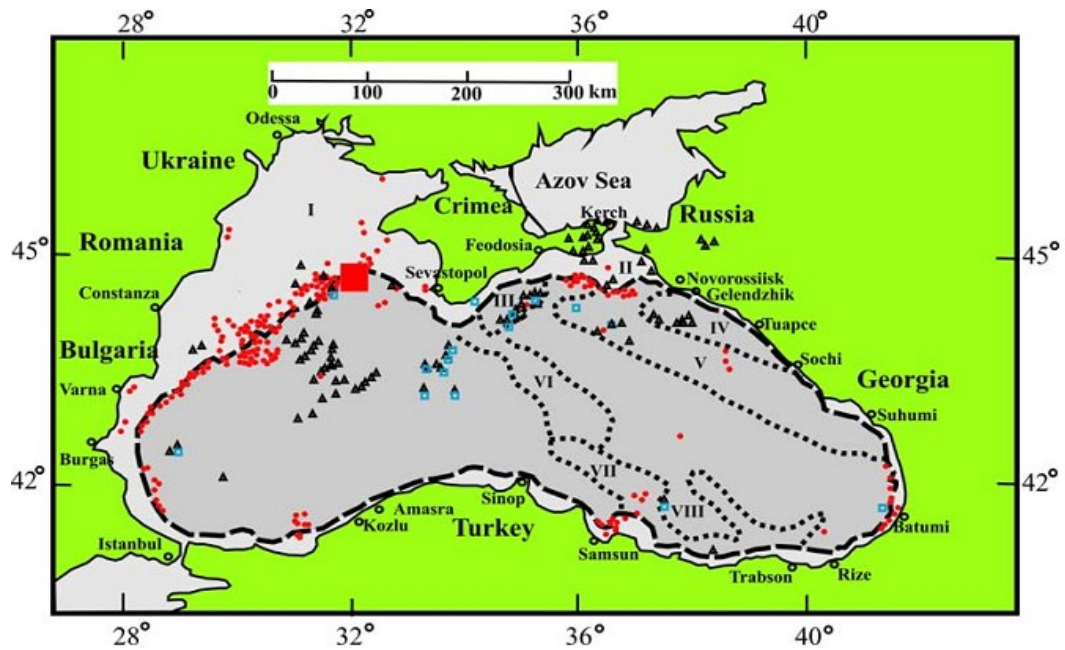


**Figure 3-14:** Location of the mud volcanoes gas seeps and gas hydrates in the Black Sea: Triangles in black, mud volcanoes; circles in red, gas seeps; squares in ice blue, gas hydrate; bold dashed lines in black, shelf edge; bold squared lines, boundaries of tectonic units; filled rectangular in red, Dnipro palaeo-delta area; I, NW Shelf; II, Kerch-Taman trough; III, Sorokin trough; IV, Tuapse trough; V, Shatsky ridge; VI, Andrusov ridge; VII, Arkhangelsky ridge; VIII, Giresuan basin (Starostenko *et al.*, 2010)

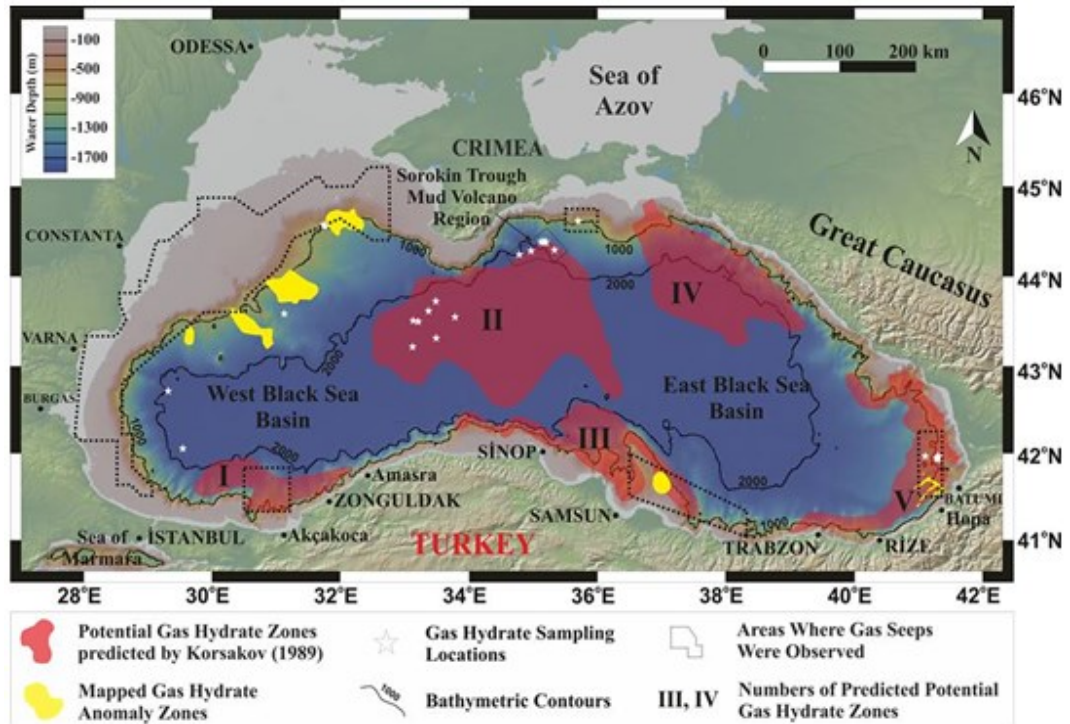


**Figure 3-15:** Gas hydrate zones in the Black Sea (Küçük, 2016)

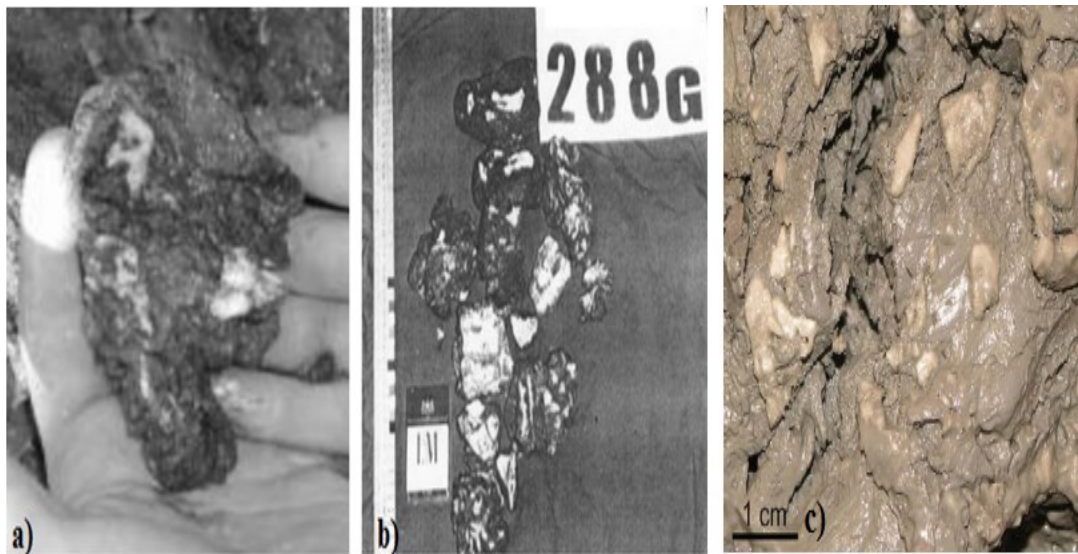


**Figure 3-16:** a) Gas hydrates in the Core BS308K in the NW of the Black Sea (Kenyon *et al.*, 2001) b) Gas hydrates in Core BS-288G in Crimean deep-water margin in the Black Sea (Ivanov *et al.*, 1998) c) Chips of gas hydrates in the core catcher in the sediment interval 10–35 cm in core GeoB 11913 taken at Vodyanitskii mud volcano in the Black Sea (Sahling *et al.*, 2009)

The gas hydrates were recovered in Batumi Region in the eastern part of the Black Sea with TV-grab (TVG) or gravity corer. The recovered gas hydrate samples contain 99.96 % of  $\text{CH}_4$  gas, which is an indication of sI type hydrate and  $\text{CH}_4$  hydrate (Heeschen *et al.*, 2011). In another recent study of Küçük *et al.* (2015), seabed samples were collected in Amasra, Bartın, Zonguldak-Kozlu in the central Black Sea by boxer corer. Headspace gas chromatography was applied to seabed samples to observe gas composition and the gas chromatography results represented hydrocarbon gases such as  $\text{CH}_4$  (mostly),  $\text{C}_2\text{H}_6$ ,  $\text{C}_3\text{H}_8$ ,  $i\text{-C}_4\text{H}_{10}$ ,  $n\text{-C}_4\text{H}_{10}$ ,  $i\text{-C}_5\text{H}_{12}$ ,  $n\text{-C}_5\text{H}_{12}$  and  $\text{C}_6\text{H}_{14}$ . Therefore, all indications show that the Black Sea has both thermogenic and biogenic gas hydrate potentials. Equations (3-5), (3-6), and (3-7) in which gas ratio intervals of gas hydrates shown are classified as thermogenic, biogenic and mixed gas hydrates (Buruss and Laughrey, 2010). As well as these gas sources, cretaceous volcanoes in the Black Sea might provide  $\text{CO}_2$  and  $\text{H}_2\text{S}$  to these shallow gas hydrates. In the study area of Küçük (2016) in the western Black Sea (Zonguldak-Amasra regions), these volcanic structures were observed.

$$C_1/(C_2 + C_3) < 100 \rightarrow \text{Thermogenic gas hydrate} \quad (3-5)$$

$$C_1/(C_2 + C_3) < 1000 \rightarrow \text{Biogenic gas hydrate} \quad (3-6)$$

$$100 < C_1/(C_2 + C_3) < 1000 \rightarrow \text{Biogenic + Thermogenic gas hydrate} \quad (3-7)$$

According to Hester and Brewer (2009)'s study, thermogenic hydrates have been found in several places worldwide, including the Gulf of Mexico, the Caspian Sea, the Black Sea, the Marmara Sea and the Sea of Japan. Moreover, the detection of i-pentane (i-C<sub>5</sub>H<sub>12</sub>) in the Black Sea near sea floor might be thought as the potential of sH hydrates in the Black Sea because i-C<sub>5</sub>H<sub>12</sub> and CH<sub>4</sub> form sH hydrate at certain concentrations. For instance, in Bush Hill, Gulf of Mexico, sH hydrate was detected, which includes 21.2 % CH<sub>4</sub> and 41.1 % i-C<sub>5</sub>H<sub>12</sub> as shown in Table 3-1 (Sassen and MacDonald, 1994).

**Table 3-1:** Gas compositions of hydrate samples taken from Bush Hill, Gulf of Mexico (Sassen and MacDonald, 1994)

Sample	C <sub>1</sub>	C <sub>2</sub>	C <sub>3</sub>	i-C <sub>4</sub>	n-C <sub>4</sub>	i-C <sub>5</sub>	n-C <sub>5</sub>
Hydrate (sH)	21.2	9.5	7.5	2.5	17.5	41.1	0.8
Hydrate (sII)	71.8	3.4	18.8	5.7	0.3	-	-
Hydrate (sII)	73.9	4.9	16.3	4.6	0.2	-	-

Although CH<sub>4</sub> and i-C<sub>5</sub>H<sub>12</sub> (very low concentration) were detected in the Black Sea, much more studies are needed whether the Black Sea has sH hydrate potential as well as sI and sII hydrate potential. It is known that the main component of gas from the Black Sea hydrates is 93.3-99.7 % CH<sub>4</sub> (Vassilev and Dimitrov, 2003). Even though it is considered that 99 % of all gas hydrate reservoirs in the world includes almost 100 % CH<sub>4</sub> (Kvenvolden, 2002; Johnson, 2011; Collett *et al.*, 2015), this percentage could be lower in the Black Sea because many samples (Sozansky, 1997; Ivanov *et al.*, 1998; Kenyon *et al.*, 2001; Dimitrov, 2002; Heeschen *et al.*, 2011; Küçük *et al.*, 2015) include thermogenic gases such as C<sub>2</sub>H<sub>6</sub>, C<sub>3</sub>H<sub>8</sub>, n-C<sub>4</sub>H<sub>10</sub>, i-C<sub>5</sub>H<sub>12</sub>, etc. These gases as impurities in CH<sub>4</sub> change gas hydrate type of CH<sub>4</sub> from sI to sII hydrate at

certain concentrations. Moreover, Vassilev and Dimitrov (2003) stated that as going deeper through the CH<sub>4</sub> hydrate stability zone in the Black sea, hydrate saturation might increase up to 45-65 %. Similarly, Nandanwar *et al.* (2016) proposed that the bottom of hydrate layers have higher gas hydrate saturations than the top layer.

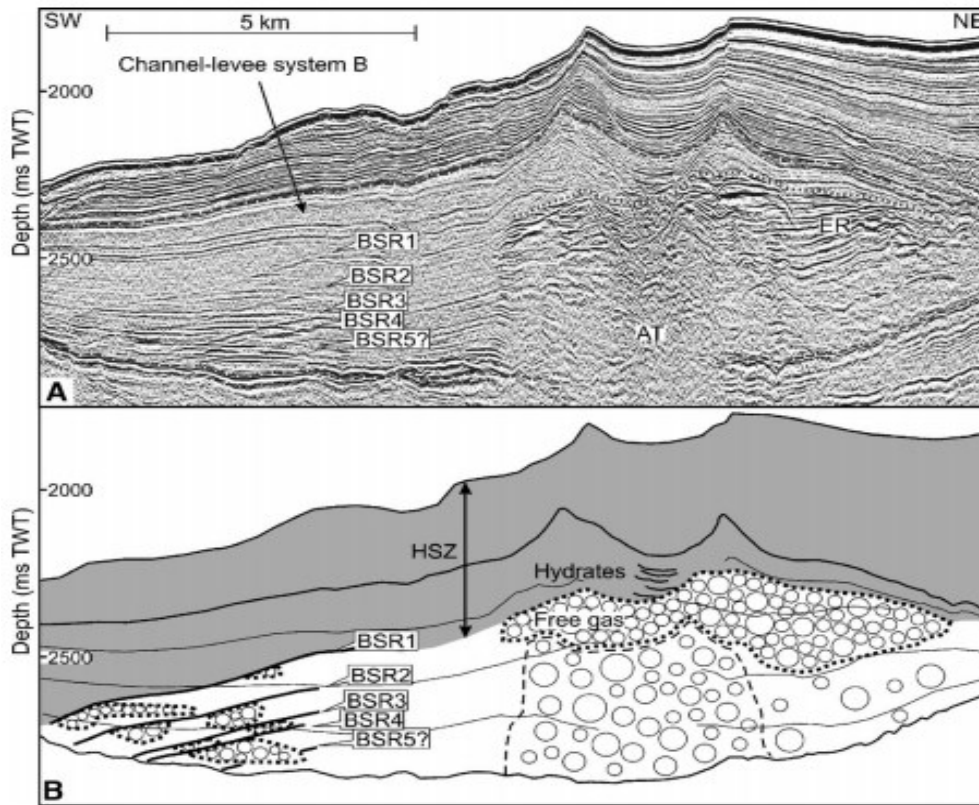


**Figure 3-17:** A) BSRs detected in the Black Sea B) Analysis of BSRs (Popescu *et al.*, 2006)

Class 1 hydrates appear to be the most promising targets for gas production. It is because its pressure is close to hydrate equilibrium conditions and it is easy to produce (only small changes in pressure and temperature are necessitated for hydrate dissociation) and the existence of a free gas zone guarantees gas production even when the hydrate contribution is small (Kurihara *et al.*, 2011; Moridis *et al.*, 2013; Xu and Li, 2015). Class 1 CH<sub>4</sub> hydrate reservoirs might be common in the Black Sea. For the determination of Class 1 hydrates, seismic studies have crucial importance. Detection of bottom-simulating reflections (BSRs) during seismic studies can give

clues about the potential of Class 1 hydrates. Bottom-simulating reflections (BSRs) are the typical seismic signature for marine gas hydrate reservoirs. They consist of a reversed polarity reflection that approximately parallels the sea floor and crosscuts the acoustic bedding structure of the sediments (Popescu *et al.*, 2006; Thakur and Rajput, 2011; Sahay and Johnson, 2014; Vadakkepuliambatta *et al.*, 2015; Küçük *et al.*, 2015). The presence of a free gas zone below the BSR is attested by high reflectivity and has been confirmed by drilling (Popescu *et al.*, 2006). Generally, BSRs mimic seafloor bathymetry (Majumdar *et al.*, 2016). In the study of Popescu *et al.* (2006), multiple BSR lines were detected and they are shown in Figure 3-17. Strong BSR reflections are preferable for gas hydrate deposited in reservoir quality sands but the strongest BSRs are observed in shales (which are not considered as good reservoir for gas production from gas hydrates) (Sahay and Johnson, 2014).

In the statistical study of Majumdar (2015), the dataset of BSR distribution from the Bureau of Ocean Energy Management with a huge dataset of gas hydrate distribution as appraised from well logs, covering an area of around 200,000 km<sup>2</sup> in the northern Gulf of Mexico were evaluated. It was found that the chances of encountering gas hydrate when drilling through a BSR is ~ 42%, while that when drilling outside the BSR is ~15%. 42 % success to find gas hydrate around the BSRs is really a good amount and this shows the importance of the BSRs for the exploration of gas hydrates. The probability of detecting gas hydrate (42%) is much higher than the probability of the exploration of conventional gas reserves (10-15%) in wildcat fields. Moreover, Majumdar *et al.* (2016) states that the chances of finding gas hydrates is increased by 2.6 times if BSRs exit according to the evaluation of 3D seismic data and well logs data of 788 wells in the northern Gulf of Mexico. Hence, BSRs are very useful for the exploration of gas hydrate reservoirs. However, BSR is not a necessary condition for the presence of hydrate, as it only occurs when there is free gas beneath the distinct gas hydrate phase boundary. If there is no free gas below gas hydrate, there will not be BSRs (Singh and Prakash, 2015). Therefore, it is hard to detect Class 3 hydrates compared to Class 1 hydrates. Although BSR is an important tool to discover gas hydrate reservoirs, currently it is not enough to predict amount of gas hydrates, free gas zone thickness and sediment type (Max and Johnson, 2016;

Dannowski *et al.*, 2016). They should be evaluated together with other indications of gas hydrates such as pockmarks, gas seepages, mud volcanoes and mounds and then drilling and well logging (Kleinberg, 2009). Furthermore, recently, controlled-source electromagnetic methods (CSEM) were reported to be very effective to determine shallow gas hydrates by imaging subsurface resistivity and these surveys might provide hydrate saturation data and free gas amount below BSRs (Darnet *et al.*, 2010; Weitemeyer *et al.*, 2011; Wang *et al.*, 2015; Zander *et al.*, 2016). For instance, in the Danube fan of the Black Sea, marine controlled source electromagnetic method was applied in 2014 for gas hydrate exploration and useful results were obtained (Jegen and Hölz, 2014; Schwalenberg *et al.*, 2016).

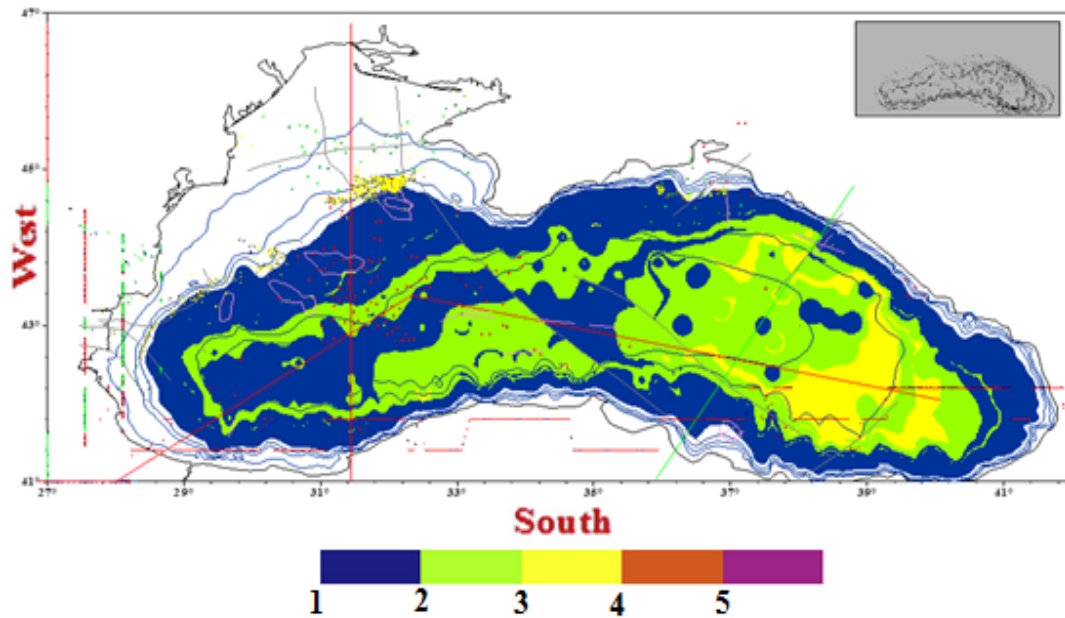


**Figure 3-18:** Gas hydrate stability zones/BSR number in the cross section (Vassilev, 2006)

In the Black Sea, multiple bottom-simulating reflections (BSR) were observed in the Danube deep-sea fan as shown in Figure 3-17 (Popescu *et al.*, 2006). Similarly, Küçük *et al.* (2015) and Küçük (2016) collected seismic data in Amasra, Bartın, Zonguldak-Kozlu in the central Black Sea represent BSRs, bright spots and transparent zones. Multiple-BSRs were also observed in the study area. There are several reasons of the multiple-BSRs, mainly it is due to (Popescu *et al.*, 2006; Jegen and Hölz, 2014; Paganoni *et al.*, 2016):

- Gas hydrate with different gas compositions (biogenic and thermogenic)
- Climate and sea level changes
- Sediment anomaly
- High sedimentation rate

In first case, top BSRs shows the sI CH<sub>4</sub> hydrate (biogenic origin or mix with thermogenic gas) and bottom BSRs shows mostly sII natural gas hydrates (thermogenic origin including C<sub>3</sub>H<sub>8</sub>). Similarly, multi-BSR was detected in paleo channel-levee system in ~1500 m water depth of the Danube Fan and sandy sediments with good reservoir properties were observed in the Danube Fan of the Black Sea (see Figure 3-14 for its location) (Dannowski *et al.*, 2016; Zander *et al.*, 2016). Scientists believed that the multiple BSRs are due to sea level changes in the past in the Danube Fan in the Black Sea (Jegen and Hölz, 2014). It should be noted that the reason of multi or double BSRs might be due to the sediments with magnetic properties such as greigite so gas hydrate related BSRs should be verified with other indications (Rogers, 2015). In the Black Sea, multiple BSRs due to gas composition and climate change are considered to exist (Popescu et al., 2006; Jegen and Hölz, 2014; Küçük, 2016). Moreover, in Figure 3-18, gas hydrate stability zones versus BSRs number in the cross section in the Black Sea is shown (Vassilev, 2006). This also shows the gas hydrate potential of the Black Sea. With the all available data about the Black Sea hydrates, there is a huge gas hydrate potential of sI and sII gas hydrates. Actually, the BTU and commercial value of natural gas including higher density gases such as C<sub>2</sub>H<sub>6</sub>, C<sub>3</sub>H<sub>8</sub> and C<sub>4</sub>H<sub>10</sub> with CH<sub>4</sub> are higher than those of natural gas including almost 100 % CH<sub>4</sub> (Max and Johnson, 2016). Therefore, this is another advantage of the Black Sea gas hydrates because of its high sI and sII gas hydrate potential.

### 3.3 Gas Hydrate Potential of the Black Sea

Gas hydrate reservoirs are considered as a potential future energy resource because it is widely available in permafrost zones and mostly marine sediments. All the evidences show that there is a huge potential of gas hydrates in the Black Sea. It is important to calculate the potential amount of gas in gas hydrates. For this reason,

there are many initial gas-in place calculations in hydrates in the world as listed in Figure 2-5 and Table 2-3.

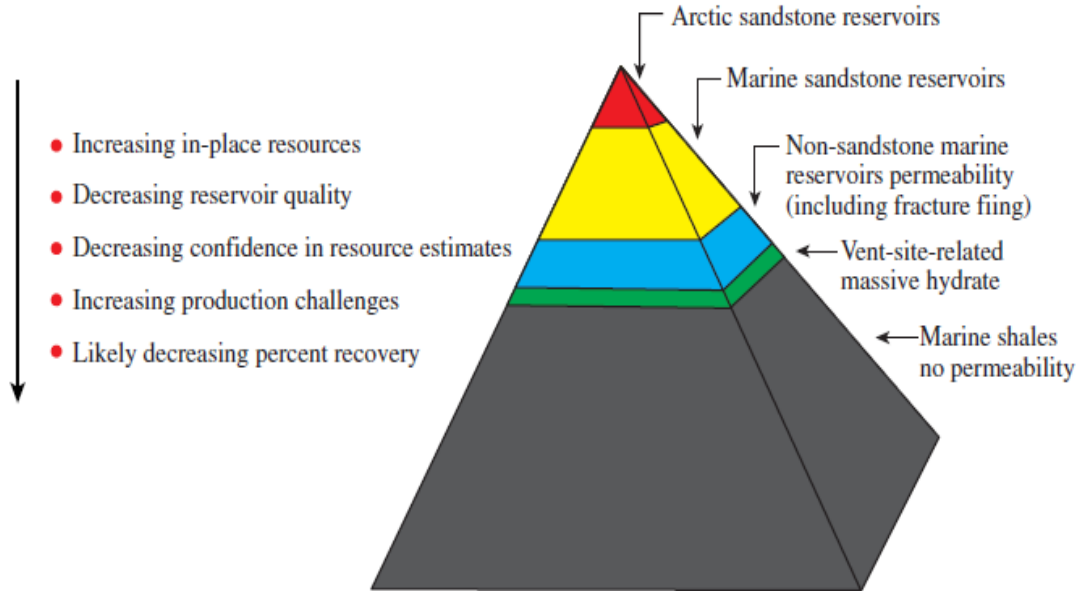


**Figure 3-19:** The hydrate resource pyramid (Zou, 2013)

Gas hydrates are found in artice sand reservoirs, marine sand reservoirs, non-sand marine reservoirs, massive sea floors, marine shales and clays as shown in Figure 3-19. However, only gas hydrates in artice sand reservoirs and marine sand reservoirs are considered as energy sources (Boswell and Collett, 2006; Boswell *et al.*, 2007; Johnson, 2011; Winters *et al.*, 2014; Boswell, 2014; Johnson and Max, 2015; Heeschen *et al.*, 2016b). Many factors such as permeability, porosity, hydrate saturation, reservoir temperature, reservoir pressure and hydrate section thickness are quite important for the production of gas from gas hydrate reservoirs (Huang *et al.*, 2016). Permeability of hydrate reservoir is one of the most important factors both during hydrate formation and hydrate dissociation. In order to prove the hydrate resource pyramid in Figure 3-19, Huang *et al.* (2015) modelled gas hydrate reservoir in Shenhu area, China for different formations: Clay reservoir (grain size<0.005 mm), silt reservoir (grain size: 0.005-0.05 mm) and sandstone reservoir (grain size: 0.05-2 mm) by using Tough + Hydrate simulator. As seen in Figure 3-20, at the same conditions, much more gas hydrate is dissociated in sand reservoirs compared to silt and clay reservoirs by 3.0 MPa depressurization. Hence, with current available

technology, sand rich reservoirs are targets for gas hydrate exploration as energy sources in Figure 3-19. Similarly, Han *et al.* (2016) conducted depressurization experiments from CH<sub>4</sub> hydrate deposited in sandy sediments (average particle size: 510.69  $\mu\text{m}$ ) and silty clay sediments (average particle size: 67.84  $\mu\text{m}$ ) in 5.6 L cubic reactor. Highest gas production is observed from hydrates deposited in sandy sediments. Moreover, it was observed that hydrate equilibrium curve in sandy sediments is same with bulk hydrate equilibrium curve whereas fine silty clay sediments shifts hydrate equilibrium curve to left.

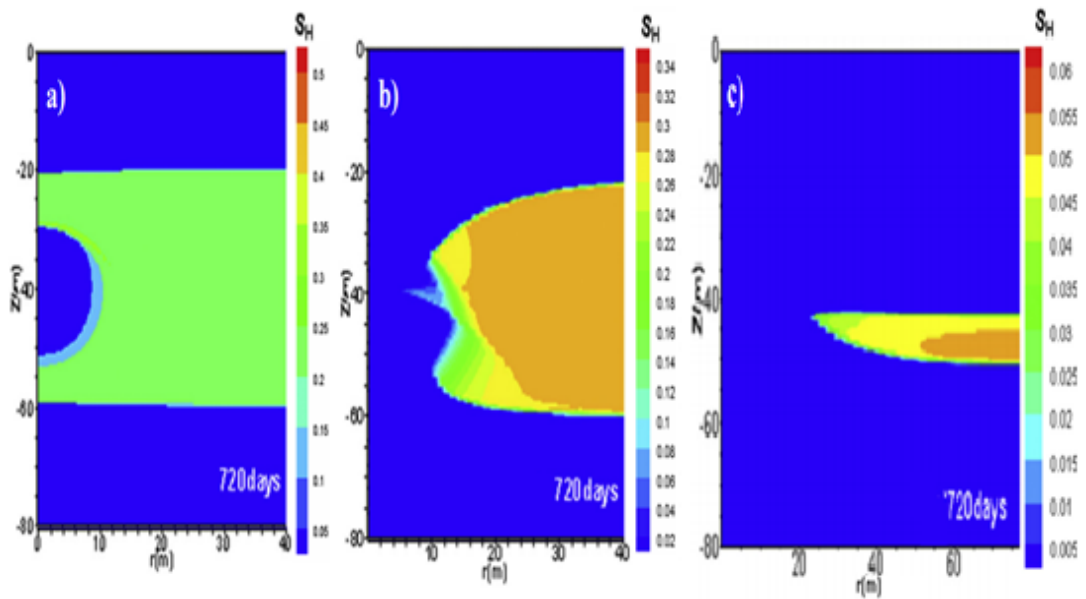


**Figure 3-20:** Hydrate saturation  $S_h$  distribution in a) Clay Reservoirs b) Silt Reservoir c) Sand Reservoir during gas production with 3.0 MPa depressurization (Huang *et al.*, 2015)

According to Boswell (2009), only 10 % or even less of all gas hydrates in the world are deposited in sands or sandstone. Gas productions from non-sand marine hydrates, massive seafloor (6 % of hydrate occurrence in nature and mostly above 11 mbsf) or shallow hydrates, and marine shale hydrates are very difficult even though there is a huge gas hydrate potential in these reservoirs compared to arctic and marine sand reservoirs (Rogers, 2015; Zhao *et al.*, 2016b). In these hydrate reservoirs, reservoir quality and fractional gas production recovery are quite low. Hence, marine sands are good reservoirs for gas hydrates because they have high porosity and high

permeability values. According to the data of sedimentation on shelves and continent slopes, sands commonly comprise 20 % of sediments with sand/silt up to 60 % (Max *et al.*, 2013). Gong *et al.* (2016) calculated that gas hydrate reservoir with hydrate saturation ( $S_h$ ) greater than 30 % has higher gas production compared to tight gas and coalbed methane reservoirs. Konno *et al.* (2015) measured the intrinsic permeability of natural sediment cores obtained from a CH<sub>4</sub> hydrate reservoir in the Eastern Nankai Trough in Japan. As seen in Figure 3-21, if clay content increases, the permeability of cores decreases. Therefore, gas flux into the cores including high clay content is difficult and generally, hydrate saturations are less than 10 % in these non-sand marine reservoirs.

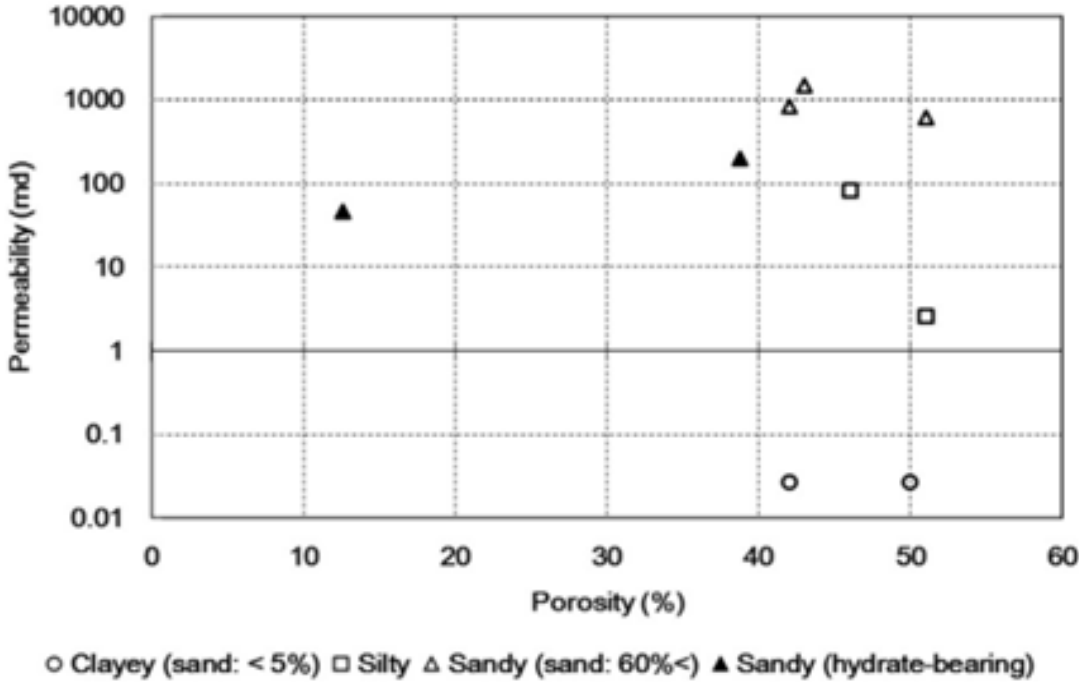


**Figure 3-21:** Relation between absolute permeability and porosity for core samples in Eastern Nankai Trough (Konno *et al.*, 2015)

According to Haeckel *et al.* (2015), high reservoir-quality in gas hydrate accumulations are expected in permeable sandy-silty deposits, such as turbidites and channel-levee-systems of the large paleo-river systems around the Black Sea. Similar observations in the Black Sea were obtained in the study of Xing (2013). Coarse sediments from the paleo-river deposited as turbidites on a wide range of the basin

floor were also observed in the eastern Nankai Trough, Japan (Ito *et al.*, 2015; Komatsu *et al.*, 2016). In ocean sediments, turbidite sand-silt systems are considered as one of the most potential places for gas hydrates because they have good reservoir properties (porous and permeable) (Max and Johnson, 2015; Su *et al.*, 2016; Max and Johnson, 2016). Therefore, the permeable sandy-silty deposits might be good targets depositing gas hydrates in the Black Sea (Haeckel *et al.*, 2015). Moreover, Max and Johnson (2015) proposed that additionally to turbidites, non-turbidite permeable sand reservoirs might be very good targets for gas hydrate reservoirs in the Black Sea and grain size of these sands might be higher than those found in marine turbidite systems. Mean grain sizes of some cores samples near seeps and mound in the Black Sea is shown in Figure 3-22.

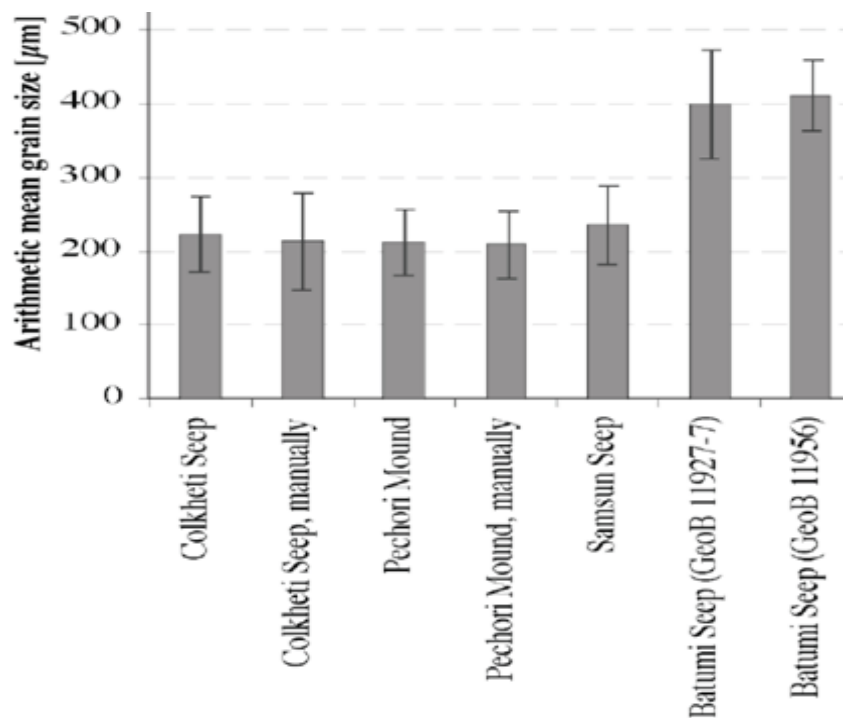


**Figure 3-22:** Mean grain sizes of gas hydrate samples in the Black Sea (Klapp, 2009)

To consider gas hydrate reservoirs as energy sources, optimum conditions of many parameters should be satisfied. Temperature gradient, pressure gradient, source gas potential, porosity, permeability, sediments types, water, gas and hydrate saturations are the most important parameters (Boswell and Collett, 2016). Even if all of these

parameters are satisfied, if the sediments do not have good reservoir properties, gas hydrates are not considered in terms of gas production. As shown in Figure 3-23, gas hydrate saturation increases if intrinsic permeability increases. However, if intrinsic permeability is very low (mostly in clay sediments), gas hydrate saturation is very low because while gas is migrating from source rock, it cannot diffuse into the sediments with very low permeability. Hence, B and C type hydrate structures in Figure 3-23 are commonly observed in sediments with low permeability. According to Boswell and Collett (2016), high saturation in poor reservoirs or low saturation in high-quality reservoirs are rarely observed. Therefore, the identification of the sediments where gas hydrates deposited are quite important.

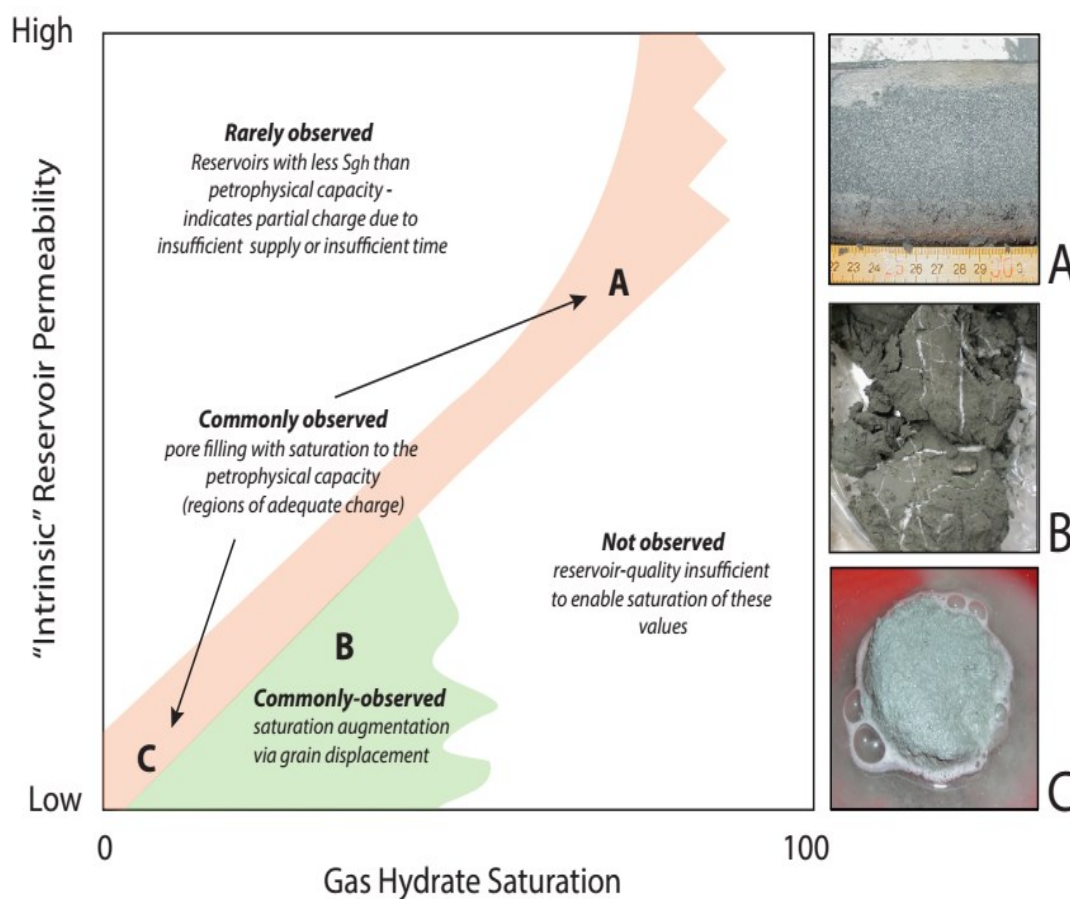


**Figure 3-23:** Gas hydrate saturation relation with intrinsic reservoir quality (Boswell and Collett, 2016)

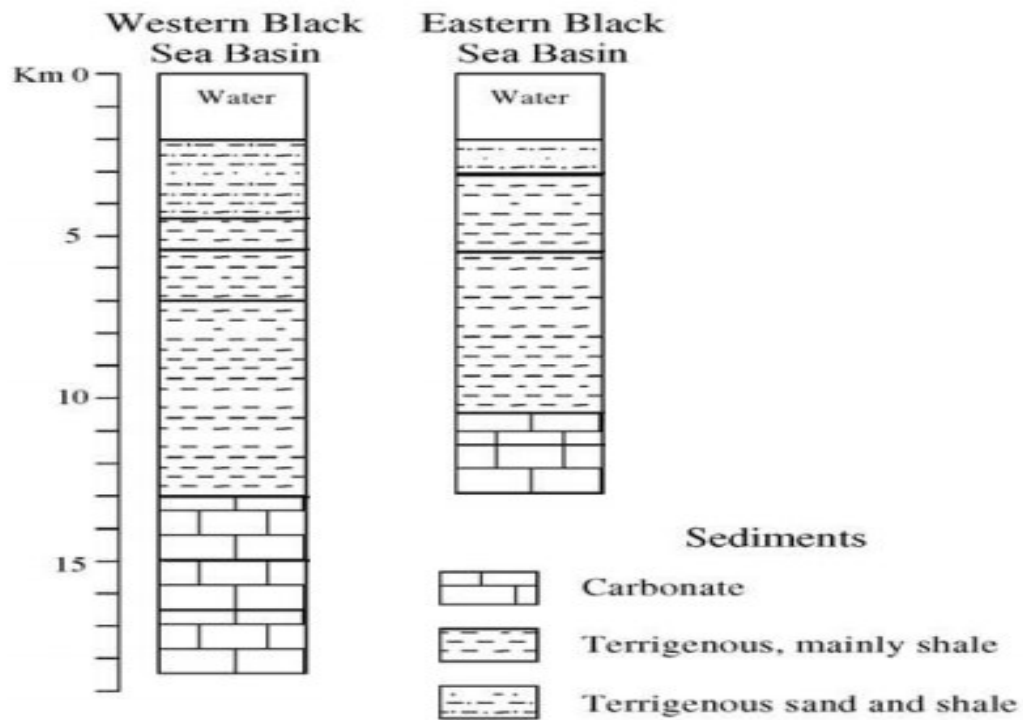


**Figure 3-24:** Black Sea Sediments (Adapted from Nikishin *et al.*, 2003)

As shown in Figure 3-1 and Figure 3-24, the Black Sea has thick sediment layers. Figure 3-24 indicates the lithology map in the western Black Sea basin and Eastern Black Sea basin. Terrigenous mud is common in gas hydrate stability zone of the Black Sea. All rocks, sands, silts, clays, etc. eroded with rivers and glaciers and then transported to the Black Sea are called as terrigenous mud. Therefore, for better gas hydrate reservoirs, coarse sand layers and coarse layers of turbidites are potential sediments (Ergun and Çifci, 1996; Max *et al.*, 2013; Max and Johnson, 2016; Rajput and Thakur, 2016). The grades of sands change from 62.5  $\mu\text{m}$  to 2000  $\mu\text{m}$  (Rogers, 2015). It is better to analyze turbidites which is considered to be common in the Black Sea.

Petroleum geologists investigate turbidites commonly because turbidites might include good reservoirs for hydrocarbons (oil and natural gas) (Bouma, 1962; Fairbridge, 1966; Walker, 1978; Melgar, 2009; Hüneke and Mulder, 2011). As seen in Figure 3-25, coarse and fine sediments form turbidites after these sediments sank.



**Figure 3-25:** Ordinary outcrop example of turbidites (alternating layers of fine and coarse sediments) (Swewe, 2016)

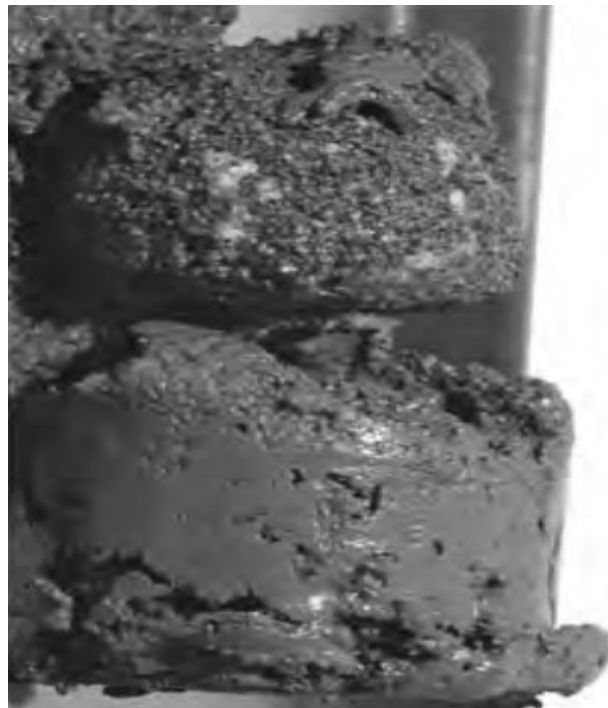


**Figure 3-26:** Typical gas hydrate bearing sand dominated turbidite layern (top) separated from gas hydrate free mud (bottom) at U1328 (Riedel *et al.*, 2009)

Because of very low permeability of fine sediments, gas cannot diffuse into fine sediment but gas can diffuse into coarse sediments because their permeability values are quite high. As clay content increases in sands, permeability decreases (Max and Johnson, 2016). Then, at high pressure and low temperature conditions, gas hydrate can form in these coarse sediments in marine environment (Long *et al.*, 2009; Jang and Santamarina, 2016). For example, during field expeditions at Sites U1326 and U1327 across the northern Cascadia in Integrated Ocean Drilling Program (ODP) Expedition 31, gas hydrate zones with exceeding 50 % hydrate saturation were determined. They were deposited in up to 20 m thick sand rich turbidite intervals (Riedel *et al.*, 2009). Figure 3-26 shows the samples taken from U1328 site. As seen in this figure, gas hydrate can be seen in coarse sediments of turbidite (top) but in fine sediment part (bottom), there is no gas hydrate. Furthermore, Max and Johnson (2014) stated that best gas hydrates are found in sands and especially in turbidites bounded with impermeable layers. Therefore, in this study, in order to understand gas production behavior from turbidites in the Black Sea conditions, gas production simulations were held for a hypothetical hydrate reservoir deposited in turbidities. Although coarse sand sediments are appropriate for gas hydrate production, more than 90 % of the global gas hydrates are deposited in fine sediments (clay, shale, muddy sediments etc.) with low gas hydrate saturation in porous media (1-5 %, rarely to 8-10 %) or inside faults, veins, nodules etc. (Jang and Santamarina, 2016; Max and Johnson, 2016).

For the Black Sea, there are a few studies aiming to calculate the amount of CH<sub>4</sub> stored in gas hydrates. In Table 3-2, the results of initial CH<sub>4</sub> in-place calculations in the Black Sea gas hydrates in several studies are shown. Figure 3-27 shows the distribution of CH<sub>4</sub> hydrate in the Black Sea (Klauda and Sandler, 2003).

**Table 3-2:** Methane potential of the Black Sea hydrates

Source	Initial gas (Methane) in place in the Black Sea hydrates, tcm
Korsakov <i>et al.</i> , 1989	40-50
Smirnov and Chumak, 1996	75-100
Parlaktuna and Erdogmus, 2001	68.9-96.6
Solov'yov, 2003	100
Klauda and Sandler, 2003	850
Shi, 2003	42
Vassilev and Dimitrov, 2003	42 to 49 (10-50)

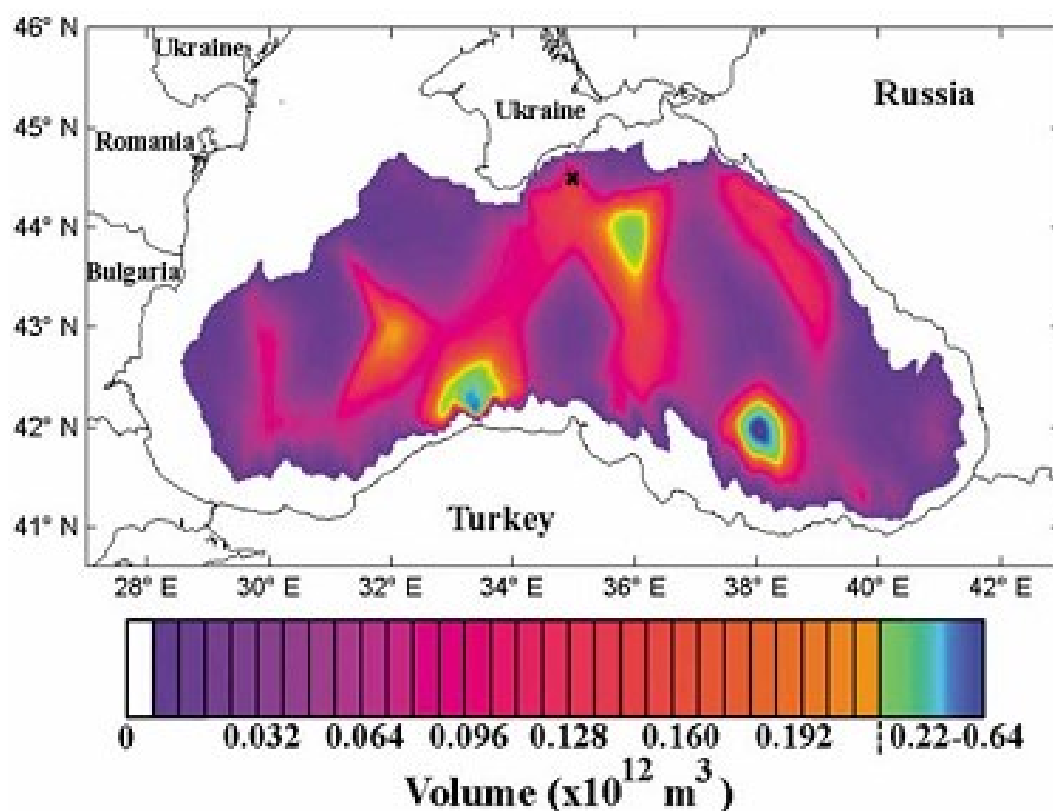


**Figure 3-27:** CH<sub>4</sub> stored in the Black Sea gas hydrates at STP (Klauda and Sandler, 2003)

Vassilev and Dimitrov (2003) calculated the amount of CH<sub>4</sub> in gas hydrates of the Black Sea as 42 to 49 tcm. In their study, they used heat flow data from their colleagues and publications; porosity is from Russian empiric formula; and density; and for the initial gas in place calculations, they used 3 variants: empirical, drills, basin analysis with the Russian "historic-genetic approach". Equation (3-8) and Equation (3-9) are commonly used to calculate CH<sub>4</sub> in-place in CH<sub>4</sub> hydrates (Adapted from Boswell and Collet, 2011):

$$OGIP = \varphi \times h \times A \times EF \times CR \quad (3-8)$$

$$EF = \frac{MW_{CH_4}}{MW_{CH_4} + N_H MW_{H_2O}} \times \frac{V_H \rho_H}{\rho_{CH_4}} \quad (3-9)$$

*Where OGIP: original CH<sub>4</sub> in-place in hydrates, standard m<sup>3</sup>;  $\varphi$ : porosity, fraction;  $h$ : thickness of hydrate zone, m;  $A$ : cross-sectional area of hydrate zone, m<sup>2</sup>;  $CR$ : cavity fill ratio of CH<sub>4</sub>;  $EF$ : Expansion factor of CH<sub>4</sub> in hydrate to surface standard conditions, ratio;  $MW_{CH_4}$ : Molecular weight of CH<sub>4</sub>, g/mol;  $MW_{H_2O}$ : Molecular Weight of H<sub>2</sub>O, g/mol;  $N_H$ : Hydration Number of CH<sub>4</sub> hydrate;  $V_H$ : unit hydrate volume (1 m<sup>3</sup>);  $\rho_H$ : CH<sub>4</sub> hydrate density, kg/m<sup>3</sup>;  $\rho_{CH_4}$ : CH<sub>4</sub> gas density at standard conditions (0.717935 kg/m<sup>3</sup> at 0 °C and 1 atm).*

The values in Table 3-2 represents all gas hydrates in all types of sediments in the Black Sea such as sands, silts, shales, clays etc. For gas production from gas hydrates, the targets are the gas hydrates deposited in sands (Kumar et al., 2015; Johnson and Max, 2015). According to Max and Johnson (2015), hydrate deposits in subaerial sediment systems in the Black Sea consist of coarser-grained sediments than those commonly found in turbidites. This is a good indication for high quality hydrate reservoirs in the Black Sea. The values in Table 3-2 are beneficial especially for the climate studies rather than energy studies. In Table 3-3, the initial CH<sub>4</sub> in-place calculations in the Black Sea hydrates deposited in sands are listed. Johnson and Max (2015) found the median figure of 2.5 tcm (gas in place in sands) for the Black Sea,

used a range of possible values for sand content, volume of the gas hydrate stability zone, and hydrate saturation. This resulted in a minimum value of 0.031 tcm and a maximum value of 20.3 tcm. In these calculations, in order to find the amount of CH<sub>4</sub> in the Black Sea hydrates deposited in sands, Equation (3-8) is multiplied by sand content.

**Table 3-3:** CH<sub>4</sub> potential of the Black Sea hydrates (in sands only)

<b>Source</b>	<b>Initial gas (Methane) in place in the Black Sea hydrates, tcm</b>
Krason and Ciesnik, 1988	6.5
Vassilev and Dimitrov, 2000	0.1-1.0
Johnson and Max, 2015	2.5 (0.031-20.3)

## CHAPTER 4

### DETERMINATION OF GAS HYDRATE PROPERTIES

It is important to understand gas hydrate properties such as hydrate equilibrium points, gas hydrate density, hydrate cage structure, hydration number, and gas hydrate enthalpy of dissociation. These parameters are useful for the studies of gas hydrates related to gas production from gas hydrate reservoirs, transportation and storage as gas hydrates, and the inhibition of hydrate formation during the transportation with pipelines (Shahnazar and Hasan, 2014). Gas mixtures are common in the Black Sea according to literature survey in Chapter 3. Therefore, the determination of hydrate properties of gas mixtures is as important as in case of pure CH<sub>4</sub> hydrate.

#### 4.1 Gas Hydrate Equilibrium Point Determination

With huge gas production from conventional natural gas reservoirs, the transportation of natural gas with pipelines started in the beginning of 20<sup>th</sup> century. However, especially in winter times, the pipelines were plugged with ice-like structures. Although at first it was considered that this plugging was due to ice formation, Hammerschmidt (1934) proved that this was due to gas hydrate formation. Then, he suggested a formula for hydrate equilibrium points. In this formula, at different temperatures, hydrate equilibrium pressures are calculated for natural gas mixtures. Then, the number of these practical formulas (Berge method, Motiee method, Sloan method, Hammerschmidt method, Katz method, etc.) increased with gas hydrate studies (Berge, 1986; Motiee, 1991; Kobayashi *et al.*, 1987; Hammerschmidt, 1934; Katz, 1959). However, those formulas are practical only in terms of engineering calculations. At high temperatures, the error margins of these equations increase and they do not fit the experimental data especially for gas mixtures (Fattah, 2004).

In this study, in HEP.m (a code written with Matlab 2014a to predict hydrate properties), the formulas of Poettmann *et al.* (1989) were used for the hydrate equilibrium point determination of sI and sII hydrates because this method has several advantages:

- These formulas cover a wide range of pressure and temperature both above and below 0 °C (32 F).
- These formulas are based on the statistical thermodynamic model developed by van der Waals and Platteeuw and they are practical for computer programming.
- The formulas can be used for the pure components (CH<sub>4</sub>, C<sub>2</sub>H<sub>6</sub>, C<sub>3</sub>H<sub>8</sub>, n-C<sub>4</sub>H<sub>10</sub>, i-C<sub>4</sub>H<sub>10</sub>, H<sub>2</sub>S, CO<sub>2</sub> and N<sub>2</sub>) and their mixtures.
- The formulas predict the structures and the conditions under which natural gas hydrate formation for the three phase equilibria, hydrate-liquid-water-vapor and hydrate-ice-vapor.

When sI and sII hydrate potentials of the Black Sea are considered, HEP.m code including Poettmann *et al.* (1989)'s formulas could be very beneficial to predict hydrate properties. The equations proposed by Poettmann *et al.* (1989) are shown in the following part:

Vapor (gas)-solid (hydrate) equilibrium ratio ( $K_{vs}$ ):

$$K_{vs} = X_i / Y_i \quad (4-1)$$

Where  $X_i$ : mole fraction of a component in the hydrate phase on a water free basis;  
 $Y_i$ : mole fraction of a component in the vapor phase on a water free basis

For gas mixtures, the equilibrium condition in Equation (4-2) should be satisfied at hydrate equilibrium pressure of any temperature (Shahnazar and Hasan, 2014):

$$\sum X_i = \sum Y_i / K_{vs} = 1.0 \quad (4-2)$$

As seen in Equation (4-2),  $K_{vs}$  values for the gas components are necessary to satisfy the equilibrium condition at hydrate formation conditions. There are different formulas for each component according to:

- sI and sII structures
- Below and above 0 °C (32 F)
- With and without H<sub>2</sub>S

Hydrate Equilibrium Ratio Equations for structure I (sI) hydrate are listed below:

For Methane (CH<sub>4</sub>):

Above 32 F:

$$\begin{aligned} \log(K_{vs}) = & 12.9293 - 0.858747\log(P) \\ & - \left[ 5086.41 + 22.2952\log(P) + 53.1254(\log(P))^2 \right. \\ & \left. - 13.3721(\log(P))^3 \right] / T \end{aligned} \quad (4-3)$$

Below 32 F:

$$\log(K_{vs}) = 5.51493 - 0.933956\log(P) - 1528.07/T \quad (4-4)$$

Correction Factor for C<sub>2</sub>H<sub>6</sub> in mixture:

$$C = 1.0088 - 0.765 \cdot Y_2 \quad (4-5)$$

Where  $Y_2$ : mole fraction C<sub>2</sub>H<sub>6</sub> in vapor phase

For Ethane (C<sub>2</sub>H<sub>6</sub>):

Above 32 F:

$$\begin{aligned} \log(K_{vs}) = & -1.47826 + 6.81400\log(P) \\ & - [3987.54\log(P) - 1923.55]/T \end{aligned} \quad (4-6)$$

Below 32 F:

$$\log(K_{vs}) = 8.1677 - 1.1939\log(P) - 2935.0/T \quad (4-7)$$

For Hydrogen Sulfide (H<sub>2</sub>S):

Above 32 F:

$$\log(K_{vs}) = 20.80520 - 8.27846\log(P) + 1.75247[\log(P)]^2 - [9114.76 - 3114.4\log(P) + 758.078[\log(P)]^2]/T \quad (4-8)$$

Below 32 F:

$$\log(K_{vs}) = 5.99384 - 0.896920\log(P) - 2458.80/T \quad (4-9)$$

For Carbon dioxide (CO<sub>2</sub>):

Above 32 F:

$$\log(K_{vs}) = 3.2538 + 3.1190\log(P) - [660.39 + 1962.5\log(P)]/T \quad (4-10)$$

Below 32 F:

$$\log(K_{vs}) = 5.22349 - 0.956062\log(P) - 1558.0/T \quad (4-11)$$

For Nitrogen (N<sub>2</sub>):

Above 32 F and no H<sub>2</sub>S:

$$\ln(K_{vs}) = 174.82 - 44553/T - 1.43 \times 10^{-6}P - 0.5996\ln(P) + 20.9/P - 7798/P^2 - 0.15963T \quad (4-12)$$

Below 32 F and no H<sub>2</sub>S:

$$\ln(K_{vs}) = 35.49 + \frac{964}{T} - 0.001396P + 5.603\ln(P) - \frac{87.46}{P} - 0.06486T - \frac{2972.6\ln(P)}{T} \quad (4-13)$$

Above 32 F with H<sub>2</sub>S:

$$\ln(K_{vs}) = 74.02 - \frac{45325}{T} + 5.56 \times 10^{-5}P - 0.32788[\ln(P)]^2 + \frac{815.4}{P} - \frac{29564}{P^2} + \frac{1185861\ln(P)}{T^2} \quad (4-14)$$

Below 32 F with H<sub>2</sub>S:

$$\ln(K_{vs}) = 8.83643 - \frac{2551.94}{T} - 0.00725046P \quad (4-15)$$

Where  $P$ : hydrate equilibrium pressure at  $T$ , psia;  $T$ : temperature, Rankine ( $R$ )

As stated earlier, even 1 % of C<sub>3</sub>H<sub>8</sub> addition to pure CH<sub>4</sub> system, sII hydrate forms if there is enough water and hydrate equilibrium conditions are satisfied. The following equations are hydrate equilibrium ratio equations for structure II (sII) hydrates and they are listed below:

Systems without H<sub>2</sub>S for sII hydrates below 32 F:

$$\ln(K_{vs}) = A + \frac{B}{T} + C.P + D.SG + E.T + \frac{F}{SG} \quad (4-16)$$

Systems without H<sub>2</sub>S for sII hydrates above 32 F excluding CO<sub>2</sub>:

$$\ln(K_{vs}) = A + B.SG + C.T + \frac{D}{P} + \frac{E}{P^2} + F.\left(\frac{P}{1000}\right)^2 + \frac{G}{SG} + H.\left(\frac{P}{1000}\right)^3 + I.SG.P + J.\ln(P) + L.P + \frac{M}{T} \quad (4-17)$$

Systems without  $H_2S$  for sII hydrates above 32 F including  $CO_2$ :

$$\ln(K_{vs}) = A + \frac{B}{T} + C.P + \frac{D}{P} + \frac{E}{P^2} + F.\left(\frac{P}{1000}\right)^2 + G.T \quad (4-18)$$

$$+ H.\ln(P) + I.\left(\frac{P}{1000}\right)^3$$

Systems with  $H_2S$  for sII hydrates below 32 F:

$$\ln(K_{vs}) = A + \frac{B}{T} + C.P + D.SG + E.T + F.MFH^2 + G.MFH^3 \quad (4-19)$$

$$+ \frac{H}{MFH} + \frac{I}{MFH^2} + J.MFH.SG + L.MFH.P$$

$$+ M.MFH$$

Systems with  $H_2S$  for sII hydrates above 32 F:

$$\ln(K_{vs}) = A + \frac{B}{T} + C.MFH + D.SG + E.\ln(P) + \frac{F}{P} + \frac{G}{P^2} \quad (4-20)$$

$$+ H.T + I.\left(\frac{P}{1000}\right)^2 + J.\left(\frac{P}{1000}\right)^3 + L.MFH^2$$

$$+ M.MFH^3 + \frac{N}{MFH} + \frac{O}{MFH^2} + Q.SG.P$$

$$+ R.MFH.SG + S.MFH.P$$

Where SG: specific gravity of hydrate former gases; MFH: mole fraction of  $H_2S$

The constants of Equations (4-16), (4-17), (4-18), (4-19) and (4-20) are listed in Table 4-1, Table 4-2, Table 4-3, Table 4-4 and Table 4-5 (Poettmann *et al.*, 1989)

**Table 4-1:** Coefficients for Equation (4-16) systems without H<sub>2</sub>S when T≤32 F

<b>Component</b>	<b>A</b>	<b>B</b>	<b>C</b>	<b>D</b>	<b>E</b>	<b>F</b>
CH <sub>4</sub>	3300.3	-2.22E-03	-2.6677	0.02057	-0.3154	-14.011
C <sub>2</sub> H <sub>6</sub>	-28667	-1.36E-02	1.1543	-0.09011	-0.4052	104.745
C <sub>3</sub> H <sub>8</sub>	-30588	-1.32E-02	1.1961	-0.09052	-0.4109	105.7
n-C <sub>4</sub> H <sub>10</sub>	-31089	-1.28E-02	1.2741	-0.099	-0.4578	112.801
i-C <sub>4</sub> H <sub>10</sub>	-32895	-1.29E-02	1.4016	-0.09955	-0.3956	113.76
CO <sub>2</sub>	-7472	-4.25E-03	-2.2995	-0.02308	-0.5126	30.294
N <sub>2</sub>	6684.3	-1.91E-03	-2.7436	0.02973	-0.2943	-24.033

**Table 4-2:** Coefficients for Equation (4-17) systems without H<sub>2</sub>S-CO<sub>2</sub> when T>32 F

<b>Component</b>	<b>A</b>	<b>B</b>	<b>C</b>	<b>D</b>	<b>E</b>	<b>F</b>
CH <sub>4</sub>	-3.8862	-2.6891	0.016296	1.098	555.2	-0.01637
C <sub>2</sub> H <sub>6</sub>	-48.4314	0.4489	0.116384	155.330	-9851.5	0.18459
C <sub>3</sub> H <sub>8</sub>	-46.0752	0.4199	0.120725	-135.638	0	-0.30192
n-C <sub>4</sub> H <sub>10</sub>	-48.23	0.0354	0.107702	351.280	-19245	0.25439
i-C <sub>4</sub> H <sub>10</sub>	-54.626	0.1238	0.115242	338.110	-18643	0.24466
N <sub>2</sub>	9.5205	-2.2112	0	-11.860	1765.3	-0.02781

**Table 4-2 (Continued):**

<b>Component</b>	<b>G</b>	<b>H</b>	<b>I</b>	<b>J</b>	<b>L</b>	<b>M</b>
CH <sub>4</sub>	-2.60E-01	0.00089	1.3690E-04	-0.337306	0	0
C <sub>2</sub> H <sub>6</sub>	-1.32568	-0.03029	-2.6146E-04	-1.48522	0	0
C <sub>3</sub> H <sub>8</sub>	-1.4989	0.01152	3.7850E-05	-2.70863	0.0020863	0
n-C <sub>4</sub> H <sub>10</sub>	-1.9692	-0.05415	3.1053E-04	-0.82554	0	0
i-C <sub>4</sub> H <sub>10</sub>	-1.889	-0.05132	2.2811E-04	-0.87306	0	0
N <sub>2</sub>	0.08466	0.00759	-2.4974E-04	-0.29777	0	-2494.9

**Table 4-3:** Coefficients for Equation (4-18) systems without H<sub>2</sub>S

Variable	Gas Gravity		
	0.6	0.7	0.8
<i>A</i>	21.3883	9.9559	-9.361
<i>B</i>	-1.08E+04	0	0
<i>C</i>	-1.35E-04	0	0
<i>D</i>	4.44E+02	81.805	1.40E+02
<i>E</i>	-3.36E+04	-3.47E+03	-5.83E+03
<i>F</i>	0.013	0.058514	0.05434
<i>G</i>	0	0.0232328	0.019155
<i>H</i>	0	-0.20857	-0.00345
<i>I</i>	0	-0.0110174	-0.011667

**Table 4-4:** Coefficients for Equation (4-19) systems with H<sub>2</sub>S when T ≤ 32 F

Component	A	B	C	D	E	F
CH <sub>4</sub>	7.996	-2005	0.0021282	-0.4281	-0.004387	101.5
C <sub>2</sub> H <sub>6</sub>	20.62	-10098	-0.0152816	1.8777	0.00132	-1131.7
C <sub>3</sub> H <sub>8</sub>	21.29	-11957	-0.0149128	1.9322	0.0012	-1106
n-C <sub>4</sub> H <sub>10</sub>	42.94	-15920	-0.0146068	1.9584	-0.02265	-1487.1
i-C <sub>4</sub> H <sub>10</sub>	39.89	-16542	-0.0142668	1.7369	-0.01792	1268.3
CO <sub>2</sub>	69.723	-17706	-0.0048472	1.3265	-0.06597	-1100.6
N <sub>2</sub>	3.507	233.3	-0.0016459	-1.15442	-0.001998	850.2
H <sub>2</sub> S	9.425	-3806.2	-0.0009575	-1.41287	-0.007137	302.41

**Table 4-4 (Continued):**

Component	G	H	I	J	L	M
CH <sub>4</sub>	-4177	-7.51E-04	1.15E-06	29.383	-0.04143	0
C <sub>2</sub> H <sub>6</sub>	17110	3.83E-03	-8.07E-06	-5.26	0.05057	0
C <sub>3</sub> H <sub>8</sub>	16705	3.80E-03	-8.04E-06	-5.39	0.04594	0
n-C <sub>4</sub> H <sub>10</sub>	23843	3.58E-03	7.14E-06	0	0.0713	0
i-C <sub>4</sub> H <sub>10</sub>	-15394	0	0	0	0	-58.996
CO <sub>2</sub>	30161	-2.78E-03	4.80E-06	0	-0.0484	0
N <sub>2</sub>	-14145	-1.66E-02	2.89E-06	0	-0.00818	0
H <sub>2</sub> S	-6280	-1.45E-03	2.81E-06	19.911	-0.01303	0

**Table 4-5:** Coefficients for Equation (4-20) systems with H<sub>2</sub>S when T >32 F

Component	A	B	C	D	E	F
CH <sub>4</sub>	22.211	-7356.5	10.2471	-0.97847	-0.21826	45.301
C <sub>2</sub> H <sub>6</sub>	-59.155	1307	-21.646	2.30741	-1.67848	173.97
C <sub>3</sub> H <sub>8</sub>	-78.909	4727	-19.501	2.72931	-1.42448	252.43
n-C <sub>4</sub> H <sub>10</sub>	-140.05	21513	-9.433	4.043	-1.0488	348.91
i-C <sub>4</sub> H <sub>10</sub>	-127.67	16795	0	3.9417	-1.13015	325.97
CO <sub>2</sub>	-3.978	-2571	9.322	-0.9707	-0.64167	40.464
N <sub>2</sub>	45.129	-11654	15.211	-1.4313	-0.19267	7.99
H <sub>2</sub> S	34.346	-11010.1	14.6441	-0.78291	-0.01803	64.734

**Table 4-5 (Continued):**

Component	G	H	I	J	L	M
CH <sub>4</sub>	-1255.9	-0.01066	0.031552	-0.0001318	-59.589	130.86
C <sub>2</sub> H <sub>6</sub>	-8926.5	0.12746	0.158916	-0.035831	130.248	-285.65
C <sub>3</sub> H <sub>8</sub>	-12792.4	0.14336	0.20902	-0.050435	125.49	-274.61
n-C <sub>4</sub> H <sub>10</sub>	-17587	0.19615	0.2749	-0.065701	242.7	-743.2
i-C <sub>4</sub> H <sub>10</sub>	-16456	0.18546	0.25326	-0.061515	93.8	91.8
CO <sub>2</sub>	-1861.8	0.02775	0.029384	-0.0078205	-156.77	739.4
N <sub>2</sub>	919.7	-0.03632	0.003146	0.009555	-112.1	375.8
H <sub>2</sub> S	-2478.2	-0.02981	0.097502	-0.0173543	-76.232	168.1

**Table 4-5 (Continued):**

Component	N	O	Q	R	S
CH <sub>4</sub>	-3.82E-04	1.00E-06	3.02E-04	4.2235	-0.00112544
C <sub>2</sub> H <sub>6</sub>	5.79E-04	-9.30E-07	3.09E-04	-9.649	0.00177421
C <sub>3</sub> H <sub>8</sub>	5.92E-04	-8.20E-07	6.02E-04	11.436	0.00161249
n-C <sub>4</sub> H <sub>10</sub>	8.20E-05	6.30E-07	6.69E-04	-34.763	0.0022188
i-C <sub>4</sub> H <sub>10</sub>	2.18E-03	-6.11E-06	6.85E-04	-35.408	0.0018496
CO <sub>2</sub>	3.31E-05	1.07E-06	2.69E-04	6.378	-0.00107529
N <sub>2</sub>	-3.33E-05	-1.40E-07	-6.05E-04	5.152	-0.00186488
H <sub>2</sub> S	-4.50E-04	1.14E-06	1.73E-04	3.2308	-0.00110619

The formulas and coefficients were explained in the article of Poettmann *et al.* (1989). However, there are some spelling errors or coefficients of some equations were mixed. Therefore, in this study, they were corrected and listed again. Moreover, when the coefficients proposed in Table 4-1 are used for Equation (4-16) (for systems without H<sub>2</sub>S when  $T \leq 32$  F), there is no convergence for each component. Then, it was concluded that these data set might be wrong because of publication error or anything else. Therefore, for HEP.m code, for sII hydrate below 32 F without H<sub>2</sub>S (Equation (4-16)), the coefficients in Table 4-4 is used and very good results were obtained. Further discussion about the results of this method is in Chapter 7.

Hydrate equilibrium formulas of Poettmann method, Berge method, Motiee method, Sloan method, Hammerschmidt method, Katz method, Kamath method and Moridis method based on the hydrate formation in the bulk system (Poettmann *et al.*, 1989; Berge, 1986; Motiee, 1991; Kobayashi *et al.*, 1987; Hammerschmidt, 1934; Katz, 1959; Fattah, 2004; Moridis *et al.*, 2005; Kamath, 1984). They were derived from the experimental data of hydrate formed during the mixing of free water and gas in the high pressure reactor (mostly constant volume method). However, when gas hydrates in nature are evaluated, they form inside the sediments at different pore sizes. In order to compare the hydrate equilibrium conditions in bulk conditions and those conditions in the sediments, Kang *et al.* (2007) conducted hydrate experiments in silica gel pore of nominal diameters 6, 30, and 100 nm. Then, they compared these data with the calculated data in the bulk.

As seen in Figure 4-1, the hydrate equilibrium values for 100 nm pore size (40 to 75  $\mu\text{m}$  mean particle diameter) are almost similar with the hydrate equilibrium in bulk phase. However, when the pore size gets smaller, the hydrate equilibrium curves are shifted to left. There is a hydrate inhibition effect in the small pores of silica gel. It is known that silica gel is hydrophilic and they attract water molecules and adsorb them. This creates the inhibition effect for the hydrate formation (Kang *et al.*, 2007; Barmavath *et al.*, 2014; Heeschen *et al.*, 2016b). Similarly, the sediments containing hydrate in the nature might include clay mineral such as illite. The adsorption capacity of illite is quite high and they attract non-polar molecules such as CH<sub>4</sub> and

CO<sub>2</sub> (Merey, 2013). Adsorption inhibits hydrate formation. This attraction is higher in small pores. Therefore, it is expected that hydrate forms in large pores first, and then it forms in the small pores of the sediments. The experimental results of Sun *et al.* (2014) support this idea. In many simulation studies, the pore size effect is ignored because 100 nm is quite small, as generally the diameter of a grain of sand is larger than this value, when hydrates are considered as energy source. However, the pore size effect below 100 nm should be considered if the pore sizes of the sediments are in this range (Jang and Santamarina, 2016). Uchida *et al.* (2004) investigated CH<sub>4</sub> hydrate formation and dissociation experimentally in the sediments (common in nature) containing silica sand, sandstone, and clays (kaolinite and bentonite) separately with different pore sizes. It was observed that pore size is the most important parameter affecting hydrate equilibrium conditions compared to adsorption mechanism in clays, mineral components and surface texture of minerals (Jang and Santamarina, 2016). Similarly, Zang *et al.* (2013) conducted CH<sub>4</sub> hydrate and mixed gas hydrate (91.85 % CH<sub>4</sub>; 5.09 % C<sub>2</sub>H<sub>6</sub>; 3.06 % C<sub>3</sub>H<sub>8</sub>) formation experiments inside sand particles with diameter of 150-250  $\mu$ m and 250-380  $\mu$ m at 275 K, 277 K and 279 K. It was observed that CH<sub>4</sub> hydrate formation is faster inside coarser sand particles (250-380  $\mu$ m). Surprisingly, the sand particle size did not have significant effect on mixed gas hydrate formation rate.

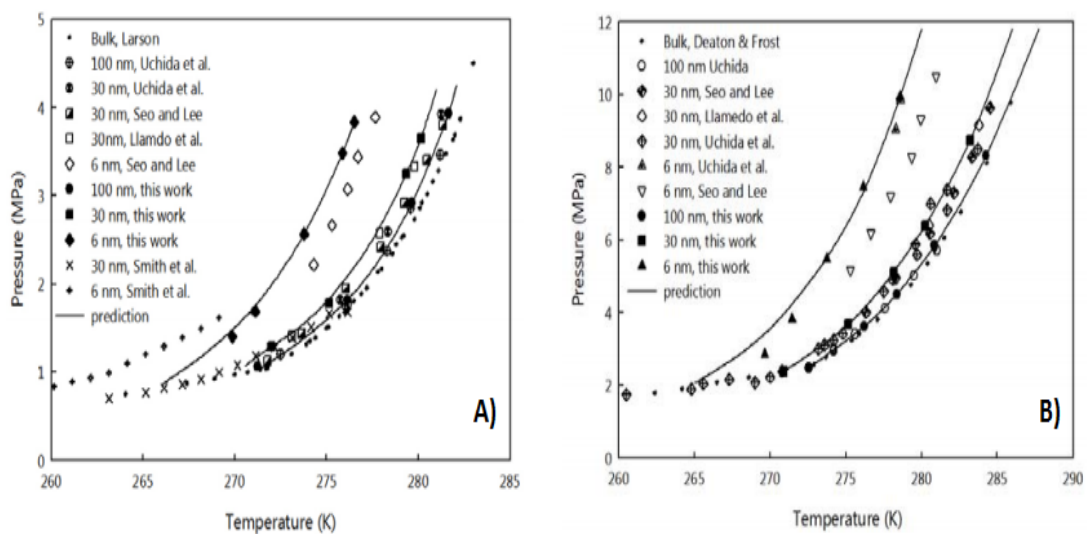


**Figure 4-1:** A) Hydrate equilibrium of CO<sub>2</sub> in silica pores B) Hydrate equilibrium of CH<sub>4</sub> in silica pores (Kang *et al.*, 2007)

In the study of Zhang *et al.* (2011), hydrate was formed in sediments having two layers: coarse sand (1-2 mm particle size) and loess (very fine sediment deposits-  $34.5 \times 10^{-3}$  mm particle size). As seen in Figure 4-2, (a) two coarse sands bounded loess and (b) two loess bounded coarse sand were used in different hydrate formation experiments. In both of them, CH<sub>4</sub> hydrate formed only or mostly inside coarse sand but not in loess sediments. Therefore, gas hydrate formation is difficult in fine sediments compared to coarse sands as described in Figure 3-19 (Jang and Santamarina, 2016). Similarly, in the study of Chong *et al.* (2015c), the behavior of CH<sub>4</sub> hydrate formed in very fine sand (0.063-0.18 mm), fine sand (0.1-0.5 mm), coarse sand (0.56-1.3), and granular pebbles (1.5-3.0 mm) were investigated. It was suggested that care must be taken to form CH<sub>4</sub> hydrate in laboratory to ensure the hydrate morphology and properties similar to that in nature because the presence of clay reduces the hydrate formation kinetics significantly (Kumar *et al.*, 2015). Fine sediments interbedded with coarse-grained sediments were observed via seismic analysis in Paleo-Don and Kuban river fan deposits of the Black Sea (Xing, 2013). Therefore, understanding Figure 3-19 is quite important.

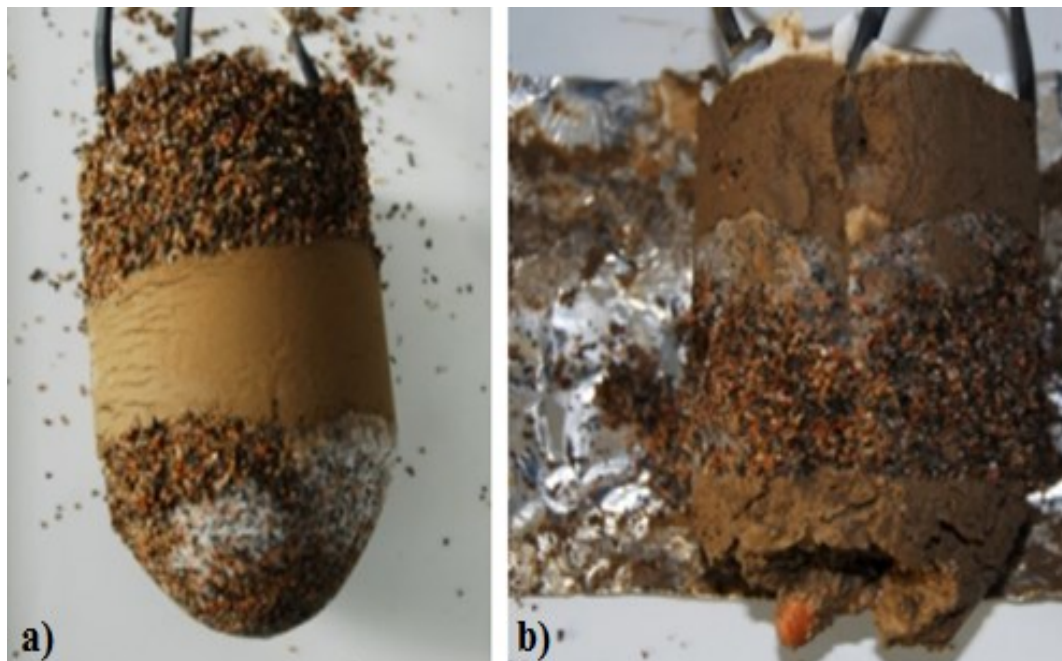


**Figure 4-2:** Hydrate configuration in different layered media (water conversion ratio is a) 23.1% b) 16.2%) (Zhang *et al.*, 2011)

## 4.2 Gas Hydrate Equilibrium Point Determination with Inhibitors

Addition of inhibitor shifts the hydrate equilibrium curve to left. These inhibitors are mainly NaCl, CaCl<sub>2</sub>, KCl, methanol, ethanol, ethylene glycol, DEG, and TEG. In this study and HEP.m code, the following formula for suppression of hydrate dissociation temperature was used for different inhibitors (Østergaard *et al.*, 2005):

$$\Delta T = [C_1 + C_2 W^2 + C_3 W^3][C_4 \ln(P) + C_5][C_6(P_0 - 1000) + 1] \quad (4-21)$$

Where  $\Delta T$ : suppression of the hydrate dissociation temperature (in K or °C);  $P$ : Pressure of the system (in kPa);  $W$ : Concentration of the inhibitor in liquid water phase (in mass %);  $P_0$ : Dissociation pressure of hydrocarbon fluid in the presence of distilled water at 273.15 K (in kPa);  $C_i$ : Constants for the inhibitor (listed in Table 4-6 and Table 4-7)

**Table 4-6:** Constants in Equation (4-21) for salts (Østergaard *et al.*, 2005)

Constants	NaCl	CaCl <sub>2</sub>	KCl
$C_1$	0.3534	0.194	0.305
$C_2$	1.375E-03	7.580E-03	6.770E-04
$C_3$	2.433E-04	1.953E-04	8.060E-05
$C_4$	4.056E-02	4.253E-02	3.858E-02
$C_5$	0.799	1.023	0.714
$C_6$	2.25E-05	2.80E-05	2.20E-05
Max.con (mol %)	26.5	40.6	31.5
Max.con (mass %)	10	10	10
AAD %	1.170	1.390	1.080

The equations for the hydrate equilibrium points with inhibitor proposed by Østergaard *et al.* (2005) are valid in the certain ranges. These ranges are shown as maximum concentration in Table 4-6 and Table 4-7. These equations are only valid when there is one type of inhibitors. However, the mixture of inhibitors might be used together to inhibit hydrate formation or to dissociate gas hydrate in nature (Mohammadi and Tohidi, 2005; Chapoy, 2014). In order to predict the hydrate equilibrium of natural gas with the mixture of inhibitors, some formulas were proposed by Ameripour (2005) for the mixtures of NaCl, CaCl<sub>2</sub>, KCl, methanol,

ethylene glycol (EG), TEG and glycerol. These formulas were integrated to HEP.m code in this study.

**Table 4-7:** Constants in Equation (4-21) for organic inhibitors (Østergaard *et al.*, 2005)

Constants	Methanol	Ethanol	Ethylene Glycol	DEG	TEG
$C_1$	0.478	1.118	38.93	0.343	0.1964
$C_2$	7.170E-02	-4.48E-03	-0.522	-3.47E-03	-5.81E-03
$C_3$	-1.440E-05	6.979E-04	1.767E-02	2.044E-04	1.393E-04
$C_4$	2.947E-02	5.85E-03	3.503E-04	1.80E-02	2.855E-02
$C_5$	0.596	0.225	5.083E-03	0.3346	0.854
$C_6$	3.10E-05	3.40E-05	2.650E-05	2.74E-05	3.24E-05
$Max.con$ (mol %)	43.3	31.2	59.6	51	59.5
$Max.con$ (mass %)	30	15	30	15	15
AAD %	1.220	1.80	1.290	1.350	1.700

### 4.3 Determination of Cage Occupancy of Gas Molecules in Hydrates

For the determination of cage occupancies in the cavities of gas hydrates, it is important to understand the thermodynamic models. The most common one was derived by van der Waals Platteeuw (vdWP). There is an analogy between this model and the Langmuir model of gas adsorption (Sloan and Koh, 2008). The following assumptions are made in the model of vdWP (Bouillot and Herri, 2015; Le Quang *et al.*, 2016):

- Each cavity contains one guest molecule at best,
- The interaction between the guest molecule and the cavity (water molecules) can be described by a pair potential function of the pair gas-molecule,
- The cavities are perfectly spherical,
- The guest molecules do not deform cavities,
- There are no interactions between the guest molecules

The equilibrium condition used in the vdWP model is the equality of the chemical potential of water in the hydrate phase, superscript H, and in the other equilibrium

phase(s),  $\beta$  representing hypothetical empty gas hydrate lattice,  $\pi$ , which might be liquid water, ice, or both, i.e. (Klauda and Sandler, 200):

$$\Delta\mu_{H_2O}^H = \mu_{H_2O}^\beta - \mu_{H_2O}^H = \Delta\mu_{H_2O}^\pi \quad (4-22)$$

The difference between the chemical potential of water in the hypothetical and real (filled) hydrate phases is given by

$$\Delta\mu_{H_2O}^H(T, P) = -RT \sum_m \vartheta_m * \ln(1 - \sum_i \theta_{mj}) \quad (4-23)$$

Where  $\vartheta_m$  is the number of cavities of type  $m$  per water molecule in the lattice

The fraction of cages occupied by a guest is given by a Langmuir adsorption relation:

$$\theta_{ml}(T, P) = \frac{C_{ml}(T)f_l(T, P)}{[1 + \sum_j C_{mj}(T)f_j(T, P)]} \quad (4-24)$$

Where  $C_{ml}$  is the Langmuir constant of gas component  $l$  in cavities of type  $m$ , and  $f_l$  is the fugacity of gas component  $l$ .

The Langmuir constant of gas component  $l$  in cavities of type  $m$ :

$$C_{ml}(T) = \frac{4\pi}{kT} \int_0^{R(cell)-a} \exp[W(r)/kT] r^2 dr \quad (4-25)$$

The solution of Equation (4-25) for the determination of the Langmuir constants of gas component is quite difficult and time consuming during the simulations. Therefore, the practical formulas for different gases were suggested by Parrish and Prausnitz (1972) and it is shown in Equation (4-26) (which is valid between 260 K and 300 K), which is an acceptable range for natural gas hydrate reservoirs. These formulas are used in this study and codes to calculate the Langmuir constants of CH<sub>4</sub>, C<sub>2</sub>H<sub>6</sub>, C<sub>3</sub>H<sub>8</sub>, n-C<sub>4</sub>H<sub>10</sub>, i-C<sub>4</sub>H<sub>10</sub>, CO<sub>2</sub>, H<sub>2</sub>S and N<sub>2</sub>.

$$C_{ml}(T) = [A_{ml}/T] \exp(B_{ml}/T) \quad (4-26)$$

Where  $C_{ml}$ : Langmuir constant;  $T$ : Temperature, K;  $A_{ml}$ : Langmuir constants for small cages of sI or sII hydrate (listed in Table 4-8);  $B_{ml}$ : Langmuir constants for large cages of sI or sII hydrate (listed in Table 4-9)

**Table 4-8:** Parameters for Equation (4-26) between 260 and 300 K for sI hydrate (Parrish and Prausnitz, 1972)

	Small Cage		Large Cage	
Gas	A <sub>ml</sub>	B <sub>ml</sub>	A <sub>ml</sub>	B <sub>ml</sub>
<i>CH</i> <sub>4</sub>	0.0037237	2708.8	0.018730	2737.9
<i>C</i> <sub>2</sub> <i>H</i> <sub>6</sub>	0.0	0.0	0.006906	3631.6
<i>C</i> <sub>3</sub> <i>H</i> <sub>8</sub>	0.0	0.0	0.0	0.0
<i>n-C</i> <sub>4</sub> <i>H</i> <sub>10</sub>	0.0	0.0	0.0	0.0
<i>i-C</i> <sub>4</sub> <i>H</i> <sub>10</sub>	0.0	0.0	0.0	0.0
<i>CO</i> <sub>2</sub>	0.0011978	2860.5	0.008507	3277.9
<i>H</i> <sub>2</sub> <i>S</i>	0.0030343	3736.0	0.016740	3610.9
<i>N</i> <sub>2</sub>	0.0038087	2205.5	0.018420	2301.3

**Table 4-9:** Parameters for Equation (4-26) between 260 and 300 K for sII hydrate (Parrish and Prausnitz, 1972)

	Small Cage		Large Cage	
Gas	A <sub>ml</sub>	B <sub>ml</sub>	Gas	A <sub>ml</sub>
<i>CH</i> <sub>4</sub>	0.002956	2695.1	0.076068	2202.7
<i>C</i> <sub>2</sub> <i>H</i> <sub>6</sub>	0.0	0.0	0.040818	3038.4
<i>C</i> <sub>3</sub> <i>H</i> <sub>8</sub>	0.0	0.0	0.012353	4406.1
<i>n-C</i> <sub>4</sub> <i>H</i> <sub>10</sub>	0.0	0.0	1.066952	2691.0
<i>i-C</i> <sub>4</sub> <i>H</i> <sub>10</sub>	0.0	0.0	0.015730	4453.0
<i>CO</i> <sub>2</sub>	0.0009091	2695.4	0.048262	2571.8
<i>H</i> <sub>2</sub> <i>S</i>	0.0023758	3750.6	0.073631	2854.1
<i>N</i> <sub>2</sub>	0.0030284	2175.0	0.075149	1860.6

The fraction of cages occupied by a guest molecule is calculated by using Equation (4-24). In this study and HEP.m code, in order to calculate the fugacity values of pure gas component or gas mixtures, modified Peng-Robinson equations of states (EOS) was used (Ahmed, 2007) and its codes were written in this study. Moreover, the vapor-liquid phase equilibrium for gas or gas mixtures are controlled by using the method of Lohrenz *et al.* (1963) and if there is liquid phase in the system, the fugacity values are calculated for both liquid and vapor phases in HEP.m by modified Peng-Robinson EOS. Then, HEP.m has ability to calculate the cage occupancy of hydrate forming pure gases or their mixtures for sI and sII hydrates.

#### 4.4 Determination of Hydration Number

Hydration number ( $N_h$ ) is defined as molar ratio of water (host) to gas (guest) molecules in hydrates (Hester *et al.*, 2007). For example, sI hydrates has 2 small cages and 6 large cages. One sI hydrate structure consists of 46 water molecules if all cages are fully filled by gas molecules. At these conditions, hydration number for sI hydrate is 5.75 (46/8) (Ye and Liu, 2013). However, in real cases, gas molecules cannot fill all the cages of hydrates. Depending on gas type, temperature, pressure, salinity etc., hydration numbers of sI and sII hydrate vary (Hester *et al.*, 2007; Sloan and Koh, 2008). Therefore, cage occupation ratio of hydrate formers is important for the determination of hydration number. By using Raman spectra, the cage occupancy and type of gas hydrate can be determined experimentally (Kida *et al.*, 2015). The following equations are also used for the hydration number ( $N_h$ ) predictions (Subramanian *et al.*, 2000; Kida *et al.*, 2009):

$$\text{For sI Hydrate: } N_h = \frac{23}{3 \sum_j \theta_{Lj} + \sum_j \theta_{sj}} \quad (4-27)$$

$$\text{For sII Hydrate: } N_h = \frac{17}{\sum_j \theta_{Lj} + 2 \sum_j \theta_{sj}} \quad (4-28)$$

Where  $\theta_{Lj}$ : Cage occupancy of gas  $j$  in the large cages of hydrate;  $\theta_{sj}$ : Cage occupancy of gas  $j$  in the small cages of hydrate.

Equation (4-27) and Equation (4-28) were also used in HEP.m code in this study to calculate the hydration numbers of pure and mixed gas hydrates.

#### 4.5 Determination of Molecular Weight and Density of Gas Hydrates

For the determination of molecular weight and density of gas hydrates, the chemical formula of hydrate should be known. However, as seen in Equation (2-1), hydrates are non-stoichiometric compounds due to varying hydration number ( $N_h$ ). Hence, after the determination of  $N_h$ , molecular weight and density of gas hydrates are calculated by using Equations (4-29), (4-30), and (4-31) (Adapted from Makogon, 1997; Sloan and Koh, 2008):

$$MW_h = N_h MW_{H_2O} + \sum_j MW_j X_j \quad (4-29)$$

Where  $MW_h$ : Molecular weight of hydrate;  $MW_j$ : Molecular weight of component  $j$ ,  
 $X_j$ : Mole fraction of component  $j$

$$\text{For sI Hydrate: } \rho_h = \frac{8MW_{H_2O}N_h + 2\sum_j MW_j \theta_{sj} + 6\sum_j MW_j \theta_{Lj}}{1040.774} \quad (4-30)$$

$$\text{For sII Hydrate: } \rho_h = \frac{24MW_{H_2O}N_h + 16\sum_j MW_j \theta_{sj} + 8\sum_j MW_j \theta_{Lj}}{3118.53} \quad (4-31)$$

Where  $\rho_h$ : Hydrate density, g/cm<sup>3</sup>;  $N_h$ : Hydration number;  $\theta_{Lj}$ : Cage occupancy of gas  $j$  in the large cages of hydrate;  $\theta_{sj}$ : Cage occupancy of gas  $j$  in the small cages of hydrate;  $MW_j$ : Molecular weight of component  $j$ ,  $X_j$ : Mole fraction of component  $j$

#### 4.6 Determination of Enthalpy of Hydrate Dissociation

Gas hydrate formation is an exothermic process. Therefore, while hydrate formation, heat is released. Reversely, gas hydrate dissociation is an endothermic process and heat is necessary for dissociation. The enthalpy of hydrate dissociation is defined as the energy needed for the dissociation per unit mole of hydrate. It changes with the type of gas and gas hydrate, salinity, temperature, and pressure (Sloan and Koh, 2008; Carroll, 2009).

**Table 4-10:** Hydrate formation enthalpy for three phase conditions of single natural gas components (Kamath, 1984)

Component	Type	T Range (°C)	a x (10 <sup>-3</sup> )	b
CH <sub>4</sub>	L <sub>w</sub> -H-V	0 to 25	13.521	-4.02
CH <sub>4</sub>	I-H-V	-25 to 0	6.534	-11.97
C <sub>2</sub> H <sub>6</sub>	L <sub>w</sub> -H-V	0 to 14	13.254	-15.00
C <sub>2</sub> H <sub>6</sub>	I-H-V	-25 to 0	8.458	-9.59
C <sub>3</sub> H <sub>8</sub>	L <sub>w</sub> -H-V	0 to 5	-37.752	250.09
C <sub>3</sub> H <sub>8</sub>	I-H-V	-25 to 0	7.609	-4.90
CO <sub>2</sub>	L <sub>w</sub> -H-V	0 to 11	19.199	-14.95
CO <sub>2</sub>	I-H-V	-25 to 0	9.290	-12.93
N <sub>2</sub>	L <sub>w</sub> -H-V	0 to 25	6.188	18.37
N <sub>2</sub>	I-H-V	-25 to 0	4.934	-9.04
H <sub>2</sub> S	L <sub>w</sub> -H-V	0 to 25	6.782	31.45
H <sub>2</sub> S	I-H-V	-25 to 0	8.488	-7.81

The enthalpy of hydrate dissociation is quite important to simulate gas production from gas hydrate reservoirs. During gas hydrate dissociation, the temperature of hydrate zone decreases because of endothermic nature of hydrate if there is no external heat supply (Kamath, 1984; Selim and Sloan, 1989; Moridis *et al.*, 2005; Alp *et al.*, 2007; Gaddipati, 2008). Hence, during gas production from hydrate reservoirs and simulation studies, the enthalpy of hydrate dissociation must be known very well. Similarly, if pipelines are plugged by gas hydrates, the amount of heat applied to pipelines is determined according to the enthalpy of hydrate dissociation. The enthalpy of hydrate dissociation and the enthalpy of hydrate formation are equal to each other if hydrate is formed by single (pure) guest (Zheng *et al.*, 2015). There are different formulas to calculate the enthalpy of hydrate dissociation. Although the effect of pressure on the enthalpy of hydrate dissociation is ignored in the formula of Kamath (1984) in Equation (4-32), it is commonly used in the simulation studies of CH<sub>4</sub> hydrate reservoirs such as in HydrateResSim and Tough+Hydrate (Gaddipati, 2008; Moridis *et al.*, 2005; Moridis, 2014).

$$\Delta H_{dis} = a + \frac{b}{T} \quad (4-32)$$

Where  $\Delta H_{dis}$ : Enthalpy of hydrate dissociation, cal/gmol;  $T$ : Temperature, K;  $a$  and  $b$ : Constants (listed in Table 4-10)

Kamath (1984)'s enthalpy of hydrate dissociation formulas is commonly used but they cannot be used for gas hydrates of natural gas mixtures. The Clausius-Clapeyron equation can be used for the hydrates of pure gases or natural gas mixtures and the effect of pressure on enthalpy is not ignored with this equation (Makogon, 1997; Sloan and Koh, 2008). In Equation (4-33), the equation of the Clausius-Clapeyron is shown:

$$\frac{d \ln P}{d(1/T)} = - \frac{\Delta H_{dis}}{zR} \quad (4-33)$$

Where  $P$ : hydrate equilibrium pressure;  $\Delta H_{dis}$ : Enthalpy of hydrate dissociation, kJ/mol;  $T$ : Temperature, K;  $R$ : Universal gas constant (8.3144621 J/mol. K);  $z$ : compressibility factor

After the determination of hydrate equilibrium pressures of CH<sub>4</sub> or natural gas mixture with/without inhibitor at different temperatures, the graph of  $\ln P$  and  $1/T$  is drawn. The slope is equal to  $\Delta H/zR$ . Gas compressibility ( $z$ ) values at different pressures and temperatures for different gas mixtures are determined with the modified Peng-Robinson EOS (Ahmed, 2007) in this study (HEP.m code). Then, the enthalpy of gas is determined. According to Sloan and Koh (2008), there is a good agreement between the enthalpy of hydrate dissociation data in literature and these data calculated with Clausius-Clapeyron equation for simple (pure) hydrates. Similar results were also obtained in the study of Nasir *et al.* (2014) for pure CH<sub>4</sub> and CO<sub>2</sub> hydrates. Moreover, the Clausius-Clapeyron equation can be used for gas mixtures. Veluswamy *et al.* (2015) used this equation to determine the enthalpy of hydrate dissociation for H<sub>2</sub> and C<sub>3</sub>H<sub>8</sub> gas mixture at different concentrations by using the experimental data and then, they obtained good results. For this reason, in this study

(HEP.m code), the Clausius-Clapeyron equation is used to calculate the enthalpy of hydrate dissociation or formation of both pure and mixed gas hydrates.

#### 4.7 Determination of the Geomechanical Properties of Gas Hydrates

In numerical simulations, some properties (i.e thermal conductivity, geomechanical properties) of CH<sub>4</sub> hydrate are necessary. These properties of CH<sub>4</sub> hydrate, tetrahydrofuran (THF) hydrate and ice are compared in Table 4-11.

**Table 4-11:** Properties of CH<sub>4</sub> and THF, their hydrates, and water ice (Adapted from Lee *et al.*, 2007)

Property	Methane	Tetrahydrofuran (THF)	Ice
Molecular Formula	CH <sub>4</sub>	C <sub>4</sub> H <sub>8</sub> O	H <sub>2</sub> O
Hydrate structure	sI	sII	-
Molecular Size, Å	4.36	6.3	1.8
Heat capacity, kJ/(kg.K), at 270 K	2.07	2.07	2.1
Heat of dissociation, kJ/ kg, at 273 K	338.7	262.9	333.5
Thermal conductivity, W/(m. K)	0.5 @ 270 K	0.5 @ 270 K	2.2 @ 263 K
Thermal diffusivity, m <sup>2</sup> /s	3e-7 @ 270 K	2.8E-7 @ 270 K	8.43E-7 @ 273 K
Density, kg/m <sup>3</sup> at 273 K	910	910	917
Adiabatic bulk compressibility, Pa, at 273 K	1.40E-10	1.40E-10	1.20E-10
Isothermal Young's modulus, Pa, at 268 K	8.40E+09	8.20E+09	9.50E+09
Strength, MPa	2 to 10	0.9 to 44	0.6 to 1

THF is in liquid phase that forms its sII hydrate at almost atmospheric conditions. Therefore, it is easy to conduct geomechanical experiments on THF hydrate compared to CH<sub>4</sub> hydrate because CH<sub>4</sub> hydrate forms at very high pressures (Le *et*

*al.*, 2007). Compressibility, Young's modulus and density values are close to each other. However, not all properties are similar. The thermal conductivity of ice is around 4.4 times higher than those in CH<sub>4</sub> and THF hydrates. Because of low thermal conductivity in gas hydrates, heat transfer is quite slow. This is a big problem because hydrate dissociation is an endothermic process. Hence, with increasing hydrate saturation, hydrate formation creates a heating barrier (Meindinyo *et al.*, 2015). The strengths of THF and CH<sub>4</sub> hydrates are higher than ice. The similar properties among these three components are commonly used for especially CH<sub>4</sub> hydrate studies (Waite *et al.*, 2009). The thermal conductivities of the sediments near gas hydrate zone are also important. For instance, if there are sediments containing salts near gas hydrate zone, it might decrease hydrate zone thickness due to high thermal conductivity of salt (approximately 6 times greater than adjacent sediments ~6 W/ m.K) (Rogers, 2015; Rajput and Thakur, 2016).

#### 4.8 Determination of Thermal Properties of Gas Hydrates

The specific heat is defined as the amount of heat per unit mass required in order to increase temperature by one degree Celsius or Kelvin depending on their unit (Waite *et al.*, 2009). For the specific heat of gas hydrate of natural gas mixtures, a formula was suggested in Equation (4-34):

$$C_p = \frac{4.5R + 18N_h[2.3 + 8.4732e^{-3}(T - 273.15)]}{M_{ng} + 18N_h} \quad (4-34)$$

Where  $C_p$ : specific heat of natural gas, J/g.K;  $N_h$ : hydration number;  $T$ : Temperature, K;  $M_{ng}$ : Molecular mass of natural gas

It is known that 99 % of gas hydrates in nature is CH<sub>4</sub> hydrate. Therefore, Waite *et al.* (2007) conducted experiments to determine the specific heat of gas hydrates at 31.5 MPa confining pressure because during thermal experiments such as thermal conductivity and specific heat, there should be no pore spaces as much as possible. Then, they suggested Equation (4-35) between 1 °C and 17 °C.

$$C_p = 6.1T + 2160 \quad (4-35)$$

Where  $C_p$ : specific heat of  $CH_4$  hydrate, J/kg.K;  $T$ : Temperature, °C

The experimental data and Equation (4-35) of Waite *et al.* (2007) were compared with the experimental data at 3.0 MPa overburden pressure and Equation (4-36) of Handa (1986) and good agreement (~5 % difference) was obtained between the results.

$$C_p = 2100 - 7.07T + 1.231e^{-2}T^2 + 5.08e^{-2}T^3 \quad (4-36)$$

Where  $C_p$ : specific heat of  $CH_4$  hydrate, J/kg.K;  $T$ : Temperature, °C

Similarly, the thermal conductivity (Equation (4-37) for -20 and 17 °C) and thermal diffusivity formulas (Equation (4-38) for 1-17 °C) of Waite *et al.* (2007) are commonly used. Equation (4-37) is only used to calculate thermal conductivity of gas hydrate (Some experimental thermal conductivity data of gas hydrates is shown in Figure 4-3-a). However, in nature, gas hydrate forms in the sediments. Hence, there are several composite thermal conductivity equations accounting thermal conductivity of gas hydrate, sediments, water and gases (Moridis *et al.*, 2005; Sloan and Koh, 2008). Some experimental composite thermal conductivity data is shown in Figure 4-3-b.

$$\lambda = -2.78e^{-4}T + 0.62 \quad (4-37)$$

Where  $\lambda$ : thermal conductivity of  $CH_4$  hydrate, W/m.K;  $T$ : Temperature, °C

$$\kappa = \frac{5.04e^{-5}}{273.15 + T} + 1.25e^{-7} \quad (4-38)$$

Where  $\kappa$ : thermal diffusivity of  $CH_4$  hydrate,  $m^2/s$ ;  $T$ : Temperature, °C

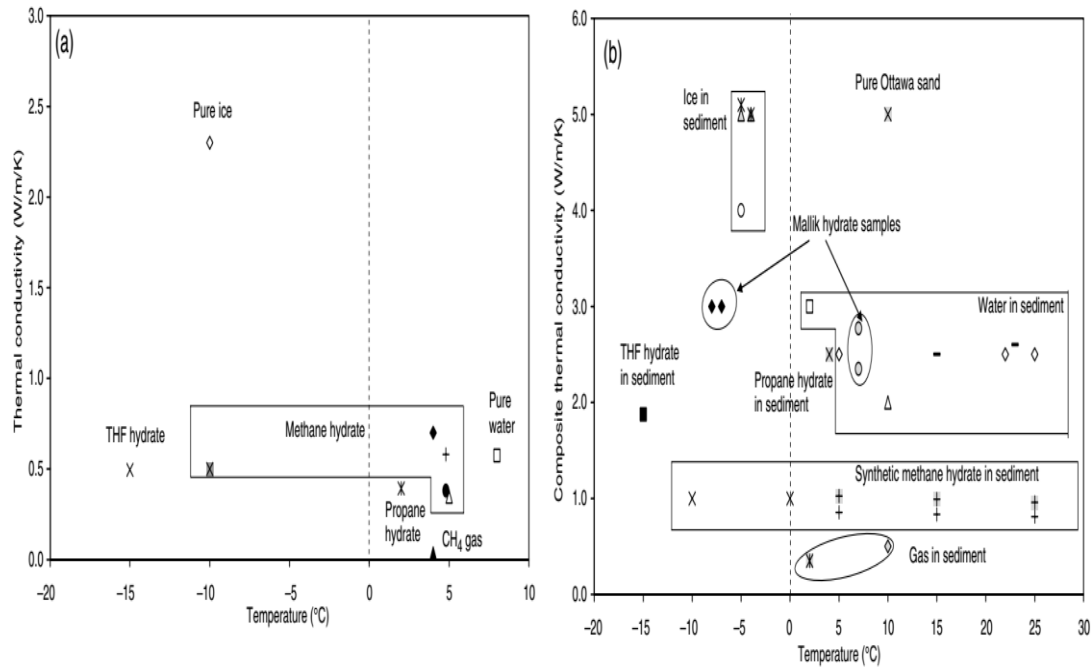


**Figure 4-3:** a) Thermal conductivities of pure ice, THF hydrate, methane hydrate, propane hydrate, pure water and methane gas in literature b) Composite thermal conductivities in sediments (Sloan and Koh, 2008)

#### 4.9 Flash Calculations in Gas Hydrates

sII hydrates can be found in the Black Sea, the Marmara Sea, Caspian Sea and Gulf of Mexico (Hester and Brewer, 2009; Bourry *et al.*, 2009). They form from natural gas mixtures. Moreover, the transportation of natural gases as in gas hydrate form is commonly studied by scientists. Therefore, it is important to understand the gas composition change of natural gas mixture during gas hydrate formation and for the determination of gas hydrate equilibrium conditions. The Rachford-Rice-form equation is commonly used in the flash calculations (Carroll, 2009):

$$f(V) = \sum \frac{z_i(1 - K_i)}{1 + V(K_i - 1)} \quad (4-39)$$

Where  $z_i$ : the composition of the feed on a water-free basis;  $V$ : vapor phase fraction;  $K_i$ : Vapor (gas)-solid (hydrate) equilibrium ratio

Equation (4-39) should be equal to zero and with the iterative solution, this equation is equalized to zero by changing V (gas-hydrate equilibrium ratio) values. However, this equation does not include non-hydrate forming gases. Therefore, the following equations are suggested (Carroll, 2009):

$$f(V) = \sum_{hydrate\ formers} \frac{z_i(1 - K_i)}{1 + V(K_i - 1)} + \sum_{non\ hydrate\ formers} \frac{z_i}{V} \quad (4-40)$$

When V is calculated by iteration, the following equation can be used to calculate vapor phase compositions ( $y_i$ ) for hydrate formers:

$$y_i = \frac{z_i K_i}{1 + V(K_i - 1)} \quad (4-41)$$

Vapor phase compositions ( $y_i$ ) for non-hydrate formers are shown in Equation (4-42):

$$y_i = \frac{z_i}{V} \quad (4-42)$$

The compositions of solid phase ( $s_i$ ) is calculated from:

$$s_i = \frac{y_i}{K_i} \quad (4-43)$$



## CHAPTER 5

### GAS HYDRATE PRODUCTION MODELLING

Numerical simulation of gas production from gas hydrate reservoirs in laboratory scale and reservoir scale is very important for gas hydrate studies because there are not many real gas production data from gas hydrate reservoirs. There are several numerical codes for the simulation of gas production from hydrate reservoirs. Those are listed in Table 5-1. Most of these codes are used to simulate gas production from hydrate reservoirs by using depressurization, thermal injection, chemical injection and combination of these production methods. Differently, STOMP-HYD-KE is used to simulate CH<sub>4</sub>-CO<sub>2</sub> swapping production method. Recently, HydrateResSim numerical simulator was modified as Mix3HydrateResSim to simulate CH<sub>4</sub>-(CO<sub>2</sub>/N<sub>2</sub>) swapping method and the results were compared with the data of Ignik Sikumi pilot project (Garapati, 2013). The assumptions, equations, formulas, etc. of these numerical codes vary. In order to compare the results of these codes (Tough+Hydrate, HydrateResSim, MH-21, CMG-Stars, STOMP and the code of University of Houston), the code comparison project of the National Energy Technology Laboratory (NETL) and the U.S Geological Survey (USGS) was held in 2008 (Moridis *et al.*, 2005; Moridis, 2014; Janicki *et al.*, 2014; Kurihara *et al.*, 2004; White, 2011; Bhade and Phirani, 2015; Gaddipati, 2008). For seven problems, these codes were run and the codes were compared. For instance, the gas production from the hydrate reservoir in a two-dimensional radial domain (10 m hydrate zone in bounded vertically by two 25 m shale zones) was simulated for depressurization at 2.7 MPa by these six codes. As seen in Figure 5-1, the cumulative and water production are not same for all codes but the production behavior is similar. Similar to the codes used in the comparison study, there are other codes written by several scientists and they are used to simulate gas production from gas hydrate reservoirs and they are used for laboratory scale simulation.

**Table 5-1:** Reservoir simulators used for hydrate reservoirs (Adapted from Garapati, 2013)

<b>Name</b>	<b>Owner</b>	<b>Capabilities</b>	<b>Source Availability</b>
HydrateResSim	Lawrence Berkeley, National Laboratory, National Energy Technology Laboratory	Kinetics and Equilibrium Model (CH <sub>4</sub> hydrate)	Free Open Source Code
CMG Starts	Computer Modelling Group Ltd.	Kinetics and Equilibrium Model (CH <sub>4</sub> /CO <sub>2</sub> hydrates)	Commercial Code
MH-21 HYDRES	National Institute of advanced Industrial Sciences and Technology, Japan.	Kinetics and Equilibrium Model (CH <sub>4</sub> hydrate)	Only MH-21 consortium
TOUGH+HYDRATE	Lawrence Berkeley National Laboratory	Equilibrium and Kinetics Model (CH <sub>4</sub> hydrate)	Free for U.S. Government, Collaborator and Available for purchase
Code from University of Houston	University of Houston	Kinetic Model (CH <sub>4</sub> hydrate)	Not Available
HYRES	German Sugar, Umsicht	Kinetic Model (CH <sub>4</sub> hydrate)	Not Available
STOMP-HYD-KE	Pacific Northwest National Laboratory	Kinetics and Equilibrium Model (CH <sub>4</sub> -CO <sub>2</sub> mixed hydrate)	Free for U.S. Government, Collaborator and Available for purchase
Mix3HydrateResSim	National Energy Technology Laboratories (NETL)	Kinetics and Equilibrium Model (CH <sub>4</sub> -CO <sub>2</sub> -N <sub>2</sub> mixed hydrate)	Not Available

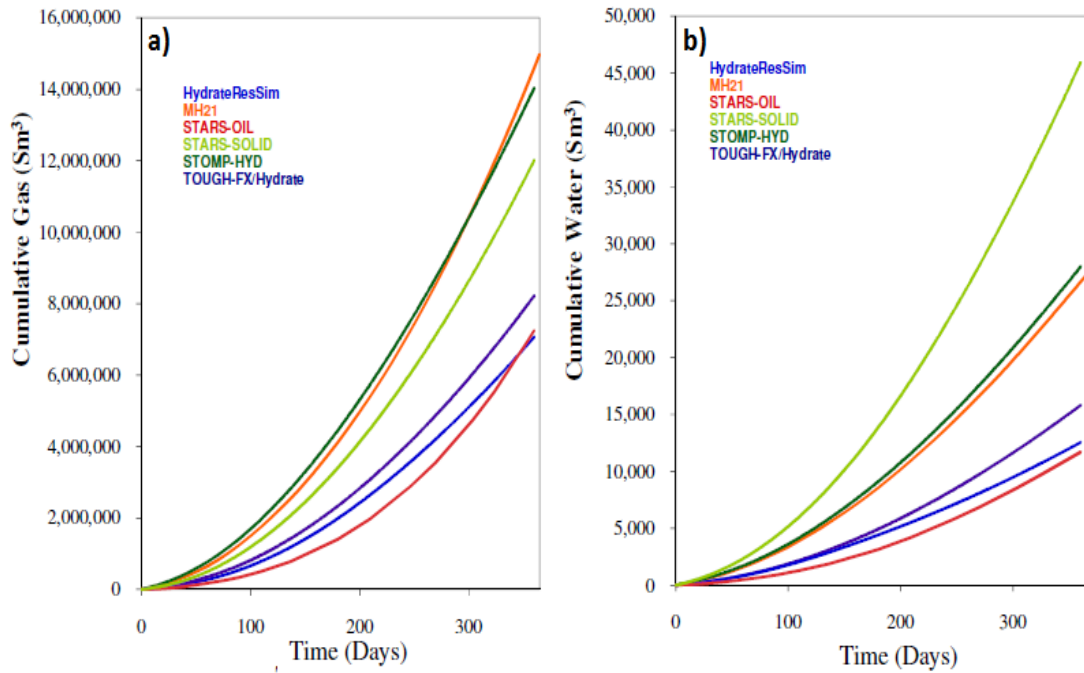


**Figure 5-1: a) Cumulative gas production b) Water production (Gaddipati, 2008)**

### 5.1 Reservoir Scale Simulations

Reservoir scale simulations are mainly conducted for Class 1, Class 2 and Class 3 CH<sub>4</sub> hydrate reservoirs. Class 1 hydrates are considered as the most important target among these three classes. Li *et al.* (2012b) developed a general-purpose simulator for gas hydrates and their simulator includes kinetics of hydrate dissociation, heat and multi-phase flow. During the simulations of depressurization for Class 1 hydrates, it was found that both free gas and hydrate dissociation have good effects on gas production rate. With hydrate dissociation, temperature, pressure, and hydrate saturation decreased. Moreover, Moridis *et al.* (2013) simulated gas production by depressurization and depressurization with wellbore heating from Class 1G (free gas in hydrate zone) and Class 1W (free water in the hydrate zone) CH<sub>4</sub> hydrate reservoirs. The results showed that there is a risk hydrate reformation along the wellbore during depressurization for Class 1W hydrate reservoir, so the wellbore heating is important. However, for the Class 1G hydrate reservoir, the gas production results with depressurization and depressurization combined with wellbore heating are almost same. This study shows that especially in Class 1G hydrate reservoirs,

depressurization is very effective. Similar observations were obtained in the study of Alp *et al.* (2007). According to Moridis *et al.* (2008), Moridis *et al.* (2008b) and Giavarini and Hester (2011), Class 1G hydrates are likely to be more common than Class 1W deposits. However, currently, there are not enough real field examples or studies to support this idea of Moridis *et al.* (2008) and Moridis *et al.* (2008b). In the other studies of Moridis and Collett (2003) and Moridis (2003), EOSHYDR2 codes were used to compare the simulation results of Class 1, Class 2 and Class 3. According to the results, depressurization method was very effective in Class 1 hydrate reservoirs. For Class 2 and 3 hydrate reservoirs, it was proposed that the combination of depressurization and thermal stimulation might be necessary if reservoirs properties are appropriate (high effective permeability) in terms of depressurization. Class 1 hydrate reservoirs are the most preferred hydrate reservoirs but there is an argument about whether Class 3 or Class 2 hydrate reservoirs are second preferred gas hydrate reservoirs. According to the simulations of Class 2 hydrate reservoir in the study of Moridis and Kowalsky (2005), if the aquifer below hydrate section is strong, depressurization is very difficult and water production rate is high. Moreover, thermal heating might be necessary. Therefore, it is obvious that depending on the hydrate properties, hydrate saturation, effective permeability of hydrate zone and bounding layers, temperature and pressure conditions, Class 3 or Class 2 hydrate reservoirs might be the most preferred between these two reservoirs (Moridis *et al.*, 2013). Yang *et al.* (2014) simulated Class 3 gas hydrate reservoir by using the data of Shenhu site SH7 area hydrate reservoirs in China with HydrateResSim numerical simulator. It was proposed that horizontal drilling and depressurization with thermal heating might provide high gas production from Class 3 hydrates. Differently, Konno *et al.* (2016) proposed that the cyclic depressurization method could be advantageous according their numerical study. The cyclic depressurization method is the alternating depressurization and shut-in periods over decades. In their numerical study for Class 3 hydrate reservoir, the recovery factor increased from 42.4 % to 71.5 % with cyclic depressurization method.

Although there may be thermodynamic reasons for the classification of Class 1 and Class 2 reservoirs, there is little difference between Class 1W, Class 1G and Class 2

in terms of geology. They all occur in sands bounded by impermeable beds and essentially pass through or are physically transitional from the gas hydrate stability zone (GHSZ) where the natural gas hydrate (NGH) is located to below, where the mineralizing solutions are migrating into the GHSZ. When depressurization is applied, all of Class 1W, Class 1G and Class 2 hydrate reservoirs will converge into a situation where free gas will tend to overlie water below NGH. Once NGH dissociates, there is going to be gas and water all over the place within the dissociation envelope - and it is all going to start to move. Some amount of free gas will be maintained within the reservoir for a number of hydraulic recovery reasons and the dissociation rate will be matched with the extraction rate to maintain a desired level of gas in the reservoir. The exception is permafrost hydrate. Where the GHSZ extends below the level of ice stability, there will be plenty of water and gas. Where the NGH is in the ice or cryo zone, persistence of water may be hard to predict, especially because dissociation is an endothermic reaction (Personal communication with Dr. Michael D. Max, 2016).

As well as the type of gas hydrate reservoirs, the properties of the boundaries of hydrate reservoirs are also important and the detailed information about them should be collected during exploration studies. During hydrate dissociation, these boundaries behave like constant temperature boundary and there are heat fluxes from these boundaries through hydrate sections and this provides additional hydrate dissociation (Alp *et al.*, 2007; Merey and Sinayuc, 2015). Li *et al.* (2013b) and Sun *et al.* (2015) conducted gas production simulations from hydrates for different types of boundaries by using Tough+Hydrate. Their study shows that gas production with the impermeable system (impermeable top and bottom boundaries of hydrate formation) is much stronger than those with the open (permeable top and bottom boundaries) and semi-open (permeable top boundary and impermeable bottom boundary) system. Especially if hydrate reservoir is close to sea floor, permeable boundaries might cause gas seepages from sea floor and this sudden release of gas can cause environmental problems. Moreover, Bahade and Phirani (2015) modelled gas production from Class 2 hydrate reservoir and their results showed that depressurization in Class 2 hydrate reservoir is inefficient if the aquifer layer permeability is high because this way, the

pressure in hydrate section cannot be decreased easily. Similarly, Boswell and Collett (2016) proposed that although impermeable boundaries are optimum for gas production from gas hydrates, also permeable boundaries above and below gas hydrate layer might exist in nature. For this reason, the detailed characterization of gas hydrate zones and their boundaries is essential.

As seen in Table 5-1, most of hydrate simulators have two options: kinetic model and equilibrium model. In equilibrium model, hydrate in a grid dissociates suddenly when pressure and temperature conditions are outside of the hydrate equilibrium curve. However, in kinetic model, hydrate dissociation rate depends on fugacity differences of equilibrium pressure and depressurization pressure. In the study of Kowalsky and Moridis (2007), the thermal stimulation-induced production from Class 3 reservoir, the simulations of the depressurization-induced production from Class 3 reservoir, the constant rate production from Class 1 reservoir and depressurization-induced production from a small core sample were run by using Tough+Hydrate. Except the simulation of small core sample, in other large scale simulations, the kinetic and equilibrium model gives similar results though small differences in the early times.

## **5.2 Laboratory Scale Simulations**

Experimental studies related to gas hydrates are quite important especially when there are not much field data available of gas hydrate reservoirs. Therefore, experimental studies are essential to investigate gas production from gas hydrates; also, they give necessary data for the simulation studies. Previously, the volumes of high pressure cells were quite small for gas production experiments from gas hydrates. Masuda *et al.* (1999) conducted depressurization experiments in a 589 cm<sup>3</sup> high pressure cylindrical cell. Similarly, the depressurization experiments on Berea sandstone were conducted in a 171 cm<sup>3</sup> cylindrical high pressure cell by Yousif *et al.* (1991). Experimental studies of Masuda *et al.* (1999) were simulated by different scientists (Ruan *et al.*, 2012; Zhao *et al.*, 2012c; Gamwo and Liu, 2010). In all these studies, with the kinetic equation of Kim *et al.* (1987), there is a good fit to the experimental study of Masuda *et al.* (1999). Moreover, Gamwo and Liu (2010) compared the

results of kinetic and equilibrium model options of HydrateResSim, and there is a big difference between the results. Similar results were obtained in the study of Kowalsky and Moridis (2007) for a small core sample. According to all of these results, the kinetic-controlled mechanism (dissociation controlled) is important for the gas production at the cases of smaller scales while the production process is more likely to be flow-controlled for the cases of larger (reservoir) simulation scale.

In order to simulate gas production from gas hydrate reservoirs experimentally, recently high volumes are preferred in high pressure cells (reactors) compared to the small high pressure cells used in the past for gas production experiments from gas hydrates. Li *et al.* (2014) conducted depressurization experiments in hydrate sediments inside a high pressure reactor (PHS~117.8 L). Moreover, they ran the simulations with the equilibrium models and kinetic models of Tough+Hydrate and they observed that the kinetic limitations are very small in the PHS because hydrate dissociation under depressurization in the PHS is mainly flow controlled, which is similar to the reservoir conditions. The laboratory scale numerical simulation is very important to compare the experimental data and numerical data. For example, Li *et al.* (2015) compared the experimental data of gas production from hydrate deposited in 4.95 L reactor by depressurization using Tough+Hydrate. Similar results were observed. This means that gas hydrate formed in the sediments almost homogenously and all equipment such as pressure transducers, thermocouples, gas flow meters, etc. run appropriately.

### **5.3 HydrateResSim**

In this study, in order to design a high pressure cylindrical reactor for gas production experiments from gas hydrate sediments at the Black Sea conditions, HydrateResSim numerical simulator was used. Similar to pilot-scale hydrate simulator (PHS~117.4 L), the aim of this study is to design a high pressure reactor which can simulate real conditions of gas hydrates in the Black Sea experimentally. Therefore, in this study, HydrateResSim was chosen to decide on the size of high pressure reactor and also other experimental set-up equipment selections. Moreover, HydrateResSim was used

to simulate gas production from the hypothetical Class 1 and Class 3 CH<sub>4</sub> hydrate reservoirs in the Black Sea.

HydrateResSim is a numerical code to predict gas production from gas hydrate reservoirs. It was written in Fortran 95/2003 language. Basically, HydrateResSim has ability to simulate non-isothermal gas production from gas hydrates, two phase flow (aqueous and gaseous) and heat transfer in CH<sub>4</sub> hydrate reservoirs by solving mass balance equation of water, mass balance equation of CH<sub>4</sub> and heat balance equation. The model equations are obtained by incorporating the multiphase Darcy's law for gas and liquid into both the mass component balances and the energy conservation equations. There are two sub-models in HydrateResSim for hydrate dissociation: the kinetic model and the equilibrium model. HydrateResSim can be used from laboratory scale simulation to reservoir scale simulation (i.e., gas hydrates in the permafrost and in marine sediments) at which Darcy's law is valid. It can be used for depressurization, thermal injection, chemical injection or their combination. HydrateResSim cannot simulate geomechanical changes during gas production from gas hydrates such as sand production and reservoir subsidence. HydrateResSim can be used when reservoir pressure is less than 100 MPa (6800 psi). HydrateResSim can only simulate gas production from CH<sub>4</sub> gas hydrate reservoirs (Moridis *et al.*, 2005).

Mass and heat balance considerations in every subdomain (grid-block) into which the simulation domain is subdivided by the integral finite difference method (Moridis *et al.*, 2005; Gamwo and Liu, 2010):

$$\frac{d}{dt} \int_{V_n} M^\kappa dV = \int_{\Gamma_n} F^\kappa \cdot n dV + \int_{V_n} q^\kappa dV \quad (5-1)$$

Where,  $V$ ,  $V_n$  : volume, volume of subdomain  $n$  ( $L^3$ );  $M_k$ : mass accumulation term of component  $\kappa$  ( $kg/m^3$ );  $A$ ,  $\Gamma_n$ : surface area, surface area of subdomain  $n$  ( $L^2$ );  $F^\kappa$  : Darcy flux vector of component ( $kg\ m^{-2}\ s^{-1}$ );  $q^\kappa$ : source/sink term of component ( $kg\ m^{-3}\ s^{-1}$ );  $t$ : time ( $T$ ), second ( $s$ )

Mass Accumulation:

$$M^\kappa = \sum_{\beta:A,G,I} \varphi S_\beta \rho_\beta X_\beta^\kappa, k: w, m, i \quad (5-2)$$

Where  $\varphi$ : porosity;  $\rho_\beta$ : density of phase  $\beta$  ( $\text{kg m}^{-3}$ );  $S_\beta$ : saturation of phase  $\beta$ ;  $X_\beta^k$ : mass fraction of component  $\kappa$ : w,m,c in phase  $\beta$  (kg/kg)

Heat Accumulation:

$$M^h = (1 - \varphi) \rho_R C_R T + \sum_{\beta=A,G,H,I}^n \varphi S_\beta \rho_\beta U_\beta + Q_{diss} \quad (5-3)$$

Where  $Q_{diss} = \begin{cases} \varphi \rho_H \Delta S_H \Delta H^o & \text{equilibrium dissociation} \\ 0 & \text{kinetic dissociation} \end{cases}$

$\varphi$ : porosity;  $\rho_R$ : rock density ( $\text{kg m}^{-3}$ );  $C_R$ : heat capacity of the dry rock ( $\text{J kg}^{-1} \text{K}^{-1}$ );  $U_\beta$ : specific internal energy of phase  $\beta$  (J/kg),  $\Delta S_h$ : change in the hydrate saturation over the current time step;  $\Delta U_H$ : specific enthalpy of hydrate dissociation / formation (J/kg)

Flux Term:

The mass fluxes of water, CH<sub>4</sub> and inhibitor include contributions from the aqueous and gaseous phases:

$$F^\kappa = \sum_{\kappa:A,G} F_\beta^\kappa \quad (5-4)$$

Where k: w, m, i For hydrate phase:  $F^c = 0$  (5-5)

For aqueous phase:  $F_A = -k \frac{k_{rA} \rho_A}{\mu_A} (\nabla P_A - \rho_A g)$  (5-6)

For gas phase:  $F_G^\kappa = -k_o \left(1 + \frac{b}{P_G}\right) \frac{k_{rG} \rho_G}{\mu_G} X_G^\kappa (\nabla P_G - \rho_G g) + J_G^\kappa, k:w,m$  (5-7)

For heat (Conduction, Advection, Radioactive heat transfers):

$$F^h = -[(1 - \phi)K_R + \phi(S_H K_H + S_i K_i + S_A K_A + S_G K_G)]\nabla T + f_\sigma \sigma_o \nabla T^4 \quad (5-8)$$

$$+ \sum_{k=A, G} h_\beta F_\beta$$

Where  $k$ : rock instrinsic permeability ( $m^2$ );  $k_{rA}$ : relative permeability of the aqueous phase;  $\mu_A$ : viscosity of the aqueous phase (Pa s);  $P_A$ : Pressure of the aqueous phase (Pa);  $g$ : gravitational accelaration vector ( $m\ s^{-2}$ );  $k_o$ : absolute permeability at large gas pressures ( $=k$ ) ( $m^2$ );  $b$ : Klinkenberg b-factor,  $k_{rG}$ : relative permeability of the gaseous phase,  $\mu_G$ : viscosity of the gaseous phase (Pa s);  $K_R$ : thermal conductivity of the rock ( $W\ m^{-1}\ K^{-1}$ );  $K_\beta$ : thermal conductivity of phase  $\beta$ : A, G, H, I ( $W\ m^{-1}\ K^{-1}$ );  $h_\beta$ : specific enthalpy of phase  $\beta$ : A, G, H, I ( $J\ kg^{-1}$ );  $f_\sigma$ : radiance emittance factor;  $\sigma_o$ : Stefan-Boltmann Constant ( $5.6687 \times 10^{-8}\ J\ m^{-2}\ K^{-4}$ )

Source and Sink Terms:

In sinks with specified mass production rate, withdrawal of the mass component  $\kappa$  is described by

$$q^\kappa = \sum_{k: A, G} X_\beta^\kappa q_\beta; \kappa: w, m \quad (5-9)$$

where  $q_\beta$ : the production rate of the phase  $\beta$  ( $kg\ m^{-3}$ );

$$q^h = q_d + \sum_{k: A, G} h_\beta q_\beta \text{ (Heat Addition or Removal)} \quad (5-10)$$

Set of first-order ordinary differential equations:

$$\frac{dM_n^\kappa}{dt} = \frac{1}{V_n} \sum_m A_{nm} F_{nm}^\kappa + q_n^\kappa \quad (5-11)$$

$F_{nm}$  in Equation (5-11) is the average value of the (inward) normal component of  $F$  over the surface segment  $A_{nm}$  between volume elements  $V_n$  and  $V_m$ . The discretization approach used in the integral finite difference method and the definition of the geometric parameters are illustrated in Figure 5-2. The discretized flux is expressed in terms of averages over parameters for elements  $V_n$  and  $V_m$ . For the basic Darcy flux term, the following equation is obtained:

$$F_{\beta,\kappa} = k_{nm} \left[ \frac{k_{r\beta} \rho_{\beta}}{\mu_{\beta}} \right]_{nm} \left( \frac{P_{\beta,m} - P_{\beta,n}}{D_{nm}} + \rho_{\beta,nm} g_{nm} \right) \quad (5-12)$$

where the subscripts (nm) denote a suitable averaging at the interface between grid blocks  $n$  and  $m$ . For the evaluation of mobility, permeability, and density at interfaces, upstream weighting was preferred in this study.  $D_{nm}$  is the distance between the nodal points  $n$  and  $m$ , and  $g_{nm}$  is the component of gravitational acceleration in the direction from  $m$  to  $n$ .

The discretization of time is done by using first-order finite difference method. The evaluation of the flux, sink, and source terms on the right-hand side of Equation (5-11) are done at the new time level,  $t_{k+1} = t_k + \Delta t$ . The time discretization results in the following set of coupled non-linear, algebraic equation (as seen in Figure 5-2):

$$R_n^{\kappa, k+1} = M_n^{\kappa, k+1} - M_n^{\kappa, k} - \frac{\Delta t}{V_n} \left( \sum_m A_{nm} F_{nm}^{\kappa, k+1} + V_n q_n^{\kappa, k+1} \right) = 0 \quad (5-13)$$

where residuals  $R_{nk}$ : residuals,  $k + 1$ .

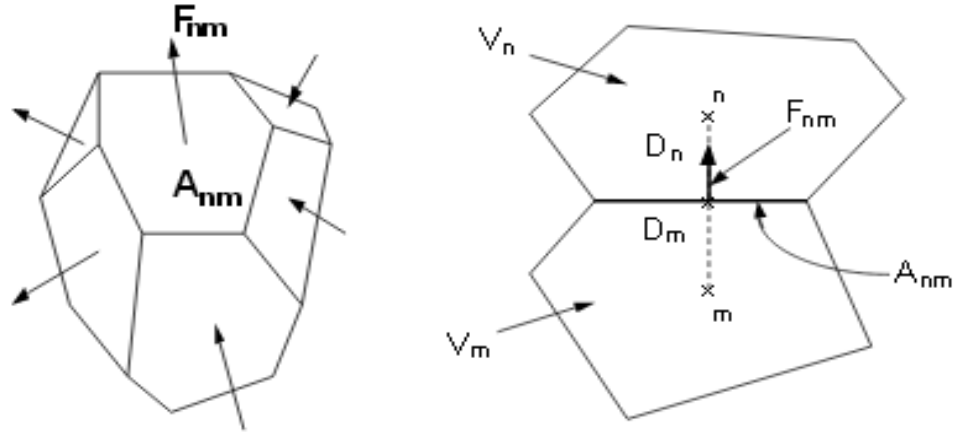


**Figure 5-2:** Space discretization and geometry data in the integral finite difference method (Moridis *et al.*, 2005)

For each volume element (grid block)  $V_n$ , there are  $N_k$  equations, so that for a system discretized into NE (number of elements) grid blocks, represents a total of  $N_k \times NE$  coupled non-linear equations. For equilibrium model, there are 3 equations (Equation

(5-13) for CH<sub>4</sub>, water, and heat) but for kinetic model, there are 4 equations (Equation (5-13) for CH<sub>4</sub>, water, heat and Equation (5-14) as kinetic equation) to be solved for each grid. The Newton-Raphson iteration and Jacobian matrix were evaluated by numerical differentiation.

Kinetic Equation of Kim *et al.* (1987):

$$Q_H = \frac{\partial M}{\partial t} = \pm K_o e^{\left(\frac{\Delta E_a}{RT}\right)} A_s (f_{eq} - f_v) \quad (5-14)$$

Where  $K_o$ : intrinsic hydrate reaction constant ( $\text{kg m}^{-2} \text{Pa}^{-1} \text{s}^{-1}$ );  $E_a$ : hydration activation energy ( $\text{J mol}^{-1}$ );  $R$ : universal gas constant ( $8.314 \text{ J mol}^{-1} \text{K}^{-1}$ );  $T$ : temperature (K);  $A_s$ : surface area participating in the reaction ( $\text{m}^2$ );  $f_{eq}$ : fugacity at equilibrium at temperature  $T$  (Pa);  $f_v$ : fugacity in the gas phase at temperature  $T$  (Pa)

In conventional oil and gas reservoirs simulations, reservoir temperature is considered as constant if there is no external heat supplied by steam/hot water injection or microwave heating. Moreover, there are certain phases such as oleic, gas, and water. However, during the simulations of gas hydrates, temperature decreases with hydrate dissociation, and phases can change. These phases can be aqueous, ice, hydrate and gaseous. Therefore, primary switching method is mostly used in gas hydrate simulations (Gamwo and Liu, 2010; Liu and Gamwo, 2012). According to temperature and pressure conditions at certain time step, the primary variables are determined (these are listed in Table 5-2 for equilibrium model and in Table 5-3 for kinetic model). Then, for next time step, new saturations values are calculated. For the other time step, these primary variables are updated again and solved in numerical simulation for other time steps. HydrateResSim has ability to determine time step automatically. Convergence criterion for relative error in HydrateResSim is  $10^{-5}$  if the default option is chosen (Moridis *et al.*, 2005) and we chose this option in this study. When converge failure occurs during simulation at chosen time step interval, time step is reduced automatically to provide convergence. Similarly, if the maximum number of iterations per time step (as default it is 8) is exceeded, automatically time step is divided by two and for new time step, the calculations are held.

**Table 5-2:** Primary variables in equilibrium hydrate simulations without inhibitor\*  
(Moridis *et al.*, 2005)

Phase	State Identifier	Primary Variable 1	Primary Variable 2	Primary Variable 3
1-Phase: G	<b>Gas</b>	P <sub>gas</sub>	Y <sub>m_G</sub>	T
1-Phase: A	<b>Aqu</b>	P	X <sub>m_A</sub>	T
2-Phase: A+G	<b>AqG</b>	P <sub>gas</sub>	S <sub>aqu</sub>	T
2-Phase: I+G	<b>IcG</b>	P <sub>gas</sub>	S <sub>ice</sub>	T
2-Phase: A+H	<b>AqH</b>	P	S <sub>aqu</sub>	T
2-Phase: I+H	<b>IcH</b>	P	S <sub>ice</sub>	T
3-Phase: A+H+G	<b>AGH</b>	S <sub>gas</sub>	S <sub>aqu</sub>	T
3-Phase: A+I+G	<b>AIG</b>	P <sub>gas</sub>	S <sub>aqu</sub>	S <sub>gas</sub>
3-Phase: A+I+H	<b>AIH</b>	P	S <sub>aqu</sub>	S <sub>ice</sub>
3-Phase: I+H+G	<b>IGH</b>	S <sub>gas</sub>	S <sub>ice</sub>	T
Quadruple Point: I+H+A+G	<b>QuP</b>	S <sub>gas</sub>	S <sub>aqu</sub>	S <sub>ice</sub>

Where the possible primary variables are:  $P$ , pressure (Pa);  $P_{\text{gas}}$ , gas pressure (Pa);  $T$ , temperature ( $^{\circ}\text{C}$ );  $X_{m_A}$ , mass fraction of  $\text{CH}_4$  dissolved in the aqueous phase;  $Y_{m_G}$ , mass fraction of  $\text{CH}_4$  dissolved in the gas phase;  $S_{\text{aqu}}$ , liquid saturation;  $S_{\text{gas}}$ , gas saturation;  $X_{i_A}$ , mass fraction of inhibitor dissolved in the aqueous phase. \*For inhibitor:  $X_{i_A}$  becomes the 3<sup>rd</sup> primary variable, and the 3<sup>rd</sup> primary variable (as listed in Table 5-2) becomes the 4<sup>th</sup> primary variable.

**Table 5-3:** Primary variables in kinetic hydrate simulations without inhibitor\*  
(Moridis *et al.*, 2005)

Phase	State Identifier	Primary Variable 1	Primary Variable 2	Primary Variable 3	Primary Variable 4
1-Phase: A	<b>Aqu</b>	P	X_m_A	S_hyd	T
2-Phase: A+G 2-Phase: A+H	<b>AqG</b> <b>AqH</b>	P_gas P	S_aqu S_aqu	S_hyd X_m_A	T T
3-Phase: A+H+G 3-Phase: A+I+G	<b>AGH</b> <b>AIG</b>	P_gas P_gas	S_aqu S_aqu	S_gas S_hyd	T S_gas
Quadruple Point: I+H+A+G	<b>QuP</b>	P_gas	S_aqu	S_gas	S_ice

Where the possible primary variables are:  $P$ , pressure (Pa);  $P_{gas}$ , gas pressure (Pa);  $T$ , temperature ( $^{\circ}C$ );  $X_{m\_A}$ , mass fraction of  $CH_4$  dissolved in the aqueous phase;  $Y_{m\_G}$ , mass fraction of  $CH_4$  dissolved in the gas phase;  $S_{aqu}$ , liquid saturation;  $S_{gas}$ , gas saturation;  $S_{hyd}$ , hydrate saturation (-);  $X_{i\_A}$ , mass fraction of inhibitor dissolved in the aqueous phase. \*For inhibitor:  $X_{iA}$  becomes the 4<sup>th</sup> primary variable, and the 4<sup>th</sup> primary variable (as listed in Table 5-3) becomes the 5<sup>th</sup> primary variable.

## 5.4 Important Parameters for Hydrate Simulations

In all gas hydrate simulators, different approximations and assumptions are used. The most important parameters during the simulations are the parameters of kinetic equation (Equation (5-14) if kinetic model option is selected), relative permeability, capillary pressure, and the formulas of thermal conductivities of hydrate in sediments. Therefore, it is better to analyze all of these separately:

### 5.4.1 The Parameters of Kinetic Equation

As seen in Equation (5-14), the kinetic model considers the difference between equilibrium temperature and bulk temperature. At those temperatures, fugacity values are calculated and subtracted. Although this difference is a driving force for hydrate formation or dissociation, the kinetics parameters such as intrinsic hydrate reaction constant and hydration activation energy are quite important (Liu and Gamwo, 2012; Li *et al.*, 2014b). If Equation (5-14) is equal to zero, hydrate is at equilibrium conditions. If it is less than zero, hydrate dissociate and in the reverse case, hydrate forms.

Previously, it was mentioned that hydrate simulators with kinetic equations are much more accurate especially in a small laboratory scale simulation because it is a dissociation-controlled system. However, the right selection of the formulas and values of the parameters in Equation (5-14) is quite important. Therefore, core samples from gas hydrate reservoirs are necessary for kinetic equation parameters, relative permeability, and capillary pressure analysis (Santamarina *et al.*, 2012). These cores should be taken without any deformation or change in their structures by using specially designed high pressure core holders (Merey, 2016).

#### 5.4.1.1 Surface Area

The surface area is defined as area involved in the reaction. In different hydrate simulators, different approximations are used to calculate the surface area of hydrate

in sediments. For example, in Tough+Hydrate and HydrateResSim, the following formulas are used for surface area calculation (Moridis *et al.*, 2005; Moridis, 2014).

$$A_s = f_A N_v (4\pi r_p^2) S_h^{2/3} \quad (5-15)$$

where  $f_A$  is the area adjustment factor,  $N_v$  is the number of voids in the porous media, and  $r_p$  is the radius of the solid grains (m),  $S_h$ : hydrate saturation

By using the radius of the solid grains, the volume of each grain is calculated for spherical shape. Then,  $N_v$  is calculated by using  $V_p$  and porosity values. According to Equation (5-15), surface area increases with  $S_h$  and there is no effect of other components to surface area in this equation. Therefore, by considering the other phases' contribution to surface area, Sun and Mohanty (2006) proposed Equation (5-16):

$$A_s = \sqrt{\frac{\phi^3 (S_A + S_G)^3}{2K}} (S_G S_A S_H)^{2/3} \quad (5-16)$$

Where  $\Phi$ : porosity,  $S_A$ : aqueous saturation;  $S_G$ : gaseous saturation;  $S_H$ : hydrate saturation;  $K$ : intrinsic permeability,  $m^2$

Li *et al.* (2014b) updated Equation (5-15) in Tough+Hydrate to Equation (5-17) for their studies.  $\beta$  is the reduction component which determines the connection degree between the reaction surface area and the water/hydrate saturations. In the study of Li *et al.* (2014b), the sensitivity analysis of hydrate formation rate to  $\beta$  was conducted.

$$A_s = S_A^\beta (1 - S_H)^\beta N_v (4\pi r_p^2) S_G^{2/3} \quad (5-17)$$

Yousif *et al.* (1991) used the following surface area equation in their simulation studies.

$$A_s = \left[ \frac{\phi_{wg}}{2K} \right]^{1/2} \quad (5-18)$$

#### 5.4.1.2 Intrinsic Hydrate Reaction Constant and Hydration Activation Energy

In order to determine the hydrate formation or dissociation rate, intrinsic hydrate reaction constant ( $K_o$ ) and hydration activation energy ( $\Delta E_a$ ) are important parameters as seen in Equation (5-14). Some of kinetic constants in literature for this equation are listed in Table 5-4.

Kim *et al.* (1987) estimated these parameters as  $K_o$ :  $1.24 \times 10^5$  mol/ (m<sup>2</sup>. Pa. s) and  $\Delta E_a$ : 78 kJ/gas mole for CH<sub>4</sub> hydrate. In another study, the particle analyzer was used to find the surface area and experimental data were used to estimate  $K_o$  and  $\Delta E_a$  (Clarke and Bishnoi, 2001).  $\Delta E_a$  values in both the studies of Clarke and Bishnoi (2001) and Kim *et al.* (1987) are similar. However,  $K_o$  ( $3.64 \times 10^4$  mol/ (m<sup>2</sup>. Pa. s)) value found in the study of Clarke and Bishnoi (2001) is approximately 10 times smaller than that value in the study of Kim *et al.* (1987).  $K_o$  and  $\Delta E_a$  values were determined from the experimental data of hydrate formed in bulk conditions. However, in nature, hydrate forms inside the sediments. There is not much experimental information about the effect of hydrates in sediments on the dissociation kinetics. However, according to some numerical studies,  $K_o$  and  $\Delta E_a$  values must be increased by two to four orders of magnitude to fit the simulation results on the experimental data of hydrates in sediments (Gupta, 2007). For this reason, Moridis *et al.* (2005b) conducted experiments on CH<sub>4</sub> hydrate in sediments by using computerized tomography (CT) to predict  $K_o$  and  $\Delta E_a$ . They found  $K_o$ :  $1.78 \times 10^6$  mol/ (m<sup>2</sup>. Pa. s) and  $\Delta E_a$ : 89.7 kJ/gas mole for CH<sub>4</sub> hydrate. Although there is not a big difference between  $\Delta E_a$  and other values in literature,  $K_o$  value is one and two orders of magnitude larger than previously reported values. The reason of this is not well known because the effect of the porous medium on the hydrate dissociation process is not yet fully understood (Moridis *et al.*, 2005b). In the recent study of Li *et al.* (2014b), they conducted depressurization experiments on hydrate formed in sediments inside 117.4 L high pressure cylindrical reactor.  $K_o$  and  $\Delta E_a$  values were calculated by fitting the experimental data as respectively, 503.75 mol/ (m<sup>2</sup>. Pa. s) and 80.9 kJ/mol for CH<sub>4</sub> hydrate in sediments.

**Table 5-4:** Hydrate kinetic constants in Equation (5-14)

Source	$K_o$ , mol/(m <sup>2</sup> .Pa.s)	$\Delta E_a$ , kJ/mol	Condition
Kim et al. (1987)	1.24e5	78	Hydrate as bulk
Clarke and Bishnoi (2001)	3.64e4	78	Hydrate as bulk
Moridis et al. (2005b)	1.78e6	89.7	Hydrate in sediments
Li et al. (2014b)	503.75	80.9	Hydrate in sediments

#### 5.4.2 Permeability and Relative Permeability

Intrinsic permeability, effective permeability and relative permeabilities are very important parameters and they should be analyzed carefully because they are key parameters in experimental studies, numerical studies and gas production from real hydrate reservoirs.

Intrinsic permeability is the permeability of hydrate sediments when they do not include hydrates. However, when hydrate forms in the sediments, the permeability decreases. Experimental results of Johnson *et al.* (2011) show that low to moderate hydrate saturations (1.5 to 36%) can significantly reduce permeability of porous media. The permeability measured or calculated at a certain  $S_h$  is defined as effective permeability. There are different formulas to calculate effective permeability. However, they differ according to the type of gas hydrate morphology in sediments. As seen in Figure 5-3 and Figure 5-4, in nature, gas hydrate can be found as filling pores in coarse grained sand, in fine-grained sands, massive lenses and nodules in muds, thin vein in muds, disseminated in muds and massive mounds on sea floor. According to Johnson and Max (2015), hydrate filling pores in sands homogenously is desirable in terms of gas production because there are less geomechanical concerns compared to others. Similar observations were obtained in the study of Santamarina and Tsouris (2007). Winters *et al.* (2004) classified the pore filling structure of hydrates in sediments as pore filling gas, nodules, disseminated and grain cementing.

Gas hydrate formation in the pores of fine sediments is quite difficult so mostly in fine sediments, gas hydrate forms as grain displacing (Liu *et al.*, 2015). Therefore, coarse grained sediments (coarse sands, coarse sandy silts and coarse silty sands) generally include higher gas hydrate saturation compared to fine-grained sediments (fine silts, clays, shales). Mostly in fine grain sediments, gas hydrates occur as low saturation disseminated, nodules or veins (Winters *et al.*, 2014; Kumar *et al.*, 2015; Jang and Santamarina, 2016; Max and Johnson, 2016).

As shown in Figure 5-3, there are different gas hydrate occurrences in sediments. Figure 5-3-A shows thin gas hydrate section in fine-grained sediment (mainly clay). In Figure 5-3-B, during high gas flux to fine grained sediment, grains were displaced and thick gas hydrate veins formed but this type of gas hydrate occurrences are not targets for gas production. This type of gas hydrate occurrences was observed in Ulleung Basin, Korea in Figure 5-4. Figure 5-3-C and Figure 5-3-F illustrate gas hydrates in coarse sands. In both of them, gas hydrates were almost equally distributed and these types of sediments are the targets for gas production from gas hydrates. Gas hydrate mound in Figure 5-3-D is in orange color because it includes oil components as well. As seen in Figure 5-4, massive gas hydrates were observed in Cascada, Gulf of Mexico. Although mounds are not targets for gas production, they should be monitored periodically in order to understand the effect of global warming on these structures with time.

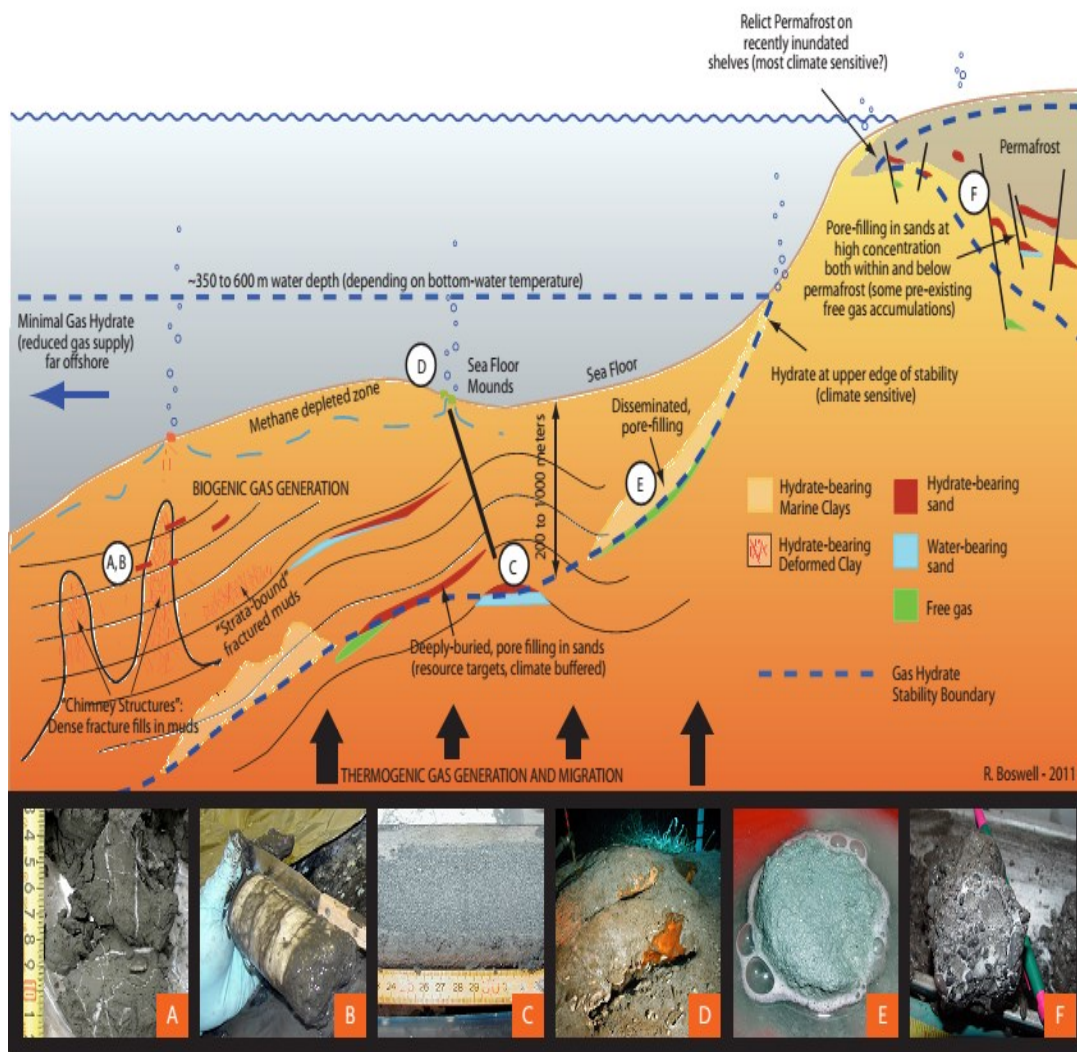
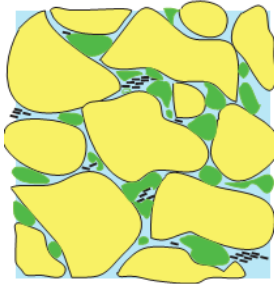


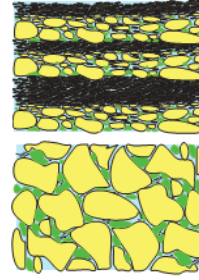
**Figure 5-3:** Gas hydrate (GH) occurrences in nature: Thin (A) and thickly veined (B) sediment-displacing GH in fine-grained sediment; (C) pore-filling GH in sand; (D) GH mounds on the sea floor; (E) Disseminated GH in fine-grained sediment; (F) GH in coarse sands (Beaudoin *et al.*, 2014)

#### Silt and Sand-rich Host Sediments



**Without Gas Hydrate**  
Porosity: 30-45%  
Permeability: 500-2000 md  
Mechanical Strength: Low

**With Gas Hydrate**  
Porosity: 10-15%  
Permeability: 0.1 - 0.5 md  
Gas Hydrate Saturation: 50-90%

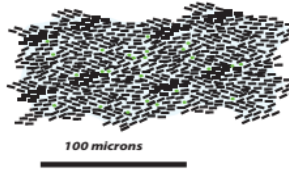


**Thinly interbedded**  
(Nankai Trough; Gulf of Mexico GC955)

**Massively-bedded**  
(Gulf of Mexico WR313; Mallik)

#### Clay-rich Host Sediments

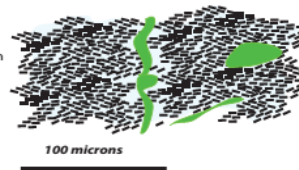
**Pore-filling in undisrupted sediments**  
(Blake Ridge)



**Without Gas Hydrate**  
Porosity: 50-70%  
Permeability: Diminishes with Depth  
to very low values (0.0001 md)  
Mechanical Strength: Very Low

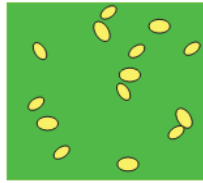
**With Gas Hydrate**  
Porosity: 45-60%  
Permeability: Nil (0.0001 md)  
Gas Hydrate Saturation: 1-10%

**Grain-displacing in disrupted, deformed sediments**  
(KG Basin, Ulleung Basin)

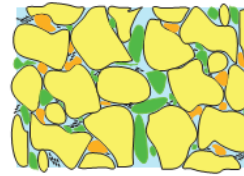


**With Gas Hydrate**  
Porosity: 45-60%  
Permeability: Nil (0.0001 md)  
Gas Hydrate Saturation: 5-40%

**Massive Occurrences (no host sediment)**  
(Gulf of Mexico, Cascadia, others)



**Consolidated host sediments (rock)**  
(Messoyahki, Barrow (AK), Qilian Mtns (Tibet))



**Variety of Lithologies**  
Porosity: Reduced due to grain  
compaction, cementation  
Permeability: Reduced 500-2000 md  
Mechanical Strength: Very high

**Figure 5-4:** Gas hydrate occurrences in sediments (Green color: hydrate, yellow color: sands) (Boswell *et al.*, 2011)

Effective permeability equations for different gas hydrate morphology in sediments are listed below (Liang *et al.*, 2011; Li *et al.*, 2014):

For the hydrate coating capillary walls model, the absolute (effective) permeability can be calculated with:

$$K = K_o(1 - S_h)^2 \quad (5-19)$$

Where  $K$ : effective permeability;  $K_o$ : intrinsic permeability;  $S_h$ : hydrate saturation

For hydrate occurring in the center of capillary model:

$$K = K_o \left[ 1 - S_h^2 + \frac{2(1 - S_h)^2}{\log(S_h)} \right] \quad (5-20)$$

For Kozeny grain models: hydrate coats the grains

$$K = K_o(1 - S_h)^{n+1} \quad (5-21)$$

Where the saturation exponent  $n$  equals 1.5 for  $0 < S_h < 0.8$ . For  $S_h > 0.8$ , the saturation exponent diverges

For Kozeny grain models: hydrate occupying the pore center

$$K = K_o \frac{(1 - S_h)^{n+2}}{(1 + \sqrt{S_h})^2} \quad (5-22)$$

Where  $n=0.7S_h+0.3$

For Masuda *et al.* (1999) model:

$$K = K_o(1 - S_h)^N \quad (5-23)$$

Where  $N$  is between 2 and 15 (When  $S_h < 35\%$ ,  $N=8$  and when  $S_h > 35\%$ ,  $N=9$  (Liang *et al.*, 2011)). Gas is produced from hydrate as  $n$  is between 2 and 11 but when  $n=20$ , gas production is not possible (Rogers, 2015).

All equations from Equation (5-19) to Equation (5-23) indicate that effective permeability is very important for gas production from gas hydrates and their modelling and experimental studies. When gas hydrate saturation ( $S_h$ ) exceeds 35 %, the absolute permeability of hydrates decreases a lot. For depressurization, thermal injection, CO<sub>2</sub> injection and chemical injection, effective permeability should be high enough. According to Konno *et al.* (2010), the absolute (effective) permeability of hydrate reservoir should be higher than 1-10 millidarcy (md) for better depressurization. However, Masuda *et al.* (2010) proposed that 50 md is the minimum preferable effective permeability when economy is considered. According to Equation (5-23), it can be concluded that when gas hydrate dissociates, effective permeability increases with time because  $S_h$  decreases with gas production from gas hydrate reservoirs. However, it should be kept in mind that if coarse sand reservoirs include certain amount of clays (i.e. smectite); released water (almost fresh water) from gas hydrate dissociation might cause the swelling of clays and certain reduction

in effective permeability (Max and Johnson, 2016). Hence, core analysis and sediment analysis are crucial.

As gas hydrate dissociates, gas and water evolve and multi-phase flow occurs in the pores. Therefore, the relative permeability of gaseous and aqueous phase should be determined for the simulation studies because they affect gas and water production rates. There are only a few experimental studies to measure the relative permeabilities in gas hydrate deposited in sediments. Johnson *et al.* (2011) measured the relative permeabilities of gas hydrate in sediments experimentally by using an unsteady state method. Based on their experiments, an unsteady state experiment was very challenging due to the mobility differences between water and gas (especially at low effective permeability conditions –as with hydrates). The displacement by gas was very piston like or channel like. Different from Johnson *et al.* (2011)’s study, Seol *et al.* (2006) conducted experiments to measure the relative permeability of CH<sub>4</sub> hydrate in sediments by using CT. In this way, the parameters of the van Genuchten relative permeability formula were determined at the desired conditions. However, these parameters can change according to type of sediments, pore structures, temperature and pressure conditions. Therefore, if the real core samples are taken from gas hydrate reservoirs, their relative permeability parameters should be measured carefully for selected relative permeability equation. Then, these data can be used in the simulations. Santamarina and Tsouris (2007) collected the most common relative permeability formulas and the values of parameters, which were used in different hydrate studies in Table 5-5.

**Table 5-5:** Relative permeability at different saturation (Santamarina and Tsouris, 2007)

	Equations	Factors and explanation	References
van Genuchten	$k_{rw} = \bar{S}_w^{0.5} \left[ 1 - \left( 1 - \bar{S}_w^{1/m} \right)^m \right]^2$	$m=0.46, S_r=0.09$ $S_r$ : irreducible water saturation	van Genuchten (1980) Parker et al. (1987)
	$k_{rg} = \sqrt{1 - \bar{S}_w} \left( 1 - \bar{S}_w^{1/m} \right)^{2m}$	$m=0.45, S_{wr}=0.2, S_{gr}=0.05$	Hong and Pooladi-Davish (2003) Uddin et al. (2008)
	$\bar{S}_w = \frac{S_w - S_r}{1 - S_r}$	$m=0.45, S_r=0.1$	Moridis (1998)
Corey	$k_{rw} = \left( \frac{S_w - S_{rw}}{1 - S_{rw}} \right)^4$	$S_m=1$	Corey (1954)
	$k_{rg} = \left( 1 - \frac{S_w - S_{rw}}{S_m - S_{rw}} \right)^2 \left( 1 - \left( \frac{S_w - S_{rw}}{1 - S_{rw}} \right)^2 \right)$	$\bar{S} = \frac{S_w - S_{rw}}{1 - S_{rw} - S_{rg}}$	Nazridoust and Ahmadi (2007)
modified Stone / Brooks-Corey	$k_{rw} = \left( \frac{S_w - S_{rw}}{1 - S_{rw}} \right)^n$ $k_{rg} = \left( \frac{S_g - S_{rg}}{1 - S_{rg}} \right)^n$	$n=3, S_{rw}=0.15, S_{rg}=0.05$ (Hydrate ResSim)	Gamwo and Liu (2010)
		$n=4, S_{rw}=0.20, S_{rg}=0.02$	Reagan and Moridis (2008) EOSHYDR
		$n=3, S_{rw}=0.25, S_{rg}=0.02$ (Class 1, Depressurization, $k=4.3 \times 10^{-14} \text{ m}^2, 10^{-12} \text{ m}^2$ )	Moridis and Kowalsky (2005) Moridis et al. (2007)
		$n=3.572, S_{rw}=0.25, S_{rg}=0.02$ (Class 2, Depressurization, $k=7.5 \times 10^{-13} \text{ m}^2$ )	Moridis and Reagan (2007)a
		$n=3.572, S_{rw}=0.25, S_{rg}=0.02$ (Class 3, Depressurization, $k=7.5 \times 10^{-13} \text{ m}^2$ )	Moridis and Reagan (2007)b
		$n=4, S_{rw}=0.2, S_{rg}=0.02$ (Class 4, Depressurization, $k=10^{-15} \text{ m}^2 = 1 \text{ mD}$ )	Moridis and Sloan (2007)
		$n=4, S_{rw}=0.2, S_{rg}=0.02$ $n=3.572, S_{rw}=0.25, S_{rg}=0.02$	Rutqvist and Moridis (2007)
		$n=4, S_{rw}=0.2, S_{rg}=0.02$	Reagan and Moridis (2008) Rutqvist and Moridis (2009)
		$n=3.572, S_{rw}=0.25, S_{rg}=0.02$ (Korea East Sea, $k=0.5 \times 10^{-13} \text{ m}^2 = 0.5 \text{ D}$ )	Moridis et al. (2009)
		$k_{rw} = \left( \frac{S_w - S_{rw}}{1 - S_{rg} - S_{rw}} \right)^{n_g}, k_{rg} = \left( \frac{S_g - S_{rg}}{1 - S_{rg} - S_{rw}} \right)^{n_g}$ $n_g=3 \text{ or } 4, S_{rw}=0.12$ (fitting from experiment)	Gupta (2007)
Grant	$k_{rw} = \bar{S}^4$ $k_{rg} = 1 - k_{rw}$	$\bar{S} = \frac{S_w - S_{rw}}{1 - S_{rw} - S_{rg}}$	Grant (1977)
Fatt	$k_{rw} = \bar{S}^3$ $k_{rg} = (1 - \bar{S})^3$	$\bar{S} = \frac{S_w - S_{rw}}{1 - S_{rw}}$	Fatt and Klikoff (1959)
Verma	$k_{rw} = \bar{S}^3$ $k_{rg} = A + B\bar{S} + C\bar{S}^3$	$\bar{S} = \frac{S_w - S_{rw}}{S_{mw} - S_{rw}}$ $A=1.259, B=-1.7615, C=0.5089, S_{rw}=0.5, S_{mw}=0.895$	Verma et al. (1985)

Where  $S_w$ : water saturation;  $S_{rw}$ : irreducible water saturation;  $S_g$ : Gas saturation;  $S_{rg}$ : irreducible gas saturation,  $k_{rw}$ : relative permeability of water;  $k_{rg}$ : relative permeability of gas;  $S_{mxw}$ : Maximum water saturation;  $A, B, C, m$ : model coefficients

### 5.4.3 Capillary Pressure

Capillary pressure is defined as the difference in pressure across the interface between two immiscible fluids.

$$P_c = P_g - P_w \quad (5-24)$$

Where  $P_c$ : Capillary pressure,  $P_g$ : gas pressure,  $P_w$ : water pressure

Santamarina and Tsouris (2007) collected the most common capillary pressure formulas and the values of parameters, which were used in different hydrate numerical studies in Table 5-6.

**Table 5-6:** Capillary pressure in hydrate-bearing sediments (Jang and Santamarina, 2014)

Factors Used in Hydrate-Bearing Sediment Study						
Equation	Relative Saturation $\bar{S}$	$S_{mxw}$	$S_{rw}$	$P_0$	$m$ or $\lambda$	References
van Genuchten [1980] $P_c = P_0 \left[ \bar{S}^{\frac{-1}{m}} - 1 \right]^{1-m}$	$\bar{S} = \frac{S_w - S_{rw}}{S_{mxw} - S_{rw}}$	1	0.14	nr	0.46	Gamwo and Liu [2010]
		nr	nr	0.1 MPa	0.45	Moridis and Reagan [2007a]
						Moridis and Reagan [2007b]
		nr	0.19	2 kPa	0.45	Moridis and Sloan [2007]
		nr	nr	0.1 MPa	0.45	Moridis et al. [2009]
		nr	nr	5 kPa	0.77	Moridis et al. [2011]
						Reagan et al. [2010]
		nr	0.19	2 kPa	0.45	Reagan and Moridis [2008]
		1	nr	2 kPa	0.45	Rutqvist and Moridis [2007]
		$\bar{S} = \frac{S_w - S_{rw}}{1 - S_{rg} - S_{rw}}$	$S_{rg} = 0.5$	0.3	1 kPa	0.45
Corey [1954] $P_c = P_0 \bar{S}^\lambda$	$\bar{S} = \frac{S_w - S_{rw}}{1 - S_{rw}}$		0.2			Uddin et al. [2008]
		nr	nr	nr	-0.5	Corey [1954]
		nr	nr	nr	-0.65	Liang et al. [2010]
		$\bar{S} = \frac{S_w - S_{rw}}{1 - S_{rg} - S_{rw}}$	$S_{rg} = 0.1$	0.1	5 kPa	-0.25

Where  $S_{mxw}$ : maximum water content,  $S_{rg}$  and  $S_{rw}$ : residual gas and water content,  $P_0$ : air entry value,  $m$ : van Genuchten equation's fitting parameter; and  $\lambda$ : pore size distribution index, nr: not reported.



## **CHAPTER 6**

### **STATEMENT OF THE PROBLEM**

Recently, especially during last decade, gas hydrates have become very popular all around the world. Many experimental studies, numerical studies and some field pilot projects have been conducted by different scientists and countries because gas hydrates are considered as future potential energy sources. However, compared to shale gas technology, gas hydrate technology is still immature. Potential gas hydrates in the Black Sea might supply an important amount of Turkey's natural gas consumption (mostly imported). However, there is no study analyzing the potential Black Sea gas hydrates in detail. Only a few seismic studies are available. Before any experimental or any field pilot projects tests in the Black Sea, the Black Sea conditions for gas hydrate should be evaluated carefully.

In this study, it is aimed to analyze the potential Black Sea gas hydrates. The investigation of thermal gradients, porosity of sediments, pressure gradients, salinity, type of sediment in the Black Sea are essential for numerical and experimental gas hydrate studies. The initial gas in place in the Black Sea gas hydrate might show the importance of the Black Sea. The target sediment types and gas hydrate reservoir types for production are needed to be determined. According to all of these data, optimum gas hydrate production method(s) in the Black Sea conditions should be selected. It is necessary to test selected gas hydrate production method(s) numerically because it is an important tool to understand the production behaviors in gas hydrates. Hence, all of these have been done in this study.

The aim of this study is also to design experimental set-up (mainly high pressure reactor) for the selected production method. This experimental set-up should mimic

gas production behavior in real gas hydrate conditions. Therefore, numerical simulations are needed while designing the experimental set-up.

In order to analyze gas hydrate properties in the Black Sea conditions, gas hydrate softwares are necessary to determine gas hydrate properties. However, available softwares are not open source and they cannot be integrated to other codes for different gas hydrate studies. Therefore, in this study, it is aimed to develop codes predicting hydrate properties, target hydrate saturations for experimental studies, gas composition change during hydrate formation and gas composition near BSRs.

Finally, as well as source gas potential and optimum pressure- temperature conditions in the Black Sea for gas hydrate formation, the types of sediments depositing gas hydrates are also important. Therefore, the characterization of the Black Sea sediments is crucial to show producible gas hydrate potential of the Black Sea. For this purpose, the DSDP Leg 42B drilling data in the Black Sea were analyzed for producible gas hydrate evaluations in this study.

## CHAPTER 7

### RESULTS AND DISCUSSION

#### 7.1 Initial Methane in-Place in the Black Sea Gas Hydrates

In Chapter 3, the detailed information about the gas hydrate potential of the Black Sea is given. Table 3-2 and Table 3-3 show initial CH<sub>4</sub> in-place calculations done in the Black Sea in all sediments within gas hydrate stability zone (GHSZ) including sands, shales, silts and clays, etc. Only gas hydrates in sands are evaluated as an energy source as seen in Figure 3-19 because they have good reservoirs properties such high permeability and high porosity. However, overall CH<sub>4</sub> in gas hydrates deposited in shales and/or clays are also important for environmental studies. Therefore, in this study, there is an attempt to calculate the possible amount of the Black Sea hydrates. For this reason, initial CH<sub>4</sub> in-place calculations in the Black Sea gas hydrates were done and compared with the data in literature. By using the literature data (Yucesoy and Ergin, 1992; Klauda and Sandler, 2003; Vassilev and Dimitrov, 2003; Vassilev, 2006; Aktosun and Varol, 2013) such as porosity distribution (Figure 7-1), hydrate filling distribution, CH<sub>4</sub> hydrate thickness information, and hydrate area, the range of these parameters were obtained in Table 7-1.

Cavity fill ratio and expansion factor in Table 7-1 were calculated in this study for CH<sub>4</sub> hydrate by using temperature distribution (Figure 7-2) and pressure gradient (which is hydrostatic pressure) of the Black Sea. Expansion factor is calculated by using Equation (3-9) and inserted into Equation (3-8) for the initial CH<sub>4</sub> amount in gas hydrates. Expansion factor is the amount of CH<sub>4</sub> at standard conditions (0°C and 1 atm) deposited in 1 m<sup>3</sup> CH<sub>4</sub> hydrate. The expansion factor of CH<sub>4</sub> hydrate was calculated as 150, 164 and 174 standard m<sup>3</sup> for 1 m<sup>3</sup> of CH<sub>4</sub> hydrate by Kvenvolden

(1993), Collett (2000), and Halliday *et al.* (1998) respectively. Gas composition, temperature and salinity affect expansion factor (Carroll, 2009; Yang *et al.*, 2010). Therefore, it is important to calculate this value for CH<sub>4</sub> hydrate in the Black Sea conditions. In Equation (3-9), there are hydrate properties such hydration number (N<sub>H</sub>) and hydrate density (ρ<sub>H</sub>) of CH<sub>4</sub>. These parameters determine expansion factor. By using HEP.m (which is written in this study and explained in detail in the following part of this chapter), N<sub>H</sub> and ρ<sub>H</sub> parameters were calculated at lowest temperature (6.5 °C), the median temperature (9 °C) and highest temperature (9.5°C) in the Black Sea. These parameters in Table 7-2 were evaluated by Monte Carlo simulation @Risk and then, expansion factors in Table 7-1 were obtained. For the Black Sea conditions, the expansion factor with cavity filling ratio of CH<sub>4</sub> molecules in the cages of sI hydrate ranges from 160.3 to 164.8 standard m<sup>3</sup> with a median value of 161.8 standard m<sup>3</sup> for 1 m<sup>3</sup> of CH<sub>4</sub> hydrate.

**Table 7-1:** Parameters calculated for the calculation of the amount of CH<sub>4</sub> in the Black Sea hydrates in this study

	<b>Lowest</b>	<b>Most Likely</b>	<b>Largest</b>
<b>Porosity, fraction</b>	0.425	0.525	0.6
<b>Average hydrate filling, fraction</b>	0.05	0.1	0.22
<b>MHSZ Thickness, m</b>	125	303	650
<b>Cavity fill ratio (cfr)</b>	0.967	0.97125	0.9885
<b>Expansion Factor without cfr</b>	165.7599	166.599299	166.7462
<b>Hydrate Area,m<sup>2</sup></b>	6.72E+07	2.79E+10	3.00E+10

**Table 7-2:** Parameters obtained from HEP.m for Monte Carlo simulation by @Risk for the evaluation of expansion factor

<b>Temperature, °C</b>	<b>ρ<sub>H</sub>, g/cm<sup>3</sup></b>	<b>Cavity filling ratio</b>	<b>N<sub>H</sub></b>
6.5	0.914	0.967	5.947
9.0	0.915	0.971	5.919
9.5	0.915	0.973	5.914

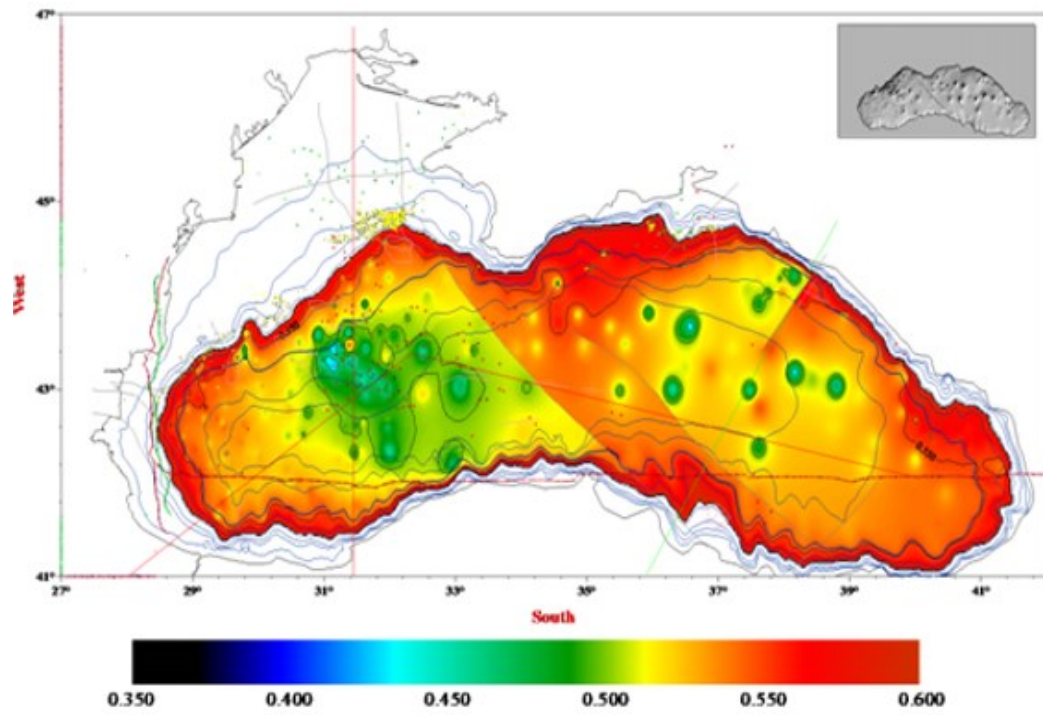


**Figure 7-1:** Porosity distribution in the Black Sea sediments (Vassilev, 2006)

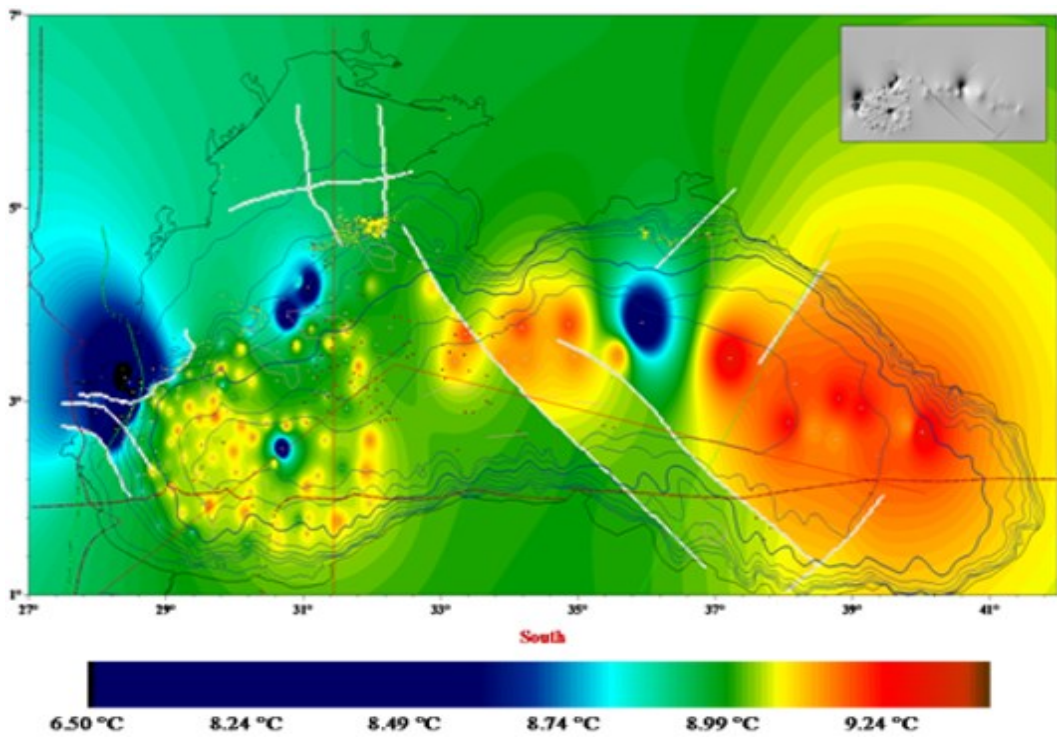


**Figure 7-2:** Temperature distribution in the Black Sea sediments (Vassilev, 2006)

Vassilev (2006) calculated porosity distribution in Figure 7-1 and temperature distribution in Figure 7-2 for the Black Sea. These parameters were very useful while calculating in initial CH<sub>4</sub> amount in CH<sub>4</sub> hydrates and simulations in this study.

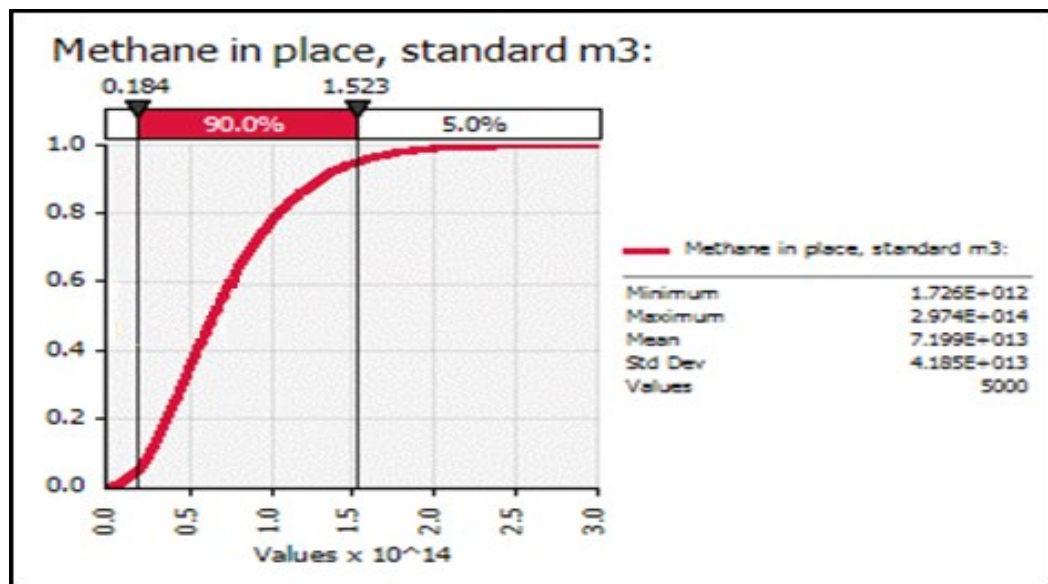
By using the parameters in Table 7-1 in @Risk program, the amount of CH<sub>4</sub> in-place in the Black Sea hydrates was calculated as 71.8 (median) standard trillion cubic meter (tcm). @RISK is the risk analysis and simulation add-in for Microsoft Excel® (Risk, 2016). Monte Carlo simulation option of @Risk was used in this study to calculate ranges of possible values. The values in Table 7-3 represent CH<sub>4</sub> hydrates deposited in all types of sediments in the Black Sea such as shales, sands, clays, etc.

**Table 7-3: CH<sub>4</sub> potential of the Black Sea hydrates**

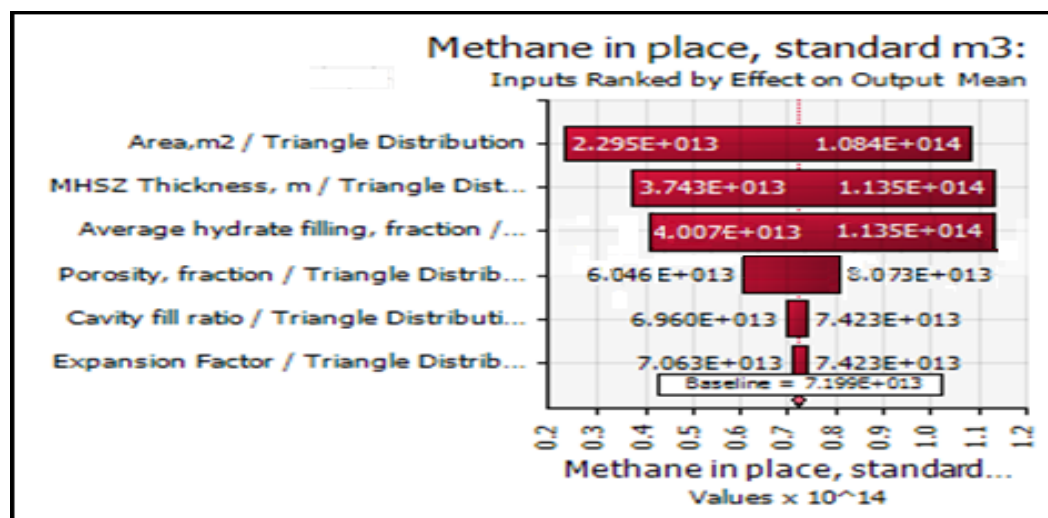
<b>Source</b>	<b>Initial gas (Methane) in place in the Black Sea gas hydrates, tcm</b>
Korsakov <i>et al.</i> , 1989	40-50
Smirnov and Chumak, 1996	75-100
Parlaktuna and Erdogmus, 2001	68.9-96.6
Klauda and Sandler, 2003	850
Solov'yov, 2003	100
Shi, 2003	42
Vassilev and Dimitrov, 2003	42 to 49 (10-50)
<b>This study</b>	<b>71.8 (1.726-297.4)</b>

Figure 7-3 and Figure 7-4 are the outputs of the Monte Carlo simulations in this study. The sensitivity analysis of model parameters such as hydrate area, methane hydrate stability zone (MHSZ) thickness, average hydrate filling or saturation, porosity, cavity fill ratio of CH<sub>4</sub> and CH<sub>4</sub> expansion factor are shown in Figure 7-4. The effects of porosity, cavity fill ratio and expansion factor with cavity filling ratio on the amount of the initial CH<sub>4</sub> in gas hydrate in the Black Sea are low compared to other

parameters because there are enough accurate data about the porosity and temperature of the Black Sea. However, as shown in Figure 7-4, the sensitivity ranges are quite wide for hydrate area, MHSZ thickness and hydrate filling ratio. Therefore, the well log data and core sample data in the Black Sea from the previously drilled wells (all for conventional oil and gas exploration) should be evaluated for most accurate initial CH<sub>4</sub> calculations in the Black Sea but mostly the companies having this well information do not intend to share their data.



**Figure 7-3:** Probability of initial CH<sub>4</sub> amount in the Black Sea hydrates



**Figure 7-4:** Sensitivity of parameters in Table 7-1

For gas production from gas hydrates, the targets are the gas hydrates deposited in sands (Boswell, 2014; Johnson and Max, 2015). However, the values in Table 7-3 are beneficial especially for the climate studies rather than energy studies because sudden release of CH<sub>4</sub> to the atmosphere might be dangerous. CH<sub>4</sub> is approximately at least 20 times more powerful greenhouse gas than CO<sub>2</sub> (Breeze, 2013; Mu and von Solms, 2016). In this study, in order to find the amount of CH<sub>4</sub> in the Black Sea gas hydrates deposited in sands (which is considered as an energy source), Equation (3-8) was multiplied by sand content. Although there are not enough data about the sand content all over the Black Sea, the sand content for the Black Sea might change from 0.9 % to 41 % (most likely value ~14.75%) (Site 379, 1978; Site 380, 1978; Site 381, 1978; Yücesoy and Ergin, 1992). By considering the sand content percentage, initial CH<sub>4</sub> in-place calculations were done with @Risk program. The amount of CH<sub>4</sub> in the Black Sea hydrates deposited in sands was found as 13.6 tcm (median). Table 7-4 shows the composition of the amount CH<sub>4</sub> deposited in sand sediments as gas hydrate in the Black Sea. Figure 7-5 and Figure 7-6 are the outputs of the Monte Carlo simulations of initial gas (CH<sub>4</sub>) in place in the Black Sea gas hydrates in this study. Similar to Figure 7-4, Figure 7-6 shows the sensitivity ranges for model parameters. Additionally, in Figure 7-6, there is another parameter called sand content. Its sensitivity range is quite wide due to unlimited data about the sand content in the Black Sea. When Table 7-3 and Table 7-4 are evaluated, the Black Sea might have a great amount of CH<sub>4</sub> in CH<sub>4</sub> hydrates as energy sources. In this study, as energy sources, it was calculated that the Black Sea might have 13.6 tcm (median) of CH<sub>4</sub> potential in CH<sub>4</sub> hydrates.

**Table 7-4:** CH<sub>4</sub> potential of the Black Sea hydrates (in sands only)

<b>Source</b>	<b>Initial gas (CH<sub>4</sub>) in place in the Black Sea gas hydrates, tcm</b>
Krason and Ciesnik, 1988	6.5
Vassilev and Dimitrov, 2000	0.1-1.0
Johnson and Max, 2015	2.5 (0.031-20.3)
<b>This study</b>	<b>13.6 (0.021-138)</b>

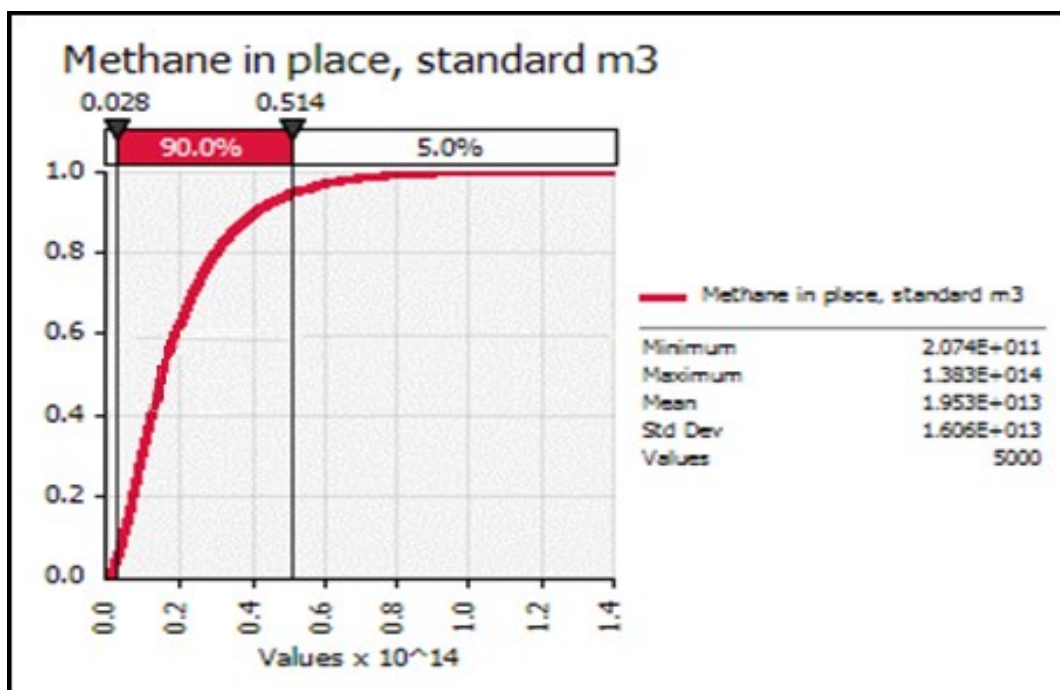


**Figure 7-5:** Probability of initial CH<sub>4</sub> amount in the Black Sea hydrates (in sands only)

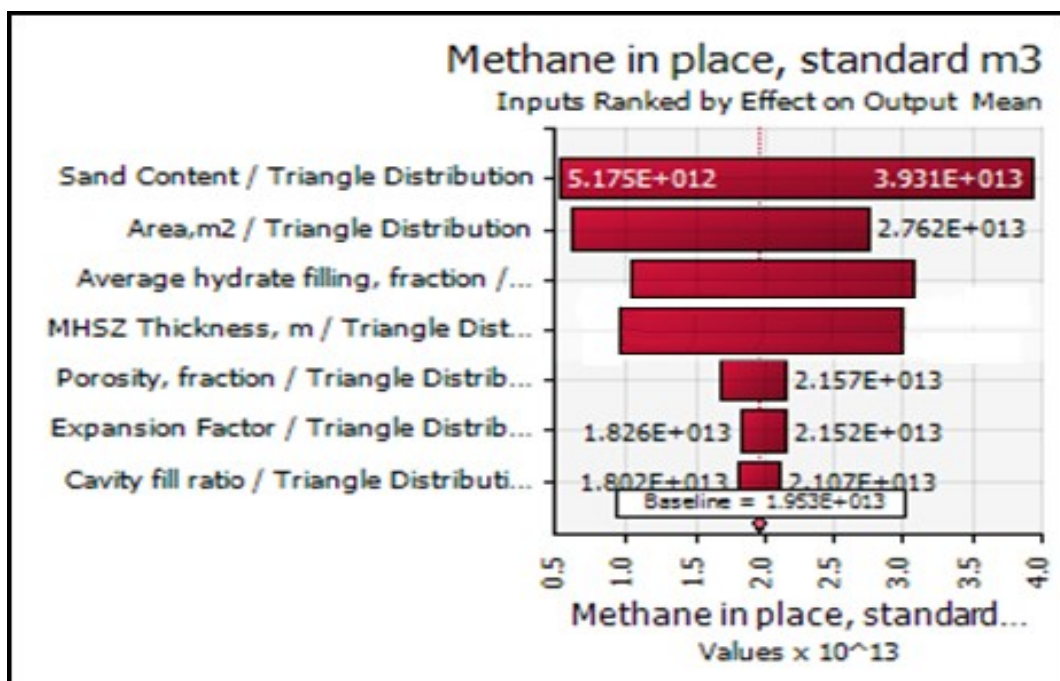


**Figure 7-6:** Sensitivity of parameters in Table 7-1 (in sands only)

## 7.2 Analysis of Gas Production Methods for the Black Sea Gas Hydrates

While designing the high pressure reactor in this study and simulating gas production from the hypothetical CH<sub>4</sub> hydrate reservoirs at the Black Sea conditions as a production method, depressurization and its combination with thermal stimulation were considered instead of CO<sub>2</sub> swapping and chemical injection methods.

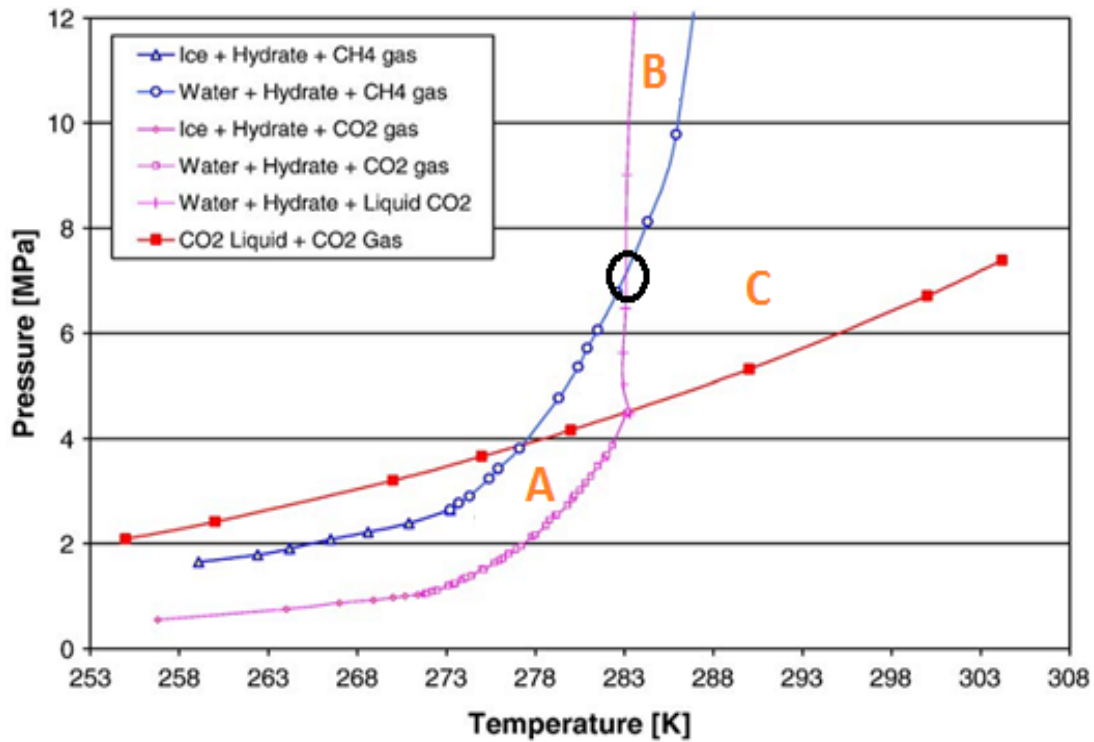


**Figure 7-7:** Hydrate equilibrium curves for pure CH<sub>4</sub> and CO<sub>2</sub> hydrates, along with phase equilibrium lines of liquid and gaseous CO<sub>2</sub> (Adapted from Goel, 2006)

As seen in Figure 3-3 and Figure 7-2, the average seafloor temperature in the Black Sea is approximately 9°C. Hence, the seafloor temperature of the Black Sea can be classified as high sea-bottom temperature compared those having low sea-bottom temperature (~4°C) in Gulf of Mexico (Küçük *et al.*, 2016b). When going deeper from seafloor, the temperature of sediments increases with thermal gradient (shown in Figure 3-6 for the Black Sea). Gas hydrates on or near seafloor is not considered as energy sources as discussed earlier in Figure 3-19. Therefore, it is expected that the temperature of potential gas hydrate zones in the Black Sea as energy sources is

higher than 10.3°C (~283.5 K). In Figure 7-7, the pure hydrate equilibrium curves of CH<sub>4</sub> and CO<sub>2</sub> in different phases are shown. Above approximately ~10.3°C, CH<sub>4</sub> hydrate is much more stable than CO<sub>2</sub> hydrate. There are two regions in Figure 7-7. In region A, CO<sub>2</sub> hydrate is much more stable than CH<sub>4</sub> hydrate but in regions B, CH<sub>4</sub> hydrate is more stable. If CO<sub>2</sub> is injected into the hydrate reservoir having temperature less than 10.3 °C (in Region A), there will be CH<sub>4</sub> and CO<sub>2</sub> swapping and also CO<sub>2</sub> can be stored as CO<sub>2</sub> hydrates. However, around Region B, only CO<sub>2</sub> injection might help the dissociation of CH<sub>4</sub> hydrate. Similar observations were done in the study of Goel (2006). Therefore, it is expected that Black Sea gas hydrates are much more likely to be in Region B and C. In region C, gas hydrates include possibly CH<sub>4</sub> and other impurities such as C<sub>3</sub>H<sub>8</sub> and H<sub>2</sub>S in the Black Sea conditions.

The first and only CO<sub>2</sub> injection field trial was conducted in Ignik Sikumi field in Alaska, USA in 2012. Instead of 100 % CO<sub>2</sub> injection, 22.5 % CO<sub>2</sub>, 77.5 % N<sub>2</sub> gas mixture was injected to Ignik Sikumi gas hydrate zone and the replacement mechanism was observed in the trial study (Schoderbek *et al.*, 2013; Kvamme, 2016). The main reasons of CO<sub>2</sub>-N<sub>2</sub> gas mixture injection were:

- To avoid the injectivity problem of CO<sub>2</sub> at high pressures
- To reduce risk of new CO<sub>2</sub> hydrate formation in the pores which decreases effective permeability
- Due to very low risk of pure N<sub>2</sub> hydrate formation because it forms sII hydrate at extremely large pressures (hydrate equilibrium of pure N<sub>2</sub> is shown in Figure 7-10)
- To increase CH<sub>4</sub> recovery because during CH<sub>4</sub>-CO<sub>2</sub> swapping, CO<sub>2</sub> enters into the large cages of sI hydrate and N<sub>2</sub> enters into the small cages of sI hydrate of CH<sub>4</sub> so CH<sub>4</sub> recovery increases

Therefore, during the analysis of CO<sub>2</sub> injection as a production method, CO<sub>2</sub> injection should be considered with N<sub>2</sub> injection. CO<sub>2</sub> sequestration as pure CO<sub>2</sub> hydrate in

sediments is an environmental issue and not discussed in this study. Figure 7-8 shows the density and phase profile of CO<sub>2</sub> at different pressures when temperature is 9°C (average sea floor temperature of the Black Sea). As the density profiles of CO<sub>2</sub> and 22.5 % CO<sub>2</sub>, 77.5 % N<sub>2</sub> mixture at different pressures and 9°C, their density and phase profiles are quite different as seen in Figure 7-8 and Figure 7-9. CO<sub>2</sub> density suddenly increases from 2.9699 mol/l to 19.733 mol/l at 639.95 psia because its phase changes from gaseous to liquid. At 9°C, hydrate equilibrium pressure of CH<sub>4</sub> is around 910.2 psia. Hence, there will be injectivity problems with pure CO<sub>2</sub> injection into the Black Sea gas hydrates. This problem increases if the effective permeability of gas hydrate reservoir is low. A solution to this injectivity problem and low CH<sub>4</sub> recovery was brought in the Ignik Sikumi field trial with CO<sub>2</sub>-N<sub>2</sub> mixture injection. As seen in Figure 7-9, the density of 22.5 % CO<sub>2</sub>, 77.5 % N<sub>2</sub> mixture increases slowly with pressure compared to the density of pure CO<sub>2</sub>.

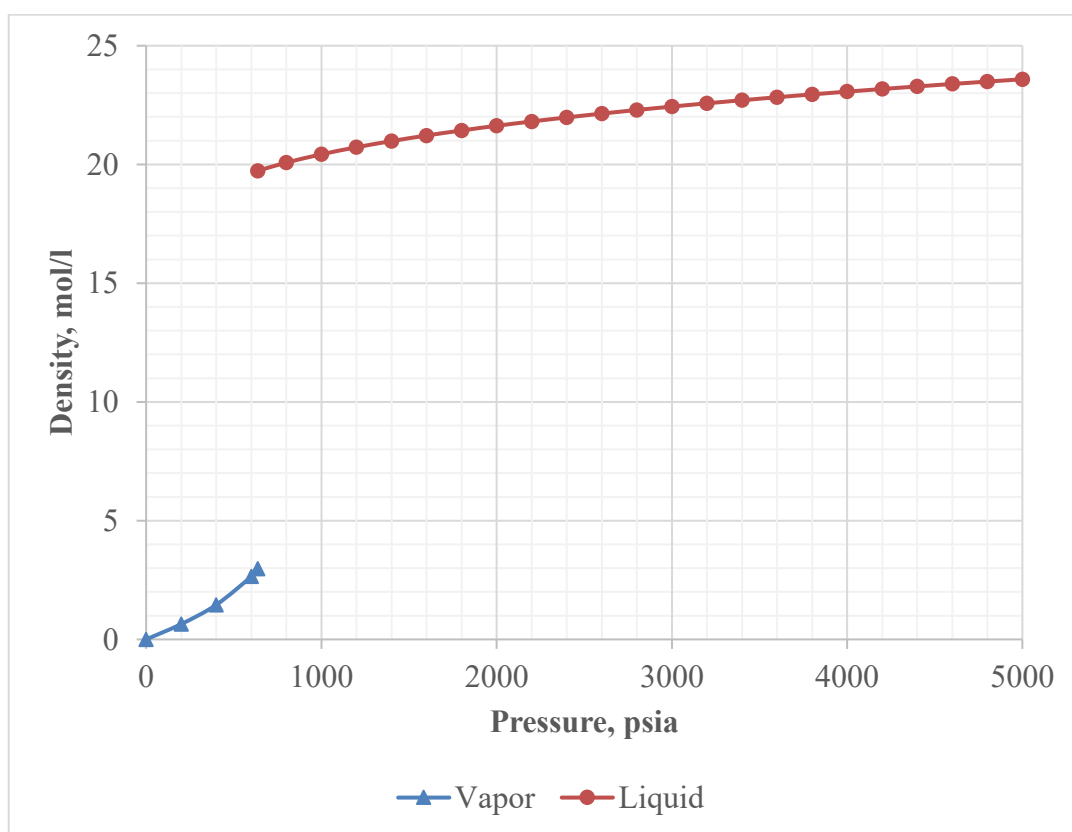


**Figure 7-8:** Density versus pressure at 9°C for CO<sub>2</sub> (Calculated with NIST)

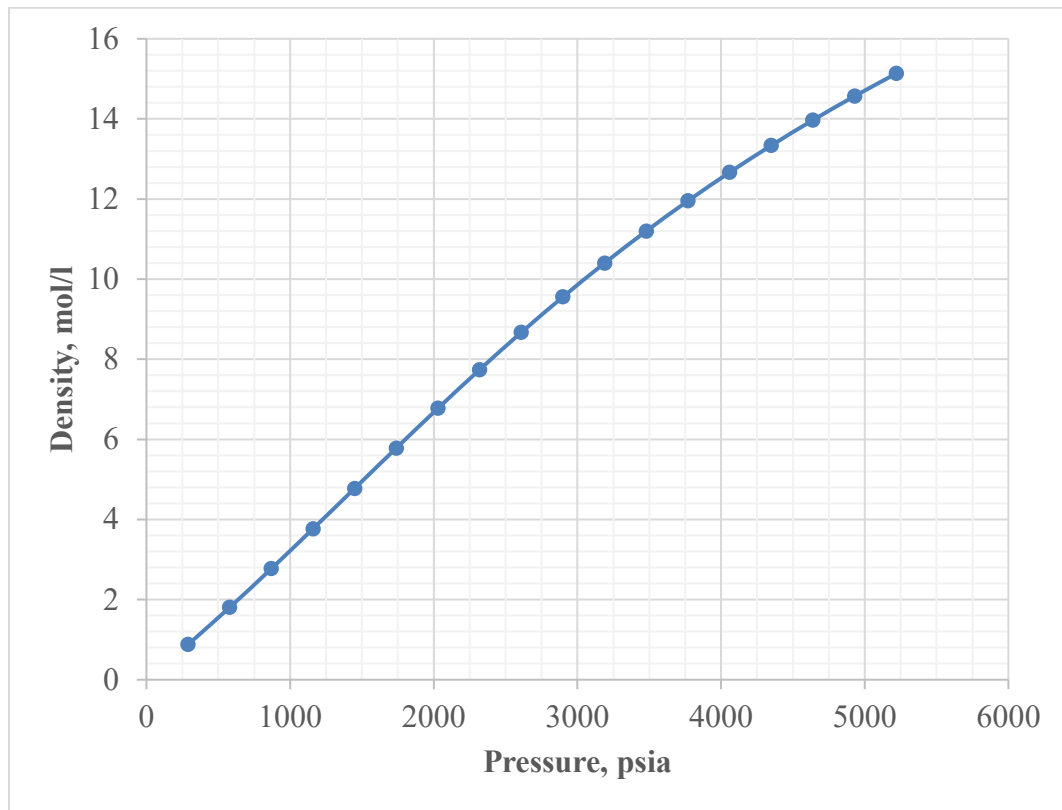


**Figure 7-9:** Density versus pressure at 9°C for 22.5 % CO<sub>2</sub>+77.5 % N<sub>2</sub> (Calculated with WebGasEOS)

While analyzing CO<sub>2</sub> injection, it should be considered with N<sub>2</sub> injection as well in the Black Sea as a production method. There are only two studies claiming to investigate CO<sub>2</sub> injection in the Black Sea. Ors (2012) observed CH<sub>4</sub>-CO<sub>2</sub> swapping after injecting pure CO<sub>2</sub> into pure CH<sub>4</sub> hydrate. Abbasov (2014) also injected CO<sub>2</sub> into natural gas hydrates but gas hydrate consisted of 95 % CH<sub>4</sub>, 3 % C<sub>3</sub>H<sub>8</sub>, and 2 % CO<sub>2</sub>. CH<sub>4</sub>-CO<sub>2</sub> swapping was also observed in the study of Abbasov (2014). In both of these studies, 4°C temperature was selected for gas hydrate formation and CH<sub>4</sub>-CO<sub>2</sub> swapping. However, when the temperature profile of the Black Sea is carefully analyzed in Figure 7-2 and Figure 3-6, there are no areas with 4°C in seafloor and in the sediments of the Black Sea, it is expected that the temperature of the sediments is higher than 9°C. Therefore, actually these studies do not represent the Black Sea conditions. Figure 7-7 obviously shows that gas hydrate reservoirs below and higher 10.3°C temperature should be evaluated separately. Hence, before any gas hydrate

production experiments and numerical simulations, the Black Sea conditions should be investigated very well and this study aims to do this.

In order to analyze CO<sub>2</sub> and CO<sub>2</sub>/ N<sub>2</sub> injection at the Black Sea conditions, Figure 7-10 was prepared in this study by using CSMGem hydrate equilibrium software of Colorado School of Mines in Sloan and Koh (2008). Pressure and temperature values for the red line in Figure 7-10 was prepared by using average thermal gradient (0.03 °C/m), average sea floor temperature (9°C) , pressure gradient of sediments (0.465 psi/ft), and average hydrate thickness (average:303 m and maximum: 650 m as shown in Table 7-1) data of Vassilev (2006) for the Black Sea. Only 38.3 meter below the Black Sea floor is in the Region A (Figure 7-7) but 264.7 m of GHSZ is in the region of B (Figure 7-7). Gas production from potential gas hydrate between seafloor and 38.3 meter below seafloor (mbsf) is not considered as an energy source as discussed in Figure 3-19. Hence, potential gas hydrates in the Black Sea as energy sources are expected to be in the region B and C when all available data in the Black Sea were analyzed in this study. Pressure ranges, temperature ranges, and hydrate types of these regions are shown in Table 7-5.

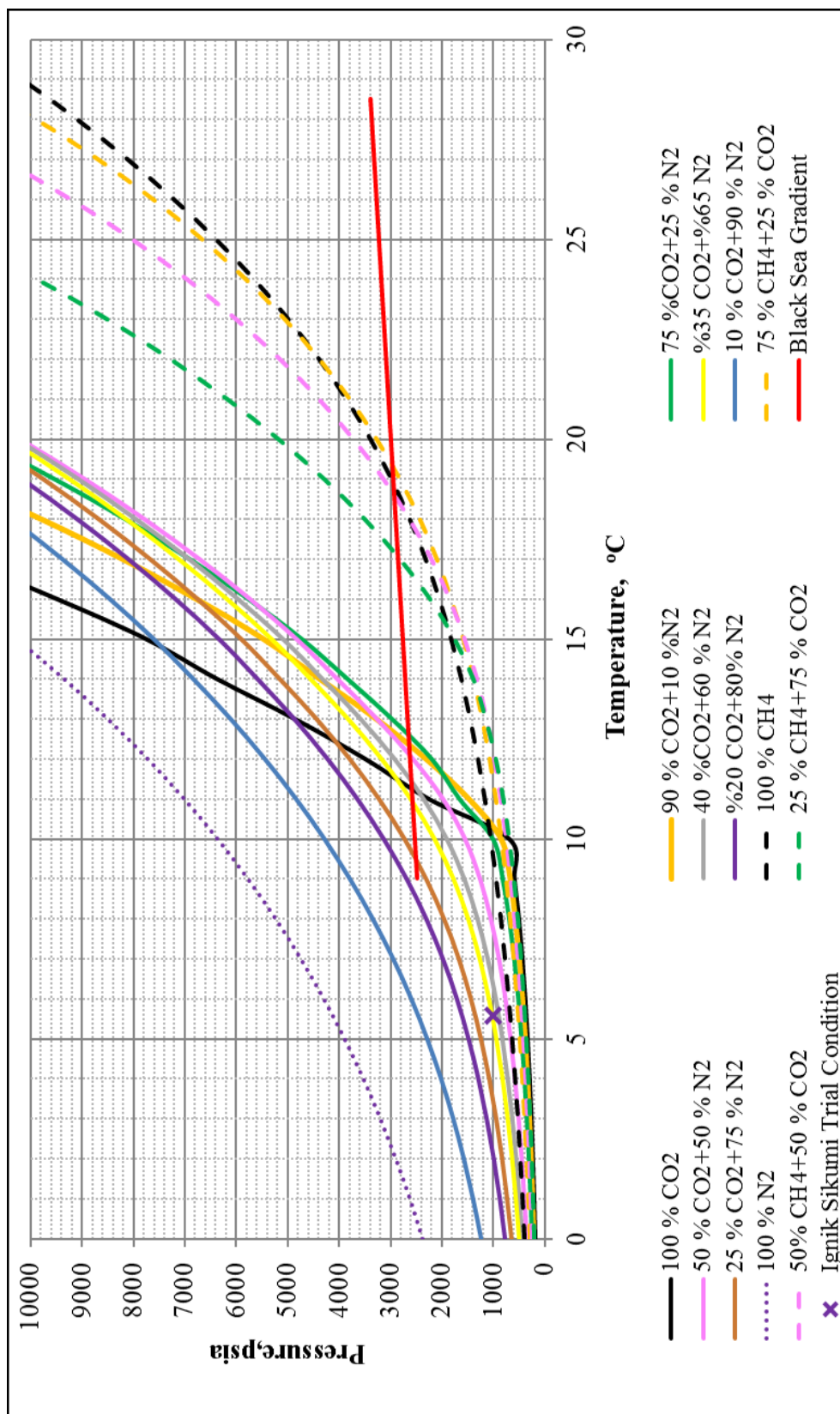


**Figure 7-10:** Hydrate equilibrium curves of CO<sub>2</sub>, CH<sub>4</sub> and N<sub>2</sub> and their mixture and potential Black Sea temperature and profile

To illustrate the field conditions of Ignik Sikumi field (first trial for CO<sub>2</sub>-N<sub>2</sub> injection to gas hydrates), pressure and temperature conditions of this field ( $P_{\text{average}}$ : 1006.2 psia;  $T_{\text{average}}$ : 5.58 °C;  $S_h$ : 66.5 %;  $P_{\text{injection}}$ : 1400 psia (Schoderbek *et al.*, 2013; Garapati, 2013)) were shown in Figure 7-10. The conditions of this field are in Region A. In this field, 22.5% CO<sub>2</sub> and 77.5 % N<sub>2</sub> was injected to swap CH<sub>4</sub> in CH<sub>4</sub> hydrate with CO<sub>2</sub> and N<sub>2</sub>. When CH<sub>4</sub> is released from sl cages, CO<sub>2</sub> enters into large cages and N<sub>2</sub> enters into small cages. After filling of the cages with new guests (CO<sub>2</sub> and N<sub>2</sub>) and release of CH<sub>4</sub> from the cages, newly formed gas hydrate should be above its hydrate equilibrium point so mixed gas hydrate stays stable. For example, as seen in Figure 7-10, if newly formed gas hydrate includes 35 % N<sub>2</sub> and 65 % CO<sub>2</sub> composition, it will be in hydrate equilibrium at the conditions of Ignik Sikumi field.

**Table 7-5:** Different zones for CO<sub>2</sub>-N<sub>2</sub> injection for the Black Sea hydrates

<b>Region</b>	<b>Interval, mbsf</b>	<b>Temperature Range, °C</b>	<b>Equilibrium Pressure Range, psia</b>	<b>Potential Hydrate Type</b>
<i>A</i>	0-38.3	9-10.3	2482-2535.4	CH <sub>4</sub> or gas mixture hydrate
<i>Transition Zone</i>	38.3-73.3	10.3-11.2	2535.4-2584.3	CH <sub>4</sub> or gas mixture hydrate
<i>B</i>	73.3-326.7	11.2-18.8	2584.3-2937.8	CH <sub>4</sub> or gas mixture hydrate
<i>C</i>	326.7-650	18.8-28.5	2937.8-3388.8	Gas mixture hydrate

Potential gas hydrates in Region A and transition zone of the Black Sea should not be considered as energy sources because they are very close to seafloor and injection pressure should be at least approximately 2500 psia. Therefore, Region B and Region C were evaluated for potential CO<sub>2</sub> and N<sub>2</sub> injection to the potential Black Sea gas hydrates. When Figure 7-10 is carefully analyzed, after 11.8 °C, higher injection pressures for CO<sub>2</sub> and N<sub>2</sub> gas hydrate mixture are needed. For example, if 75 % CO<sub>2</sub>

and 25 % N<sub>2</sub> gas mixture hydrate is formed in the gas hydrate reservoir having 15°C temperature, pressure in the reservoir should be kept at least 4700 psia. Below this pressure ( Figure 7-10), newly formed CO<sub>2</sub>-N<sub>2</sub> gas hydrate after swapping with CH<sub>4</sub> will dissociate because it is out of its hydrate stability region. The main advantage of CO<sub>2</sub>-N<sub>2</sub> injection into gas hydrate reservoirs is to avoid any geomechanical failures and to decrease water production during gas production from gas hydrates. However, over-pressurized hydrate reservoirs after increasing injection pressure upto 4700 psia might cause geomechanical failures and sudden gas releases because the Black Sea sediments are very loose and unconsolidated between 0 and 200 mbsf according to Kuprin *et al.* (1978). Similar observations were obtained about the effect of overpressurization on geomechanics of gas hydrates in the studies of Ellis *et al.* (2010), Kwon and Cho (2012), Zhang *et al.* (2015) and Priest and Grozic (2016). Therefore, after 11.8 °C (93.33 mbsf), CO<sub>2</sub>-N<sub>2</sub> injection might not be advantageous in the Black Sea gas hydrates.

**Table 7-6:** CO<sub>2</sub>-N<sub>2</sub> injection analysis between 76.67 mbsf and 120 mbsf in Figure 7-10

Number	Depth (mbsf)	Temperature, °C	Possible CO <sub>2</sub> -N <sub>2</sub> mixture	Pressure, psia
1	76.67	11.3	40 % CO <sub>2</sub> +60 % N <sub>2</sub>	2589
2	93.33	11.8	50 % CO <sub>2</sub> +50 % N <sub>2</sub>	2612
3	120	12.5	75 % CO <sub>2</sub> +25 % N <sub>2</sub>	2649
<i>At higher injection pressure (4000 psia)</i>				
1	76.67	11.3	20 % CO <sub>2</sub> +80 % N <sub>2</sub>	4000
2	93.33	11.8	25 % CO <sub>2</sub> +75 % N <sub>2</sub>	4000
3	120	12.5	35 % CO <sub>2</sub> +65 % N <sub>2</sub>	4000

In Region B, there is only limited interval between 76.67 and 120 mbsf for the evaluation of CO<sub>2</sub>-N<sub>2</sub> injection. Optimum CO<sub>2</sub>-N<sub>2</sub> gas mixture ratios for injection into this interval are shown in Table 7-6. As seen in this table, if CO<sub>2</sub>-N<sub>2</sub> mixture is injected at reservoir pressures of this depth interval, 40 % CO<sub>2</sub> + 60 % N<sub>2</sub>; 50 % CO<sub>2</sub> + 50 % N<sub>2</sub>; 75 % CO<sub>2</sub> + 25 % N<sub>2</sub> can provide CH<sub>4</sub> release and stable gas hydrate after

swapping for 11.3°C, 11.8 °C, and 12.5 °C respectively. However, CO<sub>2</sub> ratios in the Black Sea case are higher compared to 22.5 % CO<sub>2</sub> in Ignik Sikumi field. As CO<sub>2</sub> concentration increases, injectivity problem increases. CO<sub>2</sub> cannot form its pure hydrate (see Figure 7-10) in the depth interval in Table 7-6 so there is no risk of CO<sub>2</sub> hydrate formation in this depth interval of the Black Sea. When the injection pressure increases to 4000 psia, 20 % CO<sub>2</sub> + 80 % N<sub>2</sub>; 25 % CO<sub>2</sub> + 75 %, N<sub>2</sub>; 35 % CO<sub>2</sub> + 65 % N<sub>2</sub> can provide CH<sub>4</sub> release and stable gas hydrate after swapping for 11.3°C, 11.8 °C, and 12.5 °C respectively. Although necessary CO<sub>2</sub> concentration in the injected gas mixture is decreased by increasing the injection pressure, this creates another risk, which is over-pressurized reservoir and geomechanical problems.

According to all evaluations made in this study, it was concluded that CO<sub>2</sub> or CO<sub>2</sub>-N<sub>2</sub> injection methods are not completely appropriate in the Black Sea conditions due to the warm seafloor temperature of the Black Sea. Therefore, CO<sub>2</sub> (in gas and liquid phase) and N<sub>2</sub> swapping with CH<sub>4</sub> in CH<sub>4</sub> hydrate is not appropriate in the Black Sea conditions for gas production purposes. Although CO<sub>2</sub> in emulsion can provide CO<sub>2</sub>-CH<sub>4</sub> swapping in the Black Sea conditions when thermodynamic conditions are considered, the technique for preparing CO<sub>2</sub> emulsion is currently immature and consistent experimental results have not been sufficiently collected so far and also it will create injectivity problems (Koh *et al.*, 2016). Moreover, according to geophysical explorations in the western Black Sea (Zonguldak-Amasra region), many gas seepage areas and mud volcanos were observed and it was observed that the accumulated gas below gas hydrate stability zone (GHSZ) came to seafloor by cutting GHSZ due to excess pore pressure (Küçük, 2016). The main reason of this might be high rate of gas flux under impermeable sediments such as shale, clay etc. When pressure becomes very high after certain time under impermeable sediments within GHSZ, faulting in GHSZ occurs (Max and Johnson, 2016). Even somehow CO<sub>2</sub>-CH<sub>4</sub> swapping was successfully completed in the Black Sea, it is hard to say CO<sub>2</sub> hydrate would be stable there for a long time. The reasons of this can be listed as:

- High sedimentation rate in the Black Sea might cause the dissociation of CO<sub>2</sub> hydrate due to temperature increase.

- Global warming causes the increase of sea temperatures and sediment beneath seafloor.
- Below impermeable CO<sub>2</sub> gas hydrate, gas from deeper sediments might be collected and cause excess pore pressure and stability problems.
- The salinity of sea is higher than the salinity in sediments in the Black Sea so there might be salt diffusion from seawater through the sediments. Salt is a gas hydrate inhibitor and might cause the dissociation of CO<sub>2</sub> hydrate with time.

Depressurization method was successively tested in Mallik field (Canada) and Nankai (Japan) fields. As seen in Figure 7-11, when effective permeability and temperature of sediments increase, the effectiveness of depressurization method increases. According to all temperature profile and temperature gradient data, obviously the sediments of the Black Sea have higher temperature than Mallik field ( $\sim 8^{\circ}\text{C}$ , Henniges *et al.*, 2004) and Ignik Sikumi field ( $5.58^{\circ}\text{C}$ , Garapati, 2013) so this is advantageous for the application of depressurization production method to the Black Sea gas hydrates. Therefore, during the design of the experimental set-up in the Black Sea conditions, depressurization and its combinations with other techniques were considered in this study.

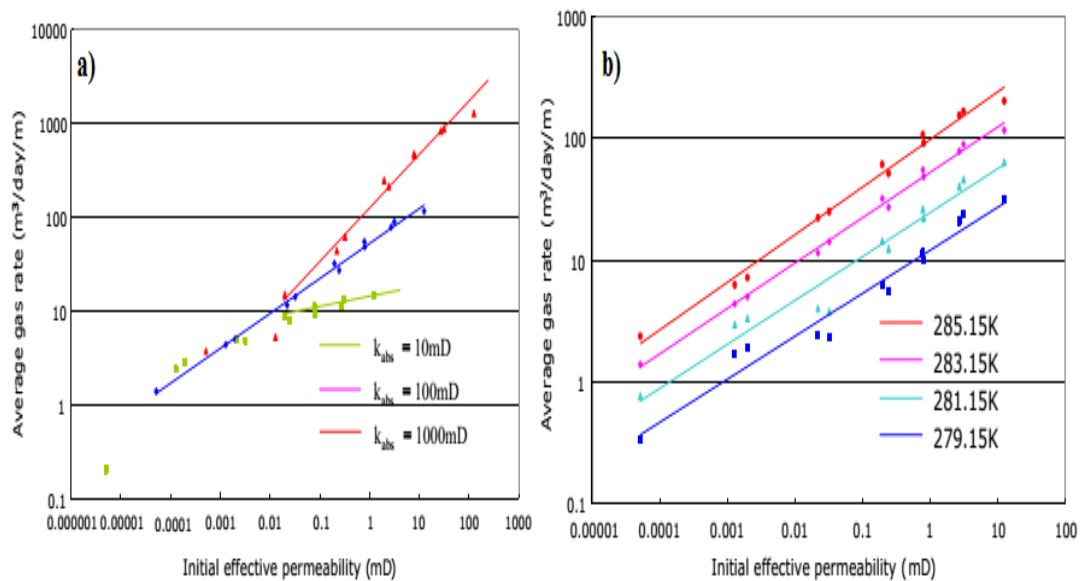


**Figure 7-11:** Relationships between the productivity using depressurization method and effective permeability and reservoir temperature (MH-21, 2008)

Gas production from gas hydrates by depressurization method can be held in two ways: Constant flow rate depressurization and constant pressure depressurization. By constant flow rate depressurization, pressure value cannot be controlled efficiently. Therefore, if pressure is above gas hydrate equilibrium point during production by constant flow rate depressurization, there is a risk of gas hydrate reformation in gas hydrate reservoirs. Moreover, if flow rate is too high, this might cause ice formation in the reservoir or along the wellbore because of the endothermic nature of hydrate dissociation and Joule Thomson cooling. In this study, constant pressure depressurization method was preferred during the design of high pressure reactor and numerical simulations of hypothetical gas hydrate reservoirs in the Black Sea conditions with HydrateResSim. Some criteria for constant pressure depressurization and constant flow rate depressurization methods are listed in Table 7-7. Constant pressure depressurization can be applied for a wide range of formation permeability values, high hydrate saturations and different gas hydrate reservoir types.

**Table 7-7:** Some criteria for constant pressure depressurization and constant flow rate depressurization methods (Adapted from Moridis *et al.*, 2008b; Sun *et al.*, 2015; Myshakin *et al.*, 2016)

<b>Constant Pressure Depressurization</b>	<b>Constant Flow Rate Depressurization</b>
Applicable to a wide range of formation permeabilities	Applicable when the intrinsic permeability of the hydrate formation is high
Only reasonable alternative when $S_h$ is high.	Applicable when the initial $S_h$ is moderate (i.e., $S_h < 0.5$ )
Reducing the risk of ice formation.	Applicable when capillary pressure is weak
Applicable to a wide range of irreducible aqueous and gas saturations	Applicable when irreducible aqueous and gas saturations are relatively low
Applicable for all types of gas hydrates	Not applicable for gas production in Class 3 hydrates

### 7.3 Experimental Set-up Design for the Black Sea Gas Hydrate Studies

In this study, a new experimental set-up was designed for gas production experiments from the Black Sea gas hydrates. The aim of these experiments are to investigate gas hydrate production, especially from Class 1 gas hydrates in the Black Sea conditions by depressurization, thermal stimulation and their combinations. As shown in Figure 7-12, the main equipment for experimental studies is listed below:

- Constant Temperature Room
- High Pressure Reactor (METU Reactor)
- Gas-Water Separator
- Backpressure Regulator
- Gas Flow Meter
- Pressure Transducers
- Thermocouples
- PC
- Data Loggers
- Methane Bottle (99.99% Purity)
- Gas Mixture Bottle if necessary
- Compressor
- Vacuum Pump
- Pumps
- Weighing Balance
- Screens
- Lines, fittings, and valves, etc.
- Gas Chromatography (if gas composition includes gas mixtures)

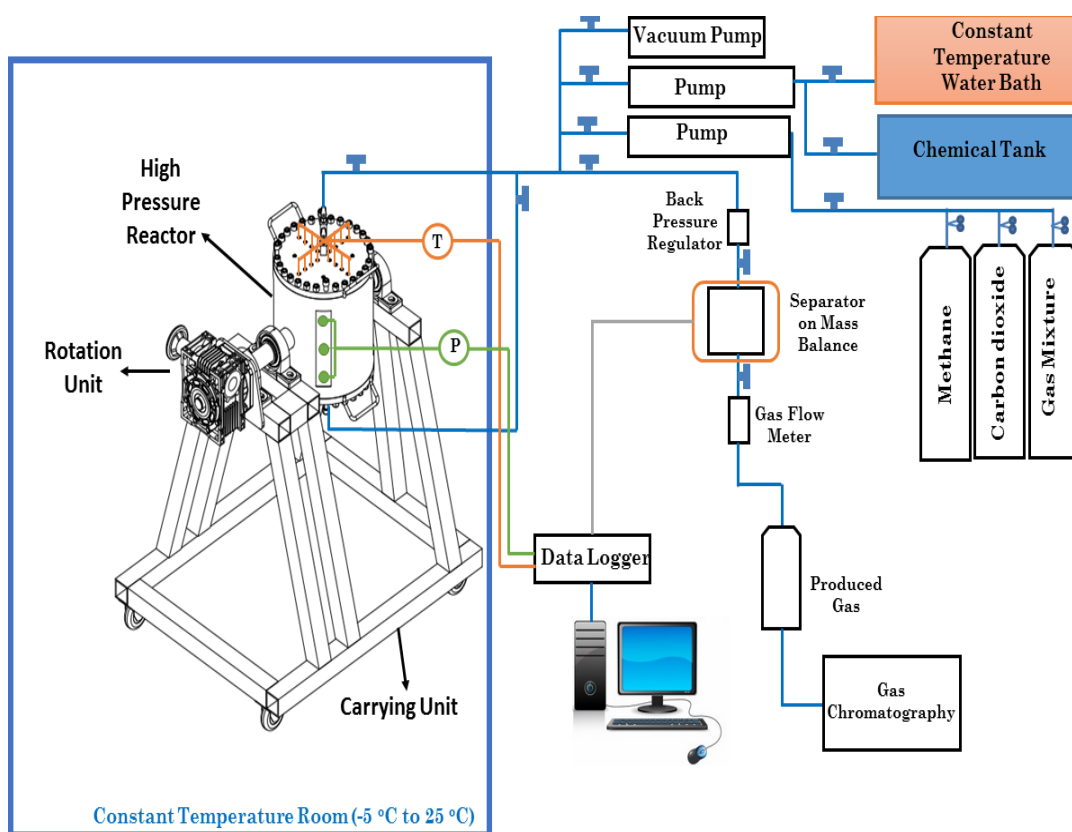


**Figure 7-12:** Schematic of the experimental setup designed in this study for gas hydrate experiments

Figure 7-12 shows the experimental set-up designed in this study. The high pressure reactor (METU reactor) is kept in the constant temperature room or cold room to keep temperature constant at desired conditions. The high pressure reactor might be coated with water jacket as well in order to keep temperature as constant as possible. When the high pressure reactor is filled with sands, air in pores is taken out by using vacuum pump. Porosity of sands can be calculated with air expansion before vacuuming or by using grain sizes because it is important for the calculation of the amount of gas and water needed to obtain target conditions. Then, sands are saturated with water or water including dissolved salt and gas according to target saturations and pressure. Syringe pumps are commonly used to inject water and or pressurize gas into small high pressure cells. Large capacity pumps and compressors are necessary to provide enough pressure in large high pressure reactors. The duration of gas hydrate formation in sediments vary with the size of high pressure reactor (mostly),

temperature, pressure, gas composition etc., but generally for small size (600 cm<sup>3</sup>) high pressure cell, it can take less than 7 days (Abbasov *et al.*, 2016). However, hydrate formation in 1710 L high pressure reactor (HIGUMA) took 30 days in the study of Konno *et al.* (2014). In the experimental study of Heeschen *et al.* (2016), mimicking Mallik field gas hydrate reservoirs (80-90 % S<sub>h</sub>) in LARS reactor (425 L) filled with 210 L sample took 3 months by forming CH<sub>4</sub> hydrate from CH<sub>4</sub> dissolved in water. After obtaining target saturations in the high pressure reactor, necessary preparations should be done according to production method. For depressurization experiments, gas production is initiated by decreasing pressure in the high pressure reactor to target depressurization pressure. It is obvious that with gas production, there will be water production because of free water in pores and water evolved after hydrate dissociation. Backpressure regulators are used to keep pressure constant at certain conditions. Therefore, they are important tools to apply constant pressure depressurization method. When gas is released after hydrate dissociation, pressure increases. If pressure inside high pressure reactor is higher than the setting pressure of backpressure regulator, gas and or water mixture are released to atmospheric conditions. In order to measure gas flow rate, dry gas should pass inside gas flow meter for accurate measurements. Therefore, the separation of water and gas is necessary. When gas and water mixture enter into gas-water separator, water is collected at the bottom of the separator and gas flow outside of the separator through gas flow meter and then, gas flow rate is recorded with time. Water flow rate is measured by recording the weight change in the separator. Therefore, separator is put on the weight balance and weight change is recorded. Water production rate and gas production at different depressurization pressures or thermal injection are important data to analyze the effectiveness of selected gas production method for gas hydrates. Hence, the size of high pressure reactor, size of gas-water separator, range of gas flow meter and weight balance are quite important. In order to select the size of gas-water separator, range of gas flow meter and weigh balance (which are most important equipment), there are two ways. One way is to make analogy with the experiments conducted in literature or to conduct simulation studies to predict water and gas production rates in laboratory scale. In this study, numerical simulations were run by HydrateResSim numerical simulator to design the size of high pressure reactor

(METU reactor), size of gas-water separator, range of gas flow meter and weight balance in the Black Sea conditions.

### **7.3.1 Design of the High Pressure Reactor (METU Reactor) and Other Equipment**

In the past, small high pressure cells were used to investigate gas production from gas hydrates by applying different production methods. For example, Yousif *et al.* (1991) conducted depressurization experiments by using 171 cm<sup>3</sup> cylindrical high pressure cell. Similarly, Masuda *et al.* (1999) conducted similar experiments in a 589 cm<sup>3</sup> cylindrical high pressure cell. However, these small high pressure cells are not enough to represent real field conditions. While producing gas from gas hydrates formed in these small cells, hydrate dissociation occurs rapidly and dissociated gas is produced very fast because gas is not exposed to follow long distances to the production valve. Therefore, during numerical simulations, the kinetic formula in Equation (5-14) should be used to predict the experimental conditions in these small high pressure cells. According to Ruan *et al.* (2012), the flow mechanism in these small high pressure cells is called “kinetic-controlled mechanism”. In these small (centimeter) scale systems, the determining factors are phase change kinetics and heat transport but not mass transport (Nagao, 2012; Konno *et al.*, 2014). However, in the cases of real gas hydrate reservoirs or large high pressure reactors, gas production process is more likely to be “flow-controlled”. The predominant factor in the early production stage is the mass transfer and in the later stages of gas production, the predominant factor becomes heat transfer. Phase change kinetics in large scale systems is negligible compared to small scale systems (Nagao, 2012; Konno *et al.*, 2014; Yang *et al.*, 2014; Wang *et al.*, 2016; Feng *et al.*, 2017). Hence, recently, there is a tendency to construct and use large high pressure reactors for gas hydrate studies mimicking the fluid flow, heat transfer, and mass transfer as in real gas hydrate reservoirs (Konno *et al.*, 2014; Wang *et al.*, 2016; Feng *et al.*, 2017). Numerical simulators are important tools to compare the experimental results with calculated results of gas production from gas hydrates. Both equilibrium and kinetic models used in these numerical simulators give quite similar results in larger scale systems

by thermal stimulation and depressurization (Kowalsky and Moridis, 2007). Moreover, they also conducted the simulation studies to determine the behavior of the core sample (Length: 3 m and Diameter: 3.13 cm) taken from the hydrate reservoir to surface with kinetic and equilibrium model of Tough + Hydrate.

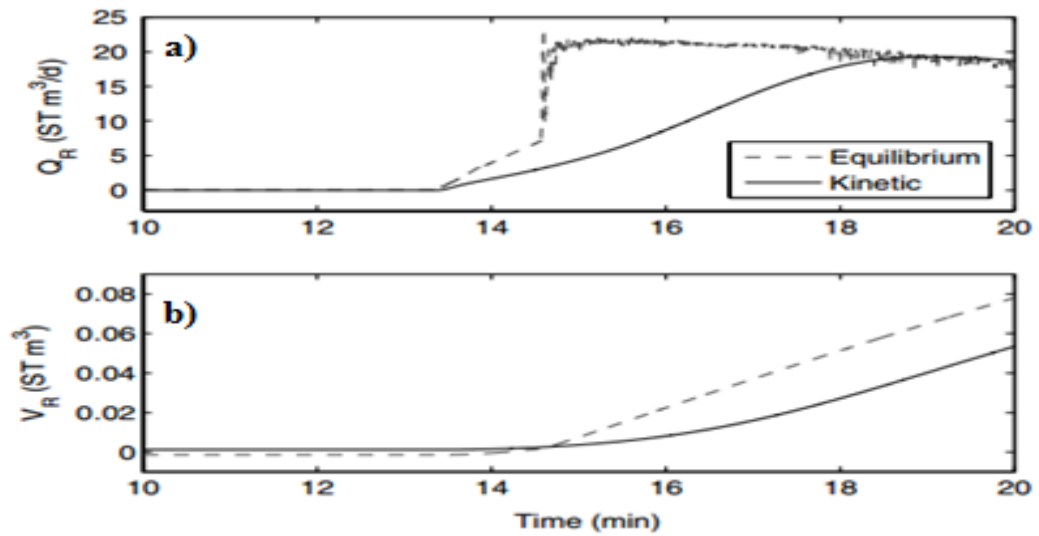


**Figure 7-13:** a) Flow rate ( $Q_R$ ) b) Total gas production ( $V_R$ ) (Kowalsky and Moridis 2007)

As shown in Figure 7-13, the gas flow rate and total gas produced are quite different with equilibrium and kinetic model. The equilibrium model overpredicts gas flow rate and total gas production. Similarly, Birkedal *et al.* (2014) proposed that kinetic reaction modeling was necessary on core scale simulations, both in terms of accuracy and computational time after conducting depressurization experiments and simulations on the core sample (Bentheim sandstone) inside a high pressure cell with a volume of  $171 \text{ cm}^3$ . For example, Li *et al.* (2014b) conducted similar study for 117.8 L cylindrical high pressure reactor (PHS) and compared the experimental results and numerical results of kinetic and equilibrium models. They proved that their high pressure reactor can be used to simulate real gas hydrate conditions because the comparisons of the kinetic and equilibrium models with the depressurization experimental data indicate that the kinetic limitations are very small in the PHS (Li *et al.*, 2014; Li *et al.*, 2014b). For this reason, large high pressure reactors are preferred in the gas production experiments from gas hydrates and some of those are shown in Table 7-8.

**Table 7-8:** High pressure reactors used for gas hydrate studies recently

Source	Type of High Pressure Reactor	Volume, L	Dimensions
Cheng <i>et al.</i> (2015)	Cylindrical	5.0	30 cm in diameter 7 cm in height 20 MPa
Feng <i>et al.</i> (2015), Feng <i>et al.</i> (2017)	Cubic	5.832	18 cm side length 30 MPa
Yang <i>et al.</i> (2012)	Cylindrical	7.0	30 cm in diameter 10 cm in height 16 MPa
Fitzgerald and Castaldi (2013)	Cylindrical	59.3	34.8 cm in diameter 91.4 cm in height 13.8 MPa
Li <i>et al.</i> (2014), Li <i>et al.</i> (2014b), Wang <i>et al.</i> (2016), Feng <i>et al.</i> (2017)	Cylindrical	117.8	50 cm in diameter 60 cm in height 30 MPa
Schicks <i>et al.</i> (2011b), Heeschen <i>et al.</i> (2016)	Cylindrical	425	60 cm in diameter 150 cm in length 25 MPa
Konno <i>et al.</i> (2014)	Cylindrical	1710	100 cm in diameter 217.8 cm in length

By considering all factors mentioned above and also the Black Sea conditions, a high pressure reactor (METU Reactor) was designed in this study. As seen in Table 7-8, most of currently available high pressure reactors are cylindrical except one cubic. Gas hydrates form at high pressures, especially if hydrate forming temperature increases, pressure increases. The resistance to high pressure is higher in cylindrical reactors compared to cubic reactors. Therefore, in this study, the cylindrical high pressure reactor was preferred.

Large size high pressure reactors are better for the representation of real gas hydrate fields. However, with extremely large size high pressure reactors, there are some certain problems such as:

- Long time of hydrate formation in the sediments (e.g. 10 hours in 288 mL reactor (Zhao *et al.*, 2016); 1 month for large high pressure reactor in 1710 L HIGUMA (Li *et al.*, 2012; Konno *et al.*, 2014)); 3 months for 90 % gas hydrate in sediments inside LARS (210 L sample) (Heeschen *et al.*, 2016)
- Long time of production experiments
- High numbers of personnels needed to deal with the experiment
- High amount of gas consumption (See Table 7-9)
- Additional costs of gas flow meter, pump, etc. with high capacity
- Safety risks

In HIGUMA reactor (1710 L), hydrate formation in the sediments took almost 30 days (Konno *et al.*, 2014). Therefore, when considering the economy, personnel number, additional costs of high pressure reactors, in this study, we tried to design the optimum high pressure reactor with low cost as much as possible and capability of representing real field gas hydrate conditions. The cold room is an important experimental equipment to keep temperature constant at desired temperatures. It is a cube with 3 m size. It keeps temperature constant between -5 °C and 25 °C. Therefore, during the size determination of the high pressure reactor, the size of the door of the constant temperature room and other external factors were also considered. Then, a

cylindrical high pressure reactor with almost 30 cm inner height and 30 cm inner diameter with an inner volume of ~21.64 L was selected.

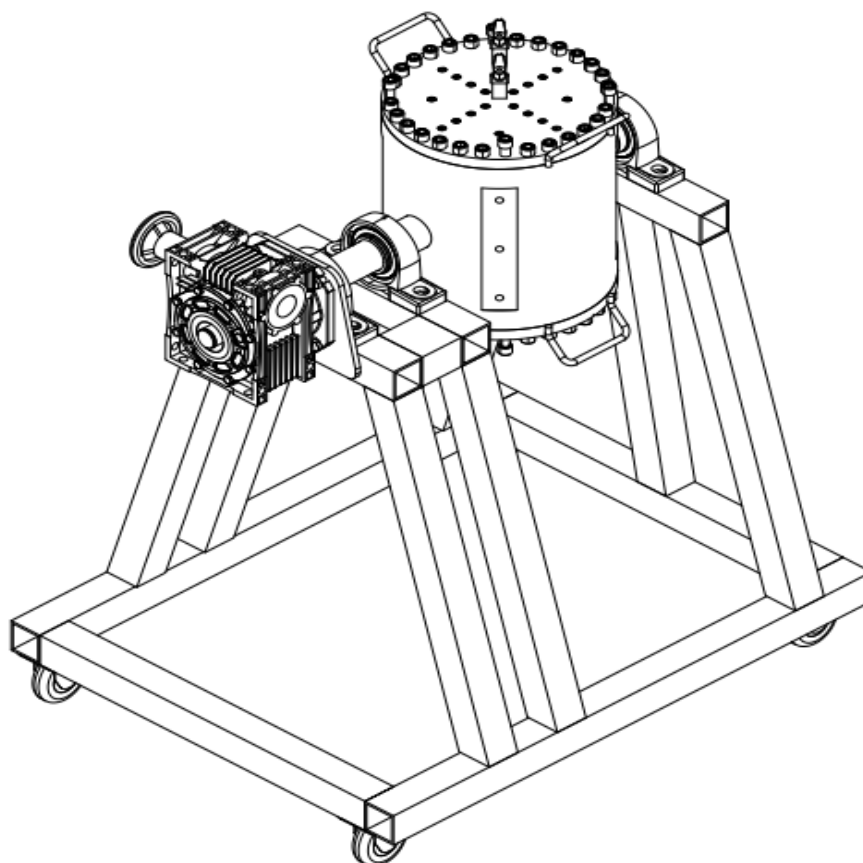


**Figure 7-14:** General view of the high pressure reactor (METU reactor)

As seen in Figure 7-14, the high pressure reactor (METU reactor) is hung on the carrying unit. There is also a rotating unit which can be used to rotate METU reactor. After making necessary connections of the thermowells and thermocouples from the top part of METU reactor, it is planned to rotate METU reactor 180°. Then, the bottom part will be on the top part after the rotation and METU reactor is filled with sediments. When mesh is inserted above the sediments and other necessary connections are completed, gas and water are injected at desired amount. Hence, it is planned to form hydrate in the rotated position by decreasing temperature of the cold room. When the target hydrate and water saturations are reached in the reactor, METU reactor is rotated to its original position. Finally, hydrate is on the top of the reactor and there is a free gas section below hydrate section when METU reactor is

in its original position. Then, at these conditions, depressurization experiments can be started by producing gas from free gas section. Generally, it is thought that gas should be produced from free gas section of Class 1 hydrate reservoirs so when pressure decreases in free gas section, dissociated gas and water flow through free gas zone. By using METU reactor with mesh, it is aimed to investigate this characteristic behavior of gas production from Class 1 hydrate reservoirs.

**Table 7-9:** Comparison of HIGUMA and METU reactor

Reactor	Diameter, cm	Length, cm	Volume of Empty Cell, L	Weight of Empty Cell, kg	Sand Weight, kg	Water Weight, kg	Gas Volume at STP, L
Higuma	100	217.8	1710	1200	1300	632.83	54830.4
METU	30.63	30.0	21.64	180	32.7	8.0	693.9

In order to compare the amount of water, sand, and gas needed to satisfy the following conditions,  $S_h$ : 39 %;  $S_w$ : 55 %;  $S_g$ : 6 % and porosity: 43 % at 10 MPa and 10 °C, these parameters were calculated by using SM.m code (code written in this study to calculate amount of gas and water needed for target saturation and explained in the following sections) for HIGUMA reactor (Konno *et al.*, 2014) and METU reactor (designed in this study in Figure 7-14). As seen in Table 7-9, the amount of sand, water and gas needed to satisfy desired conditions ( $S_h$ : 39 %;  $S_w$ : 55 %;  $S_g$ : 6 % and porosity: 43 %) are very high for HIGUMA reactor compared to METU reactor. Dealing with large systems as HIGUMA reactor is expensive and time consuming especially for universities. Therefore, in this study, it was aimed to design METU reactor with optimum volume. However, before the final decision, in order to understand whether this reactor is capable to represent the field conditions or not, the numerical simulations with HydrateResSim were conducted for different scenarios. According to the results, the 21.64 L high pressure reactor (METU reactor) designed

in this study can be used to investigate flow-controlled gas production mechanism from gas hydrate reservoirs by different production methods. Innosys Innovative Systems in Turkey drew and designed METU reactor in terms of mechanical concepts such as mechanical design, resistance to pressure, rust, etc. (Innosys, 2016). The general view of the high pressure reactor (METU reactor) is shown in Figure 7-14.

In order to check whether 21.64 L high pressure reactor in this study has dissociation controlled or flow-controlled behavior during depressurization experiments, several numerical simulations were run by using the equilibrium and kinetic model option of HydrateResSim numerical simulator. In Chapter 3, it was proposed that there is a huge potential of Class 1 hydrates in the Black Sea. Class 1 hydrates consist of hydrate in the upper section and free gas in the lower section. The saturations in the upper (hydrate) section are quite important. The upper section might consist of hydrate and free gas (Class 1G) or hydrate and free water (Class 1W). According to Alp *et al.* (2007) and Moridis *et al.* (2013), Class 1G is the most desired type of hydrate reservoirs in nature for effective gas production. Vassilev and Dimitrov (2003) stated that hydrate content in the Black Sea sediments can increase up to 45-65 % at the base of hydrate stability zone. Therefore, in the simulation study, the hydrate saturation in the upper section was selected as 50 %. As seen in Figure 3-3 and according to Klauda and Sandler (2003) and Vassilev (2006), the average temperature of the Black Sea sediments at seafloor is 9°C. It is expected that gas hydrates in the Black Sea might have higher reservoir temperatures in deeper parts below seafloor because with depth, the temperature of sediments increases by geothermal gradient. However, generally as an average temperature in the Black Sea hydrate studies, 9°C is selected. Therefore, this temperature was chosen in the simulation study. Hydrate equilibrium pressure at 9 °C for CH<sub>4</sub> is around 6.47 MPa. The conditions of the Class 1 reservoirs are close to hydrate equilibrium points. In Table 7-10, the conditions chosen for the numerical simulations of gas production from the high pressure reactor in this study by depressurization are shown.

**Table 7-10:** The conditions for the simulations of METU reactor

Simulation Set	Reactor Design	Phases	Saturations	Temperature and Pressure	Models used
1	Whole Reactor	Hydrate + Gas	Sh: 0.50; Sg: 0.50	T: 9 °C P: 6.46 MPa	Equilibrium Kinetic
2	Whole Reactor	Hydrate + Water	Sh: 0.50; Saq: 0.50	T: 9 °C P: 6.50 MPa	Equilibrium Kinetic
3	Reactor separated by mesh	Hydrate + Gas	Sh: 0.50; Sg: 0.50	T: 9 °C P: 6.46 MPa	Equilibrium
4	Reactor separated by mesh	Hydrate + Water	Sh: 0.50; Saq: 0.50	T: 9 °C P: 6.50 MPa	Equilibrium

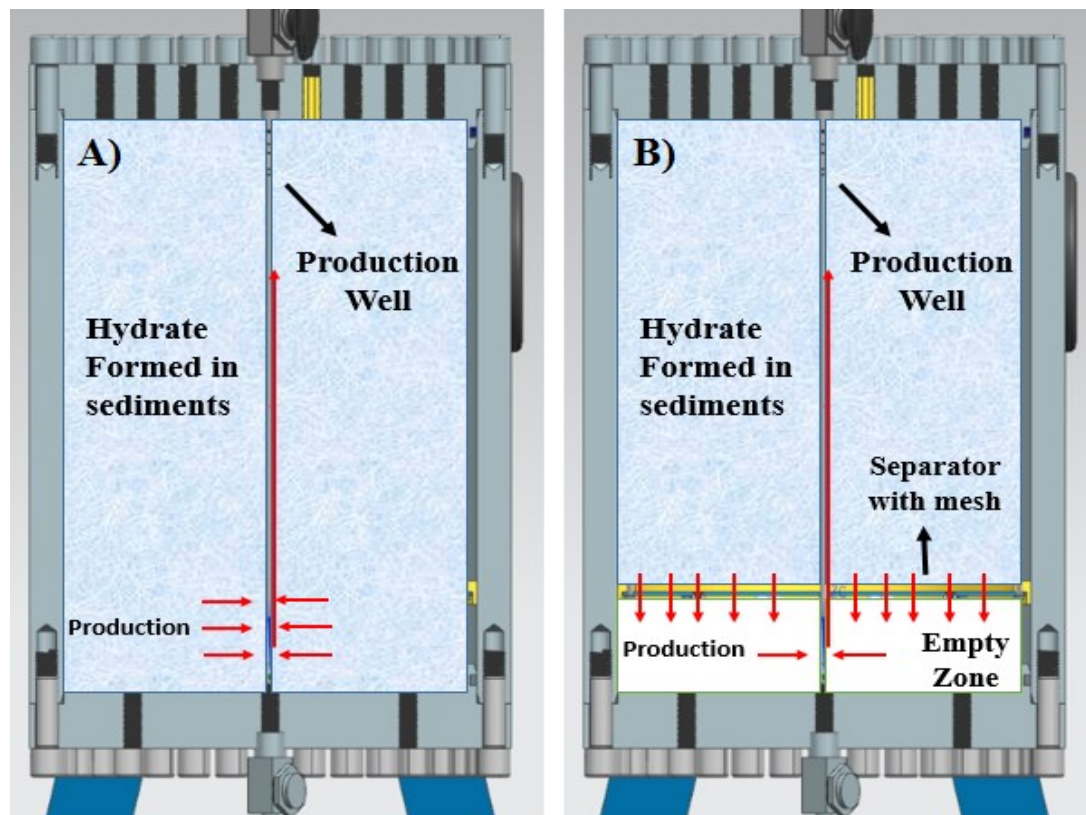


**Figure 7-15:** Schematics describing gas production behavior in METU reactor for A) Simulation set 1 and 2 B) Simulation set 3 and set 4

During the design of the high pressure reactor, as seen in Figure 7-15-B, 5 cm above the bottom of the high pressure reactor, the separator with 100 mesh (149 microns) is put and it is portable. It can be used to separate gas hydrate zone and free gas zone to mimic Class 1 hydrate reservoir as seen in Figure 7-15-B. Moreover, it is useful to avoid the blocking of the lines (pipes) by newly formed ice or hydrate during especially depressurization experiments because gas is produced through the free (empty) zone then through the well (Figure 7-15-B). In the high pressure reactors similar to the one in the Figure 7-15-A, during the gas production, the pipes were plugged by hydrate and or ice formed in the experimental studies of Ors (2012), Abbasov (2014), Wang *et al.* (2016) and the laboratory scale numerical simulation study of Merey and Sinayuc (2015) .

In order to see the effect of using the separator, the numerical simulations were run with and without separator as seen in Table 7-10 by using HydrateResSim numerical simulator. HydrateResSim was written in Fortran 95/2003. To run the source code of HydrateResSim, Simply Fortran (2.23 version) was used in all simulations in this study. Moreover, while preparing the input file of HydrateResSim, grids are rearranged if there are boundaries or constant pressure and or temperature grids. When the output file is obtained, it is needed to rearrange output data to plot output results such as pressure, temperature, gas hydrate ( $S_h$ ) saturation distribution, aqueous ( $S_{aq}$ ) saturation distribution and gas ( $S_g$ ) saturation distribution. Therefore, this procedure takes quite long time especially when grid number is high. In this study, a Matlab code was written to solve this problem. This code takes the output data of numerical simulations in HydrateResSim and automatically rearranges output data and draws necessary figures by using mesh and plot coordinates of the model.

In simulation set 1 and set 2, the high pressure reactor is assumed to be fully filled by gas hydrate containing  $S_h$ : 0.5 and  $S_g$ : 0.5 (Class 1G) and  $S_h$  and  $S_{aq}$ : 0.5 (Class 1W) and depressurization starts from the well connected to the bottom of the reactor. However, for simulation set 3 and set 4, the high pressure reactor is separated by separator with mesh. In the upper section, gas hydrate forms and it contains  $S_h$ : 0.5 and  $S_g$ : 0.5 (Class 1G) and  $S_h$  and  $S_{aq}$ : 0.5 (Class 1W) for simulation set 3 and set 4

respectively. In simulation set 3, firstly, gas is produced from the empty zone, and pressure is decreased below gas hydrate equilibrium conditions in the hydrate section. Gas evolved from hydrate dissociation flows through the empty zone and then through the well.

The details of the conditions in the high pressure reactor for simulation sets 1, 2, 3 and 4 are shown in Table 7-10 and Table 7-11. All of the parameters such as rock grain density, wet thermal conductivity, permeability and porosity for the Black sea conditions were obtained from the study of Vassilev (2006). The steel used for METU reactor, US360 and it is stainless (specific heat: 502 J/kg. K). The property of US360 steel is also included in Table 7-11.

**Table 7-11:** Simulation parameters for METU reactor at the Black Sea conditions

<i><b>Simulations</b></i>	<i><b>1</b></i>	<i><b>2</b></i>	<i><b>3</b></i>	<i><b>4</b></i>
<i><b>Radius of the Cell</b></i>	15 cm	15 cm	15 cm	15 cm
<i><b>Length of the Cell</b></i>	30 cm	30 cm	30 cm	30 cm
<i><b>Grids along r direction</b></i>	28	28	28	28
<i><b>Grids along z direction</b></i>	62	62	62	62
<i><b>Porosity</b></i>	0.50	0.50	0.50	0.50
<i><b>Permeability</b></i>	9.87E-13 m <sup>2</sup> (1 D)	9.87E-13 m <sup>2</sup> (1 D)	9.87E-13 m <sup>2</sup> (1 D)	9.87E-13 m <sup>2</sup> (1 D)
<i><b>Rock Grain Density</b></i>	2700 kg/m <sup>3</sup>	2700 kg/m <sup>3</sup>	2700 kg/m <sup>3</sup>	2700 kg/m <sup>3</sup>
<i><b>Wet Thermal Conductivity</b></i>	3.4 W/(m.K)	3.4 W/(m.K)	3.4 W/(m.K)	3.4 W/(m.K)
<i><b>Steel Thermal Conductivity</b></i>	16.2 W/(m.K)	16.2 W/(m.K)	16.2 W/(m.K)	16.2 W/(m.K)
<i><b>Capillary Pressure Parameters- van Genuchten</b></i>	S <sub>rw</sub> : 0.240 n: 1.84	S <sub>rw</sub> : 0.240 n: 1.84	S <sub>rw</sub> : 0.240 n: 1.84	S <sub>rw</sub> : 0.240 n: 1.84
<i><b>Relative Permeability Parameters- Modified Stone</b></i>	S <sub>rw</sub> : 0.250 S <sub>rg</sub> : 0.02 n: 3.0	S <sub>rw</sub> : 0.250 S <sub>rg</sub> : 0.02 n: 3.0	S <sub>rw</sub> : 0.250 S <sub>rg</sub> : 0.02 n: 3.0	S <sub>rw</sub> : 0.250 S <sub>rg</sub> : 0.02 n: 3.0

In Figure 7-16, the initial gas hydrate saturations and cartesian grids (28 grid along r direction and 62 grids along z direction) in the half of cylindrical high pressure reactor (METU reactor) for simulation sets 1, 2, 3 and 4 are shown. The blue section in Figure 7-16-A has zero hydrate concentration because it is the wall of the reactor. Figure 7-16-B has also zero hydrate concentrations as in Figure 7-16-A. However, in the free zone (or empty zone), there is no gas hydrate and initially only filled with free gas. Red arrows show the grid where the depressurization starts via production well.

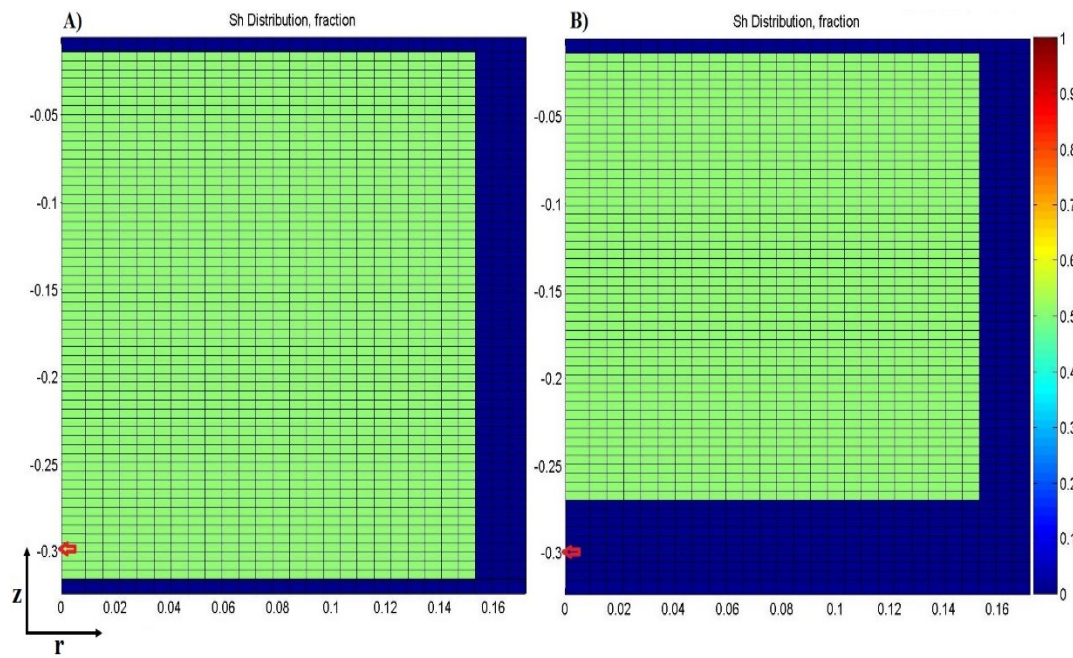


**Figure 7-16:** Gas hydrate saturation with grids in the half of the high pressure cylindrical reactor A) for simulation set 1 and set 2 B) for simulation set 3 and set 4

Both kinetic and equilibrium model were run by HydrateResSim for simulation sets 1 and 2 and the results were compared. In the kinetic model, the data of intrinsic hydrate reaction constant ( $K_o$ ) and hydrate activation energy ( $\Delta E_a$ ) are needed. However, these data for the Black Sea sediments are not available because there is no study and effort on this and also gas hydrate samples should be taken from the Black Sea sediments without any disturbance. Therefore, by analogy, the kinetic model parameters ( $K_o$ : 503.75 mol/m<sup>2</sup>. Pa. s and  $\Delta E_a$ : 80.9 kJ/mol) of the study of Li *et al.* (2014b) were used in this study.

In Figure 7-17 and Figure 7-18, the cumulative gas production and water production in simulation set 1 (Hydrate + Gas) by depressurization at different production pressures are shown. In the simulation set 1, the simulations of gas production from the high pressure reactor by depressurization at different pressures for both equilibrium and kinetic model were run by using HydrateResSim simulator. Figure 7-17-B and Figure 7-18-B show the first stages (depressurization stage) of constant pressure depressurization method for gas and water production respectively. Due to depressurization, initially most of water and or gas are produced. When pressure decreases to the depressurization pressure, hydrate dissociation becomes slower because the fugacity difference is very small as in Equation (5-14). This stage is called constant pressure stage or hydrate dissociation stage. As shown in Figure 7-17, Figure 7-18, Figure 7-19 and Figure 7-20, equilibrium and kinetic models are approximately equal to each other. This means that the high pressure reactor designed in this study have capability to investigate the gas production from real gas hydrate reservoirs in the Black Sea conditions by depressurization method.

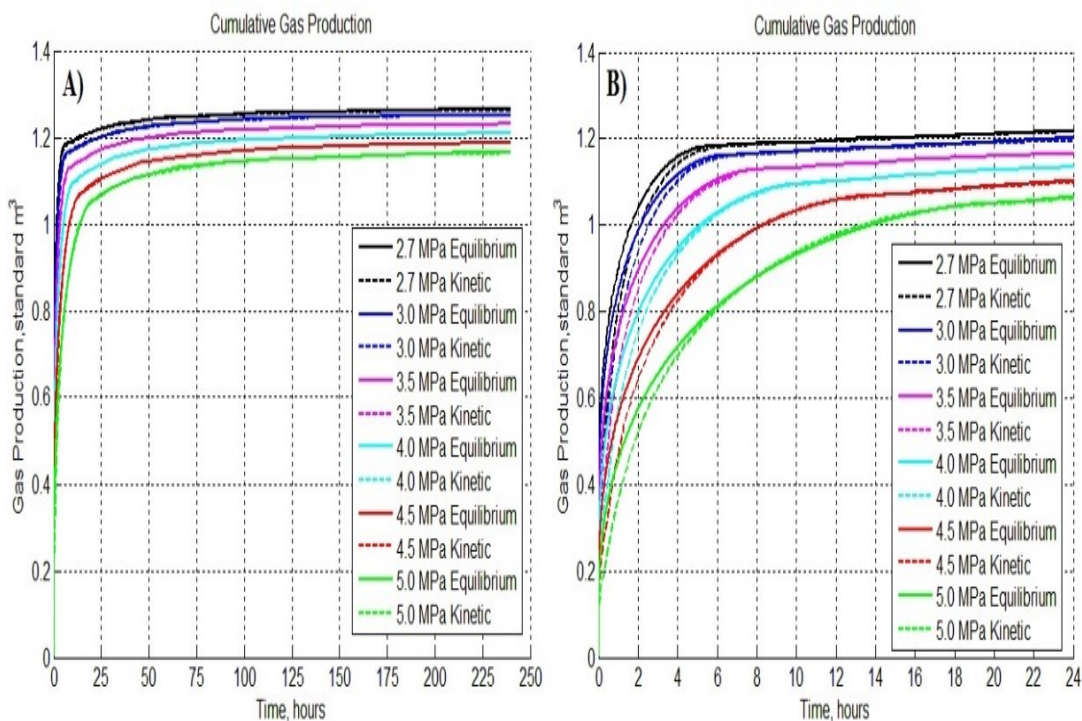


**Figure 7-17:** Cumulative gas production in simulation set 1 A) Depressurization stage + Constant pressure stage B) Depressurization stage

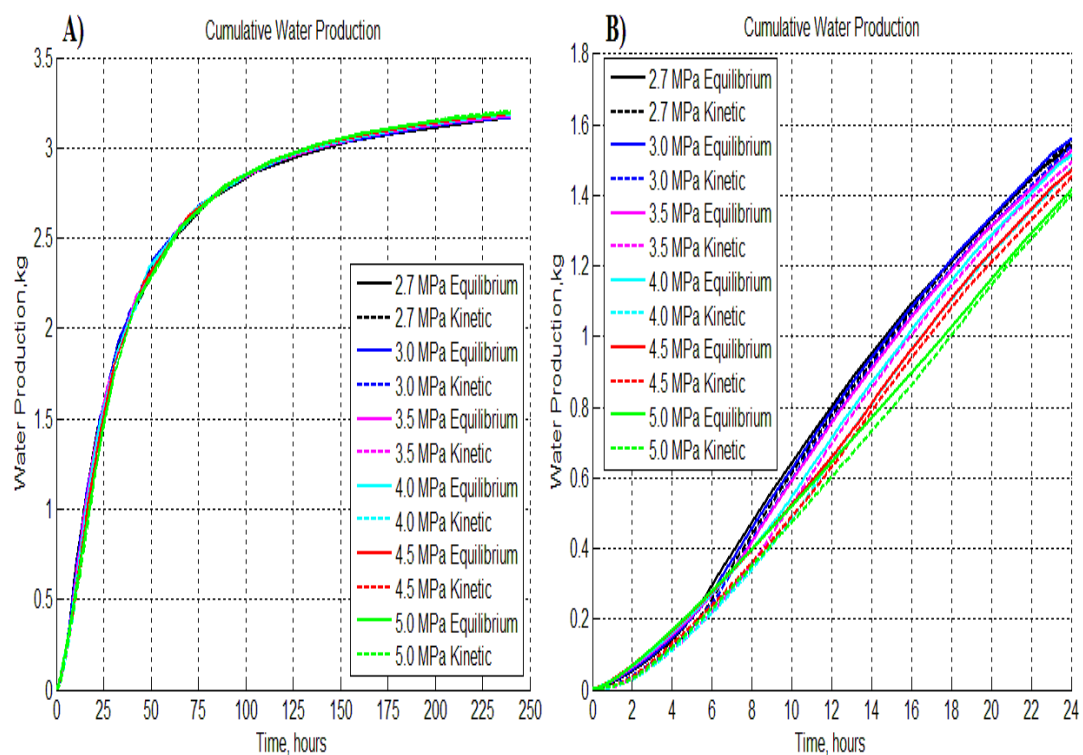


**Figure 7-18:** Cumulative water production in simulation set 1 A) Depressurization stage + Constant pressure stage B) Depressurization stage

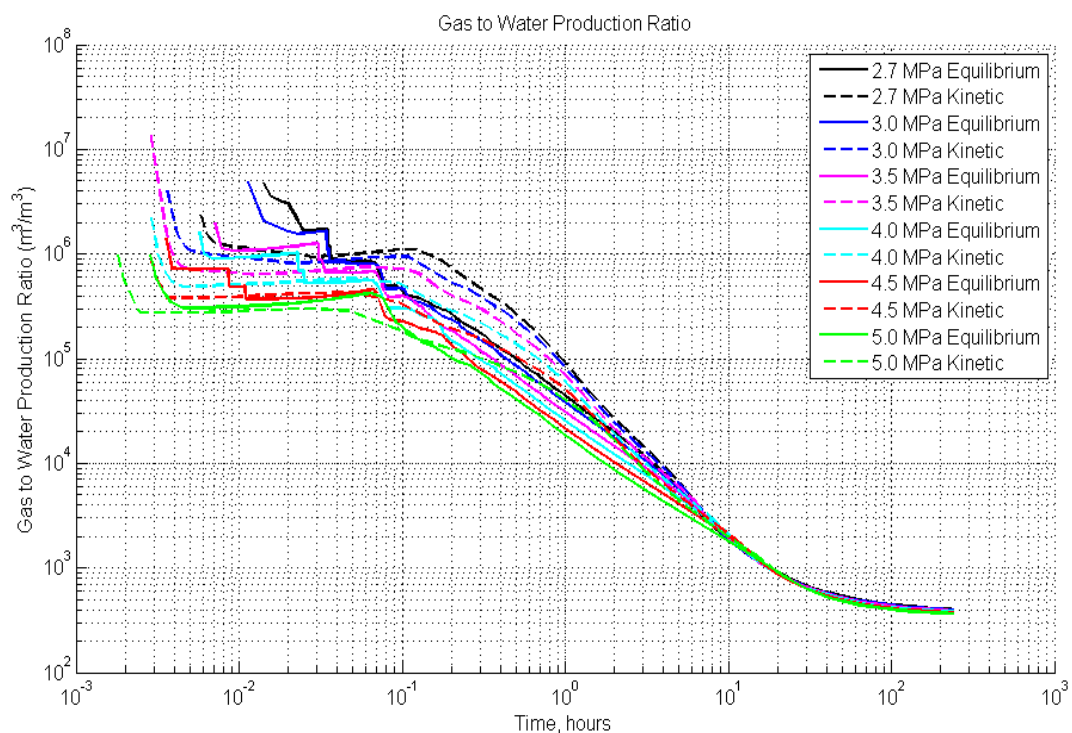


**Figure 7-19:** Gas to water production ratio in simulation set 1

Figure 7-19 indicates gas to water production ratio for simulation set 1. As seen in this figure, initially the lowest gas to water production ratio was obtained at 5 MPa because gas production at 5 MPa is lowest. As gas production continues while applying depressurization method, gas to water production ratio decreases with time. In simulation set 1, initially gas hydrate saturation is 50 % and gas saturation is 50 % as shown in Table 7-10. Therefore, water production starts with hydrate dissociation and gas to water production ratio decreases with time because initially there is no free water in pores in simulation set 1.

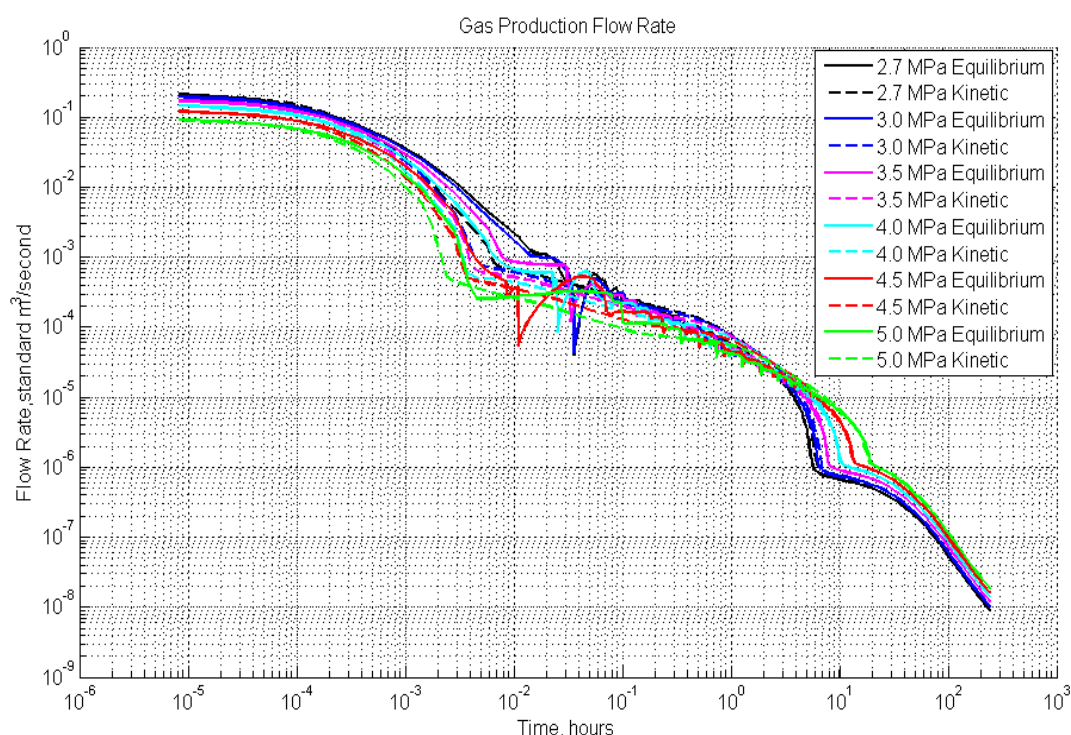
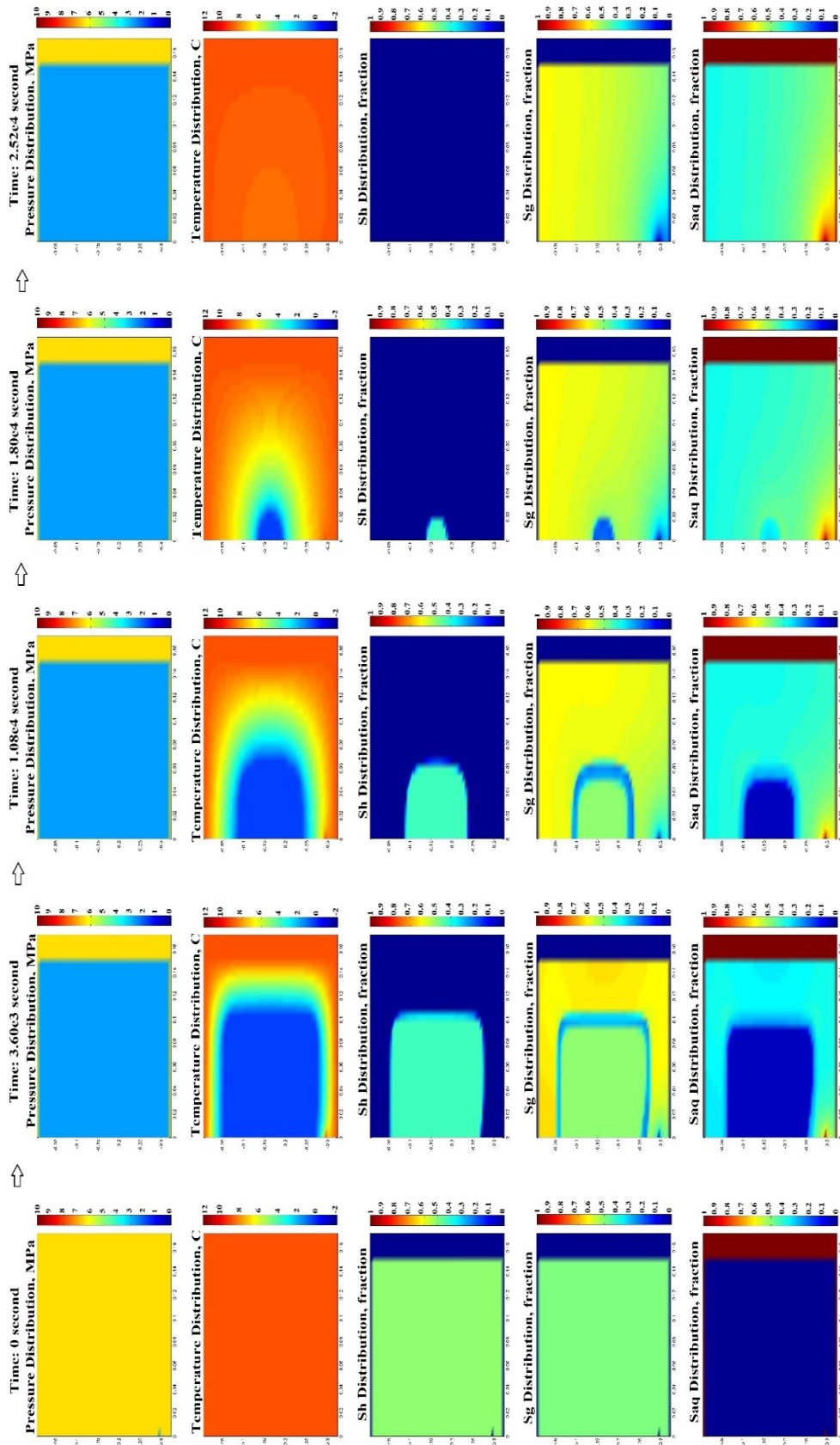


**Figure 7-20:** Gas production rate in simulation set 1

Figure 7-20 shows the gas production flow rate during depressurization at different pressures in the simulation set 1. As seen in Figure 7-20, initially gas production flow rate is quite high because the high pressure reactor includes hydrate and free gas in the pores of sediments. After the peak in the gas flow rate up to  $\sim 0.22 \text{ m}^3/\text{second}$  (13200 L/minute) for the depressurization pressure of 2.7 MPa, gas production flow rate decreases and almost become constant around  $\sim 0.000127 \text{ m}^3/\text{second}$  (7.62 L/min) until production stops. When free gas is produced from the high pressure

reactor, gas is only produced from hydrate dissociation so the gas flow rate becomes very slow. These gas production rates are important for the selection of gas flow meter. As shown in Figure 7-12, produced gas and water mixture flow through the separator and then water is separated. Gas flow meter measures the rate of gas production. Water flow rate is also measured by using weight balance. Therefore, for the selection of gas flow meter range and weight balance range, these simulations are also important before conducting any experiment.

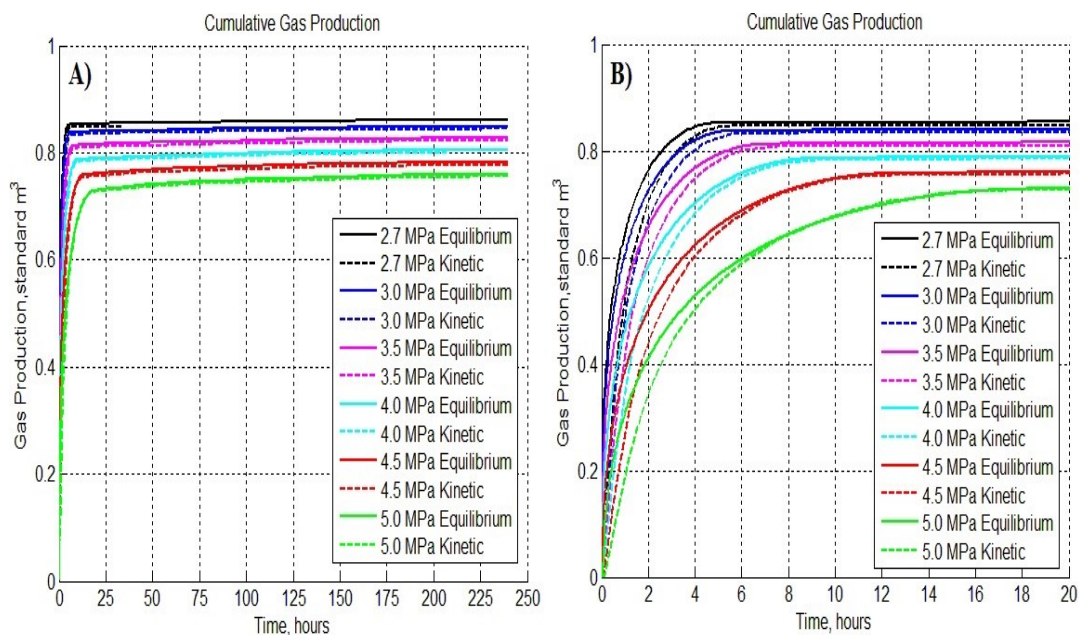
In simulation set 1, the most gas production was obtained at 2.7 MPa compared to other depressurization pressures because a larger depressurization range led to faster dissociation until certain value. Similar results were obtained in the study of Yang *et al.* (2015). As depressurization pressure decreases, gas production increases because fugacity difference in Equation (5-14) becomes larger. Below 2.7 MPa, there is a risk of ice formation in the high pressure reactor due to fast depressurization at 9°C. In some experimental studies such as in the study of Wang *et al.* (2016), the heat released due to ice formation provides additional heats to the system and increases hydrate dissociation rate, but there is also a risk of permeability reduction due to ice formation. Therefore, during the simulations for the design of high pressure reactor, we selected the depressurization pressure outside the region of ice formation because it is a controversial issue and real experimental results are needed. Moreover, in deeper part of the Black Sea sediments, almost there is no risk of ice formation except the risk of ice formations along the wellbores, which is discussed further in the hypothetical gas hydrate reservoir numerical simulations in the Black Sea conditions in this study. Figure 7-21 illustrates the changes in pressure, temperature, hydrate saturation ( $S_h$ ), gas saturation ( $S_g$ ), and aqueous saturation ( $S_{aq}$ ) with time at 2.7 MPa (depressurization pressure). As free gas is produced and pressure is decreased, hydrate dissociation starts. Temperature inside the reactor decreases to approximately 1°C because hydrate dissociation is an endothermic process. The steel wall of the high pressure reactor behaves like constant temperature boundary. When the temperature inside METU reactor decreases due to hydrate dissociation, there are heat fluxes from the walls of the high pressure reactor through hydrate section. Hence, hydrate saturation decreases through the walls of the reactor as seen in Figure 7-21.



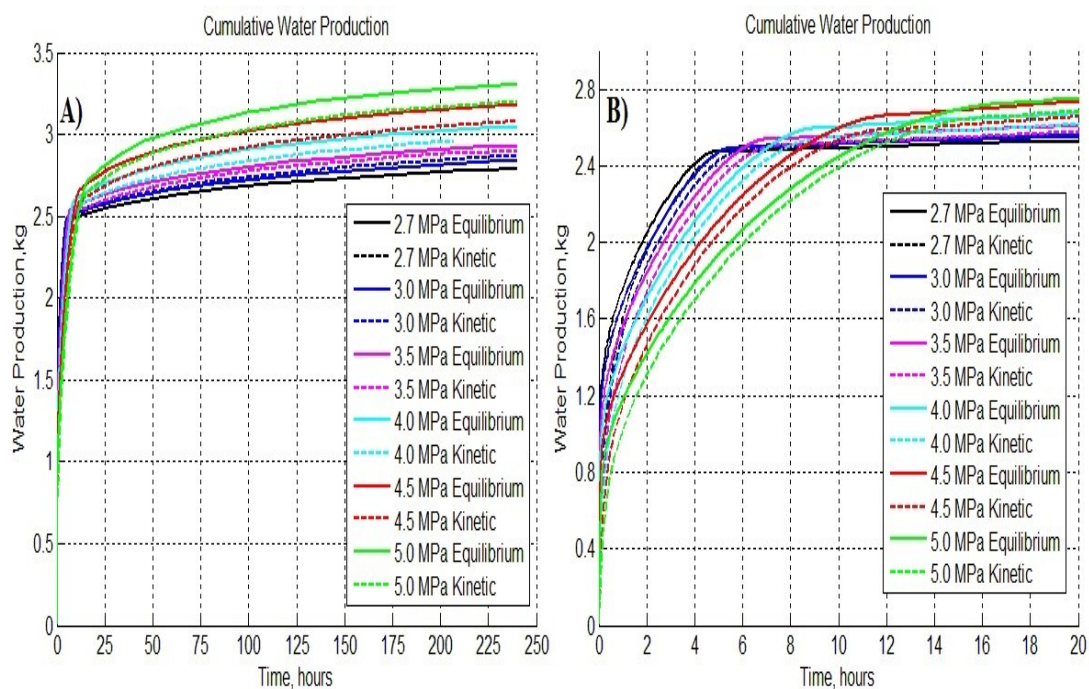
**Figure 7-21:** Pressure, temperature, hydrate saturation, and aqueous saturation in simulation set 1 of the half of the high pressure reactor at 2.7 MPa

Similar observations as in Figure 7-21 were obtained in different simulations studies in high pressure reactors such as Alexiades (2009), Konno *et al.* (2010b), Li *et al.* (2014) and Li *et al.* (2014b). When hydrate dissociation stops, the temperature inside the reactor increases to the initial temperature with the heat flux from the constant temperature boundary in Figure 7-21. In Simulation set 1, initially there are 1.29 standard m<sup>3</sup> of CH<sub>4</sub> and 4.351 kg of water in METU reactor. At 2.7 MPa, approximately 98 % of CH<sub>4</sub> and 72.8 % of water were produced.

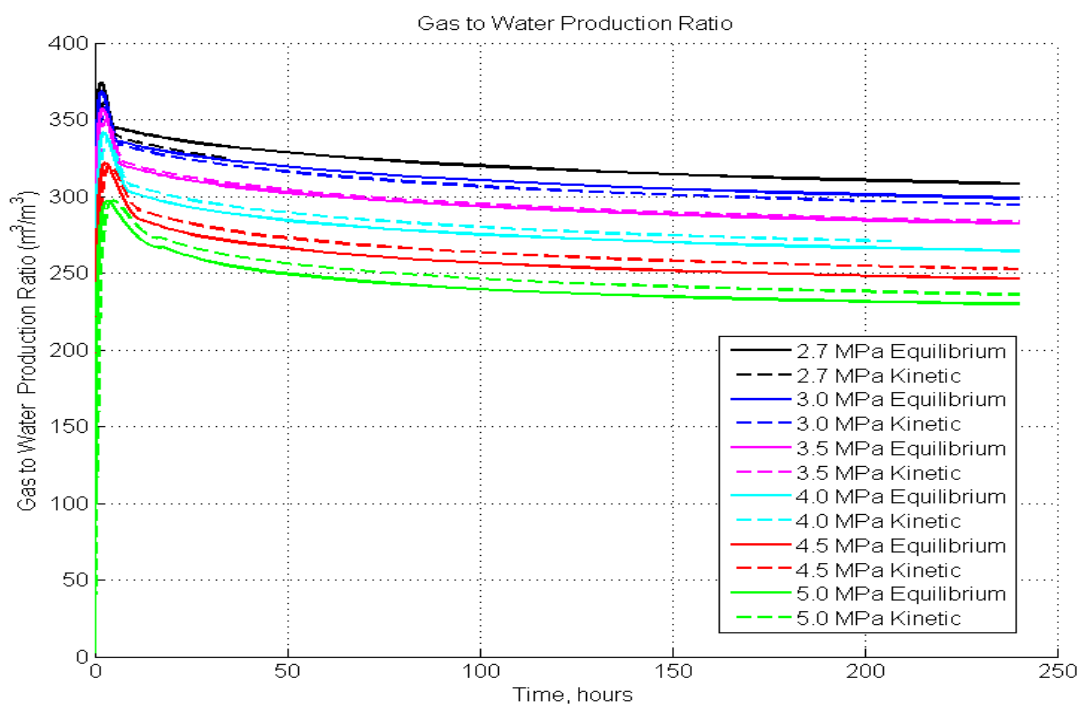
In order to check whether the high pressure reactor (METU reactor) in this study can simulate the real field conditions in Class 1W hydrates experimentally, the simulation set 2 (Hydrate + Water) were run at different depressurization pressures for both kinetic and equilibrium models. Figure 7-22, Figure 7-23, Figure 7-24 and Figure 7-25 were obtained. Similar to the simulation set 1, gas is produced in two stages as depressurization stage and constant pressure stage in Figure 7-22. In this case, initially free water is produced and pressure is decreased by applying depressurization method. Gas production and water production with equilibrium and kinetic models were almost equal to each other for each depressurization pressure. Therefore, the high pressure reactor designed in this study can represent “flow-controlled” field production.



**Figure 7-22:** Cumulative water production in simulation set 2 A) Depressurization stage + Constant pressure stage B) Depressurization stage

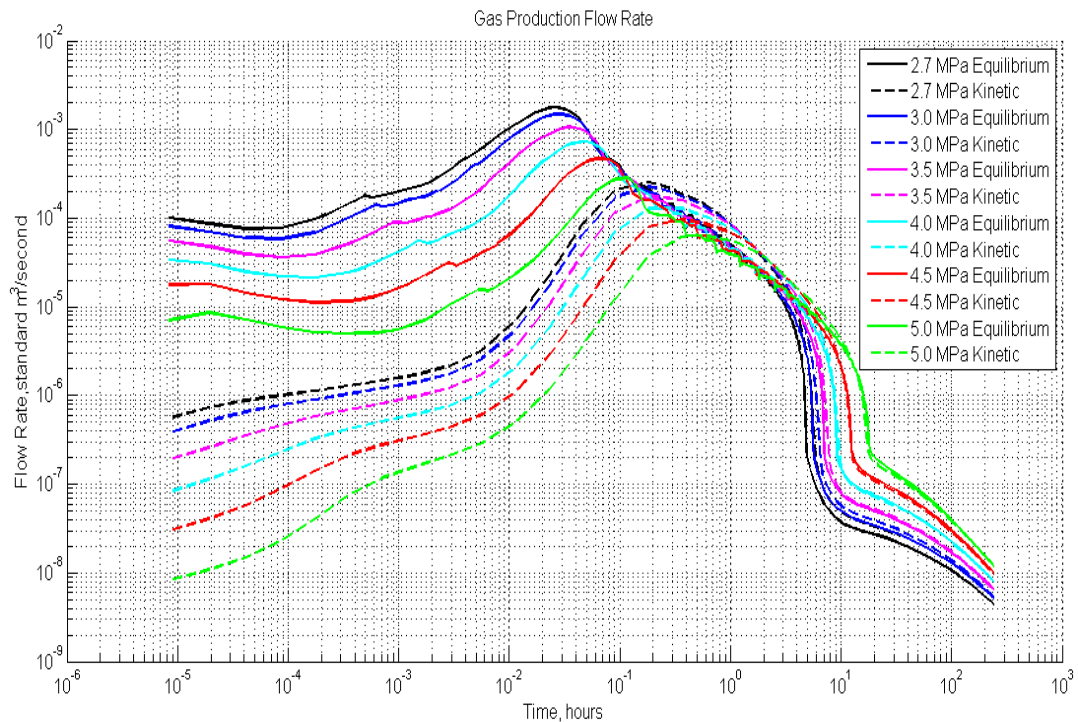


**Figure 7-23:** Cumulative water production in simulation set 2 A) Depressurization Stage + Constant pressure stage B) Depressurization stage



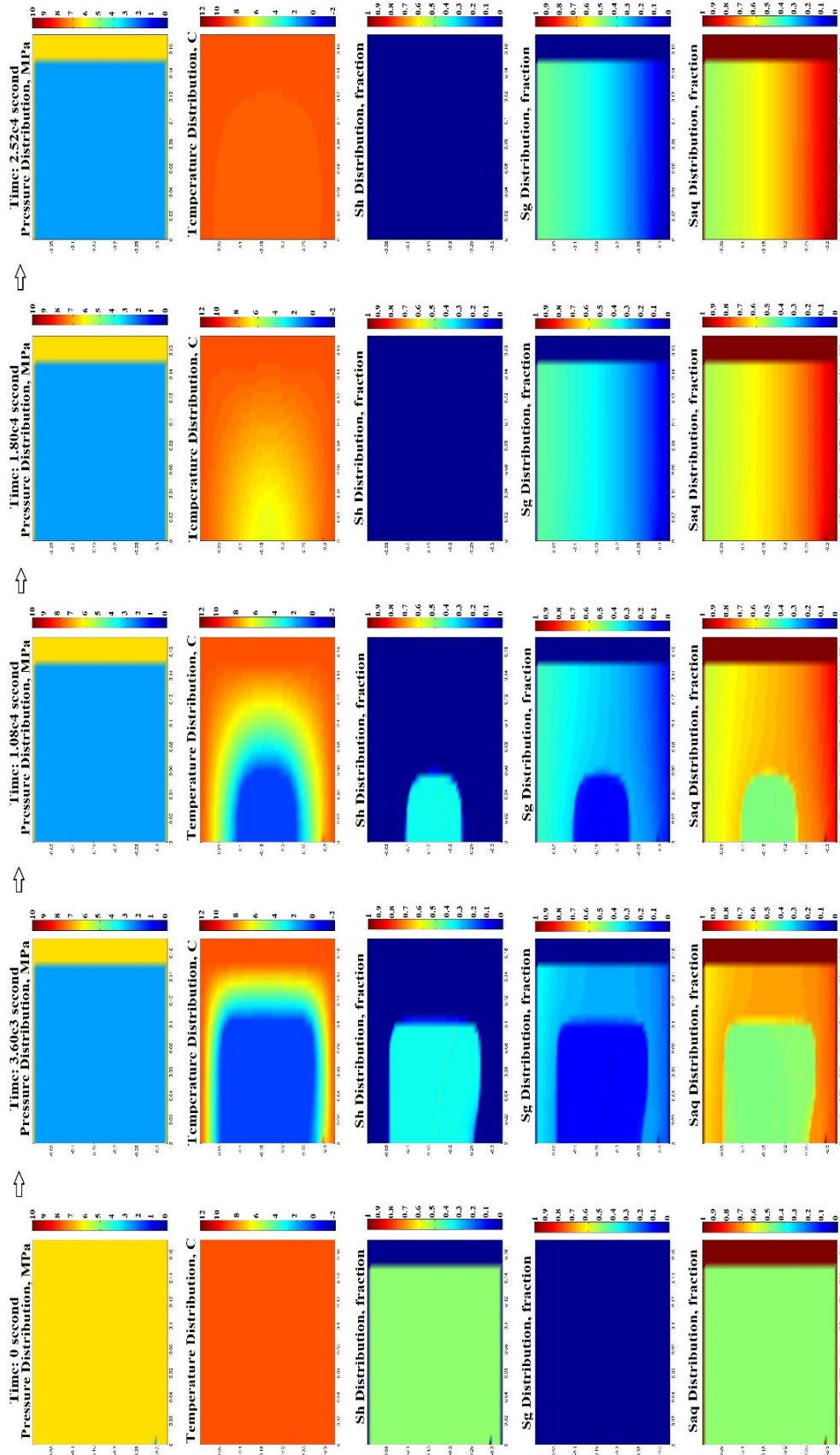
**Figure 7-24:** Gas to water production ratio in simulation set 2

Figure 7-24 indicates gas to water production ratio for simulation set 2. As seen in this figure, initially gas to water production ratio suddenly increases during depressurization because in simulation set 2, hydrate saturation is 50 % and water saturation is 50 % in Table 7-10. Therefore, with gas hydrate dissociation, gas to water production ratio increases then decreases with time because of high amount of water released after gas hydrate dissociation.



**Figure 7-25: Gas production rate in simulation set 2**

Gas production and gas flow rate are the highest at 2.7 MPa depressurization pressure in the simulation set 2 as shown in Figure 7-25. The highest gas production rate is initially around  $0.000176 \text{ m}^3/\text{second}$  (105.6 L/minute). This value is very low compared to the gas flow rate in the simulation set 1 at 2.7 MPa because in the simulation set 1, initially pores are filled with free gas but in the simulation set 2, pores are filled with free water. After the peak in the gas flow rate, the gas flow rate is as an average around  $5 \times 10^{-5} \text{ m}^3/\text{second}$  (3 L/minute).



**Figure 7-26:** Pressure, temperature, hydrate saturation, and aqueous saturation in simulation set 2 of the half of the high pressure reactor at 2.7 MPa

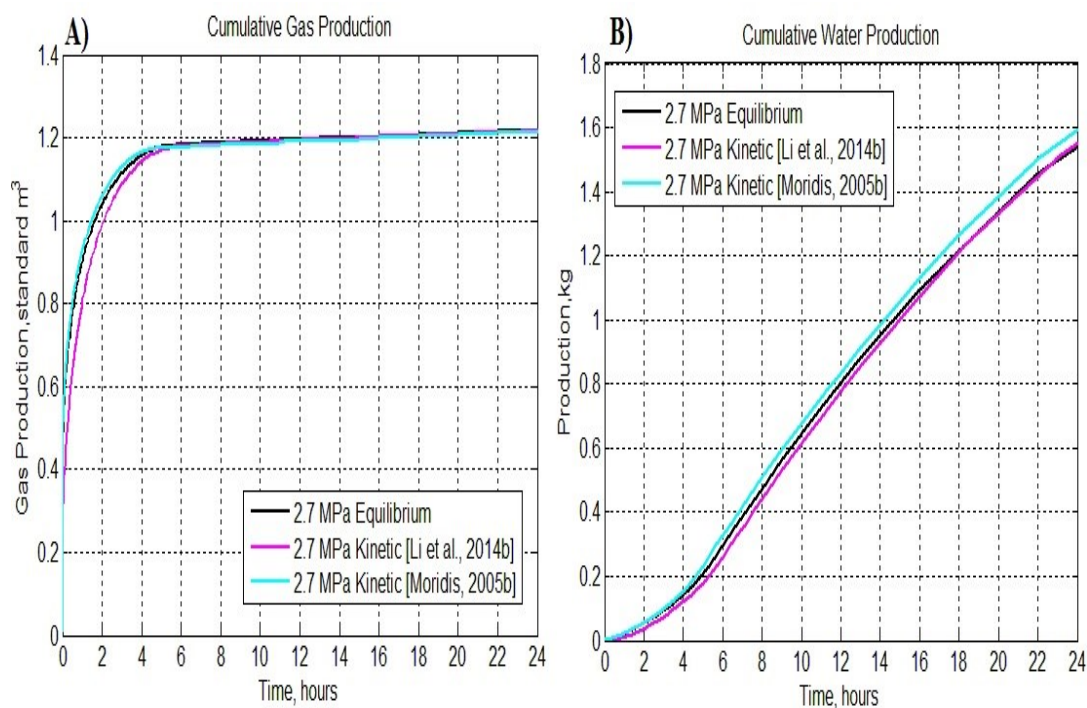
Similar to the simulation set 1 at 2.7 MPa, in this case (see Figure 7-26) also, the wall of the high pressure reactor behaves like a constant temperature boundary. Gas hydrate dissociation starts near the walls of the reactor and gas saturations increase near the walls. Temperature inside the reactor decreases below 2 °C and when gas hydrate completely disappears, the temperature of the reactor turns to its initial value after a certain time. Water saturation decreases also with time. However, as seen in Figure 7-26, water saturation in the bottom of the reactor increases with gas production from gas hydrates and this is due to gravity effect. In Simulation set 2, initially there are 0.9112 standard m<sup>3</sup> of CH<sub>4</sub> and 9.75 kg of water inside METU reactor. At 2.7 MPa, approximately 94.6 % of CH<sub>4</sub> and 28.7 % of water were produced. Water production recovery at 2.7 MPa is low in Simulation set 2 compared to Simulation Set 1 because initially water saturation is 50 % in METU reactor.

For the simulation set 1 and set 2, by analogy, the kinetic parameters of Li *et al.* (2014b) were selected to compare the kinetic model and equilibrium model. Between the equilibrium and kinetic models, there was a good agreement for all depressurization pressures because the large size (~21.64 L) of the high pressure reactor designed in this study (METU reactor) has a capability to represent “flow-controlled mechanism” as in real hydrate field conditions. It was observed that 2.7 MPa is the optimum depressurization pressure among the depressurization pressures for both simulations set 1 and set 2. In order to see the effect of kinetic parameters, different kinetic parameters of Moridis *et al.* (2005b) were used at 2.7 MPa and 3.0 MPa and the values were compared to those of Li *et al.* (2014b). Table 7-12 shows the values of intrinsic hydrate reaction constant ( $K_o$ ) and hydrate activation energy ( $\Delta E_a$ ).

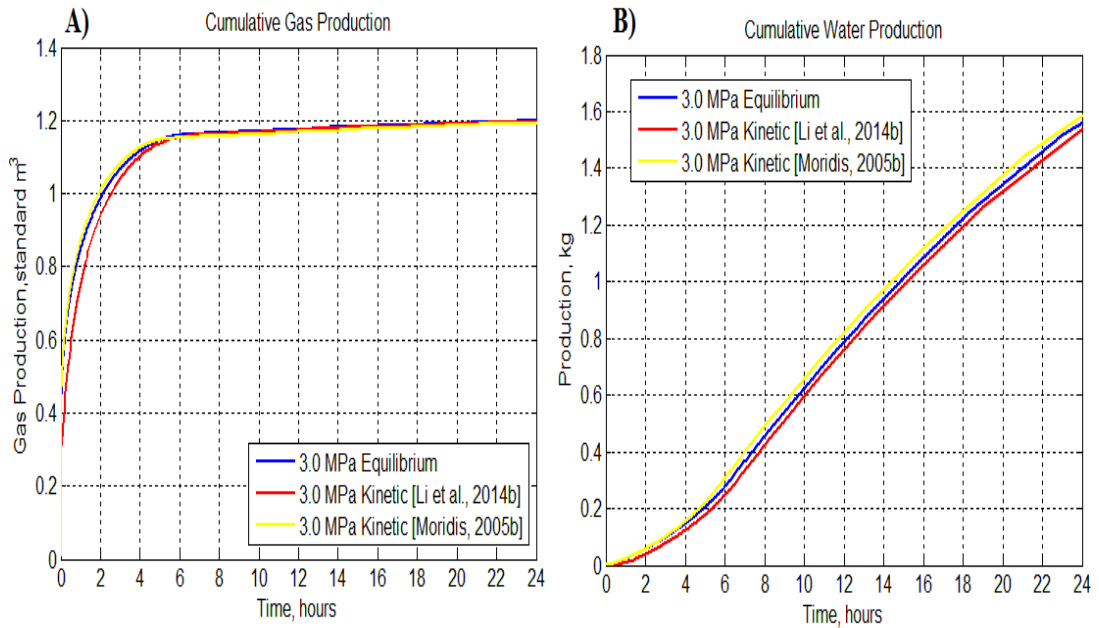
**Table 7-12:** Kinetic parameters chosen for the kinetic model comparison

Source	$K_o$ , mol/m <sup>2</sup> .Pa.s	$\Delta E_a$ , kJ/mol
Li <i>et al.</i> (2014b)	503.75	80.9
Moridis <i>et al.</i> (2005b)	1.78e6	89.7

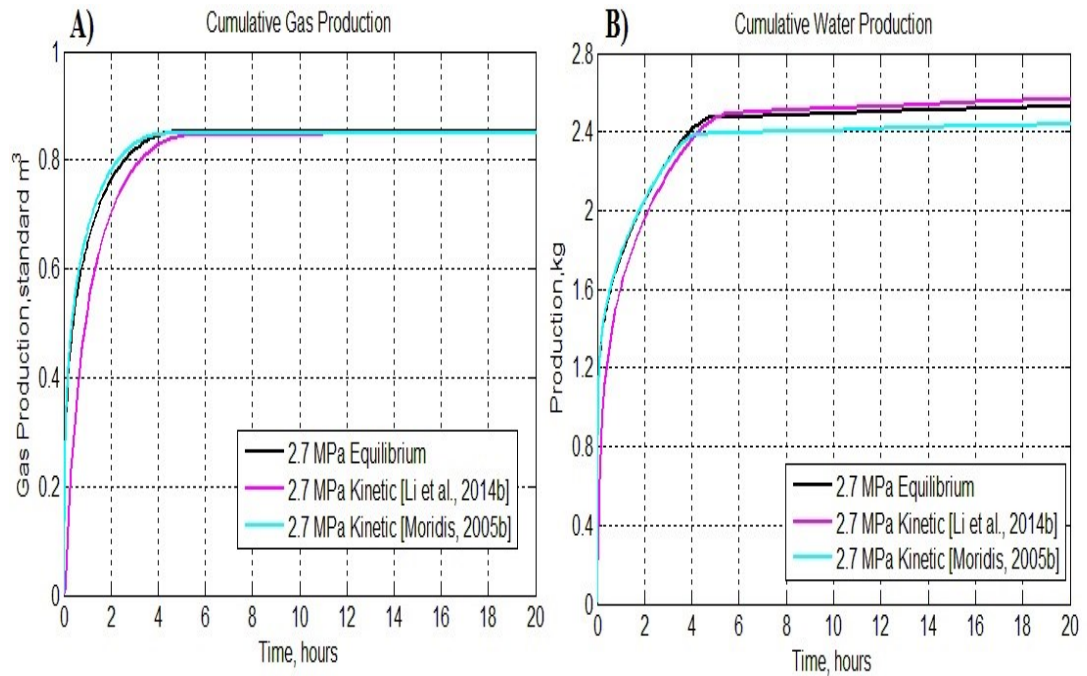
The comparisons of two kinetic models (with the data of Li *et al.*, 2014b and Moridis *et al.*, 2015b) and equilibrium models at 2.7 MPa and 3.0 MPa for both the simulation set 1 and set 2. Figure 7-27, Figure 7-28, Figure 7-29, and Figure 7-30 show the kinetic model comparisons of the cumulative gas production and water production at 2.7 MPa and 3.0 MPa for simulation set 1 and set 2. Although there are little differences between the production data of these two kinetic models, the production curves are very close to each other. Therefore, in the simulations of the high pressure reactor (METU reactor) designed in this study, the equilibrium model can be used because the flow mechanism in this reactor is not expected to be “dissociation-controlled”. Moreover, there is a confusion about the determination and selection of kinetic model parameters in the literature as stated in Chapter 5, so detailed studies on this topic are needed. Temperature, pressure, gas composition, pore size, the composition of sediments, etc. affect the parameters of the kinetic models. Hence, it is crucial to have a large high pressure reactor in which the effects of kinetic parameters on gas and water production are negligible.



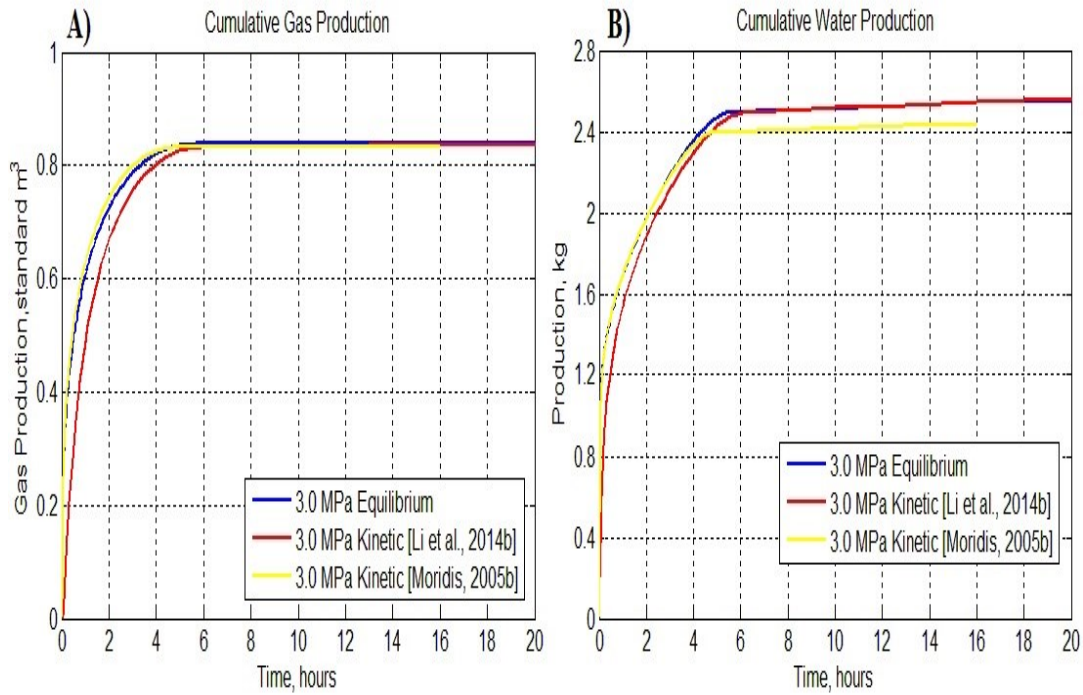
**Figure 7-27:** Equilibrium and kinetic models comparisons in simulation set 1 at the depressurization pressure of 2.7 MPa A) Cumulative gas production B) Cumulative water production



**Figure 7-28:** Equilibrium and kinetic models comparisons in simulation set 1 at the depressurization pressure of 3.0 MPa A) Cumulative gas production B) Cumulative water production

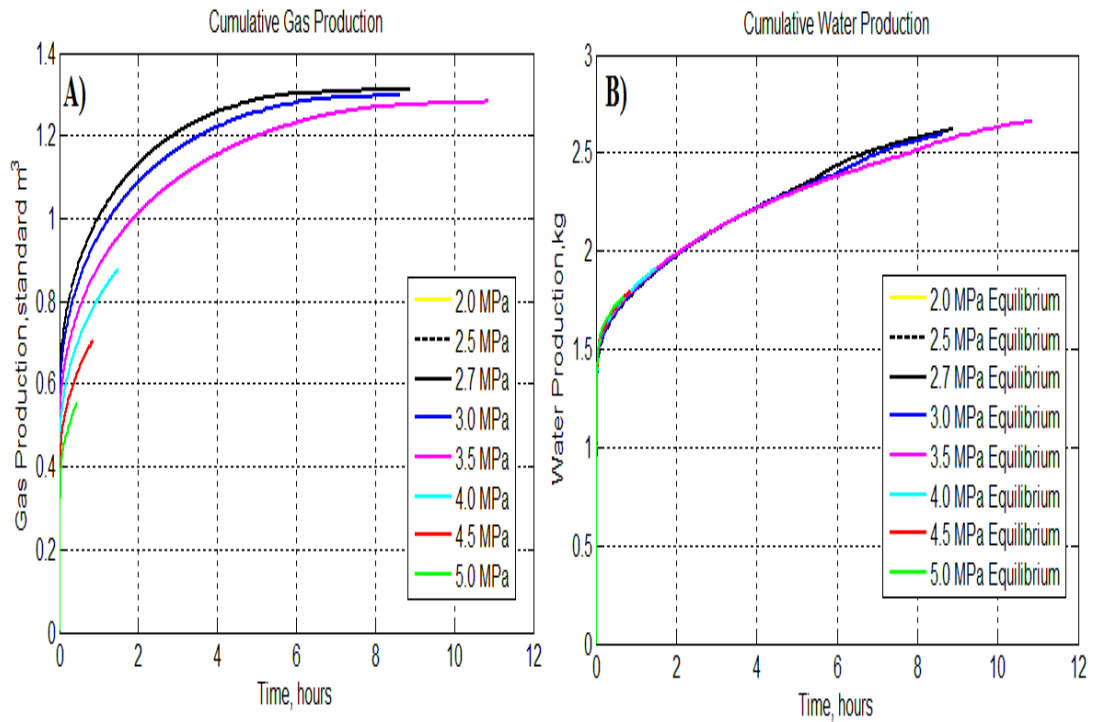


**Figure 7-29:** Equilibrium and kinetic models comparisons in simulation set 2 at the depressurization pressure of 2.7 MPa A) Cumulative gas production B) Cumulative water production



**Figure 7-30:** Equilibrium and kinetic models comparisons in simulation set 2 at the depressurization pressure of 3.0 MPa A) Cumulative gas production B) Cumulative water production

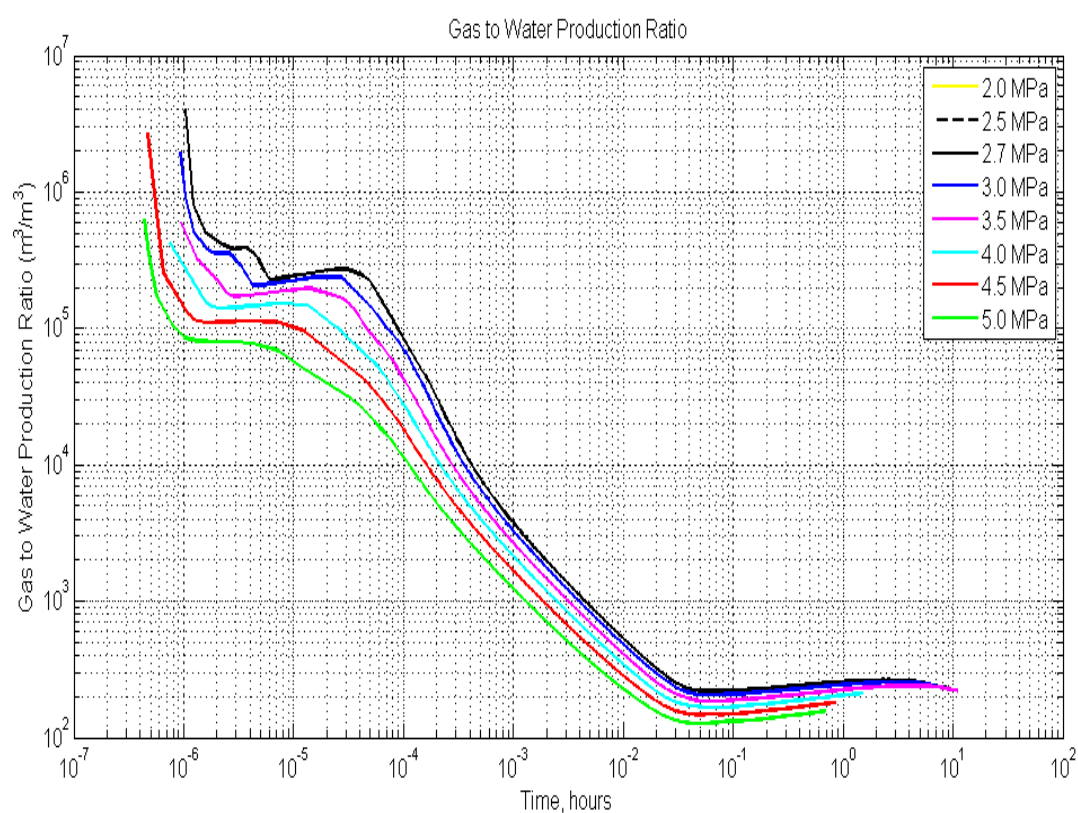
After proving the capability of the high pressure reactor (METU reactor) designed in this study for flow-controlled gas production experiments from gas hydrate reservoirs, a separator with 100 mesh size was designed as seen in Figure 7-15. The separator is portable and it is set 5 cm above the bottom of the reactor. As shown in Figure 7-15-B, when pressure is decreased by producing gas in sediment and free section in the high pressure reactor, gas hydrate dissociates in the hydrate section and gas evolved flows through the sediment free zone. The aim of this reactor with separator is to mimic Class 1 hydrate, horizontal wells and also to avoid any plugging of lines due to hydrate reformation or ice formation.



**Figure 7-31:** A) Cumulative gas production in simulation set 3 B) Cumulative water production in simulation set 3

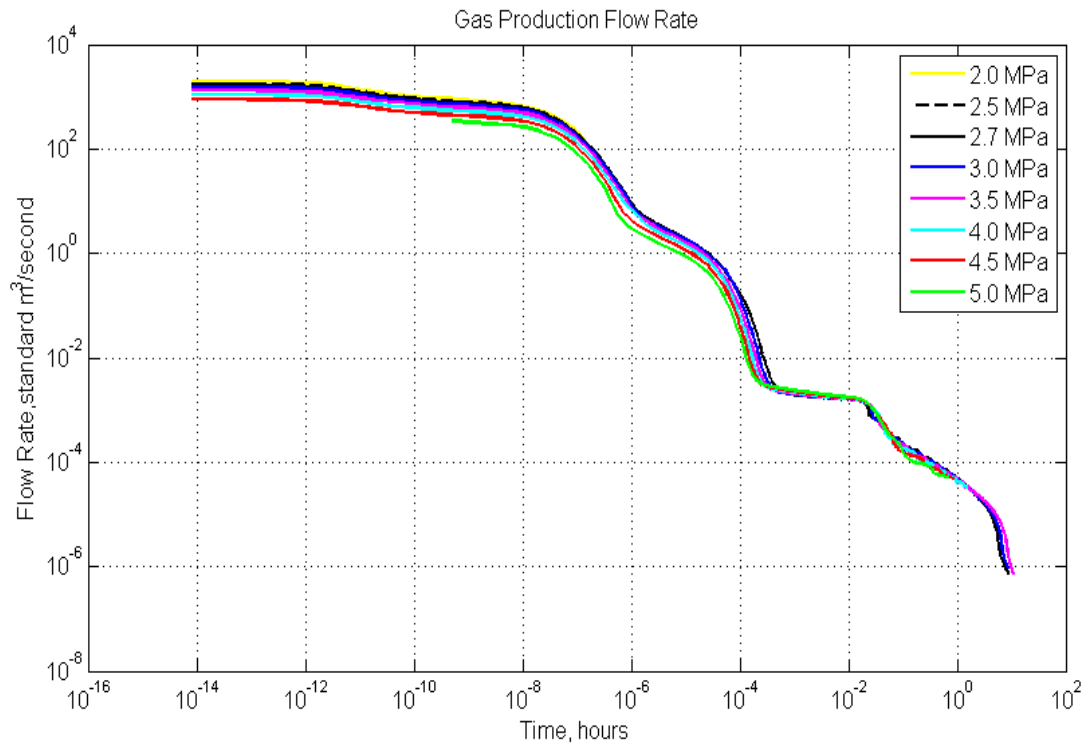
In simulation set 3, it was assumed that the reactor is divided into two sections by separator with 100 mesh as illustrated in Figure 7-15-B. The upper section of the reactor contains hydrate and free gas in pores. Initial conditions of the simulations are listed in Table 7-10. Cumulative gas and water production are shown in Figure 7-31. Below 2.7 MPa, gas production from hydrate section stops due to ice formation and plugging of the pores. As production (depressurization) pressure decreases, gas production increases. Similar to the previous simulations, in this simulation set, gas production rate is very fast at first because free gas in the sediment free zone and pores are produced first. Then, gas production rate becomes slower in the constant pressure zone. The highest gas production is at 2.7 MPa.

Figure 7-32 shows gas to water production ratio for simulation set 3. As seen in this figure, initially gas to water production ratio is quite high due to free gas in lower section of the high pressure reactor (METU reactor) and free gas in the pores of the sediments during depressurization. Table 7-10 indicates that hydrate saturation is 50 % and gas saturation is 50 % in hydrate section of simulation set 3 (see Figure 7-15-B). Gas to water production ratio decreases with time because the high amount of water is released with gas hydrate dissociation.



**Figure 7-32:** Gas to water production ratio in simulation set 3

Due to sudden pressure decrease from 6.5 MPa to desired depressurization pressure, in simulation set 3, at very early time of the production, gas production rate peak is more than 1600 m³/second (9.6e7 L/min) (see Figure 7-33). This is very high. However, when pressure is around the desired depressurization pressure, gas production rate decreases to below 1e-3 m³/second (60 L/min) and gas evolved from hydrate dissociation is the main source of gas production in the constant pressure stage.



**Figure 7-33:** Gas production rate in simulation set 3

In Figure 7-34, the changes of pressure, temperature, gas hydrate saturation ( $S_h$ ), gas saturation ( $S_g$ ) and aqueous saturation ( $S_{aq}$ ) with time at 2.7 MPa are shown. Similar to simulation set 1 and set 2, the walls of the high pressure reactor (METU reactor) behave like a constant temperature boundary and when the temperature inside the reactor decreases with time due to endothermic hydrate dissociation, there is a heat flux from boundaries. In simulation set 3, the high pressure reactor has an empty zone (where there is no sediments). Therefore, water evolved from hydrate dissociation flows through the zone and fills the bottom of the reactor with water with time. In Simulation set 3, initially there are 1.338 standard  $m^3$  of  $CH_4$  and 3.63 kg of water inside METU reactor. At 2.7 MPa, approximately 98.1 % of  $CH_4$  and 35.9 % of water were produced. Water production recovery at 2.7 MPa is low in Simulation set 3 compared to Simulation Set 1 because some of water was collected in the bottom (free section below portable mesh) of METU reactor

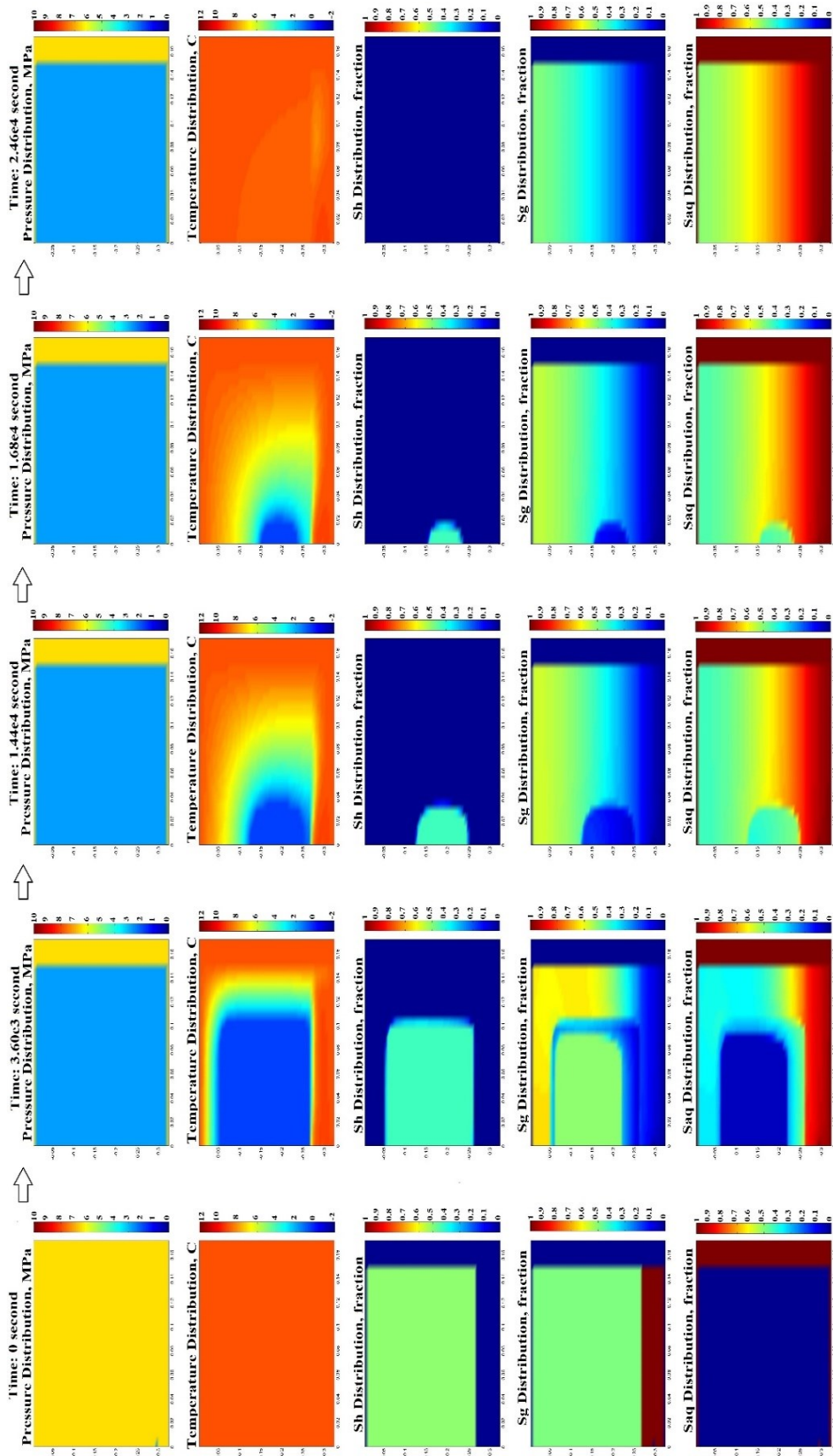


**Figure 7-34:** Pressure, temperature, hydrate saturation, gas saturation, and aqueous saturation in simulation set 3 of the half of the high pressure reactor at 2.7 MPa

The cumulative gas production, water production, gas to water production ratio, and gas flow rate of the simulation set 4 at different depressurization pressures are shown in Figure 7-35, Figure 7-36 and Figure 7-37 respectively.

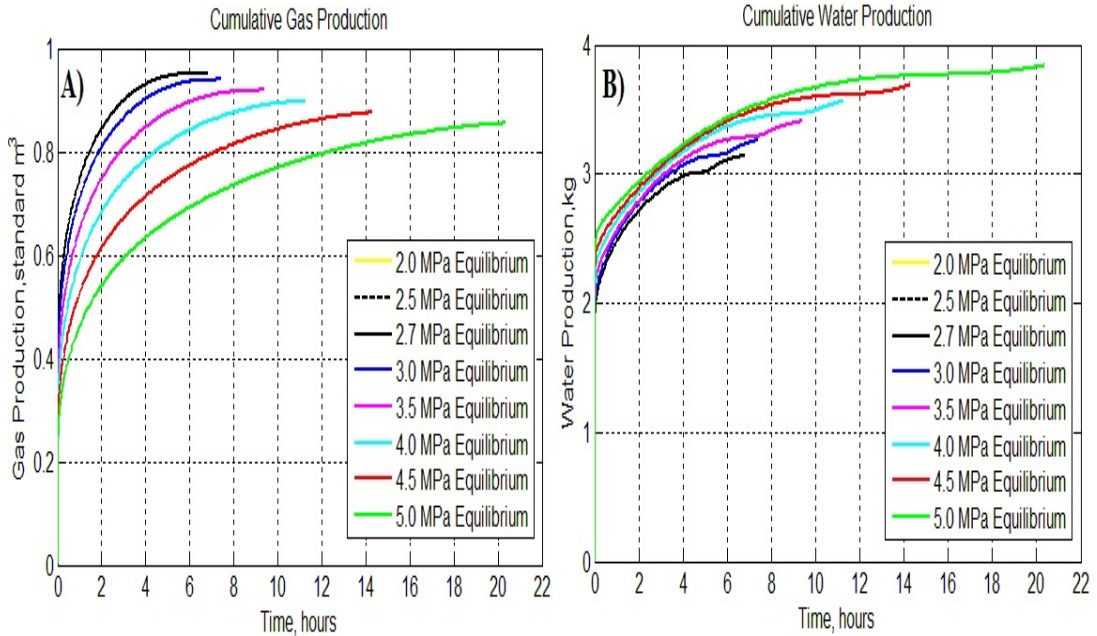


**Figure 7-35:** A) Cumulative gas production in simulation set 4 B) Cumulative water production in simulation set 4

In the gas hydrate section of simulation set 4, water saturation and gas saturation are 50 % while in the lower part of the high pressure reactor, gas saturation is 100 %. Hence, initially gas to water production is high in Figure 7-36. However, after depressurization of free gas from the pores and the lower part of the high pressure reactor (free zone), gas to water production ratio decreases due to the high amount of water released with gas hydrate dissociation. Initially gas production rate is very high and the maximum gas flow rate is approximately  $1262 \text{ m}^3/\text{second}$  ( $7.6\text{e}7 \text{ L/min}$ ) as seen in Figure 7-37 at 2.7 MPa and average gas production rate is nearly  $9.0\text{e-}4 \text{ m}^3/\text{second}$  (54 L/min). Figure 7-38 shows the changes of pressure, temperature and saturations with time are shown. Similar to other simulation sets, temperature decreases with hydrate dissociation and gas hydrate dissociates from boundaries to the interior of the high pressure reactor. Moreover, as gas is produced from free section (empty zone), it is filled by water due to gravity so water saturation in free zone increases with time.

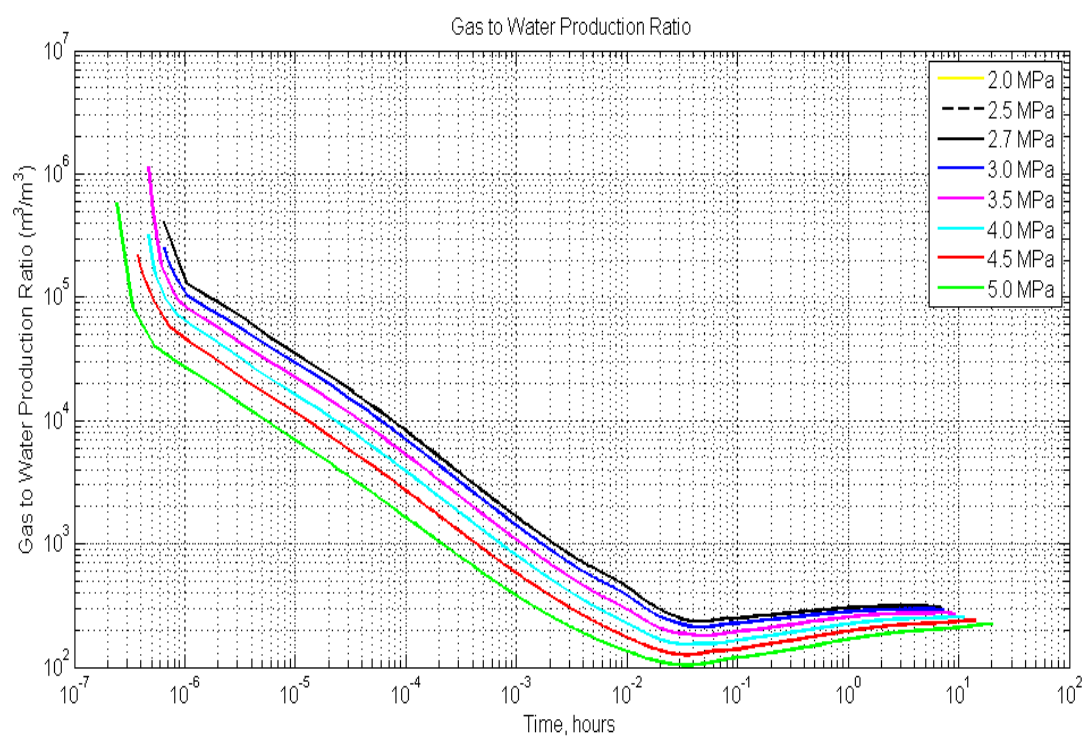


**Figure 7-36:** Gas to water production ratio in simulation set 4

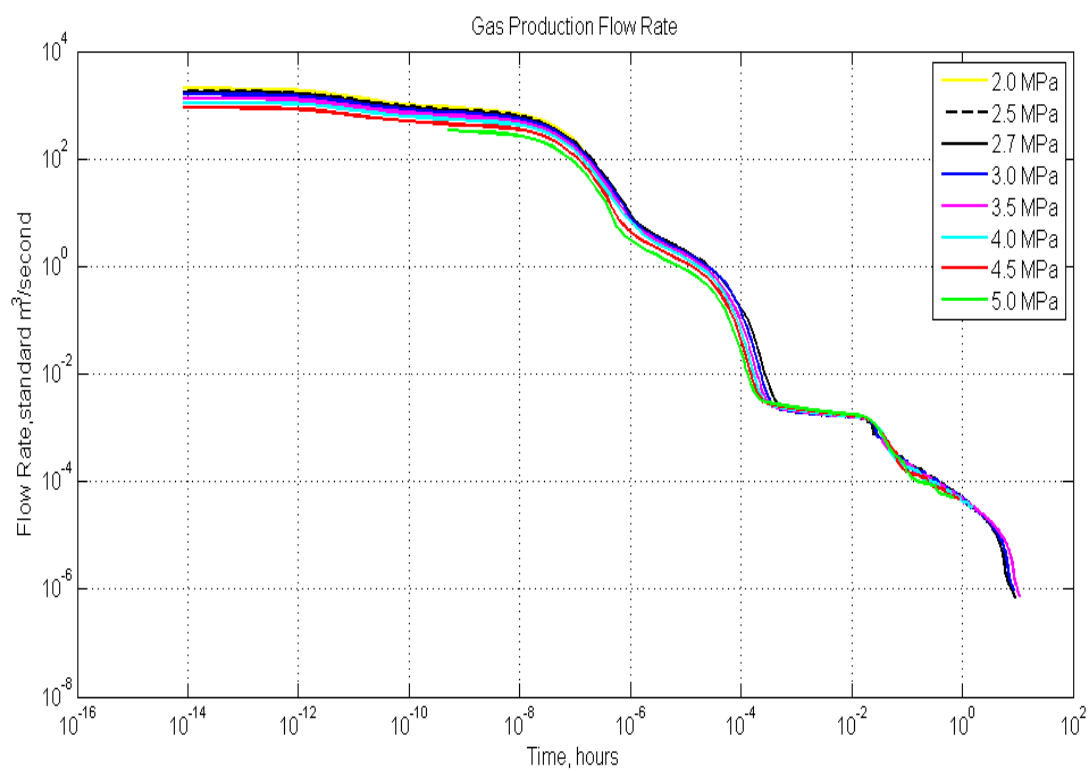


**Figure 7-37:** Gas production rate in simulation set 4

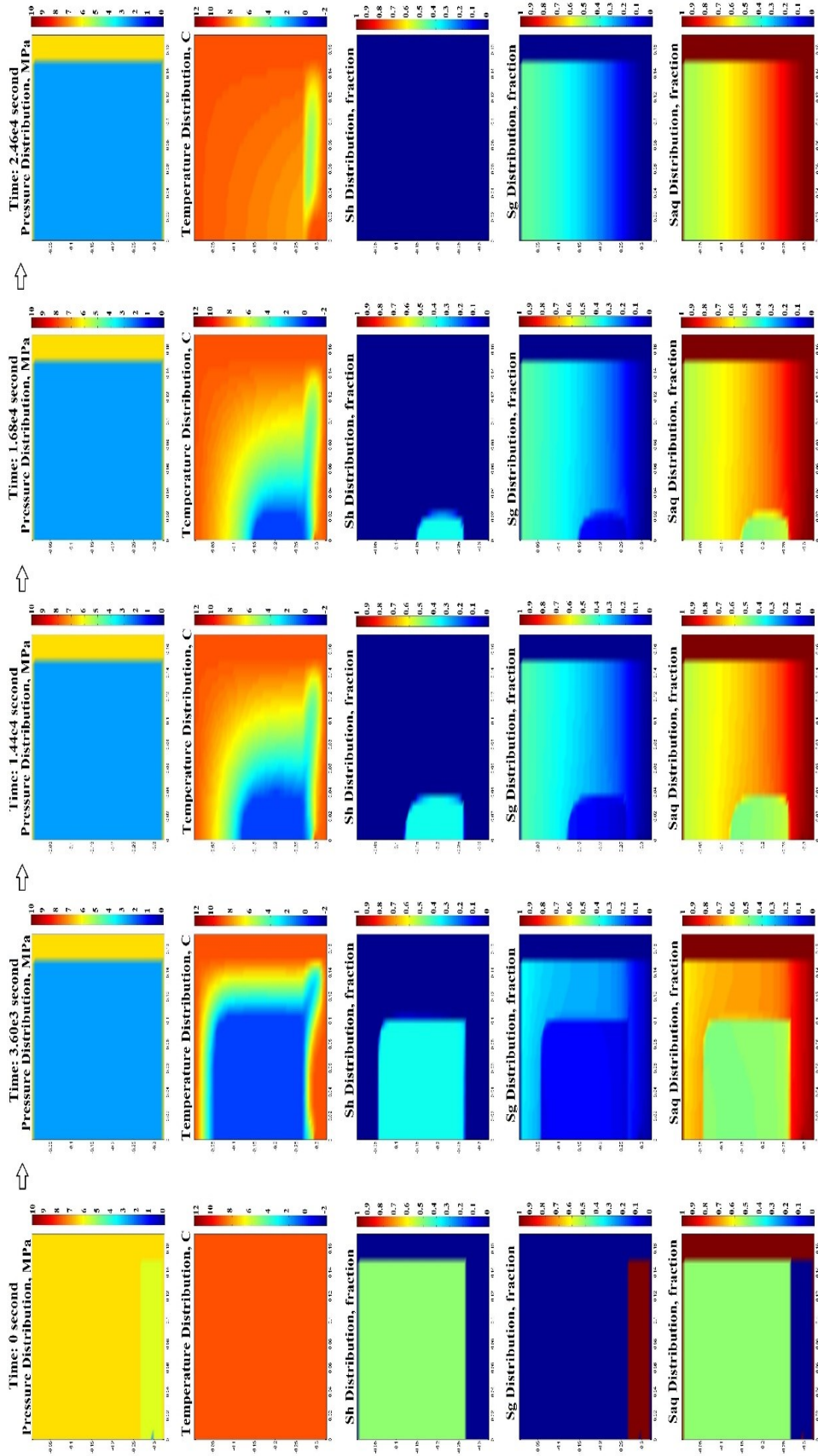


**Figure 7-38:** Pressure, temperature, hydrate saturation, and aqueous saturation in simulation set 4 of the half of the high pressure reactor at 2.7 MPa

In Simulation set 4, initially there are 0.992 standard m<sup>3</sup> of CH<sub>4</sub> and 8.12 kg of water inside METU reactor. At 2.7 MPa, approximately 74.8 % of CH<sub>4</sub> and 38.7 % of water were produced. Water production recovery at 2.7 MPa is low because some of water was collected in the bottom (free section below portable mesh) of METU reactor.

**Table 7-13:** Maximum gas flow rate, average gas flow rate and maximum water production in the simulations of the high pressure reactor (METU reactor)

<b>Simulation</b>	<b>Maximum Gas Flow Rate</b>	<b>Average Gas Flow Rate</b>	<b>Maximum Cumulative Water Produced, kg</b>
<i>1</i>	0.22 m <sup>3</sup> /second (13200 L/min)	1.27e-4 m <sup>3</sup> /second (7.62 L/min)	3.20
<i>2</i>	0.0134 m <sup>3</sup> /second (804 L/min)	5e-5 m <sup>3</sup> /second (3 L/min)	2.80
<i>3</i>	1681 m <sup>3</sup> /second (1e8 L/min)	6.1e-4 m <sup>3</sup> /second (36.6 L/min)	2.66
<i>4</i>	1262 m <sup>3</sup> /second (7.6e7 L/min)	9.0e-4 m <sup>3</sup> /second (54 L/min)	3.84

Table 7-13 lists the maximum gas flow rates, average gas flow rates and maximum water production during the simulations of the high pressure reactor by using HydrateResSim numerical simulator. As shown in Figure 7-12, during depressurization, gas and water produced through the production well are sent to the gas-water separator. Gas-water separator is on the weight balance and the amount of produced water with time is recorded. After leaving the produced water in gas-water separator, gas flow through gas flow meter and gas flow rate is recorded. Table 7-13 is very useful for the design of gas-water separator and the selection of gas flow rate. In the laboratory facility, there is a weight balance with 0-100 kg (with 1-gram accuracy) and which can be used for the planned experiments. Due to fast depressurization in the simulations studies, in the very early times, gas flow rates are very high as seen in Table 7-13. However, in real case, it is planned to decrease the initial pressure (6.5 MPa) to desired pressure in controlled way by regulating the production valve. Therefore, it is better to use the average gas flow rate for the

selection of gas flow rates. A gas flow meter with  $\text{CH}_4$  100 L/minute is highly enough for the experimental studies for Black Sea gas hydrates.

As seen in Figure 7-21, Figure 7-26, Figure 7-34, and Figure 7-38, the temperature inside the high pressure reactor (METU reactor) decreases with hydrate dissociation by depressurization. When all gas hydrate dissociates, temperature inside the reactor goes to its original temperature by heat flux from the walls of the high pressure reactor. It is known that hydrate formation is exothermic and hydrate dissociation is endothermic. Therefore, temperature changes give clues about hydrate formation or hydrate dissociation. Furthermore, in the experimental conditions, it is difficult to form uniform gas hydrate saturation in the reactor. There are certain procedures to form homogenous gas hydrates in sediments. For this reason, it is important to check homogenous gas hydrate formation inside sediments, gas hydrate dissociation and any ice formation by measuring temperatures at different locations in the high pressure reactor. For this purpose, 16 thermocouples are suggested to be distributed equally inside the high pressure reactor (METU reactor).

## **7.4 Depressurization Simulations in Field Cases in the Black Sea**

### **7.4.1 Class 1 Hydrate Reservoir Simulations**

All BSRs, seafloor samples and gas hydrate samples recovered indicate that there is a huge potential of  $\text{CH}_4$  hydrates in the Black Sea. As stated earlier, Class 1 hydrates are the most preferred hydrate reservoirs among Class 1, 2, and 3 because of its free gas potential below hydrate zone and the ease of dissociation of hydrate by depressurization. BSRs detected by seismic studies are the most important proof of Class 1 hydrate potential in the Black Sea.

In this study, firstly, a hypothetical Class 1 methane ( $\text{CH}_4$ ) hydrate reservoir was selected for the simulation study. For the simulation of gas production from the hypothetical reservoir, HydrateResSim numerical simulator were used in this study. Klauda and Sandler (2003) estimated that the greatest amount of  $\text{CH}_4$  hydrate can be

found in the southern Black Sea bordering Turkey as seen in Figure 7-39. The area shown inside a black circle in Figure 7-39 was selected for a hypothetical Class 1 CH<sub>4</sub> hydrate reservoir. This area is also close to the BSRs detected by Küçük *et al.* (2015). Porosity, rock grain density, wet thermal conductivity, and temperature gradient data in the selected area were found from the study of Vassilev (2006) and other data used for the simulations in this study are shown in Table 7-14.

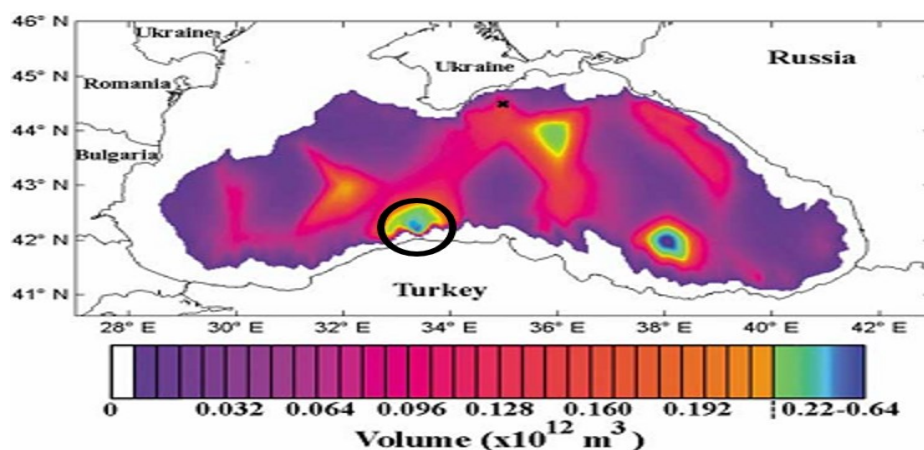


**Figure 7-39:** CH<sub>4</sub> at standard conditions in the Black Sea hydrates (Klauda and Sandler, 2003)

The properties of the hypothetical Class 1 CH<sub>4</sub> hydrate in the Black Sea conditions are shown in Table 7-14. Class 1 hydrate reservoir is bounded by two impermeable shale or clay boundaries with 5 m thickness. Gas production from hydrate zone bounded with impermeable layers is better than in the other conditions (permeable boundary layers) because pressure can diffuse upward and downward to the boundaries and the released gas cannot escape when there are impermeable layers (Sun *et al.*, 2015). Therefore, the hypothetical reservoir (Class 1) was assumed to be bounded by impermeable shale or clay layers. Thicknesses of the hydrate layer and free gas layer in the hypothetical reservoir are 20 m each. For the Black Sea, there is no well drilled for the exploration of gas hydrates. Therefore, it is hard to predict the thickness of gas hydrate zone and free gas zone in Class 1 reservoirs. For the hypothetical hydrate simulations, Alp *et al.* (2007) simulated gas production from Class 1W and Class 1G reservoir with 16 m hydrate zone and 16 m free zone by using Tough-Fx/Hydrate numerical simulator. Similarly, Moridis and Kowalsky (2006) made simulations studies for Class 1 hydrate with 30 m hydrate zone and 30 m free

zone by using Tough-Fx/Hydrate numerical simulator. In this study, 20 m hydrate zone and 20 m free zone were selected. Moreover, in order to see the effect of shale or clay boundaries on hydrate dissociation, the hydrate zone thickness should not be very large for effective heat transfers because the thermal conductivity of hydrate is quite low (0.5 W/m.K (Sloan and Koh, 2008)). When hydrate thickness increases, the effect of heat fluxes from the impermeable shale boundary decreases because of low thermal conductivity of gas hydrates. Moreover, as discussed in Chapter 4, the Black Sea does not have possibility to have very thick gas hydrate sections. As seen in Table 7-14, hydrate saturation in the hydrate zone was chosen as 65 % and gas saturation in the free gas zone was chosen as 75 % because Vassilev and Dimitrov (2003) stated that as going deeper through the CH<sub>4</sub> hydrate stability zone in the Black sea, hydrate saturation might increase up to 45-65 %. Similarly, in the Danube fan in the western Black Sea, it was detected that above gas hydrate stability zone, gas hydrate saturation is up to 50 % by electric dipole-dipole system when water depth is 1335 m and 300 mbsf (15-19.5°C) (Schwalenberg *et al.*, 2016). Equilibrium model option of HydrateResSim was selected because at the reservoir conditions, kinetic model and equilibrium models give similar results (Kowalsky and Moridis, 2007; Ruan *et al.*, 2012). For 2D grids for the cylindrical reservoir, 53 grids (Cartesian) along z direction and 75 grids (logarithmic) along r direction are placed and it is shown in Figure 7-40. When number of grids increases, simulation time also increases. In this study, for 2D grids of the cylindrical reservoir, 86 grids (Cartesian) along z direction and 100 grids (logarithmic) along r direction were placed at 3.0 MPa and almost similar results were obtained with 53 grids (Cartesian) along z direction and 75 grids (logarithmic) along r direction. 53 grids (Cartesian) along z direction and 75 grids (logarithmic) along r direction were selected for faster simulation because the number of simulations is high in this study for different cases. Therefore, 11,925 equations (mass balance equation for water, mass balance equation for CH<sub>4</sub> and heat balance equation) were solved for 3,975 elements (grids) at each time step. For time step, 3.60e4 second was chosen in this study. However, HydrateResSim has ability to determine time step automatically. If the maximum number of iterations per time step (as default it is 8) is exceeded, automatically time step is divided by two and for new time step, the calculations are held.

**Table 7-14:** Properties of the hypothetical Class 1 CH<sub>4</sub> hydrate in the Black Sea

<i>Radius</i>	500 m
<i>Thickness of Hydrate Zone</i>	20 m
<i>Thickness of Free Gas Zone</i>	20 m
<i>Thickness of Each Shale Layer</i>	5 m
<i>Porosity</i>	0.50
<i>Permeability</i>	9.869e-13 m <sup>2</sup> (1 D)
<i>Rock Grain Density</i>	2700 kg/m <sup>3</sup>
<i>Wet Thermal Conductivity</i>	2.4 W/(m.K)
<i>Average Pressure</i>	6.7 MPa
<i>Temperature Gradient</i>	0.06 °C/m
<i>Temperature Interval</i>	7.98-10.68 °C
<i>Hydrate Zone Saturations</i>	S <sub>h</sub> :0.65; S <sub>aq</sub> :0.35
<i>Free Gas Zone Saturations</i>	S <sub>gas</sub> :0.75; S <sub>aq</sub> :0.25
<i>CH<sub>4</sub> in Hydrate Zone, m<sup>3</sup></i>	8.44E+08
<i>CH<sub>4</sub> in Free Gas Zone, m<sup>3</sup></i>	4.43E+08
<i>Total CH<sub>4</sub> Amount, m<sup>3</sup></i>	1.30E+09
<i>Total Water Amount, kg</i>	8.806E+09
<i>Relative Permeability Parameters- Modified of Stone Equation</i>	S <sub>ar</sub> :0.25 S <sub>gr</sub> :0.02 n: 3.0
<i>Capillary Pressure Parameters- Van Genuchten function</i>	S <sub>ar</sub> : 0.24 n: 1.84 a:10.0

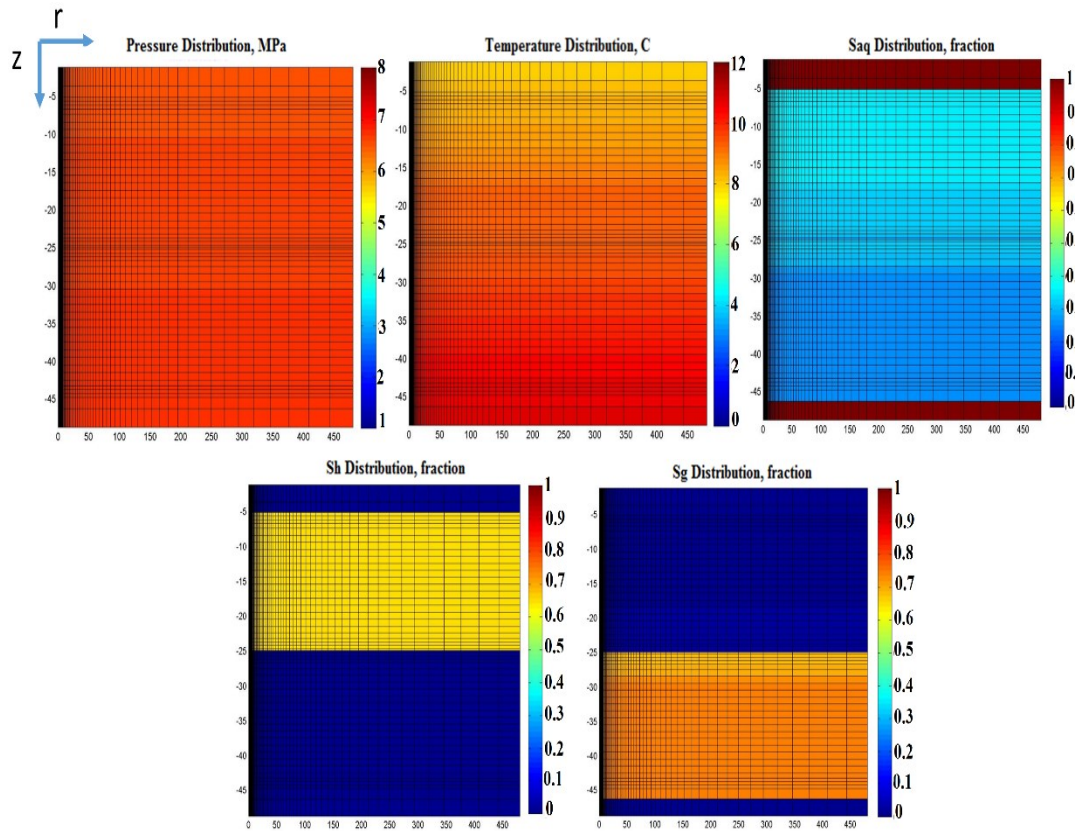


**Figure 7-40:** Grid structure of the hypothetical Class 1 hydrate reservoir in the Black Sea conditions

Without having any log data and other information from the real Class 1 hydrate reservoirs, it is very difficult to obtain steady-state conditions for hypothetical Class 1 hydrate reservoirs by using only limited data such as thermal gradient, porosity, hydrostatic pressure, thermal conductivity etc. Hence, before the gas production simulations of Class 1 hydrate reservoirs, it is important to have steady-state conditions. For this purpose, Class 1 hydrate reservoir is separated into upper and lower parts (just in the intersection between hydrate zone and free gas zone). Then, initial conditions of these two parts are prepared separately. When both parts have almost equal rates of heat fluxes, they are joined together. Then, the simulation is run without any production or injection wells at steady-state conditions. If there is no hydrate dissociation or hydrate formation during the simulation, it means that the steady-state conditions are provided for the Class 1 hydrate reservoir. Similar studies

were done by Moridis *et al.* (2005b), Alp *et al.* (2007), and Kowalsky and Moridis (2007).

After obtaining the steady-state Class 1 hydrate reservoir, gas production simulations from the hypothetical reservoir by depressurization method at different pressures were run by using HydrateResSim numerical simulator. 1.0 MPa, 1.5 MPa, 2.0 MPa, 2.7 MPa, 3.0 MPa, 3.5 MPa, 4.2 MPa and 5.0 MPa were selected as production pressures. In Class 1 hydrate reservoirs, perforations are opened in the free gas section and by the production of free gas, the pressure of the hydrate section is lowered as well. When pressure is below the hydrate equilibrium pressure, hydrate starts to dissociate and gas and water move through the wellbore via the free gas section. Therefore, the wellbore was assumed to be perforated below the hydrate layer from -26 to -42 m in our model.

At constant wellbore pressures, simulations were run by HydrateResSim numerical simulators. The cumulative gas production versus time at different production pressures are shown in Figure 7-41. As seen in Figure 7-41, when production pressure is lower, much more gas is produced but until certain value. As gas is produced and with the decrease of the pressure below the hydrate equilibrium pressure, hydrate dissociates. Hydrate dissociation is an endothermic process and it decreases temperature. However, when the temperature of the hydrate zone decreases with endothermic hydrate dissociation, the impermeable shale/clay boundary provides heat flux through the hydrate zone. The higher the depressurizing range is, the faster the dissociation rate is. Figure 7-42 shows the contribution of upper hydrate section of Class 1 hydrate reservoir to the cumulative gas production. Gas production rates during depressurization are shown in Figure 7-45. Gas production rates at all depressurization pressures were quite high within half year because the contribution of free gas zone was high during the decrease of reservoir pressure. Later, the gas flow rates decreased a lot because the pressure became almost equal to depressurization pressure and most of gas was produced via hydrate dissociation. Moreover, the cumulative water production is shown in Figure 7-43. Much water was produced when the production pressure is 3.0 MPa because most hydrate dissociation

occurred at this production pressure. When the depressurization pressure is equal to 2.7 MPa or below it, it was observed that there is hydrate formation along the wellbore. Fast production in the wellbore decreases the temperature because of the Joule-Thomson effect. Class 1 hydrate reservoir conditions are very close to the equilibrium conditions even in the free gas section. Hence, with the decrease of the temperature along the wellbore due to Joule Thomson effect, hydrate was formed along the wellbore when the depressurization pressure is equal to or below 2.7 MPa. Then, the simulation stopped because of no gas production. Figure 7-44 and Figure 7-45 show gas to water production ratio and gas flow rate respectively. In very early stage of depressurization, gas to water production ratio is quite high because gas production starts from free gas zone of Class 1 hydrate reservoir. However, when depressurization in free gas zone near the target pressure, gas to water production ratio decreases because with gas hydrate dissociation, water released from hydrate section of Class 1 reservoir is produced.

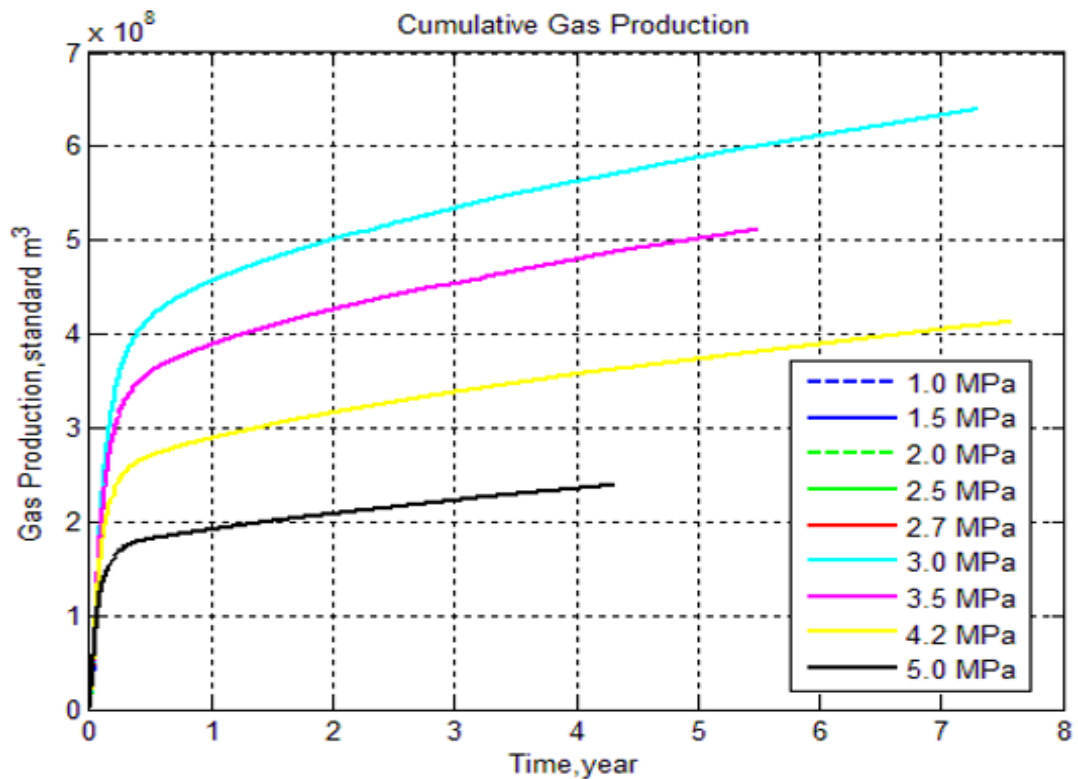


**Figure 7-41:** Cumulative gas production from the Class 1 CH<sub>4</sub> hydrate by depressurization at different pressures

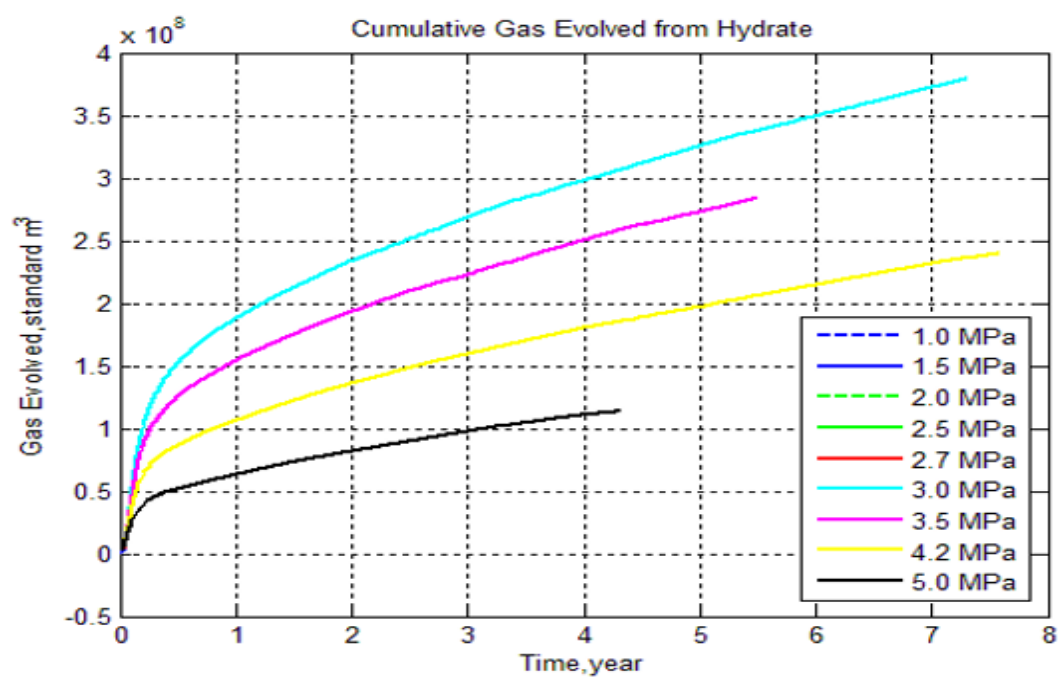


**Figure 7-42:** Cumulative gas production from the upper hydrate section of the Class 1 CH<sub>4</sub> hydrate by depressurization at different pressures

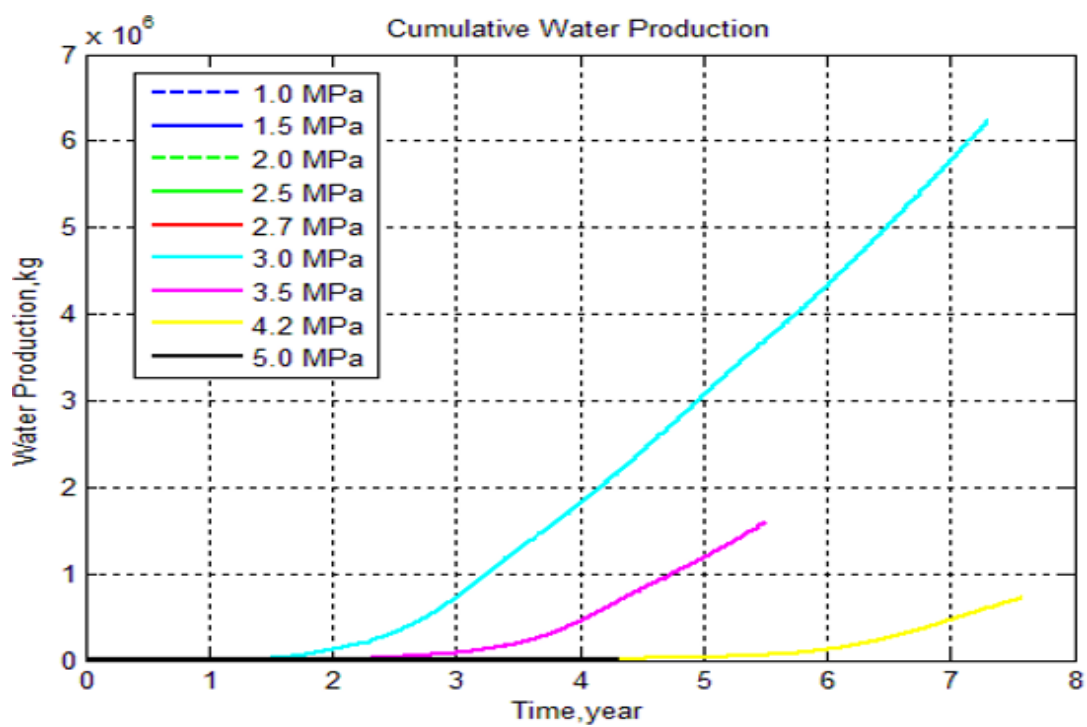


**Figure 7-43:** Cumulative water production from the Class 1 CH<sub>4</sub> hydrate by depressurization at different pressures

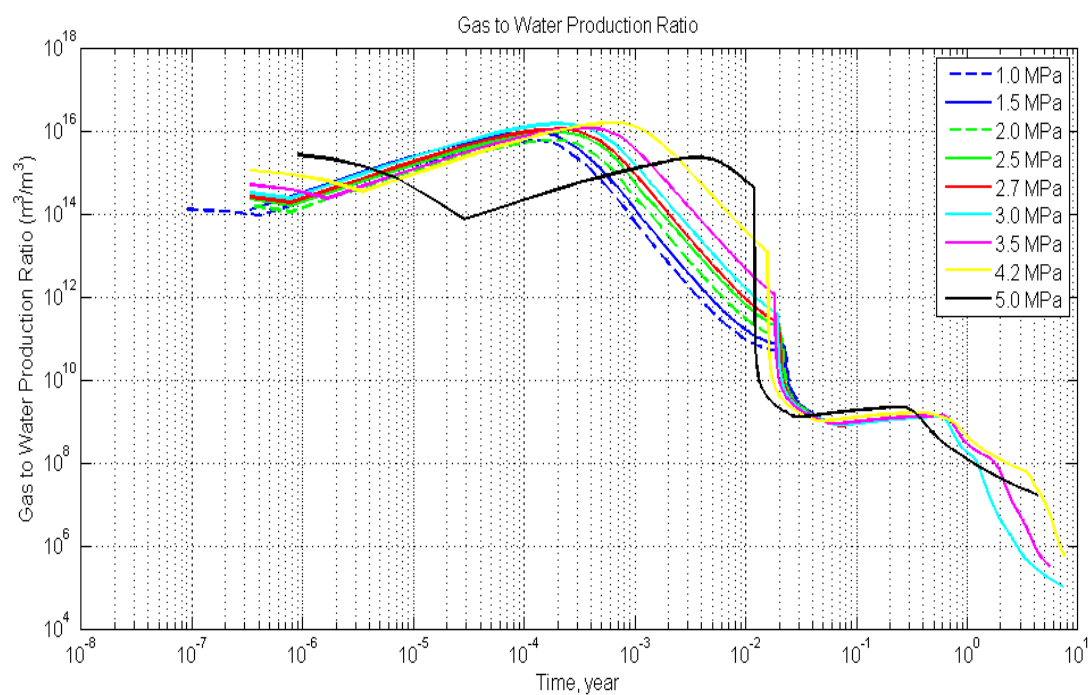


**Figure 7-44:** Gas to water production ratio of the Class 1 CH<sub>4</sub> hydrate by depressurization at different pressures

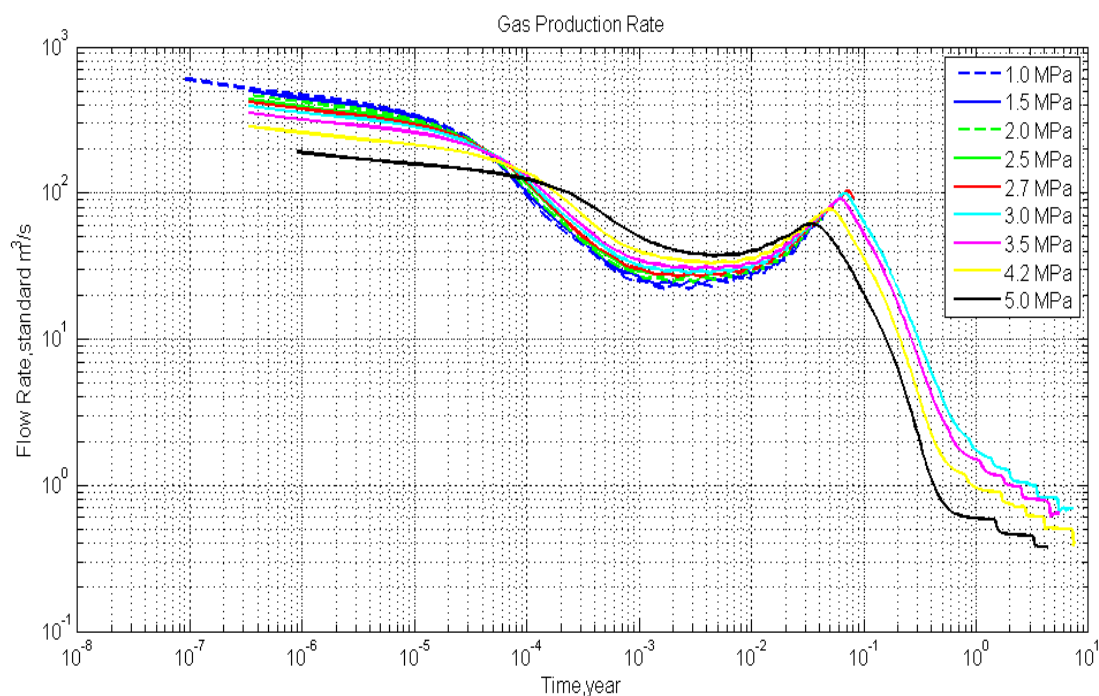


**Figure 7-45:** Gas production flow rate from the Class 1 CH<sub>4</sub> hydrate by depressurization at different pressures

After gas production at 3.0 MPa depressurization from the hypothetical Class 1 gas hydrate reservoir, 49.2 % of total CH<sub>4</sub> was produced. Table 7-14 shows the initial CH<sub>4</sub> in free gas and hydrate sections. 58.7 % of CH<sub>4</sub> in free gas section and 44.9 % of CH<sub>4</sub> in gas hydrate section were produced at 3.0 MPa depressurization pressure.

Figure 7-46 shows the gas hydrate formed along the wellbore during gas production when the depressurization pressure is 2.0 MPa. Hydrate formation near wellbore was also observed in the study of Alp *et al.* (2007).

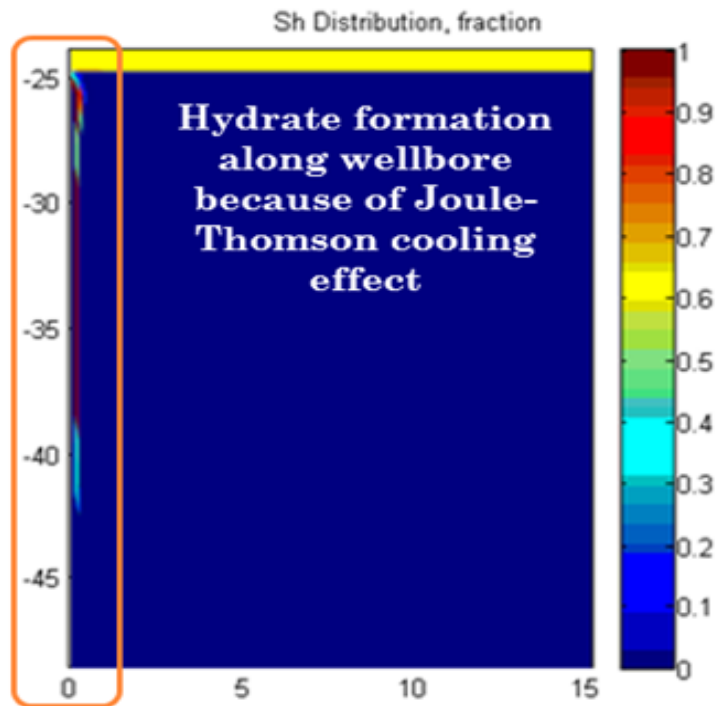


**Figure 7-46:** Hydrate formation along the wellbore during depressurization at 2.0 MPa after 16 days

In Figure 7-47, the changes in pressure, temperature, hydrate saturation ( $S_h$ ), gas saturation ( $S_g$ ) and aqueous saturation ( $S_{aq}$ ) are shown between the steady-state condition and after 7.3 years of production at 3.0 MPa. Temperature of the hydrate section decreased below 2.0 °C although its original temperature was approximately 10 °C. This is due to endothermic hydrate dissociation during gas production. Hydrate zone thickness decreased from 20 m to below 15 m and  $S_h$  decreased below 0.55. As expected,  $S_g$  increased in the hydrate section because of hydrate dissociation. Hydrate

just below the overburden impermeable shale zone dissociated completely and  $S_g$  increased a lot in this section. This is because the overburden impermeable shale/clay layer behaves like a constant temperature boundary. During depressurization at 3.0 MPa, gas production stopped at 7.3 year because hydrate dissociation ceased. At 7.3 year, the temperature of the hydrate zone is below 2 °C. Therefore, the heat flux provided by the constant temperature shale/clay layer is not enough to dissociate the hydrate further. Even though many reservoir parameters and other cost analysis are necessary for different gas hydrate reservoirs, Max and Johnson (2016) proposed that 0.983 standard  $m^3/s$ -1.639 standard  $m^3/s$  (3-5 MMscf/d) gas production rates might be commercial for shallow water or onshore gas fields. When gas flow rate at 3.0 MPa in Figure 7-45 is analyzed, gas production might be feasible according to the rough cost proposal of Max and Johnson (2016).

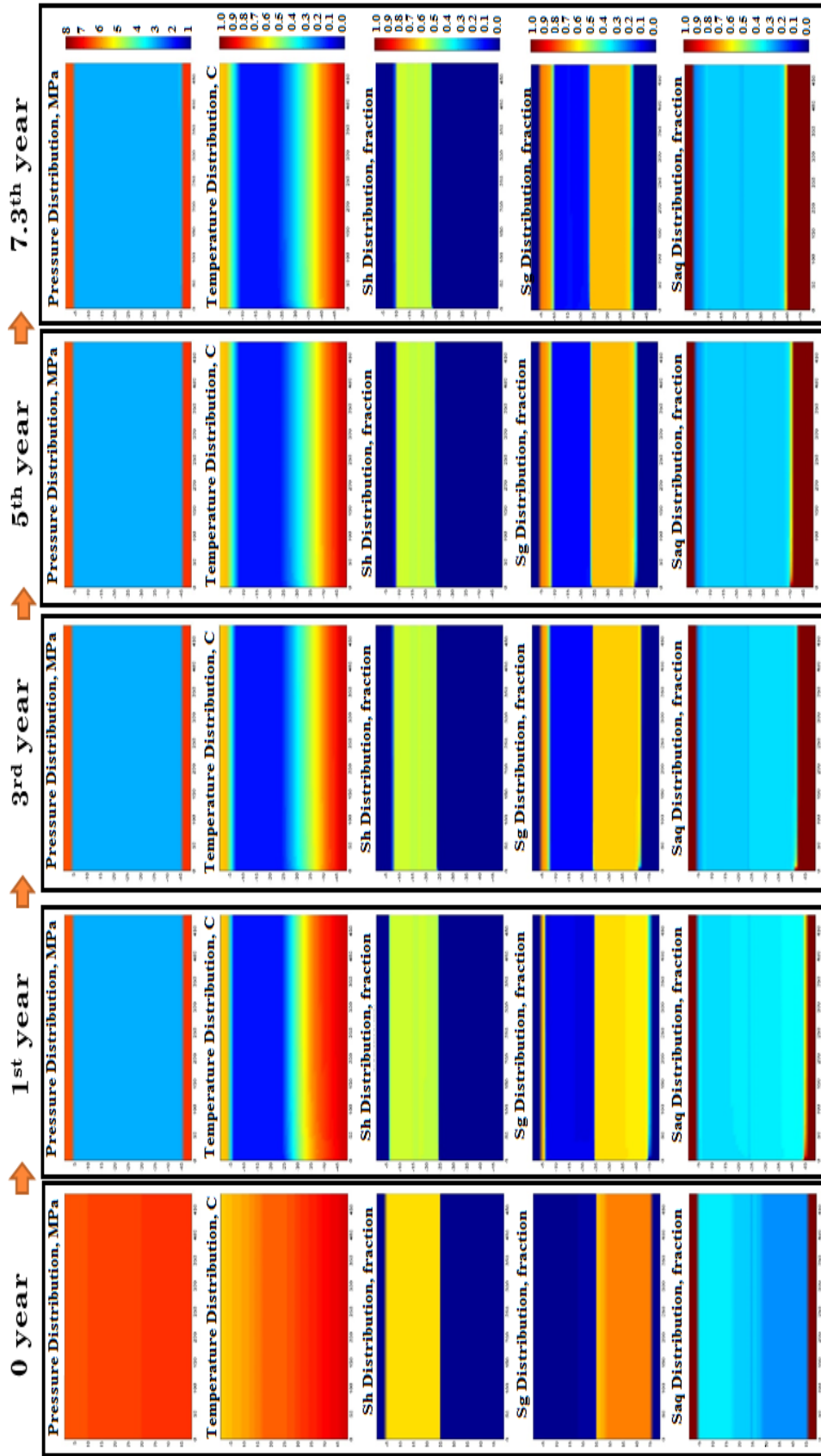


**Figure 7-47:** Changes in pressure, temperature,  $S_h$ ,  $S_g$  and  $S_{aq}$  from initial conditions to 7.3 years production from the Class 1 CH<sub>4</sub> hydrate with depressurization at 3.0 MPa

During depressurization without any external heat, 3.0 MPa is the most appropriate production pressure for the hypothetical hydrate reservoir in this study. At 2.7 MPa and below 2.7 MPa, gas production stopped because of hydrate formation along the wellbore due to Joule Thomson effect. With wellbore heating, hydrate reformation might be avoided and much gas can be produced below 3.0 MPa. For this purpose, similar depressurization simulations at different pressures (2.0 MPa, 2.5 MPa, 2.7 MPa and 3.0 MPa) were run with wellbore heating. Between -20 m to -42 m, total heat of 5,400 J/s was applied along the wellbore during the simulations. This heating rate was selected with trial and error method by running same simulations at different heating rate. When the hydrate formation was avoided along the wellbore, trial and error was stopped and final heating rate (5,400 J/s) was considered as an optimum one. Different from thermal stimulation in gas hydrates, the aim of wellbore heating is just to avoid any hydrate and/or ice formation along the wellbore. As shown in Figure 7-46, hydrate formation along the wellbore stopped the simulation. After the simulations with wellbore heating, Figure 7-48 was obtained. At early stages, gas production at 2.0 MPa is higher. However, after some time, the gas productions at 2.0 MPa and 2.5 MPa stopped. Then, 2.7 MPa has the highest gas production until 8.4 years. Although there is no hydrate and ice formation along the wellbore because of wellbore heating, the gas productions at 2.0 MPa and 2.5 MPa stopped. This is due to ice formation in the hydrate zone and ice plugged the flow channels. Fast depressurization at 2.0 MPa and 2.5 MPa caused the temperature decrease in the hydrate zone. The reasons of this temperature decrease are Joule-Thomson cooling and endothermic dissociation of gas hydrates. Gas production from hydrate section and cumulative water production at different pressures with wellbore heating are also shown in Figure 7-49 and Figure 7-52 respectively. Water production at 2.7 MPa is higher than water production at 3.0 MPa because water production increases with hydrate dissociation. Similarly, highest gas flow rates were obtained at 2.7 MPa as seen in Figure 7-51. Figure 7-50 shows gas to water production ratio. Initially, free gas was produced from the free gas section of the Class 1 CH<sub>4</sub> hydrate reservoir and then gas and water were produced with the dissociation of the gas hydrate section. Hence, initially gas to water production ratio is high but then decreases with high amount of water production with hydrate dissociation as seen in Figure 7-50.

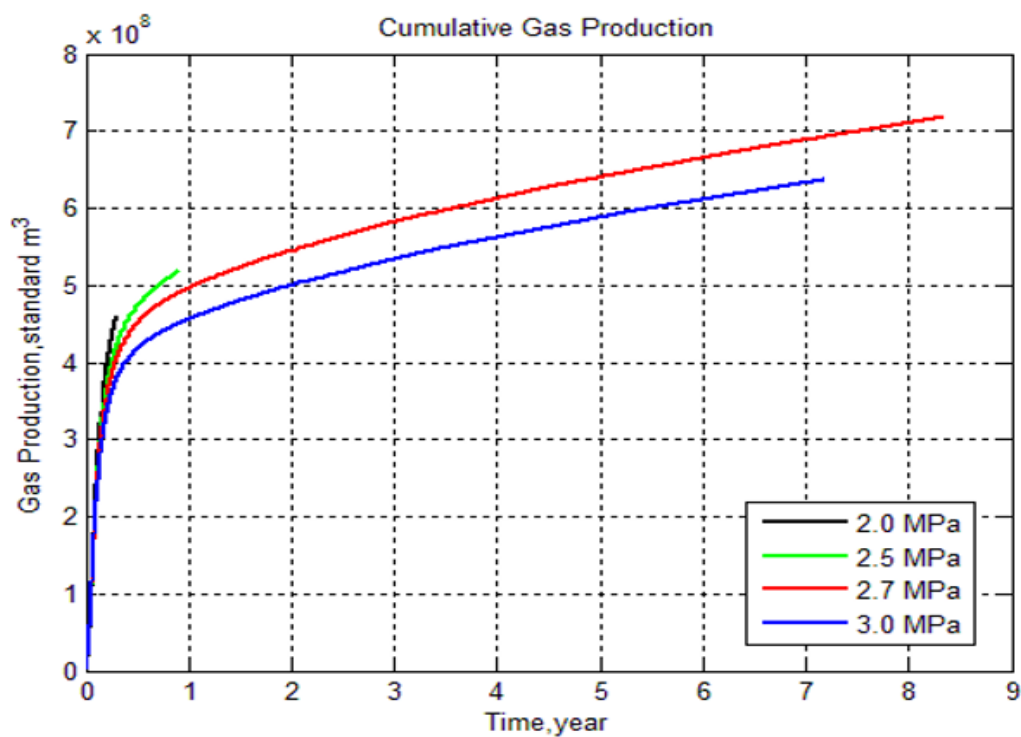


**Figure 7-48:** Cumulative gas production by depressurization with wellbore heating

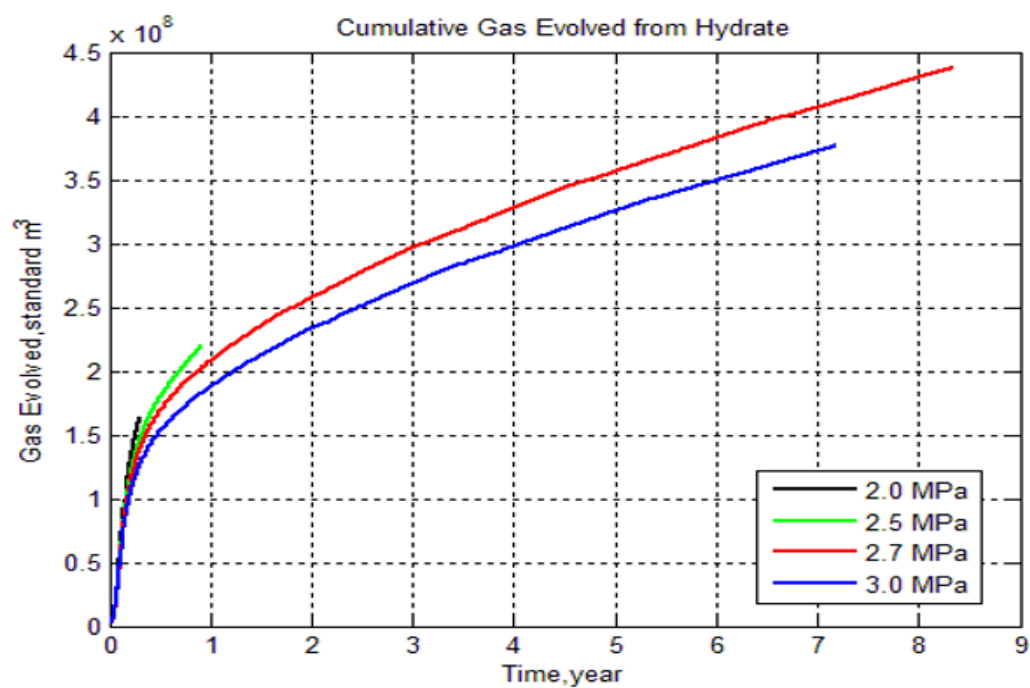


**Figure 7-49:** Cumulative gas production from the upper hydrate section of the Class 1 CH<sub>4</sub> hydrate by depressurization at different pressures with wellbore heating

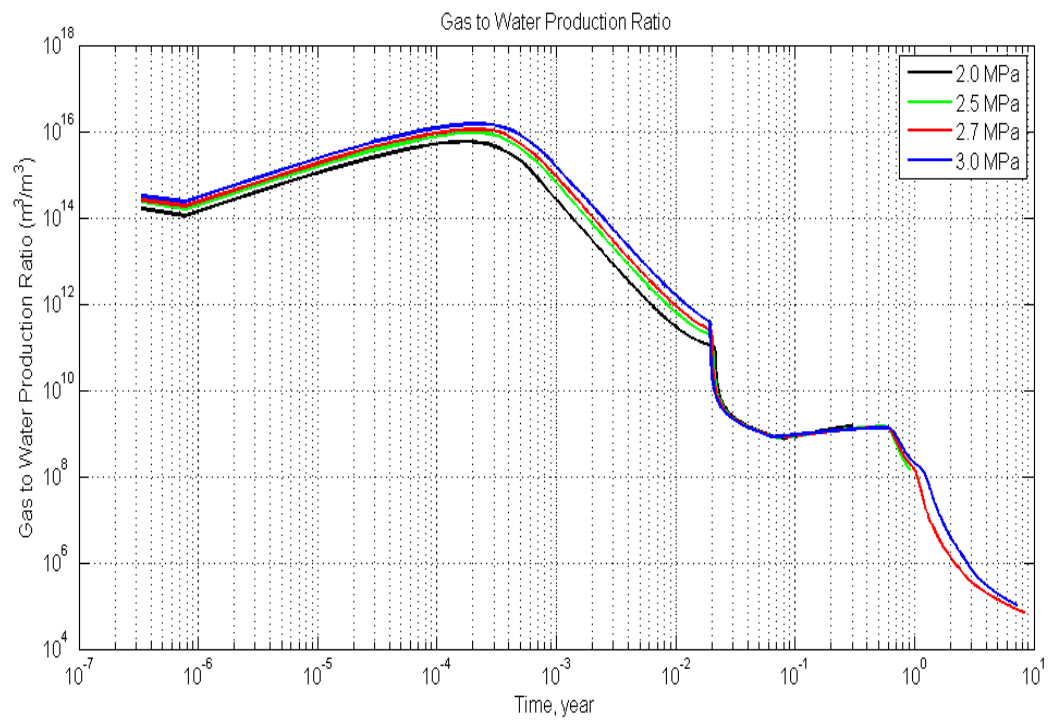


**Figure 7-50:** Gas to water production ratio of depressurization with wellbore heating

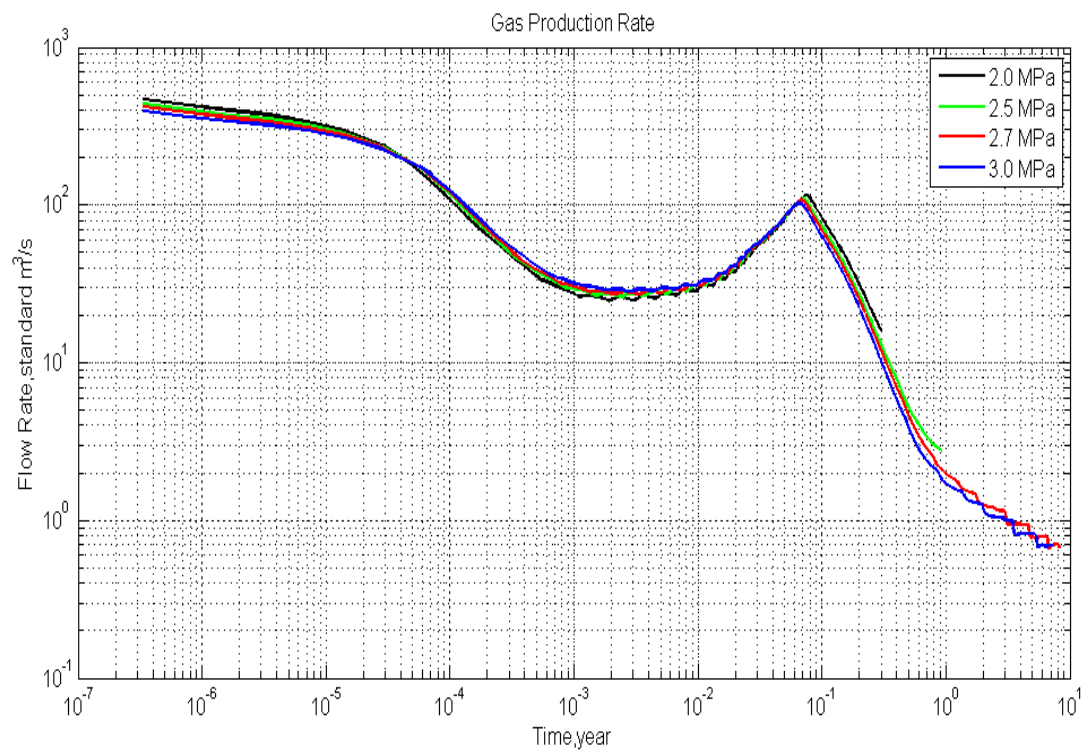


**Figure 7-51:** Gas production flow rate by depressurization with wellbore heating

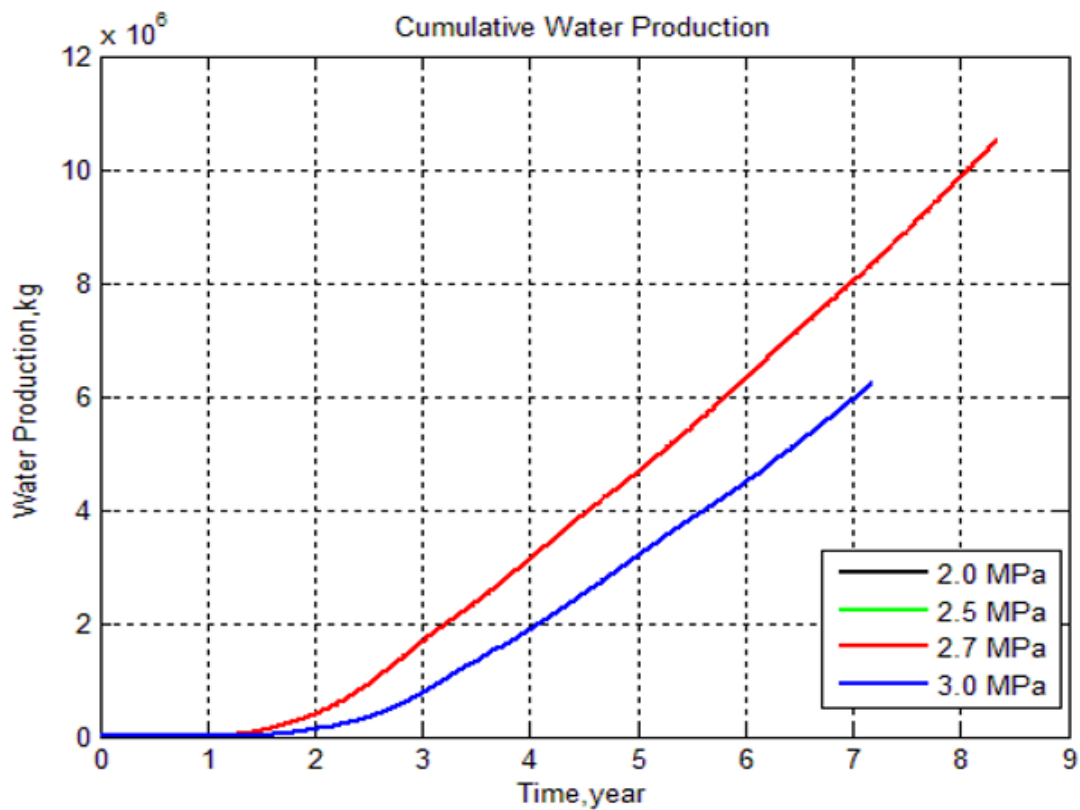


**Figure 7-52:** Cumulative water production by depressurization with wellbore heating

Figure 7-53 and Figure 7-54 show the ice formation in the reservoir during gas production at 2.5 MPa with wellbore heating. Hence, the most appropriate depressurization pressure is 2.7 MPa if wellbore heating is applied to avoid any hydrate formation along the wellbore at the conditions of the hypothetical Class 1 reservoir in this study. However, cost analysis is necessary to decide whether wellbore heating is economical or not. If it is not economical, depressurization at 3.0 MPa or 4.0 MPa without wellbore heating might be selected. Gas production at 2.7 MPa with wellbore heating is shown in Figure 7-55. During 8.4 year-production time, approximately 55.2 % of all gases in the free section and hydrate section of the hypothetical Class 1 gas hydrate reservoir (Table 7-14) was produced. 63.2 % of CH<sub>4</sub> in free gas section and 51.9 % of CH<sub>4</sub> in gas hydrate section were produced at 2.7 MPa depressurization pressure. These results show that both hydrate and free gas section of Class 1 hydrate reservoir provide large amount of gas production.

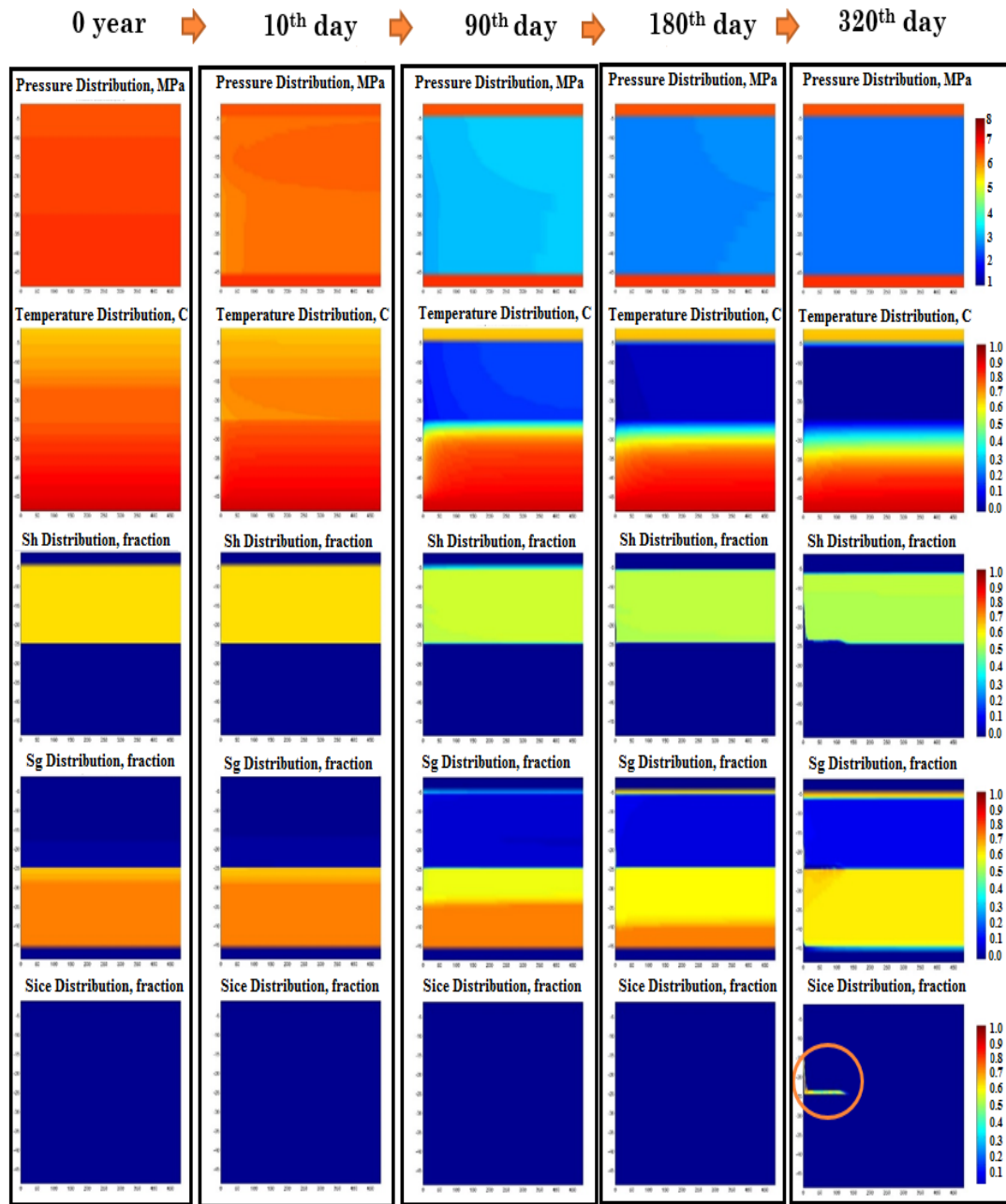


**Figure 7-53:** Changes in pressure, temperature,  $S_h$ ,  $S_g$  and  $S_{aq}$  from initial conditions to 320 days for the Class 1  $\text{CH}_4$  hydrate with depressurization at 2.5 MPa with wellbore heating

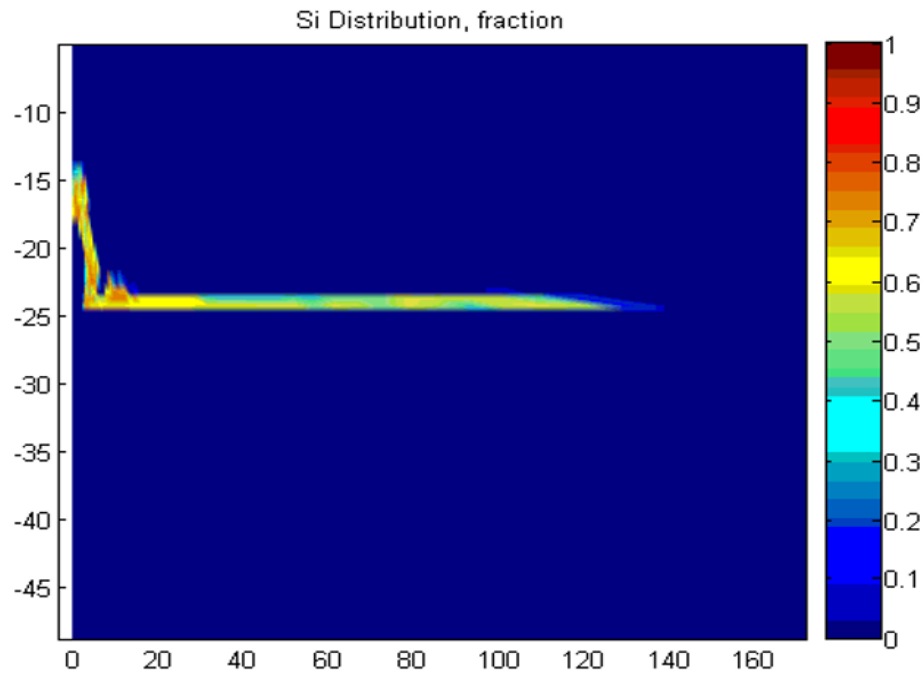


**Figure 7-54:** Ice formation due to fast depressurization at 2.5 MPa with wellbore heating

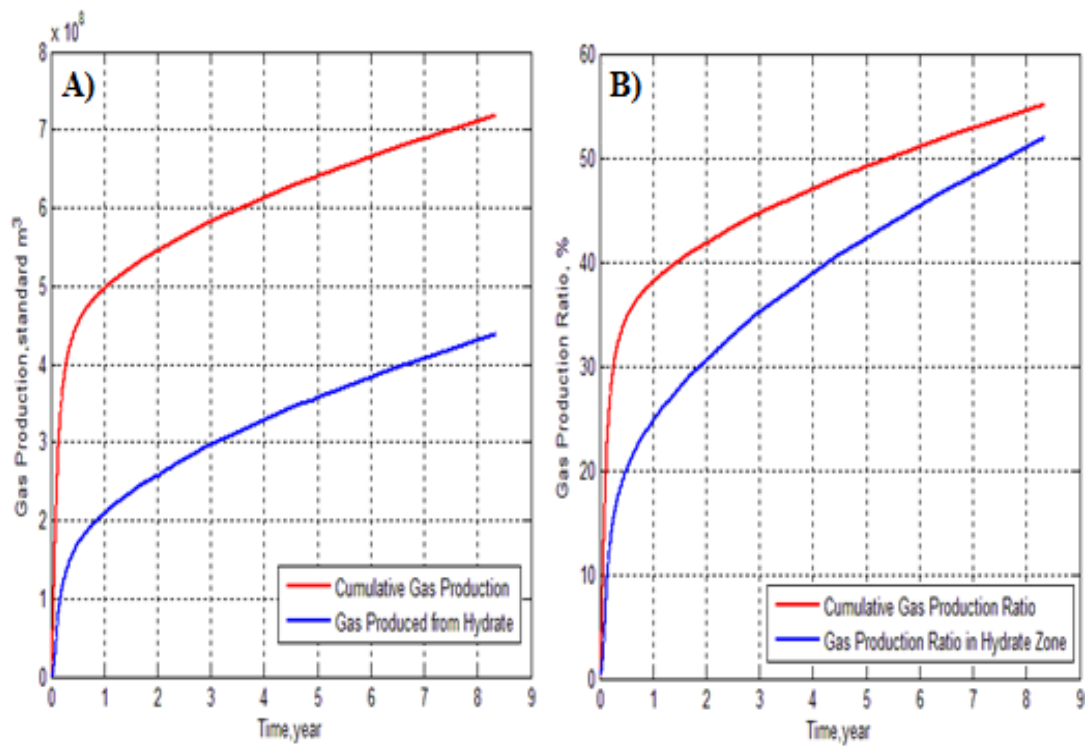


**Figure 7-55:** A) Gas production B) Gas production ratio by depressurization at 2.7 MPa with wellbore heating

Although there is some information in the literature about the porosity, thermal gradient, and thermal conductivity data of the Black Sea, there is not enough data about the permeability of the sediments in the selected area for the hypothetical Class 1 hydrate reservoir. For the simulation, the intrinsic permeability of the sediments in the selected area was assumed as 1.0 Darcy (D). In order to see the effect of the intrinsic permeability of the sediments on gas production from the Class 1 hydrate reservoir, the simulations for 2.7 MPa with wellbore heating at different permeability values (100 mD, 250 mD, 400 mD, 500 mD, 750 mD, 1000 mD) were run. In Figure 7-56, the results of these simulations are shown. As intrinsic permeability increases from 400 mD to 1000 mD, gas production increased little and gas production values are close to each other. However, when the permeability is 250 mD, gas production stopped during the simulation. In order to understand whether this is due to numerical instability or hydrate reservoir characteristics, another numerical simulation at similar conditions was run when intrinsic permeability is 100 mD. As seen in Figure 7-56, gas production stopped within 100 days during depressurization at 2.7 MPa. HydrateResSim numerical simulator gives generally error warnings if there is any numerical instability. Moreover, when the output files were investigated in detail, we did not observe any failed iteration. Hence, the production might stop at early stages for 100 mD and 250 mD due to hydrate reservoir characteristics. Intrinsic permeability is the permeability of the sediments when there is no hydrate. Hydrate saturation decreases the permeability of sediments. The relation between hydrate saturation ( $S_h$ ) and absolute permeability is shown in Equation (7-1) (Masuda *et al.*, 1999). For effective depressurization, the absolute permeability should be higher than 10 mD (Konno *et al.*, 2010). However, in this study, when the intrinsic permeability is 250 mD, the absolute permeability becomes below 10 mD for  $S_h=0.65$ . By using the simulation data in this study for 250 mD, Equation (7-1) and the range of effective permeability suggested by Konno *et al.* (2010), it was calculated that  $N$  is equal to approximately 3.1. Similarly, in the study of Kumar *et al.* (2010),  $N$  was found as 3.0. According to the study of Kumar *et al.* (2010), it was observed that hydrates preferentially formed as grain coating for hydrate saturations below 35% and above 35 %, hydrates formed in the center of the pores. In this study,  $S_h$  and  $N$  were 0.65 and 3.1 respectively so it might be expected that hydrate is in the center of the pores

at the conditions of the hypothetical Class 1 hydrate in the Black Sea. Due to low absolute permeability in hydrate zone, depressurization is not effective when the intrinsic permeability below 400 mD for the hypothetical Class 1 reservoir in the Black Sea conditions.

$$k_d = k_{do} \times [1 - S_h]^N \quad (7-1)$$

$k_d$ : permeability of the methane hydrate layer;  $k_{do}$ : original absolute (intrinsic) permeability;  $N$ : permeability reduction index (changes 2 to 10 according pore structure)

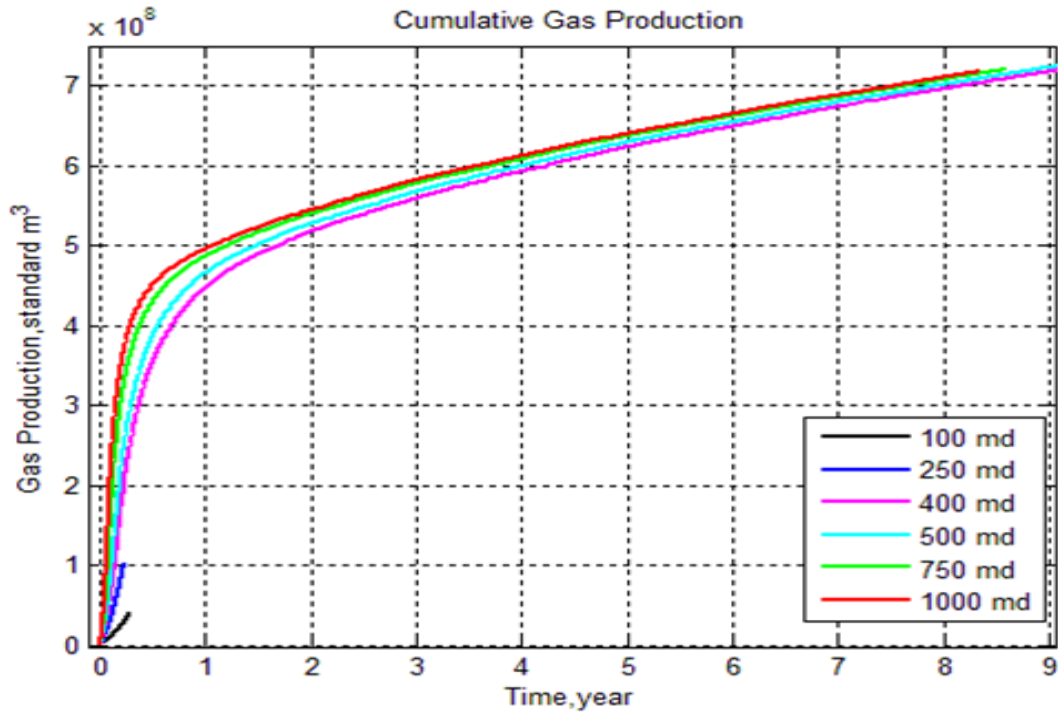


**Figure 7-56:** Depressurization at 2.7 MPa with wellbore heating at different intrinsic permeabilities

#### 7.4.2 Class 3 Hydrate Reservoir Simulations

In this study, the importance of Class 1 gas hydrates was emphasized and it was stated that there is a high potential of Class 1 CH<sub>4</sub> hydrates in the Black Sea. In the Class 1 hydrate simulations in the Black Sea conditions in this study, it was shown that both free gas zone and hydrate zone have important effect on gas production. However, in the Class 3 reservoirs, there is no free gas zone to ease the depressurization or at least

guarantees gas production from only free gas section. Therefore, in order to see these differences between Class 1 and Class 3 hydrate reservoirs in the Black Sea conditions, gas production simulations in the hypothetical Class 3 CH<sub>4</sub> hydrate reservoir in the Black Sea conditions were run. Similar with the Class 1 hydrate simulations, the area shown inside a black circle in Figure 7-39 was selected for a hypothetical Class 3 CH<sub>4</sub> hydrate reservoir. Porosity, rock grain density, wet thermal conductivity, and temperature gradient data in the selected area were found from the study of Vassilev (2006) and other data used for the simulations in this study are shown in Table 7-15.

**Table 7-15:** Properties of the Hypothetical Class 3 CH<sub>4</sub> Hydrate in the Black Sea

<i>Radius</i>	500 m
<i>Thickness of Hydrate Zone</i>	40 m
<i>Thickness of Each Shale Layer</i>	10 m
<i>Porosity</i>	0.50
<i>Permeability</i>	9.869e-13 m <sup>2</sup> (1 D)
<i>Rock Grain Density</i>	2700 kg/m <sup>3</sup>
<i>Wet Thermal Conductivity</i>	2.4 W/(m.K)
<i>Average Pressure</i>	9.9 MPa
<i>Temperature Gradient</i>	0.04 °C/m
<i>Temperature Interval</i>	8.9-11.35°C
<i>Hydrate Zone Saturations</i>	S <sub>h</sub> : 0.55; S <sub>aq</sub> : 0.45
<i>Total CH<sub>4</sub> Amount, m<sup>3</sup></i>	1.233E+09
<i>Total Water Amount, kg</i>	1.432E+10
<i>Relative Permeability Parameters- Modified of Stone Equation</i>	S <sub>ar</sub> : 0.25 S <sub>gr</sub> : 0.02 n: 3.0
<i>Capillary Pressure Parameters- Van Genuchten function</i>	S <sub>ar</sub> : 0.24 n: 1.84 a: 10.0

Hydrate saturation in the hypothetical Class 3 reservoir was chosen as 0.55 in Table 7-15. It was assumed that 40 m hydrate section was bounded by 10 m impermeable

shale or clay sections. Equilibrium model option of HydrateResSim was selected because in the field simulations, there is no difference between equilibrium and kinetic model. Moreover, for kinetic model, many parameters such as intrinsic hydrate reaction constant, hydration activation energy and surface area are needed as shown in Equation (5-14) and these data are not available in the Black Sea because the studies related to gas hydrates in the Black Sea are still immature. For 2D grids of the cylindrical reservoir, 36 grids (Cartesian) along z direction and 75 grids (logarithmic) along r direction are placed and it is shown in Figure 7-57. Therefore, 8,100 equations were solved for 2,700 elements (grids) at each time step.

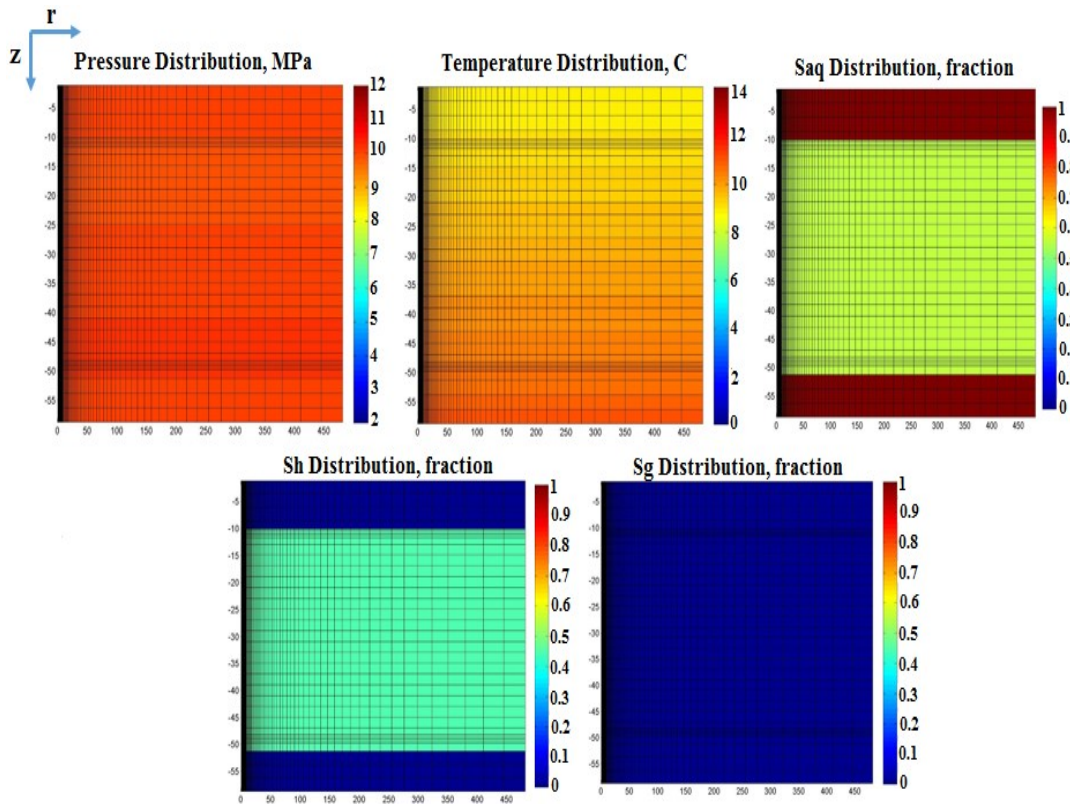


**Figure 7-57:** Grid structure of the hypothetical Class 3 reservoir

The hypothetical reservoir model was constructed by using limited data of Vassilev (2006) because currently, there is no well drilled so there is no available well log data or core sample data. Temperatures at each depth of the hypothetical Class 3 reservoir were calculated by HydrateResSim. Temperature and pressure in the top section of the Class 3 hydrate and those values in the bottom section were entered into the input

file. When HydrateResSim was run without any production at steady state conditions, temperatures and pressures at each grids were found automatically. This is a commonly used method if there is no huge data set for modelling studies (i.e. Kowalsky and Moridis, 2007). After obtaining the steady-state Class 3 hydrate reservoir, gas production simulations from the reservoir by depressurization at different pressures were run with HydrateResSim. 2.0 MPa, 2.7 MPa, 3.0 MPa, 3.5 MPa, 4.2 MPa and 5.0 MPa were selected as production pressures. In Class 3 hydrate reservoirs, perforations are opened in 36 m section of hydrate zone (2 m below and above shale/clay layers). When the pressure is below the hydrate equilibrium pressure, firstly, pressure in the reservoir is decreased by producing water in free pores and then, hydrate starts to dissociate and gas and water flow through the wellbore.

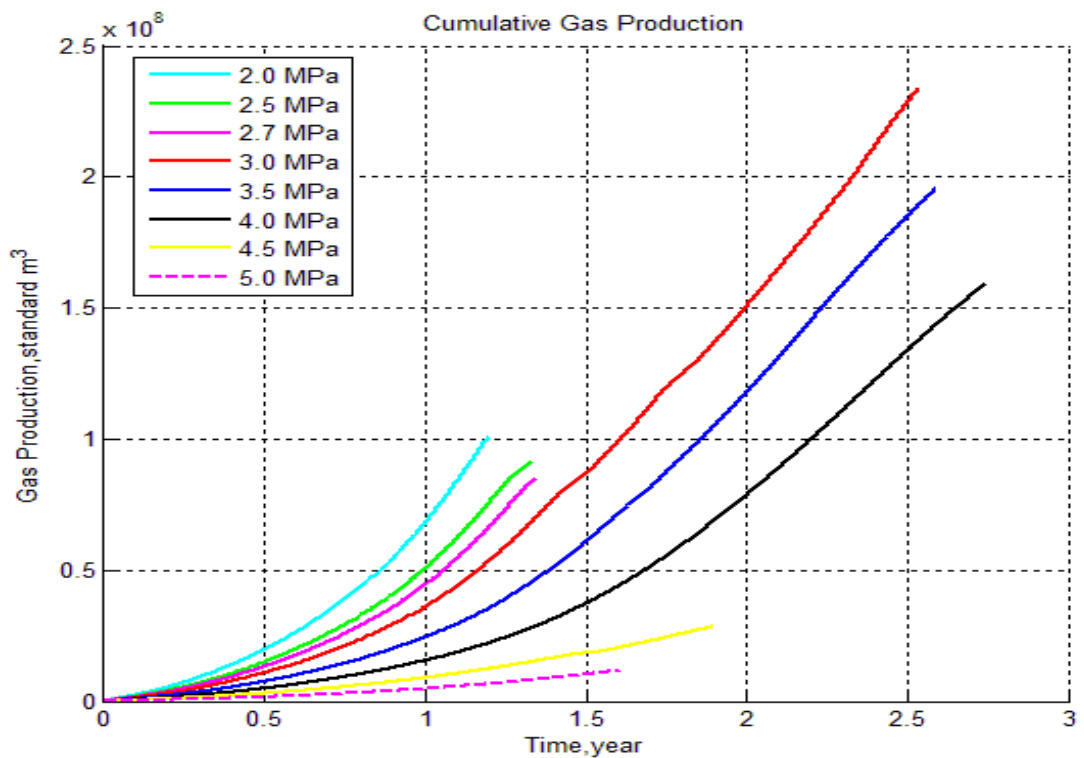


**Figure 7-58:** Cumulative gas production from the Class 3 CH<sub>4</sub> hydrate by depressurization at different pressures

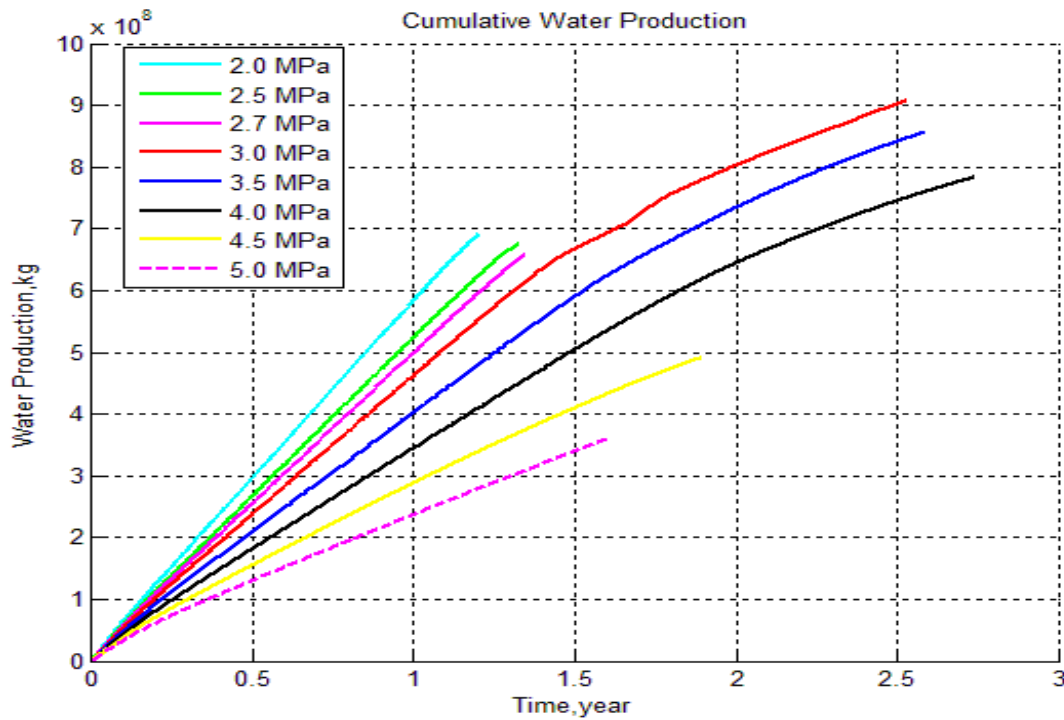


**Figure 7-59:** Cumulative water production from the Class 3 CH<sub>4</sub> hydrate by depressurization at different pressures

At constant wellbore pressures, simulations were run by HydrateResSim. In Figure 7-58 and Figure 7-59, the cumulative gas production and cumulative water production versus time at different production pressures are shown respectively. Highest gas production was obtained at 3 MPa. As seen in Figure 7-58, when the production pressure is lower, much more gas produced but until certain value (2.7 MPa in this case). As gas is produced and with the decrease of the pressure below the hydrate equilibrium pressure, hydrate dissociates. The dissociation of hydrate is endothermic process and it decreases the temperature. However, when the temperature of the hydrate zone decreases with endothermic hydrate dissociation, the impermeable shale/clay boundary provides heat flux through the hydrate zone. As seen in Figure 7-60, gas to water production ratio of Class 3 reservoir increases with gas hydrate dissociation because the main sources of gas and water are stored in Class 3 hydrate so compared to Class 1 hydrate reservoir, gas to water production is low in this case. Gas to water production ratio in Nankai Trough 2013 6-day depressurization test was approximately 100 (Yamamoto *et al.*, 2017).

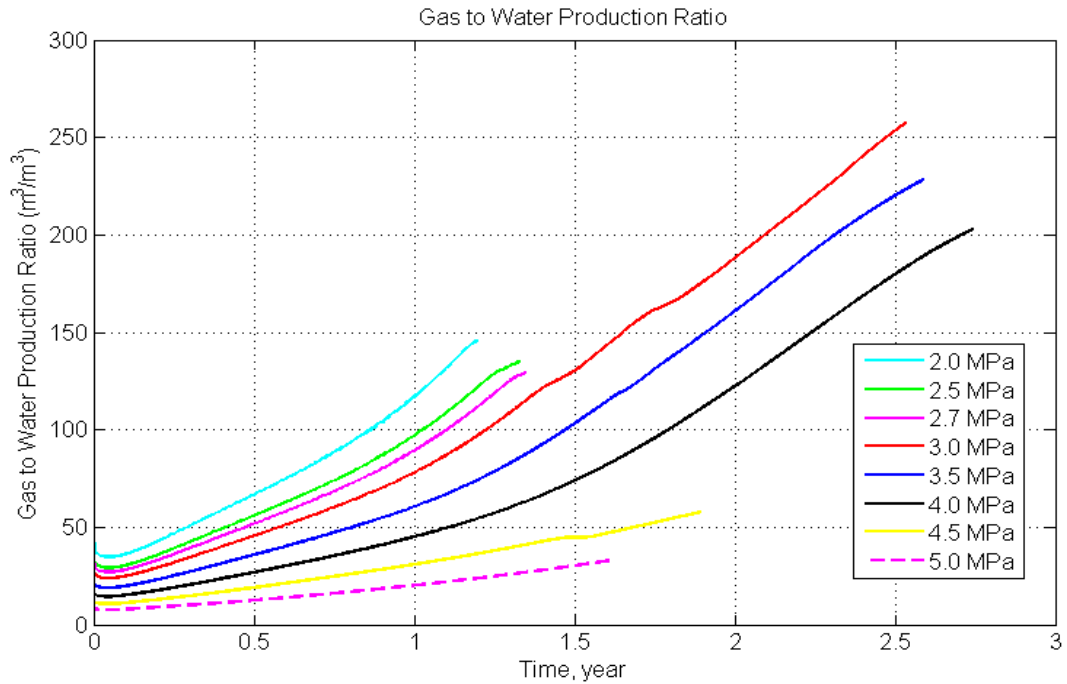


**Figure 7-60:** Gas to water production ratio of the Class 3 CH<sub>4</sub> hydrate by depressurization at different pressures

Gas production rates during depressurization are shown in Figure 7-61. Gas production rate increases exponentially at every depressurization pressure and then they sharply decrease and stop, this is because depressurization decreases temperature significantly due to its endothermic nature. Although impermeable shale boundaries provide heat flux through hydrate section, this might not be enough after a certain time. As the thickness of hydrate section increases, the effect of these heat fluxes disappear because the thermal conductivity of gas hydrates is quite low. Therefore, there is always a risk of hydrate reformation. During depressurization, high amount of water is released to pores with hydrate dissociation. The decrease in the reservoir temperature eases hydrate reformation at lower pressures.

In Figure 7-61, especially at 3.0 MPa between 1.3 year and 2 year, there are sudden decreases in gas flow rates. There might be two reasons of these sudden variations in gas production rates: Hydrate reformation and water blocking in the wellbore. In Figure 7-59, the cumulative water production is shown. When gas flow rates decreased at 3 MPa, water production rate decreased as well. Therefore, the reason

of sudden changes in gas flow rates is hydrate reformation near wellbore. Moreover, when wellbore heating was applied at 50°C, these sudden changes in gas flow rates disappeared as shown in Figure 7-66 because hydrate reformation near wellbore was avoided with heating along the wellbore.

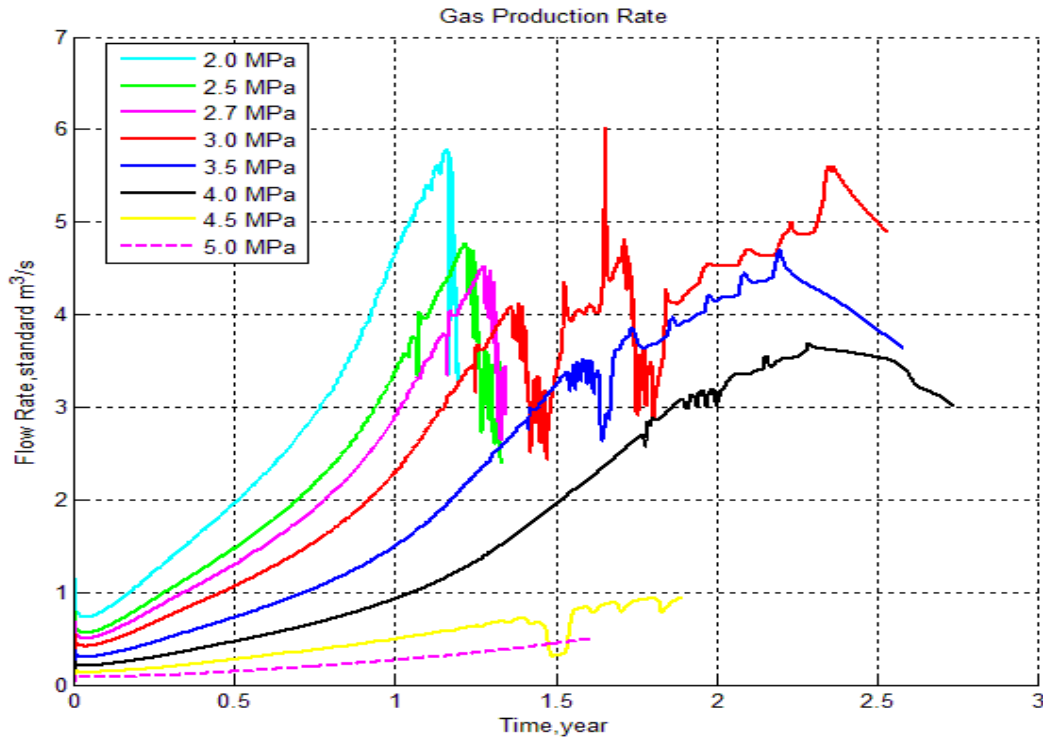


**Figure 7-61:** Gas production flow rate from the Class 3 CH<sub>4</sub> hydrate by depressurization at different pressures

As seen in Figure 7-62, hydrate just below the overburden impermeable shale zone dissociated completely and  $S_g$  increased a lot in this section. This is because the overburden impermeable shale zone behaves like a constant temperature boundary. During depressurization at 3.0 MPa, gas production stopped at 2.5<sup>th</sup> year because hydrate dissociation ceased. At 2.5<sup>th</sup> year, the temperature of the hydrate zone is around 2 °C. Therefore, the heat flux provided by the constant temperature shale/clay zone is not enough to dissociate the hydrate further. With depressurization at 3.0 MPa without any external heat, only 19 % ( $2.337\text{E}+8 \text{ m}^3$ ) of CH<sub>4</sub> in place was produced according to the simulation study. Moreover, the produced water is 6.4 % ( $9.1\text{E}+8 \text{ kg}$ ) of water in place in the hypothetical Class 3 hydrate reservoir.

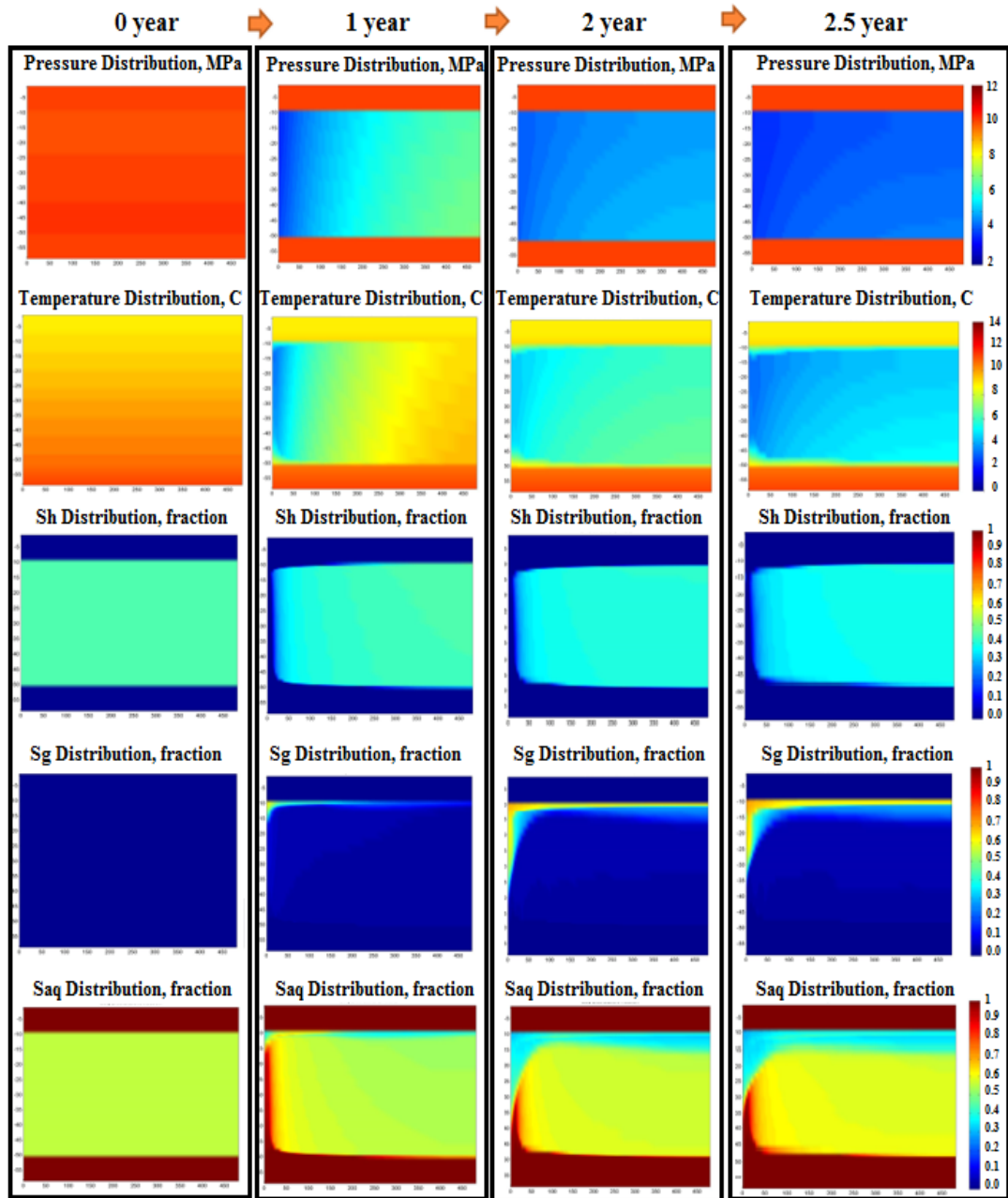


**Figure 7-62:** Changes in pressure, temperature,  $S_h$ ,  $S_g$  and  $S_{aq}$  with depressurization at 3.0 MPa without wellbore heating

After gas production at 3.0 MPa depressurization from the Class 3 hydrate reservoir, approximately 19 % of total CH<sub>4</sub> was produced. Table 7-15 shows the initial CH<sub>4</sub> in the hypothetical Class 3 hydrate reservoir.

As seen in Figure 7-61, there are sudden variations in gas flow rates at different depressurization pressures but most obviously at 3.0 MPa. This is because hydrate reformation near wellbore. Therefore, hydrate formed near wellbore directly blocks water and gas. Wellbore heating is an effective way to avoid any hydrate reformation along wellbore (Kowalsky and Moridis, 2007). However, it should not be considered as another method of gas production from gas hydrates because the effective area of wellbore heating is only along wellbore and near wellbore. For the hypothetical Class 3 CH<sub>4</sub> hydrate in this study, the simulations at different depressurization pressures were run by using HydrateResSim with wellbore heating at 50°C and the results of the simulations were compared with depressurization without wellbore heating. The comparisons of cumulative gas production, water production, gas to water production ratio, and gas production rate are shown in Figure 7-63, Figure 7-64, Figure 7-65 and Figure 7-66 respectively. Cumulative gas productions at 2 MPa, 2.5 MPa, 2.7 MPa, and 4.0 MPa are almost similar but for 3.0 MPa and 3.5 MPa, they are different due to hydrate reformation. The prevention of hydrate reformation along the wellbore with 50°C wellbore heating can be seen obviously when the gas production rates in Figure 7-66 are compared. Similar behaviors were obtained for water production as seen in Figure 7-64. Therefore, wellbore heating might be necessary when there are sudden variations in gas production and water production rates. However, the effect of wellbore heating is just valid near wellbore because thermal conductivity is very low in gas hydrates (around 0.5 W/m. K).

After gas production at 3.0 MPa depressurization with wellbore heating at 50 °C from the Class 3 hydrate reservoir, approximately 25.7 % of total CH<sub>4</sub> (Table 7-15) was produced.

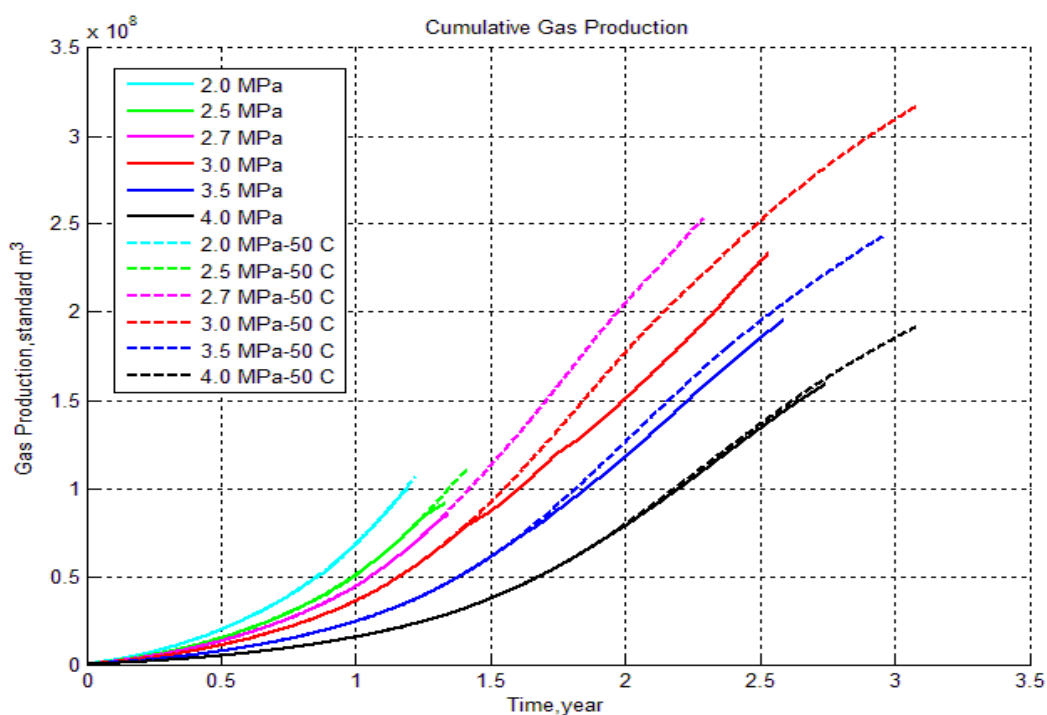


**Figure 7-63:** Comparison of cumulative gas production from the Class 3 CH<sub>4</sub> hydrate by depressurization and depressurization with 50 C wellbore heating

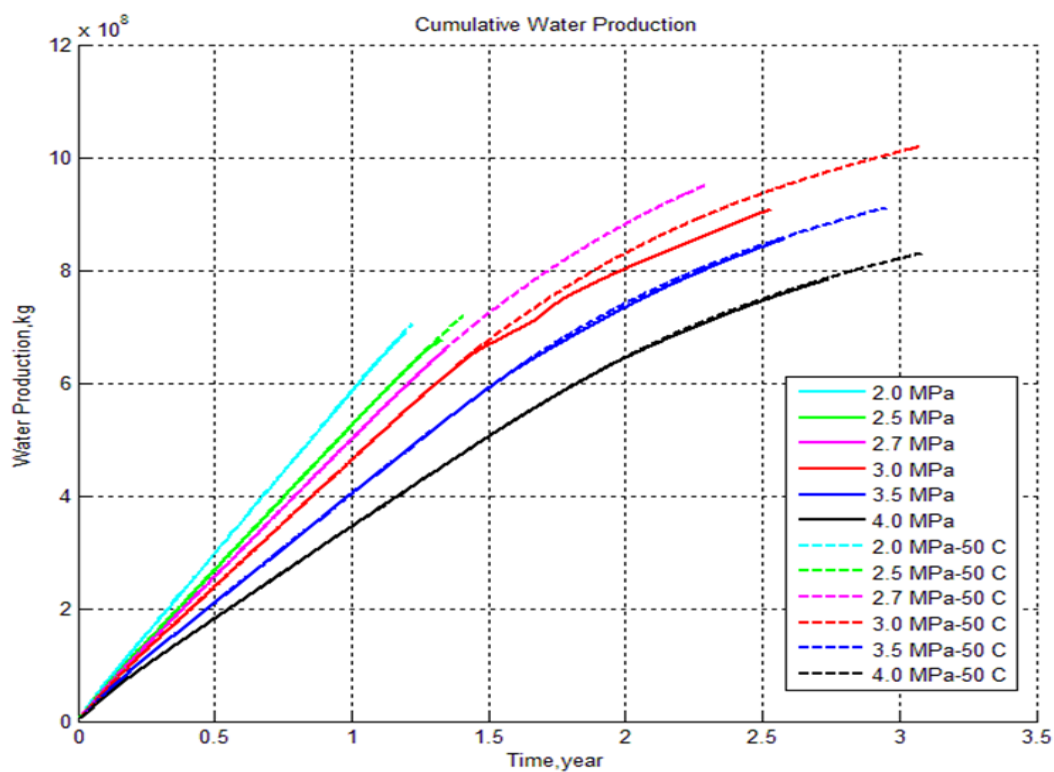


**Figure 7-64:** Comparison of cumulative water production from the Class 3 CH<sub>4</sub> hydrate by depressurization and depressurization with 50 C wellbore heating

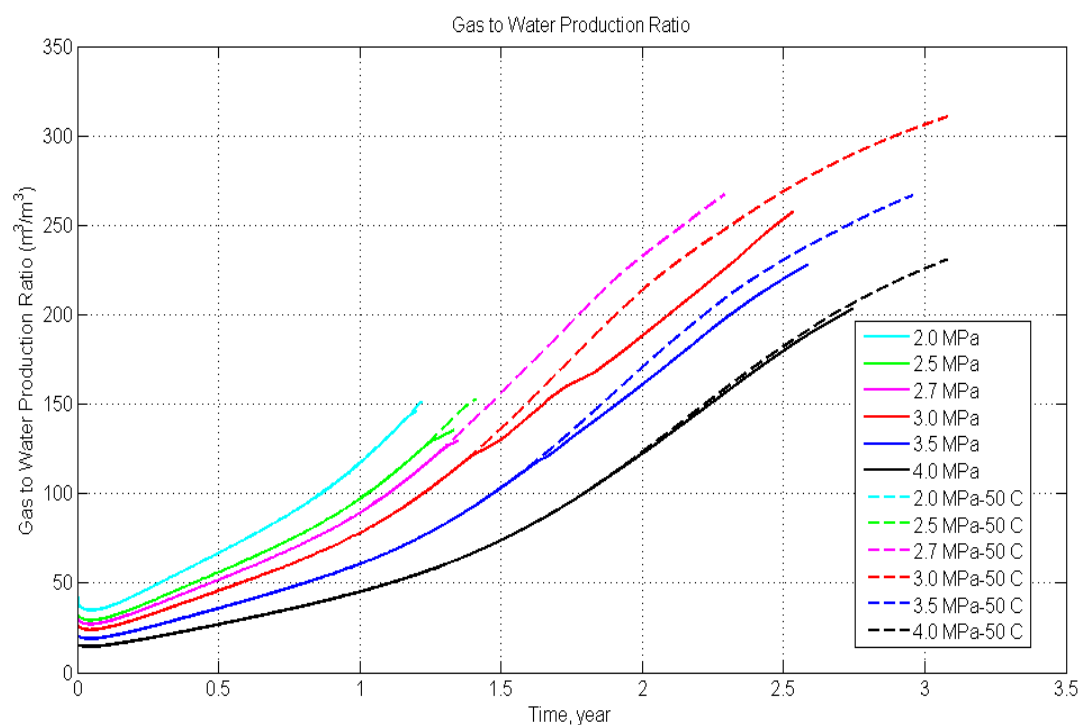


**Figure 7-65:** Comparison of gas to water production ratio of the Class 3  $\text{CH}_4$  hydrate by depressurization and depressurization with 50 C wellbore heating

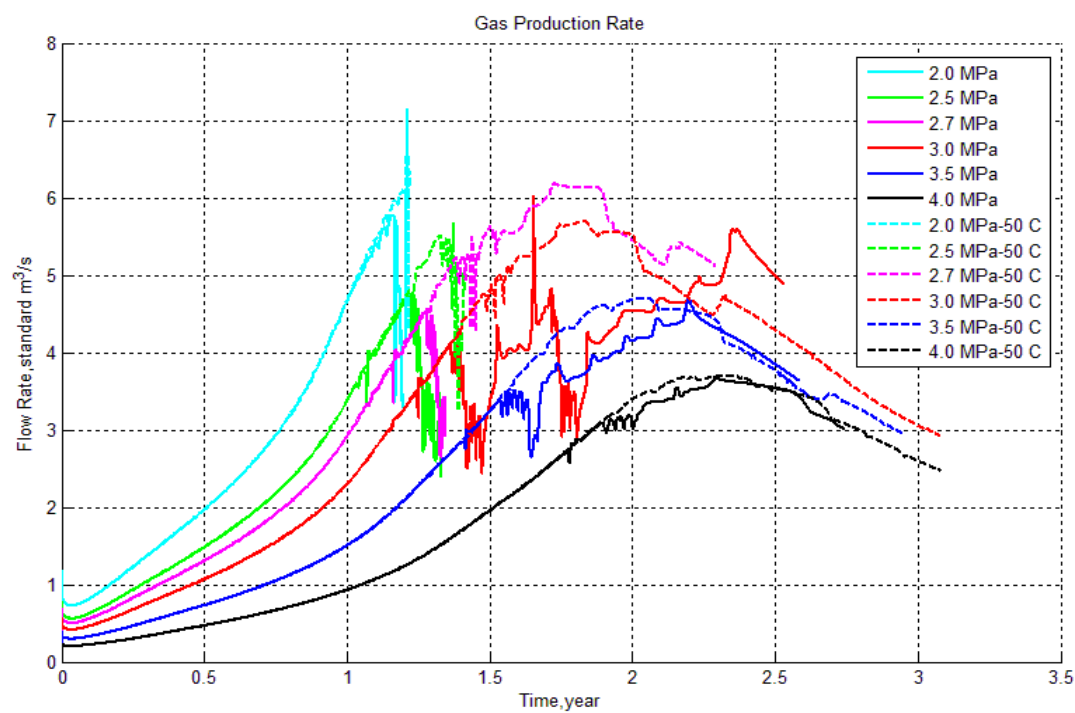


**Figure 7-66:** Comparison of Cumulative gas production flow rates from the Class 3  $\text{CH}_4$  hydrate by depressurization and depressurization with 50 C wellbore heating

In the hypothetical Class 1 hydrate reservoir, gas production was almost equal for every permeability values from 1 Darcy (D) to 400 mD as shown in Figure 7-56. Below 400 mD, it was observed that production has stopped early. There are some gas production differences at 1 Darcy, 750 mD, 500 mD, and 400 mD especially at early times but their effects seem little because of large gas production from free gas zone and hydrate zone. However, when gas production is low, this difference might be important. In Figure 7-67, gas production from Class 3 hypothetical reservoir by depressurization at 3.0 MPa without and with wellbore heating (50 °C) at different intrinsic permeability are shown. Because of hydrate reformation, there are some differences in gas production at same permeability values with and without wellbore heating. When gas production values at different permeability values (1000 mD, 750 mD, 500 mD, 400 mD, 250 mD, 100 mD) are compared, it is obvious that there are big differences. However, this is because of production stop at early times. The main reason of production stop is very low reservoir temperature after hydrate dissociation.

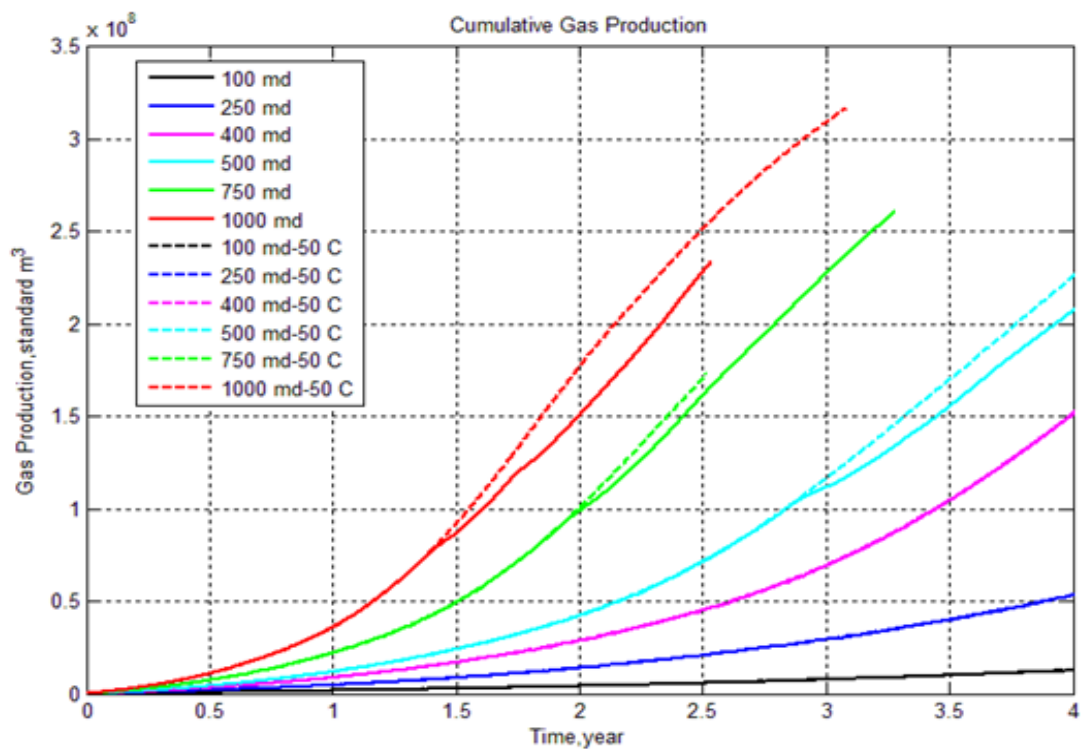


**Figure 7-67:** Gas production from Class 3 hypothetical reservoir by depressurization at 3.0 MPa without and with wellbore heating (50 °C) at different intrinsic permeability

When the results of the hypothetical Class 3 reservoir were compared with the hypothetical Class 1 reservoir, Class 1 hydrates are advantageous. There are important contributions of free gas zone and hydrate zone to gas production. Moreover, BSRs are quite helpful to determine the potential Class 1 gas hydrates. In this study, it was emphasized that Class 1 hydrate might be common in the Black Sea. For better simulation studies, more data such as well log data (obtained during logging while drilling), hydrate saturation data, porosity, permeability, sediment type, etc. are needed. In the future, these data can be obtained from exploration wells and better simulation studies can be held for the Black Sea gas hydrates.

#### **7.4.3 Gas Production Simulations from Gas Hydrate Reservoirs deposited in Turbidites in the Black Sea**

In nature, generally gas hydrate reservoirs are not very thick. Mostly they have alternating layers. To illustrate this, Figure 7-68 was drawn in this study for illustration purpose. In well logs, gas hydrates (with different hydrate saturations, permeability, porosity, etc.) in different layers of pilot hydrate wells in Mallik field, Ignik Sikumi field and Nankai field were observed (Collett and Lee, 2005; Schoderbek *et al.*, 2013; Ito *et al.*, 2015; Sun *et al.*, 2016). The main reason of this is alternating layers from fine sediments (clay and shale) to coarse sediments (sands). Therefore, these types of sediments in the Black Sea might be common because turbidites are common. During logging while drilling (LWD) and coring operations in the sediments as shown in Figure 7-68, many information about their porosities, permeability, and hydrate saturations, etc. are collected. Then, optimum perforation strategy is developed for gas hydrate zones (i.e. zone 1, zone 2, zone 3, etc.). In the study of Sun *et al.* (2016), different well completion strategies were developed and simulated by using Tough + Hydrate for hydrate layers with different hydrate saturations (0.6, 0.35, 0.70) in 1<sup>st</sup> offshore test site in the eastern Nankai Trough. For example, if all hydrate zones are perforated in Figure 7-68 with 0.7, 0.7, and 0.3 hydrate saturation for zone 1, zone 2 and zone 3 respectively, in early stages, gas production will be mostly from zone 3 because it is easy to dissociate due to its low hydrate saturation. However, when hydrate in zone 1 and zone 2 start to dissociate

later, water produced from these perforations might avoid gas production from zone 3. Hence, for similar analysis in the Black Sea, drilling data, well logging data (such as resistivity log), permeability of layers, porosity of layers, temperature profile, type of sediments, gas type, etc., are needed to decide on optimum well completion strategy for the Black Sea gas hydrates having similar characteristics as seen in Figure 7-68.

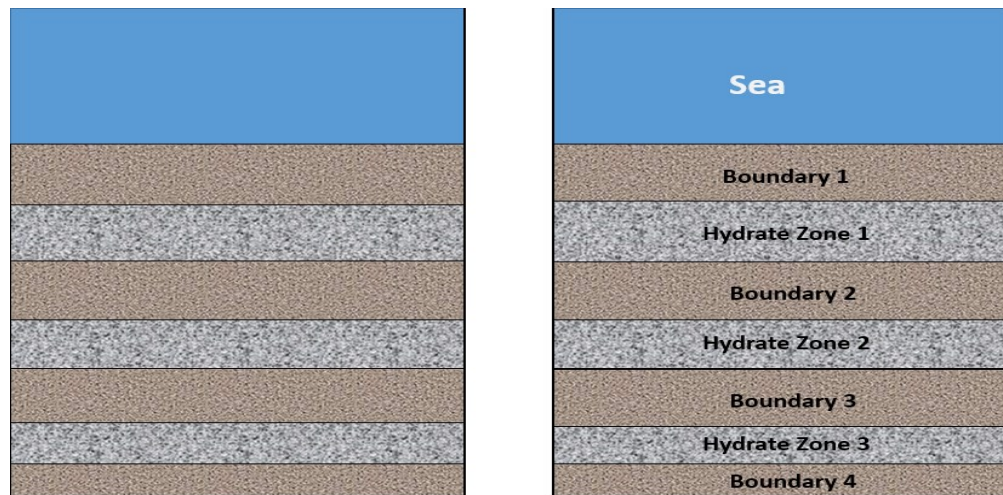


**Figure 7-68:** Alternating gas hydrate layers in turbidites (for illustration purpose)

In this study, in order to understand the differences between gas hydrate reservoirs deposited in different layers of turbidites and Class 3 reservoirs having one thick hydrate zone in the Black Sea conditions, their gas production simulations were compared. As discussed earlier, Class 1 hydrate reservoirs might be common in the Black Sea because many BSRs were detected in seismic studies. However, these seismic studies do not describe the types of sediments below and above this BSR lines well. If there are fine clay or shaly formation just above BSR lines and hydrate zone is above fine silty, clay or shaly formation, classical gas production method from Class 1 hydrate reservoirs cannot be applied. In Class 1 hydrates, perforations are opened in the free gas zone below hydrate zone and this way, hydrate zone dissociates but clay or shaly zone at or just above BSR line in turbidites might avoid this production method. However, compared to Class 3 hydrate reservoirs with one thick hydrate section, turbidites might be advantageous because turbidites have generally thin hydrate sections so heat transfer is very effective from impermeable layers (clay

and shaly layers) of turbidites. It is known that heat conductivity of gas hydrates is low so when hydrate zone is thicker, heat conductivity is lower.

According to Boswell and Collett (2016), in many deep water systems, the sediments are thinly bedded. Moreover, similar tendency was observed in the sediments of the Black Sea in Leg 42B drilling program held in the Black Sea (DSDP, 2016). Therefore, in order to investigate gas production difference between Class 3 and hydrate deposited in turbidites, hypothetical hydrate reservoirs were formed in this study. In the study of Küçük *et al.* (2015), BSR lines were observed at 305 mbsf when sea depth is around 2010 m in Amasra, Bartın, Zonguldak-Kozlu in the central Black Sea. Moreover, several indications were observed that interlayers might exist in this region (Küçük, 2016). Therefore, just above this BSR line, two hypothetical hydrate reservoirs were formed in the Black Sea conditions by using the necessary data for simulation studies in this study. These data are listed in Table 7-16 by using thermal gradient, pressure gradient, porosity etc. gained from the study of Küçük *et al.* (2015) and Vassilev (2006).

As seen in Table 7-16, hydrate saturation in the hydrate zone was chosen as 0.50 and free water saturation in pores was chosen as 0.50. Equilibrium model option of HydrateResSim was selected because at the reservoir conditions, kinetic model and equilibrium models give similar results (Kowalsky and Moridis, 2007; Ruan *et al.*, 2012). For 2D grids of the cylindrical reservoir in turbidites, 65 grids (Cartesian) along z direction and 75 grids (logarithmic) along r direction are placed. 10 grids (cartesian) along z direction and 5 grids (cartesian) along z direction are placed for each hydrate and impermeable boundary respectively. For 2D grids of the Class 3 cylindrical reservoir, 50 grids (cartesian) along z direction and 75 grids (logarithmic) along r direction are placed. 40 grids (cartesian) along z direction and 10 grids (cartesian) along z direction are placed for hydrate and impermeable boundaries respectively. Grids for both hydrate deposited in turbidites and Class 3 reservoir are shown in Figure 7-69. Therefore, 14,625 equations were solved for 4,875 elements at each time step for hydrate deposited in turbidites and 11,250 equations were solved for 3,750 elements at each time step for hydrate deposited Class 3 reservoir.

**Table 7-16:** Properties of the hypothetical CH<sub>4</sub> hydrate deposited in turbidites and Class 3 CH<sub>4</sub> hydrate in the Black Sea conditions

<b>Parameters</b>	<b>Hydrate Deposited in Turbidites</b>	<b>Class 3</b>
<i>Radius</i>	500 m	500 m
<i>Thickness of Hydrate Zone</i>	20 m (Separated 4 layers with 5 m thickness each)	20 m
<i>Thickness of Each Shale Layer</i>	50 m (Separated 5 layers with 10 m thickness each)	50 m (Top and bottom boundary with 25 m thickness)
<i>Porosity</i>	0.50	0.50
<i>Permeability of Hydrate Zone</i>	9.869e-13 m <sup>2</sup> (1 D)	9.869e-13 m <sup>2</sup> (1 D)
<i>Rock Grain Density</i>	2700 kg/m <sup>3</sup>	2700 kg/m <sup>3</sup>
<i>Wet Thermal Conductivity</i>	2.4 W/(m.K)	2.4 W/(m.K)
<i>Average Pressure</i>	24 MPa	24 MPa
<i>Temperature Gradient</i>	0.034 °C/m	0.034 °C/m
<i>Temperature Interval</i>	16.514-18.724°C	16.514-18.724°C
<i>Hydrate Zone Saturations</i>	S <sub>h</sub> :0.50; S <sub>aq</sub> :0.50	S <sub>h</sub> :0.50; S <sub>aq</sub> : 0.50
<i>Total CH<sub>4</sub> Amount, m<sup>3</sup></i>	6.7959113E+08	6.7969273E+08
<i>Total Water Amount, kg</i>	7.11004176E+09	7.10990760E+09
<i>Relative Permeability Parameters- Modified of Stone Equation</i>	S <sub>ar</sub> :0.25 S <sub>gr</sub> :0.02 n: 3.0	S <sub>ar</sub> :0.25 S <sub>gr</sub> :0.02 n: 3.0
<i>Capillary Pressure Parameters- Van Genuchten function</i>	S <sub>ar</sub> : 0.24 n: 1.84 a:10.0	S <sub>ar</sub> : 0.24 n: 1.84 a:10.0

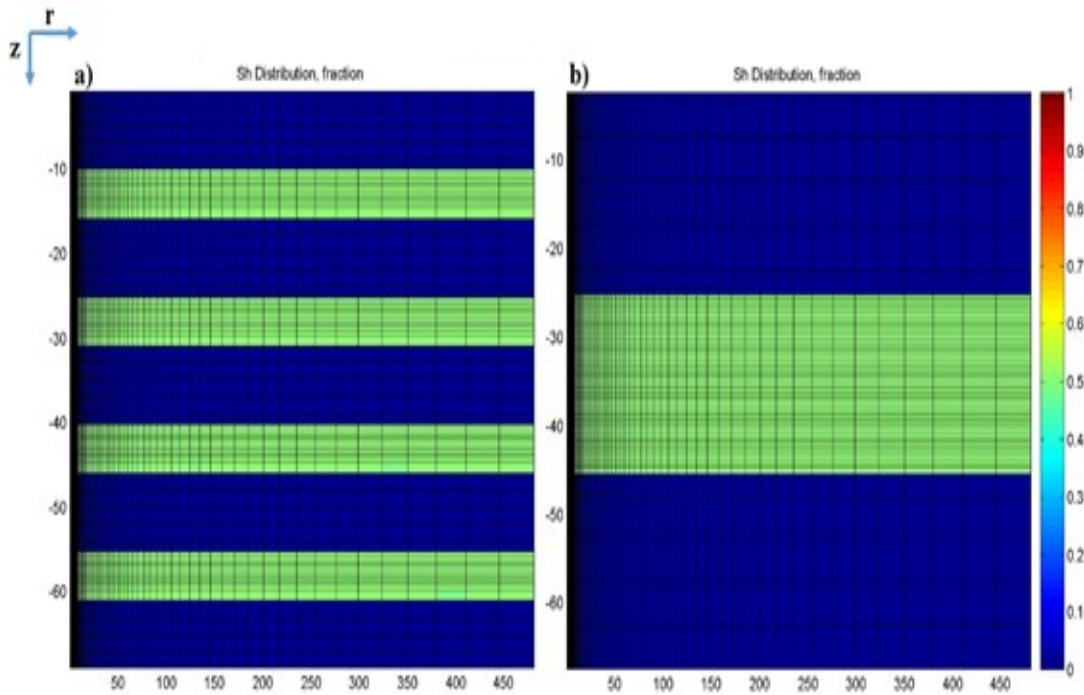


**Figure 7-69:** Hydrate saturations and grids in a) Turbidites b) Class 3 reservoir

For both hypothetical hydrate reservoirs, perforations are opened in hydrate sections and gas production simulations were held by using depressurization with and without wellbore heating methods. HydrateResSim numerical simulator was used in the simulations. When cumulative gas production, cumulative water production, gas to water production ratio and gas production rates of two reservoirs are compared in Figure 7-70, Figure 7-71, Figure 7-73, Figure 7-74, Figure 7-75, Figure 7-76 and Figure 7-77, it is obvious that gas production in the hypothetical gas hydrate reservoirs deposited in turbidites are quite higher than gas production in the hypothetical gas hydrate reservoirs deposited in turbidites because heat flow from boundaries are higher in thin hydrate zones in turbidites. Therefore, this can be advantageous for the Black Sea.

Table 7-16 shows the initial  $\text{CH}_4$  in the hypothetical Class 3 hydrate reservoir. After gas production at 4.0 MPa depressurization with wellbore heating at  $50^\circ\text{C}$  from the hypothetical hydrate sections deposited in turbidites, approximately 95.5 % of total  $\text{CH}_4$  was produced because of wellbore heating and thin gas hydrate sections.

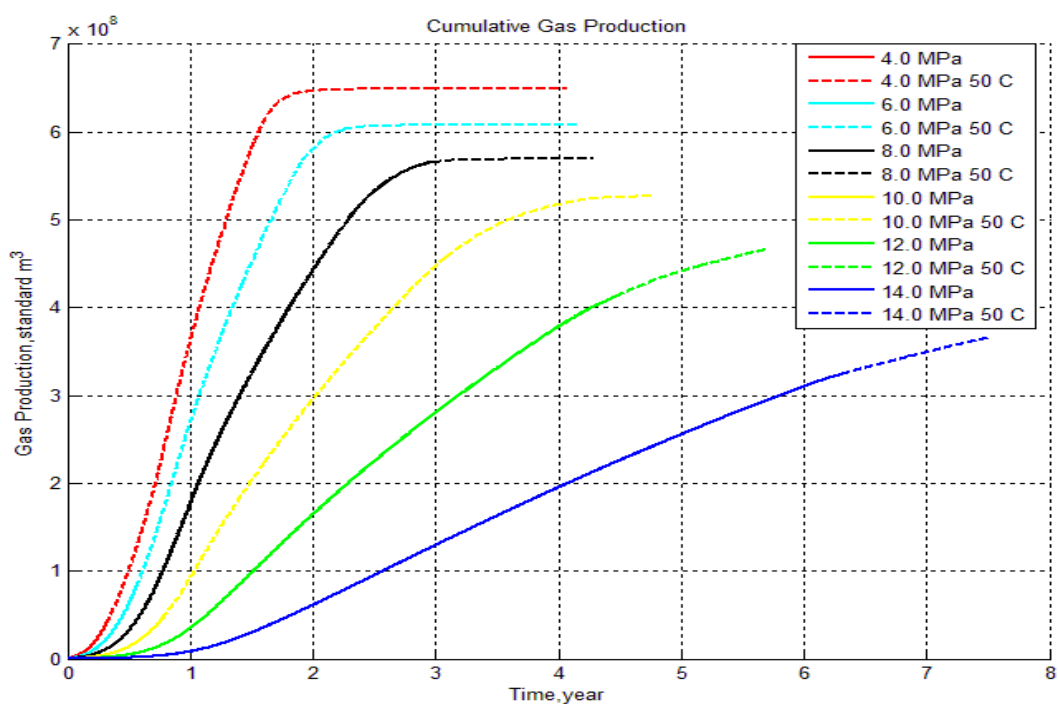


**Figure 7-70:** Cumulative gas production by depressurization in the hypothetical hydrate deposited in turbidites

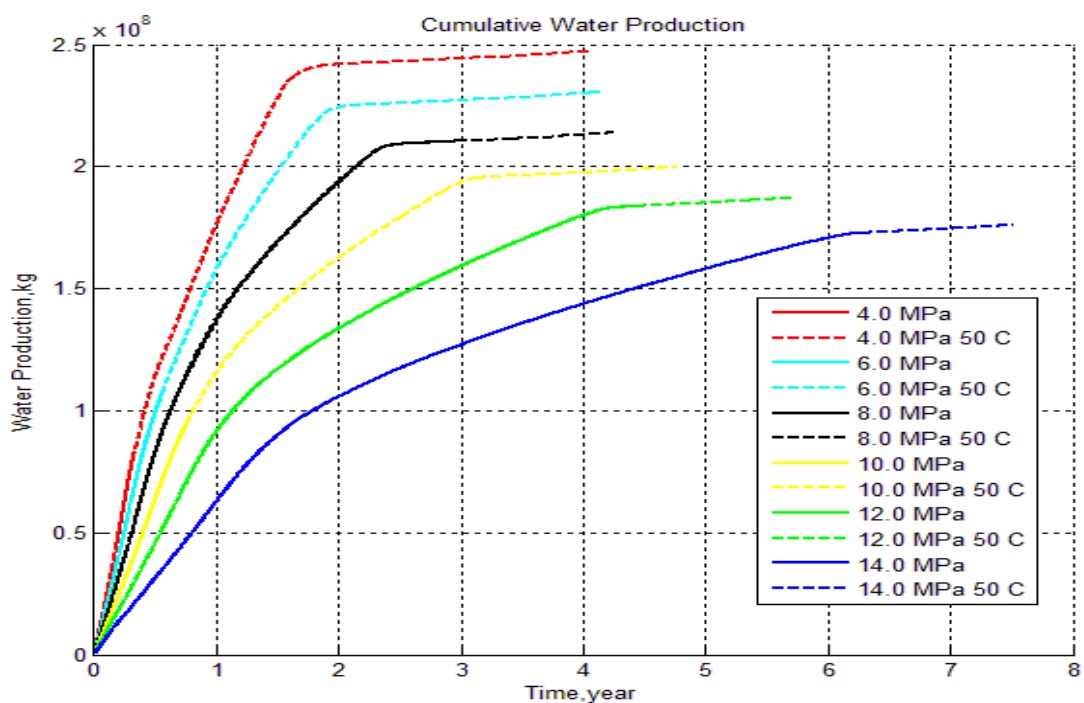


**Figure 7-71:** Cumulative water production by depressurization in the hypothetical hydrate deposited in turbidites

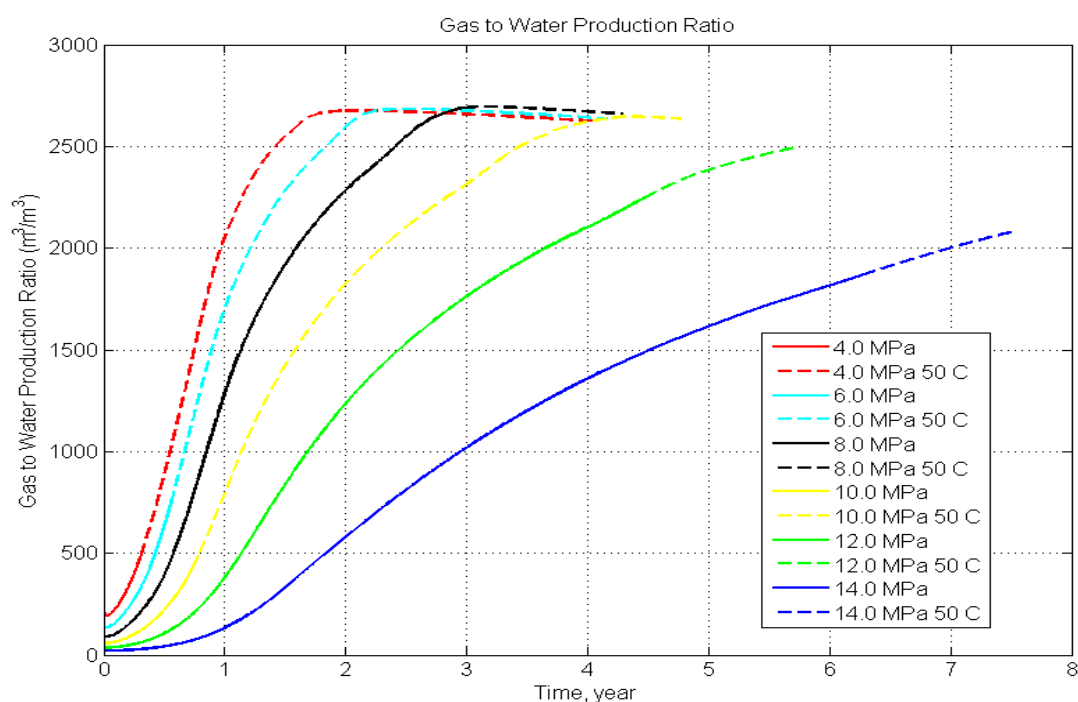


**Figure 7-72:** Gas to water production ratio of depressurization in the hypothetical hydrate deposited in turbidites

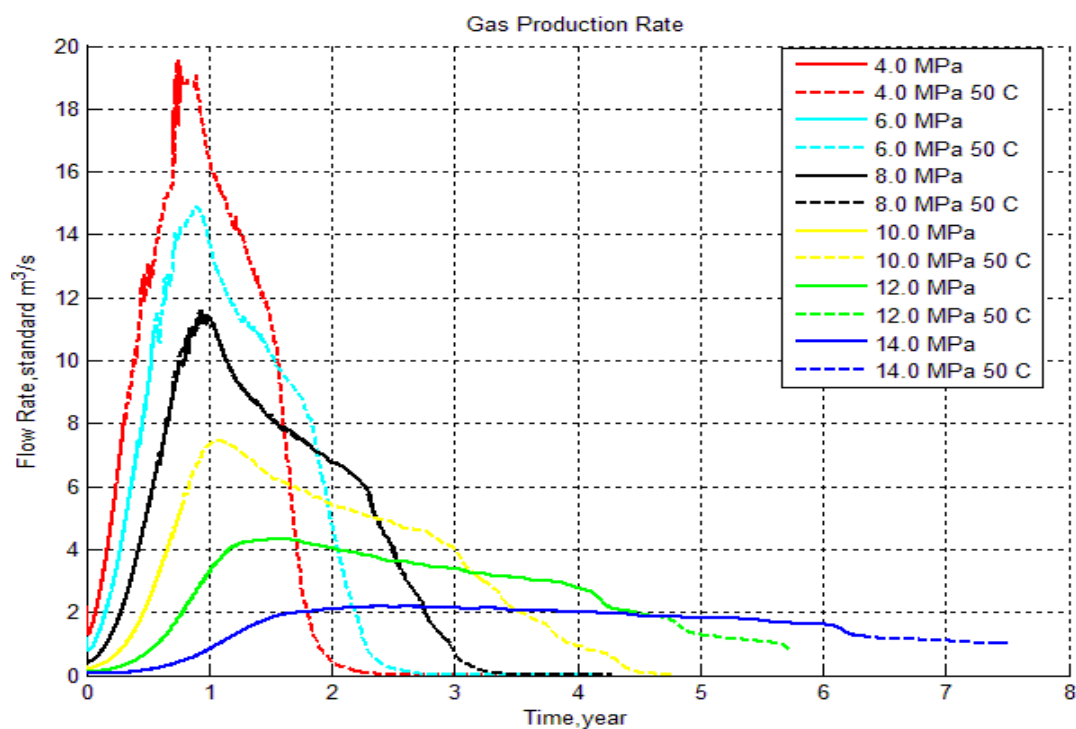


**Figure 7-73:** Gas production rate by depressurization in the hypothetical hydrate deposited in turbidites

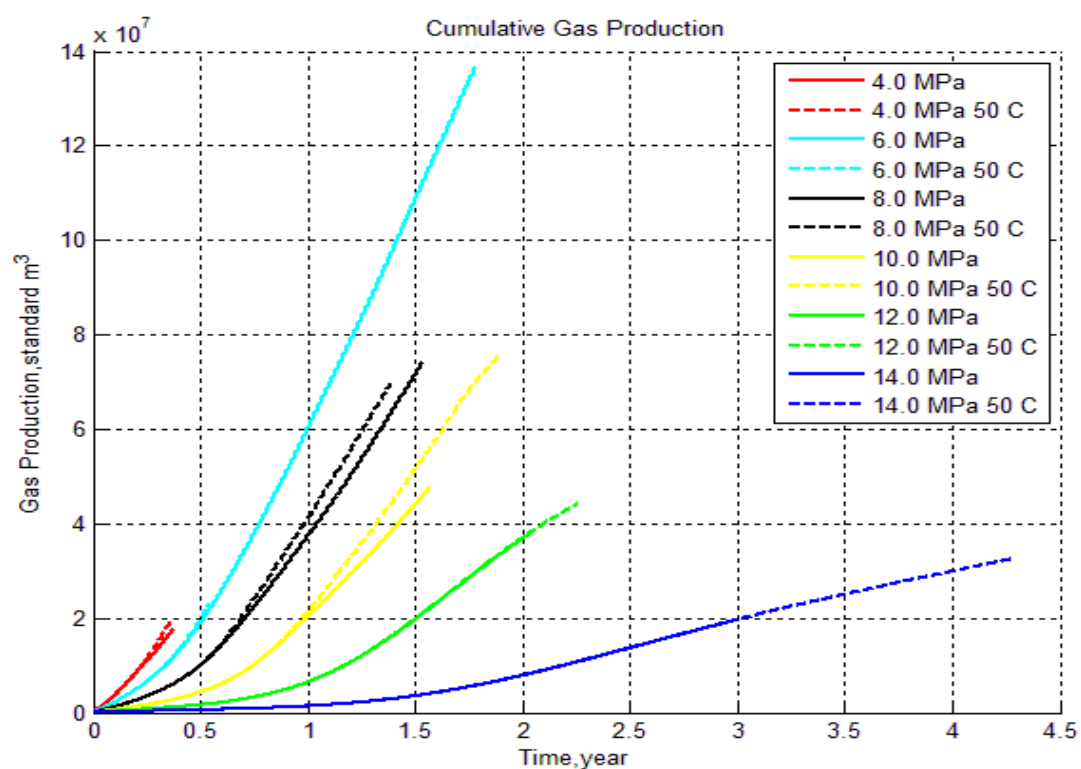


**Figure 7-74:** Cumulative Gas Production by depressurization in the hypothetical Class 3 reservoir

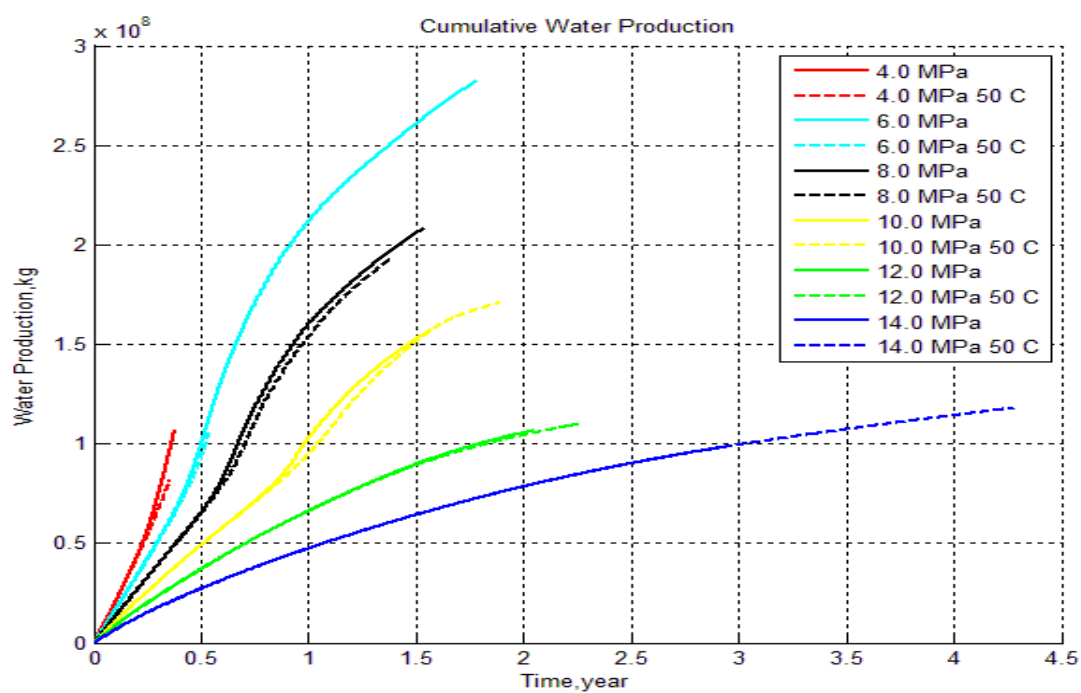


**Figure 7-75:** Cumulative Water Production by depressurization in the hypothetical Class 3 reservoir

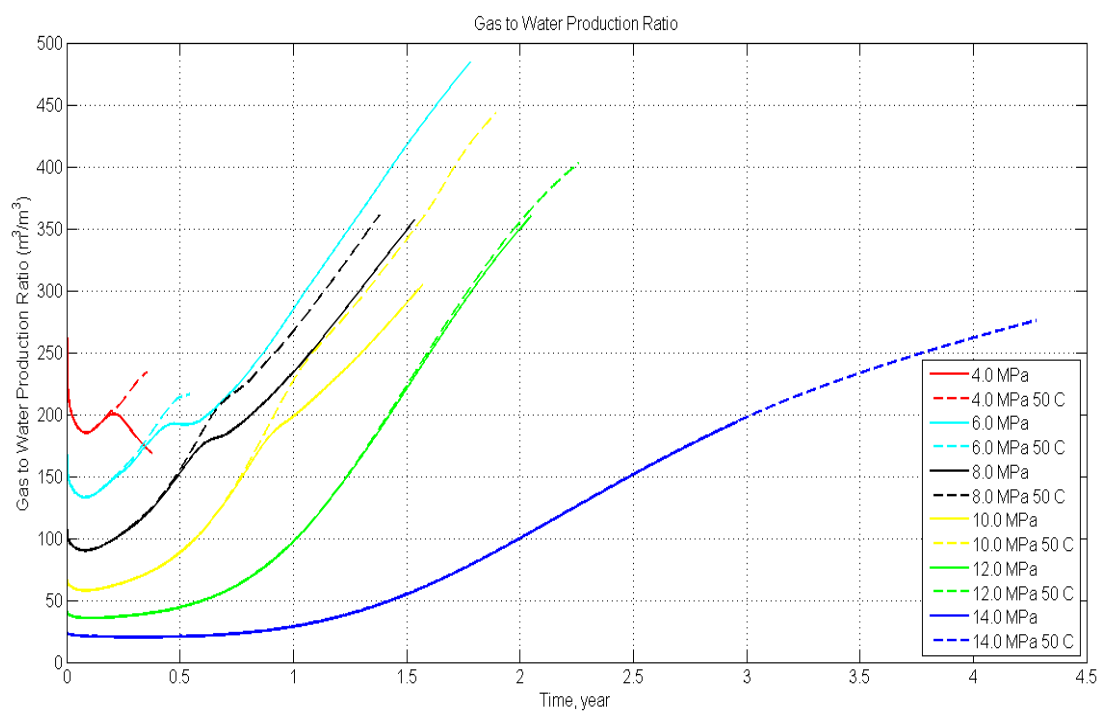


**Figure 7-76:** Gas to water production ratio of depressurization in the hypothetical Class 3 reservoir

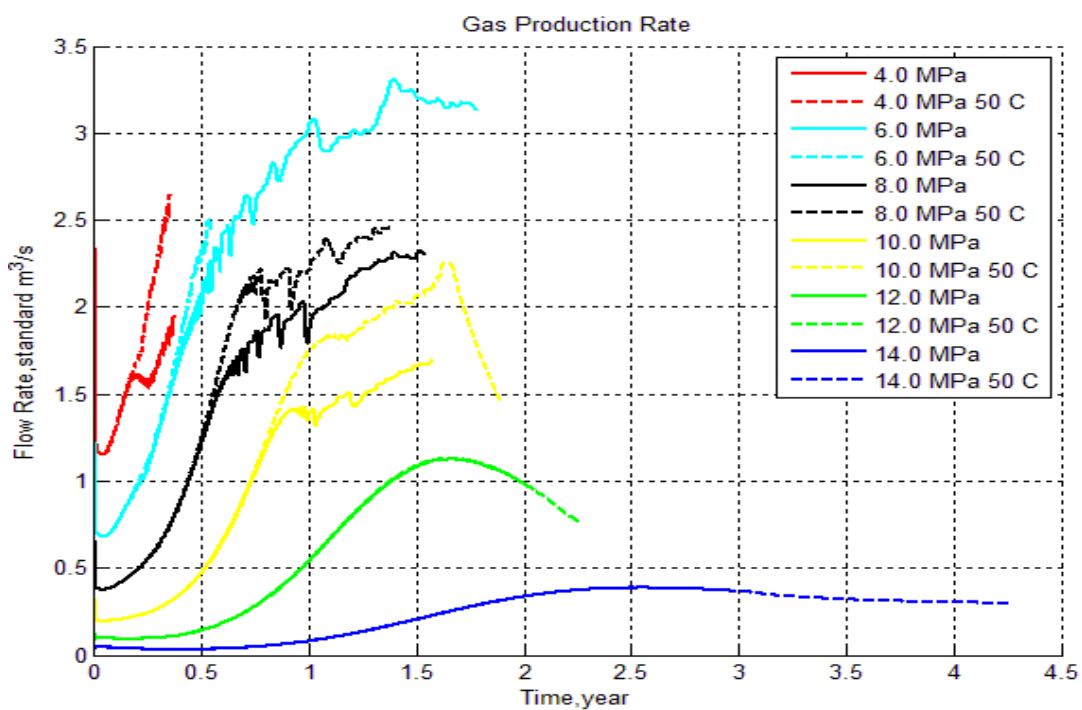


**Figure 7-77:** Gas production rate by depressurization in the hypothetical Class 3 reservoir

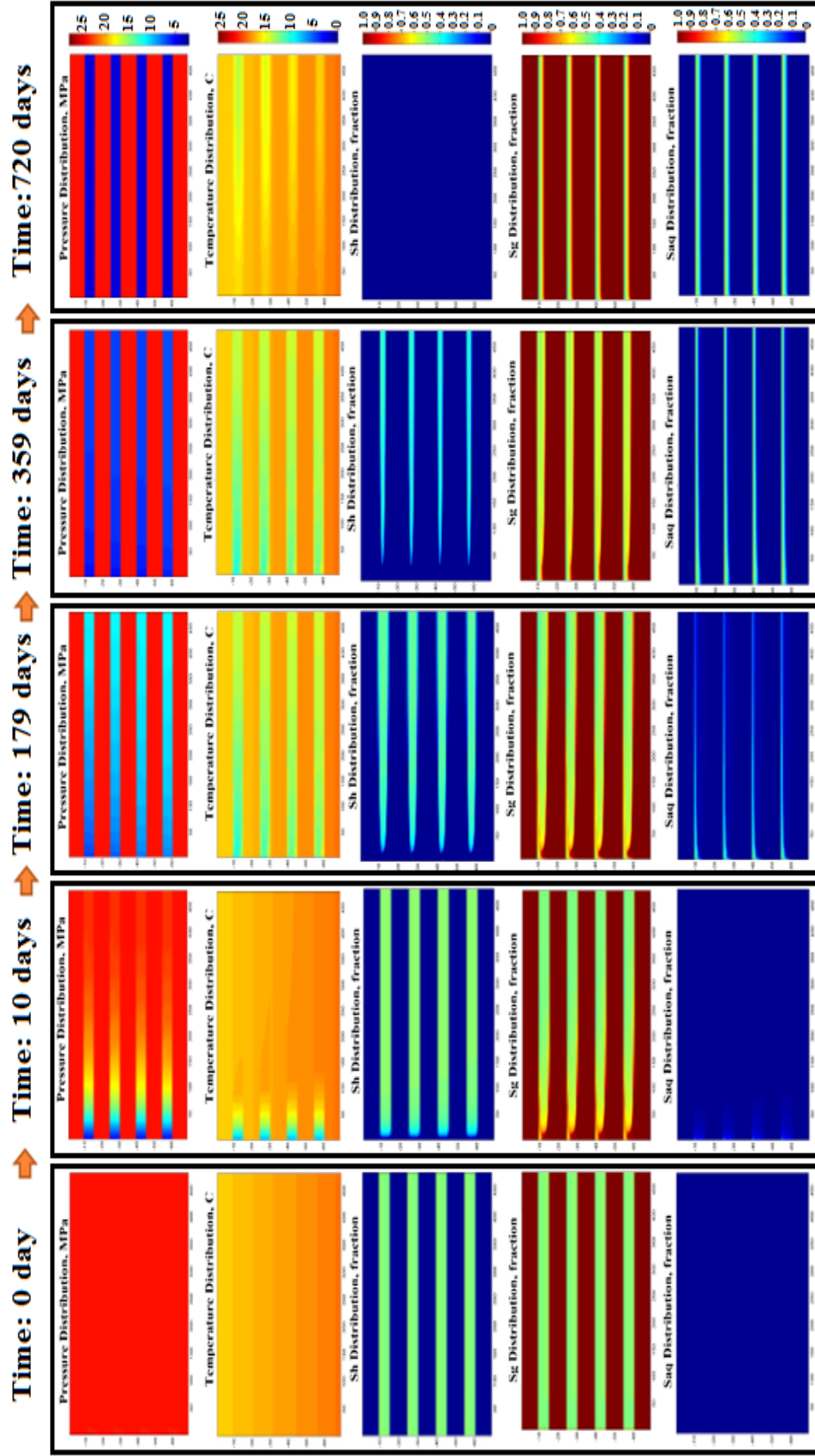


**Figure 7-78:** Changes in pressure, temperature,  $S_h$ ,  $S_g$  and  $S_{aq}$  with depressurization at 4.0 MPa with wellbore heating at 50 °C in turbidite hydrate reservoirs

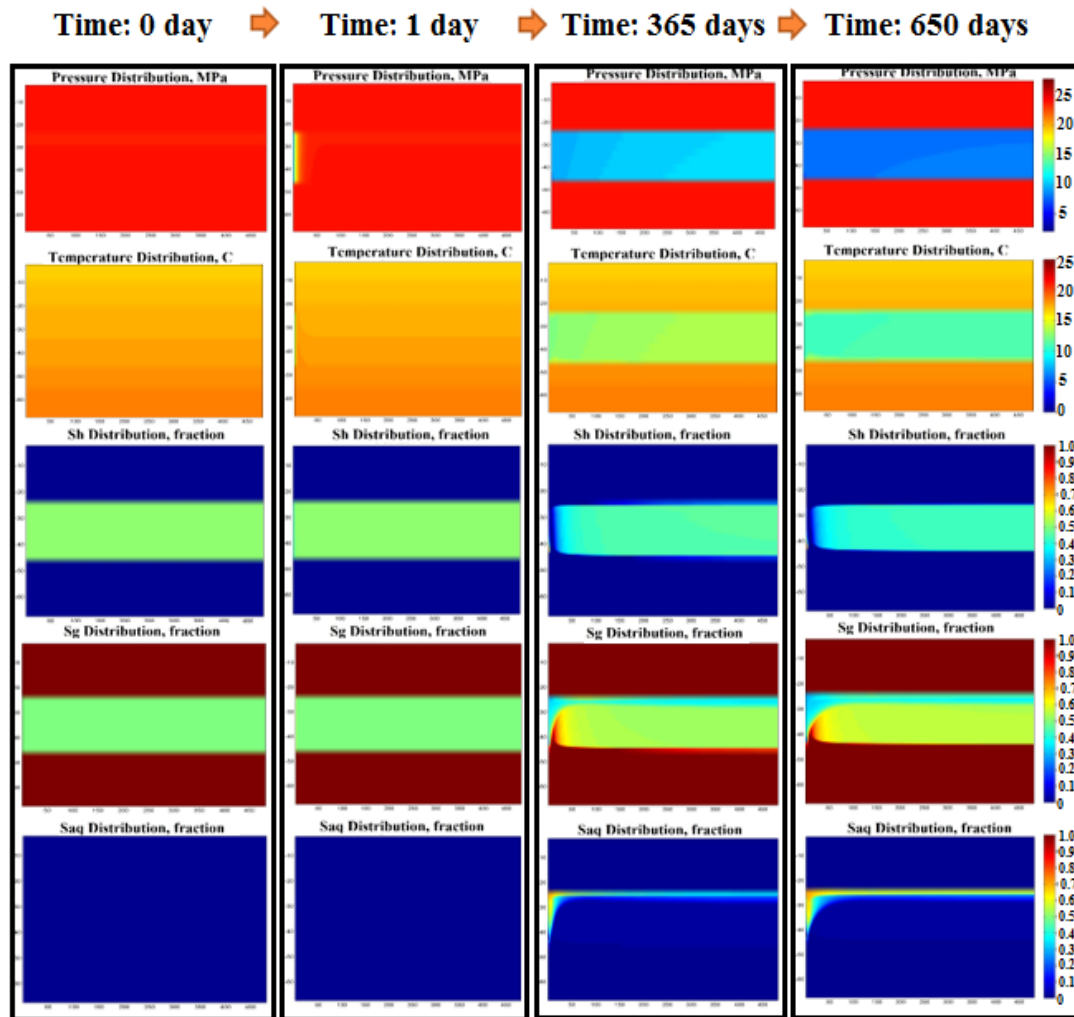


**Figure 7-79:** Changes in pressure, temperature,  $S_h$ ,  $S_g$  and  $S_{aq}$  with depressurization at 6.0 MPa without wellbore heating in Class 3 hydrate reservoir

After gas production at 6.0 MPa depressurization without wellbore heating from the Class 3 hydrate reservoir in Table 7-16 and Figure 7-79, approximately 20.1 % of total  $CH_4$  was produced. Compared to thin gas hydrate sections of the hypothetical hydrate reservoir in turbidites, gas production recovery from the thick Class 3 hydrate reservoir is quite low because low heat fluxes through thick hydrate section from the boundaries.

Gas production behavior during depressurization for hydrates deposited in turbidites and Class 3 reservoirs are shown in Figure 7-78 and Figure 7-79 respectively. As seen in these figures, the temperatures of hydrate sections decrease while gas production.

The reason of this is mainly endothermic nature of hydrate dissociation. However, as an average, temperature decreases from 17.5 °C to 10 °C. Therefore, in the Black Sea conditions, ice formation in hydrate reservoirs is not possible when sediments are around 50-100 m below seafloor. For hydrate deposited in turbidites, it was assumed that hydrate sections have uniform hydrate saturation as 50 %. However, in real cases, their saturations might be different. Hence, well completion strategies should be developed for these cases. In this study, it was only aimed to show that gas hydrate deposited in turbidites as thin sections can be advantageous compared to Class 3 hydrate reservoirs in the Black Sea conditions. It is because heterogeneous thin hydrate layers cause faster hydrate dissociation and higher gas production rate due to fast heat transport. Similar observations were reported in the study of Myshakin *et al.* (2012), Janicki *et al.* (2014) and Max and Johnson (2016) for gas hydrates in the world.

#### **7.4.4 Gas Production Simulations from Gas Hydrates in the Danube Delta of the Black Sea**

Even though there are high gas fluxes in the different parts of the Black Sea, almost of all these gases do not reach to atmosphere. Mainly, these gases are consumed by oxidation, sulfate reduction, carbonate precipitation and benthic ecosystems as discussed in Chapter 4 (Kessler *et al.*, 2006). Tinivella (2016) proposed that the Black Sea might be a good site for gas hydrate production tests due to its low environmental risks. Recently, the activities related to the Black Sea gas hydrates have increased. For example, in Turkey, the seismic surveys have been taken in the southwestern part of the Black Sea for gas hydrate exploration (Max and Johnson, 2016). Moreover, detailed exploration analysis such as BSR detection, ocean bottom seismometer survey and marine controlled source electromagnetic (CSEM) survey have been done in the Danube Delta in the Black Sea (Popescu *et al.*, 2006; Schwalenberg and Engels, 2011; Schwalenberg *et al.*, 2015; Schwalenberg *et al.*, 2016; Dannowski *et al.*, 2016). According to Haeckel *et al.* (2015), the Paleo-Danube river system in the western Black Sea, located in the economic zones of Bulgaria and Romania is a good candidate for the first gas hydrate production test in the Black Sea because gas

hydrates in coarse sand sections were detected in this region. Therefore, in the late of 2017, the drilling with seafloor drilling unit MeBo (200-300 m drilling capability from seafloor) in this region under SUGAR Project is planned (Vasilev, 2015; Merey, 2016). There are enough data (gas hydrate saturation, location and thickness of gas hydrate sections, seafloor temperature, sea salinity, etc.) to simulate gas production from this region. Therefore, in this study, it is aimed to simulate short-term gas production from this region and provide useful results for possible short-term production tests from the gas hydrates in this region. In this study, for the first time, it was shown that CO<sub>2</sub>-CH<sub>4</sub> swapping is not appropriate in the Black Sea conditions, especially due to the high temperature of the Black Sea. Moreover, in Ignik Sikumi field, CO<sub>2</sub>-CH<sub>4</sub> swapping could not be proved completely and it is considered that for a long time, depressurization method will stay the primary basis for future gas hydrate field production tests (Boswell *et al.*, 2016). As temperature increases, the effectiveness of depressurization method increases and the Black Sea sediments are warm compared to those in oceans. Hence, in the numerical simulations in this study, depressurization production method was chosen.

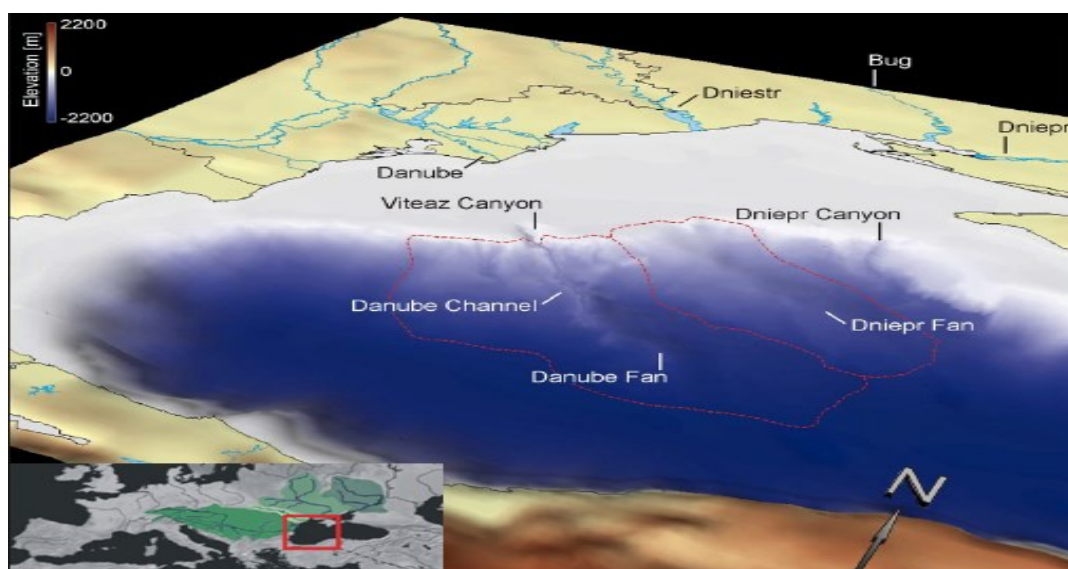


**Figure 7-80:** 3D view of a digital elevation model of the western Black Sea (Konerding, 2009)

The Danube deep-sea fan (or turbidite system) is developed in the northwestern part of the Black Sea, fed by sediments from the Danube river (having freshwater) (Popescu *et al.*, 2004). Figure 7-80 shows 3D of Danube channel and Danube fan.

Popescu *et al.* (2006) determined multiple-BSRs in the Danube system. There are several reasons of multiple BSRs: different gas composition at each BSR, the effect of climate change (sea level changes), rapid sedimentation and some different lithology (Popescu *et al.*, 2006; Paganoni *et al.*, 2016; Zander *et al.*, 2017). According to Jegen and Hölitz (2014), multiple BSRs in the Danube fan are thought to be due to climate related sea level changes in the past. However, Zander *et al.* (2017) proposed that the reason of the multiple BSRs in Danube delta is the temperature effect due to rapid sedimentation rather than bottom-water temperature change, sea level variations and different gas composition. The expelled gas in the Danube delta is mainly composed of CH<sub>4</sub> of biogenic origin with concentrations of 99.1–99.9% (Bialas, 2004; Zander *et al.*, 2017). Hence, in this study, it was assumed that 100 % CH<sub>4</sub> exists in gas hydrate deposited in coarse-grained sediments in this region during numerical simulations.

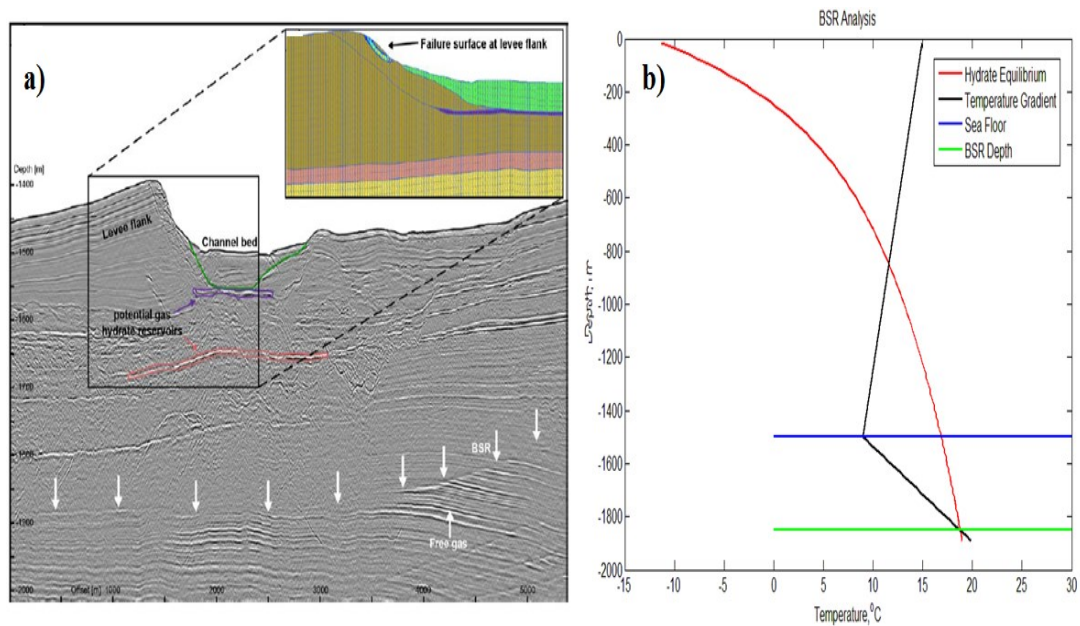


**Figure 7-81:** a) A seismic section in the Danube Delta (coarse grained sediments are highlighted with purple and light red) (Zander *et al.*, 2016) b) BSR analysis by BSR.m code in this study for 100 % CH<sub>4</sub> hydrate for the system in Figure 7-81-a

Figure 7-81-a shows two gas hydrate sections in coarse grained sediments (upper one is 6 m thick at 60 mbsf and the lower one is 30 m thick at 140 mbsf) within CH<sub>4</sub> gas hydrate stability zone in the Danube fan of the Black Sea (at 350 mbsf) (Zander *et*

*al.*, 2015; Zander *et al.*, 2016). Marine controlled source electromagnetic methods are useful to reveal the electrical properties of the shallow seafloor. In the Danube Delta, western Black Sea, these methods were implemented at where there are not any gas seepages and the sections with high resistivity were detected as shown in Figure 7-81-a. The reason of high resistivity was due to highly fresh pore water (Danube river's water is fresh) and up to 50 % gas hydrate saturation (Schwalenberg and Engels, 2011; Schwalenberg *et al.*, 2015; Schwalenberg *et al.*, 2016). Moreover, in the study area in Figure 7-81-a, no gas seepage was observed even though many gas seepages were observed in different parts of the Danube fan (Zander *et al.*, 2015). Seafloor temperature at 1500 m sea depth is nearly 9°C and geothermal gradient ranges from 27 to 35 °C/km in the Danube delta (Haeckel *et al.*, 2015). By using BSR.m code (which is described in the following sections of this chapter) in this study in Figure 7-81-b, it was found that in the region of Figure 7-81-a, geothermal gradient should be nearly 27.8 °C/km to cut the BSR line at 350 mbsf for 100 % CH<sub>4</sub> hydrate. When hydrate equilibrium curve of CH<sub>4</sub> (pressure versus temperature graph) is investigated, it is an exponential curve so small changes in temperature causes large differences in hydrate equilibrium pressures (especially at high temperatures). The Black Sea sediments are warm compared to those in oceans. Hence, highly accurate heat flow and geothermal gradient determination is necessary in the Black Sea to determine the thickness of CH<sub>4</sub> hydrate stability zone correctly.

The porosity of coarse sediments in the study area are expected to be approximately 0.5 (Schwalenberg *et al.*, 2015). Seawater density is nearly 1030 kg/m<sup>3</sup> and sediment thermal conductivity is nearly 1.27 W/m.K (Vasilev, 2015). Generally, the formation pressure of gas hydrate reservoirs is essentially hydrostatic with a light sediment load whereas deeper conventional hydrocarbon deposits can be highly pressurized with respect to seafloor pressure (Berndt, 2005; Max and Johnson, 2016). Hence, for upper hydrate section (Hydrate Zone 1) in Figure 7-81-a and Figure 7-82, average reservoir pressure was calculated as 15.83 MPa. For lower hydrate section (Hydrate Zone 2) in Figure 7-81-a and Figure 7-82, average reservoir pressure was calculated as 16.79 MPa.

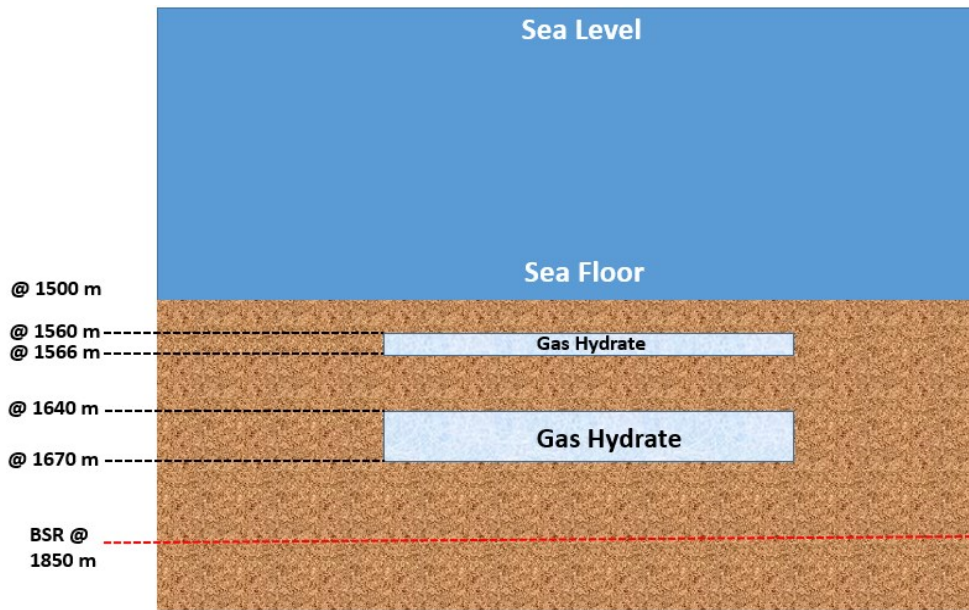


**Figure 7-82:** Scheme of gas hydrate sections in the Danube fan in the Black Sea

From Figure 7-81-a, it was assumed that the gas hydrate reservoirs are cylindrical and its radius is 250 m. Moreover, the boundaries of gas hydrate sections (mainly clays) are considered as impermeable and in different studies, it was also assumed that clay boundaries are impermeable (Lim *et al.*, 2016). Hence, their permeabilities are assumed to zero. For intrinsic permeability of gas hydrate reservoirs, there is no available data but it is known that these sections have coarse grained sediments according to all exploration studies in this study area. Therefore, by using the permeability versus grain size (coarse sand) correlations of Shepherd (1989), it was decided that permeability of sediments might be around 1 Darcy ( $9.869\text{e-}13 \text{ m}^2$ ). During Ignik Sikumi 1 well  $\text{CO}_2\text{-N}_2/\text{CH}_4$  swapping test, no core sample is taken and permeability is calculated by using Carman-Koseny type models where porosity and surface area/volume information are used (Boswell *et al.*, 2016). Similar assumptions are necessary when there is no information. For instance, for relative permeability, the modified of Stone equation was used and for capillary pressure, the formula of Van Genuchten was used in this study. For parameters of these equations, the values frequently used in the literature were preferred due to lack of these data for the Black Sea sediments and they are shown with all other parameters in Table 7-17 for numerical simulations by depressurization with HydrateResSim numerical simulator in the Danube Fan of the Black Sea.

**Table 7-17:** Properties of CH<sub>4</sub> Hydrates in the Danube Fan of the Black Sea

<i>Sea Water Density</i>	1030 kg/m <sup>3</sup>
<i>Radius</i>	250 m
<i>Thickness of Hydrate Zone 1 (Upper Zone)</i>	6 m (12 grids)
<i>Thickness of Hydrate Zone 2 (Lower Zone)</i>	30 m (60 grids)
<i>Thickness of Impermeable Layers of Hydrate Zone 1</i>	60 m (12 grids) 74 m (15 grids)
<i>Thickness of Impermeable Layers of Hydrate Zone 2</i>	74 m (15 grids) 90 m (18 grids)
<i>Total CH<sub>4</sub> Amount in Hydrate Zone 1, m<sup>3</sup></i>	5.009E+07
<i>Total CH<sub>4</sub> Amount in Hydrate Zone 2, m<sup>3</sup></i>	2.505E+08
<i>Porosity</i>	0.50
<i>Permeability</i>	9.869e-13 m <sup>2</sup> (1 D)
<i>Rock Grain Density</i>	2680 kg/m <sup>3</sup>
<i>Sediment Thermal Conductivity</i>	1.27 W/m.K
<i>Average Pressure and Average Temperature</i>	15.83 MPa (Hydrate Zone 1) 16.79 MPa (Hydrate Zone 2)
<i>Sea Floor Temperature, Temperature Gradient</i>	9°C ; 0.0278°C/m
<i>Hydrate Zone Saturations</i>	S <sub>h</sub> :0.5; S <sub>aq</sub> :0.5
<i>Relative Permeability Parameters- Modified of Stone Equation</i>	S <sub>ar</sub> :0.25 S <sub>gr</sub> :0.02 n: 3.0
<i>Capillary Pressure Parameters- Van Genuchten function</i>	S <sub>ar</sub> : 0.24 n: 1.84 a:10.0

The most important part of the simulation studies is to determine reservoir properties and to decide on grid numbers before simulations. If some data are unavailable, it is important to make necessary assumptions. In this study, by using the literature data available related to gas hydrates in the Danube Fan of the Black Sea and those are listed in Table 7-17. Many information such as porosity, temperature gradient, hydrate section thickness and their locations, hydrate saturation, pore water salinity, etc. are known in the Danube Fan of the Black Sea after many geophysical studies such as BSR determination, electromagnetic surveys and ocean seismometer techniques. Hence, currently, the Danube Fan is the only place where there is many information about the gas hydrate reservoirs in the Black Sea so in 2017, drilling with MeBo seafloor drilling unit is planned in this region. Then, first gas production test from gas hydrates in the Black Sea with depressurization method are planned to be conducted in the Danube Fan after analysis of drilling and coring operations (Vasilev, 2015). As shown Figure 7-81 and Figure 7-82, gas hydrates (up to 50 % hydrate saturation) are deposited in coarse sands and silts in the Danube Fan and these hydrate sections are bounded with clay sections. Generally, clays have very low permeability (Konno *et al.*, 2015). Therefore, in this study, it is assumed that the clays bounding hydrate sections are impermeable and fully water saturated.

Grid numbers are also important to predict gas production accurately as much as possible. Generally, as you increase grid numbers, the accuracy of the simulations increases but the cost of simulation (time) increases as well. In the study of Long *et al.* (2016), numerical simulations of two cases with different size meshes were run by using HydrateResSim. In vertical direction, the 35 m-thick hydrate bearing sandy silt reservoir was meshed with 2 or 3 m vertical layers in case 1 and 1 m vertical layers in case 2. Case 2 provided enough fineness of mesh (grid) for the 35 m-thick hydrate bearing sandy silt reservoir according to the numerical simulations in the study of Long *et al.* (2016). In this study, 0.5 m thick grids in vertical direction in gas hydrate sections were chosen for better results. In these simulations, it is aimed to put much more grids and make simulations for only 60-day short-term depressurization test instead of long-term production tests. The aim of these simulations in the Danube Fan is to make analysis and provide results before short-term production tests are

planned to be held in this region. In the first gas production test from marine gas hydrates in Nankai Trough in 2013, the production stopped within 6 days due to several operation difficulties mainly sand production (Uchida *et al.*, 2016). During the selection of the location of production test well in Nankai Trough, many seismic and geological studies were conducted. The characterization of the sediments bounding gas hydrate section is as important as those of gas hydrate sections for effective depressurization (Fujii *et al.*, 2013). The location with 200 m GHSZ thickness was preferred in Nankai Trough for effective depressurization and safety (Max and Johnson, 2016).

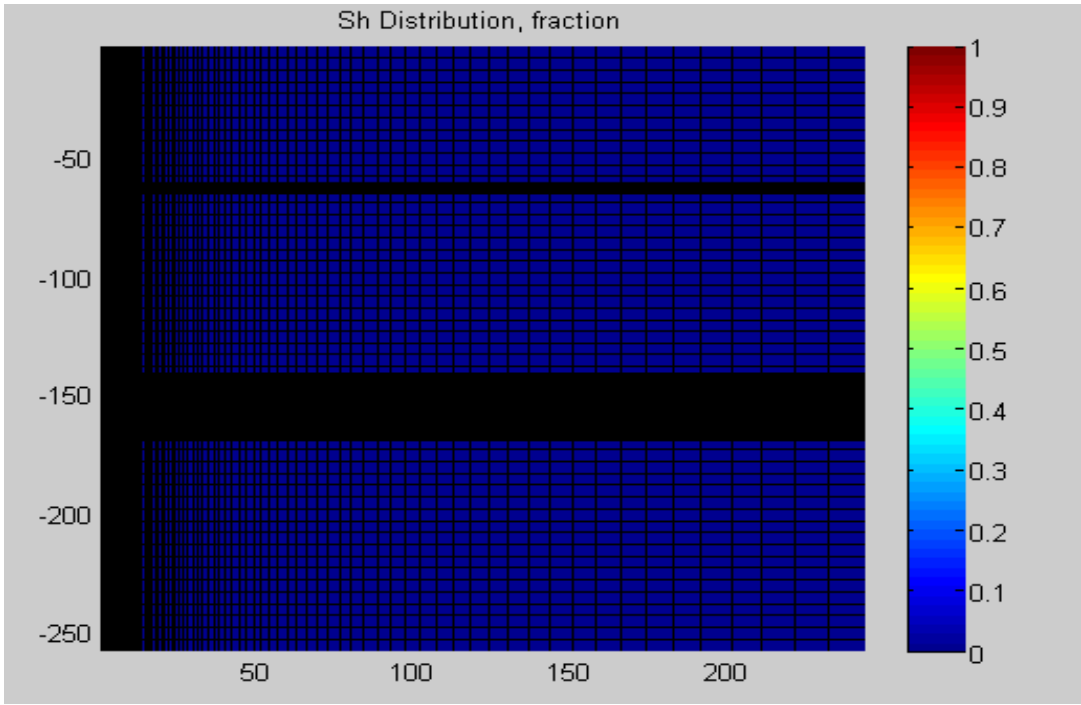


**Figure 7-83:** Grid structure in the Danube Fan in Figure 7-82

The grid structures for gas hydrate sections in Figure 7-81 and Figure 7-82 are shown in Figure 7-83. As seen in Figure 7-83, the grids are denser in gas hydrate sections and near wellbore compared to clay sections because with gas hydrate dissociation within 60-day depressurization test, most changes will occur in gas hydrate sections and near wellbore. As seen in Table 7-17, in gas hydrate sections along vertical direction, each grid thickness is 0.5 m and the vertical size of grids in clay section is nearly 5 m (the number of all grids along vertical direction for one section along

horizontal section is 117). In horizontal direction, logarithmic 100 grids were put. Hence, the total number of grids is 11,700. Equilibrium model of HydrateResSim was used in this study and 3 equations (mass balance for CH<sub>4</sub>, mass balance for water and heat balance equation) are solved for each grid at each time. 35,100 equations were solved in each time interval.

The aim of short production tests from gas hydrate reservoirs is not to produce gas commercially. It is to understand:

- The effect of depressurization or any other method preferred
- Gas flow rate and water flow rate changes with time
- The distance of gas hydrate dissociation front
- Temperature changes during gas hydrate dissociation
- Sand production amount and geomechanical stability

After obtaining all of these data, future long-term production tests can be designed and then conducted after many years of preparation as in Nankai field. For gas hydrates in Figure 7-82, it is not logical to test these two gas hydrate sections at the same time because water production from gas hydrate zone 1 (upper gas hydrate) might surpass gas production from gas hydrate zone 2 (lower gas hydrate) and this is not advisable for short term production tests and detailed well completion studies are essential (Sun *et al.*, 2016). The boundaries where there are no gas hydrates behave like heat sources and provide heat flux through gas hydrate sections. In this study, the grids between 0-5 mbsf and grids between 255-260 mbsf are assumed to have constant temperature but the temperature of other grids are calculated during simulations with heat balance equations (from Equations (5-1) to (5-14)). Hence, in this study, depressurization production simulations at 2 MPa, 2.5 MPa, 3 MPa, 4 MPa, 5 MPa and 6 MPa were conducted for each gas hydrate section in Figure 7-82 separately.

Figure 7-84, Figure 7-85, Figure 7-86 and Figure 7-87 show cumulative gas production, cumulative water production, gas to water production ratio and gas flow rate respectively from upper gas hydrate section (6 m-thick gas hydrate reservoir) in Figure 7-82 at different depressurization pressures. In 2013-Nankai Trough test, reservoir pressure decreased from 11.5 MPa to 4 MPa near wellbore within 6 days by using electrical submersible pump (ESP) (Kawamoto, 2014). ESP pumps might be also used in the production test of the Danube Fan. As shown in Figure 7-84 and Figure 7-85, when depressurization pressures decrease from 6 MPa to 2 MPa, gas and water production increase. This is an expected result in depressurization tests.

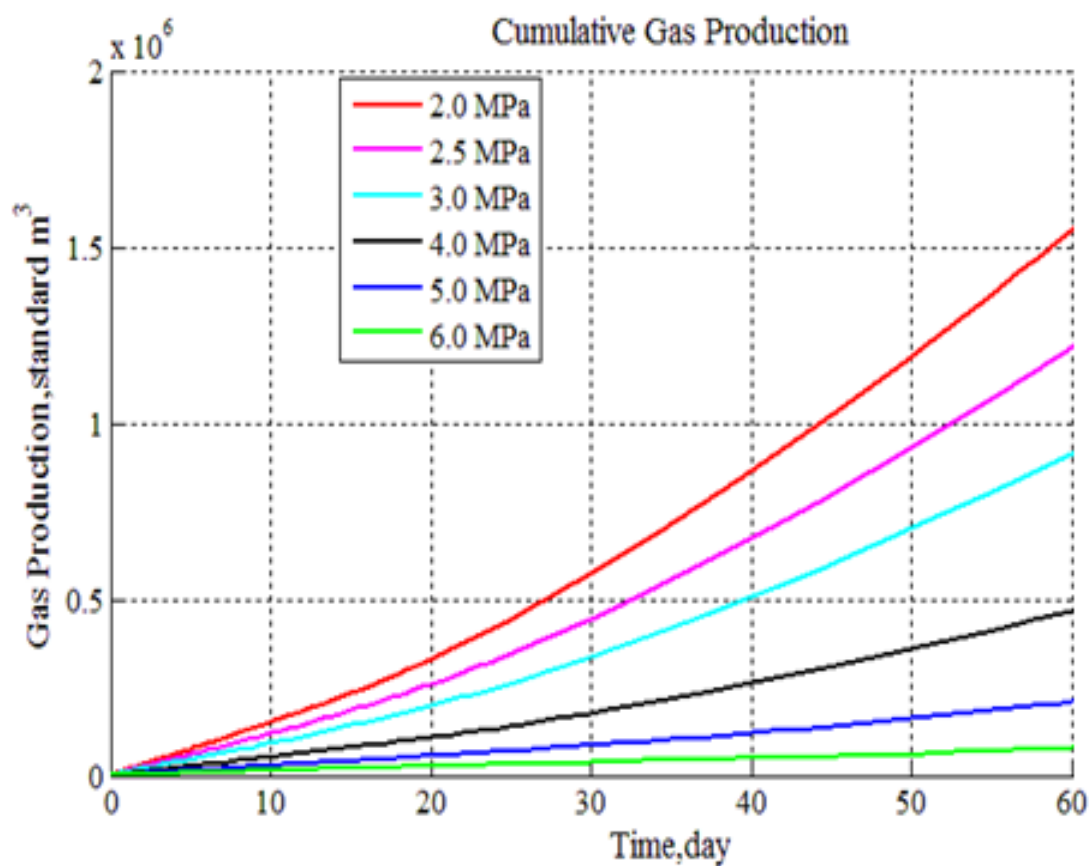


**Figure 7-84:** Cumulative gas production for upper gas hydrate section

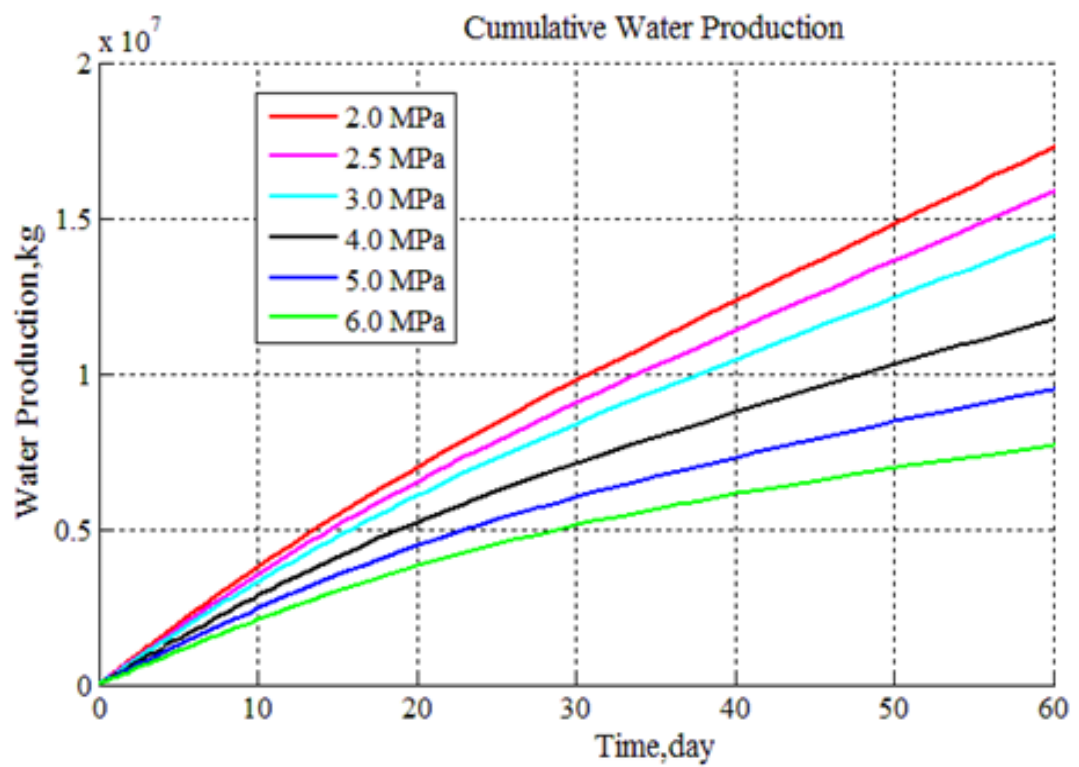


**Figure 7-85:** Cumulative water production for upper gas hydrate section at different depressurization pressures

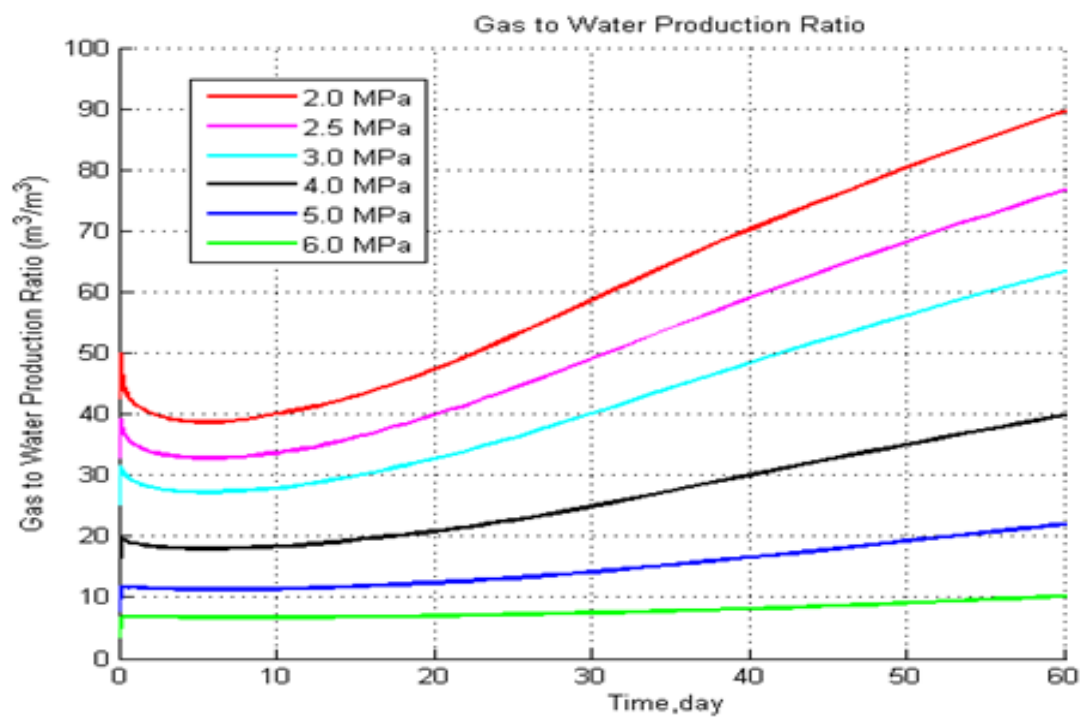


**Figure 7-86:** Gas to water production ratio of upper gas hydrate section

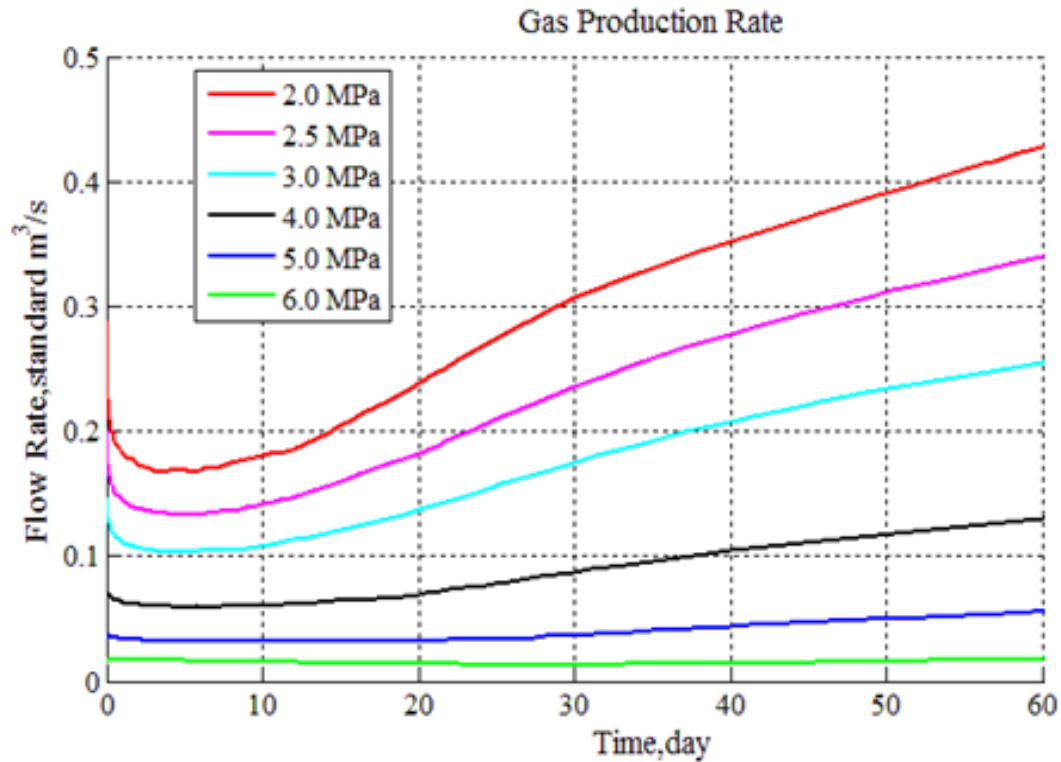


**Figure 7-87:** Gas flow rate for upper gas hydrate section

During 60-day production test from the upper gas hydrate section, initially gas to water production ratio in Figure 7-86 decreases within first 8 days because of the production of free water in pores. However, with gas hydrate dissociation, this ratio increases with time. Similar behavior is observed in gas flow rate versus time graph in Figure 7-87.

Fast depressurization might cause two problems: ice formation (due to endothermic nature of gas hydrate dissociation) and sand production (Uchida *et al.*, 2016). Ice formation might plug the pores and can cause reduction in permeability and gas production (Seol and Myshakin, 2011). However, in different experimental studies, it was observed that heat released during ice formation provides additional heat to gas hydrate dissociation and increased gas production (Konno *et al.*, 2014). In this study, within 60-day production simulation with depressurization tests, no ice was observed in simulations of upper gas hydrate section. However, ice formed in the latest stages of the production at especially for 2.0 MPa for this section. For example, as shown in Figure 7-88, at the 420<sup>th</sup> day of gas production at 2 MPa from upper gas

hydrate section, long ice section formed with gas hydrate dissociation. Although in this simulation, ice formation did not cause reduction in gas production, it is better to be far from ice formation in pores during production tests. Ice did not form within 60 days and also the Black Sea seafloor sediment temperature is classified as high sea bottom temperature ( $\sim 9^{\circ}\text{C}$ ) compared to low sea bottom temperature of the Gulf of Mexico (Küçük *et al.*, 2016). Moreover, 2 MPa depressurization pressure might cause high sand production as in Nankai Trough (Uchida *et al.*, 2016). Therefore, it is much better to choose depressurization pressure for the first production tests in the Danube Fan as 3 MPa or 4 MPa.

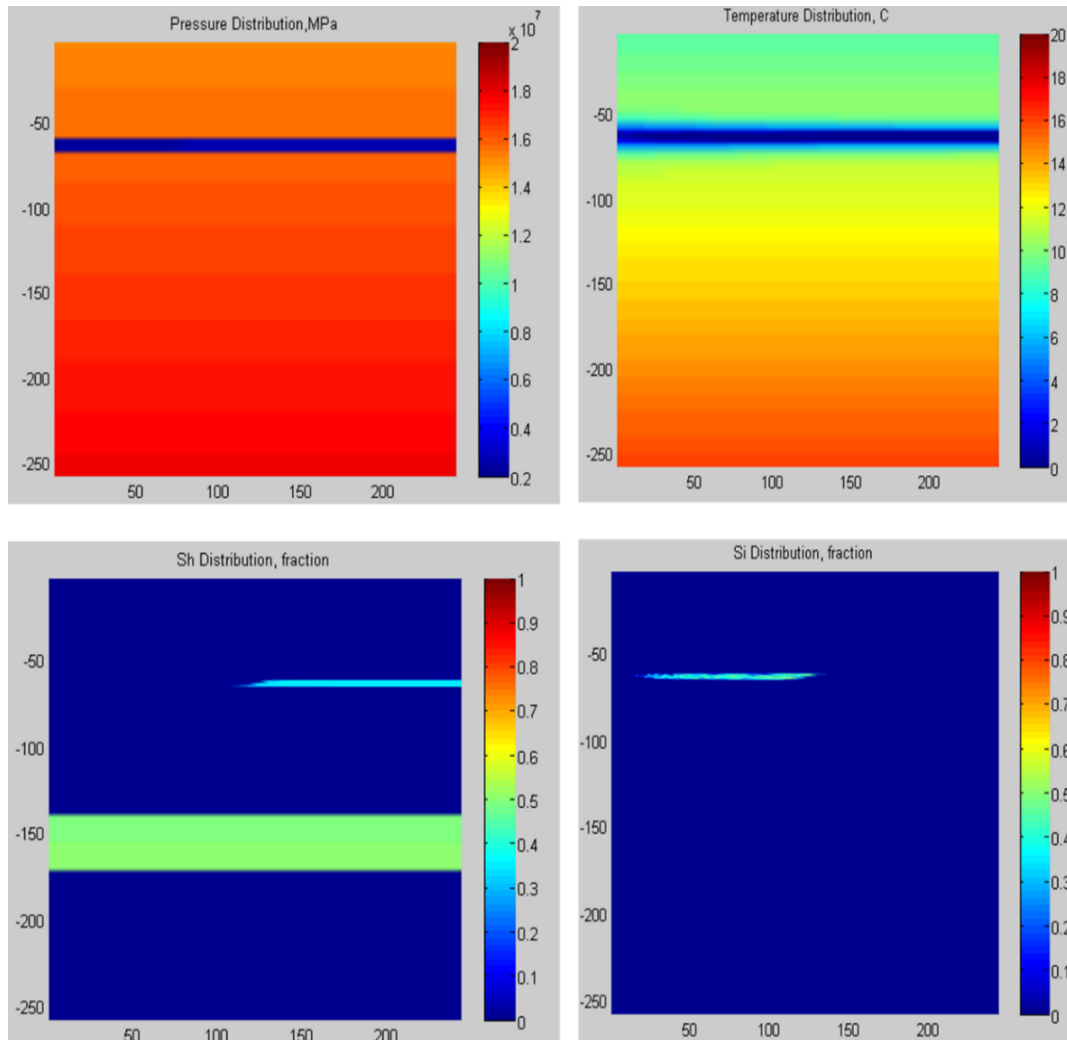


**Figure 7-88:** Pressure, temperature, hydrate saturation ( $S_h$ ), and ice saturation ( $S_i$ ) at 2.0 MPa depressurization for upper gas hydrate section at 420<sup>th</sup> day of gas production

In order to visualize the changes in pressure, temperature, hydrate saturation, aqueous saturation, gas saturations during 60-day depressurization test at 3 MPa, Figure 7-89 was prepared. As seen in this figure, gas hydrate dissociation occurred within 60 days. Gas hydrate dissociation front reached to 20-25 m far from wellbore. Moreover, temperature decreased to 2-3°C near wellbore. In Nankai Trough, two observation wells were drilled 20 m from the production well to measure temperature and pressure changes during gas hydrate dissociation (Kawamoto, 2014; Yamamoto *et al.*, 2017). Similar wells might be drilled in this region as well. The dissociation of 6 m-thick gas hydrate section did not affect the temperature of clay boundaries a lot within 60-day test and also did not affect lower 30 m-gas hydrate section. Due to gravity difference, aqueous saturation is highest at the bottom and gas hydrate saturation is highest at the top in gas hydrate dissociation front. Thin gas hydrates dissociate faster compared to thick gas hydrate sections due to low heat conduction in gas hydrates at similar conditions according to the results in this study. Therefore, upper gas hydrate section in the Danube Fan in the Black Sea could be a good candidate for first gas hydrate production test compared to lower thick gas hydrate section. However, the permeability of the clay sediments above upper clay section should be very low. Upper gas hydrate section is very close to seafloor (60 mbsf) and if seawater goes through upper gas hydrate section, the depressurization test and its quality might be affected negatively due to high flux of seawater. However, if the impermeable property and geomechanical stability of clay section above 6 m-gas hydrate section are proved after drilling and coring, this section could bring many clues about the efficiency of gas production by depressurization method in the Black Sea conditions.

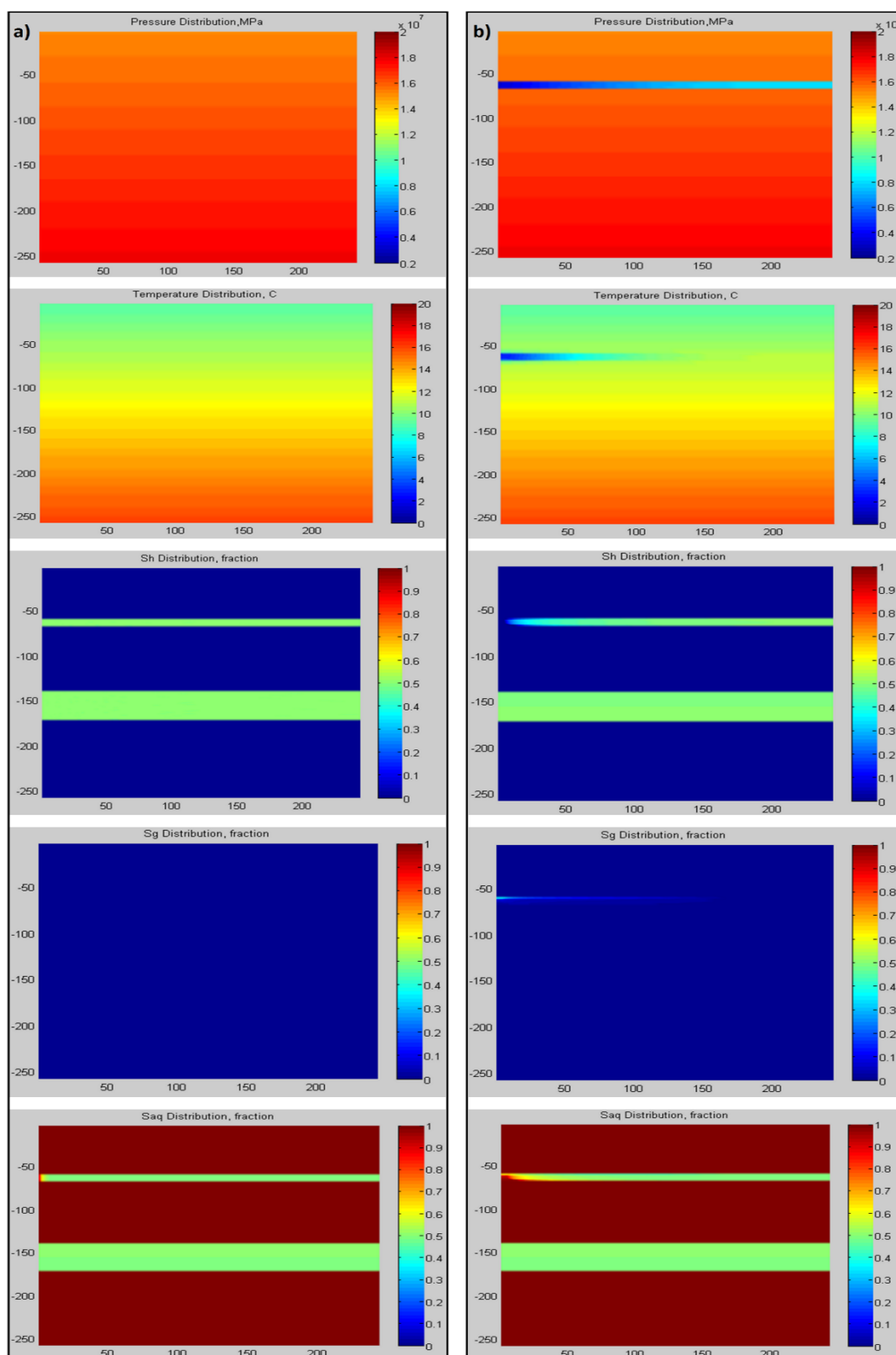


**Figure 7-89:** Pressure, Temperature, hydrate saturation, gas saturation, and aqueous saturation at a) 0-day b) 60 days at 3 MPa depressurization pressure for upper gas hydrate section

Permeability is a key parameter determining the efficiency of depressurization-dissociation and natural gas production (Masuda *et al.*, 1999; Mahabadi and Jang, 2014). In this study, due to unavailability of intrinsic permeability of coarse sands, some assumptions were made and permeability is assumed to be equal to 1000 mD (1 D). In order to calculate effective permeability, equation (5-23) of Masuda *et al.* (1999) is commonly used. To determine N value, experimental analysis is necessary from sediment samples. In Nankai Trough sediments, this value is 6 (Uchida *et al.*, 2016). Hence, effective permeability in the Danube Fan with 50 % hydrate saturation might be around 15.625 mD for 1 D intrinsic permeability and with gas hydrate dissociation, this value increases.

Numerical simulations for different intrinsic permeability (100 mD, 250 mD, 500 mD, 750 mD, 1000 mD, 1500 mD, and 2000 mD) at 3 MPa depressurization pressure were run in order to understand the effect of permeability on gas production from the upper gas hydrate section. The results (cumulative gas production, cumulative water production and gas flow rate) are compared in Figure 7-90, Figure 7-91 and Figure 7-92 respectively. As permeability increases, gas production and water production increases as in Figure 7-90 and Figure 7-91 . However, the differences of cumulative productions are narrow when going through from higher permeability to lower permeability as seen in Figure 7-90. Therefore, core samples should be taken with special coreholder without affecting hydrate structure and in laboratory necessary permeability and geomechanical analysis should be done.

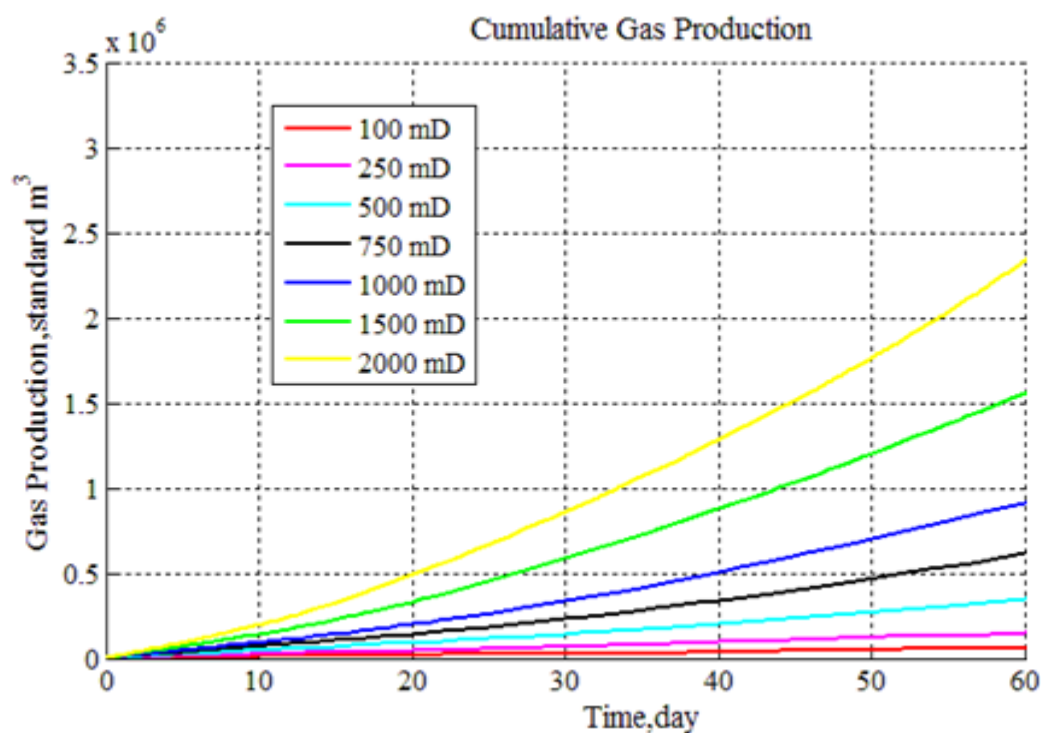


**Figure 7-90:** Effect of absolute permeability on gas production at 3 MPa depressurization pressure from upper gas hydrate

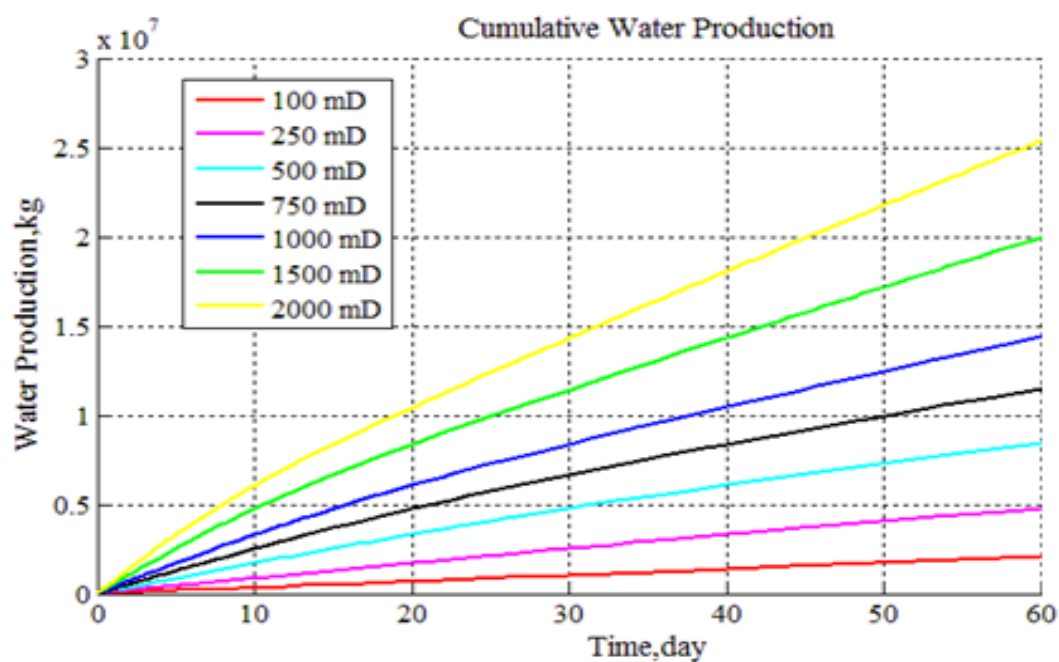


**Figure 7-91:** Effect of absolute permeability on water production at 3 MPa depressurization pressure from upper gas hydrate

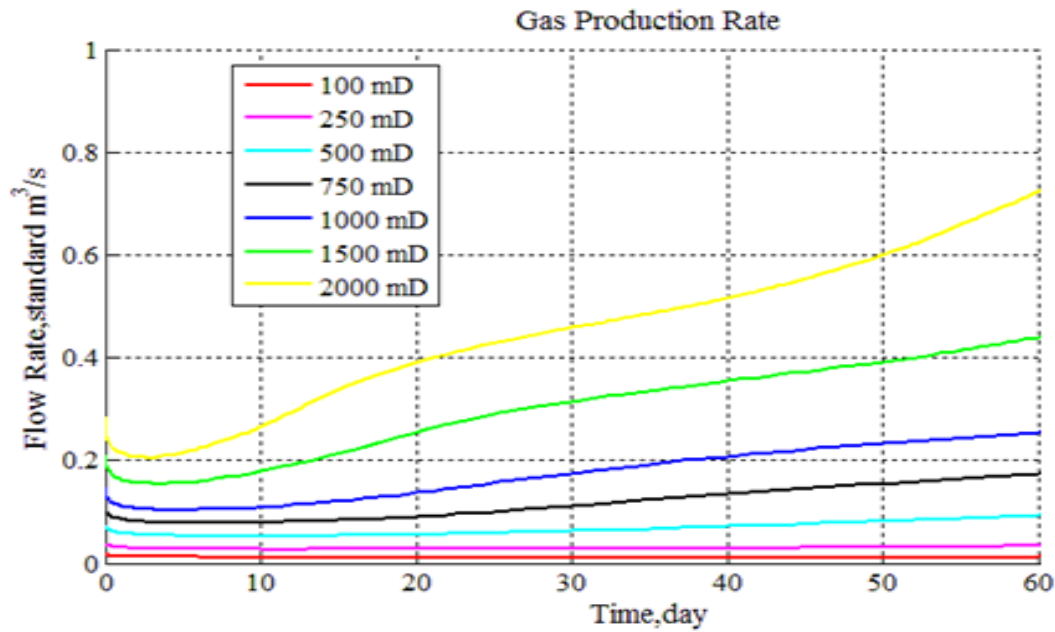


**Figure 7-92:** Effect of absolute permeability on gas flow rate at 3 MPa depressurization pressure from upper gas hydrate

If the clay layer above 6 m-thick gas hydrate layer is permeable and geomechanically weak, production test might be conducted in the lower 30m-thick gas hydrate layer. Although Zander *et al.* (2016) made geomechanical simulations in this area and showed maximum seafloor subsidence is 12-15 cm after depressurization, more experimental and numerical geomechanical studies should be conducted at the same time. Moreover, 74 m clay layer above this hydrate layer and also 6 m-thick gas hydrate layer create good seals and it is not possible seawater to reach the lower hydrate section. For this reason, depressurization simulations were held at 2 MPa, 2.5 MPa, 3 MPa, 4 MPa, 5 MPa, and 6 MPa for gas production from 30 m-thick gas hydrate layer. Figure 7-93, Figure 7-94, Figure 7-95, and Figure 7-96 show the cumulative gas production, cumulative water production, gas to water production ratio and gas production flow rate at different depressurization pressures respectively. The highest gas production within 60 day-production test was obtained at 2 MPa. At 2.0 MPa, the cumulative gas production from the lower gas hydrate section within 60 day-production test is approximately 4.5 times higher than the cumulative gas production from the upper gas hydrate section because the thickness and perforation interval of the lower gas hydrate section is higher.

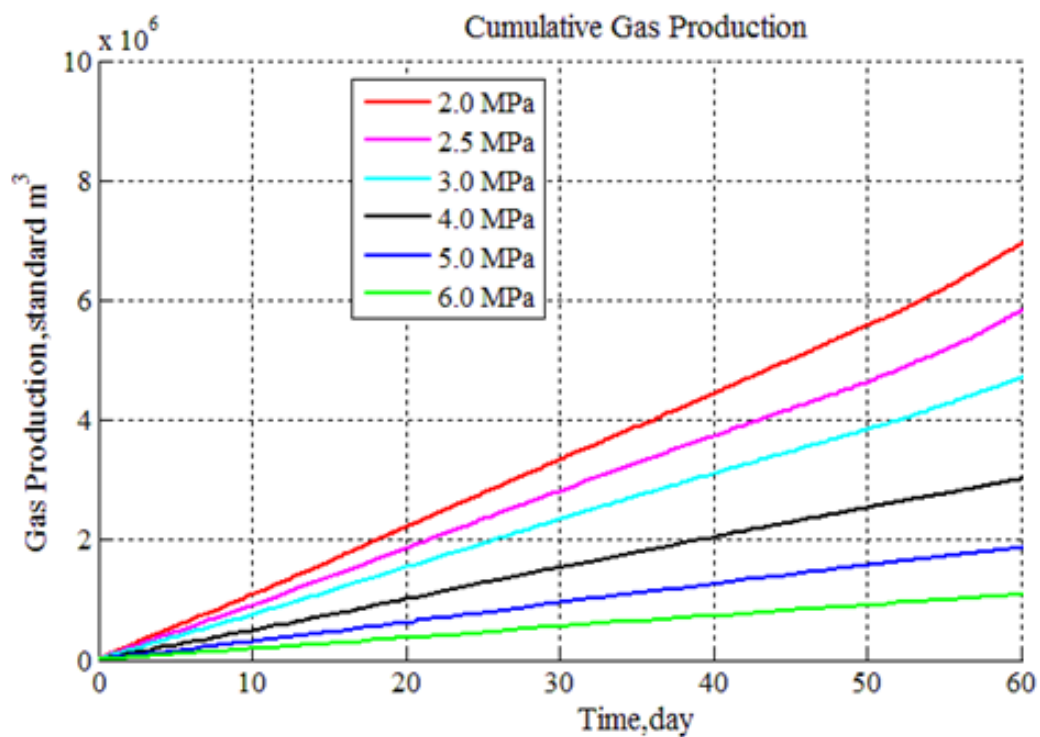


**Figure 7-93:** Cumulative gas production for lower gas hydrate section

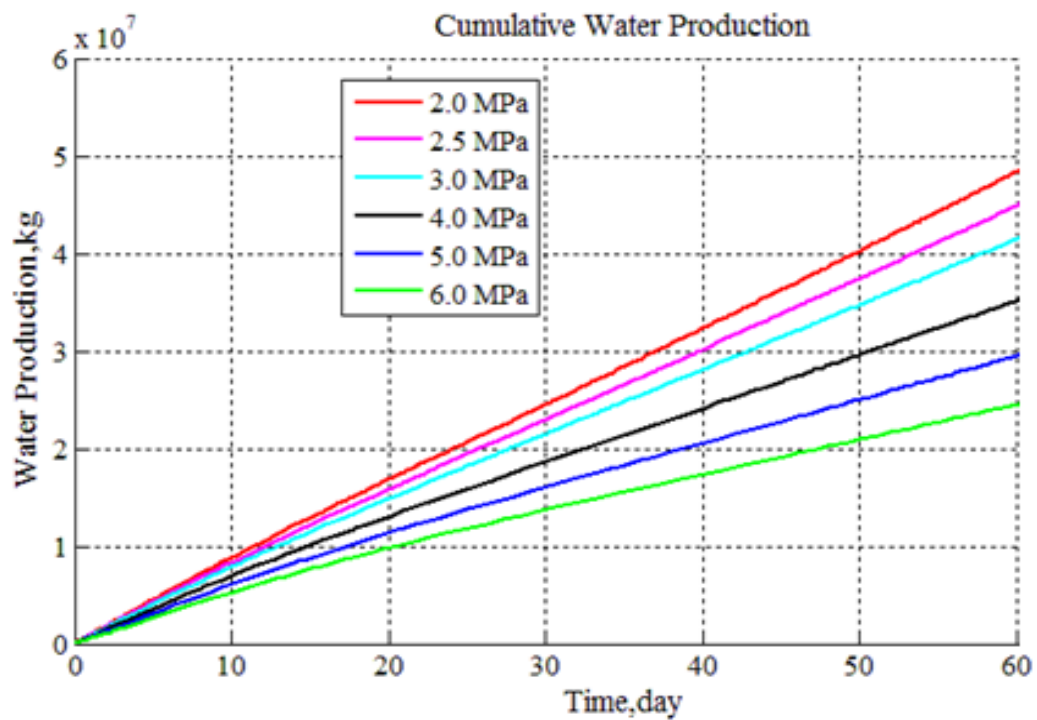


**Figure 7-94:** Cumulative water production for lower gas hydrate section at different depressurization pressures

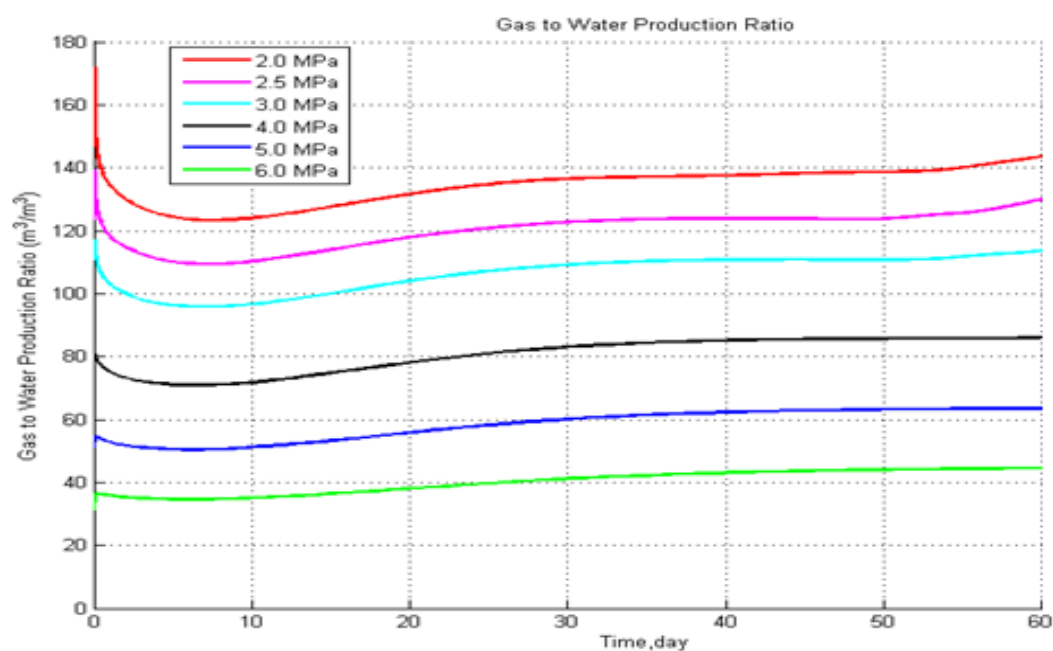


**Figure 7-95:** Gas to water production ratio of lower gas hydrate section at different depressurization pressures

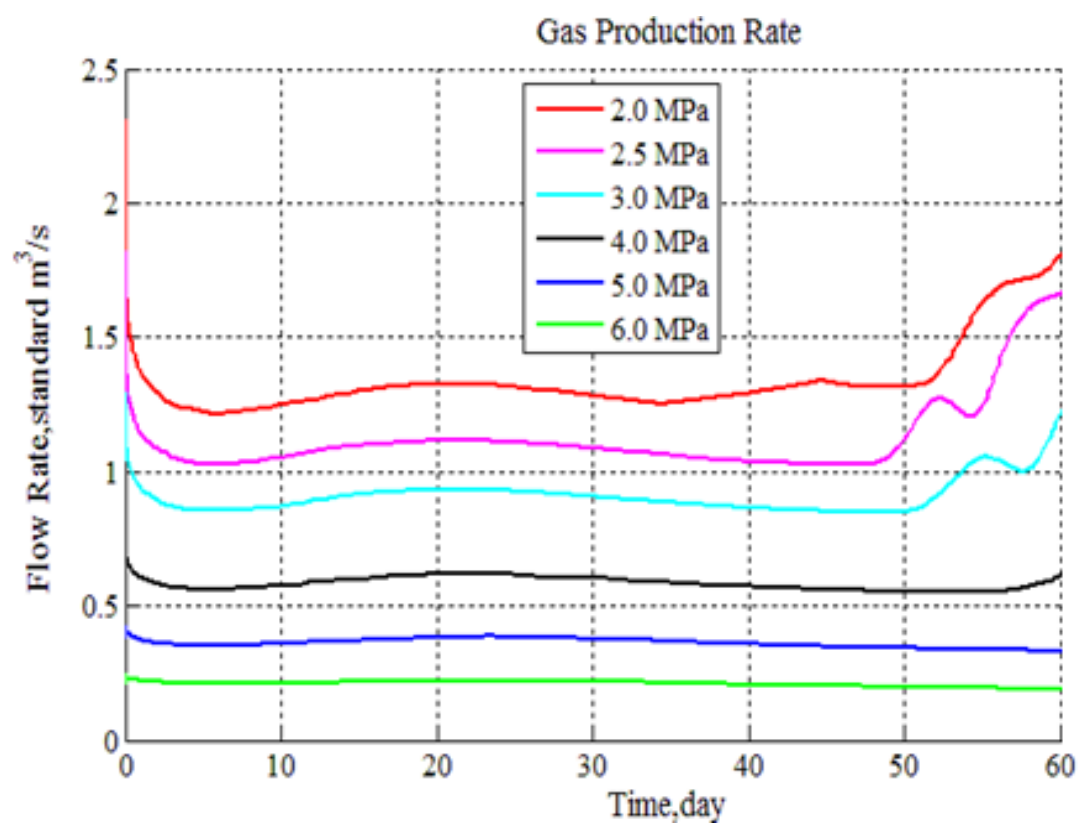


**Figure 7-96:** Gas flow rate for lower gas hydrate section

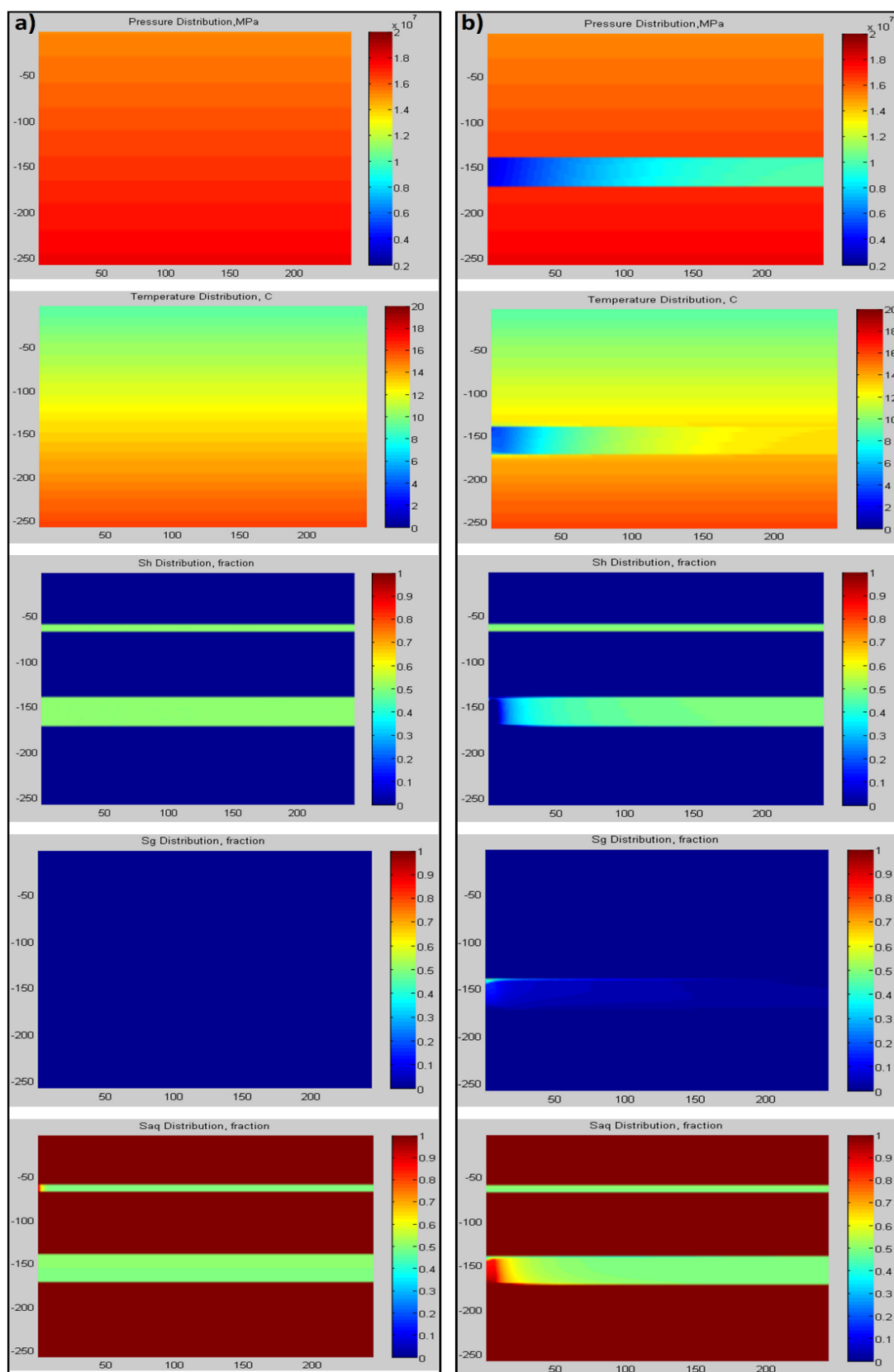


**Figure 7-97:** Pressure, Temperature, hydrate saturation, gas saturation, and aqueous saturation at a) 0-day b) 60 days at 3 MPa depressurization pressure

Compared to upper thin gas hydrate section, no ice formation was observed during depressurization test of lower gas hydrate section (hydrate zone 2) at 2 MPa even in 2 year-long-term simulation. The reason of this is that the temperature of lower gas hydrate zone (13.3°C in the middle) is higher than the temperature of upper gas hydrate zone (10.75°C in the middle). However, to avoid high sand production and lower risk of ice formation along wellbore and in pores, it is better to choose 3 or 4 MPa as a test pressure. In order to visualize the changes in pressure, temperature, aqueous saturation, hydrate saturation and gas saturation after 60 day-short-term production test, Figure 7-97 was shown for 3 MPa depressurization. If upper gas hydrate section and lower gas hydrate section are at similar temperature conditions, it is expected that upper (thin) gas hydrate section would dissociate faster because heat conduction is quite low in thick gas hydrate reservoirs compared to thin gas hydrate reservoirs. However, in this study, lower gas hydrate section has higher temperature compared to upper gas hydrate section. Hence, gas hydrate dissociation fronts in Figure 7-89 and Figure 7-97 close to each other. At least 20 m far from production test well, two observation wells might be necessary to prove gas hydrate dissociation and also to measure temperature and pressure changes in gas hydrate sections. Furthermore, geomechanical gauges might be inserted to these observation wells to record geomechanical changes during depressurization.

For lower gas hydrate section, numerical simulations for different intrinsic permeability (100 mD, 250 mD, 500 mD, 750 mD, 1000 mD, 1500 mD, and 2000 mD) at 3 MPa depressurization pressure were run and their results are shown in Figure 7-98, Figure 7-99, and Figure 7-100. As permeability increases, gas production and water production increases. However, the differences of productions are narrow when going through from high permeability to low permeability as seen in Figure 7-98, Figure 7-99, and Figure 7-100. Therefore, the determination of permeability is quite important for accurate prediction of gas and water production. Many core samples should be collected from the Danube fan and the Black Sea before any short-term production test and production experiments. The sediment type, grain size, pore water properties, porosity, permeability, and geomechanical properties of core samples should be analyzed carefully.

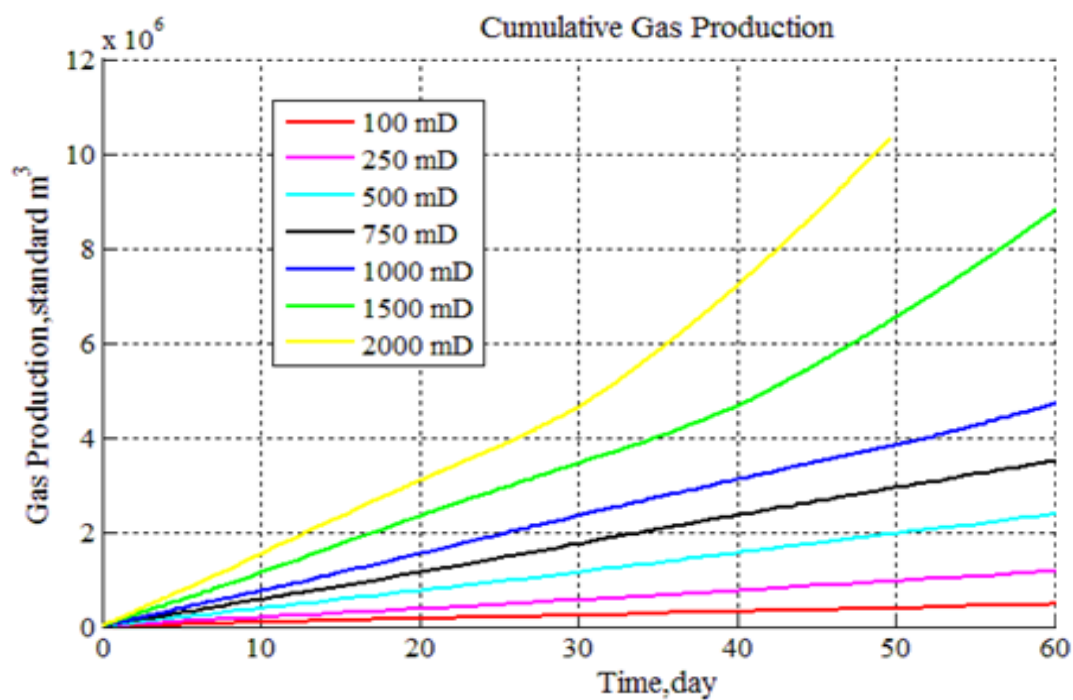


**Figure 7-98:** Effect of absolute permeability on gas production at 3 MPa depressurization pressure from lower gas hydrate

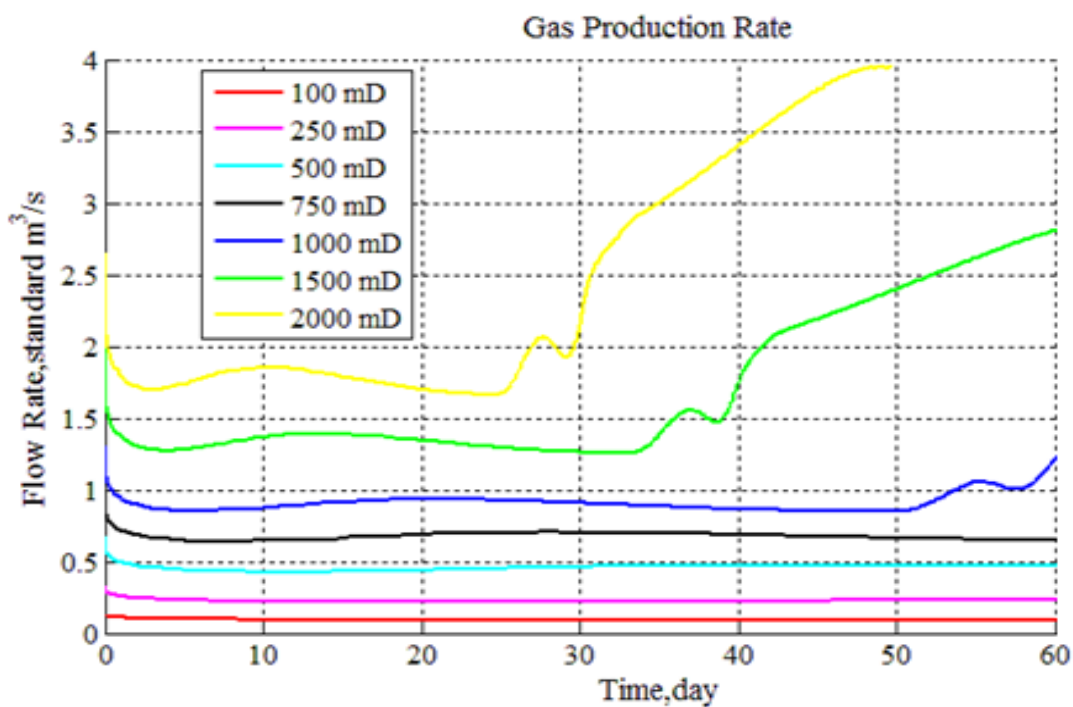


**Figure 7-99:** Effect of absolute permeability on gas flow rate at 3 MPa depressurization pressure from lower gas hydrate

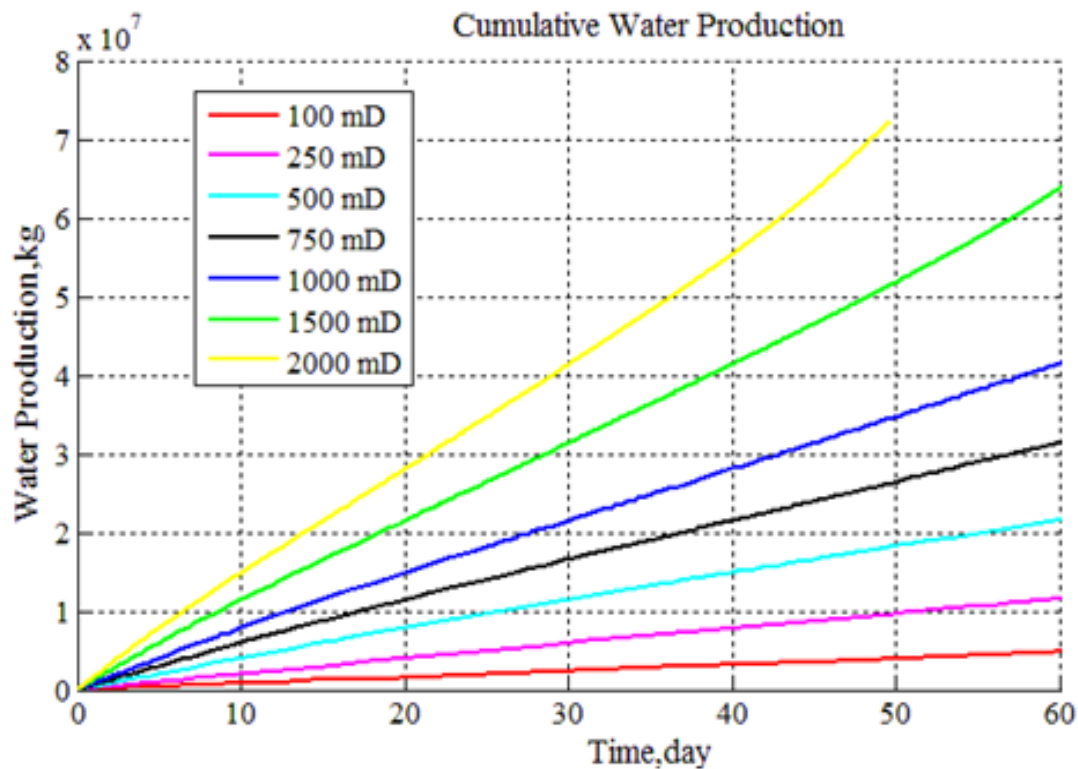


**Figure 7-100:** Effect of absolute permeability on water production at 3 MPa depressurization pressure from lower gas hydrate

60-day depressurization test in Danube Fan might give many clues about sand production, pressure changes, temperature changes, gas and water production. According to the results of this first short-term production test, better designs of drilling, well completion and production from the Black Sea gas hydrate might be made. Hence, after 60-day depressurization tests, the production and observations wells might be easily plugged either by cement plugs or drillable permanent packers. After plugging, it is expected that gas and free water in pores will form gas hydrate again and gas hydrate zones become stable again after short-term production tests. As seen Figure 7-101, after stopping production test and plugging the well in Nankai Trough first gas hydrate depressurization test in 2013, pressure near wellbore increased to near initial pressure conditions in a short time.

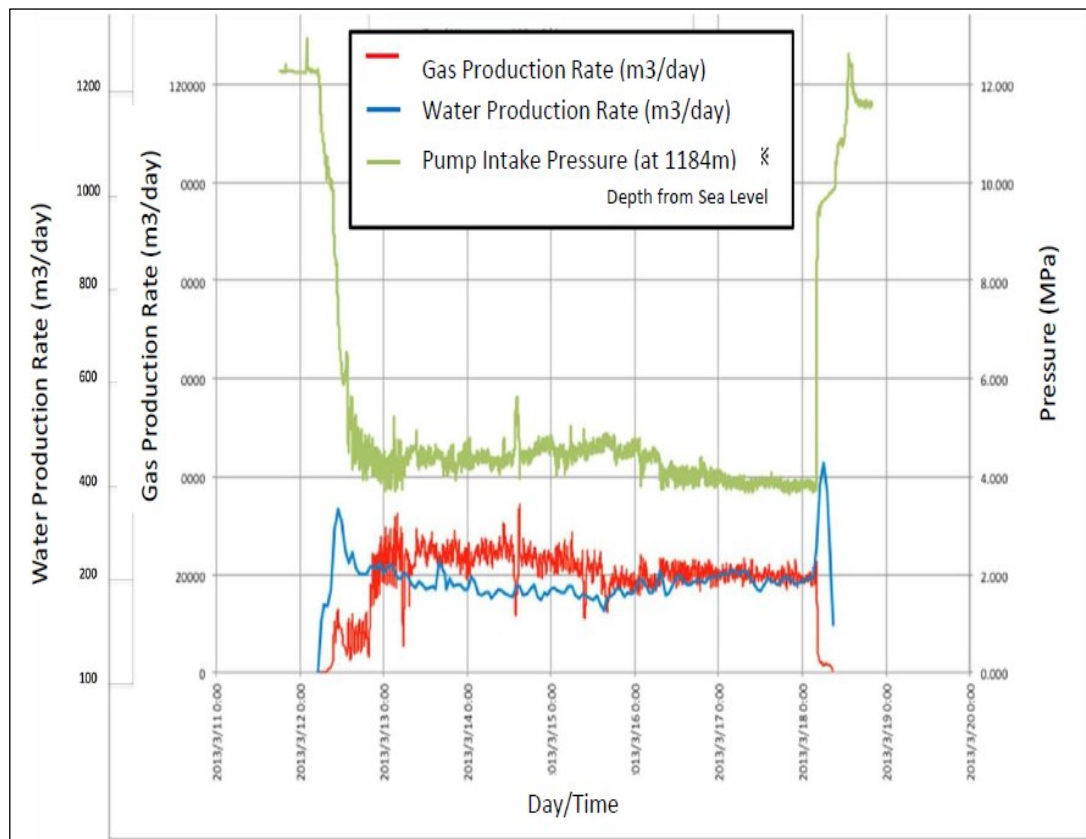


**Figure 7-101:** Pressure, gas production rate and water production rate during 6-day depressurization test in Nankai Trough, Japan (Kawamoto, 2014)

## 7.5 A New Gas Hydrate Software (HEP) to Predict Gas Hydrate Properties

Gas hydrate software is necessary for natural gas hydrate transportation through pipelines, the experimental studies and the prediction of gas compositions of gas hydrate detected by BSRs. Gas produced from gas reservoirs include always water and also especially in winter times, there is a risk of pipe plugging due to hydrate formation. Therefore, the hydrate formation conditions of natural gas transported should be known and then necessary preventions can be taken. Moreover, before experimental studies, at certain temperature, the hydrate forming pressure of gas or gas mixtures such as  $\text{CH}_4$ ,  $\text{C}_2\text{H}_6$ ,  $\text{C}_3\text{H}_8$ ,  $n\text{-C}_4\text{H}_{10}$ ,  $i\text{-C}_4\text{H}_{10}$ ,  $n\text{-C}_5\text{H}_{12}$ ,  $i\text{-C}_5\text{H}_{12}$ ,  $n\text{-C}_6\text{H}_{14}$ ,  $\text{H}_2\text{S}$ ,  $\text{N}_2$  and  $\text{CO}_2$  should be known to calculate the amount of gas injected into the high pressure cell or reactor. As stated earlier in Chapter 2, bottom simulation reflectance (BSR) seismic data are commonly used to find Class 1 hydrate reservoirs. With gas hydrate software, gas compositions can be determined at the location of BSR by using some information of BSR such as sea depth, temperature, and pressure gradient.

Gas hydrate software is quite useful. The most commonly used gas hydrate software is CSMHYD. It is a code of Colorado Schools of Mines. It predicts the thermodynamics of stable hydrate structures at given pressure, temperature and composition conditions (CSM, 2016). Although it is a free software, it is not an open source code so it cannot be used in other codes by adaptation for different purposes. Similarly, CSMGem codes of Colorado Schools of Mines are commonly used to predict hydrate properties with and without inhibitors. Moreover, there is another gas hydrate software called HydraFLASH (software of HYDRAFACT Group in Institute of Petroleum Engineering, Heriot-Watt University) predicting PVT properties of gas hydrates (Hydrafact, 2016).

The Black Sea consists of sI and sII gas hydrates. Although sI hydrate includes mostly 100 %  $\text{CH}_4$  in nature, sII hydrates include  $\text{CH}_4$  and other impurities such as  $\text{C}_3\text{H}_8$ . Therefore, the gas hydrate software for gas mixtures is essential in this study because

many core samples and gas samples collected in the Black Sea include thermogenic gases.

In the experimental studies, in order to form gas hydrate at specific gas, water and hydrate saturations in the high pressure cell or reactor, some calculations (i.e mass equilibrium) are essential. For these calculations, the density of gas hydrate and gas hydrate equilibrium pressure of pure gas or gas mixture are needed. Moreover, for the prediction of gas compositions at the BSRs detected in the Black Sea conditions, a good hydrate software is needed and these codes can be connected to other codes to get gas hydrate properties.

In this study, Matlab 2014a was used to write the codes of a gas hydrate program to predict the hydrate properties of pure CH<sub>4</sub>, C<sub>2</sub>H<sub>6</sub>, C<sub>3</sub>H<sub>8</sub>, n-C<sub>4</sub>H<sub>10</sub>, i-C<sub>4</sub>H<sub>10</sub>, n-C<sub>5</sub>H<sub>12</sub>, i-C<sub>5</sub>H<sub>12</sub>, n-C<sub>6</sub>H<sub>14</sub>, H<sub>2</sub>S, N<sub>2</sub>, CO<sub>2</sub> and the mixtures of these components with/without pure or mixtures of NaCl, CaCl<sub>2</sub>, KCl, Methanol, Ethanol, Ethylene Glycol, DEG, TEG. The name of the code is called “HEP” (**H**ydrate **E**quilibrium **P**roperties) in m file of Matlab 2014a. The algorithm of the code of HEP is briefly described in Figure 7-102. In this study by using HEP.m, it is aimed to predict:

- Hydrate equilibrium pressures of pure CH<sub>4</sub>, C<sub>2</sub>H<sub>6</sub>, C<sub>3</sub>H<sub>8</sub>, n-C<sub>4</sub>H<sub>10</sub>, i-C<sub>4</sub>H<sub>10</sub>, n-C<sub>5</sub>H<sub>12</sub>, i-C<sub>5</sub>H<sub>12</sub>, n-C<sub>6</sub>H<sub>14</sub>, H<sub>2</sub>S, N<sub>2</sub>, CO<sub>2</sub> and the mixtures of these components
- The type of gas hydrate structure (sI or sII) of pure gas or gas mixtures
- Hydrate properties of pure gas or gas mixtures such as density, molecular weight, hydration number, and enthalpy of hydrate dissociation
- Gas compositional fractions (cavity filling ratio) in the small and large cages of sI and sII hydrates
- All values mentioned above with inhibitors: NaCl, CaCl<sub>2</sub>, KCl, Methanol, Ethanol, Ethylene Glycol, DEG, TEG and their mixtures

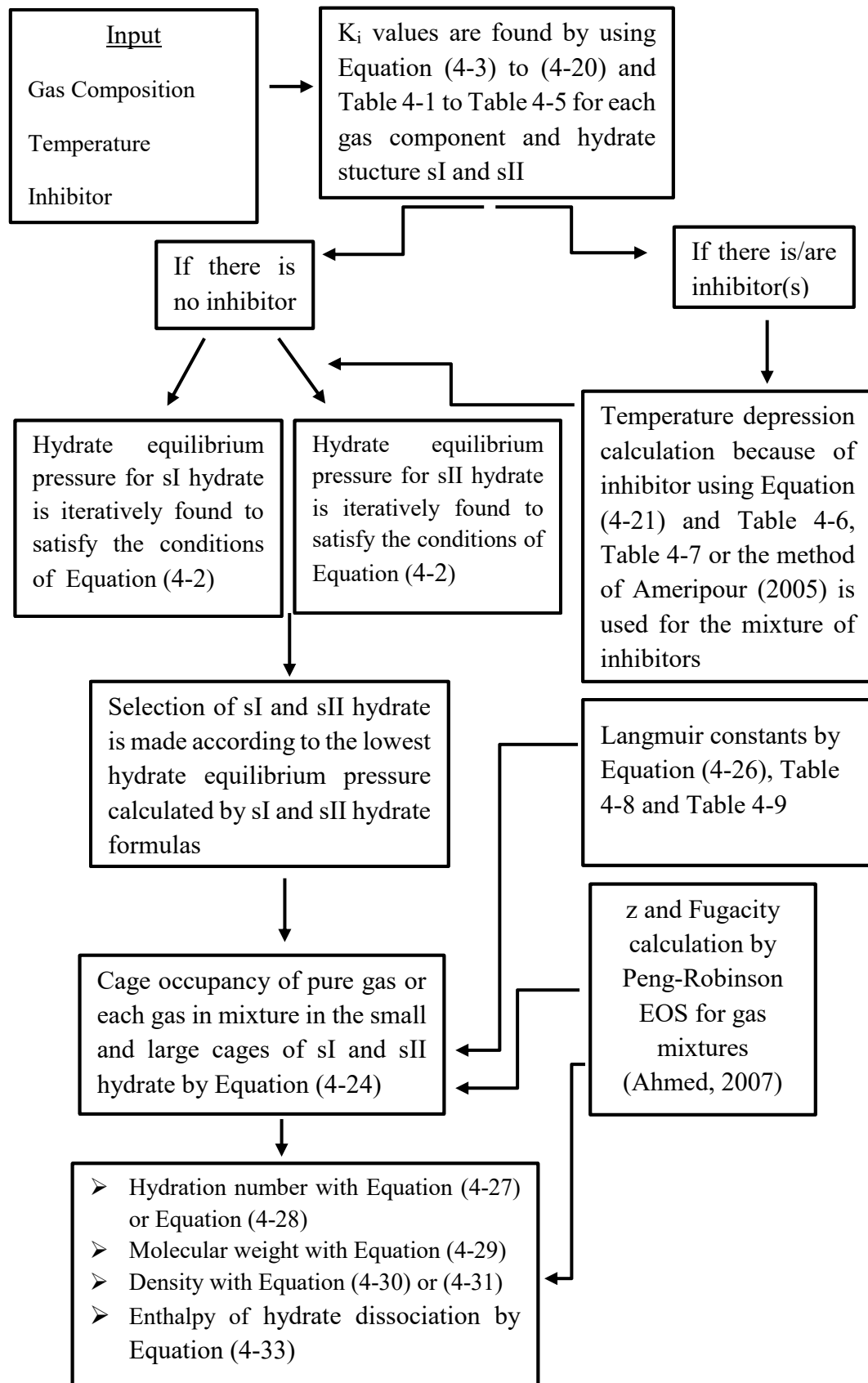


**Figure 7-102: Algorithm of HEP code**

**Table 7-18:** Error Analysis from Figure 7-103 to Figure 7-115 with Minitab 17

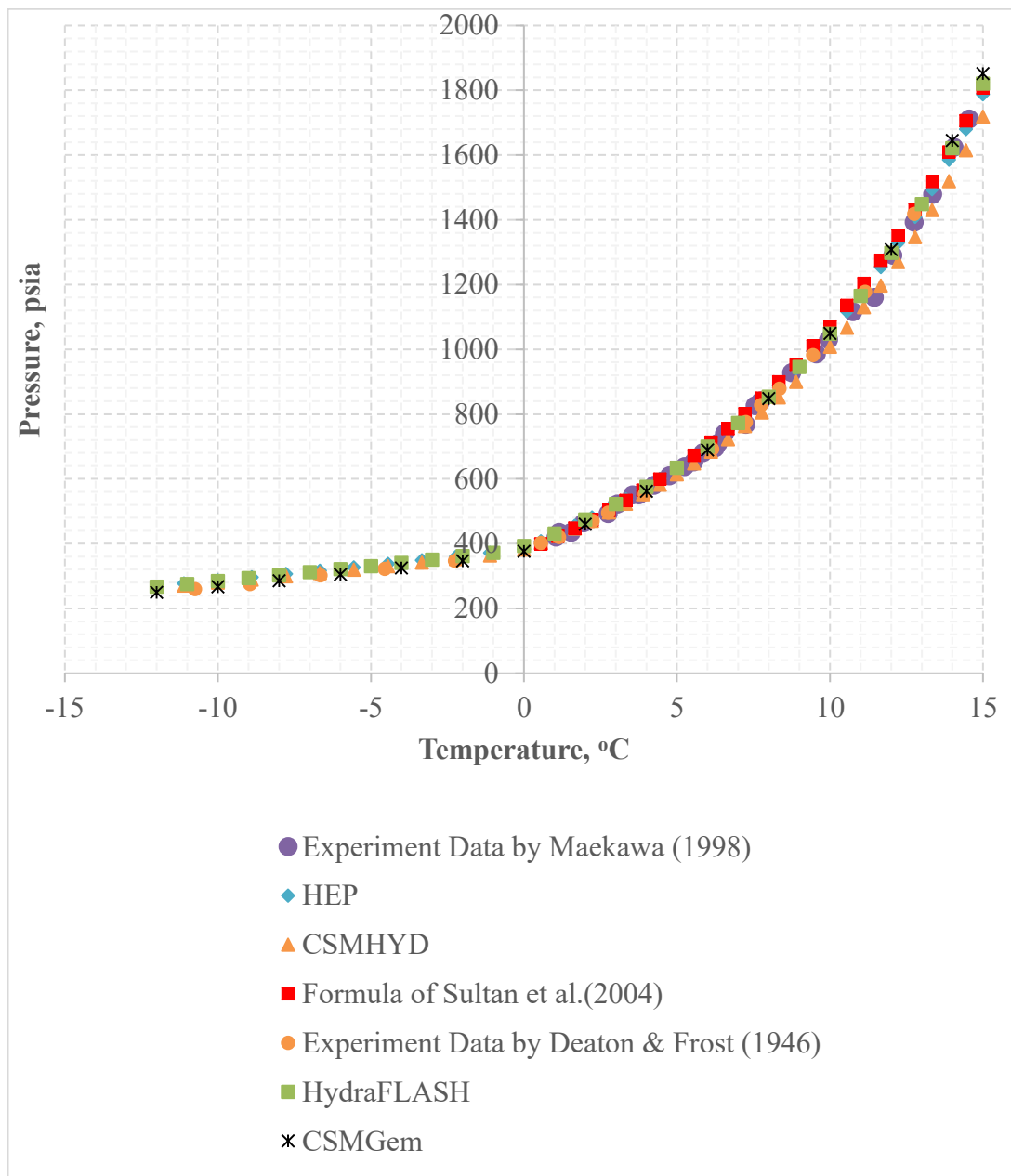
Figures	R <sup>2</sup> (%)			
	HEP <sup>+</sup>	CSMHYD	HydraFLASH	CSMGem
<i>Figure 7-103</i>	99.75	99.76	99.4	99.64
<i>Figure 7-104</i>	94.07	89.77	95.86	94.98
<i>Figure 7-105</i>	86.46	NA	NA	NA
<i>Figure 7-106</i>	C <sub>2</sub> H <sub>6</sub> - 99.59	C <sub>2</sub> H <sub>6</sub> - 99.68	C <sub>2</sub> H <sub>6</sub> - 98.25	C <sub>2</sub> H <sub>6</sub> - 96.04
	CO <sub>2</sub> - 98.47	CO <sub>2</sub> - 98.45	CO <sub>2</sub> - 99.12	CO <sub>2</sub> - 98.42
	C <sub>3</sub> H <sub>8</sub> - 88.95	C <sub>3</sub> H <sub>8</sub> - 88.96	C <sub>3</sub> H <sub>8</sub> - 86.27	C <sub>3</sub> H <sub>8</sub> - 88.95
<i>Figure 7-107</i>	99.9	99.8	99.8	99.8
<i>Figure 7-108</i>	99.62	99.09	99.08	99.63
<i>Figure 7-109</i>	99.49	99.85	99.78	99.46
<i>Figure 7-110</i>	87 % CH <sub>4</sub> +13% CO <sub>2</sub> : 99.12; 88.3 % CH <sub>4</sub> + 11.7 % C <sub>3</sub> H <sub>8</sub> : 99.68	87 % CH <sub>4</sub> + 13% CO <sub>2</sub> : 99.12; 88.3 % CH <sub>4</sub> + 11.7 % C <sub>3</sub> H <sub>8</sub> : 99.87	87 % CH <sub>4</sub> + 13% CO <sub>2</sub> : 99.93; 88.3 % CH <sub>4</sub> + 11.7 % C <sub>3</sub> H <sub>8</sub> : 99.11	87 % CH <sub>4</sub> + 13% CO <sub>2</sub> : 99.98; 88.3 % CH <sub>4</sub> + 11.7 % C <sub>3</sub> H <sub>8</sub> : 99.11
<i>Figure 7-111</i>	99.01	NA	99.61	99.63
<i>Figure 7-112</i>	99.23	NA	99.04	99.03
<i>Figure 7-113</i>	98.98	NA	98.66	99.02
<i>Figure 7-114</i>	97	NA	97.13	NA
<i>Figure 7-115</i>	96.48	NA	97.36	96.16

\*NA: Not Applicable; <sup>+</sup> The code written in this study

In order to check the reliability of HEP.m code, the results should be compared with the experimental data and the data predicted with HEP, CSMHYD, CSMGem and HydraFLASH. Therefore, from Figure 7-103 to Figure 7-115, the experimental hydrate equilibrium results in literature and the predicted results by HEP, CSMHYD, CSMGem, and HydraFLASH for different pure gases and gas mixtures with and without inhibitors are compared.

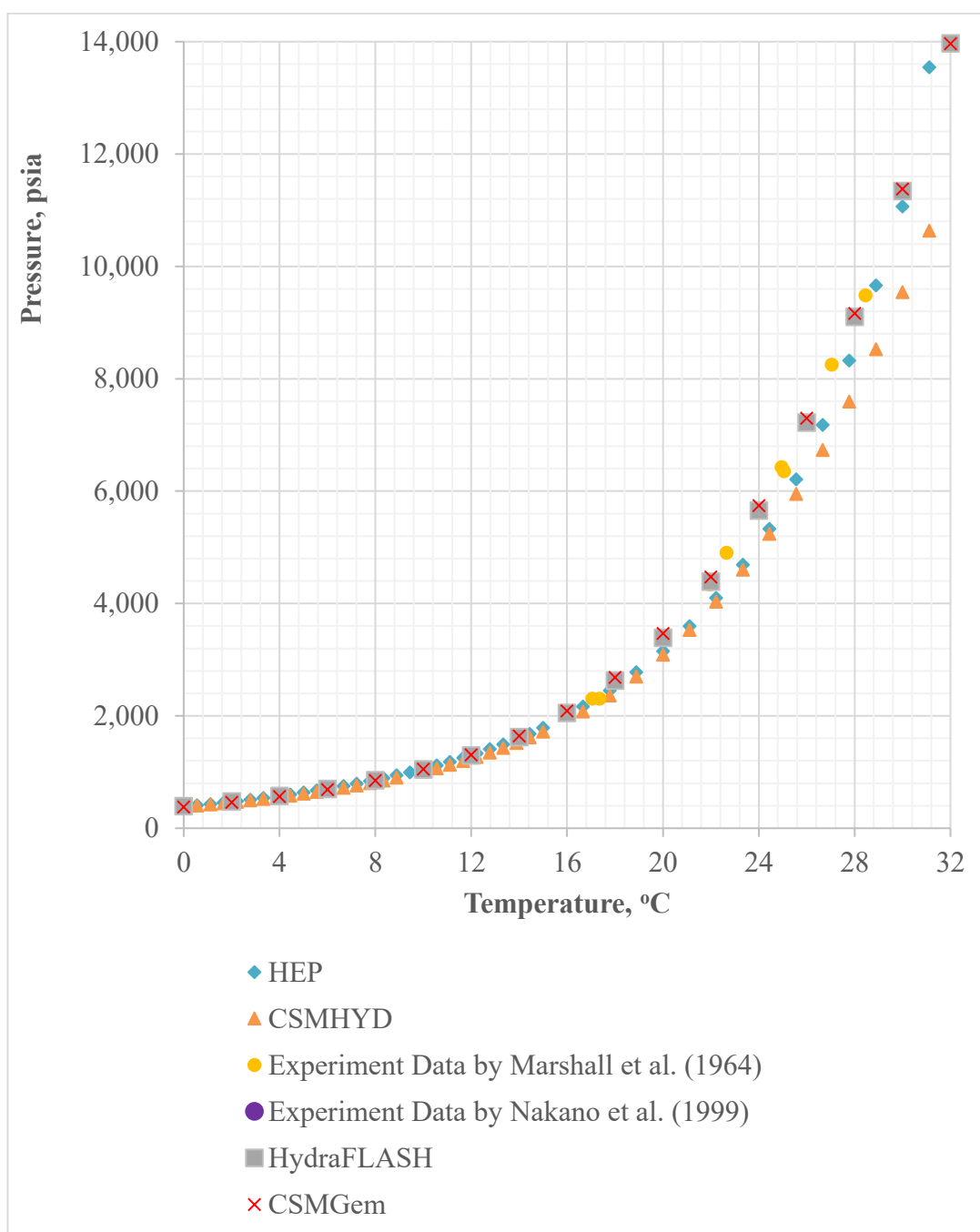
The fitting of predicted results by HEP, CSMHYD, CSMGem, and HydraFLASH to the experimental data were analyzed statistically by using Minitab 17, which is powerful statistical software (Minitab, 2016).  $R^2$  values of these statistical evaluations were shown in Table 7-18.

In Figure 7-103, the experimental result of CH<sub>4</sub> hydrate equilibrium curve between -10.8 °C and 15 °C are compared with those curve predicted by HEP, CSMHYD, CSMGem, HydraFLASH and the formula of Sultan *et al.*(2004). CH<sub>4</sub> hydrate is the most common hydrate in nature so it is important to predict its equilibrium pressure and its properties. Figure 7-103 shows that there is a very good agreement between the experimental CH<sub>4</sub> hydrate equilibrium data of Maekawa (1998), Deaton and Frost (1946) and the predicted data by HEP, CSMHYD, CSMGem, HydraFLASH and the formula of Sultan *et al.* (2004). When  $R^2$  values in Table 7-18 are compared, all softwares fit to the pure CH<sub>4</sub> experimental hydrate equilibrium data very well.



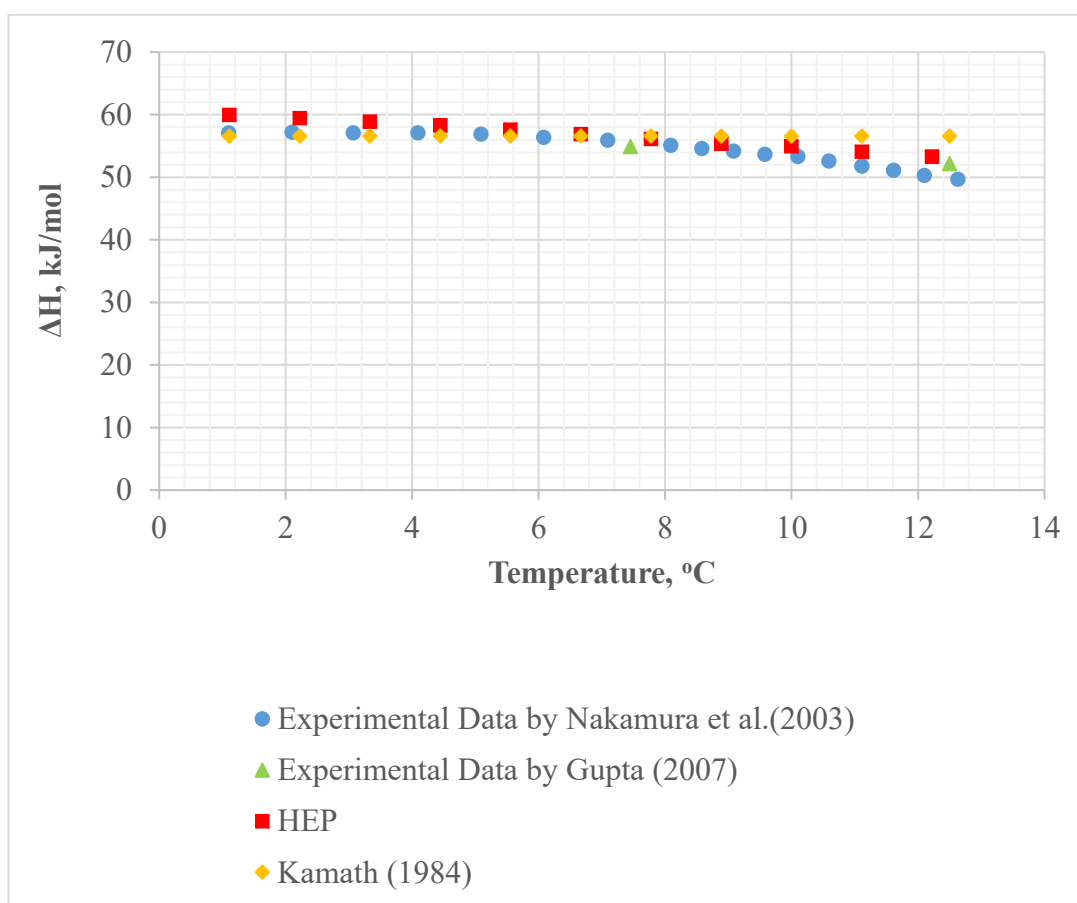
**Figure 7-103:** Comparison of CH<sub>4</sub> hydrate equilibrium curve of HEP, CSMHYD, CSMGem and HydraFLASH with experimental and other software data

The experimental CH<sub>4</sub> hydrate equilibrium curves of Marshall *et al.* (1964) and Nakano *et al.* (1999) were measured between 0 °C and 47°C. As these results are compared with the calculated data by HEP, CSMHYD, CSMGem and HydraFLASH in Figure 7-104, all values are close to each other until 24 °C. However, after 24 °C (higher temperatures), the calculated data by CSMHYD are quite different from the experimental CH<sub>4</sub> hydrate equilibrium data. For the formation of CH<sub>4</sub> hydrate after 20-30 °C, high pressure values are needed. Although it is possible to form CH<sub>4</sub> hydrate after 20-30 °C in the laboratory conditions, in nature (both gas hydrate reservoirs and during the transportation of natural gas hydrate), these conditions (i.e., at 30 °C, 10,000 psia) cannot be reached easily (Max and Johnson, 2016). According to Moridis *et al.* (2005), the largest pressure at which natural gas hydrates are known to exist (i.e., about 1595.4 psia). Moreover, Kirby *et al.* (2004) stated that hydrate usually occurs in sediments where temperature of 0 to 20 °C (Hydrate equilibrium pressure of CH<sub>4</sub> ranges from 382.3 psia to 3087.1 psia between these temperatures). Hence, HEP, CSMHYD, CSMGem, and HydraFLASH can be used to predict the hydrate formation conditions of CH<sub>4</sub>. R<sup>2</sup> value for CSMHYD is lowest (89.77) but R<sup>2</sup> values of HEP, CSMGem, and HydraFLASH change from 94.07 to 95.86 as seen in Table 7-18.



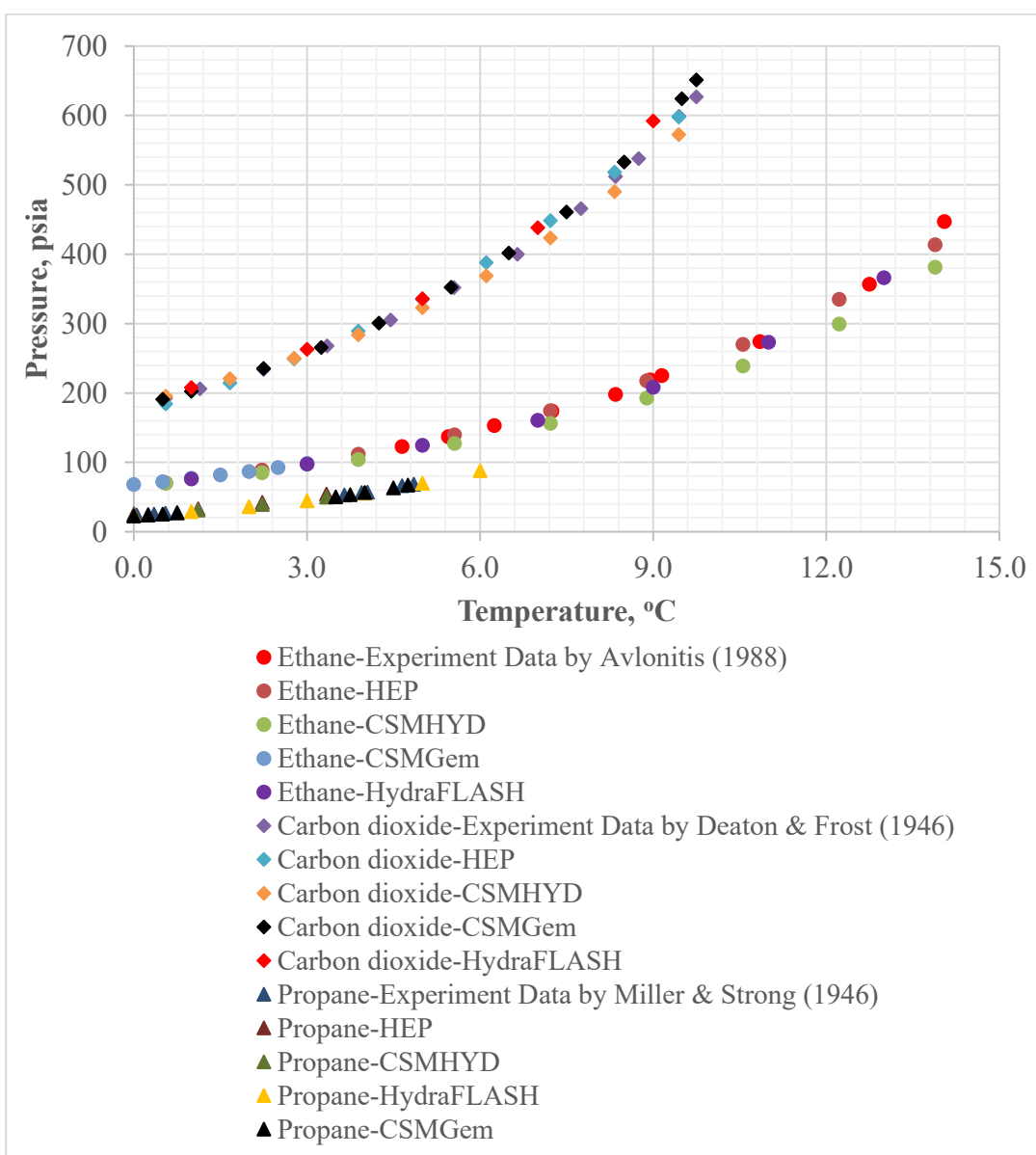
**Figure 7-104:** Comparison of CH<sub>4</sub> hydrate equilibrium curve of HEP, CSMHYD, CSMGem and HydraFLASH with experimental and other software data at high temperatures

As well as hydrate equilibrium pressure of CH<sub>4</sub> at certain temperatures, the determination of enthalpy of hydrate dissociation is also quite important. Especially, during the hydrate formation or dissociation in the sediments inside the high pressure cells or reactors, the temperature of the system decreases or increases because the formation of hydrate is exothermic and the dissociation of hydrate is endothermic. Although CSMHYD, CSMGem and HydraFLASH cannot predict the enthalpy of hydrate dissociation, HEP calculates the enthalpy of hydrate dissociation by using Equation (4-33) (Clausius-Clapeyron equation) for pure CH<sub>4</sub>, C<sub>2</sub>H<sub>6</sub>, C<sub>3</sub>H<sub>8</sub>, n-C<sub>4</sub>H<sub>10</sub>, i-C<sub>4</sub>H<sub>10</sub>, n-C<sub>5</sub>H<sub>12</sub>, i-C<sub>5</sub>H<sub>12</sub>, n-C<sub>6</sub>H<sub>14</sub>, H<sub>2</sub>S, N<sub>2</sub>, CO<sub>2</sub> and the mixtures of these components. The equation of Kamath (1984) in Equation (4-32) is also commonly used for the calculation of the enthalpy of hydrate dissociation for different pure gases such as pure CH<sub>4</sub>, C<sub>2</sub>H<sub>6</sub>, C<sub>3</sub>H<sub>8</sub>, H<sub>2</sub>S, N<sub>2</sub>, and CO<sub>2</sub>. Moreover, in HydrateResSim and Tough + Hydrate numerical simulators, this equation is used to calculate enthalpy of pure CH<sub>4</sub> hydrate dissociation (Moridis *et al.*, 2005; Moridis, 2014). The experimental data of the enthalpy of CH<sub>4</sub> hydrate dissociation in the studies of Gupta (2007) and Nakamura *et al.* (2003) were compared to those values calculated by HEP and the formula of Kamath (1984). As shown in Figure 7-105, there is a good agreement with the results. In Table 7-18, the error analysis for HEP to predict the experimental enthalpy of dissociation of CH<sub>4</sub> hydrate is shown. R<sup>2</sup> value was calculated as 86.46 % by Minitab 17. This value is 81.14 % with Kamath (1984)'s equation (Equation (4-32)). Similar to pure CH<sub>4</sub> hydrates, HEP also can predict the hydrate equilibrium pressure, hydrate density, hydrate molecular weight, hydration number, and enthalpy of hydrate dissociation of pure CH<sub>4</sub>, C<sub>2</sub>H<sub>6</sub>, C<sub>3</sub>H<sub>8</sub>, n-C<sub>4</sub>H<sub>10</sub>, i-C<sub>4</sub>H<sub>10</sub>, n-C<sub>5</sub>H<sub>12</sub>, i-C<sub>5</sub>H<sub>12</sub>, n-C<sub>6</sub>H<sub>14</sub>, H<sub>2</sub>S, N<sub>2</sub>, and CO<sub>2</sub> hydrate (some these components cannot form their pure gas hydrates as shown in Figure 2-1 but they might enter to cages of mixed gas hydrates).



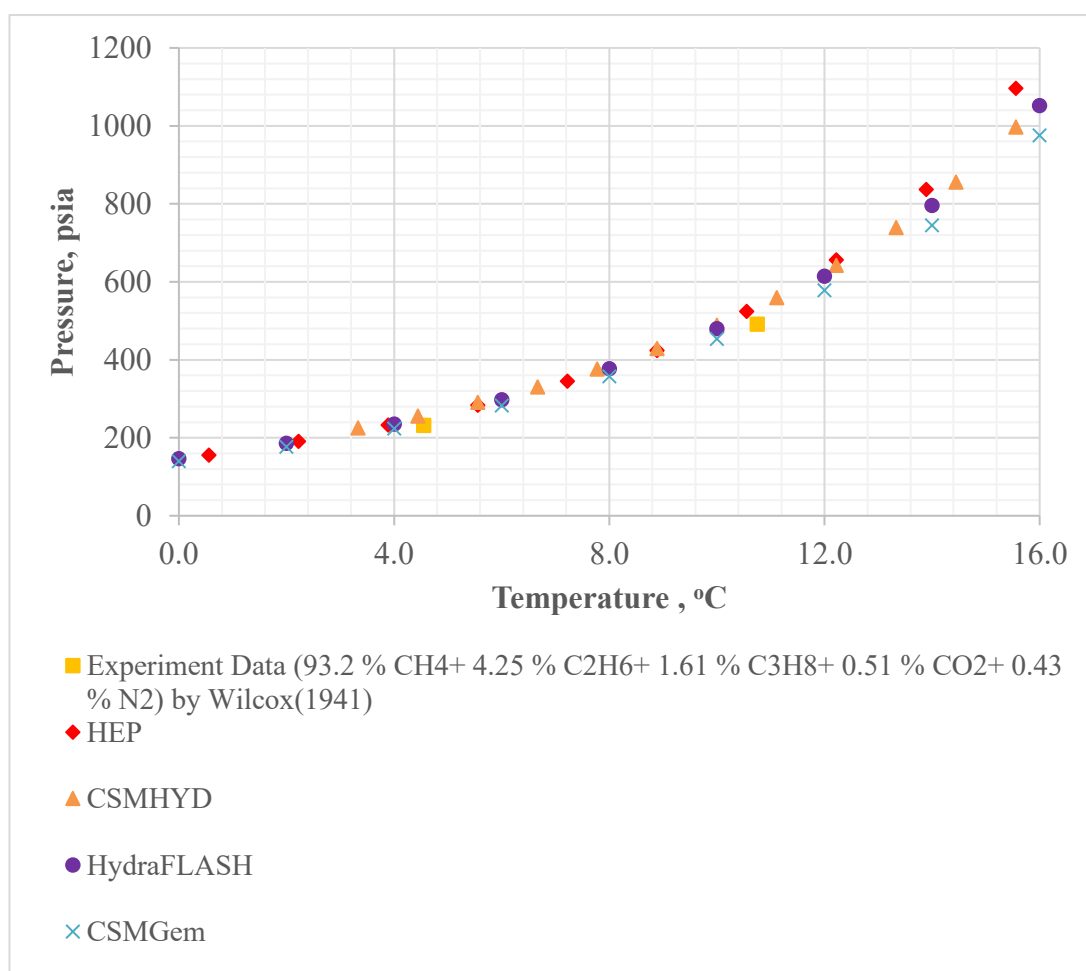
**Figure 7-105:** Comparison of enthalpy of CH<sub>4</sub> hydrate of HEP and Kamath (1984)'s equation with experimental data

Figure 7-106 shows the comparison of hydrate equilibrium of pure C<sub>2</sub>H<sub>6</sub>, C<sub>3</sub>H<sub>8</sub>, and CO<sub>2</sub> with HEP, CSMHYD, CSMGem, HydraFLASH and experimental data. The results are quite close to each other. Therefore, HEP is capable of predicting hydrate equilibrium pressure or temperature of pure hydrates or non-hydrate formers of CH<sub>4</sub>, C<sub>2</sub>H<sub>6</sub>, C<sub>3</sub>H<sub>8</sub>, n-C<sub>4</sub>H<sub>10</sub>, i-C<sub>4</sub>H<sub>10</sub>, n-C<sub>5</sub>H<sub>12</sub>, i-C<sub>5</sub>H<sub>12</sub>, n-C<sub>6</sub>H<sub>14</sub>, H<sub>2</sub>S, N<sub>2</sub>, and CO<sub>2</sub>. Table 7-18 shows R<sup>2</sup> values for HEP, CSMHYD, CSMGem and HydraFLASH. These values for pure C<sub>2</sub>H<sub>6</sub>, C<sub>3</sub>H<sub>8</sub>, and CO<sub>2</sub> with HEP, CSMHYD, CSMGem and HydraFLASH are approximately equal to each other. 99.59 %, 98.47 %, and 88.95 % R<sup>2</sup> for HEP were calculated by Minitab 17 for pure C<sub>2</sub>H<sub>6</sub>, CO<sub>2</sub>, and C<sub>3</sub>H<sub>8</sub> respectively.



**Figure 7-106:** Comparison of hydrate equilibrium of pure  $C_2H_6$ ,  $C_3H_8$ , and  $CO_2$  with HEP, CSMHYD, CSMGem and HydraFLASH and experimental data

The hydrate properties of natural gas mixtures are also important for checking any possible hydrate plugging during the transportation of natural gas with pipeline and understanding sII hydrate (thermogenic) reservoirs in nature. It is obvious that Black Sea has high potential of gas hydrates formed from gas mixtures. Samples were collected in Amasra, Bartın, Zonguldak-Kozlu in the central Black Sea by gravity corer (Küçük et al., 2015b). These samples consist of CH<sub>4</sub> (mostly), C<sub>2</sub>H<sub>6</sub>, C<sub>3</sub>H<sub>8</sub>, n-C<sub>4</sub>H<sub>10</sub>, i-C<sub>4</sub>H<sub>10</sub>, n-C<sub>5</sub>H<sub>12</sub>, i-C<sub>5</sub>H<sub>12</sub>, n-C<sub>6</sub>H<sub>14</sub>, H<sub>2</sub>S, and CO<sub>2</sub>. Therefore, the prediction of thermogenic hydrate properties is as important as the prediction of pure CH<sub>4</sub> hydrate properties. HEP code written in this study with Matlab 2014a can be used to predict these properties.



**Figure 7-107:** Comparison of hydrate equilibrium of 93.2 % CH<sub>4</sub>, 4.25% C<sub>2</sub>H<sub>6</sub>, 1.61 % C<sub>3</sub>H<sub>8</sub>, 0.51% CO<sub>2</sub>, 0.43% N<sub>2</sub> with HEP, CSMHYD, CSMGem and HydraFLASH and experimental data

Wilcox (1941) formed hydrate as bulk by using the gas mixture of 93.2 % CH<sub>4</sub>, 4.25% C<sub>2</sub>H<sub>6</sub>, 1.61 % C<sub>3</sub>H<sub>8</sub>, 0.51% CO<sub>2</sub> and 0.43% N<sub>2</sub> between 4.4°C to 16°C. The hydrate equilibrium curves of HEP, CSMHYD, CSMGem, and HydraFLASH for the gas mixture are shown in Figure 7-107. There is a good agreement between the predicted values and experimental results and R<sup>2</sup> values are listed in Table 7-18. Similarly, good fitting results were obtained by using HEP, CSMHYD, CSMGem and HydraFLASH for gas mixtures 78 % CH<sub>4</sub> , 2 % C<sub>3</sub>H<sub>8</sub> , 20% CO<sub>2</sub> (Bishnoi and Dholabhani, 1999); 88.36 % CH<sub>4</sub>, 6.82 % C<sub>2</sub>H<sub>6</sub>, 2.54 % C<sub>3</sub>H<sub>8</sub>, 0.38 % i-C<sub>4</sub>H<sub>10</sub>, 0.89 % n-C<sub>4</sub>H<sub>10</sub>, 1.01 % n-C<sub>5</sub>H<sub>12</sub> (Sloan, 1990); 87 % CH<sub>4</sub>, 13% CO<sub>2</sub> (Adisasmito *et al.*, 1991) and 88.3 % CH<sub>4</sub>, 11.7 % C<sub>3</sub>H<sub>8</sub> (Deaton and Frost, 1946). The results of HEP, CSMHYD, CSMGem and HydraFLASH are shown in Figure 7-108, Figure 7-109, and Figure 7-110, respectively. There is a good agreement between the predicted values and experimental results and R<sup>2</sup> values are listed in Table 7-18.

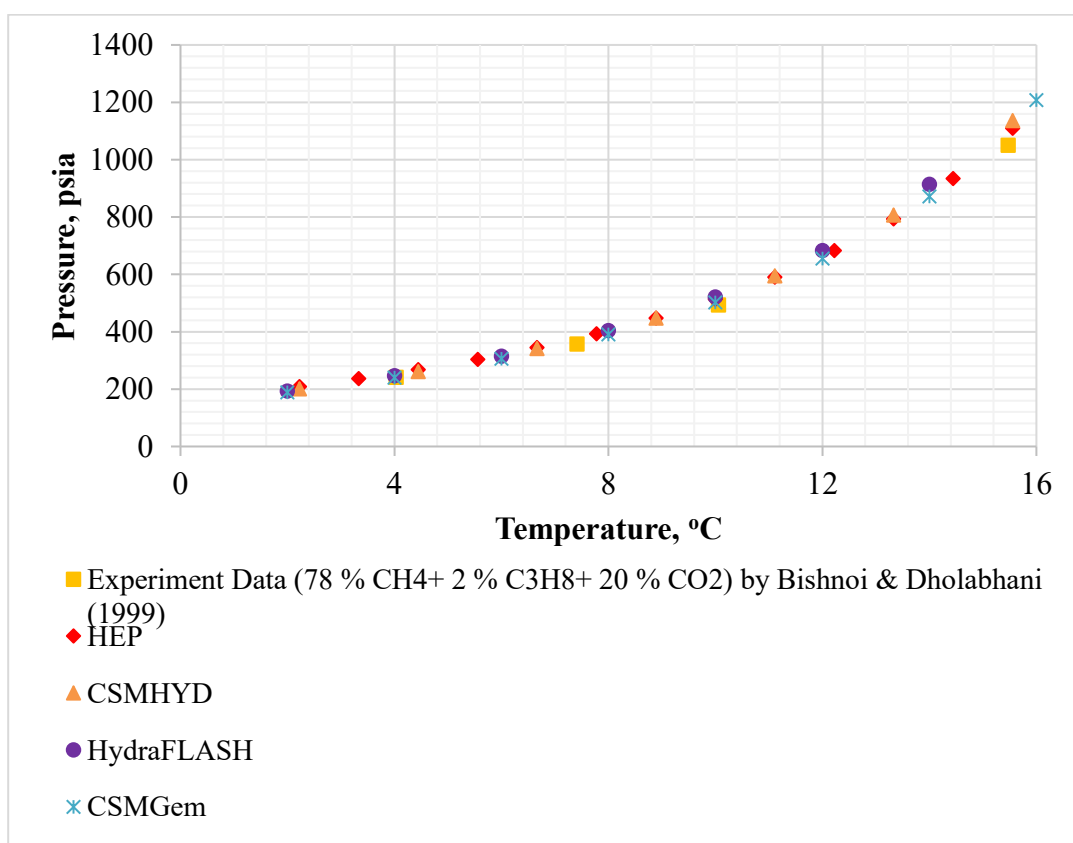


**Figure 7-108:** Comparison of hydrate equilibrium of 78 % CH<sub>4</sub>, 2 % C<sub>3</sub>H<sub>8</sub>, 20% CO<sub>2</sub> with HEP, CSMHYD, CSMGem and HydraFLASH and experimental data

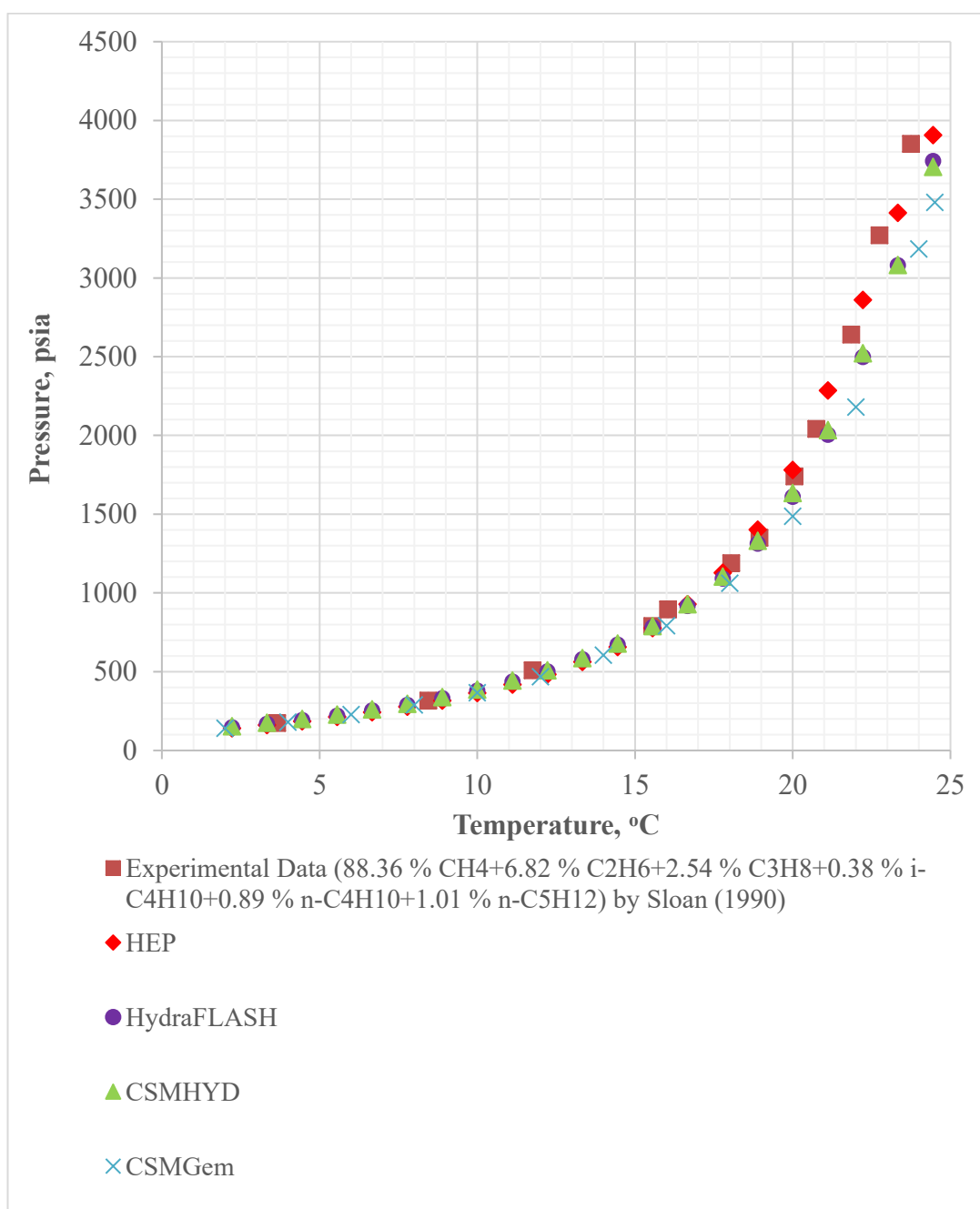


**Figure 7-109:** Comparison of hydrate equilibrium of 88.36 % CH<sub>4</sub>, 6.82 % C<sub>2</sub>H<sub>6</sub>, 2.54 % C<sub>3</sub>H<sub>8</sub>, 0.38 % i-C<sub>4</sub>H<sub>10</sub>, 0.89 % n-C<sub>4</sub>H<sub>10</sub>, 1.01 % n-C<sub>5</sub>H<sub>12</sub> with HEP, CSMHYD, CSMGem and HydraFLASH and experimental data

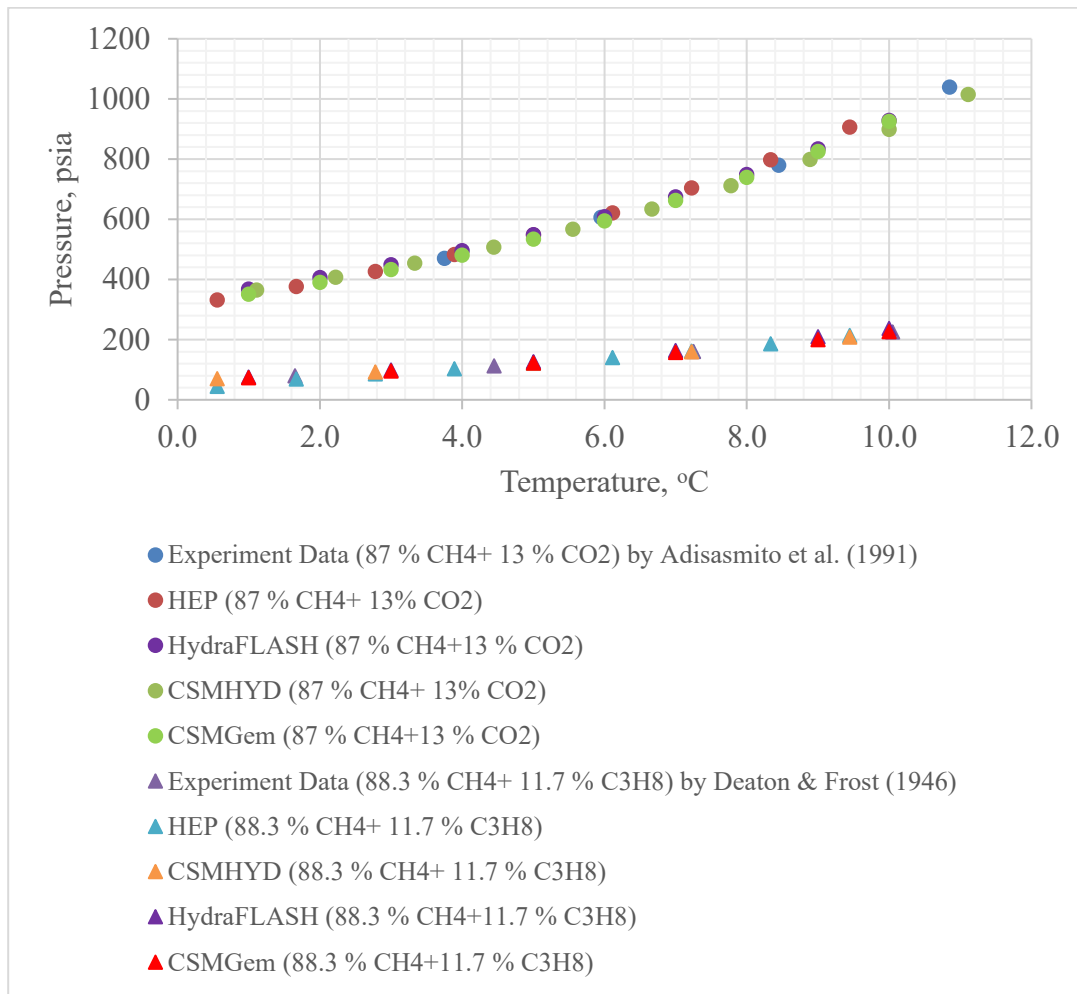


**Figure 7-110:** Comparison of hydrate equilibrium of gas mixture (87 % CH<sub>4</sub>, 13% CO<sub>2</sub>) and gas mixture (88.3 % CH<sub>4</sub>, 11.7 % C<sub>3</sub>H<sub>8</sub>) with HEP, CSMHYD, CSMGem and HydraFLASH and experimental data

When gas pipelines are plugged by hydrate formation, different hydrate inhibitors such as methanol are added to the system to solve plugging problem. Moreover, chemical injection is considered as a gas production method from gas hydrate reservoirs. Therefore, the prediction of hydrate equilibrium curve shifts and hydrate properties with inhibitors are quite important. HEP can be used to calculate hydrate properties after the addition of inhibitors: NaCl, CaCl<sub>2</sub>, KCl, Methanol, Ethanol, Ethylene Glycol, DEG, TEG and their mixtures. CSMHYD cannot predict hydrate properties with inhibitors but those can be predicted by CSMGem and HydraFLASH. In Figure 7-111, the experiment data of CH<sub>4</sub> hydrate with 10 % methanol is compared

with the data of HEP, CSMGem and HydraFLASH and very similar results were obtained with  $R^2$  values higher than 99 % (Table 7-18).

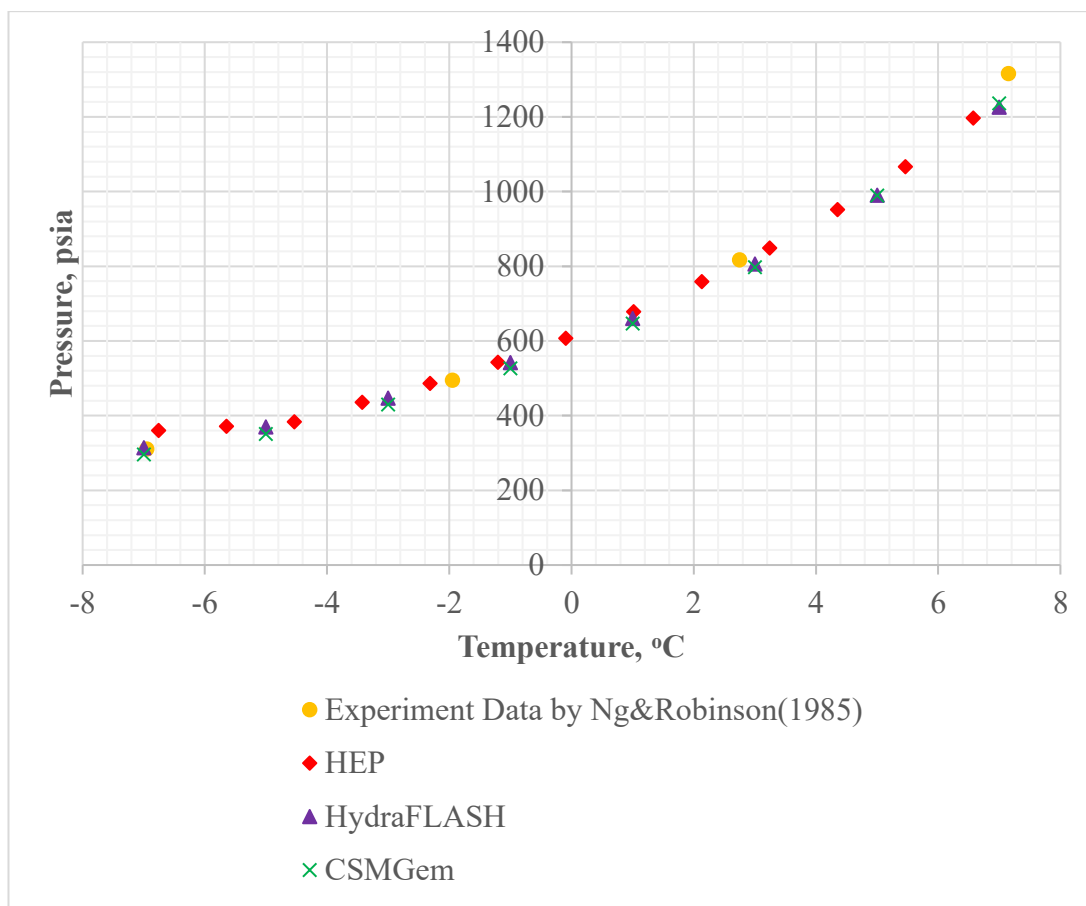


**Figure 7-111:** CH<sub>4</sub> hydrate equilibrium curve with 10 weight % Methanol with HEP, CSMGem and HydraFLASH and experimental data

Gas hydrate reservoir in both permafrost and marine environment might contain water with different salinity values. Therefore, the prediction of hydrate equilibrium with NaCl is also important. In Figure 7-112, the experimental results of Jager and Sloan (2001) were compared with those values calculated with HEP, CSMGem, and HydraFLASH for 10.81 % NaCl and the results are very similar with  $R^2$  values higher than 99 % (Table 7-18).

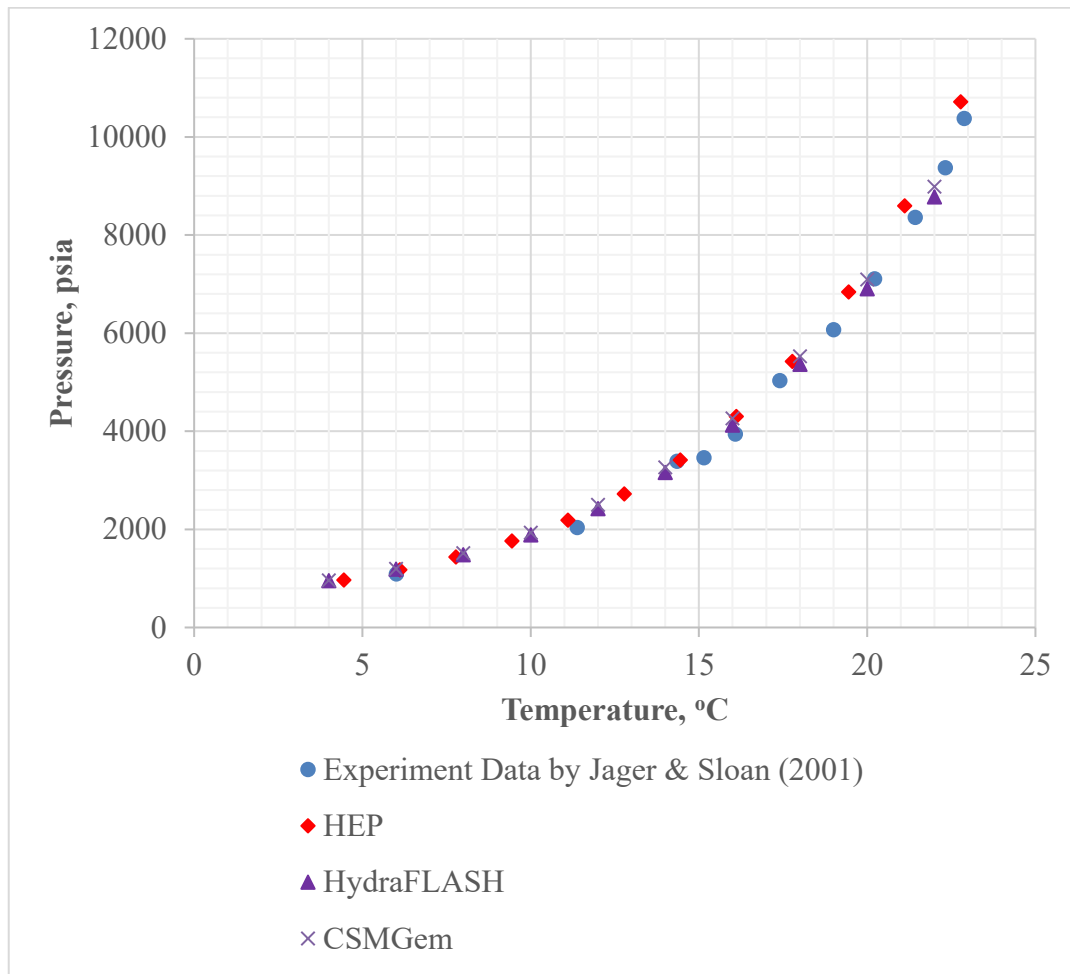


**Figure 7-112:** CH<sub>4</sub> hydrate equilibrium curve with 10.81 weight % NaCl with HEP, CSMGem and HydraFLASH and experimental data

Some inhibitors are mixed at different concentrations to increase the hydrate inhibition effect. Jager *et al.* (2002) measured hydrate equilibrium of CH<sub>4</sub> with inhibitor solution including 6.21 % NaCl and 10 % Methanol. CSMGem, HEP and HydraFLASH can predict hydrate properties with mixtures of inhibitors. In Figure 7-113, the comparison of hydrate equilibrium of this composition with the results of HEP, CSMGem and HydraFLASH. Very similar results were obtained with  $R^2$  values higher than 98 % (Table 7-18).

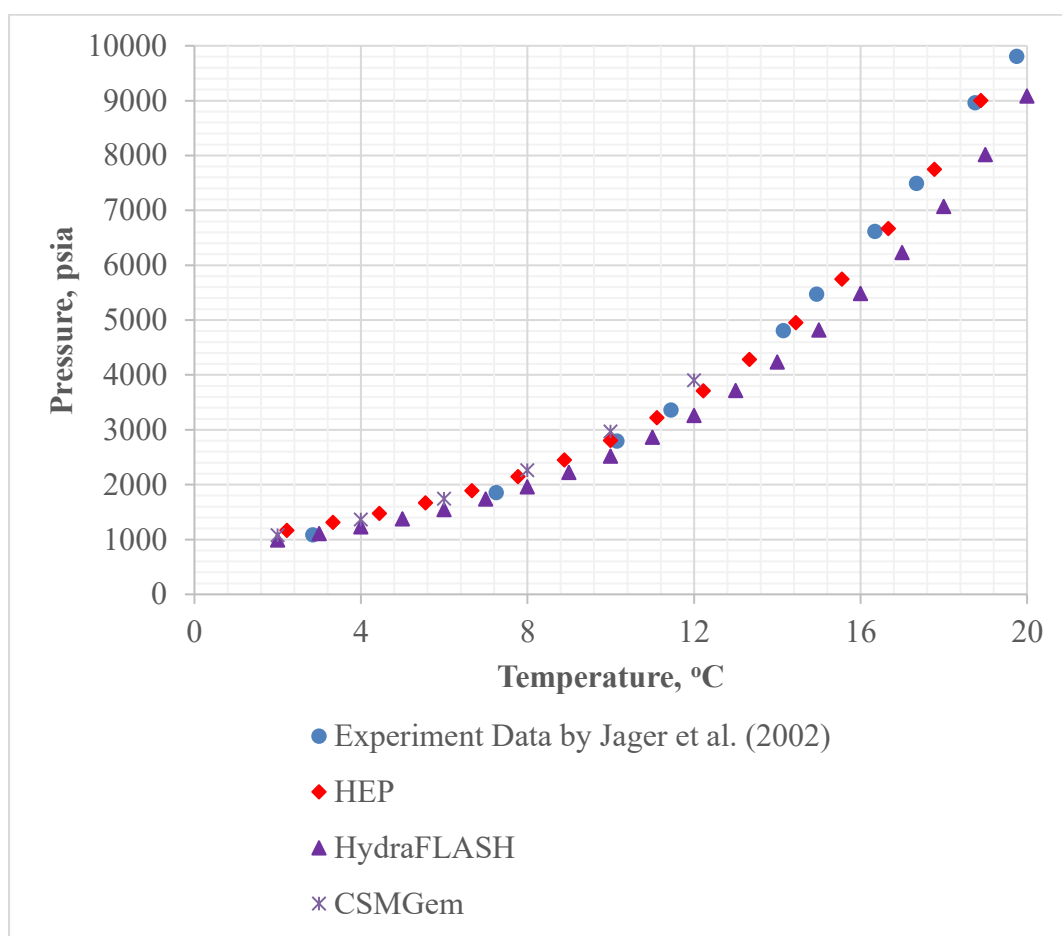


**Figure 7-113:** Comparison of hydrate equilibrium of CH<sub>4</sub> with inhibitors (6.21 % weight NaCl and 10.0 weight % Methanol) with HEP, CSMGem and HydraFLASH and experimental data

In the study of Bishnoi and Dholabhani (1999), the mixture of 9.99 % NaCl and 10.01 % Methanol was used to shift the hydrate equilibrium curve of gas mixture of 78 % CH<sub>4</sub>, 2 % C<sub>3</sub>H<sub>8</sub>, and 20 % CO<sub>2</sub>. CSMGem could not converge with this mixture. However, by applying the method of Ameripour (2005) in HEP, the hydrate inhibition for the mixture of 9.99 % NaCl and 10.01 % Methanol was predicted and compared with the experimental data of Bishnoi and Dholabhani (1999). Moreover, HydraFLASH could predict hydrate properties for this mixture. As seen in Figure 7-114, a good agreement was obtained between the experimental data and modelled data. However, at different points where there is no experimental data, HEP and HydraFLASH gave quite different results. All of CSMHYD, CSMGem, HEP and HydraFLASH have certain assumptions and the formulas used in these software were

generated from the experimental data. For very complex mixtures, these software might not converge. For example, CSMGem could not converge for the gas mixture with inhibitor mixture in Figure 7-114. Moreover, the experimental errors of these gas mixture and inhibitor mixture could be higher compared to other simple mixtures. Therefore, it is better to test this software with experimental data as much as possible. HEP is newly written code in this study. It was aimed to test its reliability by comparing its results with many experimental data and other similar software (CSMHYD, CSMGem and HydraFLASH), which are commonly used in hydrate studies and projects (Sloan and Koh, 2008; Hydrafact, 2016).

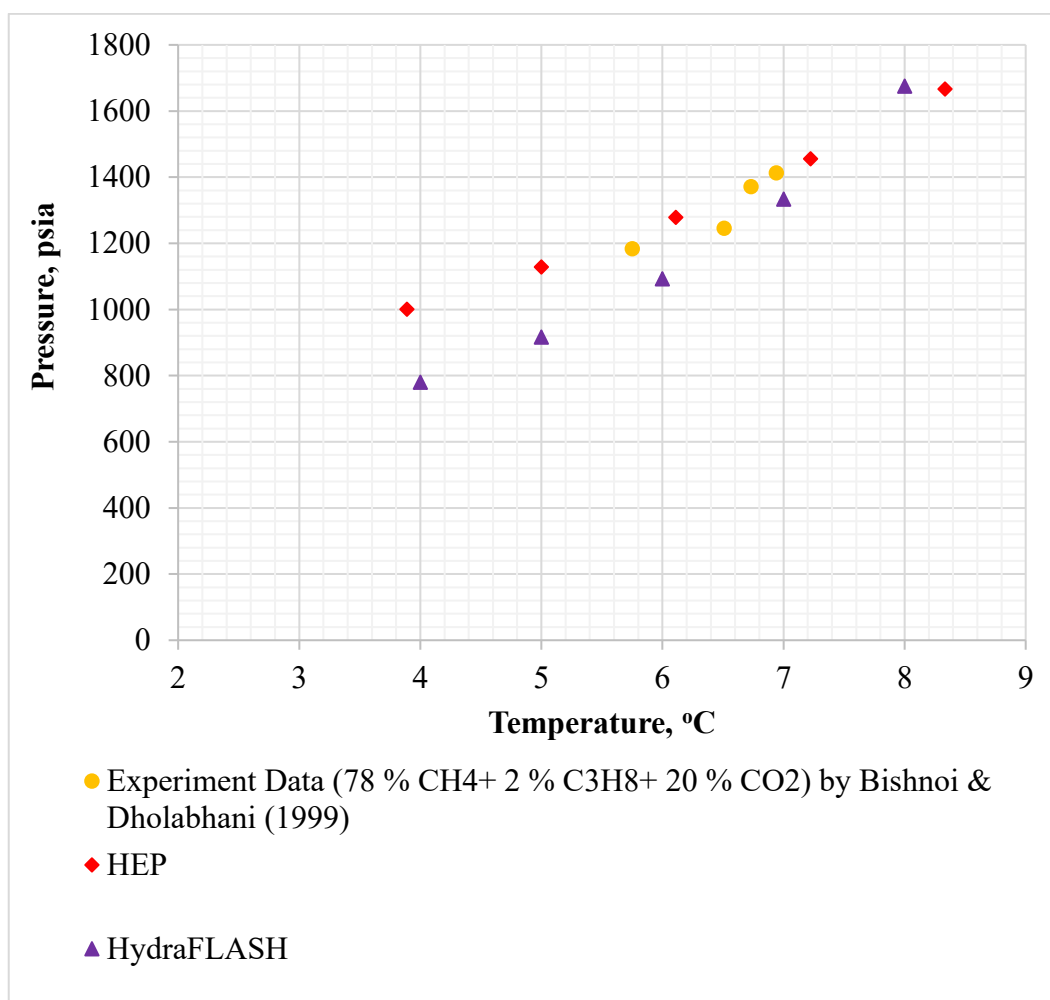


**Figure 7-114:** Comparison of hydrate equilibrium of 78 % CH<sub>4</sub>, 2 % C<sub>3</sub>H<sub>8</sub>, 20% CO<sub>2</sub> with inhibitors (9.99 % NaCl and 10.01 % Methanol) with HEP and HydraFLASH and experimental data

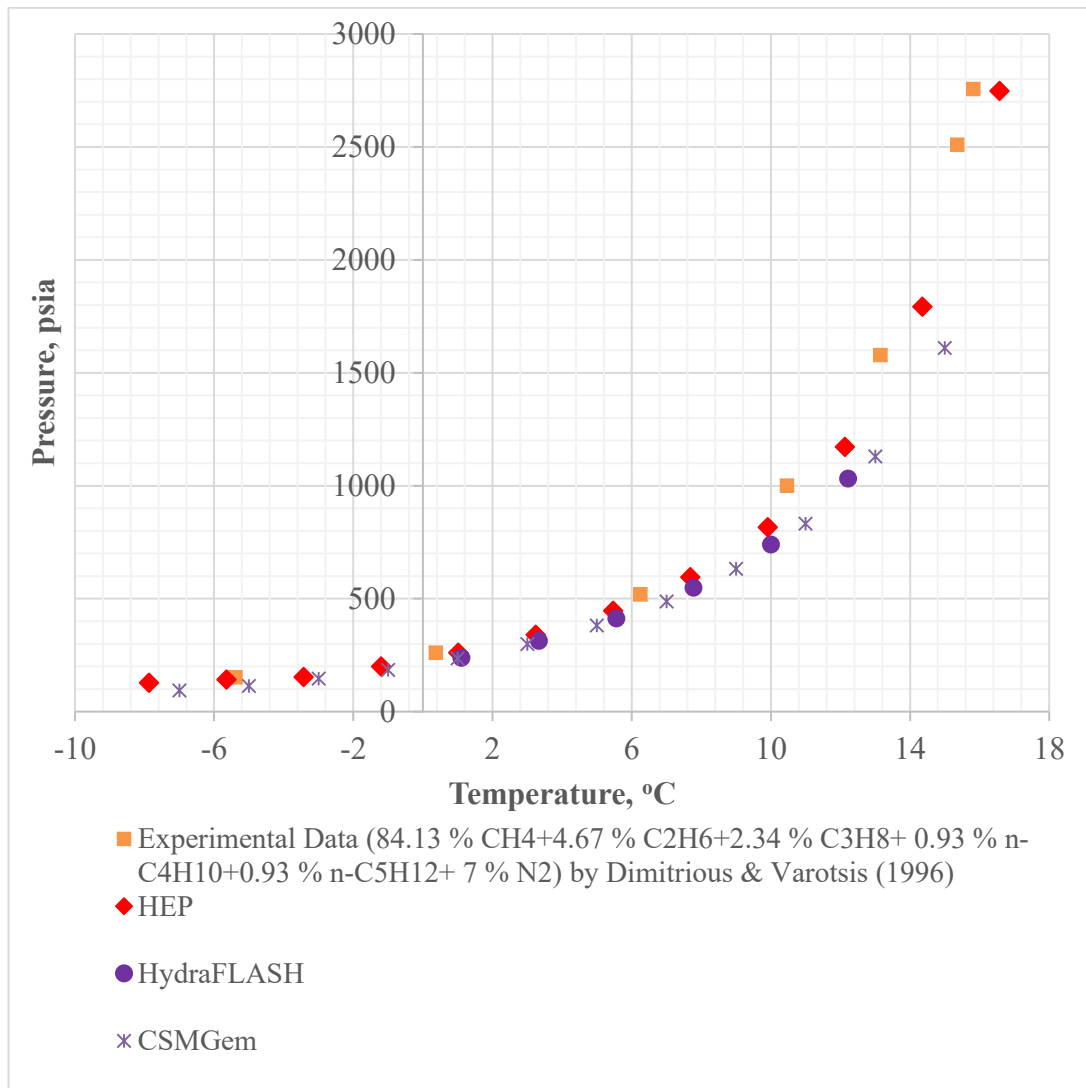


**Figure 7-115:** Comparison of hydrate equilibrium of 84.13 % CH<sub>4</sub>, 4.67 % C<sub>2</sub>H<sub>6</sub>, 2.34 % C<sub>3</sub>H<sub>8</sub>, 0.93 % n-C<sub>4</sub>H<sub>10</sub>, 0.93 % n-C<sub>5</sub>H<sub>12</sub>, 7% N<sub>2</sub> with 10.0 % Methanol with HEP, CSMHYD, CSMGem and HydraFLASH and experimental data

Finally, in order to test HEP code, the experimental hydrate equilibrium data of 84.13 % CH<sub>4</sub>, 4.67 % C<sub>2</sub>H<sub>6</sub>, 2.34 % C<sub>3</sub>H<sub>8</sub>, 0.93 % n-C<sub>4</sub>H<sub>10</sub>, 0.93 % n-C<sub>5</sub>H<sub>12</sub>, 7% N<sub>2</sub> with 10.0 % Methanol mixture (Dimitriou and Varotsis, 1996) was selected because it includes many components that the Black Sea consists of according to the study of Küçük *et al.* (2015b). HEP fits to the experimental data very well with 99.23 % R<sup>2</sup> as seen in Table 7-18.

By using HEP.m code, the enthalpy of natural gas hydrate, density, hydrate type and the cage occupation by each gas are also predicted as well as pure gases. Table 7-19 shows the comparisons of the enthalpy values of natural gas hydrate between HEP and experimental data. The calculated values by HEP is quite close to those values measured in the experiments.

**Table 7-19:** Comparison of enthalpy of hydrate dissociation of gas mixtures

Gas Mixture	$\Delta H$ , kJ/mol (Sarshar <i>et al.</i> , 2009)	$\Delta H$ , kJ/mol (This Study with HEP)
65.02 % CH <sub>4</sub> , 2.39% C <sub>2</sub> H <sub>6</sub> , 26.62 % C <sub>3</sub> H <sub>8</sub> , 1.5 % i-C <sub>4</sub> H <sub>10</sub> , 1.5% CO <sub>2</sub> , 4.26 % O <sub>2</sub> , 0.22% N <sub>2</sub>	73.9 @ 286 K	74.107 @ 286 K
70 % CO <sub>2</sub> , 30 % N <sub>2</sub>	63.41 @ 273.65 K	60.829 @ 273.65 K

In Table 7-20, some of hydrate properties calculated by CSMHYD by Sloan and Koh (2008) and those calculated by HEP and CSMGem were compared. Free gas concentration at hydrate equilibrium conditions (277 K) are 90 % CH<sub>4</sub>, 7 % C<sub>2</sub>H<sub>6</sub> and 3 % C<sub>3</sub>H<sub>8</sub>. Gas hydrate of this gas mixture was guessed as sII by CSMHYD, CSMGem and HEP. Although pure CH<sub>4</sub> and pure C<sub>2</sub>H<sub>6</sub> form sI hydrate, C<sub>3</sub>H<sub>8</sub> forms sII hydrate at appropriate conditions for hydrate formation. Therefore, even if 1 % of C<sub>3</sub>H<sub>8</sub> is added to the system where CH<sub>4</sub> gas exist, sII hydrate starts to form. When free C<sub>3</sub>H<sub>8</sub> concentration decreases to almost zero and if there is still free water and free CH<sub>4</sub> gas in the system, sI hydrate starts to form. In order to understand all of these, the type of gas hydrate of gas mixture or pure gas and the ratio of the molecular diameter to cavity diameters of each gas for each cages should be known. As seen in Table 7-20 with HEP calculation, CH<sub>4</sub> molecules fill 66.5 % of small cages of sII hydrate and 6.5 % of large cages. However, C<sub>2</sub>H<sub>6</sub> only fills 5.2 % of large cages of sII hydrate but it cannot fit to the small cages of sII hydrate. Similarly, C<sub>3</sub>H<sub>8</sub> fills 84 % of the large cages of sII hydrate because it is sII hydrate former but it cannot fit

into the small cages of sII hydrate. Hence, sII hydrate of pure C<sub>3</sub>H<sub>8</sub> has empty small cages and sII hydrate of gas mixture in Table 7-20 does not have empty cages. Therefore, compared to pure sII hydrate of C<sub>3</sub>H<sub>8</sub>, sII hydrate of this gas mixture is much more stable and it is hard to dissociate these gas hydrates. Table 2-2 is useful to understand the ratio of the molecular diameter to cavity diameters of each gas for each cages of sI and sII hydrate. The hydrate equilibrium pressure of the gas mixture in Table 7-20 was calculated by HEP as 187.6 psia at 277 K (3.85 °C). For example, if there is a gas hydrate reservoir with the composition in Table 7-20 in nature, in order to produce gas from this reservoir, pressure should be decreased below 187.6 psia (for depressurization production method) so for this type of reservoirs, other methods such thermal stimulation might be essential because depressurization is quite difficult for this case.

**Table 7-20:** Comparison of some hydrate properties determined with HEP and CSMHYD

		<b>CH<sub>4</sub></b>	<b>C<sub>2</sub>H<sub>6</sub></b>	<b>C<sub>3</sub>H<sub>8</sub></b>
<b>CSMHYD, Sloan and Koh (2008)</b>	<i>Concentration</i>	90	7	3
	$\theta_s$	0.67	0	0
	$\theta_L$	0.057	0.096	0.84
	<i>Hydrate Density, g/cm<sup>3</sup></i>	0.94		
	<i>Hydrate Type</i>	sII		
	<i>Equilibrium Pressure, psia @ 277 K</i>	189.58		
<b>CSMGem</b>	$\theta_s$	0.698	0.0004	0
	$\theta_L$	0.0434	0.1455	0.8046
	<i>Hydrate Density, g/cm<sup>3</sup></i>	-		
	<i>Hydrate Type</i>	sII		
	<i>Equilibrium Pressure, psia @ 277 K</i>	176.33		
<b>In this study with HEP</b>	$\theta_s$	0.665	0	0
	$\theta_L$	0.065	0.052	0.876
	<i>Hydrate Density, g/cm<sup>3</sup></i>	0.945		
	<i>Hydrate Type</i>	sII		
	<i>Equilibrium Pressure, psia @ 277 K</i>	187.6		

In order to calculate the initial gas in place in gas hydrate reservoirs, Equation (3-9) is commonly used. Hydration number is also used in this equation for the calculation of expansion factor. By using HEP, hydration number of 99.97 % CH<sub>4</sub>, 0.03 % C<sub>2</sub>H<sub>6</sub> gas mixture was calculated at the conditions of the experimental study of Kida *et al.* (2009) and close values are obtained as listed in Table 7-21.

**Table 7-21:** Comparison of some hydrate properties determined with HEP and the experimental study of Kida *et al.* (2009)

		CH <sub>4</sub>	C <sub>2</sub> H <sub>6</sub>
Kida <i>et al.</i> (2009)	Concentration	99.97	0.03
	$\theta_s$	0.853 ± 0.030	0
	$\theta_L$	0.975 ± 0.002	-
	Hydration Number	6.09 ± 0.04	
In this study with HEP	Concentration	99.97	0.03
	$\theta_s$	0.890	0
	$\theta_L$	0.976	0.002
	Hydration Number	6.013	

## 7.6 Prediction of Gas Mixture Composition Change during Hydrate Formation with HEPComp

In order to predict hydrate formation conditions of natural gas transmitted by pipelines, there are several experimental studies (Daraboina *et al.*, 2013). In these experiments, when hydrate formation starts with the decrease of temperature in the high pressure cell or reactor, gas composition changes with time. Similar observations were obtained in the experimental studies of Abbasov (2014), Abbasov *et al.* (2016), Küçük *et al.* (2013) and Schicks *et al.* (2011). Different from these studies, Bouillot

and Herri (2015) and Le Quang *et al.* (2016) analyzed gas compositional change during hydrate formation experimentally and mathematically.

The coring operations in gas hydrate reservoirs are quite difficult. As temperature increases or pressure decreases, hydrate core sample dissociates (Abid *et al.*, 2015). Therefore, generally, when gas hydrate sample taken with the closed core barrel to the surface, gas hydrate dissociates and free gas composition in gas mixture can be determined with GC (Gas Chromatography) analysis. The gas mixture composition before hydrate formation and after hydrate formation are quite different. By using the overall gas mixture, hydrate in sediments can be formed at the conditions of hydrate reservoir experimentally. As temperature decreases, hydrate forms and free gas composition in pores changes with hydrate formation. In Table 7-22, the results of the compositional change of feed gas during hydrate formation with experimental data of Küçük *et al.* (2013) and Abbasov (2014) and software (HEPComp) are listed. HEPComp.m (**HEP Computational**) matlab code was written in this study to predict gas compositional change during hydrate formation of gas mixtures. In the study of Küçük *et al.* (2013), gas composition of 94.84 % CH<sub>4</sub>, 2.04 % C<sub>3</sub>H<sub>8</sub>, and 3.12 % CO<sub>2</sub> was injected into the sediments saturated with water in a 200 cm<sup>3</sup> cylindrical high pressure cell at room temperatures and then temperature of the system was decreased to 4°C. When the decrease of system pressure stopped, this means that hydrate equilibrium conditions were satisfied at 4°C. Then, GC analysis of free gas was done and the gas mixture includes 97.784 % CH<sub>4</sub>, 0.206 % C<sub>3</sub>H<sub>8</sub> and 2.01 CO<sub>2</sub> %. The reason of this compositional change is similar to those explained in detailed for Table 7-20. During gas hydrate formation of feed gas, because of C<sub>3</sub>H<sub>8</sub> concentration, sII hydrate forms. Therefore, there is a decrease in the composition of C<sub>3</sub>H<sub>8</sub> in free gas of the system and this makes the increase of the composition of CH<sub>4</sub> in the system. However, CO<sub>2</sub> cannot enter into the small cages of sII hydrate and the large cages of sII hydrate are mostly filled by C<sub>3</sub>H<sub>8</sub> and CH<sub>4</sub>. Hence, the composition of CO<sub>2</sub> decreased slightly. Similarly, in the study of Yang *et al.* (2015b), when combined the hydrate phase equilibrium pressure and relative CO<sub>2</sub> gas uptake decrease with C<sub>3</sub>H<sub>8</sub> concentration increase.

**Table 7-22:** Composition change of feed gas during hydrate formation with experimental data and software (HEPComp)

Source	Initial Feed Gas Composition			After Hydrate Formation at Equilibrium @ 4°C		
	CH <sub>4</sub> %	C <sub>3</sub> H <sub>8</sub> %	CO <sub>2</sub> %	CH <sub>4</sub> %	C <sub>3</sub> H <sub>8</sub> %	CO <sub>2</sub> %
Küçük <i>et al.</i> (2013)	94.84	2.04	3.12	97.784	0.206	2.01
HEPComp in this study (1)	94.84	2.04	3.12	96.437	0.343	3.22
Abbasov (2014)	95.2	2.97	1.83	98.71	0.357	0.933
HEPComp in this study (2)	95.2	2.97	1.83	97.619	0.469	1.912

**Table 7-23:** Hydrate properties at the equilibrium conditions in Table 7-22 with HEPComp

					CH <sub>4</sub>		C <sub>3</sub> H <sub>8</sub>		CO <sub>2</sub>	
	Type	N <sub>H</sub>	$\rho_H$ g/cm <sup>3</sup>	$\Delta H$ , kJ/mol	$\theta_s$	$\theta_L$	$\theta_s$	$\theta_L$	$\theta_s$	$\theta_L$
HEP (1)	sII	6.4	0.934	73.07	0.825	0.431	0	0.517	0.008	0.032
HEP (2)	sII	6.5	0.938	73.173	0.812	0.360	0	0.606	0.005	0.016

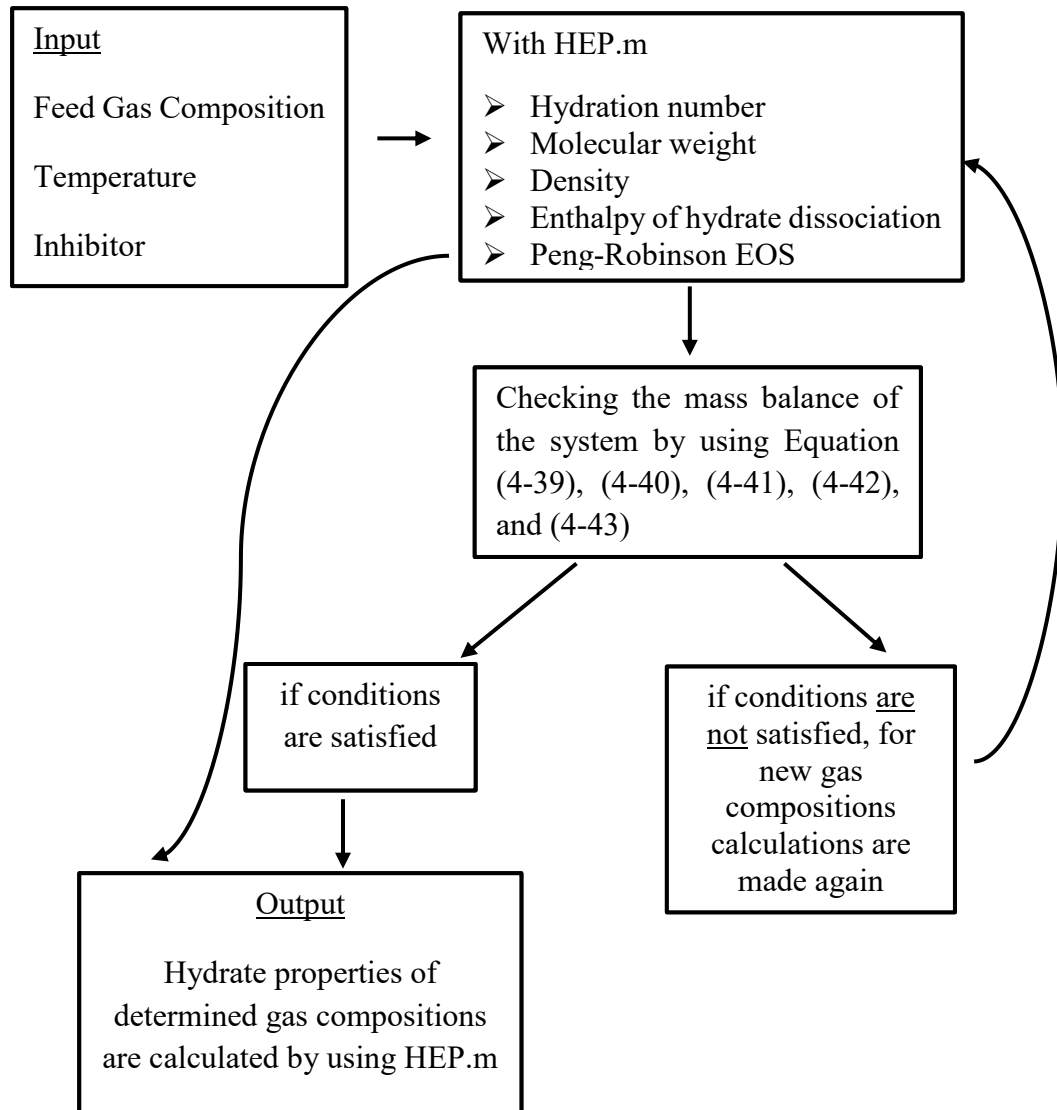


**Figure 7-116:** Algorithm of HEPComp code

HEPComp.m code was written in this study by Matlab 2014a to predict the gas compositional change during hydrate formation of gas mixture. The description of this code is briefly shown in Figure 7-116. When the experimental data of Abbasov (2014) and Küçük *et al.* (2013) were used to predict the compositional change of gas mixture after hydrate formation with HEPComp, very close results were obtained with HEPComp and the experimental results. However, as seen in Table 7-22, CO<sub>2</sub> concentration increases with HEPComp after gas hydrate formation but it decreased in the studies of Abbasov (2014) and Küçük *et al.* (2013). It is obvious that CO<sub>2</sub> molecules cannot enter 16 small cages of one sII hydrate structure but it can fit into

8 large cages of one sII hydrate structure. Therefore, CO<sub>2</sub> only can enter to the large cages but C<sub>3</sub>H<sub>8</sub> is sII hydrate former and it wins the competition with CH<sub>4</sub> and CO<sub>2</sub> gas molecules to enter the large cages. Moreover, the gas composition ratio of CH<sub>4</sub> is quite high and serious amount of CH<sub>4</sub> fills some large cages as well. This made the increase of CO<sub>2</sub> concentration after formation with HEPComp. In both studies of Abbasov (2014) and Küçük *et al.* (2013), gas samples were taken by gas sample injector and then gas was transferred to GC lab for the analysis. Hence, the air in the gas sample injector consists of CO<sub>2</sub> and they made correction for air while analyzing CO<sub>2</sub> concentration in GC results. CO<sub>2</sub> concentration reduction in these experiments might be related to this mistake. Table 7-23 shows the cavity filling ratio in the cages of sII hydrate by HEP. As seen in this table, CO<sub>2</sub> concentration in small cages is less than 0.5 % and in large cages is less than 3.2 %. Even though the molecule size of CO<sub>2</sub> is higher than the average diameter of the small cages of sII hydrate (Table 2-2), small amount of CO<sub>2</sub> might enter into these small cages by distorting them. Similar observations were obtained in the experimental study of Park *et al.* (2006) by using Raman and NMR spectra.

In the study of Le Quang *et al.* (2016), hydrate formation experiments were conducted by using different gas feed compositions. Some of these gas mixtures are listed in Table 7-24. After hydrate formation as bulk hydrate, free gas mixtures were analyzed in gas chromatography (GC). GC results for gas composition A, B, and C were used to calculate experimental hydrate composition, which is shown in Table 7-25. These experimental results were compared with the predicted hydrate composition with HEPComp.m. As seen in Table 7-25, the results are approximately equal to each other. Gas hydrate saturation in marine sediments can be calculated from pressure core degassing data (Wang *et al.*, 2011). Table 7-26 shows the feed gas composition of CH<sub>4</sub>/N<sub>2</sub>/CO<sub>2</sub> before hydrate formation at 1°C and gas composition after hydrate formation measured with GC in the study of Lim *et al.* (2017). With HEPComp, gas composition changes were predicted very well as seen in Table 7-26. Hence, HEPComp.m code can be used to calculate gas hydrate saturation and gas mixture composition at hydrate reservoir conditions by using surface gas composition recovered from the core sample.

**Table 7-24:** Feed gas composition in the study of Le Quang *et al.* (2016)

	CO <sub>2</sub>	N <sub>2</sub>	CH <sub>4</sub>	C <sub>2</sub> H <sub>6</sub>
Gas A	0.24	-	0.76	-
Gas B	0.225	-	0.775	-
Gas C	0.055		0.917	0.028

**Table 7-25:** Comparison of experimental hydrate composition of feed gas in Table 7-24 and predicted hydrate composition with HEPComp

Type	Conditions		Experimental hydrate composition (Le Quang <i>et al.</i> , 2016)			Predicted hydrate composition with HEPComp		
	P, bar	T, °C	CO <sub>2</sub>	CH <sub>4</sub>	C <sub>2</sub> H <sub>6</sub>	CO <sub>2</sub>	CH <sub>4</sub>	C <sub>2</sub> H <sub>6</sub>
Gas A	33.3	3.4	0.29	0.71	-	0.277	0.723	-
Gas B	29.1	2.2	0.292	0.708	-	0.302	0.698	
Gas C	37.75	4.6	0.081	0.799	0.12	0.086	0.823	0.091

**Table 7-26:** Experimental (Lim *et al.*, 2017) and predicted compositions of CH<sub>4</sub>/N<sub>2</sub>/CO<sub>2</sub> for gas phase after hydrate formations

Gas Composition	Feed Gas Mixture	Gas Compositions			Predicted Gas Compositions with HEPComp		
		CH <sub>4</sub>	N <sub>2</sub>	CO <sub>2</sub>	CH <sub>4</sub>	N <sub>2</sub>	CO <sub>2</sub>
CH <sub>4</sub> /N <sub>2</sub> /CO <sub>2</sub>	0.9/0.08/0.02	0.8435	0.1365	0.0201	0.84843	0.11519	0.03638
	0.8/0.16/0.04	0.7144	0.2459	0.0397	0.71837	0.2588	0.02283
	0.7/0.24/0.06	0.5936	0.3567	0.0498	0.59542	0.37191	0.03267
	0.6/0.32/0.08	0.4765	0.4663	0.0573	0.48059	0.47879	0.0462

### 7.7 Calculations to Form Target Hydrate, Gas and Water Saturation in the High Pressure Reactor for CH<sub>4</sub> Hydrates

By well log data and the core data taken (coring in hydrate reservoirs is quite difficult) from gas hydrate reservoirs, initial hydrate, gas and water saturations of gas hydrate reservoirs can be determined. Even with the seismic data (i.e. electromagnetic survey) and analysis of the acoustic impedance on BSRs detected, the saturations in the gas hydrate reservoirs can be predicted (Lu and McMechan, 2002; Wang *et al.*, 2011b; Shankar, 2015). In order to simulate the gas production experimentally from gas hydrate reservoirs with known saturations, the target saturations should be satisfied in high pressure cell or reactor. When the target saturations are satisfied in high pressure cell or reactor after hydrate formation, the desired production method such as depressurization can be applied. By combining Equation (7-2) to (7-5), the amount of gas (simple gas: CH<sub>4</sub>) and water injected are calculated in order to obtain the target gas, hydrate and water (aqueous) saturations. When these saturations are obtained in high pressure cell or reactor, during depressurization, gas, hydrate and water saturations change with time. By using the gas and water production data at certain time, gas, water and gas hydrate saturations at that time are calculated by combining Equations (7-6), (7-8), (7-7) and (7-8).

In all studies of Li *et al.* (2012), Wang *et al.* (2013b), Li *et al.* (2014) and Feng *et al.* (2015), the mass balance and saturation equations are used for the determination of the target saturations. Peng and Robinson EOS is used to calculate gas molar density and the hydrate equilibrium method of Li *et al.* (2008b) were used. Moreover, the constant values listed in Table 7-27 were used for the determination of target saturations.

$$S_G + S_A + S_H = 1.0 \quad (7-2)$$

Where  $S_G$ : gas saturation;  $S_A$ : aqueous saturation;  $S_H$ : hydrate saturation

Target saturations are as follows (Li *et al.*, 2012; Wang *et al.*, 2013b; Li *et al.*, 2014; Feng *et al.*, 2015):

$$S_G = \frac{v_m + n_{m,G}}{V_{pore}} \quad (7-3)$$

$$S_A = \frac{m_{w,inj} - N_H(n_{m0} - n_{m,G} - n_{m,W})M_W}{\rho_w V_{pore}} \quad (7-4)$$

$$S_H = \frac{(n_{m0} - n_{m,G} - n_{m,W})M_H}{\rho_H V_{pore}} \quad (7-5)$$

where  $v_m$ : molar volume of  $CH_4$  (mL/mol) calculated by an equation of states with PVT data;  $n_{m,G}$ : the amount of the remaining  $CH_4$  existing in gas phase;  $n_{m,W}$ : the amount of dissolved  $CH_4$  in aqueous phase;  $m_{w,inj}$ : the total injected water mass, gram;  $n_{m0}$ : the total  $CH_4$  amount, mol (Note: the sand grains are assumed to be incompressible under high pressure conditions so  $V_{pore}$ : pore volume,  $cm^3$  is constant any time.);  $\rho_w$ : density of water, g/mL;  $\rho_H$ : density of hydrate, g/mL;  $N_H$ : hydration number;  $M_w$ : molecular weight of water, g/mol,  $M_H$ : molecular weight of hydrate, g/mol

Saturations in the high pressure cell or reactor at different percentage of hydrate dissociation (Li *et al.*, 2012; Wang *et al.*, 2013b; Li *et al.*, 2014; Feng *et al.*, 2015):

$$S_H = S_{H00}(1 - x) \quad (7-6)$$

$$S_G = \frac{(n_{m00} + \rho_H S_{H00} V_{pore} x / M_H - n_{m,W} - V_p / 22.4) v_m}{V_{pore}} \quad (7-7)$$

$$S_A = S_{A00} + \frac{N_H M_W \rho_H S_{H00} x}{M_H \rho_w} - \frac{m_w}{\rho_w V_{pore}} \quad (7-8)$$

Where  $n_{m00}$ : the total amount of free  $CH_4$  before hydrate dissociation, mol;  $V_p$ : the volume of the produced  $CH_4$ , L;  $m_w$ : the mass of the produced water, gram;  $S_{H00}$ : hydrate saturation before hydrate dissociation;  $S_{A00}$ : aqueous saturation before hydrate dissociation;  $x$ : percentage of hydrate dissociation

**Table 7-27:** Some constants used in the studies of Li *et al.* (2012), Wang *et al.* (2013b), Li *et al.* (2014) and Feng *et al.* (2015)

Density of Water ( $\rho_w$ ), g/cm <sup>3</sup>	1.0
Density of CH <sub>4</sub> Hydrate ( $\rho_H$ ), g/cm <sup>3</sup>	0.94
CH <sub>4</sub> Hydration Number ( $N_H$ )	5.75
Molecular Weight of CH <sub>4</sub> Hydrate, g/mol	124

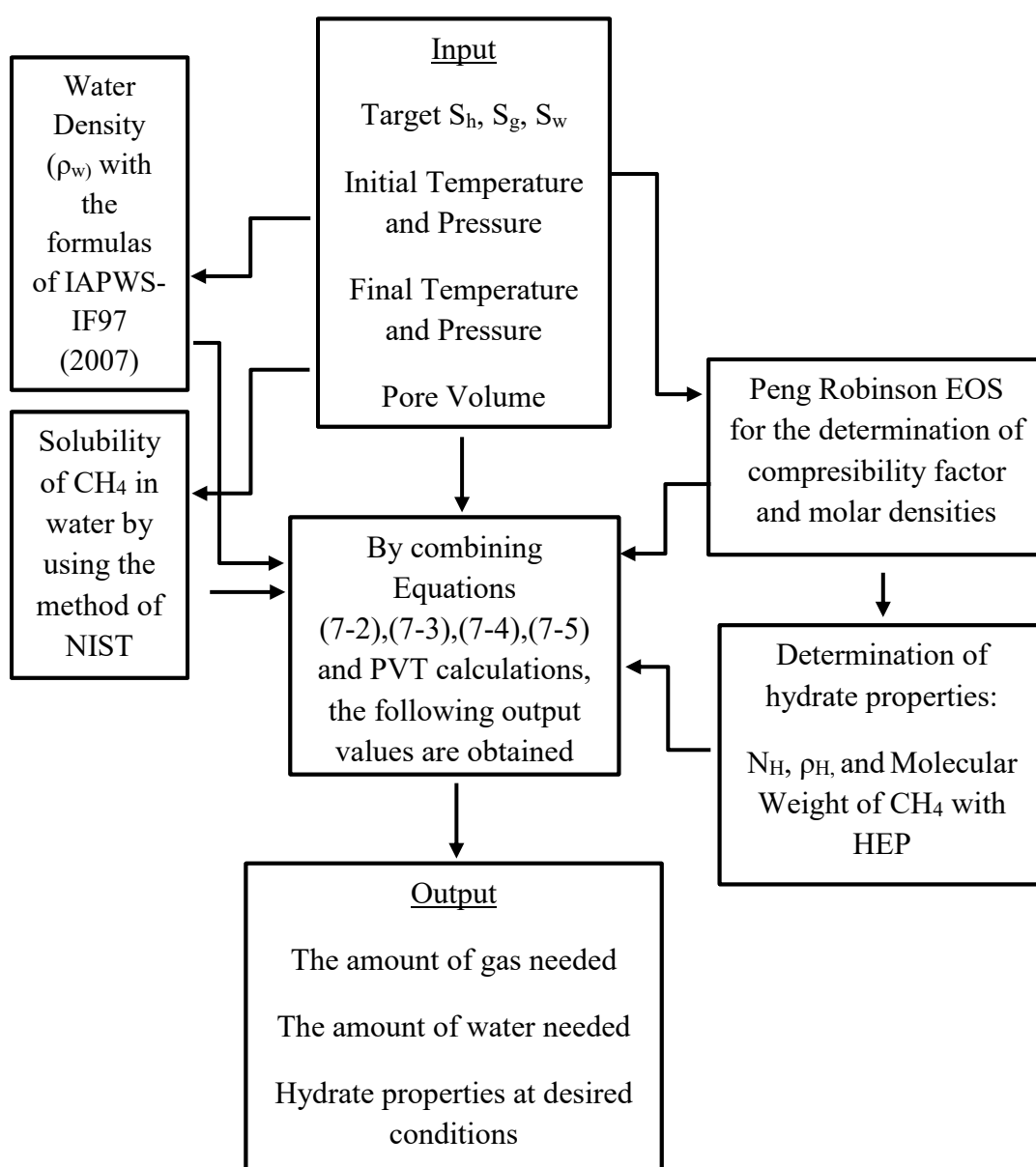


**Figure 7-117:** Algorithm of SM code

Although Li *et al.* (2012), Wang *et al.* (2013b), Li *et al.* (2014) and Feng *et al.* (2015) assumed that the hydrate properties in Table 7-27 are constant and they do not change with pressure and temperature. However, the hydration number of gas hydrate changes with temperature and pressure as explained in Chapter 5. With hydration number, molecular weight of gas hydrate also changes. Moreover, water density changes with pressure and temperature. In this study, for the saturation determination of CH<sub>4</sub> hydrate (SM.m), SM (Saturation of Methane hydrates) codes were written with Matlab 2014a. The procedure of this code is briefly described in Figure 7-117. Different from previous studies, in this study, hydration number, water density, CH<sub>4</sub> hydrate density and CH<sub>4</sub> hydrate molecular weight at different pressures and temperatures are calculated in SM code.

**Table 7-28:** Target saturations, pressure and temperature data in the study of Li *et al.* (2014)

Source	S <sub>H</sub>	S <sub>G</sub>	S <sub>A</sub>	V <sub>pore</sub> , cm <sup>3</sup>	T <sub>initial</sub> , °C	P <sub>initial</sub> , psia	T <sub>final</sub> , °C	P <sub>final</sub> , psia
Run#1- Li <i>et al.</i> (2014)	0.436	0.097	0.467	51069	22.8	2935.564	7.0	1588.163
Run#3- Li <i>et al.</i> (2014)	0.455	0.085	0.460	51069	21.54	2915.259	7.0	1535.95

In order to check the accuracy of SM code for calculating the amount of gas and water injected to reach target gas, hydrate and water saturations in high pressure cell or reactor, the data of Li *et al.* (2014) was used in SM code and the results of both study were compared. Table 7-28 shows the target saturations, pressure and temperature values before hydrate formation and at final conditions in the study Li *et al.* (2014). For example, for Run#1, initially, CH<sub>4</sub> and water injected into 51069 cm<sup>3</sup> pore volume of the sediments in the high pressure (PHS) reactor at 22.8 °C and then temperature decreased to 7.0 °C. When pressure of the system decreased to 1588 psia,

target hydrate ( $S_H$ : 0.436), gas ( $S_G$ : 0.097), and aqueous ( $S_A$ : 0.467 water) saturations were obtained for Run#1.

**Table 7-29:** The amount of gas and water needed for the target saturations in the study of Li *et al.* (2014)

Source	Gas injected, L	Water injected, g
Run#1-Li <i>et al.</i> (2014)	4622	42210
Run#1-SM code with constant $N_H$ , $\rho_w$ , $\rho_H$ , Molecular Weight of $CH_4$	4564.298	42078.681
Run#1- SM code in this study	4485.253	41530.449
Run#3-Li <i>et al.</i> (2014)	4688.1	42632
Run#3-SM code with constant $N_H$ , $\rho_w$ , $\rho_H$ , Molecular Weight of $CH_4$	4617.756	42515.601
Run#3- SM code in this study	4535.648	41945.749

The amount of gas and water needed for the target calculations in Table 7-28 were compared for both Run#1 and Run#3 by Li *et al.* (2014), SM code with constant hydrate and water properties as in the study of Li *et al.* (2014) and SM code as described in Figure 7-117. As seen in Table 7-29, the amount of gas and water needed for injection by Li *et al.* (2014) and SM code with constant hydrate and water properties as in the study of Li *et al.* (2014) are close to each other. The small differences between the results are due to different approximations and different hydrate equilibrium methods used. When the similar results were obtained with SM code with the constant hydrate and water properties, the original SM code does not neglect the change in water density, hydration number, hydrate density and hydrate molecular weight with pressure and temperature. Therefore, SM code is very helpful to simulate real gas hydrate conditions experimentally in the high pressure cells or reactors.

In the study of Li *et al.* (2014), when target saturations in Table 7-28 were obtained in the high pressure reactor at desired temperature and pressure, depressurization experiments were conducted at 687.5 psia for Run#1 and 541 psia for Run#3. By

using the measured produced gas and water amount, saturations and hydrate dissociation percentages in the high pressure reactor were determined at different stages of depressurization by using Equation (7-2) to (7-8). These calculations in the study of Li *et al.* (2014) were compared to the calculations in this study to check the reliability of our codes. By combining SM.m code and HEP.code, for the determination of gas, hydrate and water saturation, the code “SMProd.m” (**SM** after **Production**) were written in Matlab 2014a. It is briefly described in Figure 7-118. By using the gas and water production data in Table 7-30, final gas, water, hydrate saturations and hydrate dissociation percentage were calculated by Li *et al.* (2014) and SMProd.m codes in the high pressure reactor at this stage of depressurization. Very close results were obtained as listed in Table 7-31.

**Table 7-30:** Experimental Data in the study of Li *et al.* (2014) during depressurization

	<b>Depressurization Pressure, psia</b>	<b>Dissociation Temperature, °C</b>	<b>Produced Gas, L</b>	<b>Produced Water, g</b>
Run#1	687.5	6.07	558.9	5528
Run#3	541	4.35	769.3	7163

**Table 7-31:** Calculated saturations during depressurization in Table 7-30

	<b>Hydrate Dissociation % (x)</b>	<b>S<sub>h</sub></b>	<b>S<sub>g</sub></b>	<b>S<sub>w</sub></b>
Run#1 Li <i>et al.</i> (2014)	11.42	0.386	0.214	0.400
Run#1- SMProd.m with constant N <sub>H</sub> , ρ <sub>w</sub> , ρ <sub>H</sub> , Molecular Weight of CH <sub>4</sub>	12.5	0.382	0.215	0.403
Run#1 with SMProd.m	13.5	0.377	0.217	0.406
Run#3 Li <i>et al.</i> (2014)	16.84	0.378	0.239	0.383
Run#3- SMProd.m with constant N <sub>H</sub> , ρ <sub>w</sub> , ρ <sub>H</sub> , Molecular Weight of CH <sub>4</sub>	18.0	0.373	0.240	0.386
Run#3 with SMProd.m	19.0	0.369	0.243	0.389

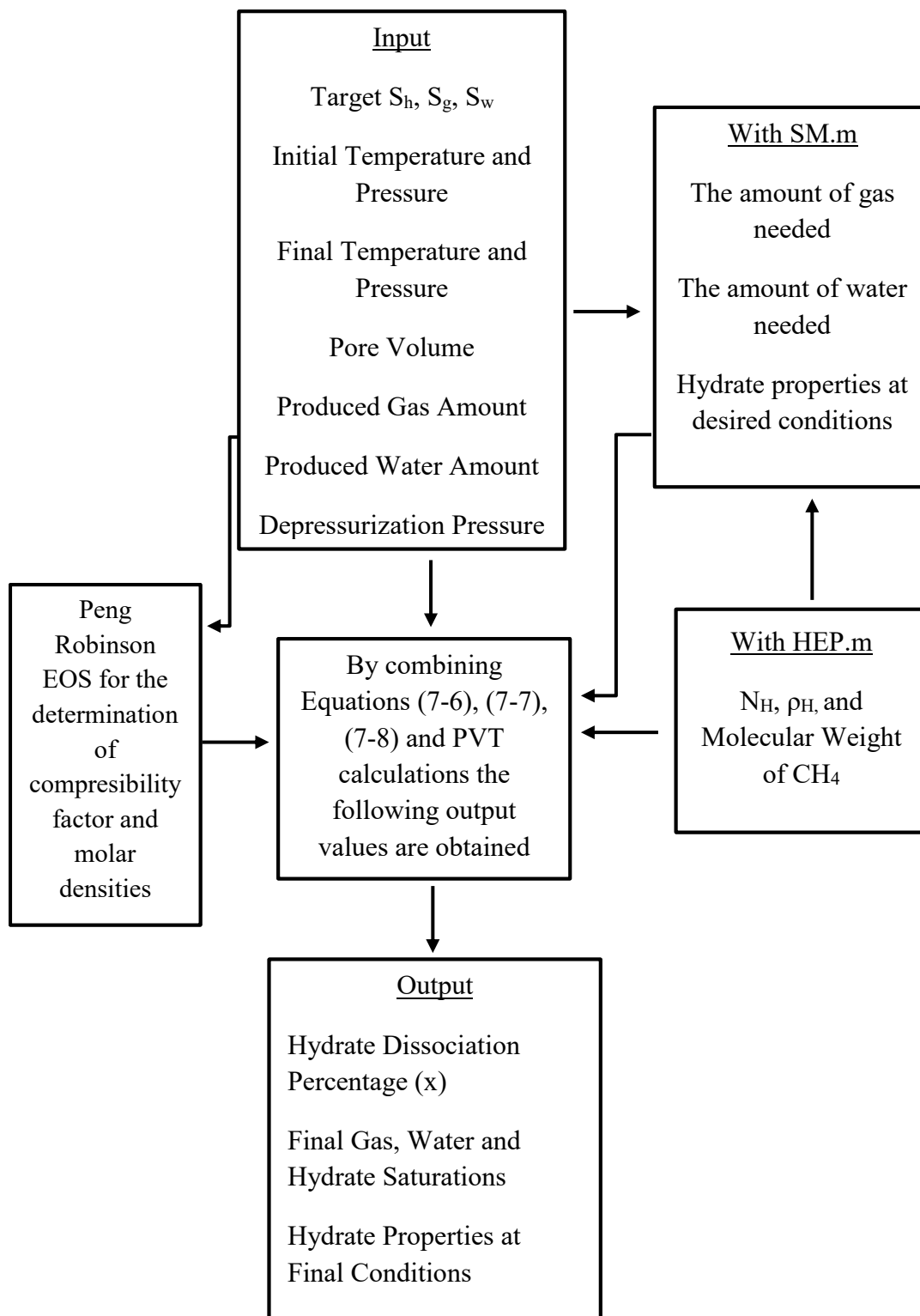


**Figure 7-118:** Algorithm of SMProd code

## **7.8 Calculations to Form Target Hydrate, Gas and Water Saturation in the High Pressure Reactor for Natural Gas Hydrates**

The Black Sea has sI and sII gas hydrate potential. Therefore, thermogenic (sII) hydrates include gas mixtures. Different from previous studies, in this study, it is also aimed to propose a code calculating target hydrate, gas and water saturation in high pressure cell or reactor for natural gas hydrates. The description of SMmix.m code written by Matlab 2014a is shown in Figure 7-119.

There is no similar example in literature to test the reliability of SMmix code. The gas composition (94.84 % CH<sub>4</sub>, 2.04 % C<sub>3</sub>H<sub>8</sub>, and 3.12 % CO<sub>2</sub>) of Küçük *et al.* (2013) was used to run SMmix code in the Black Sea conditions. The initial conditions and target saturations were assumed according to the Black Sea conditions for the analysis of SMmix code.

After using the input data given in Table 7-32, the output results in Table 7-33 were obtained by SMmix code. As seen in this table, SMmix data gives the amount of gas mixture and water needed to reach the target experimental saturations in the high pressure reactor (METU reactor) designed in this study. First, the sediments in the high pressure reactor should be saturated with 4148.354 gr water after vacuuming air from the high pressure reactor. Then, gas mixture (94.84 % CH<sub>4</sub>, 2.04 % C<sub>3</sub>H<sub>8</sub>, and 3.12 % CO<sub>2</sub>) should be injected inside the high pressure reactor until 2043.717 psia. It was assumed that room temperature is initially around 25°C. Then, the temperature of cold room is decreased to 9°C and hydrate forms inside the reactor and it was assumed that the equilibrium pressure is approximately 610 psia. SMmix.m code gives the final gas composition in free pores, the number of moles of gas inside hydrate and water, their fractions and final hydrate properties as seen in Table 7-33.

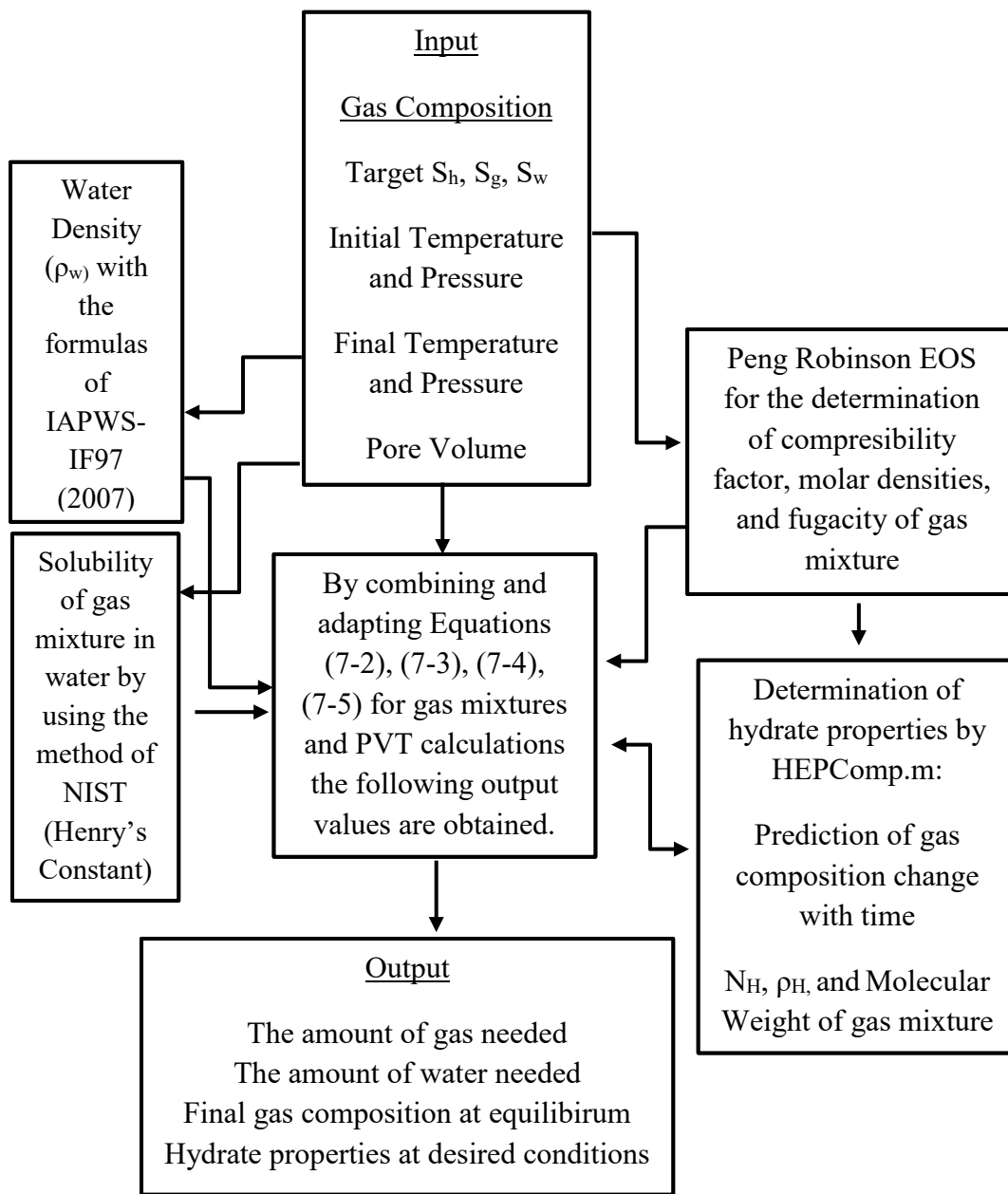


**Figure 7-119:** Algorithm of SMmix code

**Table 7-32:** Initial conditions for SMMix code analysis

Source	$\phi$ , %	V <sub>pore</sub> , cm <sup>3</sup>	S <sub>H</sub> , %	S <sub>G</sub> , %	S <sub>A</sub> , %	T <sub>initial</sub> , °C	T <sub>final</sub> , °C	P <sub>final</sub> , psia
Assumed data in this study	38.8	8400	0.5	0.4	0.1	25	9.0	610

**Table 7-33:** Output results of SMmix code

Gas and Water Amount to be injected			
<i>Gas amount, mol</i>	<i>Gas volume, L</i>	<i>Water amount, g</i>	<i>Initial Pressure, psia</i>
35.541	795.090	4148.354	2043.717
Mole % in Dissolved Gas at Final Conditions			
<i>Mole</i>	<i>CH<sub>4</sub>, %</i>	<i>C<sub>3</sub>H<sub>8</sub>, %</i>	<i>CO<sub>2</sub>, %</i>
0.125	49.824	0.571	49.605
Mole % in Free Gas at Final Conditions			
<i>Mole</i>	<i>CH<sub>4</sub>, %</i>	<i>C<sub>3</sub>H<sub>8</sub>, %</i>	<i>CO<sub>2</sub>, %</i>
6.655	95.983	0.819	3.198
Mole % in Hydrate at Final Conditions			
<i>Mole</i>	<i>CH<sub>4</sub>, %</i>	<i>C<sub>3</sub>H<sub>8</sub>, %</i>	<i>CO<sub>2</sub>, %</i>
28.76	94.771	2.329	2.90
Gas Occupancy in Hydrate at Final Conditions			
<i>CH<sub>4</sub></i>	<i>C<sub>3</sub>H<sub>8</sub></i>	<i>CO<sub>2</sub></i>	
<i>θ<sub>s</sub></i>	<i>θ<sub>s</sub></i>	<i>θ<sub>s</sub></i>	
0.834	0	0.008	
<i>θ<sub>L</sub></i>	<i>θ<sub>L</sub></i>	<i>θ<sub>L</sub></i>	
0.294	0.673	0.021	
Hydrate Properties at Final Conditions			
Hydration Number	Density, g/cm <sup>3</sup>	Molecular Weight, g/mol	
6.365	0.946	138.343	

## 7.9 Prediction of Natural Gas Hydrate Composition by using BSR data

Bottom simulating reflectance (BSR) data in ocean sediments are important to detect Class 1 gas hydrate reservoirs, which is considered as the most promising gas hydrate reservoir in nature (See Chapter 2). As stated by Majumdar (2015), gas hydrates were found after drilling at the region of 42 % of BSRs detected. Hence, it is important to analyze BSRs. By using BSR depth, sea depth, salinity, geothermal gradient and pressure gradient in the study area, many information about expected Class 1 hydrate reservoir near BSR lines can be found. Therefore, in this study, a code (**BSR.m**) was written by Matlab 2014a. In Figure 7-120, BSR.m code is briefly described. BSR.m predicts the composition of gas hydrate, its type, density, hydration number, cavity ratio, etc. In order to check the reliability of this code, multiple BSRs detected by Popescu *et al.* (2006) in the Danube deep-sea fan of the Black Sea was investigated. Although CH<sub>4</sub> hydrate (biogenic-sI hydrate) is common in nature, there are also thermogenic (sII hydrate) gas hydrates consisting gas mixtures. sII hydrates are much more stable compared to sI hydrates so in deeper sediments (higher temperatures) sII hydrates form when appropriate hydrate formation conditions are reached. Hence, multiple BSRs are commonly observed where there is biogenic and thermogenic gases (Paganoni *et al.*, 2016).

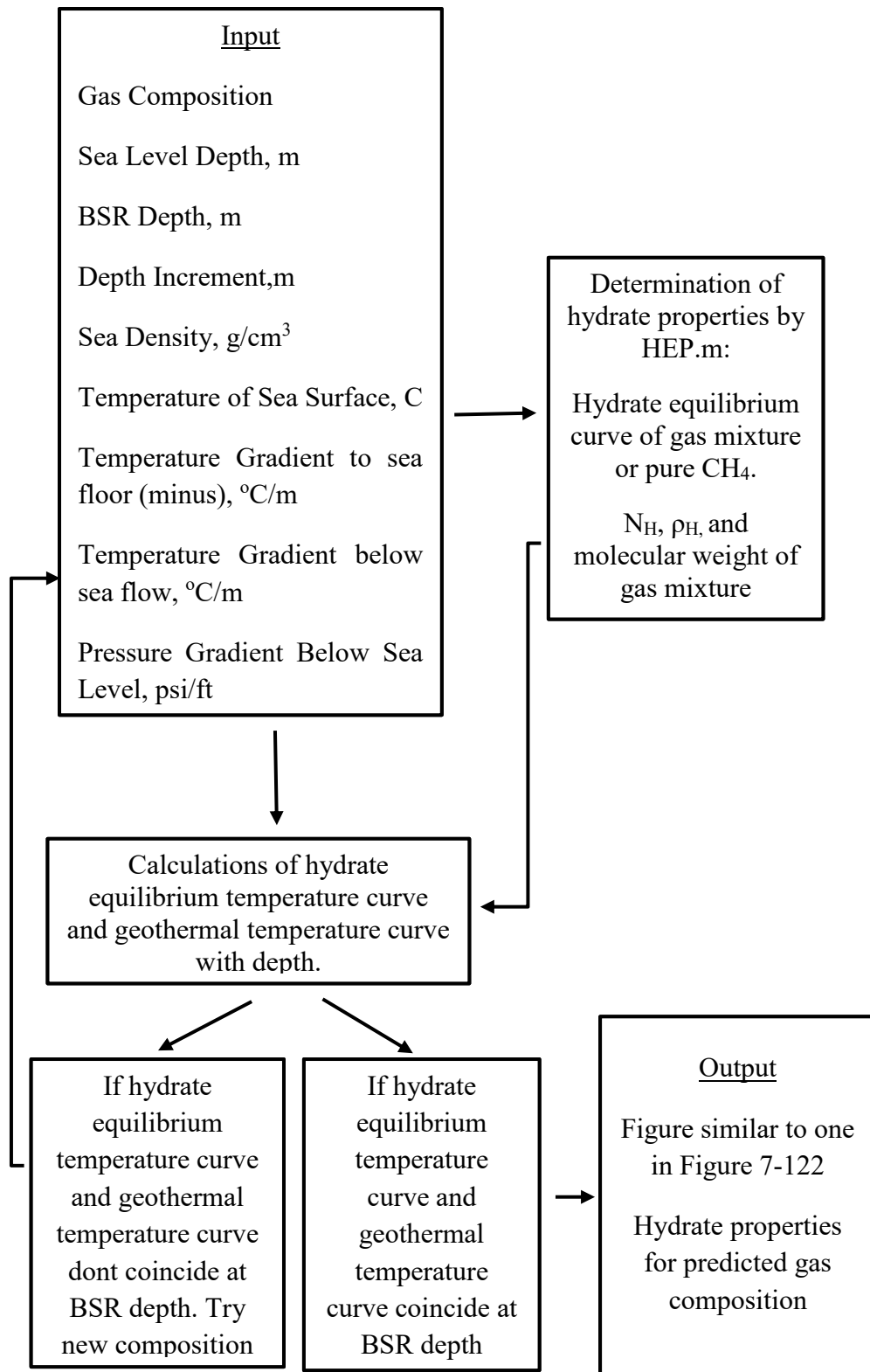


**Figure 7-120:** Algorithm of BSR.m code

Figure 7-121 shows the seismic profile in the study of Popescu *et al.* (2006). As seen in the figure, at least 4 BSRs were detected. The composition analysis is quite important for simulation studies and production method selection. All BSRs along the red line in Figure 7-121 was selected for gas composition analysis with BSR.m code.

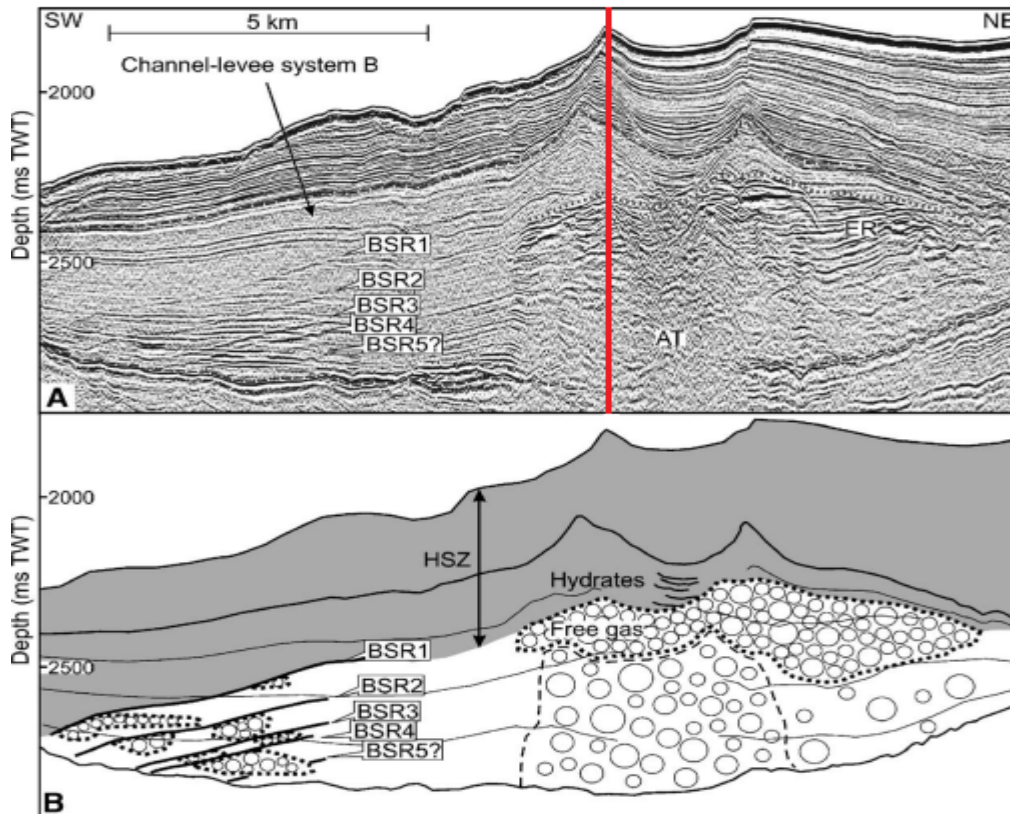


**Figure 7-121:** Detail of the multiple BSRs observed by Popescu *et al.* (2006)

For BSR 1, the analysis was done with BSR.m code by using data listed in Table 7-34. Pore water salinity, sea depth, BSR depth, pressure gradient below sea floor, thermal gradient from sea surface to sea floor, and thermal gradient from sea floor to the bottom of formations are given in Table 7-34. Then, as outputs, Figure 7-122 and Table 7-35 were obtained for all BSR analysis. As seen in Figure 7-122, when gas composition is 100 % CH<sub>4</sub> because hydrate equilibrium curve and temperature gradient curve intersect at BSR 1 depth (2507 m). The detailed properties of the gas hydrate near BSR 1 are shown in Table 7-35 about hydrate properties at this section. Therefore, BSR 1 most probably includes sI CH<sub>4</sub> hydrate.

**Table 7-34:** The data available for BSRs in the study of Popescu *et al.* (2006)

Name	Pore Salinity, %	Sea Depth, m from Sea Level	BSR Depth, m from Sea Level	Pressure Gradient below Sea Floor, psi/ft	Thermal gradient from sea surface to bottom, °C/m	Thermal gradient below sea floor °C/m
BSR1	0	1707	2057	0.465	-3.456e-3	0.03
BSR2	0	1707	2128	0.465	-3.456e-3	0.03
BSR3	0	1707	2183	0.465	-3.456e-3	0.03
BSR4	0	1707	2207	0.465	-3.456e-3	0.03

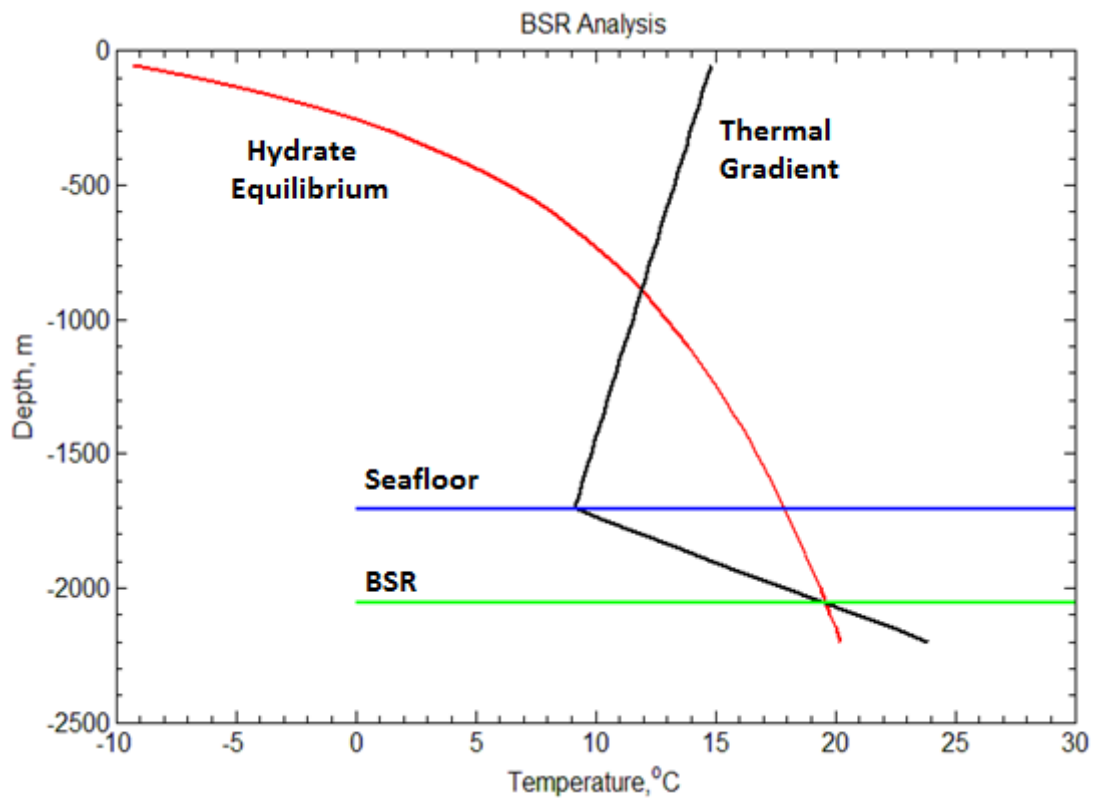


**Figure 7-122:** BSR analysis by BSR.m code for BSR 1 with CH<sub>4</sub> hydrate

**Table 7-35:** Scenario 1: Output of BSR.m code for BSRs detected in the study of Popescu *et al.* (2006)

BSR	Composition Selected	Hydrate Type	T, °C	Pressure, psia	Density, g/cm <sup>3</sup>	N <sub>h</sub>	Molecular Weight, g/mol
1	100 % CH <sub>4</sub>	sI	19.6	3016	0.917	5.829	121.065
2	97.86 % CH <sub>4</sub> , 2.14% H <sub>2</sub> S	sI	21.7	3124	0.938	5.848	123.782
3	95.54% CH <sub>4</sub> , 4.46% H <sub>2</sub> S	sI	23.38	3208	0.955	5.837	125.507
4	94.31% CH <sub>4</sub> , 5.69% H <sub>2</sub> S	sI	24.1	3244	0.961	5.833	126.251

By using geothermal gradient data, salinity, temperature gradient from sea level to sea floor and pressure gradient, it was found that BSR 1 might contain CH<sub>4</sub> hydrate and CH<sub>4</sub> hydrate properties at BSR 1 found with BSR.m code are shown in Table 7-35. If gas hydrate reservoir contains CH<sub>4</sub> with other impurities such as C<sub>2</sub>H<sub>6</sub>, C<sub>3</sub>H<sub>8</sub>, H<sub>2</sub>S and CO<sub>2</sub>, hydrate formation stability increases. Therefore, especially thermogenic gas hydrates form in deeper sediments. In the seismic study of Popescu *et al.* (2006), 4 BSRs were detected. It was shown that CH<sub>4</sub> hydrate only can form at BSR 1 in this study and also in the study of Popescu *et al.* (2006). Below BSR 1, it is obvious that there might be gas hydrates containing gas mixtures. Hence, compared to BSR 1, it is very hard to predict the gas composition for BSR 2, BSR 3 and BSR 4 without any core data because there are many gas composition scenarios. Therefore, two scenarios (CH<sub>4</sub> and H<sub>2</sub>S gas mixture and CH<sub>4</sub> and C<sub>3</sub>H<sub>8</sub> gas mixture) were evaluated for BSR 2, BSR 3 and BSR 4 separately by using BSR.m code in this study. Gas seepages near BSR area might give information about gas components in gas mixtures. The predicted gas compositions are listed in Table 7-35 for BSR 1, BSR 2, BSR 3, and BSR 4 for scenario 1. For BSR 2, BSR 3 and BSR 4, it was assumed that gas mixtures mainly contain CH<sub>4</sub> and H<sub>2</sub>S. As seen in Figure 7-123, Figure 7-124, and Figure 7-125, hydrate equilibrium curve of predicted gas mixture intersects with geothermal gradient at each BSR's location.

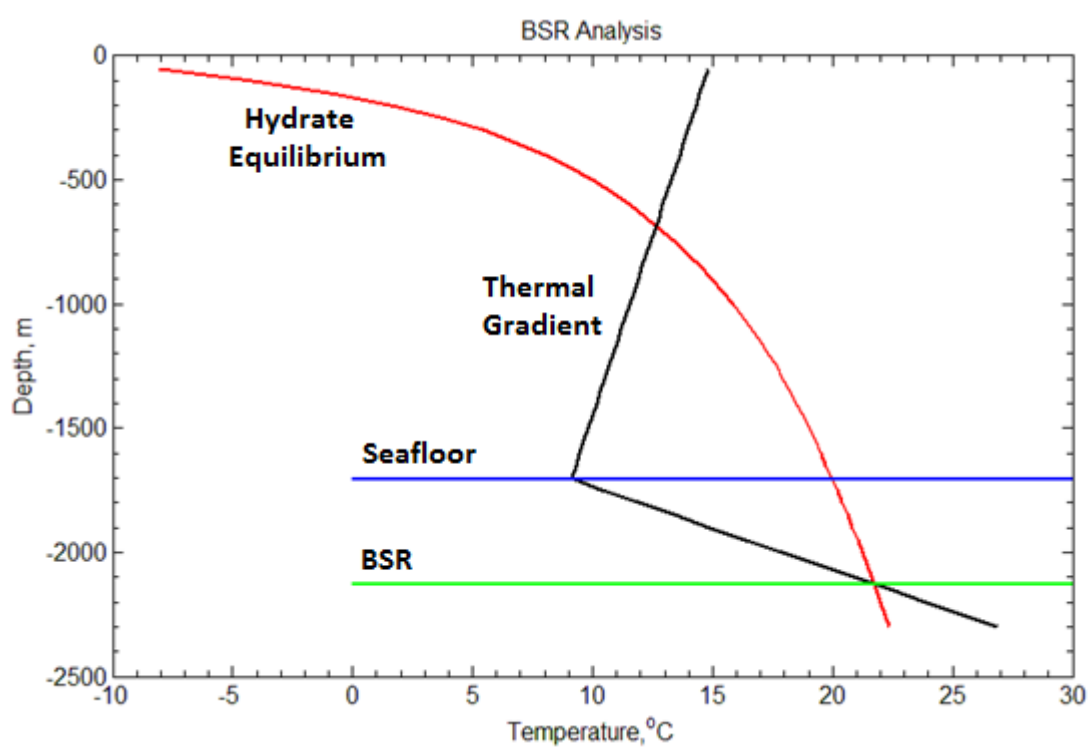


**Figure 7-123:** BSR analysis by BSR.m code for BSR 2 with 97.86 % CH<sub>4</sub>, 2.14% H<sub>2</sub>S hydrate

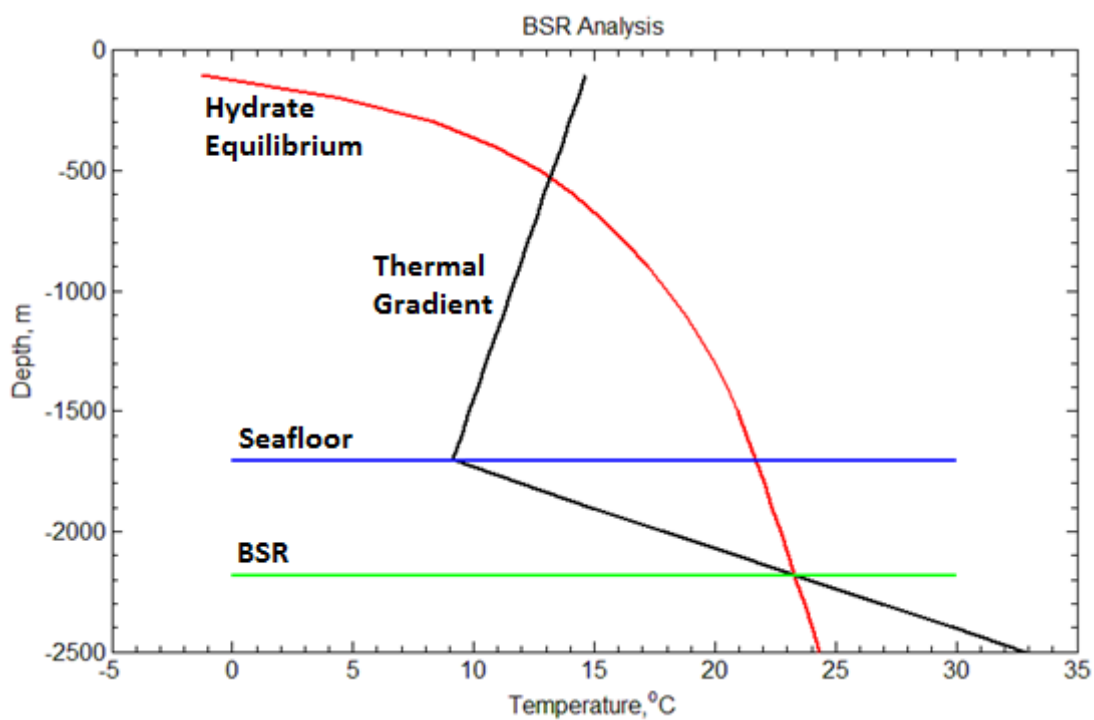


**Figure 7-124:** BSR analysis by BSR.m code for BSR 3 with 95.54 % CH<sub>4</sub>, 4.46% H<sub>2</sub>S hydrate

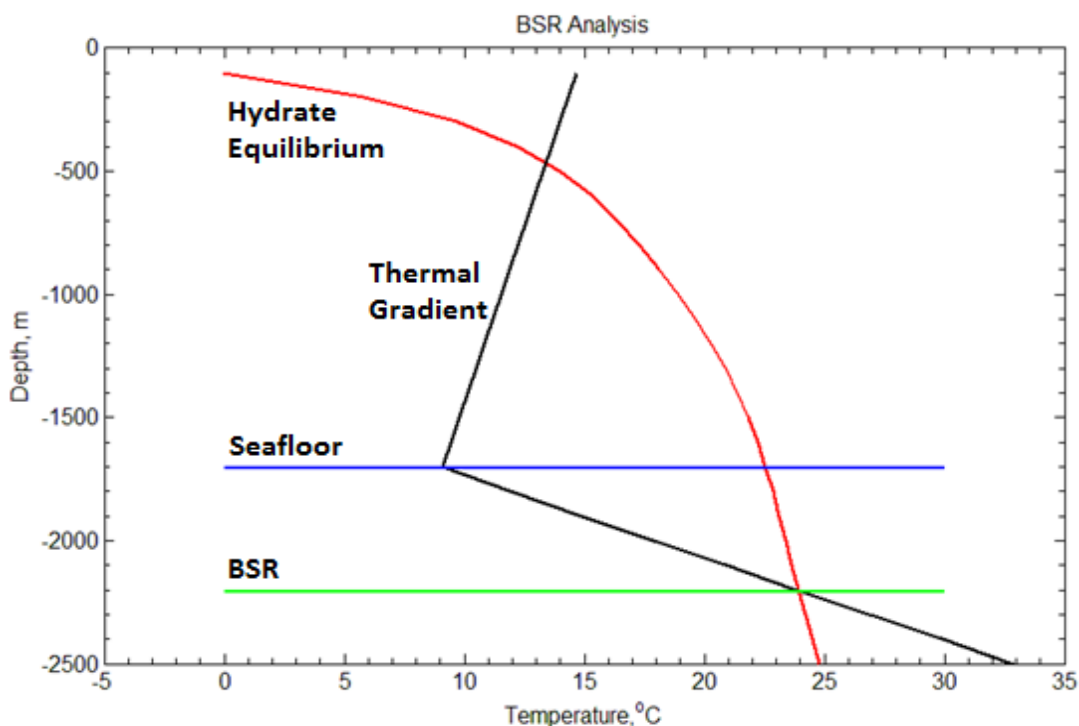


**Figure 7-125:** BSR analysis by BSR.m code for BSR 4 with 94.31 % CH<sub>4</sub>, 5.69% H<sub>2</sub>S hydrate

As shown in Table 7-35, Figure 7-123, Figure 7-124, and Figure 7-125, BSR 1, BSR 2, BSR 3 and BSR 4 might contain 100 % CH<sub>4</sub>; 97.86 % CH<sub>4</sub> and 2.14% H<sub>2</sub>S; 95.54 % CH<sub>4</sub> and 4.46% H<sub>2</sub>S ; 94.31 % CH<sub>4</sub> and 5.69% H<sub>2</sub>S gas mixtures at equilibrium conditions respectively. This scenario might be possible because the Black Sea has suitable conditions for hydrate formation of CH<sub>4</sub>-H<sub>2</sub>S mixtures according to the study of Bülbül *et al.* (2014). CH<sub>4</sub>-H<sub>2</sub>S mixture form sI type of gas hydrate.

BSR 2, BSR 3, and BSR 4 might consist of other gases such as C<sub>3</sub>H<sub>8</sub>. Therefore, as second scenario, CH<sub>4</sub> and C<sub>3</sub>H<sub>8</sub> gas mixture was analyzed for BSRs. As seen in Table 7-36, Figure 7-126, Figure 7-127 and Figure 7-128, BSR 1, BSR 2, BSR 3 and BSR 4 might contain 100 % CH<sub>4</sub>; 98.02 % CH<sub>4</sub> and 1.98% C<sub>3</sub>H<sub>8</sub>; 96.58 % CH<sub>4</sub> and 3.42% C<sub>3</sub>H<sub>8</sub>; 95.65 % CH<sub>4</sub> and 4.35% C<sub>3</sub>H<sub>8</sub> gas mixtures at equilibrium conditions respectively. CH<sub>4</sub>-C<sub>3</sub>H<sub>8</sub> mixture form sII type of gas hydrate and hydrate properties at BSRs are shown in Table 7-36. Therefore, thermogenic gas hydrates might be commonly found in the Black Sea.

**Table 7-36:** Scenario 2: Output of BSR.m code for BSRs detected in the study of Popescu *et al.* (2006)

BSR	Composition Selected	Hydrate Type	Density, g/cm <sup>3</sup>	N <sub>h</sub>	Molecular Weight, g/mol
1	100 % CH <sub>4</sub>	sI	0.917	5.829	121.065
2	98.02 % CH <sub>4</sub> , 1.98% C <sub>3</sub> H <sub>8</sub>	sII	0.943	5.946	127.857
3	96.58 % CH <sub>4</sub> , 3.42% C <sub>3</sub> H <sub>8</sub>	sII	0.951	5.956	128.816
4	95.65 % CH <sub>4</sub> , 4.35% C <sub>3</sub> H <sub>8</sub>	sII	0.954	5.961	129.228

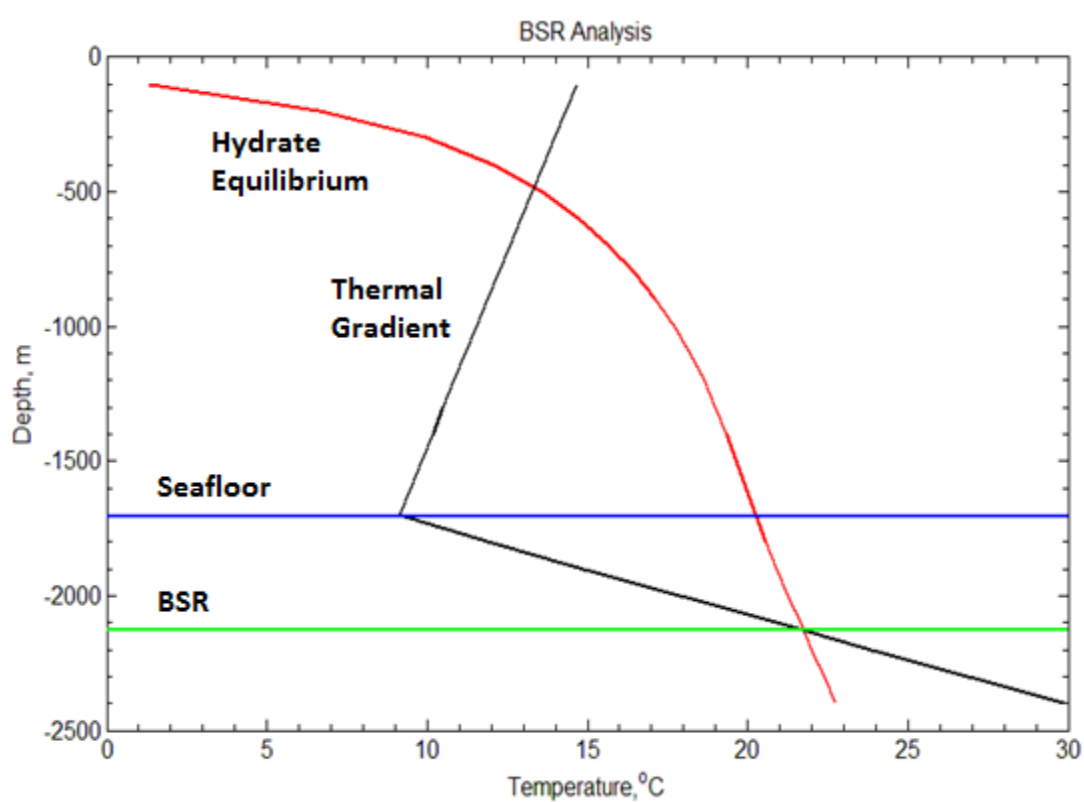


**Figure 7-126:** BSR analysis by BSR.m code for BSR 2 with 98.02 % CH<sub>4</sub>, 1.98% C<sub>3</sub>H<sub>8</sub> hydrate

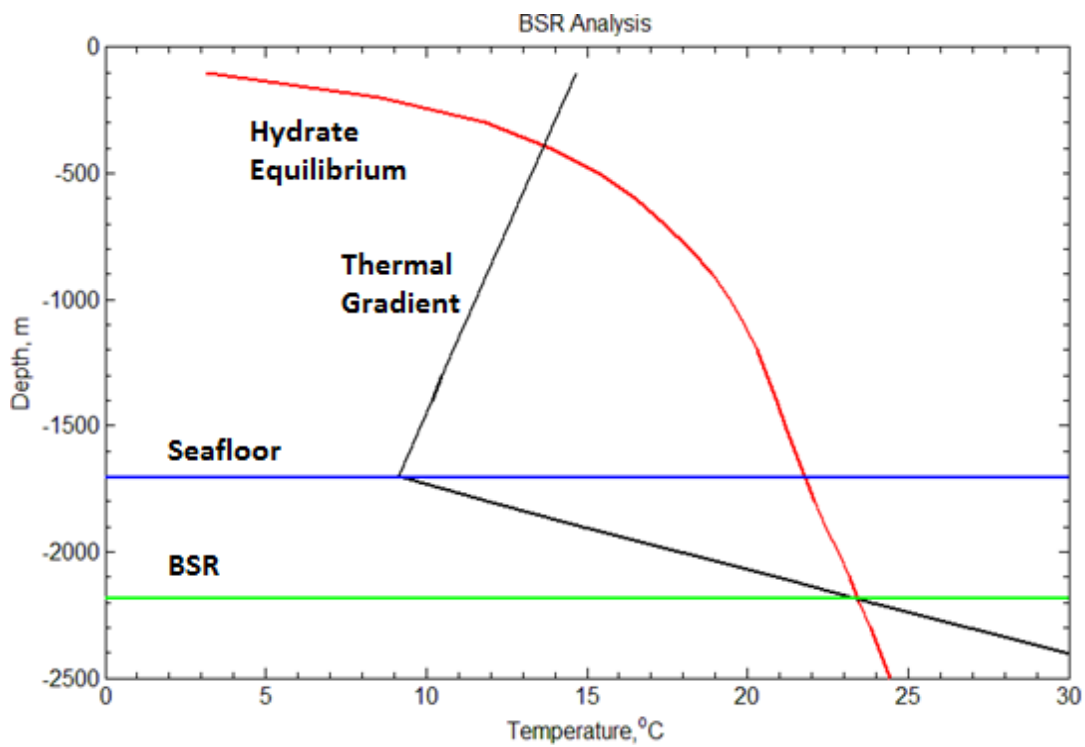


**Figure 7-127:** BSR analysis by BSR.m code for BSR 3 with 96.58 % CH<sub>4</sub>, 3.42% C<sub>3</sub>H<sub>8</sub> hydrate

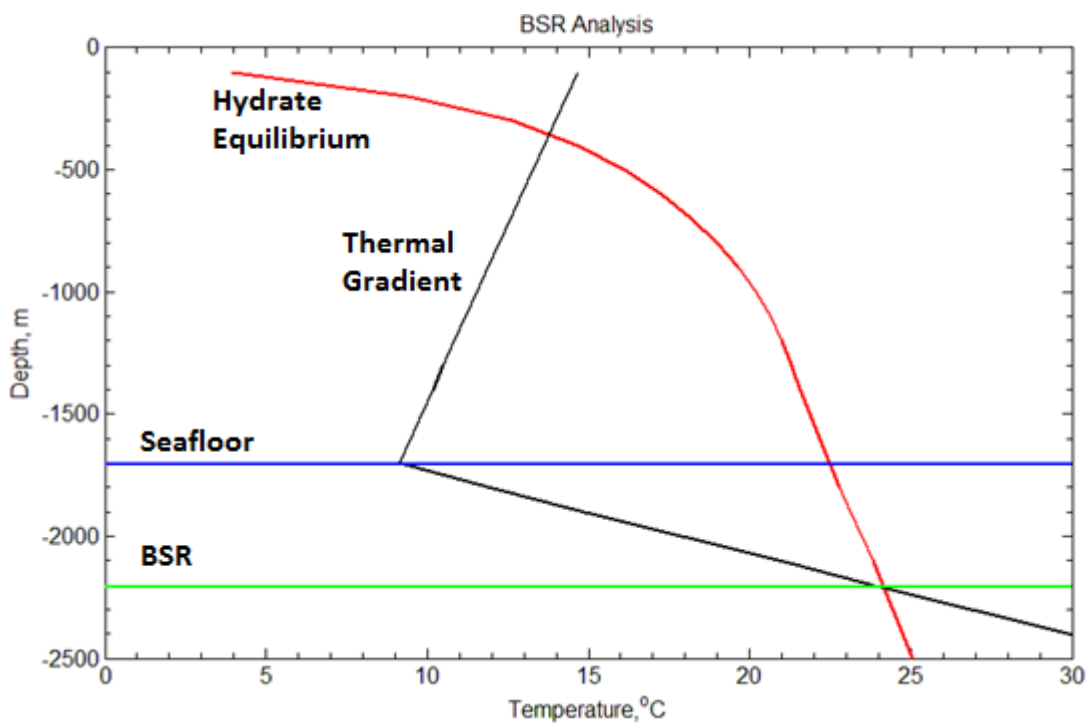


**Figure 7-128:** BSR analysis by BSR.m code for BSR 4 with 95.65 % CH<sub>4</sub>, 4.35% C<sub>3</sub>H<sub>8</sub> hydrate

### 7.10 Analysis of the Black Sea Sediments in terms of Gas Hydrate Potential by using the Core Data of Deep Sea Drilling Project (DSDP) Leg 42B program

According to all investigations in this study, there are several essential elements to consider a gas hydrate reservoir as an energy source. Figure 7-129 describes these elements. Firstly, source gas is essential, this might be from biogenic or thermogenic source rocks. Especially, for thermogenic source gases, migration paths such as faults or permeable formations are essential for the movement of gas from source rock through the sediments inside gas hydrate stability zone (GHSZ). The sufficient amount of water in the sediments inside GHSZ should be satisfied. According to the all evaluations of the Black Sea in this study, all of these elements are available. There are high sedimentation rates, high amounts of source gas because of its anoxic environment, enough thickness of GHSZ, etc. However, there is no much data evaluation in the Black Sea related to the Black Sea sediments. As shown in Figure 7-129, porous and permeable sediments (mostly coarse sands) inside GHSZ is a must for gas production from the Black Sea gas hydrates with current technology.

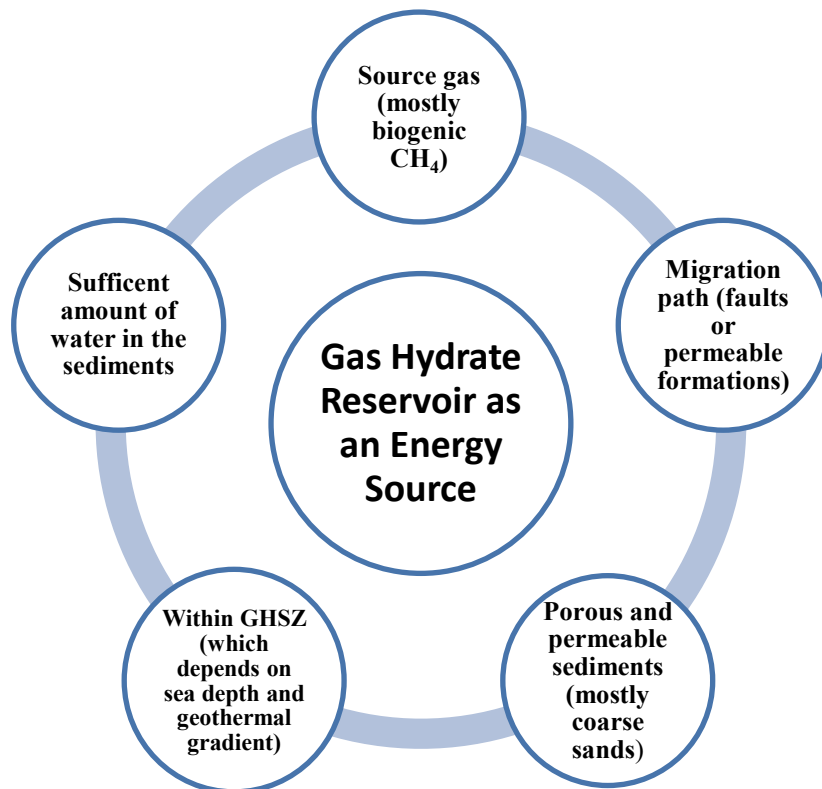


**Figure 7-129:** Essential elements for gas hydrate reservoir as an energy source

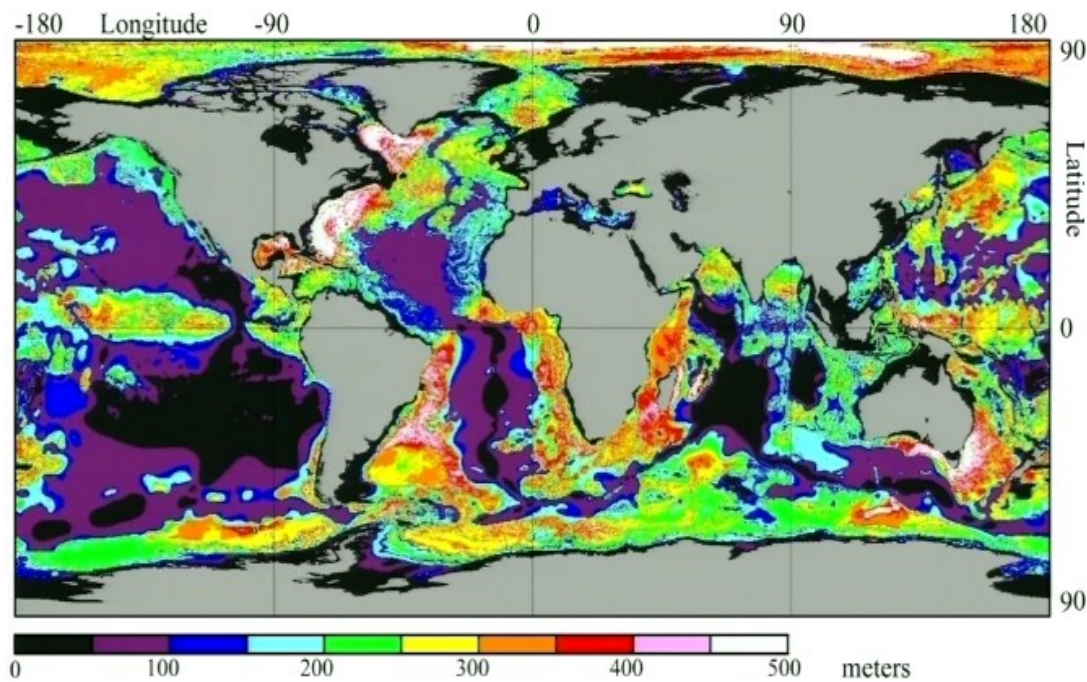


**Figure 7-130:** CH<sub>4</sub> hydrate stability zone thickness (Wood and Jung, 2008)

Wood and Jung (2008) estimated CH<sub>4</sub> hydrate stability thickness in the world as shown in Figure 7-130. The Black Sea average CH<sub>4</sub> hydrate stability thickness was calculated as approximately 300 m. These calculations are based on sea depth, hydrostatic pressure and thermal gradient but not on type of sediments in these sections. Hence, although gas hydrate stability zone calculations are important but without sediment information, they are not meaningful. Therefore, for the Black Sea, it is important to investigate the type of sediments within gas hydrate stability zone (GHSZ). The Deep Sea Drilling Project (DSDP) Leg 42B program in the Black Sea gives much information about the Black Sea and its sediments but there is not any analysis of these sediments in terms of gas hydrates. Hence, the aim of this study is to analyze this huge data set (mainly core, water and gas sample data). In 1975, several holes were drilled in the Black Sea in order to understand its geological, geochemical and sediment history with DSDP Leg 42B program. The aim of DSDP is to drill holes in marine sediments and to collect core samples. The collected core data are analyzed geologically and geochemically and these data are shared with different scientists from all over the world. With this way, many questions are answered related to marine geology (DSDP, 2016). As seen in Figure 7-131, DSDP

Legs were distributed all around the world. In the Black Sea, in 42B leg drilling program, 6 holes were drilled at Site 379, Site 380, and Site 381 (orange arrow shows their location in Figure 7-131).

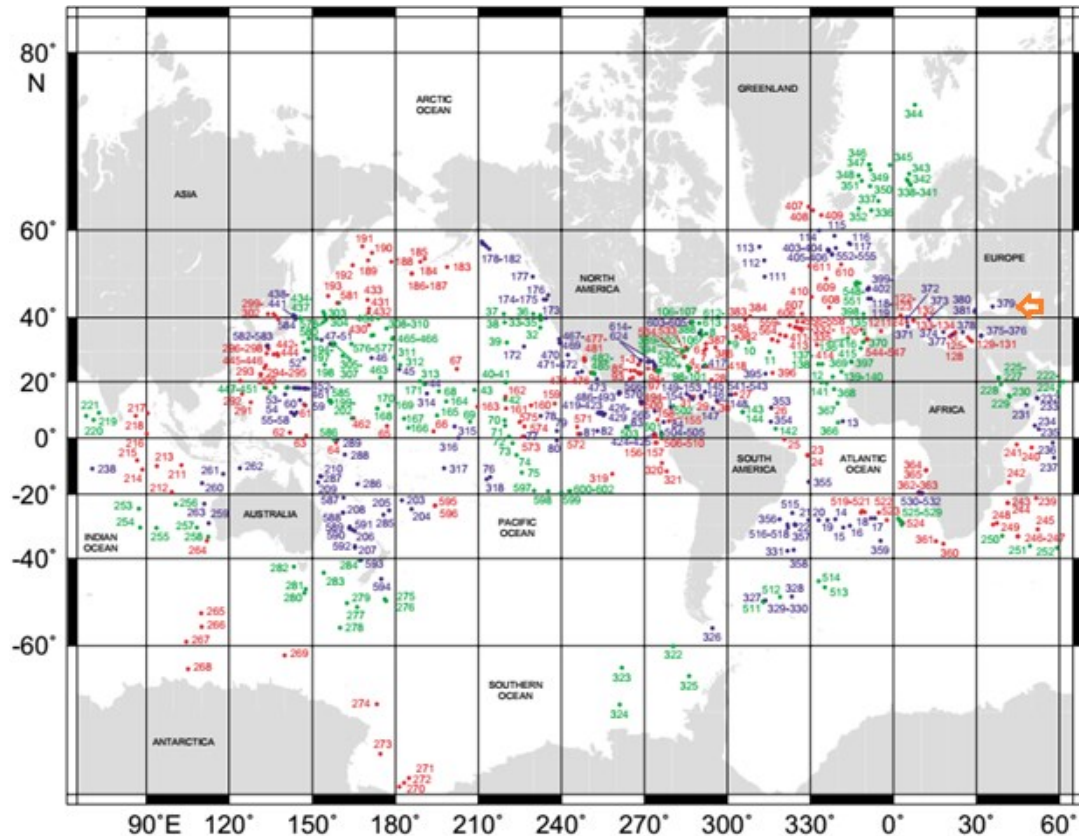


**Figure 7-131: DSDP Legs 1-96, Sites 1-624 (DSDP, 2016)**

In 1975, 6 holes were drilled and many cores were taken in the Black Sea sediments with the Glomar Challenger offshore rig. The location and details of these holes are shown in Figure 7-132 and Table 7-37 (DSDP, 2016). Because of conventional coring operations, gas hydrate could not be recovered with cores in the surface conditions. Moreover, the aim of DSDP Leg 42B drilling program in the Black Sea was only for geological investigations not for gas hydrate or hydrocarbon explorations. Hence, by using the available data of Leg 42B in the Black Sea, we tried to analyze gas hydrate potential of the Black Sea in this study.

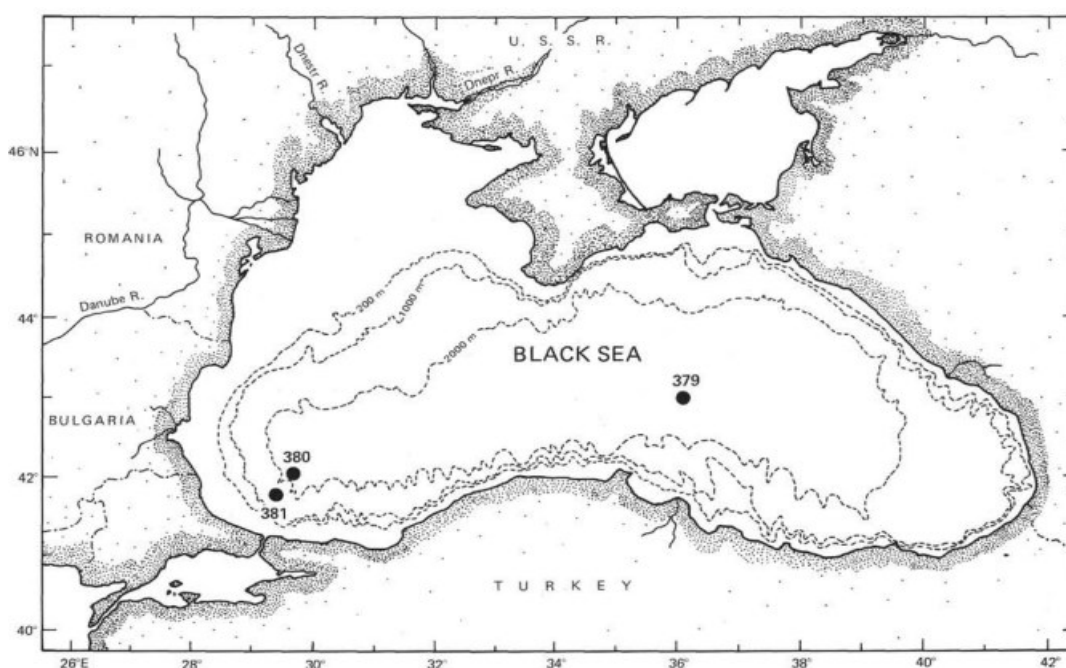


**Figure 7-132:** Drilling sites in Leg 42B in the Black Sea (Supko *et al.*, 1978)

**Table 7-37:** The details of the holes drilled in Leg 42B in the Black Sea (Supko *et al.*, 1978)

Hole	Latitude (N)	Longitude (E)	Sea Depth (m)	MBSF	# of Core	Meters cored	Recovery %
379	43°00.29'	36°00.68'	2171	7	1	7	57
379A	43°00.29'	36°00.68'	2171	624.5	68	622	61.3
379B	43°00.29'	36°00.68'	2171	159	9	80.5	36.4
380	42°05.98'	29°36.90'	2115	370.5	40	370.5	45.7
380A	42°05.94'	29°36.82'	2115	1073.5	79	734.5	57.4
381	41°40.25'	29°24.96'	1750.5	503.5	54	1503.5	55

Although many data such as geology, mineralogy, geochemical, grain size, thermal gradient, salinity, geomechanical, etc. were gained from the cores taken from the Black Sea with Leg 42B program, these data were not evaluated in terms of gas hydrate potential of the Black Sea and producible gas hydrate potential of the Black Sea sediments. Hence, in this study, we tried to analyze these vast amounts of core data to investigate gas hydrate reservoir potential of the Black Sea sediments as energy sources. One of the aims of drilling the holes in Table 7-37 was to understand the thickness of Pleistocene period in the Black Sea. However, although scientists expected that the end of this period was a few hundred meter below sea floor, after drilling data, it was understood that the end of Pleistocene period might be more than a kilometer of sediments due to high sedimentation rate in the Black Sea (Ross, 1978). The age of Pleistocene is around 1.8 million years (Stoffers and Müller, 1978). According to the drilling data of Leg 42B, it was found that the mean deposition is  $20 \text{ cm}/10^3 \text{ years}$  during Pleistocene period. With slumping and turbidity currents, the amount of sedimentation rate was thought to be doubled (Degens *et al.*, 1978).

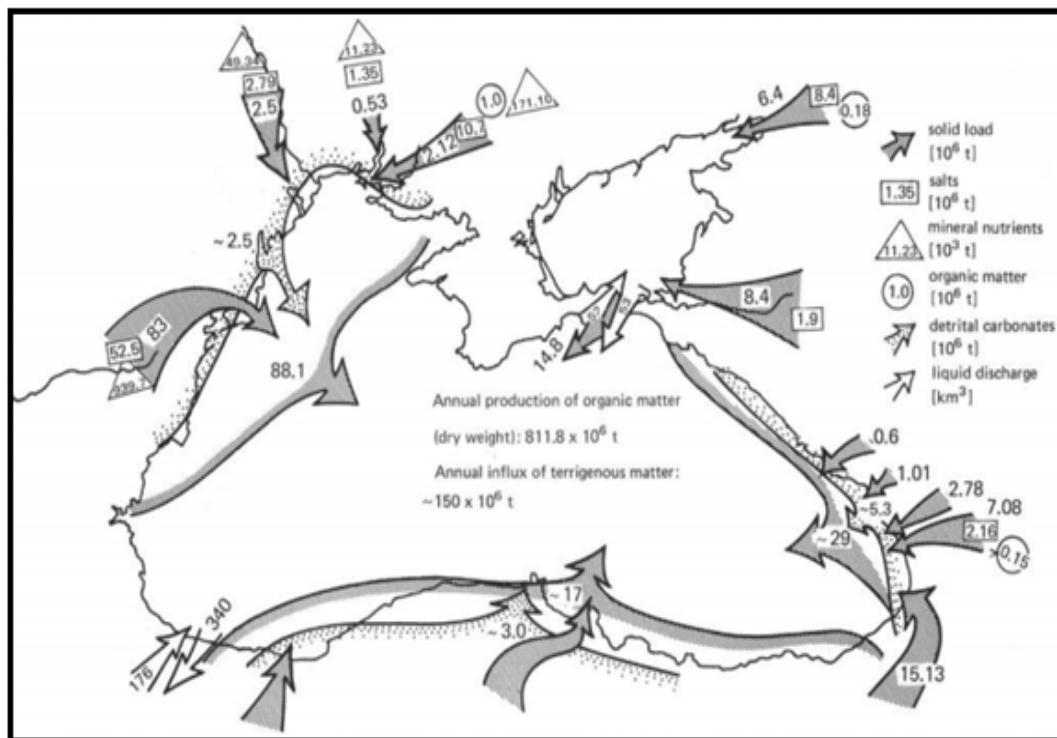


**Figure 7-133:** Supply of sedimentary material to the Black Sea on annual basis (Shimkus and Trimonis, 1974)

As seen in Figure 7-133, different types of sediments are collected in the Black Sea via many rivers. The deltas where sediments brought by rivers in the Black Sea are potential places for gas hydrate exploration (Max and Johnson, 2016). Furthermore, there is only narrow connection of the Black Sea to the Mediterranean Sea. With the rise of the sea level around 15000 years ago, the lacustrine environment of the Black Sea returned to marine environment around 3000 years ago (Supko *et al.*, 1978; Ross, 1978b). Hence, the dense (saline) water of the Mediterranean Sea sank and less dense water of the Black Sea was above the halocline (see Figure 3-3 and Figure 3-4). In the anoxic environments of the Black Sea, the preservation of organic materials brought by many rivers is possible compared to oxic environment. This is one of the basic information of petroleum geochemistry (Hunt, 1995). The core data of Site 379 (as shown in Figure 7-132 and Table 7-37) such as sulphur weight percentage and organic carbon percentage show the organic material rich sediments of the Black Sea in Figure 7-134. Especially between 50 mbsf and 100 mbsf at Hole 379A, the organic carbon % is quite high. Hence, the sediments in this region are sapropels which are dark colored organic rich sediments (Calvert and Batchelor, 1978)

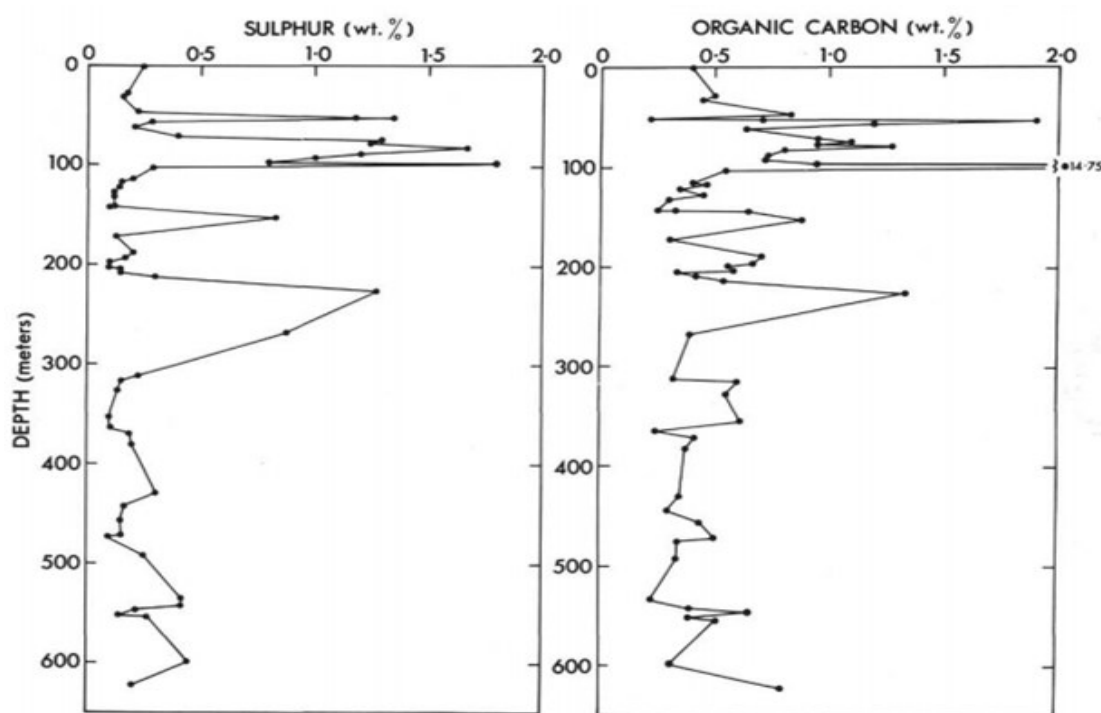


**Figure 7-134:** Vertical distribution of total Sulphur and organic carbon content at Hole 379A (Calvert and Batchelor, 1978)

Chlorine content of pore water of sediments are commonly used to calculate gas hydrate saturation in sediments and these saturation values are compared with hydrate saturations calculated with well logs. If hydrate saturations calculated by Cl concentration and well logs are close to each other, it can be concluded that the results are reliable. However, if they are quite different, the reasons of this difference are investigated, which might be due to wrong core handling and or unreliable logging while drilling operations. To illustrate, the hydrate saturations calculated by Cl concentration and well log data in the Ulleung Basin (UBGH2), East Sea are shown in Figure 7-135-b (Kim *et al.*, 2013). Figure 7-135-a shows Cl anomaly in the sediments containing gas hydrates. During the formation of gas hydrate with guest molecule (mostly CH<sub>4</sub>) and host molecules (water), only pure water molecules are selected from the pore water and free pore water Cl increases. However, in nature hydrate formation takes long times (~ 1000s years), so with time high Cl diffuse away from free water. Hence, when Cl concentration of gas section was measured after dissociation, mostly Cl concentration is low compared to chlorine baseline of marine environment.

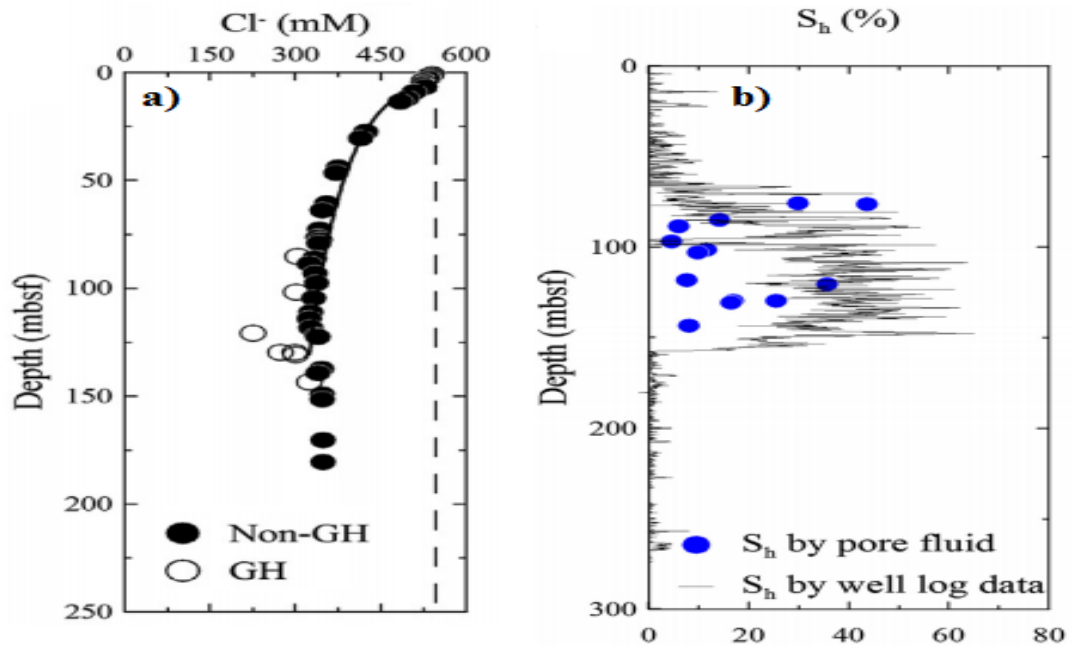


**Figure 7-135:** a) Core profiles of Cl at Site UBGH2-2\_1 b) Estimates of gas hydrate saturation (S<sub>h</sub>) from Cl concentration at Site UBGH2-2\_1, compared with S<sub>h</sub> estimates based on well log resistivity data (black line) (Kim *et al.*, 2013)

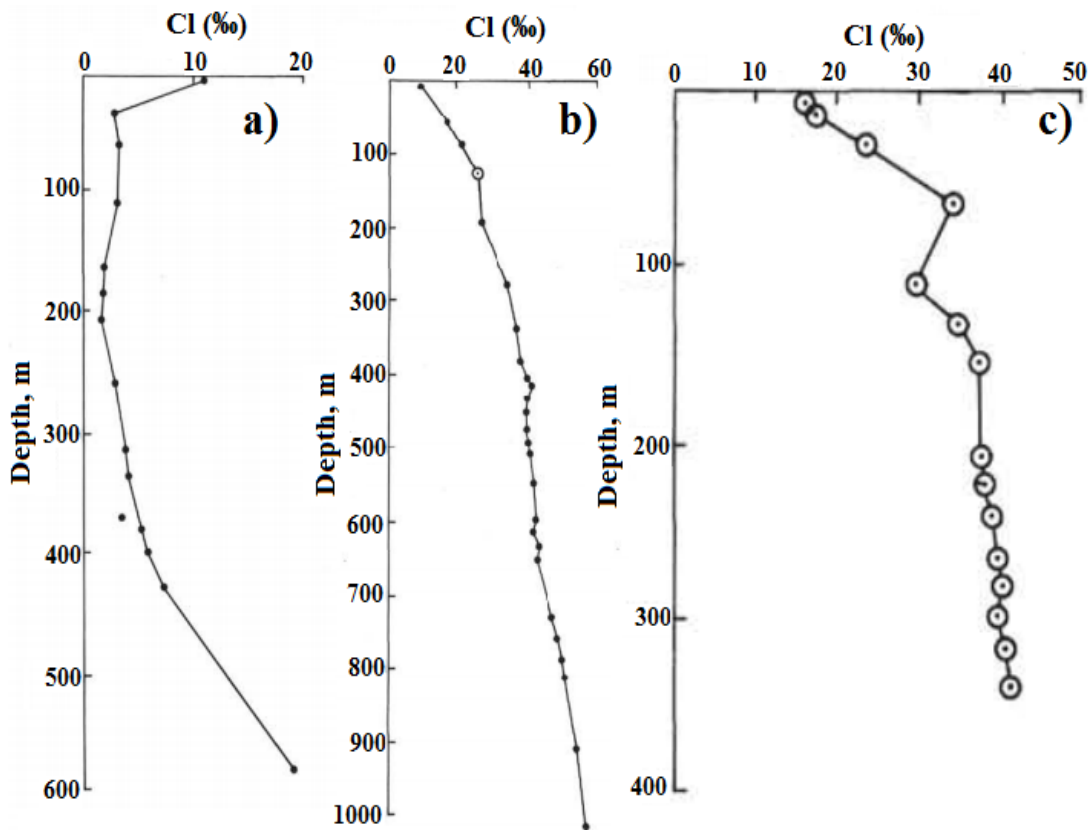


**Figure 7-136:** Distribution of Cl in a) Sites 379A/B b) Sites 380/380A c) Site 381 (Adapted from Shishkina, 1978)

The analysis of Cl profiles of pore water of the Black Sea sediments can be also helpful to determine the intervals where there might be gas hydrates in sediments. One of the disadvantages of the Black Sea is that most of the wells drilled for deep-sea explorations targeting conventional oil and gas reservoirs. Furthermore, the companies do not share their drilling data and well log data. Therefore, Leg 42B drilling program in the Black Sea provides many useful data for gas hydrate analysis although the aim of this program was only for geological and geochemical purposes. As shown in Figure 7-136, Cl profiles of Sites 380/380A and Sites 381 are similar. However, there is a sharp decrease in Cl profile of Site 381 at around 125 mbsf. The reason of this might be Cl anomaly due to gas hydrate in sediments. When the data of Core 14 of Site 381 was analyzed, gas expansions and voids in the core due to gas expansion were observed. Moreover, 125 mbsf is in methane ( $\text{CH}_4$ ) hydrate stability zone (MHSZ). In Figure 7-137, Core 14 was shown and white sponges illustrates

voids formed after gas expansion. This core includes more than 50 % clay content, sandy silt, quartz and other minerals. Especially in clay sediments, mostly gas hydrate forms as nodules and veins (See Figure 5-3 and Figure 5-4) (Li *et al.*, 2016c). Therefore, in Core 14, there might be gas hydrates as nodules. However, in order to consider gas hydrate reservoirs as an energy source, they should be in sand-dominated sediments as pore filling because these sand-dominated sediments have good reservoir properties such as coarse grains, high porosity, and high permeability (Li *et al.*, 2016c). When clay content increases, hydrate saturation and reservoir quality decrease (Kumar *et al.*, 2015). Therefore, hydrate stability zone (HSZ) and sediment types of the Black Sea should be investigated carefully.

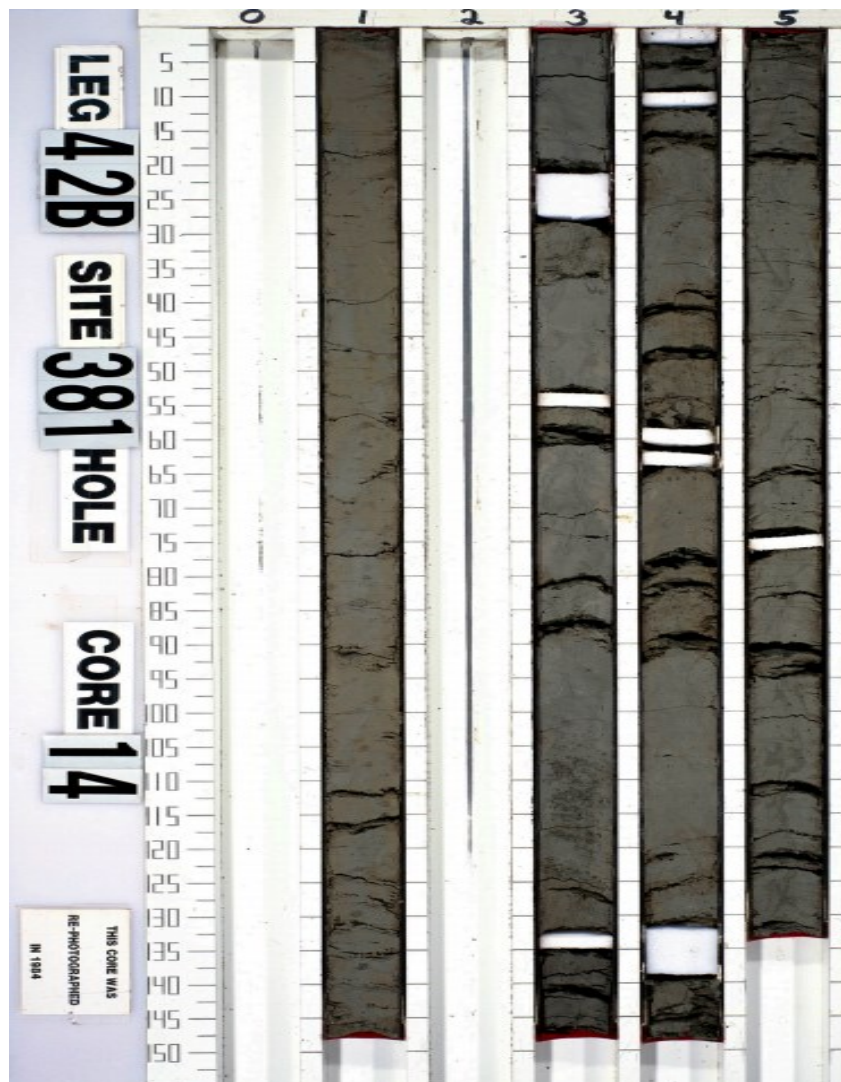


**Figure 7-137:** Core 14 at Site 381 (Site 381, 1978)

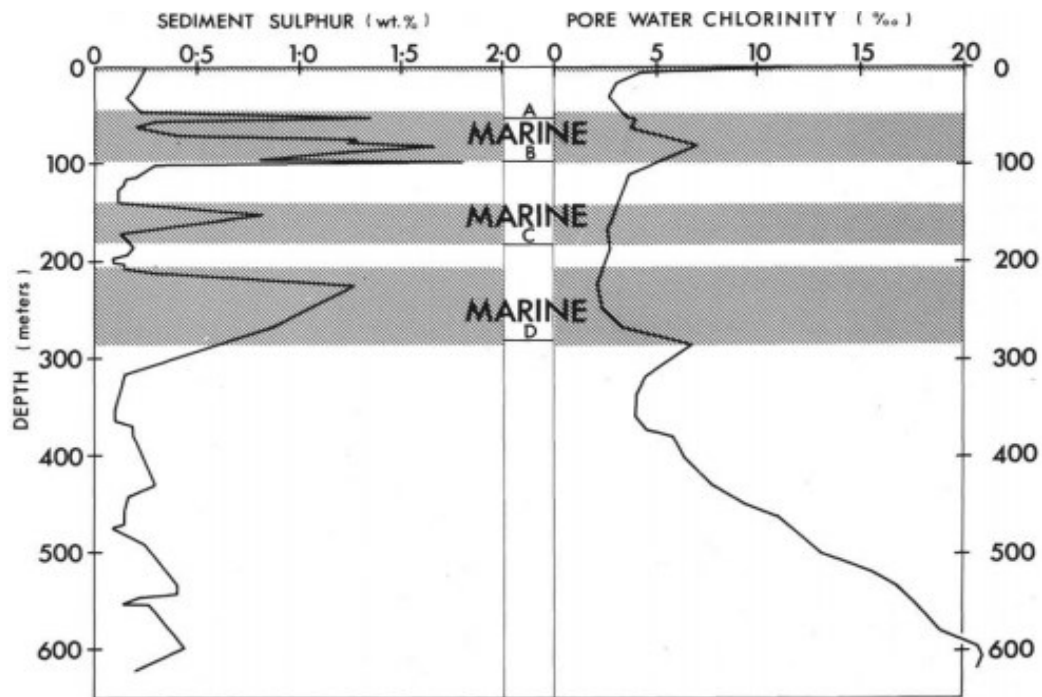


**Figure 7-138:** Tentative identification of marine and lacustrine horizons at Hole 379A based on the distribution of sulfur in the bulk sediment (left), the chlorinity of the pore water (Calvert and Batchelor, 1978)

In Site 379/379A, Cl profile is quite different from those at Sites 380 and 381. As seen in Figure 7-136-a, there is a Cl anomaly especially between around 40 mbsf and 400 mbsf. However, the reason of this anomaly is not only the occurrence of gas hydrates. As mentioned earlier, around 15000 years ago, the seawater of Mediterranean Sea and the Black Sea mixed via narrow Bosphorus connection. Hence, lacustrine environment of the Black Sea returned to marine environment with time. High saline water of Mediterranean Sea sank in the bottom below the fresh water of the Black Sea, which created anoxic environment. When all geological and geochemical analysis of the cores of Hole 379A at Site 379 were done, it was observed that the anomaly of Cl is due to marine and lacustrine horizons so this is because of unique geological history of the Black Sea (Calvert and Batchelor, 1978) as shown in Figure 7-138. Therefore, especially for this site (Site 379), it is difficult to observe Cl anomaly due to gas hydrate in sediments. Similarly, in the expedition of Schwalenberg *et al.* (2015) in Danube fan in the western Black Sea, generally it was observed that pore water salinity is low due to isolation in the past. For more

reliable gas hydrate analysis, well log data from logging while drilling, core data (taken by specially designed high pressure core holder) and pore water Cl in the Black Sea should be evaluated together for future gas hydrate expeditions and explorations in the Black Sea.

As discussed earlier, the Black Sea has both biogenic and thermogenic gas hydrate potential. Even though gas recovered during Leg 42B drilling program includes mostly CH<sub>4</sub>, there are also other thermogenic gas impurities such as C<sub>2</sub>H<sub>6</sub>, C<sub>3</sub>H<sub>8</sub>, C<sub>4</sub>H<sub>10</sub>, i-C<sub>5</sub>H<sub>14</sub>, 3,3-dimethylpentane and 2,2-dimethylbutane (Hunt and Whelan, 1978). i-C<sub>5</sub>H<sub>12</sub>, 3,3-dimethylpentane and 2,2-dimethylbutane might form sH hydrate with help gas (mostly CH<sub>4</sub>) (Sassen and MacDonald, 1994; Sloan and Koh, 2008; Makogon *et al.*, 1996). These molecules were observed at very low level in the cores of Leg 42B drilling program and also in the study of Küçük *et al.* (2015, 2016) but they might be at high concentration in different parts of the Black Sea so sH hydrates might be observed in the Black Sea in future as in Gulf of Mexico and Caspian Sea.

One of the advantages of Leg 42B drilling program, all holes were drilled in Turkey's border. Moreover, Site 379 is almost in the center of the Black Sea. Sites 380 and 381 are near the Bosphorus as seen in Figure 7-132. All investigations, expeditions, and seismic surveys show that there are huge gas fluxes (mostly CH<sub>4</sub>) in the Black Sea because anoxic environment of the Black Sea is appropriate for the generation of gas. Hence, these gas sources and appropriate temperature of the Black Sea and overburden pressure (mostly 2000 m water head) make the Black Sea as potential location in terms of gas hydrates. However, there is another important criterion in order to consider gas hydrate as an energy source. This is the type of sediments where gas hydrate deposited. There is no doubt of the existence of gas hydrate in the Black Sea but the important question should be "in which types of sediments are gas hydrates deposited in the Black Sea?" As shown in Figure 3-19, sand-dominated sediments are the targets for gas hydrate exploration for gas production purposes because as clay content and silt increases, permeability of sediments decreases enormously. Mostly, gas hydrate saturation is low in clay sediments and hydrates in clays are found as nodules and veins. The evaluation of the Black Sea sediments for

gas production from gas hydrates is crucial important. Leg 42B drilling program of DSDP provides many information about the sediments in the Black Sea and all data are open sources. By using measured salinity, temperature, and water depth data of Sites 379, 380 and 381 (Table 7-37 and Figure 7-136) (Site 379, 1978; Site 380, 1978; Site 381, 1978; Erickson and Von Herzen, 1978), CH<sub>4</sub> hydrate equilibrium curves and 93.3 % CH<sub>4</sub>, 6.7 % C<sub>3</sub>H<sub>8</sub> hydrate equilibrium curves were drawn with HEP.m (code written in this study) and these figures were combined with the lithostratigraphic section of Sites 379, 380 and 381 (Site 379, 1978; Site 380, 1978; Site 381). The aim of selecting 93.3 % CH<sub>4</sub>, 6.7 % C<sub>3</sub>H<sub>8</sub> is to understand the approximate depth of mixed gas hydrate stability depth for thermogenic gases. According to Vassilev and Dimitrov (2003), the main component of the gas from the Black Sea hydrates is CH<sub>4</sub> 93.3-99.7 %. Hence, we selected thermogenic gas including 93.3 % CH<sub>4</sub> + 6.7 % C<sub>3</sub>H<sub>8</sub> so the approximate range of mixed gas hydrate stability depth for thermogenic gases were predicted for Sites 379, 380 and 381. Hydrate equilibrium curves and lithostratigraphy of Sites 379, 380 and 381 are shown in Figure 7-139, Figure 7-143 and Figure 7-145, respectively

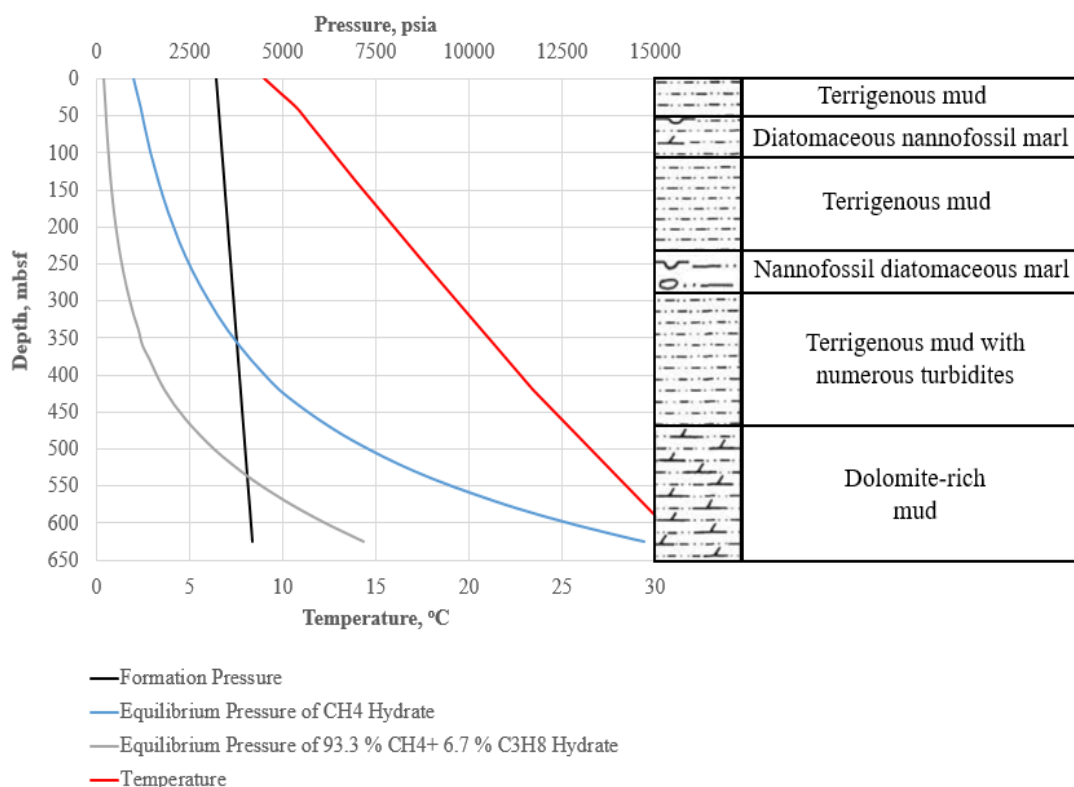


**Figure 7-139:** Hydrate equilibrium curves and lithostratigraphy at Site 379

As seen in Figure 7-139, for Site 379, 100 % CH<sub>4</sub> and 93.3 % CH<sub>4</sub>, 6.7 % C<sub>3</sub>H<sub>8</sub> hydrate stability zones are at nearly 360 mbsf and 540 mbsf respectively. The sediments in this site include terrigenous mud, generally with turbidite sequences. Sources of terrigenous mud consists of weathering of rocks, wind blown dust, abrasion by glaciers and carried by glaciers. Mostly, they include mud, clays, silts and fine sands (Bridge and Demicco, 2008). The sediments observed in the core samples of Site 379 are mostly a dark greenish-gray to dark gray terrigenous mud, with occasional interbeds of clays, silts, sandy silts, and fine sands (Site 379, 1978). Although only a few hole data are not enough to make a decision for the Black Sea, the sediments observed in Site 379 do not have good reservoirs properties for gas hydrates. This is because the muds are silty clays to clayey silts with intercalations of very thin sandy silt to sand laminae (up to 8 cm as shown in Figure 7-140) (Site 379, 1978). Moreover, turbidite units were observed but compared to nearly 1 m thick coarse sand sections (alternating sand layers less than 1 m, with cumulative thickness of the hydrate bearing-sands around 12-14 m) in turbidites of Nankai field (Tsuji *et al.*, 2004), the turbidites of Site 379 mostly include silty clay and very thin sandy silts as shown in Figure 7-141. The clays in terrigenous mud consist of illite (mostly) and smectite (Stoffers and Müller, 1978). Because of high adsorption capacity of illite (Merey, 2013), gas hydrate formations in these type of clays are much more difficult.



**Figure 7-140:** Sand layer intercalated in a terrigenous mud sequence (Site 379, 1978)



**Figure 7-141:** a) Core 28 (254-263.5 mbsf) of Site 379: Dark greenish gray terrigenous mud with abundant muddy sand to sandy mud layers suggesting turbidites b) Core 43 of Site 379: Dark greenish gray terrigenous mud with numerous silt and sandy mud layers, some indicating turbidite deposits. (Site 379, 1978)

It is hard to see gas hydrates in sediments if the core samples are taken to the surface with conventional coring techniques instead of new pressurized coring techniques. However, the appearance of the sediments after conventional coring can be a proxy for the presence of gas hydrates. With gas hydrate dissociation after conventional coring, “soupy” and “mousse-like” sediments are seen as a proxy for the gas hydrate existence (Holditch *et al.*, 2008; Melgar, 2009). In the cores of Leg 42B drilling program in the Black Sea, soupy and mousse-like sediments were also observed as

shown in Figure 7-142. Soupy sediments include high amount of water, and high hydrate content might be reason of this when nodular and massive gas hydrate exists. Different from soupy sediments, mousse like sediments are considered to include disseminated gas hydrates in fine sediments (Melgar, 2009). Therefore, core samples are one of good indicators of gas hydrates even if they are conventional core samples.



**Figure 7-142:** a) Soupy sediments from Hole 381 Core 18 (170 mbsf) b) Mousse-like sediments from Hole 379A Core 11 (100 mbsf) (Site 379, 1978; Site 381, 1978)

As shown in Figure 7-143, for Site 380, 100 % CH<sub>4</sub> and 93.3 % CH<sub>4</sub>, 6.7 % C<sub>3</sub>H<sub>8</sub> hydrate stability zones are around 216 mbsf and 365 mbsf respectively. Compared to Site 379, the thicknesses of gas hydrate stability zones of Site 380 are less because the sea depth of Site 380 (1750.5 m) is shallower than this in Sites 379 (2171 m) and 380 (2115 m) and thermal gradient is higher. Similar to Site 379, in the gas hydrate stability zones of Site 380, terrigenous sediments which include muds, sandy silts, and silty sands are between 0 mbsf and 332.5 mbsf as shown in Figure 7-144. In this region, silty sands might include gas hydrate and they might be good gas hydrate reservoir but the problem is their thickness in a few centimeter scale interbedded with

clays and silts. Almost all cores obtained during Leg 42B drilling program in the Black Sea have heterogeneous structure. In this study, it was shown that gas production is higher in gas hydrate in sands interbedded with clays in turbidites compared to gas hydrates deposited in thick sand sediments. However, in Sites 379, 380 and 381, sand sediments are only found in centimeter scale, even perforations of these intervals are difficult. However, in different parts of the Black Sea, thicker sand dominated zones might be found but it is obvious that the Black Sea sediments are very heterogenous and they include high clay content.

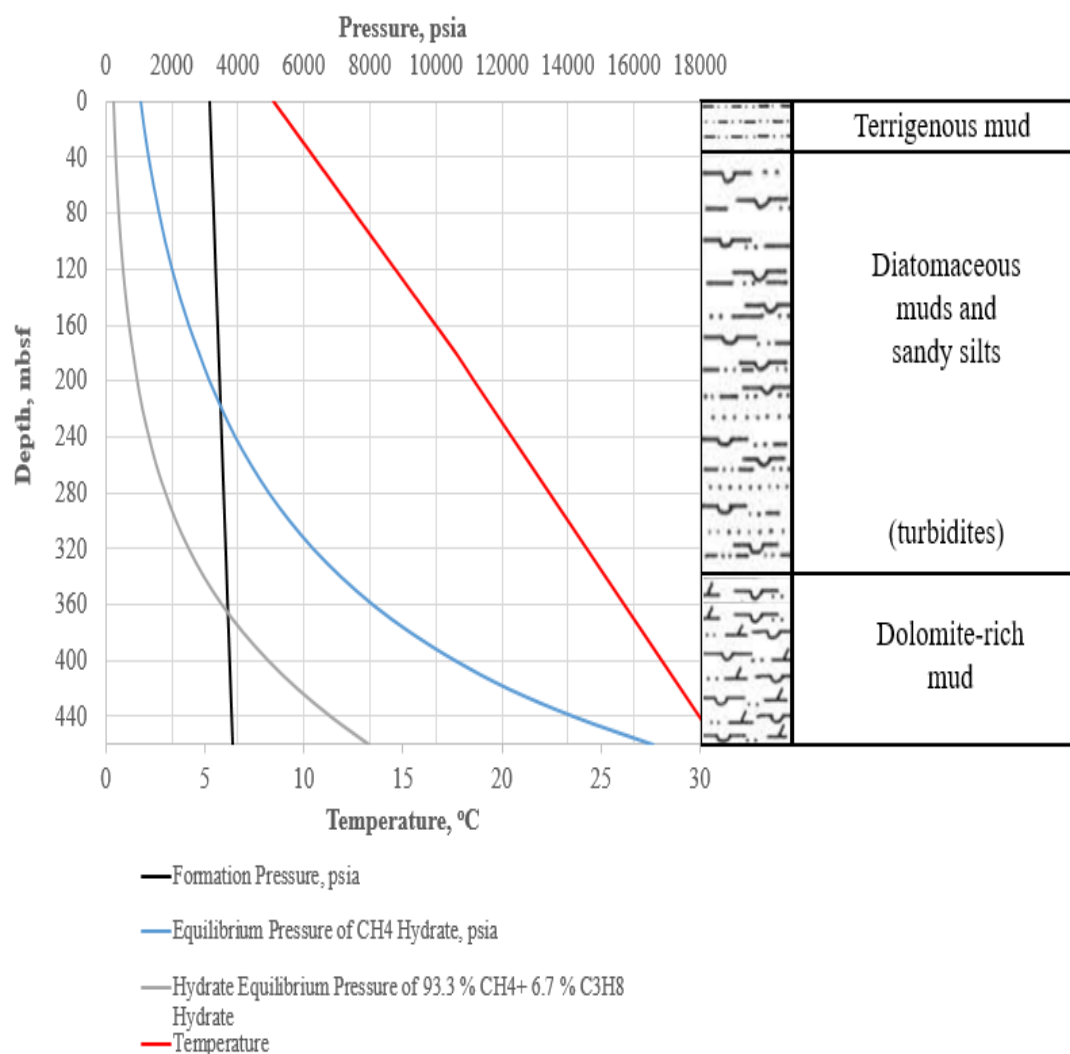


**Figure 7-143:** Hydrate equilibrium curves and lithostratigraphy at Site 380

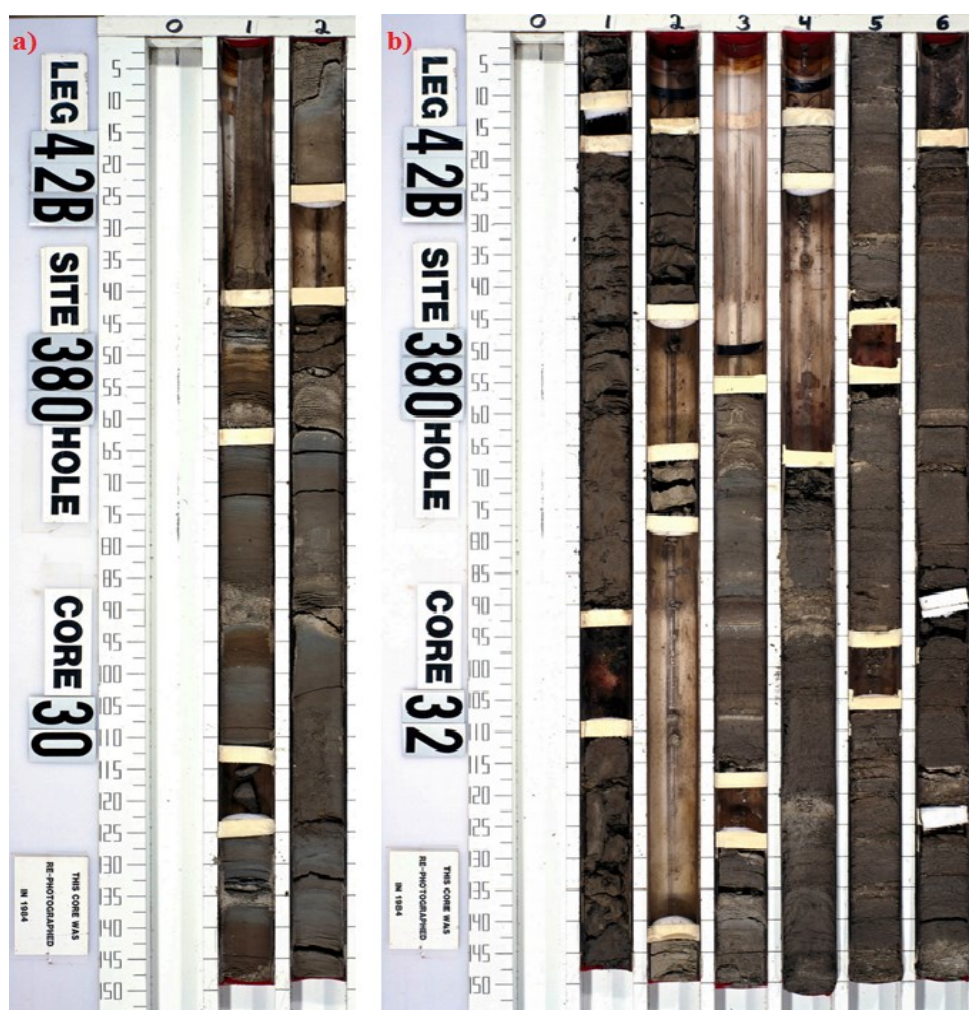


**Figure 7-144:** a) Core 30 of Site 380 (275.5-285 mbsf): interbedded sandy silt layers deposited by turbidite currents b) Core 32 of Site 380 (294.5-305.0 mbsf) in muds, dark greenish gray, greenish black, color variation attributed to the varying abundance of pyrite with intercalation of sandy silt, deposited by turbidity currents (Site 380, 1978)

As seen in Figure 7-145, for Site 380, 100 % CH<sub>4</sub> and 93.3 % CH<sub>4</sub>, 6.7 % C<sub>3</sub>H<sub>8</sub> hydrate stability zones are approximately 235 mbsf and 432 mbsf respectively. According to the lithological analysis of core samples of Site 381, the turbidites in this region include higher silt and clay content compared to Site 379 and Site 380 (Site 381, 1978). However, there are sandy silt and sand sections at Site 381 in gas hydrate stability zones of 100 % CH<sub>4</sub> and 93.3 % CH<sub>4</sub>, 6.7 % C<sub>3</sub>H<sub>8</sub>. During handling of Core 18 at Site 380, huge gas expansions and voids were observed as shown in

Figure 7-146-a. Unfortunately, there is no explanation of whether gas hydrates were observed in the pores of Core 18 because this study was only for geological purposes. The interval of Core 18 is between 161.5 and 171 mbsf, which is in both CH<sub>4</sub> and 93.3 % CH<sub>4</sub>, 6.7 % C<sub>3</sub>H<sub>8</sub> hydrate stability zones as seen in Figure 7-145. Therefore, most probably, gas hydrate exists in sandy silt sediments of Core 18 but high silt content might be disadvantageous during gas hydrate production because its lower permeability characteristic compared to sands (See Figure 3-21). Soupy sediments of Hole 381 Core 18 illustrated in Figure 7-146-a shows that there might be nodular type of gas hydrates in the pores. Furthermore, Core 42 recovered between 380 mbsf and 399.5 mbsf includes pebble, sand, mud as shown in Figure 7-146-b. Core 42 is not in the CH<sub>4</sub> hydrate stability zone but it is in the 93.3 % CH<sub>4</sub>, 6.7 % C<sub>3</sub>H<sub>8</sub> hydrate zone so Core 42 might be a good thermogenic gas hydrate reservoir for gas production. Even though high gas release from Core 42 was not reported in Leg 42B drilling program, the sediments have optimum properties for gas production from gas hydrates. Hence, these sand zones should be targets during gas exploration studies in the Black Sea. Turbidites in the Black Sea should be second targets although they consist of fine silts, sandy silts and silty sands at Sites 379, 380 and 381.

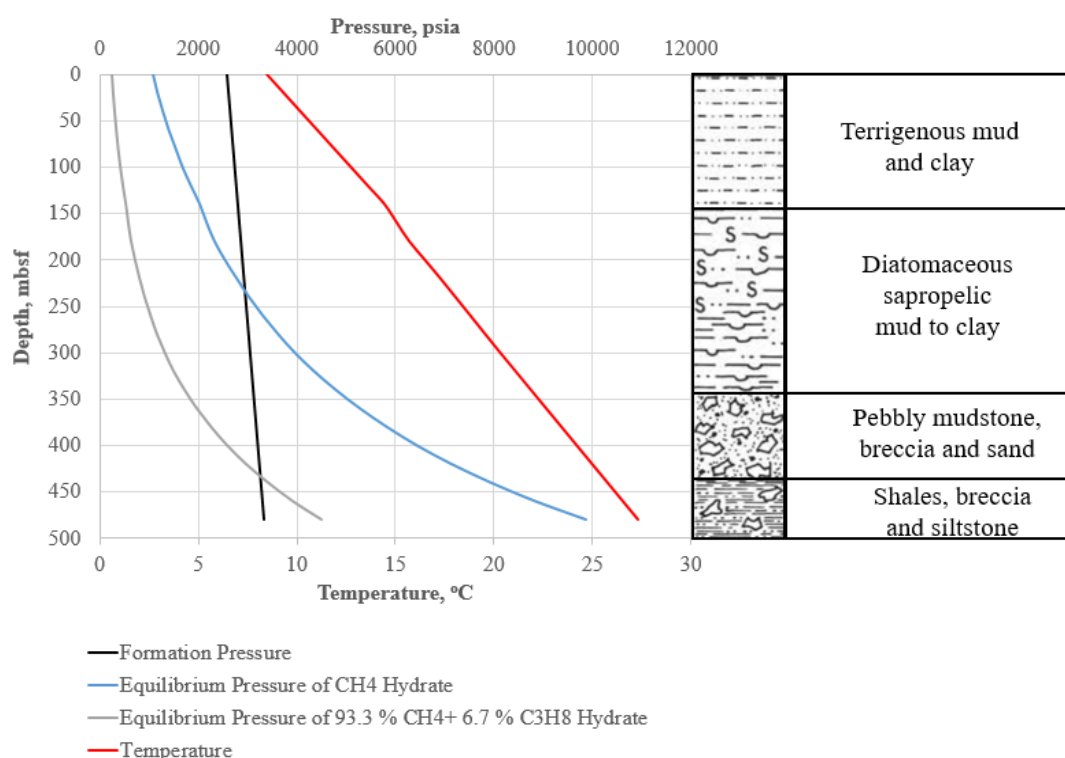


**Figure 7-145:** Hydrate equilibrium curves and lithostratigraphy at Site 381

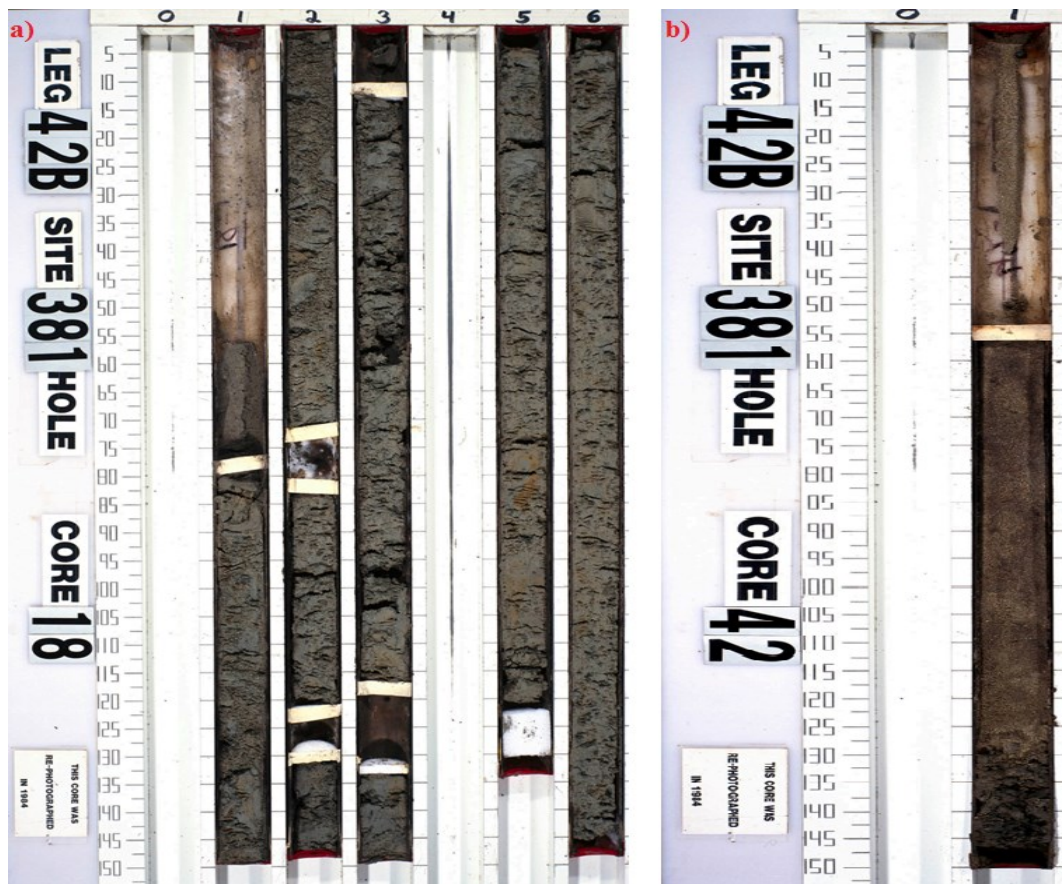


**Figure 7-146:** a) Core 18 of Site 381 (161.5-171 mbsf) Coarse medium gray terrigenous calcareous silt with abundant mollusc fragments. Lower part of the core is a finer greenish gray terrigenous carbonate mud. Several 5-10 cm voids due to gas expansion b) Core 42 of Site 381 (380-399.5 mbsf): Pebble, sand, mud (Site 381, 1978)

Pleistocene sediments at all three sites (379, 380, and 381) are mainly represented by terrigenous muds, clays, silts, and fine sandy interbeds (Muratov *et al.*, 1978). It is considered that Pleistocene glacial sediments predominantly host gas hydrates within 1000 m (Max *et al.*, 2011). Grain size is quite important both for the formation of gas hydrates and gas production from gas hydrates. Figure 7-147 shows the grain size fractions and clay contents of the sediments at Sites 379, 380 and 381. As seen in this figure as clay content increases, grain size decreases. However, when sand content increases, grain size increases as well. Therefore, Figure 7-147 is quite useful to determine coarse sections, which might be a good gas hydrate reservoir as energy source.

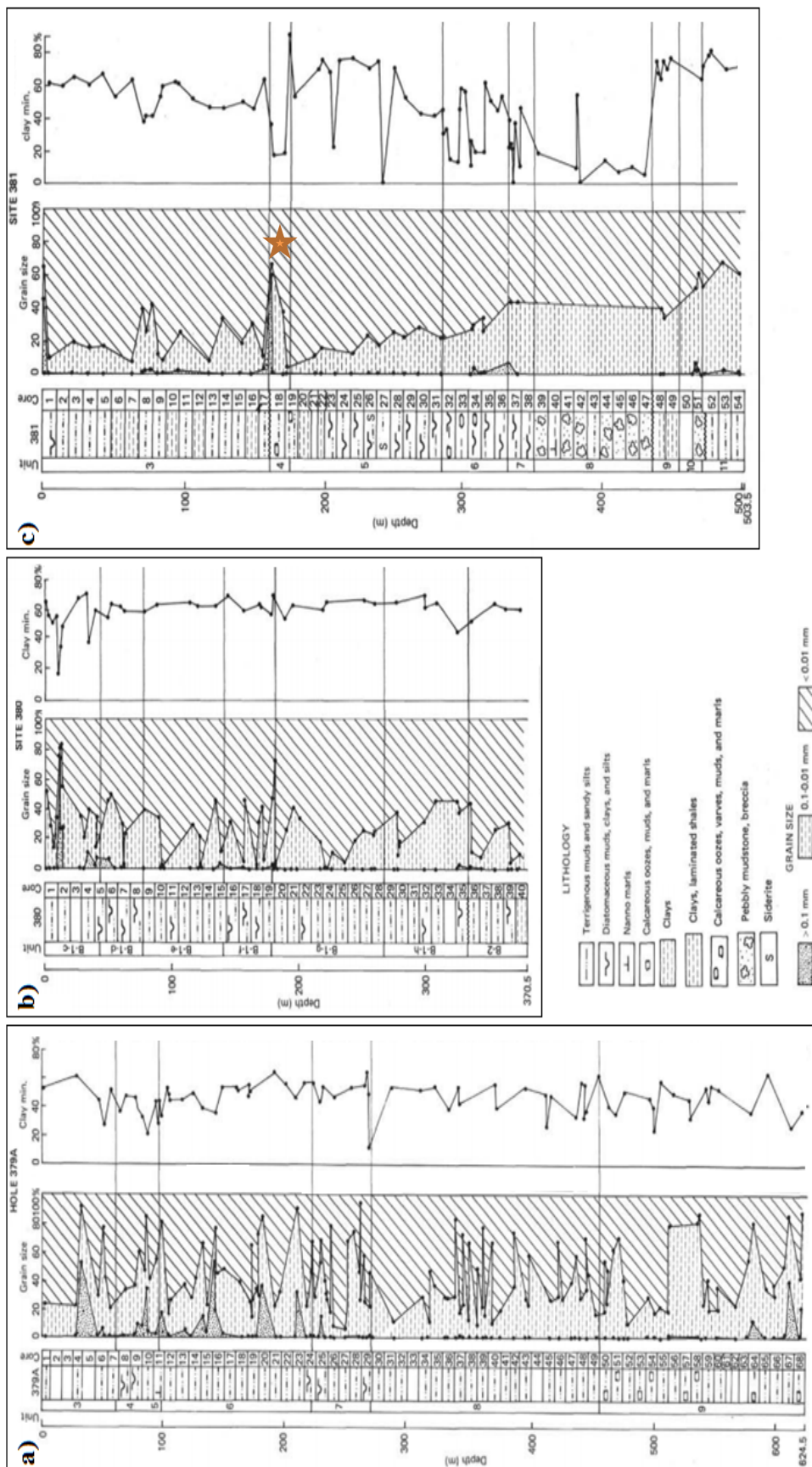


**Figure 7-147:** Grain size fractions and clay contents of Sites 379 (1978), Site 380 (1978), Site 381 (1978), and Trimonis *et al.* (1978))

Core 18 at Site 381 in Figure 7-146-a includes less clay content as shown in Figure 7-147 with star mark so grain size of Core 18 is higher compared to average grain size of the sediments at Site 381. Similar to Figure 7-147, gas hydrates were observed in the core sections where sand content is high in DSDP Site 570, Middle America Trench and DSDP Site 635, Peru Trench (Ginsburg, 1998). Although it includes high silt content, this core might include gas hydrates. Similarly, Core 13 of Site 379 in Figure 7-148 consists of coarser silt to sandy silt, and gas expansion was observed during handling of this core.



**Figure 7-148:** Core 13 of Site 379 (111.5-121 mbsf): Patches of coarser silt to sandy silt occur throughout the core (high gas expansion and voids are due to gas expansion) (Site 379, 1978)

Kuprin *et al.* (1978) conducted mechanical experiments on the core samples recovered during Leg 42B drilling program of DSDP. The mechanical properties of the sediments at Sites 380 and 381 are shown in Figure 7-149. As seen in this figure, the sediments between 0 mbsf and 200 mbsf are unlithified or unconsolidated sediments and their mechanical strength is very low. However, during gas production with depressurization, there might be geomechanical problems (i.e. reservoir subsidence) in this interval of the Black Sea. Although CO<sub>2</sub>/N<sub>2</sub> injection method is alternative to depressurization method because of its geomechanical advantage, the Black Sea does not have appropriate conditions because the Black Sea sediments are warm and high injection pressure is necessary for stable CO<sub>2</sub>/N<sub>2</sub> hydrate which might cause also geomechanical problems in the Black Sea (See Figure 7-10, Table 7-5 and Table 7-6). Furthermore, until now, CO<sub>2</sub>/N<sub>2</sub> injection has not been tried in marine sediments. Underneath 300 mbsf, the deposits can be considered as true rock.

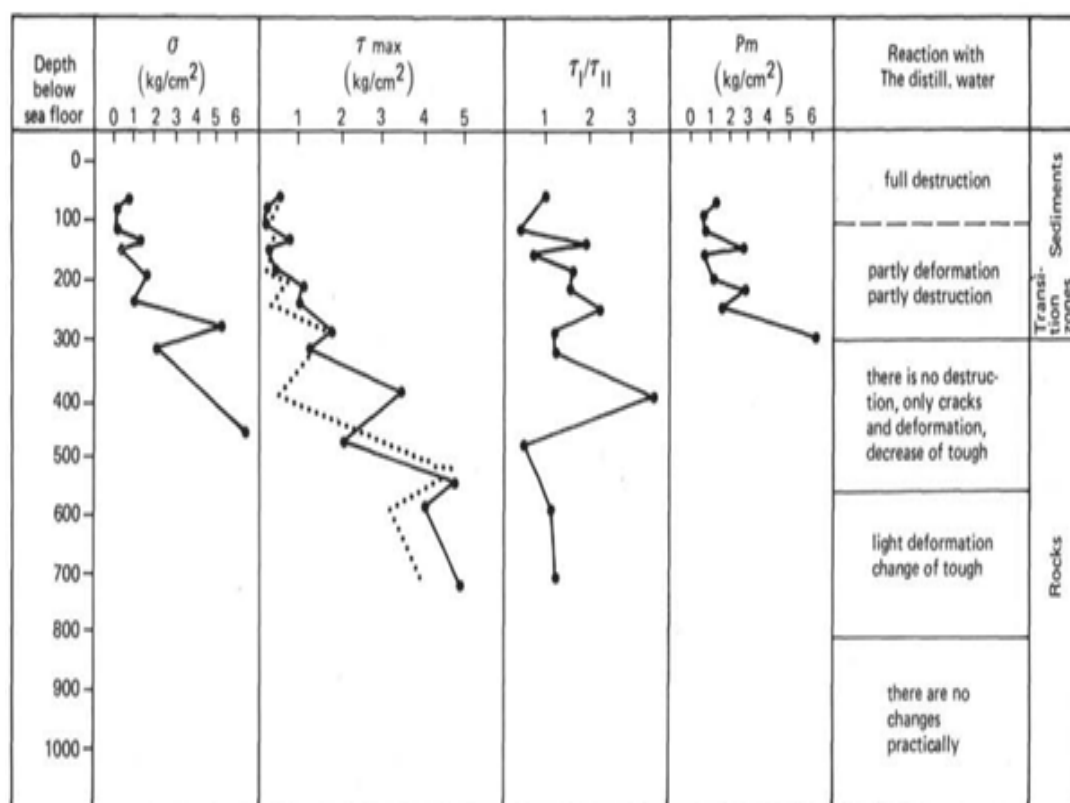


**Figure 7-149:** Changes in the mechanical (deformative) properties of the deposits from Site 381 and Hole 380A and their reaction with the distillate water downsection (Kuprin *et al.*, 1978)

To summarize, the Leg 42B of DSP provides enormous data about the sediments of the Black Sea and their geology and geochemistry. The Black Sea has many parameters needed for potential gas hydrates such as huge gas sources, appropriate temperature and pressure conditions. However, the sediments of the Black Sea include high clay contents and silt contents. Moreover, turbidites in the Black Sea includes as coarse material, fine silty sand or sandy silts. There are centimeter scale sand sections in the cores recovered. Hence, in different parts of the Black Sea, these sands sections might be thicker and include gas hydrates as pore filling as in the Danube fan of the Black Sea. With 2D and 3D high resolution reflection seismic datasets from a paleo channel-levee system in ~1500 m water depth of the Danube Fan, the Black Sea, coarse sandy sediments with good reservoir properties were observed within GHSZ (Zander *et al.*, 2016). It was considered that gas hydrate saturation might be around 50 % at 140 mbsf with 30 m thickness which was determined by marine controlled source electromagnetic (CSEM) survey (Zander *et al.*, 2016). Moreover, in around November 2017, drilling operations are planned to collect more data from this region and after the analysis of core samples, depressurization test method is planned to be conducted in this site (Personal communication with Dr. Timo Zander and Dr. Matthias Haeckel, 2016). Many new exploration holes should be drilled because the Black Sea is mostly unexplored marine basin for both for deep and shallow hydrocarbon exploration. Current pressurized coring equipment are very useful and hydrate section in cores can be recognized. Moreover, as well as core data, well log data are essential. Logging while drilling is commonly preferred in gas hydrate expeditions such as in Gulf of Mexico Gas Hydrate Joint Industry Project (Collett *et al.*, 2009b). Hence, all core and well log data should be evaluated together.



## CHAPTER 8

### CONCLUSION

In this study, the gas hydrate potential of the Black Sea was investigated. Detailed analysis was made by using literature data related to the Black Sea and potential Black Sea gas hydrates. After determining properties and conditions of the Black Sea and the Black Sea gas hydrates, the optimum gas production method was selected for the Black Sea conditions by numerical analysis, which are depressurization or depressurization combined with thermal stimulation. Then, for the selected production method, the experimental set-up (especially high pressure reactor) were designed with numerical studies. To compare the laboratory scale simulation with reservoir scale simulations, gas production simulations from gas hydrates were conducted for hypothetical Class 1 and Class 3 reservoirs. Finally, several codes were written to understand and calculate hydrate properties, especially for the Black Sea gas hydrates. In this study, the following concluding remarks were obtained:

- ✓ The Black Sea has a gas hydrate potential and in this study its potential was calculated as ~71.8 tcm (median). However, this amount should not be considered as only energy resource. Turbidites (layering of coarse to medium sediments and fine sediments alternatively) are thought be common in the Black Sea sediments. Gas hydrate in sands are considered as potential source of energy compared to the gas hydrate deposited in shales and clays because sand sediments have higher permeability compared to clay and shale sediments. The average sand content was selected as 14.75 % for average 303 m thick of gas hydrate section in the Black Sea. CH<sub>4</sub> amount in the CH<sub>4</sub> hydrates found in the sands of the Black Sea was calculated as 13.6 tcm (median) in this study.

- ✓ In this study, optimum gas production methods for the potential Black Sea gas hydrates were investigated by using the Black Sea literature data. Moreover, the experimental set-up to be used in future studies in the Black Sea conditions were designed for the Black Sea gas hydrates. Mainly, HydrateResSim numerical simulator output data were quite useful to decide on the design of high pressure reactor (METU reactor) and the selection of the ranges of gas flow meter, separator and mass weigh balance.
- ✓ According to the analysis of hydrate equilibrium curves of CH<sub>4</sub>, CO<sub>2</sub>, N<sub>2</sub> and their mixtures in this study, the Black Sea conditions are not favorable for CO<sub>2</sub> or CO<sub>2</sub>/N<sub>2</sub> injection as a production method for potential Black Sea gas hydrates due to the warm temperature of its sediments.
- ✓ Depressurization might be a good production method from the Black Sea because the temperature of potential hydrate reservoirs and their boundaries are expected to be higher than 9°C. The main reason of this is that when temperature is higher, depressurization is much more effective.
- ✓ Cylindrical high pressure reactor (METU reactor) was designed in 30 cm inner length and 30 cm inner diameter with a volume of 21.64 L. The simulation results (cumulative gas production and water production) with equilibrium and kinetic models are quite close to each other. Therefore, METU reactor is likely to have “flow-controlled” system in the Black Sea conditions as it is in real hydrate reservoirs. Portable 100 mesh size separator which is located 5 cm above the bottom of METU reactor might be quite useful to mimic horizontal well production, gas production from Class 1 hydrate reservoirs and to avoid any plugging due to possible hydrate reformation and ice formation in the production lines. Higher gas productions were obtained when METU reactor includes 100 mesh separator according to the simulations done with HydrateResSim. 0-100 L/min gas flow meter, 5 kg water-gas separator, 5 kg mass balance, 250 bar pressure transducer, and 0-

100°C thermocouples might be enough for the gas production experiments from the potential Black Sea gas hydrates.

- ✓ Gas production simulations from a hypothetical Class 1 CH<sub>4</sub> hydrate reservoir in the Black Sea were run by depressurization and depressurization with wellbore heating. The higher the depressurizing range is, the faster the dissociation rate is as long as there is no ice formation or hydrate reformation. The highest gas production was obtained at 3.0 MPa with only depressurization but 2.7 MPa was the optimum production pressure by depressurization combined with wellbore heating at the conditions of the hypothetical Class 1 CH<sub>4</sub> hydrate reservoir in this study. Both with and without wellbore heating, below 2.7 MPa depressurization pressure, ice formations were observed inside the reservoir and ice plugged the pores so the production periods below 2.7 MPa were very short. Wellbore heating might be necessary to avoid hydrate reformation near perforations. In the Black Sea conditions, huge amount of gas (more than 50 % of gas) can be produced from the Class 1 hydrate reservoirs both from the hydrate zone and free gas zone by depressurization. If the intrinsic permeability of the hydrate zone is less than 400 mD, the depressurization might not be effective for the hypothetical Class 1 reservoir. Hence, the determination of the intrinsic and absolute permeability is very important.
- ✓ When the results of the hypothetical Class 3 reservoir were compared with the hypothetical Class 1 reservoir, Class 1 hydrates are advantageous. There are important contribution of free zone and hydrate zone to gas production. The intrinsic permeability has quite important effect on gas production in Class 3 reservoir different from Class 1 reservoir. The production behavior of laboratory scale simulations and reservoir scale simulations are quite close to each other in this study.
- ✓ Impermeable clay or shale boundaries of gas hydrates are very important to increase gas production from both Class 1 and Class 3 gas hydrate reservoirs

because with the decrease of temperature during dissociation of gas hydrates, these boundaries supply heat through gas hydrate sections. High temperature of the Black Sea sediments (more than 9°C) are quite advantageous to supply heat while depressurization method is applied.

- ✓ In order to compare gas productions from thick Class 3 hydrate and thin hydrate sections in turbidites in the Black Sea conditions, several depressurization numerical simulations were run with HydrateResSim. Because of faster thermal flux from impermeable boundaries to thin hydrate section in turbidites, much more gas might be produced compared to thick hydrate sections in the same conditions.
- ✓ The Black Sea has a high potential of gas hydrates and the only well-known gas hydrate prospect in the Black Sea are gas hydrates in the Danube Fan. Moreover, several drilling and production tests are planned in this region. Hence, in this study, depressurization simulations were conducted by using HydrateResSim at different depressurization pressures. If the clay above the upper gas hydrate section is geomechanically stable and impermeable, this upper section is appropriate for first depressurization test in the Black Sea at 3 or 4 MPa within 60-day depressurization test. However, if this clay is permeable and is geomechanically weak, the lower gas hydrate section is also appropriate short-term depressurization test at 3 or 4 MPa. Moreover, observation wells at least 20 m far from the production test well are necessary to measure temperature, pressure and geomechanical changes in gas hydrate section during production test. With further drilling and coring data, detailed well completion and production test design is necessary.
- ✓ In this study, HEP.m (Hydrate Equilibrium Properties code) code was written with Matlab 2014a. This code can be very useful to predict hydrate properties (pure CH<sub>4</sub>, C<sub>2</sub>H<sub>6</sub>, C<sub>3</sub>H<sub>8</sub>, n-C<sub>4</sub>H<sub>10</sub>, i-C<sub>4</sub>H<sub>10</sub>, H<sub>2</sub>S, N<sub>2</sub>, CO<sub>2</sub> and the mixtures of these components and other heavy hydrocarbon molecules such as i-C<sub>5</sub>H<sub>12</sub>, n-C<sub>5</sub>H<sub>12</sub>, i-C<sub>6</sub>H<sub>14</sub>, n-C<sub>6</sub>H<sub>14</sub>) such as hydrate equilibrium pressure, hydrate

density, hydrate molecular weight, cage occupancy and enthalpy of dissociation of pure or mixed hydrates with/without inhibitors (NaCl, CaCl<sub>2</sub>, KCl, Methanol, Ethanol, Ethylene Glycol, DEG, TEG and their mixtures). This code can be used for hydrate studies related to energy source, hydrate inhibition conditions during transportation of natural gases from gas fields and transportation of natural gas as gas hydrates. In order to understand the reliability of this code, hydrate equilibrium pressure, enthalpy and density with the experimental studies and those calculated with HEP.m and other software were compared and very good fitting results were obtained.

- ✓ HEPComp.m code was written with Matlab 2014a in this study. Generally, gas hydrate samples dissociate when they are taken from ocean sediments to surface. Gas compositions are measured with GC. By using GC results and temperature in ocean sediments, HEPComp.m code can predict gas composition at initial reservoir conditions. Therefore, this code is also quite useful.
- ✓ Gas hydrates are considered as potential future energy sources. Therefore, for hydrate experimental studies to represent field conditions (especially hydrate is formed in sediments inside high pressure reactors), SM.m and SMmix.m codes are useful to calculate the amount of water and gas needed to satisfy target hydrate saturations for pure CH<sub>4</sub> and gas mixtures respectively. The results calculated with SM.m were compared with the data in literature and very close results were obtained.
- ✓ By using BSR depth, sea depth, salinity, geothermal gradient and pressure gradient in the study area, many information about expected Class 1 hydrate reservoir near BSR lines can be found. Therefore, in this study, a code (BSR.m) was written by Matlab 2014a. BSR.m predicts the composition of gas hydrate, its type, density, hydration number, cavity ratio, etc. In order to check the reliability of this code, multiple BSRs detected by Popescu et al.

(2006) in the Danube deep-sea fan of the Black Sea was investigated. Similar results were obtained with the study of Popescu *et al.* (2006).

- ✓ As well as numerical simulations and codes written in this study, it was also aimed to understand and characterize the potential Black Sea gas hydrates and Black Sea sediments. After evaluating all available geology, temperature, pressure, salinity, geochemistry, and sediment data of the Black Sea, it was observed that the Black Sea has appropriate conditions for gas hydrates. Due to gas flux from biogenic sources and thermogenic sources, sI and sII gas hydrates are thought to be common in this study. Moreover, although CH<sub>4</sub> recovered from the samples taken in the Black Sea include other impurities i-C<sub>5</sub>H<sub>12</sub>, 3,3-dimethylpentane and 2,2-dimethylbutane, if these components are high content in different places of the Black Sea, sH gas hydrates might be observed in the Black Sea.
- ✓ High amount of gas source potential, temperature and hydrostatic pressure of the Black Sea are optimum for gas hydrate formation. The last most important parameter for producible gas hydrate reservoirs is that the existence of coarse sand dominated sediments depositing gas hydrates as pore filling. However, according to all core data in different studies and the core data taken during Leg 42B drilling program of DSDP in the Black Sea, the sediments in the Black Sea include high clay content, which is not good for gas hydrate formation or gas production from hydrates due to their low permeability.
- ✓ Although coarse layers of turbidites are considered as potential reservoirs, the cores taken from the Black Sea turbidites include very fine to fine silt and sandy silt layers. Moreover, very thin sand sections up to 8 cm were observed in the cores of Leg 42B drilling program, these sand sections might be thicker in different locations of the Black Sea and they might be good hydrate reservoirs in terms of gas production.

## **CHAPTER 9**

### **RECOMMENDATION**

Based on the experience gained in the present study, the following suggestions are recommended for future researches in this area:

In this study, it is aimed to analyze the general properties and behaviors of potential gas hydrates in the Black Sea. However, gas hydrate reservoirs in different places of the Black Sea should be evaluated separately. There are seismic studies in the Black Sea and these studies should be completed with drilling of many holes in the Black Sea sediments. As in many places of the world, the first aim of these drillings should not be immediate gas production tests. Firstly, many holes with logging while drilling should be drilled at sections where strong BSR lines are observed. Moreover, core samples should be taken and necessary experiments should be conducted to characterize the Black Sea gas hydrates. Drilling, coring and well logging will bring many new data and these data are crucial to develop a production method for that case. Therefore, it is important to conduct gas production experiments and relative permeability experiments for a specific hydrate reservoir compared to general hydrate studies. Moreover, numerical simulations will be very helpful to predict and choose appropriate production method, well testing and well completion for a specific gas hydrate reservoir in the Black Sea.



## REFERENCES

- Abbasov, A. (2014). Experimental Verification of CH<sub>4</sub>-CO<sub>2</sub> Swap in Methane-Propane-Carbon Dioxide Mixture Hydrates. MSc. Thesis. Middle East Technical University, Turkey.
- Abbasov, A., Merey, S., Parlaktuna, M. (2016). Experimental Investigation of Carbon Dioxide Injection Effects on Methane-Propane-Carbon Dioxide Mixture Hydrates. *Journal of Natural Gas Science and Engineering*, 34 (2016) 1148-1158.
- Abid, K., Spagnoli, G., Teodoriu, C., Falcone, G. (2015). Review of pressure coring systems for offshore gas hydrates research. *Underwater Technology*, Vol. 33, No. 1, pp. 19–30, 2015.
- Adisasmito, S., Frank, R.J., Sloan, E.D., (1991). Hydrates of carbon dioxide and methane mixtures. *J. Chem. Eng. Data* 36, 68–71.
- Ahmed, T. (2007). *Equations of State and PVT Analysis: Applications for Improved Reservoir Modeling*. Gulf Publishing Company Houston, Texas, USA.
- Ahn, Y., Kang, H., Koh, D., and Lee, H. (2015). Production of Natural Gas Hydrate by Using Air and Carbon Dioxide. *International Journal of Chemical, Molecular, Nuclear, Materials and Metallurgical Engineering* Vol:9, No:7, 2015; 749-753.
- Aktosun, A., Varol, B. (2013). Concretions in Akçakoca Sandstone Member of Kusuri Formation (Lower-Middle Eocene), Western Black Sea. 19<sup>th</sup> International Petroleum and Natural Gas Congress and Exhibition, May 15-17, 2013, Ankara, Turkey.
- Alexiades, V. (2009). Methane hydrate formation and decomposition. *Electronic Journal of Differential Equations*, Conference 17 (2009), pp. 1–11. ISSN: 1072-6691.
- Alp, D., Parlaktuna, M., Moridis, G.J. (2007). Gas Production by Depressurization from Hypothetical Class 1G and Class 1W Hydrate Reservoirs. "Energy Conversion and Management", 48, (2007), p.1864-1879.

- Ameripour, S. (2005). Prediction of Gas-Hydrate Formation Conditions in Production and Surface Facilities. MSc. Thesis, Texas AandM University, TX, USA.
- Avlonitis, D., Danesh, A., Todd, A.C., (1988). Measurement and Prediction of Hydrate Dissociation Pressure of Oil-Gas Systems. Presented at BHRA Conference on Operational Consequences of Hydrate Formation an Inhibition Offshore, Crainfield, UK, November 3, 1988.
- Barmavath, T., Mekala, P., and Sangwai, J. S. (2014). Prediction of phase stability conditions of gas hydrates of methane and carbon dioxide in porous media. *Journal of Natural Gas Science and Engineering*, 18, 254–262.
- Beaudoin, Y. C., Waite, W., Boswell, R. and Dallimore, S. R. (eds), (2014). *Frozen Heat: A UNEP Global Outlook on Methane Gas Hydrates*. Volume 1. United Nations Environment Programme, GRID-Arendal. ISBN: 978-92-807-3429-4.
- Berge, B. K. (1986). Hydrate Prediction on a Microcomputer. SPE 15306 Presented at the 1986 Symposium On Petroleum Industry Applications of Microcomputers, SilverCreek, CO, June 18-20, 1986.
- Berndt, C. (2005). Focused fluid flow in passive continental margins. *Philos. Trans. R. Soc. Lond. A* 363, 2855–2871.
- Bhade, P., and Phirani, J. (2015). Effect of geological layers on hydrate dissociation in natural gas hydrate reservoirs. *Journal of Natural Gas Science and Engineering*, 26 (2015), 1549-1560.
- Bialas, J. (Ed.), 2014. FS Maria S. Merian Fahrtbericht/Cruise Report MSM-34/1 & 2 SUGAR Site. Berichte aus dem GEOMAR Helmholtz-Zentrum für Ozeanforschung Kiel Nr. 15.
- Birkedal, K., Freeman, C. M., Moridis, G. J., and Graue, A. (2014). Numerical Predictions of Experimentally Observed Methane Hydrate Dissociation and Reformation in Sandstone. *Energy and Fuels*, 28(9), 5573–5586.
- Bishnoi, P.R. and Dholabhai, P.D. (1999). “Equilibrium Conditions for Hydrate Formation for a Ternary Mixture of Methane, Propane and Carbon Dioxide, and a Natural Gas Mixture in the Presence of Electrolytes and Methanol,” *Fluid Phase Equilibria* (1999) 158-160, 821.

- Breeze, N. (2013). CO<sub>2</sub>? Let Me Introduce You to My Little Friend: CH<sub>4</sub> (Methane)! Retrieved from (Accessed on February 12, 2016): <http://envisionation.co.uk/index.php/blogs/72-co2-let-me-introduce-you-to-my-little-friend-ch4-methane>.
- Burruss, R.C., Laughrey, C.D. (2010). Carbon and hydrogen isotopic reversals in deep basin gas: Evidence for limits to the stability of hydrocarbons. *Org Geochem* 41:1285-1296.
- Bülbül, S., Parlaktuna, M., Mehmetoglu, T., Karabakal, U. (2014). Black Sea Hydrate Formation Conditions of Methane Hydrogen Sulfide Mixtures. *Energy Sources, Part A: Recovery, Utilization, and Environmental Effects*. Volume 36, Issue 16, 2014 pages 1738-1748.
- Bridge, J., Demicco, R. (2008). *Earth Surface Processes, Landforms and Sediment Deposits*. Cambridge University Press, New York.
- Bohrmann, G., Torres, M.E. (2006). Gas Hydrates in Marine Sediments. In book: *Marine Geochemistry*, pp.481-512. [http://dx.doi.org/10.1007/3-540-32144-6\\_14](http://dx.doi.org/10.1007/3-540-32144-6_14)
- Bouma, A. H. (1962) *Sedimentology of some Flysch deposits: A graphic approach to facies interpretation*. Elsevier, Amsterdam, 168 p.
- Bouillot, B., and Herri, J. M. (2015). Framework for clathrate hydrate flash calculations and implications on the crystal structure and final equilibrium of mixed hydrates. *Fluid Phase Equilibria*, 413, 184–195.
- Bourry, F., Chazallon, B., Charlou, J.L., Donval, J.P., Ruffine, L., Henry, P., Geli, L., Çağatay, M.N., İnan, S., Moreau, M. (2009). Free gas and gas hydrates from the Sea of Marmara, Turkey Chemical and structural characterization. *Chemical Geology* 264 (2009) 197–206.
- Boswell, R., Collett, T.S. (2006). The gas hydrates resource pyramid: Fire in the ice, Methane hydrate newsletter, US Department of Energy, Office of Fossil Energy, National Energy Technology Laboratory, Fall Issue, p. 5-7.
- Boswell, R., Kleinberg, R., Collett, T., Frye, M. (2007). Exploration Priorities for Marine Gas Hydrate Resources. *Methane Hydrate Newsletter: Fire in Ice*, Vol.7, Iss.2, 2007.
- Boswell, R (2009). Is gas hydrate energy within reach? *Science* 2009, 325 (5943), 957–958.

- Boswell, R., Collett, T.S. (2011). Current perspectives on gas hydrate resources. *Energy Environ. Sci.*, 2011, 4, 1206–1215.
- Boswell, R., Moridis, G., Reagan, M., Berkeley, L., and Collett, T. S. (2011). Gas hydrate accumulation types and their application to numerical simulation. *Proceedings of the 7<sup>th</sup> International Conference on Gas Hydrates, (Icgh)*, 12. Retrieved from (Accessed on February 12, 2016):  
<http://www.pet.hw.ac.uk/icgh7/papers/icgh2011Final00130.pdf>
- Boswell, R. (2014). Developments in Marine Gas Hydrate Exploration. The Offshore Technology Conference held in Houston, Texas, USA, 5–8 May 2014.
- Boswell, R., Collett, T. (2016). Emerging Issues in The Development of Geologic Models for Gas Hydrate Numerical Simulation. *Fire in Ice, Hydrate News Letter*, 2016 Vol. 16, Issue 1.
- Boswell, R., Schoderbek, D., Collett, T.S., Ohtsuki, S., White, M.D., Anderson, B.J. (2016). The Ignik Sikumi Field Experiment, Alaska North Slope: Design, Operations, and Implications for CO<sub>2</sub>-CH<sub>4</sub> Exchange in Gas Hydrate Reservoirs. *Energy & Fuels*. DOI: 10.1021/acs.energyfuels.6b01909
- Calvert, S.E., Batchelor, C.H. (1978). Major and Minor Element Geochemistry of Sediments from Hole 379A, Leg 42B, Deep Sea Drilling Project. <http://dx.doi.org/10.2973/dsdp.proc.42-2.116.1978>
- Carroll, J. J. (2009). *Natural Gas Hydrates: A Guide for Engineers*; Gulf Professional Publishing: Houston, 2009.
- Chapoy, A. (2014). HSZ in the Presence of Organic Inhibitor. SFGP Seminar - La Thermodynamique des phases solides- Paris, December, 2014.
- Cheng, C., Zhao, J., Yang, M., Liu, W., Wang, B., and Song, Y. (2015). Evaluation of Gas Production from Methane Hydrate Sediments with Heat Transfer from Over-Underburden Layers. *Energy Fuels*, 2015, 29, 1028–1039.
- Chong, Z. R., Hern, S., Yang, B., Babu, P., Linga, P., and Li, X. (2015). Review of natural gas hydrates as an energy resource: Prospects and challenges. *Applied Energy*, 162, 1633–1652.
- Chong, Z. R., Chan, A. H. M., Babu, P., Yang, M., and Linga, P. (2015b). Effect of NaCl on methane hydrate formation and dissociation in porous media. *Journal of Natural Gas Science and Engineering*, 27 (1), 178–189.

- Chong, Z.R., Yang, M., Khoo, B.C., Ling, P. (2015c). Size effect of porous media on methane hydrate formation and dissociation in an excess gas environment. *Ind. Eng. Chem. Res.*, 55, 7981–7991.
- Chuvilin, E., Buhanov, B., Guryeva, Istomin, V., Takeya, S., Hachikubo, A., (2011). Experimental Study of Self-Preservation Mechanisms during Gas Hydrate Decomposition in Frozen Sediments. *Proceedings of the 7<sup>th</sup> International Conference on Gas Hydrates (ICGH 2011)*, Edinburgh, Scotland, United Kingdom, July 17-21, 2011.
- Clarke, M.A, Bishnoi, P.R. (2001). Determination of the activation energy and intrinsic rate constant of methane gas hydrate decomposition. *Can.J.Chem.Eng.*, 79:143-147, 2001.
- Cremiere, A., Pierre, C., Aloisi, G., Blanc-Valeron, M.M., Henry, P., Zitter, T., Çağatay, N. (2011). Uthigenic Carbonates Related to Thermogenic Gas Hydrates in The Sea Of Marmara (Turkey). *Proceedings of the 7th International Conference on Gas Hydrates (ICGH 2011)*, Edinburgh, Scotland, United Kingdom, July 17-21, 2011.
- Collett, T. S., Survey, U. S. G., Ginsburg, G. D., and Petersburg, S. (1998). Gas Hydrates in the Messoyakha Gas Field of the West Siberian Basin — A Re-Examination of the Geologic Evidence. *International Journal of Offshore and Polar Engineering*, 8(1), 5381.
- Collins, P.C., Carlsson, J., Rowcroft, P., Tibbles, B. (2016). Ecosystem status of the deep Black Sea, soft sediment, benthic community. *Marine Policy* 73 (2016) 216–223.
- Collett, T.S. (2000). Natural gas hydrate as a potential energy source, in M.D. Max, ed., *Natural gas hydrate in oceanic and permafrost environments*: Boston, Klu Academic, p. 123-136.
- Collett, T.S. and Lee, M.W., (2005): Electrical-resistivity well-log analysis of gas hydrate saturations in the JAPEx/JNOC/GSC et al. Mallik 5L-38 gas hydrate production research well; in *Scientific Results from the Mallik 2002 Gas Hydrate Production Research Well Program, Mackenzie Delta, Northwest Territories, Canada*, (ed.) S.R. Dallimore and T.S. Collett; Geological Survey of Canada, Bulletin 585, 8 p.

- Collett, T., Johnson, A., Knapp, C., Boswell, R. (2009). Natural Gas Hydrates-Energy Resource Potential and Associated Geologic Hazards. The American Association of Petroleum Geologists (AAPG) Memoir 89.
- Collett, T., Boswell, R., Frye, M., Shedd, W., Godfriaux, P., Dufrene, R., McConnell, D., Mrozewski, S., Guerin, G., Cook, A., Jones, E., Roy, R. (2009b). Gulf of Mexico Gas Hydrate Joint Industry Project Leg II : Operational Summary. Retrieved from (Accessed on April 12, 2016): <http://www.netl.doe.gov/File%20Library/Research/Oil-Gas/methane%20hydrates/OpSum.pdf>
- Collett, T., Bahk, J. J., Baker, R., Boswell, R., Divins, D., Frye, M., Goldberg, D., Husebø, J., Koh, C., Malone, M., Morell, M., Myers, G., Shipp, C., Torres, M. (2015). Methane hydrates in nature-current knowledge and challenges. *Journal of Chemical and Engineering Data*, 60(2), 319–329.
- CSM (2016). "CMSHYD and CSM Software" Retrieved from (Accessed on July 11, 2016): <http://hydrates.mines.edu/CHR/Software.html>
- Dahlmann, A., de Lange, G.J. (2003). Fluid–sediment interactions at Eastern Mediterranean mud volcanoes: a stable isotope study from ODP Leg160. *Earth and Planetary Science Letters* 212 (3–4), 377–391.
- Dannowski, A., Bialas, J., Zander, T., Kläschen, D., Koch, S. (2016). High Resolution Shear Wave Modelling of Obs Data in a Gas Hydrate Environment in the Danube Deep-Sea Fan, Black Sea. CIESM, At Kiel, Germany, September 2016.
- Daraboina, N., Malmos, C., and Von Solms, N. (2013). Synergistic kinetic inhibition of natural gas hydrate formation. *Fuel*, 108, 749–757.
- Darnet, M., Van Der Sman, P., Plessix, R.E., Johnson, J.L., Rosenquist, M. (2010). Exploring with Controlled Source Electro-Magnetic (CSEM) methods: from 2D profiling to 3D multi-azimuth surveying. EGM 2010 International Workshop, Adding new value to Electromagnetic, Gravity and Magnetic Methods for Exploration, Capri, Italy, April 11-14, 2010.
- Deaton, W.M., Frost, E.M., Jr., (1946). Gas Hydrates and Their Relation to the Operation of Natural-Gas Pipe Lines, U.S. Bureau of Mines Monograph 8, p. 101 (1946).

- Degens, E.T., Stoffers, P., Golubic, S., Dickman, M.D. (1978). Varve Chronology: Estimated Rates of Sedimentation in the Black Sea Deep Basin. <https://doi.org/10.2973/dsdp.proc.42-2.114.1978>
- DSDP. Deep Sea Drilling Project. Retrieved from (Accessed on April 23, 2016): <http://www.deepseadrilling.org/about.htm>.
- Deuser, W. G. (1974). “Evolution of Anoxic Conditions in Black Sea during Holocene”, in the Black Sea-Geology, Chemistry, and Biology, Degens, E. T. and Ross, A. D., ed., the American Association of Petroleum Geologists, United States (1974), 133-136.
- Dimitrios, A. and Varotsis, N. (1996). Modeling Gas Hydrate Thermodynamic Behavior: Theoretical Basis and Computational Methods. *Fluid Phase Equilibria* (1996) 123, 107.
- Dimitrov, L. (2002). Contribution to atmospheric methane by natural seepages on the Bulgarian continental shelf. *Continental Shelf Research* 22(2002) 2429–2442.
- Donohoue, D., and College, A. (2000). Effects of Hydrate Formation on Gas Composition: A physical chemistry and environmental science question. *Structure*, 1–12. Retrieved from (Accessed on November 1, 2015): <http://www.mbari.org/education/internship/00interns/00internpapers/deanna.pdf>
- Ellis, S., Pecher, I., Kukowski, N., Xu, W., Henrys, S., and Greinert, J. (2010). Testing proposed mechanisms for seafloor weakening at the top of gas hydrate stability on an uplifted submarine ridge (Rock Garden), New Zealand. *Marine Geology*, 272(1-4), 127–140.
- Ergun, M., Cifci, G. (1999). Gas-Saturated Shallow Sediments in the Eastern Black Sea and Geohazard Effects. The 1999 Offshore Technology Conference, Houston, Texas, 3–6 May 1999.
- Erickson, A.J., Von Herzen, R.P. (1978). Downhole Temperature Measurements and Heat Flow Data in the Black Sea—DSDP Leg42B. <https://doi.org/10.2973/dsdp.proc.42-2.152.1978>
- Eslamimanesh, A., Mohammadi, A.H., Richon, D., Naidoo, P., Ramjugernath, D. (2012). Application of gas hydrate formation in separation processes: A review of experimental studies. *The Journal of Chemical Thermodynamics*, Volume 46, March 2012, Pages 62–71.

- Fairbridge, R. W. (ed.) (1966) *The Encyclopedia of Oceanography*, Encyclopedia of earth sciences series 1, Van Nostrand Reinhold Company, New York, p. 945-946.
- Falser, S., Uchida, S., Palmer, a. C., Soga, K., and Tan, T. S. (2012). Increased gas production from hydrates by combining depressurization with heating of the wellbore. *Energy and Fuels*, 26(10), 6259–6267.
- Fan, S., Zhang, Y., Tian, G., Liang, D., and Li, D. (2006). Natural gas hydrate dissociation by presence of ethylene glycol. *Energy and Fuels*, 20(8), 324–326.
- Fattah, K. (2004). Evaluation of empirical correlations for natural gas hydrate predictions. *Oil and Gas Business*, 1–12. Retrieved from (Accessed on March 13, 2016): [http://www.ogbus.ru/eng/authors/Fatahh/Fatahh\\_1.pdf](http://www.ogbus.ru/eng/authors/Fatahh/Fatahh_1.pdf)
- Feng, J.C., Wang, Y., Li, X.S., Li, G., and Zhang, Y. (2015). Three dimensional experimental and numerical investigations into hydrate dissociation in sandy reservoir with dual horizontal wells. *Energy*, 90 (1), 2015, 836–845.
- Feng, J.C., Wang, Y., Li, X.S., Li, G., Zhang, Y., and Chen, Z.Y. (2015b). Effect of horizontal and vertical well patterns on methane hydrate dissociation behaviors in pilot-scale hydrate simulator. *Applied Energy*, 145, 69–79.
- Feng, J.C., Wang, Y., Li, X.S. (2017). Entropy Generation Analysis of Hydrate Dissociation by Depressurization with Horizontal Well in Different Scales of Hydrate Reservoirs. *Energy*, 125, (2017), 62–71.
- Fitzgerald, G. C., and Castaldi, M. J. (2013). Thermal stimulation based methane production from hydrate bearing quartz sediment. *Industrial and Engineering Chemistry Research*, 52, 6571–6581.
- Fujii, T., Noguchi, S., Takayama, T., Suzuki, K., Yamamoto, K., Saeki, T. (2013). Site Selection and Formation Evaluation at the first Offshore Methane Hydrate Production Test Site in the Eastern Nankai Trough, Japan. 75th EAGE Conference & Exhibition incorporating SPE EUROPEC 2013, London, UK, 10-13 June 2013.
- Gaddipati, M. (2008). Code Comparison of Methane Hydrate Reservoir Simulators using CMG STAR. MSc Thesis. Department of Chemical Engineering, West Virginia University, USA.

- Gamwo, I. K., and Liu, Y. (2010). Mathematical Modeling and Numerical Simulation of Methane Production in a Hydrate Reservoir. *Industrial and Engineering Chemistry Research*, 49(11), 5231–5245.
- Garapati, N. (2013). Reservoir Simulation for Production of CH<sub>4</sub> from Gas Hydrate Reservoirs Using CO<sub>2</sub>/CO<sub>2</sub>+N<sub>2</sub> by HydrateResSim. PhD Thesis. Department of Chemical Engineering Morgantown, West Virginia.
- Geng, C.-Y., Wen, H., and Zhou, H. (2009). Molecular simulation of the potential of methane reoccupation during the replacement of methane hydrate by CO<sub>2</sub>. *The Journal of Physical Chemistry. A*, 113(18), 5463–5469.
- Giavarini, C., Hester K. (2011). *Gas Hydrates: Immense Energy Potential and Environmental Challenges*. Springer, New York.
- Ginsburg, G. D. (1998). Gas hydrate accumulation in deep-water marine sediments. In: Henriot, J.-P. and Mienert, J. (eds) *Gas Hydrates: Relevance to World Margin Stability and Climate Change*. Geological Society, London, Special Publications, 137, 51-62.
- Gudmundsson, J.S., Hveding, F., Bomhaug, A. (1995). Transport of Natural Gas as Frozen Hydrate. *Proceedings of the Fifth (1995) International Offshore and Polar Engineering Conference*, The Hague, The Netherlands, June 11-16, 1995.
- Gupta, A. (2007) *Methane Hydrate Dissociation Measurements and Modelling: The Role of Heat Transfer and Reaction Kinetics*. PhD Thesis. Colorado School of Mines, USA.
- Goel, N. (2006). In situ methane hydrate dissociation with carbon dioxide sequestration: Current knowledge and issues. *Journal of Petroleum Science and Engineering*, 51(3-4), 169–184.
- Gong, Z., Zhang, L., Cheng, H., Wang, Y., Qi, D. and Ren, S. (2016) ‘Productivity and feasibility analysis of gas production from subsea sediment bearing with natural gas hydrate’, *Int. J. Oil, Gas and Coal Technology*, Vol. 11, No. 3, pp.229–248.
- Haeckel, M., Bialas, J., Klaucke, I., Wallmann, K., Bohrmann, G., Schwalenberg, K., SUGAR participants, (2015). Gas Hydrate Occurrences in the Black Sea – New Observations from the German Sugar Project. *Fire in the Ice. Methane Hydrate Newsletter*. 2015 Vol. 15, Issue 2.

- Halliday, W., Dennis, K., Clapper, Smalling, M., (1998): “New Gas Hydrate Inhibitors for Deepwater Drilling Fluids”, SPE 39316, Proc. of the 1998 IADC/SPE Drilling Conference, Dallas, Texas 3-6 March, pp. 201-211.
- Hammerschmidt, E.G. (1934). Formation of Gas Hydrates in Natural Gas Transmission Lines. *Ind. Eng. Chem.*, 1934, 26 (8), pp 851–855.
- Han, H., Wang, Y., Li, X.S., Yu, J.X., Feng, J.C., Zhang, Y. (2016). Experimental study on sediment deformation during methane hydrate decomposition in sandy and silty clay sediments with a novel experimental apparatus. *Fuel* 182 (2016) 446–453.
- Handa, Y.P., (1986). Compositions, enthalpies of dissociation, and heat capacities in the range 85 to 270 K for clathrate hydrates of methane, ethane, and propane, and enthalpy of dissociation of isobutane hydrate, as determined by a heat-flow calorimeter, *J. Chem. Thermodynamics*, 18, 915–921.
- Hao, W., Wang, J., Fan, S., Hao, W. (2008). Evaluation and analysis method for natural gas hydrate storage and transportation processes. *Energy Conversion and Management* 49 (2008) 2546–2553.
- Hao, Y., Xu, C., and Li, S. (2012). Study on the Effect of Heat Injection Rate during NGH Exploitation by Thermal Stimulation. *International Journal of Advancements in Computing Technology* 4, 2012, 550–557.
- Heeschen, K. U., Haeckel, M., Klaucke, I., Ivanov, M. K., and Bohrmann, G. (2011). Quantifying in-situ gas hydrates at active seep sites in the eastern Black Sea using pressure coring technique. *Biogeosciences*, 8(12), 3555–3565.
- Heeschen, K.U., Abendroth, S., Priegnitz, M., Spangenberg, E., Thaler, J., Schicks, J.M. (2016). Gas Production from Methane Hydrate: A Laboratory Simulation of the Multistage Depressurization Test in Mallik, Northwest Territories, Canada. *Energy Fuels* 2016, 30, 6210–6219.
- Heeschen, K.U., Schicks, J.M., Oeltzschner, G. (2016b). The promoting effect of natural sand on methane hydrate formation: Grain sizes and mineral composition. *Fuel* 181 (2016) 139–147.
- Henningses, J., J. Schroetter, K. Erbas, and E. Huenges (2004), Temperature field of the Mallik gas hydrate occurrence - implications on phase changes and thermal properties, in *Scientific Results from Mallik 2002 Gas Hydrate Production*

- Research Well Program, Mackenzie Delta, Northwest Territories, Canada, edited by S.R. Dallimore, and T.S. Collett, Geological Survey of Canada.
- Hesse, R., Schacht, U. (2011), Early Diagenesis of Deep-Sea Sediments. In Hüneke, H., Mulder, T., editors: *Developments in Sedimentology*, Vol. 63, Amsterdam: The Netherlands, 2011, pp. 557-713.
- Hester, K. C., Dunk, R. M., White, S. N., Brewer, P. G., Peltzer, E. T., and Sloan, E. D. (2007). Gas hydrate measurements at Hydrate Ridge using Raman spectroscopy. *Geochimica et Cosmochimica Acta*, 71(12), 2947–2959.
- Holditch, S.A., Patzek, T., Rutqvist, J., Moridis, G., Plumb, R. (2008). *Geomechanical Performance of Hydrate-Bearing Sediment in Offshore Environments*. United States: N. p., 2008. Doi: 10.2172/947014.
- Huang, L., Su, Z., Wu, N.Y. (2015). Evaluation on the gas production potential of different lithological hydrate accumulations in marine environment. *Energy* 91 (2015) 782-798.
- Huang, L., Su, Z., Wu, N., Cheng, J., (2016). Analysis on geologic conditions affecting the performance of gas production from hydrate deposits, *Marine and Petroleum Geology*, 77 (2016), 19-29.
- Hester, K.C. and Brewer, P.G., (2009). Clathrate Hydrates in Nature. *Annu. Rev. Marine. Sci.* 2009.1:303-327.
- Huang, Y.J., Wu, C.Y., Hsieh, B.Z. (2016). Effect of Fluid Saturation on Gas Recovery from Class-3 Hydrate Accumulations Using Depressurization: A Case Study of the Yuan-An Ridge Site in Southwestern Offshore Taiwan. *Energy Procedia* 97 (2016) 310 – 317.
- Hunt, J.M., Whelan, J.K. (1978). Dissolved Gases in Black Sea Sediments. <https://doi.org/10.2973/dsdp.proc.42-2.125.1978>
- Hunt, J. M., (1995), *Petroleum Geochemistry and Geology*: Freeman, New York, 1995.
- Hutta, H. (2012). “Is the Black Sea the Next North Sea?” presented in: IENE 2012-6<sup>th</sup> South East Europe Energy Dialogue, Thessaloniki, Greece, May 30-31, 2012.
- Hüneke, H., Mulder, T. (2011), *Deep-Sea Sediments. Developments in Sedimentology*, Vol. 63, Amsterdam: The Netherlands, 2011.

- Hydrafact (2016). “HydraFLASH Software”. Retrieved from (Accessed on May 17, 2016): <http://www.hydrafact.com/>
- Hyodo, M., Yoneda, J., Yoshimoto, N., and Nakata, Y. (2013). Mechanical and dissociation properties of methane hydrate-bearing sand in deep seabed. *Soils and Foundations*, 53(2), 299–314.
- Hyodo, M., Li, Y., Yoneda, J., Nakata, Y., Yoshimoto, N., and Nishimura, A. (2014). Effects of dissociation on the shear strength and deformation behavior of methane hydrate-bearing sediments. *Marine and Petroleum Geology*, 51, 52–62.
- Hyodo, M., Nakata, Y., Yoshimoto, N., Orense, R., Yoneda, J., Nakagawa, M., and Luding, S. (2009). Bonding Strength by Methane Hydrate Formed among Sand Particles. *AIP Conference Proceedings*, 79(2015), 79–82.
- Hyodo, M., Li, Y., Yoneda, J., Nakata, Y., Yoshimoto, N., Kajiyama, S., Nishimura, A., Song, Y. (2014b). A comparative analysis of the mechanical behavior of carbon dioxide and methane hydrate-bearing sediments. *American Mineralogist*, 99(1), 178–183.
- IAPWS-IF97 (2007). The International Association for the Properties of Water and Steam, Lucerne, Switzerland August 2007. Retrieved from (Accessed on November, 1, 2015): <http://www.iapws.org/relguide/IF97-Rev.pdf>
- Innosys (2016). Innosys Innovative Systems, contact: [cemal@innosys.com.tr](mailto:cemal@innosys.com.tr)
- Ito, T., Komatsu, Y., Fujii, T., Kiyofumi, S., Egawa, K., Nakatsuka, Y., Konno, Y., Yoneda, J., Jin, Y., Kida, M., Nagao, J., Minagawa, H. (2015). Lithological features of hydrate-bearing sediments and their relationship with gas hydrate saturation in the eastern Nankai Trough, Japan. *Marine and Petroleum Geology*, 66 (2015) 368-378.
- Ivanov, M.K., Limonov, A.F., Woodside, J.M. (1998) Extensive deep fluid flux through the sea floor on the Crimean continental margin (Black Sea) In: Henriot, J.-P. and Mienert, J. (eds) 1998. *Gas Hydrates: Relevance to World Margin. Stability and Climate Change*. Geological Society, London, Special Publications, 137.
- Jager, M.D. and Sloan, E.D. (2001). The Effect of Pressure on Methane Hydration in Pure Water and Sodium Chloride Solutions, *Fluid Phase Equilibria* (2001) 185, 89-99.

- Jager, M.D., Peters, C.J., and Sloan, E.D., (2002). Experimental Determination of Methane Hydrate Stability in Methanol and Electrolyte Solutions. *Fluid Phase Equilibria* (2002) 193, 17.
- Janicki, G., Schlüter, S., Hennig, T., Deerberg, G. (2014). Simulation of subsea gas hydrate exploitation. *Energy Procedia* 59 (2014), 82-89.
- Jang, J., Santamarina, J.C. (2014), Evolution of gas saturation and relative permeability during gas production from hydrate-bearing sediments: Gas invasion vs. gas nucleation, *J. Geophys. Res. Solid Earth*, 119, 116–126.
- Jang, J., Santamarina, J.C. (2016). Hydrate bearing clayey sediments: Formation and gas production concepts. *Marine and Petroleum Geology* 77 (2016) 235-246.
- Jegen, M., Hölz, S. (2014). Marine CSEM gas hydrate exploration in the Danube Delta, Black Sea. Retrieved from (Accessed on December 1, 2016): [http://www.giraf-network.org/EN/Themen/MarineRohstoffforschung/Projekte/HC-Potential-of-continental-margins/Laufend/MSM35\\_BlackSea\\_Merian.html](http://www.giraf-network.org/EN/Themen/MarineRohstoffforschung/Projekte/HC-Potential-of-continental-margins/Laufend/MSM35_BlackSea_Merian.html)
- Johnson, A.H. (2011). Global Resource Potential of Gas Hydrate—A New Calculation. *Proceedings of the 7<sup>th</sup> International Conference on Gas Hydrates (ICGH 2011)*, Edinburgh, Scotland, United Kingdom, July 17-21, 2011.
- Johnson, A., Patil, S., and Dandekar, A. (2011). Experimental investigation of gas-water relative permeability for gas-hydrate-bearing sediments from the Mount Elbert Gas Hydrate Stratigraphic Test Well, Alaska North Slope. *Marine and Petroleum Geology*, 28(2), 419–426.
- Johnson, A., Max, M.D. (2015), Natural Gas Hydrate Workshop, Dokuz Eylul University Marine Sciences Institute, February 23-24, 2015, Izmir, Turkey.
- Kang, H., Koh, D., and Lee, H. (2014). Nondestructive natural gas hydrate recovery driven by air and carbon dioxide. *Scientific Reports*, 4, 6616.
- Kang, S., Ryu, H., and Seo, Y. (2007). Phase Behavior of CO<sub>2</sub> and CH<sub>4</sub> Hydrate in Porous Media, *International Journal of Chemical, Nuclear, Metallurgical and Materials Engineering* Vol: 1, No: 9, 2007.
- Kamath, V.A., (1984). Study of Heat Transfer Characteristics during Dissociation of Gas Hydrates in Porous Media, Ph.D. Dissertation, University of Pittsburgh, PA.

- Kawamura, T., Ohtake M., Sakamoto, Y., Yamamoto, Y., Haneda, H., Komai, T., Higuchi, S. (2007). Experimental Study on Steam Injection Method using Methane Hydrate Core Samples., 83–86. Proceedings of the Seventh (2007) ISOPE Ocean Mining Symposium Lisbon, Portugal, July 1-6, 2007.
- Kawamoto, T. (2014). Methane Hydrate R&D in Japan. CSIS Seminar, September 17, 2014. Retrieved from (Accessed on January 1, 2017): [sis-prod.s3.amazonaws.com](http://sis-prod.s3.amazonaws.com)
- Kenyon, N.H., Ivanov, M.K., Akhmetzhanov, A.M., Akhmanov, G.G., (2001). Geological Processes in the Mediterranean and Black Seas and North East Atlantic- Preliminary results of investigations during the TTR-11 cruise of RV Professor Logachev July-September, 2001. Intergovernmental Oceanographic Commission technical series 62. SC-2002/WS/62.
- Katz, D.I (1959). Handbook of Natural Gas Engineering, McGraw-Hill, New York, 1959.
- Kessler J.D., Reeburgh W.S., Southon J., Seigert R., Michaelis, W., Tyler, S.C., (2006) Basin-wide estimates of the input of methane from seeps and clathrates to the Black Sea. *Earth and Planet. Sci. Letts.* 2006; 243:366-375.
- Kida, M., Hachikubo, A., Sakagami, H., Minami, H., Krylov, A., Yamashita, Takahashi, N., Shoji, H., Narita, H. (2009). Natural gas hydrates with locally different cage occupancies and hydration numbers in Lake Baikal. *Geochemistry, Geophysics, Geosystems*, 10 (2009), 1–8.
- Kida, M., Jin, Y., Watanabe, M., Konno, Y., Yoneda, J., Egawa, K., Ito, T., Nakatsuka, Y., Suzuki, K., Fujii, T., Nagao, J. (2015). Chemical and crystallographic characterizations of natural gas hydrates recovered from a production test site in the eastern Nankai Trough. *Marine and Petroleum Geology*, 66, 396–403.
- Kim, H.C., Bishnoi, P.R., Heidemann, R.A., Rizvi, S.H., (1987). Kinetics of methane hydrate decomposition. *Chem.Eng.Sci.* 42, 7:1645-1653, 1987.
- Kim, J. H., Torres, M. E., Hong, W. L., Choi, J., Riedel, M., Bahk, J. J., and Kim, S. H. (2013). Pore fluid chemistry from the Second Gas Hydrate Drilling Expedition in the Ulleung Basin (UBGH2): Source, mechanisms and consequences of fluid

- freshening in the central part of the Ulleung Basin, East Sea. *Marine and Petroleum Geology*, 47, 99–112.
- Kim, A.R., Cho, G.C., Song, K.I., Kim, S.J. (2014). Settlement Prediction in The Ulleung Basin Due to Gas Hydrate Production. The Offshore Technology Conference (OTC-25308-MS), Houston, Texas, USA, 5–8 May 2014.
- Kirby, S.H., Circone, S., Stern, L.A., Pinkston, J. (2004). USGS Laboratory Studies Shed Light on Hydrate Decomposition Behavior under Possible Gas Production Scenarios. *Methane Hydrate Newsletter*. Vol.4 Iss.3, 2004.
- Klapp, S.A. (2009). Natural Gas Hydrates – from the Microstructure towards a Geological Understanding. PhD Thesis, im Fachbereich Geowissenschaften der Universität Bremen, Germany.
- Klaucke, I., Sahling, H., Weinrebe, W., Bohrmann, G., Ivanov, M.K. (2005). Mud volcanoes and other types of cold seeps in the Black Sea: morphologies, settings and processes. *Fluid Seepages / Mud Volcanism in the Mediterranean and Adjacent Domains – Bologna*, 19 - 22 October 2005.
- Klauda, J. B., and Sandler, S. I. (2000). A Fugacity Model for Gas Hydrate Phase Equilibria. *Industrial and Engineering Chemistry Research*, 39, 3377–3386.
- Klauda, J. B., and Sandler, S. I. (2003). Predictions of gas hydrate phase equilibria and amounts in natural sediment porous media. *Marine and Petroleum Geology*, 20(5), 459–470.
- Kleinberg, R.L. (2009). Exploration strategy for economically significant accumulations of marine gas hydrate. *Geological Society, London, Special Publications* 2009; v. 319; p. 21-28.
- Krason, J., Ciesnik, M. (1988). Basin analysis, formation, and stability, in the Black Sea. In: *Geological Evolution and Analysis of Confirmed or Suspected Gas Hydrate Localities*, v.11. US Department of Energy, p. 88. DOE/MC/21181e1950(DE80001057).
- Kumar, A., Maini, B., Bishnoi, P.R., Clarke, M., Zatsepina, O., Srinivasan, S. (2010). Experimental determination of permeability in the presence of hydrates and its effect on the dissociation characteristics of gas hydrates in porous media. *Journal of Petroleum Science and Engineering* 70 (2010) 114–122.

- Kumar, A., Sakpal, T., Roy, S., Kumar R. (2015). Methane hydrate formation in a test sediment of sand and clay at various levels of water saturation. *Canadian Journal of Chemistry*, 2015, 93(8): 874-881.
- Kumar, P., Collett, T., Vishwanath, K., Shukla, K.M., Nagalingam, J., Lall, M.V., Yamada, Y., Schultheiss, P., Holland, M. (2016). Gas Hydrate-Bearing Sand Reservoir Systems in the Offshore of India: Results of the India National Gas Hydrate Program Expedition 02. *Fire in Ice, Hydrate News Letter*, 2016 Vol. 16, Issue 1.
- Kumar, P. (2016). Gas Hydrates: An Unconventional Resource Horizon for India. Retrieved from (Accessed on January 11, 2017): <https://www.spe.org/en/twa/twa-article-detail/?art=2143>
- Kungrani, S., Joshi, K., Prof, G., and Jadhao, P. R. S. (2016). Applications of Hydrate Technology in Food Industry: A Review of Experimental Studies. *International Conference on Global Trends in Engineering, Technology and Management (ICGTETM-2016)*, 215–219. ISSN: 2231-5381.
- Kuprin, P.N., Stecherbakov, F.A., Poljakov, A.S., Shlikov, V.G., Nesterova, M.P. (1978). Physical and Mechanical Properties of the Black Sea's Pliocene–Quaternary Sediments (Sites 380 and 381). <https://doi.org/10.2973/dsdp.proc.42-2.153.1978>
- Kurihara, M., Ouchi, H., Narita, H., Masuda, Y. (2011). “Gas Production from Methane Hydrate Reservoirs”. *Proceedings of the 7th International Conference on Gas Hydrates (ICGH 2011)*, Edinburgh, Scotland, United Kingdom, July 17-21, 2011.
- Küçük, H.M., Dondurur, D., Özel, Ö. Parlaktuna, M., Sınyuç, Ç., Çiftçi, G., Merey, Ş., Darılmaz, E. (2013). “Gas Hydrate Potential Offshore Amasra-Zonguldak and Possible Reasons for Multiple BSR Reflection Occurrence”, 20th International Geophysical Congress and Exhibition, November 25-27, 2013, Antalya, Turkey.
- Küçük, H.M., Dondurur, D., Özel, Ö., Sınyuç, Ç., Merey, Ş., Parlaktuna, M., Çiftçi, G., the SeisLab Team, (2015). Gas and Gas Hydrate Potential Offshore Amasra, Bartın and Zonguldak and Possible Agent for Multiple BSR Occurrence *Geophysical Research Abstracts Vol. 17, EGU2015-10310-1*, 2015 EGU General Assembly 2015.

- Küçük, H.M., Dondurur, D., Özel, Ö., Sınayuç, Ç., Merey, Ş., Parlaktuna, M., Çifçi, G. (2015b). “Acoustic Investigations of Gas and Gas Hydrate Formations, offshore southwestern Black Sea.”. American Geophysical Union-Fall Meeting, December 14-18, 2015, San Francisco, USA.
- Küçük, H.M. (2016). Geological and Geophysical Investigations of Gas and Gas Hydrates Offshore Zonguldak - Amasra, The Western Black Sea. PhD Thesis, Institute of Marine Sciences and Technology - Dokuz Eylul University, İzmir, Turkey.
- Küçük, H.M., Goldberg, D.S., Haines, S.S., Dondurur, D., Guerin, G., Çifçi, G. (2016b). Acoustic Investigations of Shallow Gas and Gas Hydrates: Comparison Between the Black Sea and the Gulf of Mexico. Gordon Research Seminars - Natural Gas Hydrate Systems, February 28 - March 4, 2016, At Galveston, Houston, Texas.
- Kobayashi, R., Song, K.Y., and Sloan, E.D (1987). Phase Behavior of Water/Hydrocarbon Systems. Quoted in Bradley, H.B., Petroleum Engineers Handbook, and Richardson: Society of Petroleum Engineers, 1987.
- Koh, C.A., Sloan, E.D., Sum, A.K. and Wu, D.T (2012). Unconventional energy sources: gas hydrates. In Ginley, D. S., and Cahen, D. (2012). Fundamentals of materials for energy and environmental sustainability. (pp 137-146.) Cambridge University Press and Materials Research Society.
- Koh, D.-Y., Kang, H., Lee, J.-W., Park, Y., Kim, S.-J., Lee, J., Park, Y., Kim, S., Lee, H. (2016). Energy-efficient natural gas hydrate production using gas exchange. *Applied Energy*, 162, 114–130.
- Korsakov, O., Byakov, U., Stupak, S., (1989). Gas Hydrates in the Black Sea. Basin. -Sov.Geologia 12, 3-10.
- Konerding, P. (2009). Quaternary tectonics and seismic stratigraphy of the western Black Sea shelf. PhD Thesis. zur Erlangung des Doktorgrades der Naturwissenschaften im Department Geowissenschaften der Universität Hamburg.
- Konno, Y., Masuda, Y., Hariguchi, Y., Kurihara, M., and Ouchi, H. (2010). Key factors for depressurization-induced gas production from oceanic methane hydrates. *Energy and Fuels*, 24(3), 1736–1744.

- Konno, Y., Oyama, H., Nagao, J., Masuda, Y., and Kurihara, M. (2010b). Numerical Analysis of the Dissociation Experiment of Naturally Occurring Gas Hydrate in Sediment Cores Obtained at the Eastern Nankai Trough, Japan. *Energy and Fuels*, 24(12), 6353–6358.
- Konno, Y., Uchiumi, T., Oyama, H., Jin, Y., Nagao, J., Masuda, Y., and Ouchi, H. (2012). Dissociation behavior of methane hydrate in sandy porous media below the quadruple point. *Energy and Fuels*, 26(7), 4310–4320.
- Konno, Y., Jin, Y., Shinjou, K., and Nagao, J. (2014). Experimental evaluation of the gas recovery factor of methane hydrate in sandy sediment. *RSC Adv.*, 4, 51666–51675.
- Konno, Y., Yoneda, J., Egawa, K., Ito, T., Jin, Y., Kida, M., Suzuki, K., Fuji, T., Nagao, J. (2015). Permeability of sediment cores from methane hydrate deposit in the Eastern Nankai Trough. *Marine and Petroleum Geology*, 66, 487–495.
- Konno, Y., Masuda, Y., Akamine, K., Naiki, M., and Nagao, J. (2016). Sustainable gas production from methane hydrate reservoirs by the cyclic depressurization method. *Energy Conversion and Management*, 108, 439–445.
- Komatsu, H., Ota, M., Smith, R. L., and Inomata, H. (2013). Review of CO<sub>2</sub>–CH<sub>4</sub> clathrate hydrate replacement reaction laboratory studies – Properties and kinetics. *Journal of the Taiwan Institute of Chemical Engineers*, 44(4), 517–537.
- Komatsu, Y., Suzuki, K., and Fujii, T. (2016). Sequence stratigraphy and controls on gas hydrate occurrence in the eastern Nankai Trough, Japan. *Interpretation*, 4(1), SA73-SA81.
- Kowalsky, M. B., and Moridis, G. J. (2007). Comparison of kinetic and equilibrium reaction models in simulating gas hydrate behavior in porous media. *Energy Conversion and Management*, 48(6), 1850–1863.
- Kvamme, B. (2015). Feasibility of simultaneous CO<sub>2</sub> storage and CH<sub>4</sub> production from natural gas hydrate using mixtures of CO<sub>2</sub> and N<sub>2</sub>. *Canadian Journal of Chemistry*, 93(8), 897–905.
- Kvamme, B. (2016). Thermodynamic Limitations of the CO<sub>2</sub>/N<sub>2</sub> Mixture Injected into CH<sub>4</sub> Hydrate in the Ignik Sikumi Field Trial. *J. Chem. Eng. Data*. DOI: 10.1021/acs.jced.5b00930.

- Kvenvolden, K.A. (1993). Geological Perspective and Global Change. *Reviews of Geophysics*. Pp 173-187 (93RG00268)
- Kvenvolden K., (1995). A review of the geochemistry of methane in natural gas hydrate. *Org. Geochem.* 1995, 23, 997–1008.
- Kvenvolden, K.A. (2002). Methane hydrate in the global organic carbon cycle. *Terra Nova*, Vol 14, No. 5, 302–306.
- Kwon, T. H., and Cho, G. C. (2012). Submarine slope failure primed and triggered by bottom water warming in oceanic hydrate-bearing deposits. *Energies*, 5(8), 2849–2873.
- Laherrere, J. (2000). Oceanic Hydrates: More Questions than Answers. *Energy Exploration and Exploitation*, 18: 349-383.
- Le Quang, D., Le Quang, D., Bouillot, B., Herri, J.-M., Glenat, P., and Duchet-Suchaux, P. (2016). Experimental procedure and results to measure the composition of gas hydrate, during crystallization and at equilibrium, from N<sub>2</sub>–CO<sub>2</sub>–CH<sub>4</sub>–C<sub>2</sub>H<sub>6</sub>–C<sub>3</sub>H<sub>8</sub>–C<sub>4</sub>H<sub>10</sub> gas mixtures. *Fluid Phase Equilibria*, 413, 10–21.
- Lee, J. Y., Yun, T. S., Santamarina, J. C., and Ruppel, C. (2007). Observations related to tetrahydrofuran and methane hydrates for laboratory studies of hydrate-bearing sediments. *Geochemistry, Geophysics, Geosystems*, 8, 1–10.
- Lee, Y., Kim, Y., and Seo, Y. (2015). Enhanced CH<sub>4</sub> Recovery Induced via Structural Transformation in the CH<sub>4</sub>/CO<sub>2</sub> Replacement That Occurs in sH Hydrates. *Environmental Science and Technology*, 49(14), 8899–8906.
- Li, X.-S., Wan, L.-H., Li, G., Li, Q.-P., Chen, Z.-Y., and Yan, K.-F. (2008). Experimental Investigation into the Production Behavior of Methane Hydrate in Porous Sediment with Hot Brine Stimulation. *Industrial and Engineering Chemistry Research*, 47(23), 9696–9702.
- Li, X. S.; Zhang, Y.; Li, G.; Chen, Z. Y.; Yan, K. F.; Li, Q. P. (2008b). Gas hydrate equilibrium dissociation conditions in porous media using two thermodynamic approaches. *J. Chem. Thermodyn.* 2008, 40 (9), 1464– 1474.
- Li, X. Sen, Zhang, Y., Li, G., Chen, Z. Y., and Wu, H. J. (2011). Experimental investigation into the production behavior of methane hydrate in porous sediment by depressurization with a novel three-dimensional cubic hydrate simulator. *Energy and Fuels*, 25, 4497–4505.

- Li, B., Li, G., Li, X., Li, Q., Yang, B., Zhang, Y., and Chen, Z. (2012). Gas Production from Methane Hydrate in a Pilot-Scale Hydrate Simulator Using the Huff and Puff Method by Experimental and Numerical Studies. *Energy and Fuels*, 29, 7183–7194.
- Li, S., Jiang, X., and Liu, C. (2012b). The simulation of gas production from hydrates by depressurization at a constant pressure. *Petroleum Science and Technology*, 30(9), 855–863.
- Li, W., Gong, J., Lü, X., Zhao, J., Feng, Y., Yu, D. (2013). A study of hydrate plug formation in a subsea natural gas pipeline using a novel high-pressure flow loop. *Petroleum Science*, March 2013, Volume 10, Issue 1, pp 97-105.
- Li, G., Li, X.-S., Zhang, K., Li, B., and Zhang, Y. (2013b). Effects of Impermeable Boundaries on Gas Production from Hydrate Accumulations in the Shenhu Area of the South China Sea. *Energies*, 6(8), 4078–4096.
- Li, B., Li, X. Sen, Li, G., Feng, J. C., and Wang, Y. (2014). Depressurization induced gas production from hydrate deposits with low gas saturation in a pilot-scale hydrate simulator. *Applied Energy*, 129, 274–286.
- Li, B., Li, X. Sen, and Li, G. (2014b). Kinetic studies of methane hydrate formation in porous media based on experiments in a pilot-scale hydrate simulator and a new model. *Chemical Engineering Science*, 105, 220–230.
- Li, C. H., Zhao, Q., Xu, H. J., Feng, K., and Liu, X. W. (2014c). Relation between relative permeability and hydrate saturation in Shenhu area, South China Sea. *Applied Geophysics*, 11(2), 207–214.
- Li, B., Liang, Y. P., Li, X. Sen, and Wu, H. J. (2015). Numerical analysis of methane hydrate decomposition experiments by depressurization around freezing point in porous media. *Fuel*, 159, 925–934.
- Li, S., Shen, Y., Liu, D., Fan, L., Zhang, Z., Li, W., Tan, Z., Li, W., Bai, J. (2016). Measurement and Prediction of Hydrate Phase Equilibrium of Orange Juice + CO<sub>2</sub>, C<sub>2</sub>H<sub>4</sub> or C<sub>2</sub>H<sub>6</sub> for Orange Juice Concentration. *Advance Journal of Food Science and Technology*, 10(12), 890–893.
- Li, S., Zheng, R., Xu, X., and Hou, J. (2016b). Energy efficiency analysis of hydrate dissociation by thermal stimulation. *Journal of Natural Gas Science and Engineering*, 30, 148–155.

- Li, X.-S., Xu, C.-G., Zhang, Y., Ruan, X.-K., Li, G., and Wang, Y. (2016c). Investigation into gas production from natural gas hydrate: A review. *Applied Energy*, 172, 286–322.
- Liang, D. L., Liang, D. Q., Fan, S. S., Li, X. S., Tang, L. G., and Huang, N. S. (2008). In situ hydrate dissociation using microwave heating: Preliminary study. *Energy Conversion and Management*, 49, 2207–2213.
- Liang, H., Song, Y., and Chen, Y. (2010). Numerical simulation for laboratory-scale methane hydrate dissociation by depressurization. *Energy Conversion and Management*, 51(10), 1883–1890.
- Liang, H., Song, Y., Chen, Y., and Liu, Y. (2011). The Measurement of Permeability of Porous Media with Methane Hydrate. *Petroleum Science and Technology*, 29(1), 79–87.
- Lim, D., Ro, H., Seo, Y., Lee, J.Y., Lee, J., Kim, S.J., Park, Y., Lee, H. (2016). Electrical Resistivity Measurements of Methane Hydrate during N<sub>2</sub>/CO<sub>2</sub> Gas Exchange. *Energy Fuels*. DOI: 10.1021/acs.energyfuels.6b01920
- Lim, D., Ro, H., Seo, Y., Seo, Y., Lee, J.Y., Kim, S., Lee, J., Lee, H. (2017). Thermodynamic stability and guest distribution of CH<sub>4</sub>/N<sub>2</sub>/CO<sub>2</sub> mixed hydrates for methane hydrate production using N<sub>2</sub>/CO<sub>2</sub> injection. *J. Chem. Thermodynamics* 106 (2017) 16–21.
- Liu, Y., Gamwo, I.K. (2012). Comparison between equilibrium and kinetic models for methane hydrate dissociation. *Chemical Engineering Science* 69 (2012) 193–200.
- Liu, C., Meng, Q., He, X., Li, C., Ye, Y., Lu, Z., Zu, Y., Li, Y., Liang, J. (2015). Comparison of the characteristics for natural gas hydrate recovered from marine and terrestrial areas in China. *Journal of Geochemical Exploration*, 152 (2015), 67–74.
- Liu, W., Luo, T., Li, Y., Song, Y., Zhu, Y., Liu, Y., Zhao, J., Wu, Z., Xu, X., (2016). Experimental study on the mechanical properties of sediments containing CH<sub>4</sub> and CO<sub>2</sub> hydrate mixtures, *Journal of Natural Gas Science and Engineering*, 32 (2016), 20-27.
- Lu, S., and McMechan, G. (2002). Estimation of gas hydrate and free gas saturation, concentration, and distribution from seismic data. *Geophysics*, 67(2), 582.

- Lohrenz, J., Clark, G.C., and Francis, R.J. (1963). "A Compositional Material Balance for Combination Drive Reservoirs with Gas and Water Injection," JPT (November 1963) 1233; Trans., AIME, 228.
- Long, D., Lovell, M. A., Rees, J. G. and Rochelle, C. A. (2009). Sediment Hosted Gas Hydrates: New Insights on Natural and Synthetic Systems. Geological Society, London, Special Publications, 319.
- Long, X., Tjok, K., Adhikari, S. (2016). Numerical Investigation on Gas Hydrate Production by Depressurization in Hydrate-Bearing Reservoir. Proceedings of the ASME 2016 35th International Conference on Ocean, Offshore and Arctic Engineering, OMAE2016, June 19-24, 2016, Busan, South Korea.
- Ma, Y.Z, Holditch, S.A. (2016). Unconventional Oil and Gas Resources Handbook: Evaluation and Development. Gulf Professional Publishing, USA.
- Majumdar, U (2015). The Role of Bottom Simulating Reflectors in Gas Hydrate Assessment. AGU Fall Meeting 2015. Retrieved from (Accessed on February 14, 2015):  
<https://fallmeeting.agu.org/2015/abstract/the-role-of-bottom-simulating-reflectors-in-gas-hydrate-assessment/>
- Majumdar, U., Cook, A.E., Shedd, W., Frye, M. (2016). The connection between natural gas hydrate and bottom simulating reflectors. Geophysical Research Letters, 43, 7044–7051.
- Mahabadi, N., Jang, J. (2014). Relative water and gas permeability for gas production from hydrate-bearing sediments. Geochemistry, Geophysics, Geosystems 15, 2346–2353.
- Maekawa, T. (1998) Equilibrium conditions of gas hydrate from mixtures of methane and ethane and out-line of experimental apparatus for gas hydrate synthesis in porous sediment. Bull. Geol. Surv. Japan 49, 501–507.
- Makogon, T. Y., Mehta, A. P., and Sloan, E. D. (1996). Structure H and Structure I Hydrate Equilibrium Data for 2,2-Dimethylbutane with Methane and Xenon. Journal of Chemical and Engineering Data, 41(2), 315–318.
- Makogon, Y. (1997). Hydrates of Hydrocarbons. PennWell Publishers Company, Tulsa, OK, USA.

- Makogon, Y. F., S. A. Holditch, and T. Y. Makogon, (2005), Russian field illustrates gas-hydrate production: *Oil and Gas Journal*, v. 103, p. 43-47.
- Marinakis, D., Varotsis, N., and Perissoratis, C. (2015). Gas hydrate dissociation affecting the permeability and consolidation behaviour of deep sea host sediment. *Journal of Natural Gas Science and Engineering*, 23, 55–62.
- Marshall, D. R., S. Saito and R. Kobayashi, (1964) “Hydrates at High Pressures: Part I. Methane–Water, Argon–Water, and Nitrogen–Water Systems,” *AIChE J.* 10, 202–205(1964).
- Maslin, M., Owen, M., Betts, R., Day, S., Jones, T.D., Ridgwell, A. (2010). Gas hydrates: past and future geohazard? *Phil. Trans. R. Soc. A* (2010) 368, 2369–2393.
- Masuda, Y.; Fujinaga, Y.; Naganawa, S. (1999). Modeling and experiment studies on dissociation of methane gas hydrates in Berea sandstone cores. *Proceedings of the 3rd International Conference on Gas Hydrate*, Salt Lake City, UT, 1999.
- Masuda, Y., Hariguchi, Y., Konno, Y., Kurihara, M., Ouchi, H. (2010). Calculation on Economics of Depressurization-Induced Gas Production from Oceanic Methane Hydrates. *OTC 20787. 2010 Offshore Technology Conference*, Houston, Texas, USA, 3–6 May 2010.
- Matsumoto, R., Okuda, Y., Hiruta, A., Tomaru, H., Takeuchi, E., Sanno, R., Suzuki, M., Tsuchinaga, K., Ishida, Y., Ishizaki, O., Takeuchi, R., Komatsubara, J., Freire, A.F., Machiyama, H., Aoyama, C., Joshima, M., Hiromatsu, M., Snyder, G., Numanami, H., Satoh, M., Matoba, Y., Nakagawa, H., Kakuwa, Y., Ogihara, S., Yanagawa, K., Sunamura, M., Goto, T., Lu, H., Kobayashi, T. (2009). Formation and Collapse of Gas Hydrate Deposits in High Methane Flux Area of the Joetsu Basin, Eastern Margin of Japan Sea. *Journal of Geography* 118 (1) 43-71 2009.
- Max, M.D., (2003). *Natural Gas Hydrate in Oceanic and Permafrost Environments*. Kluwer Academic Publishers, Netherlands.
- Max, M.D., Johnson, A.H., Dillon, W.P. (2006). *Economic Geology of Natural Gas Hydrate*. Published by Springer.

- Max, M.D., Johnson, A.H., Dillon, W.P. (2013). Natural Gas Hydrate – Arctic Ocean Deepwater Resource Potential. Springer Cham Heidelberg New York Dordrecht London. <https://doi.org/10.1007/978-3-319-02508-7>
- Max, M.D.; Johnson, A.H. (2014). Hydrate petroleum system approach to natural gas hydrate exploration. *Petrol. Geosci.* 2014, 20, 187–199.
- Max, M. D.; Johnson, A. H. (2015). A fresh look at the Mediterranean and Black Sea Basins: Potential for high quality hydrate reservoirs. *Fire in the Ice* 2015, 15, (1), 15-18.
- Max, M.D., Johnson, A.H. (2016). Exploration and Production of Oceanic Natural Gas Hydrate. Springer, Switzerland. ISBN 978-3-319-43384-4.
- McNutt, M.K., R. Camilli, T.J. Crone, G.D. Guthrie, P.A. Hsieh, T.B. Ryerson, O. Savas, F. Shaffer. (2012). Review of flow rate estimates of the Deepwater Horizon oil spill. *Proceedings of the National Academy of Sciences* 109(50): 20260–20267.
- Meindinyo, R.E., Bøe, R., Svartås, T.M., Bru, S. (2015). Experimental Study on the Effect of Gas Hydrate Content on Heat Transfer. *Proceedings of the ASME 2015 34th International Conference on Ocean, Offshore and Arctic Engineering OMAE2015*, May 31-June 5, 2015, St. John's, Newfoundland, Canada.
- Melgar, E.P. (2009). Sedimentology and Geochemistry of Gas Hydrate-rich Sediments from the Oregon Margin (Ocean Drilling Program Leg 204). PhD Thesis, Universitat de Barcelona, Spain.
- Merey, S. (2013), Experimental Analysis of Adsorption Capacities and Behaviors of Shale Samples, MSc Thesis, Middle East Technical University, Ankara, Turkey, 2013.
- Merey, S., Sinayuc, C. (2015). “Simulation of Gas Production from Hydrate Reservoirs by using HydrateResSim Numerical Simulator”. 20<sup>th</sup> International Petroleum and Natural Gas Congress and Exhibition, May 29, 2015, Ankara, Turkey.
- Merey, S. (2016). Drilling of Gas Hydrate Reservoirs. *Journal of Natural Gas Science and Engineering*, 35, 1167-1179.

- Meyer, D. W., and Flemings, P. B. (2014). Thermodynamic State of Gas Hydrate in the Krishna-Godavari Basin Inferred from Well Log Analysis. OTC-25139-PT, Offshore Technology Conference, Houston, 5-8 May 2014.
- MH-21 Project Report (2008). Phase 1: Comprehensive Report of Research Results. August 2008 Edition. Retrieved from (Accessed on August 25, 2016): <http://www.mh21japan.gr.jp/english/wp/wp-content/uploads/ca434ff85adf34a4022f54b2503d86e92.pdf>
- Miller, B. and E.R. Strong, Jr, (1946). Hydrate storage of natural gas. Am. Gas Assoc. Monthly, 28: 63-67.
- Minagawa, H., Ito, T., Kimura, S., Kaneko, H., Noda, S., and Narita, H. (2015). Depressurization and Electrical Heating of Hydrate Sediment for Gas Production, 82–88.
- Minitab (2016). Minitab 17 Statistical Software. <https://www.minitab.com/en-us/products/minitab/>.
- Miyazaki, K., Yamaguchi, T., Sakamoto, Y., and Aoki, K. (2011). Time-dependent behaviors of methane-hydrate bearing sediments in triaxial compression test, 7(1), 43–48.
- Miwa, M., Yamashita, S., Itaya, K., Hachikuba, A., Sakagami, H., Yamasaki, S., Konishi, M., Minami, H., Kataoka, S. (2016). Tomaru, H., Honda, Y., Matsumoto, R. (2016). Japan Geoscience Union Meeting, May 22-26, 2016, Chiba, Japan.
- Mohammadi, A. H., and Tohidi, B. (2005). Prediction of Hydrate Phase Equilibria in Aqueous Solutions of Salt and Organic Inhibitor Using a Combined Equation of State and Activity Coefficient-Based Model. The Canadian Journal of Chemical Engineering, 83(5), 865–871.
- Moridis, G. J., Collett, T. S., (2003). From Hydrate Accumulations under Various Geological and Reservoir Conditions. Proceedings, Tough Symposium 2003. Lawrence Berkeley National Laboratory, Berkeley, California, May 12–14, 2003.
- Moridis, G. J. (2003). Numerical Studies of Gas Production from Methane Hydrates. SPE Journal, 8(4), 359–370.

- Moridis, G.J., Kowalsky, M.B, Pruess, K. (2005). ‘HydrateResSim User’s Manual: A Numerical Simulator for Modeling the Behavior of Hydrates in Geologic Media’. Earth Sciences Division, Lawrence Berkeley National Laboratory, Berkeley, CA 94720.
- Moridis, G. J., Seol, Y., Kneafsey, T. J. (2005b). Studies of Reaction Kinetics of Methane Hydrate Dissociation in Porous Media. Retrieved from (Accessed on April 1, 2015): <http://escholarship.org/uc/item/8q50w5cn>.
- Moridis, G.J. and Kowalsky, M.B. (2005). Gas Production from Unconfined Class2 Hydrate Accumulations in the Oceanic Subsurface. Report LBNL-57299, Lawrence Berkeley Natl. Laboratory, Berkeley, California.
- Moridis, G. J., Reagan, M. T., and Zhang, K. (2008). The Use of Horizontal Wells in Gas Production from Hydrate Accumulations. Proceedings of the 6<sup>th</sup> International Conference on Gas Hydrates (ICGH 2008), Vancouver, British Columbia, Canada, July 6-10, 2008.
- Moridis, G. J., Collett, T. S., Ray Boswell, Kurihara, M., Reagan, M. T., Koh, C., Sloan, E. D. (2008b). Toward production from gas hydrates: Current status, assessment of resources, and simulation-based evaluation of technology and potential. SPE Unconventional Reservoirs Conference, Keystone, Colorado, U.S.A., 10–12 February 2008.
- Moridis, G.J., Collett, T.S., Boswell, R., Hancock, S., Rutqvist, J., Santamarina, C., Kneafsey, T., Reagan, M.T., Darvish, M.P., Kowalsky, M., Sloan, E.D., Coh, C. (2013) Chapter 37: Gas Hydrates as a Potential Energy Source: State of Knowledge and Challenges-Lee, W.J. (ed.) Advanced Biofuels and Bioproducts, Springer Science+Business Media, New York 2013.
- Moridis, G. J., Kowalsky, M. B., and Pruess, K. (2013b). Depressurization-Induced Gas Production from Class-1 Hydrate Deposits. SPE Reservoir Evaluation and Engineering, 10(05), 458–481.
- Moridis, G.J. (2014). TOUGH+HYDRATE v1.2 User's Manual: A Code for the Simulation of System Behavior in Hydrate-Bearing Geologic Media. LBNL Paper LBNL-0149E-Rev.
- Motiee, M. (1991), “Estimate Possibility of Hydrates”, Hyd. Proc., P.98, July 1991.

- Mu, L., von Solms, N. (2016). Methane Production and Carbon Capture by Hydrate Swapping. *Energy & Fuels*, doi: 10.1021/acs.energyfuels.6b01638
- Murray, J. W. (1991). Black Sea oceanography. Results from the 1988 Black Sea expedition. *Deep Sea Res.* 38: S655–S126.
- Muratov, M.V., Neprochnov, Y.P., Ross, D.A., Trimonis, E.S. (1978) Basic Features of the Black Sea Late Cenozoic History Based on Results of Deep-Sea Drilling, Leg42B. <https://doi.org/10.2973/dsdp.proc.42-2.156.1978>
- Myshakin, E., Gaddipaati, M., Rose, K., Anderson, B. (2012). Numerical Simulation of Depressurization-Induced Gas Production from Gas Hydrate Reservoirs at the Walker Ridge 313 Site, Northern Gulf of Mexico. *Journal of Marine and Petroleum Geology*, 34, 169-185.
- Myshakin, E.M., Ajayi, T., Anderson, B.J., Seol, Y., Boswell, R. (2016). Numerical simulations of depressurization-induced gas production from gas hydrates using 3-D heterogeneous models of L-Pad, Prudhoe Bay Unit, North Slope Alaska. *Journal of Natural Gas Science and Engineering*, 35 (A), 1336–1352.
- Nagao, J. (2012). Development of methane hydrate production method- A large-scale laboratory reactor for methane hydrate production tests. *Synthesiology*, Vol.5 No.2 pp.89-97 (May 2012).
- Nago, A., and Nieto, A. (2011). Natural Gas Production from Methane Hydrate Deposits Using CO<sub>2</sub> Clathrate Sequestration: State-of-the-Art Review and New Technical Approaches. *Journal of Geological Research*, 2011, 1–6. <http://doi.org/10.1155/2011/239397>.
- Nakamura, T., Makino, T., Sugahara, T., Ohgaki, K. (2003) "Stability boundaries of gas hydrates helped by Methane-Structure-H hydrates of methylcyclohexane and cis-1,2-dimethylcyclohexane", *Chem. Eng.Sci*, vol. 58, pp. 269-273, 2003.
- Nakano, S., Moritoki, M., Ohgaki, K. (1999). High-Pressure Phase Equilibrium and Raman Microprobe Spectroscopic Studies on the Methane Hydrate System. *J. Chem. Eng. Data* 1999, 44, 254-257.
- Nandanwar, M.S., Anderson, B.J., Ajayi, T., Collett, T.S., Zyrianova, M.V. (2016) Evaluation of gas production potential from gas hydrate deposits in National Petroleum Reserve Alaska using numerical simulations, *Journal of Natural Gas Science & Engineering*, 36, Part A, November 2016, 760–772.

- Nasir, Q., Lau, K. K., and Lal, B. (2014). Enthalpies of Dissociation of Pure Methane and Carbon Dioxide Gas Hydrate. *International Journal of Chemical, Nuclear, Metallurgical and Materials Engineering*, 8(8), 785–788.
- Naudts L, Greinert J, Artemov Y, Staelens P, Poort J, Van Rensbergen P, and De Batist M., 2006. Geological and morphological setting of 2778 methane seeps in the Dnepr paleo-delta, northwestern Black Sea. *Marine Geology* 227:177-199.
- Naudts, L., Greinert, J., Artemov, Y., Beaubien, S.E., Borowski, C., De Batist, M. (2008). Anomalous sea-floor backscatter patterns in methane venting areas, Dnepr paleo-delta, NW Black Sea. *Marine Geology* 251 (2008) 253–267.
- Naudts, L., De Batist, M., Greinert, J., Artemov, Y. (2009). Geo and hydro-acoustic manifestations of shallow gas and gas seeps in the Dnepr paleodelta, northwestern Black Sea. *The Leading Edge* (2009), 28(9):1030.
- Neprochnov, Y. P. and Ross, D. A. (1978): Black Sea geophysical framework. <https://doi.org/10.2973/dsdp.proc.42-2.147.1978>.
- NIST. Thermophysical Properties of Fluid Systems (Accessed on February 11, 2016): <http://webbook.nist.gov/chemistry/fluid/>
- Nikishin, A. M., Korotaev, M. V., Ershov, A. V., and Brunet, M. F. (2003). The Black Sea basin: Tectonic history and Neogene-Quaternary rapid subsidence modelling. *Sedimentary Geology*, 156(1-4), 149–168.
- Ng, H.J., Chen, C.-J., Robinson, D.B., (1985). Gas Processors Association Research Report 92, September (1985).
- Ocakoğlu, N. (2009). Gaz Hidratlar ve Önemi: Türkiye Çevresi Denizlerde Gaz Hidrat ve Sığ Gaz Aramaları. *İstanbul Yerbilimleri Dergisi*, C. 22, S. 1, SS. 29-47, Y. 2009.
- Ohgaki, K.; Takano, K.; Sangawa, H.; Matsubara, T.; Nakano, S. (1996) Methane exploitation by carbon dioxide from gas hydrates-phase equilibria for CO<sub>2</sub>-CH<sub>4</sub> mixed hydrate system. *J. Chem. Eng. Jpn.* 1996, 29, 478–483.
- Okay, S. (2008). İstanbul Boğazı Karadeniz Çıkışının İncelenmesi. PhD. Thesis. Dokuz Eylül University, İzmir, Turkey.

- Ors, O. (2012). Investigation of the Interaction of CO<sub>2</sub> and CH<sub>4</sub> Hydrate for the Determination of Feasibility of CO<sub>2</sub> Storage in the Black Sea Sediments. Msc Thesis. Middle East Technical University, Ankara, Turkey.
- Ors, O., Sinayuc, C. (2014). An experimental study on the CO<sub>2</sub> - CH<sub>4</sub> swap process between gaseous CO<sub>2</sub> and CH<sub>4</sub> hydrate in porous media. "Journal of Petroleum Science and Engineering", 119, (2014), p.156 - 162.
- Oyama, H., Konno, Y., Masuda, Y., and Narita, H. (2009). Dependence of depressurization-induced dissociation of methane hydrate bearing laboratory cores on heat transfer. *Energy and Fuels*, 23(4), 4995–5002.
- Overmann, J., and Manske, A. K. 2006. Past and Present Water Column Anoxia. Leiden, the Netherlands: Springer.
- Østergaard, K.K., Masoudi, R., Tohidi, B., Danesh, A., Todd, A.C. (2005). A general correlation for predicting the suppression of hydrate dissociation temperature in the presence of thermodynamic inhibitors. *Journal of Petroleum Science and Engineering* 48 (2005) 70– 80.
- Özgür, E. (2016). Upstream Petroleum Law and activities in Turkey. *Energy Policy*, 88, 131–137.
- Paganoni, M., Cartwright, J. A., Foschi, M., Shipp, R. C., and Rensbergen, P. Van. (2016). Structure II gas hydrates found below the bottom simulating reflector. *Geophysical Research Letters*, 43, 11, 5696–5706.
- Pape, T., Bahr, A., Klapp, S.A., Abegg, F., Bohrmann, G. (2011). High-intensity gas seepage causes rafting of shallow gas hydrates in the southeastern Black Sea. *Earth and Planetary Science Letters* 307 (2011) 35–46.
- Park, Y., Kim, D.-Y., Lee, J.-W., Huh, D.-G., Park, K.-P., Lee, J., and Lee, H. (2006). Sequestering carbon dioxide into complex structures of naturally occurring gas hydrates. *Proceedings of the National Academy of Sciences of the United States of America*, 103(34), 12690–12694.
- Parlaktuna, M., Erdogmus, T. (2001) Natural Gas Hydrate Potential of the Black Sea, *Energy Sources*, 23:3, 203-211.
- Parrish, W.R., Prausnitz, J.M., (1972). Dissociation Pressures of Gas Hydrates Formed by Gas Mixtures. *Ind. Eng. Chem. Process Des. Develop.* Vol. 11, No. 1, 1972.

- Pasynkov A.A., Pozachenyuk E.A., Pasynkova L.A. (2014). Gas Seeps at The Black Sea Bottom. Retrieved from (Accessed on March 7, 2016):  
[www.symposia.gr/wp-content/uploads/2014/10/10S2012\\_143\\_Pasynkov.pdf](http://www.symposia.gr/wp-content/uploads/2014/10/10S2012_143_Pasynkov.pdf)
- Priegnitz, M., Thaler, J., Spangenberg, E., Rücker, C., and Schicks, J. M. (2013). A cylindrical electrical resistivity tomography array for three-dimensional monitoring of hydrate formation and dissociation. *Review of Scientific Instruments*, 84, 104502 (2013).
- Priegnitz, M., Thaler, J., Spangenberg, E., Schicks, J. M., Schrötter, J., and Abendroth, S. (2015). Characterizing electrical properties and permeability changes of hydrate bearing sediments using ERT data. *Geophysical Journal International*, 202(3), 1599–1612.
- Priest, J.A., Grozic, J.L.H. (2016). Stability of Fine-Grained Sediments Subject to Gas Hydrate Dissociation in the Arctic Continental Margin. *Submarine Mass Movements and their Consequences*, Volume 41 of the series *Advances in Natural and Technological Hazards Research* pp 427-436.
- Poettmann, F.H., Sloan, E.D., Mann, S.L., McClure, L.M., (1989). Vapor-solid equilibrium ratios for structure I and II natural gas hydrates. In: *Proceedings 68th annual GPA convention*, March 13-14, 1989 San Antonio, Texas.
- Popescu, I., Lericolais, G., Panin, N., Norman, A., Dinu, C., Le Drezeni E. (2004). The Danube submarine canyon (Black Sea): morphology and sedimentary processes. *Marine Geology*, May 2004; 206 (1-4): 249-265
- Popescu, I., De Batist, M., Lericolais, G., Nouzé, H., Poort, J., Panin, N., Versteeg, W., Gillet, H. (2006). Multiple bottom-simulating reflections in the Black Sea: Potential proxies of past climate conditions. *Marine Geology*, 227 (3-4), 163–176.
- Poort, J., Vassilev, A., Dimitrov, L. (2005). Did postglacial catastrophic flooding trigger massive changes in the Black Sea gas hydrate reservoir? *Terra Nova*, Vol 17, No. 2, 135–140.
- Rajput, S., Thakur, N.K. (2016). *Geological Controls for Gas Hydrates and Unconventionals*. Elsevier, Amsterdam.
- Railsback, B. (2010). The Black Sea IIIa: Variation with depth. Retrieved from (Accessed on April 23, 2016):  
<http://www.gly.uga.edu/railsback/Fundamentals/BlackSeaTSOPProfile01.pdf>

- Riedel, M., Collett, T., Malone, M.J., IODP Expedition 311 Scientists, (2009). Geological Society, London, Special Publications 2009; v. 319; p. 11-19.
- Risk (2016), @Risk, Palisade. <http://www.palisade.com/risk/>
- Rogers, R. (2015). Offshore Gas Hydrates: Origins, Development, and Production. Gulf Professional Publishing, USA.
- Ross DA, Uchupi E, Prada KE, MacIlvaine JC (1974) Bathymetry and microtopography of Black Sea. In: Degens ET, Ross DA (eds) The Black Sea-geology, chemistry and biology. AAPG Memoir 20. Tulsa, Oklahoma: 1-10.
- Ross, D.A. (1978). Summary of Results of Black Sea Drilling. <https://doi.org/10.2973/dsdp.proc.42-2.157.1978>
- Ross, D.A., (1978b). Black Sea Sedimentary Framework. <https://doi.org/10.2973/dsdp.proc.42-2.106.1978>
- Ruan, X., Song, Y., Liang, H., Yang, M., and Dou, B. (2012). Numerical Simulation of the Gas Production Behavior of Hydrate Dissociation by Depressurization in Hydrate-Bearing Porous Medium. *Energy and Fuels*, 26(3), 1681–1694.
- Rutqvist, J., and Moridis, G. (2009). Numerical Studies on the Geomechanical Stability of Hydrate-Bearing Sediments. *SPE Journal*, 14(2), 267–282.
- Rutqvist, J., Moridis, G. J., Grover, T., Silpngrmlert, S., Collett, T. S., and Holdich, S. a. (2012). Coupled multiphase fluid flow and wellbore stability analysis associated with gas production from oceanic hydrate-bearing sediments. *Journal of Petroleum Science and Engineering*, 92-93, 65–81.
- Ruppel, C., 2011, Methane hydrates and the future of natural gas, Supplementary Paper #4, The Future of Natural Gas, MIT Energy Initiative study, 25 pp.
- Sahay, V.K., Johnson, A. (2014). Gas Hydrate Deposits of Krishna Godavari Basin, India: Issues and Potentiality in Exploration and Commercial Production, Offshore Technology Conference, OTC-25137-PT, OTC.
- Sahling, H., Bohrmann, G., Artemov, Y.G., Bahr, A., Bruning,N., Klapp, S.A., Klaucke,I., Kozlova, E., Nikolovska, A., Pape, T., Reitz, A., Wallmann, K. (2009). Vodyanitskii mud volcano, Sorokin trough, Black Sea: Geological characterization and quantification of gas bubble streams. *Marine and Petroleum Geology*, 26, 9, 1799-1811.

- Sangwai, J.S, Patel, R.S., Mekala, P., Mech, D., Busch, M. (2013). Desalination of Seawater using Gas Hydrate Technology – Current Status and Future Direction. XVIII Conference on Hydraulics, Water Resources, Coastal and Environmental Engineering, 4-6 Dec 2013, IIT Madras, Chennai, INDIA.
- Santamarina, J. C., Tsouris, C. (2007). Methane Recovery from Hydrate-bearing Sediments, (May), 1–22. Quarterly Report: September 2010. Funding Number: DE-FC26-06NT42963, USA.
- Santamarina, J.C., Dai, S., Jang, J., Terzariol, M. (2012). Pressure Core Characterization Tools for Hydrate-Bearing Sediments. *Sci. Dril.*, 14, 44-48, doi:10.2204/iodp.sd.14.06.2012, 2012.
- Sarshar, M., Fathikaljahi, J., Esmailzadeh, F. (2009). Developing Correlations for Calculating Dissociation Enthalpies of Simple and Mixed Hydrates. *Iranian Journal of Science and Technology, Transaction B, Engineering*, Vol. 33, No. B3, pp 279-284.
- Sassen, R., and MacDonald, I. R. (1994). Evidence of structure H hydrate, Gulf of Mexico continental slope. *Organic Geochemistry*, 22(6), 1029–1032.
- SBC Energy Institute, (2015). Natural Gas Series Factbook: Gas Hydrates-Taking the heat out of the burning-ice debate Potential and future of Gas Hydrates. Retrieved from (Accessed on January 1, 2016):  
[https://www.sbc.slb.com/~media/Files/SBC%20Energy%20Institute/SBC%20Energy%20Institute\\_Gas%20Hydrates\\_FactBook.pdf](https://www.sbc.slb.com/~media/Files/SBC%20Energy%20Institute/SBC%20Energy%20Institute_Gas%20Hydrates_FactBook.pdf)
- Schicks, J.M. (2010). Review: Gas hydrates. *Annu. Rep. Prog. Chem., Sect. C*, 2010, 106, 101–117 | 101.
- Schicks, J. M., Luzi, M., and Beeskow-Strauch, B. (2011). The conversion process of hydrocarbon hydrates into CO<sub>2</sub> hydrates and vice versa: Thermodynamic considerations. *Journal of Physical Chemistry A*, 115(46), 13324–13331.
- Schicks, J.M., Spangenberg, E., Giese, R., Steinhauer, B., Klump, J., Luzi, M. (2011b) “New approaches for the production of hydrocarbons from hydrate bearing sediments,” *Energies*, vol. 4, no. 1, pp. 151–172, 2011.
- Schicks, J. M., and Luzi-Helbing, M. (2013). Cage occupancy and structural changes during hydrate formation from initial stages to resulting hydrate phase.

- Spectrochimica Acta - Part A: Molecular and Biomolecular Spectroscopy*, 115, 528–536.
- Schindler, M., Batzle, M., Prasad, M. (2015) Pore-Scale Imaging of Tetrahydrofuran-Hydrate Bearing Porous Media. SEG Technical Program Expanded Abstracts 2015: pp. 3140-3145. doi: 10.1190/segam2015-5924868.1
- Schoderbek, D., Farrell, H., Hester, K., Howard, J., Raterman, K., Silpngarm, S., Martin, K.L., Smith, B., Klein, P. (2013). ConocoPhillips Gas Hydrate Production Test Final Technical Report (October 1, 2008–June 30, 2013). Oil and Natural Gas Technology. DOE Award No.: DE-NT0006553.
- Schwalenberg, K., Engels, M. (2011). Marine Controlled Source Electromagnetic Methods for Gas Hydrate Assessment: New Instrumentation and First Results from The Black Sea Test Cruise. 24. Schmucker-Weidelt-Kolloquium Neustadt an der Weinstraße, 19. –23. September 2011.
- Schwalenberg, K., Rippe, D., Gehrmann, R., Hoelz, S. (2015). Marine CSEM Site Survey on Gas Hydrate Targets in the Danube Delta, western Black Sea. 26. Schmucker-Weidelt-Kolloquium Dassel, 21–25 September 2015.
- Schwalenberg, K., Müller, H., Engels, M., Rippe, D., Gehrmann, R.A.S. (2016). Marine Electromagnetic and Electrical Case Studies of Seafloor Massive Sulfide Systems and Submarine Gas Hydrates. Near Surface Geoscience, 4-8 September 2016, Barcelona, Spain.
- Selim, M., and Sloan, E. (1989). Heat and mass transfer during the dissociation of hydrates in porous media. *AIChE Journal*, 35(6), 1049–1052.
- Seol, Y., Kneafsey, T.J., Tomutsa, L., Moridis, G.J. (2006). Preliminary Relative Permeability Estimates of Methane Hydrate-Bearing Sand. PROCEEDINGS, TOUGH Symposium 2006 Lawrence Berkeley National Laboratory, Berkeley, California, May 15–17, 2006.
- Seol, Y., and Myshakin, E. (2011). Experimental and numerical observations of hydrate reformation during depressurization in a core-scale reactor. *Energy and Fuels*, 25, 1099–1110.
- Shahnazar, S., and Hasan, N. (2014). Gas hydrate formation condition: Review on experimental and modeling approaches. *Fluid Phase Equilibria*, 379, 72–85.

- Shankar, U. (2015). Gas hydrate saturation from seismic data constrained by log data in the Krishna-Godavari Basin. *Journal of Petroleum Exploration and Production Technology*. J Petrol Explor Prod Technol, (2016) 6: 13.
- Shepherd, R.G. (1989). Correlations of Permeability and Grain Size. Vol. 27, No. 5-  
Groundwater September-October 1989, 633-638.
- Shi, D., (2003). Evaluating the resources of hydrate gas in the Black Sea. *Nat. GasGeosci.* 14, 519-524.
- Shimkus, K.M. and Trimonis, E.S., (1974). Modern sedimentation in Black Sea. In  
Degens, E.T. and Ross, D.A. (Eds.), *The Black Sea-geology, chemistry and  
biology*: Am. Assoc. Petrol. Geol. Mem. 20, p. 249-278.
- Shishkina, O.V. (1978). Distribution of Bromine, Cl/Br Relationships and Iodine in  
Interstitial Water of the Black Sea, Based on DSDP Leg 42B.  
<https://doi.org/10.2973/dsdp.proc.42-2.122.1978>
- Singh, N.P., Prakash, A. (2015). Natural Gas Hydrate in India: Prospect  
Identification, Production Technologies and Associated Challenges. *Journal of  
Geography, Environment and Earth Science International* 3(2): 1-24, 2015; Article  
no.JGEESI.18860.
- Sira, J.H., Patil, S.L., Kamath, V.A. (1990). Study of Hydrate Dissociation by  
Methanol and Glycol Injection. *SPE* 20770, 977–984.
- Site 379 (1978). The Shipboard Scientific Party.  
<https://doi.org/10.2973/dsdp.proc.42-2.103.1978>
- Site 380 (1978). The Shipboard Scientific Party.  
<https://doi.org/10.2973/dsdp.proc.42-2.104.1978>
- Site 381 (1978). The Shipboard Scientific Party.  
<https://doi.org/10.2973/dsdp.proc.42-2.105.1978>
- Sloan, E.D. Jr (1990). *Clathrate Hydrates of Natural Gases*, Marcel Dekker, New  
York.
- Sloan E.D. (1998). “Clathrate hydrates of natural gases”. 2<sup>nd</sup> ed. New York: Marcel  
Dekker.
- Sloan, E.D.J. (2003). “Fundamental principles and applications of natural gas  
hydrates”, *Nature* 426, 353-363.

- Sloan, E.D. and Koh, C.A., (2008) “Clathrate Hydrates of Natural Gases”, 3rd Edition, Taylor and Francis/CRC Press, Boca Raton.
- Smirnov, L.F., Chumak, I. (1996) Investment project Methane-from Black Sea gas hydrate. 2<sup>nd</sup> Int. Conf. on Gas Hydrate, Toulouse, France.
- Spangenberg, E., Priegnitz, M., Heeschen, K., and Schicks, J. M. (2015). Are laboratory-formed hydrate-bearing systems analogous to those in nature? *Journal of Chemical and Engineering Data*, 60(2), 258–268.
- Soloviev, V. and Ginsburg, G.D. (1994): Formation of submarine gas hydrates. *Bulletin of the Geological Society of Denmark*, Vol. 41, pp. 86-94. Copenhagen, 1994-03-30.
- Solov'yov, V.A. (2003). Natural gas hydrates as potential mineral. *Russian chemical magazine*. Volume 48:59-69.
- Sozansky, V.I. (1997). Gaseous Regime of the Black Sea. *Proc. Intern. Workshop on “Continental Margins and Sea Level Changes”* in Tescani, Romania, Oct. 6-12, 1997.
- Starostenko, V.I., Rusakov, O.M., Shnyukov, E.F., Kobolev, V.P., Kutas, R.I. (2010). Methane in the northern Black Sea: characterization of its geomorphological and geological environments. *Geological Society, London, Special Publications-2010-Starostenko-57-75*.
- Stanev, E. V., He, Y., Staneva, J., and Yakushev, E. (2014). Mixing in the black sea detected from the temporal and spatial variability of oxygen and sulfide andndash; Argo float observations and numerical modelling. *Biogeosciences*, 11(20), 5707–5732.
- Stern, L., Circone, S., Kirby, S. H., and Durham, W. B. (2003). Temperature, pressure, and compositional effects on anomalous or “self” preservation of gas hydrates. *Canadian Journal of Physics*, 81(1-2), 271–283.
- Stoffers, P., Müller, G. (1978). Mineralogy and Lithofacies of Black Sea Sediments, Leg 42B Deep Sea Drilling Project. <https://doi.org/10.2973/dsdp.proc.42-2.107.1978>
- Su, M., Yang, R., Wang, H., Sha, Z., Liang, J., Wu, N., Qiao, S., Cong, X. (2016). Gas hydrates distribution in the Shenhu area, northern South China Sea: comparisons between the eight drilling sites with gas hydrate petroleum system.

- Geologica Acta, Vol.14, N°2, June 2016, pgs-pgs. DOI: 10.1344/Geologica Acta 2016.14.2. n°manuscript.
- Subramanian, S., Kini, R., Dec, S. F., Sloan, E. D. (2000). Evidence of structure II hydrate formation from methane+ethane mixtures. *Chemical Engineering Science*, 55, 1981–1999.
- Sultan, N., P. Cochonat, J.P. Foucher, J. Mienert, 2004. Effect of gas hydrates melting on seafloor slope instability. *Marine Geology*, 213 (2004), 379-401.
- Supko, P., Ross, D.A., Neprochnov, Y.P. (1978). Introduction and Explanatory Notes, Leg 42B, Deep Sea Drilling Project. <https://doi.org/10.2973/dsdp.proc.42-2.101.1978>.
- Sun, X., and Mohanty, K. K. (2006). Kinetic simulation of methane hydrate formation and dissociation in porous media. *Chemical Engineering Science*, 61(11), 3476–3495.
- Sun, S. C., Liu, C. L., Ye, Y. G., and Liu, Y. F. (2014). Phase behavior of methane hydrate in silica sand. *Journal of Chemical Thermodynamics*, 69, 118–124.
- Sun, J., Ning, F., Li, S., Zhang, K., Liu, T., Zhang, L., Jiang, G., (2015). Numerical simulation of gas production from hydrate-bearing sediments in the Shenhu area by depressurising: The effect of burden permeability. *Journal of Unconventional Oil and Gas Resources*, 12 (2015), 23-33.
- Sun, J., Ning, F., Zhang, L., Liu, T., Peng, L., Liu, Z., Li, C., Jiang, G. (2016). Numerical simulation on gas production from hydrate reservoir at the 1st offshore test site in the eastern Nankai Trough. *Journal of Natural Gas Science and Engineering*, 30, 64–76.
- Swewe (2016). *Türbiditler*. Retrieved from (Accessed on May 11, 2016): [http://tr.swewe.org/word\\_show.htm/?297188\\_1andT%C3%BCrbiditler](http://tr.swewe.org/word_show.htm/?297188_1andT%C3%BCrbiditler)
- Tang, L. G., Xiao, R., Huang, C., Feng, Z. P., and Fan, S. S. (2005). Experimental investigation of production behavior of gas hydrate under thermal stimulation in unconsolidated sediment. *Energy and Fuels*, 19(12), 2402–2407.
- Tinivella, U. (2016). MIGRATE Working Group (WG) 3: Environmental challenges First annual report, Feb. 2016. Retrieved from (Accessed on December 7, 2016):

- [https://www.migrate-cost.eu/documents/1134909/1134981/Report\\_WG3\\_26feb2016.pdf/9d12d6d4-659b-426c-991a-bdb17f775259](https://www.migrate-cost.eu/documents/1134909/1134981/Report_WG3_26feb2016.pdf/9d12d6d4-659b-426c-991a-bdb17f775259)
- Thakur, N.K., Rajput, S. (2011). Exploration of Gas Hydrates: Geophysical Techniques. Springer, New York.
- Tohidi, B., Danesh, A., and Todd, A. C. (1997). On the mechanism of gas hydrate formation in subsea sediments. In Preprints of Symposia-Division of Fuel Chemistry American Chemical Society Vol. 42, pp. 485-489.
- Tomaru, H., Honda, Y., Matsumoto, R. (2016). Concentration of anomalies of pore waters collected from shallow gas hydrate deposits in the eastern margin of the Japan Sea. Japan Geoscience Union Meeting, May 22-26, 2016, Chiba, Japan.
- TPAO (2015). Ham Petrol ve Doğalgaz Sektör Raporu. May 2015. Retrieved from (Accessed on March 1, 2016):
- [http://www.tpao.gov.tr/tp5/docs/imaj/HP\\_DG\\_SEKTOR\\_RPR\\_040515.pdf](http://www.tpao.gov.tr/tp5/docs/imaj/HP_DG_SEKTOR_RPR_040515.pdf)
- Trimonis, E.S., Shimkus, K.M., Ross, D.A. (1978) Mineral Composition of Coarse-Silt Fraction of the Black Sea Late Cenozoic Sediments.
- <https://doi.org/10.2973/dsdp.proc.42-2.108.1978>
- Tsuji, Y., Ishida, H., Nakamizu, M., Matsumoto, R., and Shimizu, S. (2004). Overview of the MITI Nankai Trough wells: A milestone in the evaluation of methane hydrate resources. Resource Geology, 54(1), 3–10.
- Uchida, T., Takeya, S., Chuvilin, E.M., Ohmura, R., Nagao, J., Yakushev, V.S., Istomin, V.A., Minagawa, H., Ebinuma, T., Narita, H. (2004). Decomposition of methane hydrates in sand, sandstone, clays, and glass beads. Journal of Geophysical Research, Vol. 109, B05206, 1-12.
- Uchida, T.; Ikeda, I.Y.; Takeya, S.; Kamata, Y.; Ohmura, R.; Nagao, J.; Zatsepina, O.Y.; Buffett, B.A. (2005). Kinetics and stability of CH<sub>4</sub>-CO<sub>2</sub> mixed gas hydrates during formation and long-term storage. Chem Phys Chem 2005, 6, 646–654.
- Uchida, S., Klar, A., Yamamoto, K. (2016). Sand production modeling gas hydrate-bearing sediments. International Journal of Rock Mechanics & Mining Sciences 86(2016) 303–316.
- Uddin, M., Wright, F., Dallimore, S., and Coombe, D. (2014). Gas hydrate dissociations in Mallik hydrate bearing zones A, B, and C by depressurization:

- Effect of salinity and hydration number in hydrate dissociation. *Journal of Natural Gas Science and Engineering*, 21, 40–63.
- Vadakkepuliambatta, S., Hornbach, M.J., Bünz, S., Phrampus, B.J., (2015). Controls on gas hydrate system evolution in a region of active fluid flow in the SW Barents Sea, *Marine and Petroleum Geology*, 66 (4), 861-872.
- Vassilev, A., Dimitrov, L. (2000). Spatial and qualitative evaluation of methane hydrates in the Black Sea. *Geology and Geophysics*. 43(7): 672-684.
- Vassilev, A., Dimitrov, L., (2003). Model Evaluation of the Black Sea Gas Hydrates. Tome 56, No.3, 2003.
- Vassilev, A., (2006). Black Sea Gas Hydrates Stability Zone Model (Optimistic and Pessimistic Assessment). CRIMEA Final Project Meeting, January 19-21, 2006, Gent, Belgium.
- Vasilev, A. (2015). Geothermal study of gas hydrates from Danube paleodelta – BEEZ of the Black Sea. 7<sup>th</sup> BGGGS National Conference with International Participation “Geophysics 2015”, Sofia, 20-22 May 2015.
- Veluswamy, H. P., Yew, J. C., and Linga, P. (2015). New Hydrate Phase Equilibrium Data for Two Binary Gas Mixtures of Hydrogen and Propane Coupled with a Kinetic Study. *J. Chem. Eng. Data* 2015, 60, 228–237.
- Waite, W. F., Stern, L. a., Kirby, S. H., Winters, W. J., and Mason, D. H. (2007). Simultaneous determination of thermal conductivity, thermal diffusivity and specific heat in sI methane hydrate. *Geophysical Journal International*, 169(2), 767–774.
- Waite, W. F., Santamarina, J. C., Cortes, D. D., Dugan, B., Espinoza, D. N., Germaine, Jang, J., Jung, W., Kneafsey, T.J., Shin, H., Soga, K., Winters, W. J., Yun, T.S. (2009). Physical Properties of Hydrate-Bearing Sediments. *Rev. Geophys.*, 47, 4, RG4003, 2009. <https://doi.org/10.1029/2008RG000279>
- Walker, R.G. (1978) "Deep-water sandstone facies and ancient submarine fans: model for exploration for stratigraphic traps", *American Association of Petroleum Geologists Bulletin*, 62 (6), p. 932-966.
- Wang, X., Hutchinson, D. R., Wu, S., Yang, S., and Guo, Y. (2011). Elevated gas hydrate saturation within silt and silty clay sediments in the Shenhu area, South China Sea. *Journal of Geophysical Research: Solid Earth*, 116(5), 1–18.

- Wang, X., Wu, S., Lee, M., Guo, Y., Yang, S., and Liang, J. (2011b). Gas hydrate saturation from acoustic impedance and resistivity logs in the shenhu area, south china sea. *Marine and Petroleum Geology*, 28(9), 1625–1633.
- Wang, Y., Li, X. Sen, Li, G., Zhang, Y., Li, B., and Chen, Z. Y. (2013). Experimental investigation into methane hydrate production during three-dimensional thermal stimulation with five-spot well system. *Applied Energy*, 110, 90–97.
- Wang Y, Li XS, Xu WY, Li QP, Zhang Y, Li G, (2013b) Experimental investigation into factors influencing methane hydrate formation and a novel method for hydrate formation in porous media. *Energy Fuels* 2013; 27:3751–7.
- Wang, M., Deng, M., Zhao, Q., Luo, X. and Jing, J. (2015), Two types of marine controlled source electromagnetic transmitters. *Geophysical Prospecting*, 63: 1403–1419.
- Wang, Y., Feng, J.-C., Li, X.-S., Zhang, Y., and Li, G. (2016). Large scale experimental evaluation to methane hydrate dissociation below quadruple point in sandy sediment. *Applied Energy*, 162, 372–381.
- WebGasEOS. <http://lnx.lbl.gov/gaseos/gaseos.html>
- Weitemeyer, K.A., Constable, S., Trehu, A.M. (2011). A marine electromagnetic survey to detect gas hydrate at Hydrate Ridge, Oregon. *Geophys. J. Int.* (2011) 187 (1): 45-62.
- White, M., Lee, W.S., (2014). Guest Molecule Exchange Kinetics for the 2012 Ignik Sikumi Gas Hydrate Field Trial. The Offshore Technology Conference held in Houston, Texas, USA, 5–8 May 2014.
- White, M., 2011. Impact of kinetics on the injectivity of liquid CO<sub>2</sub> into Arctic hydrates. In: OTC Arctic Technology Conference.
- Wood, W.T., and W.Y. Jung, (2008). Modeling the Extent of Earth’s Marine Methane Hydrate Cryosphere, Proceedings of the 6<sup>th</sup> International Conference on Gas Hydrates (ICGH 2008), July 6-10, 2008, Vancouver, British Columbia, Canada, 8.
- Worthington, P.F. (2010). Petrophysical evaluation of gas-hydrate formations. *Petroleum Geoscience*, Vol. 16 2010, pp. 53–66.
- Wikipedia. Black Sea relief location map with exclusive economic zones. Retrieved from (Accessed on April 1, 2016):

[https://commons.wikimedia.org/wiki/File:Black\\_Sea\\_relief\\_location\\_map\\_with\\_exclusive\\_economic\\_zones.svg](https://commons.wikimedia.org/wiki/File:Black_Sea_relief_location_map_with_exclusive_economic_zones.svg)

- Wilcox, W.I., Carson, D.B., Katz, D.L. (1941). Natural Gas Hydrates. *Ind. Eng. Chem.*, 33, 662-671.
- Winters, W. J., Pecher, I. A., Waite, W. F., and Mason, D. H. (2004). Physical properties and rock physics models of sediments containing natural and laboratory formed methane gas hydrate. *Am. Mineral.* 89:1221–1227.
- Winters, W. J., Wilcox-Cline, R. W., Long, P., Dewri, S. K., Kumar, P., Stern, L., and Kerr, L. (2014). Comparison of the physical and geotechnical properties of gas-hydrate-bearing sediments from offshore India and other gas-hydrate-reservoir systems. *Marine and Petroleum Geology*, 58(PA), 139–167.
- Wu, M., Wang, S., Liu, H., (2007). A Study on Inhibitors for the Prevention of Hydrate Formation in Gas Transmission Pipeline. *Journal of Natural Gas Chemistry* Volume 16, Issue 1, March 2007, Pages 81–85.
- Xing, J. (2013). Seismoacoustic Study of the Shallow Gas Transport and Reservoirs in the Vicinity of Seabed Fluid Seepage of the Black Sea. PhD Thesis, Im Fachbereich der Geowissenschaften der Universität Bremen, Germany.
- Xiong, L., Li, X., Wang, Y., and Xu, C. (2012). Experimental study on methane hydrate dissociation by depressurization in porous sediments. *Energies*, 5, 518–530.
- Xu, C.-G., and Li, X. (2015). Research Progress on Methane Production from Gas Hydrates. *RSC Adv.* 2015, 5, 54672-54699.
- Xu, C., Cai, J., Lin, F., Chen, Z., and Li, X. (2015). Raman analysis on methane production from natural gas hydrate by carbon dioxide e methane replacement. *Energy*, 79, 111–116.
- Yamamoto, K., Kanno, T., Wang, X., Tamaki, M., Fujii, T., Chee, S., Wang, X., Pimenov, V., Shako, V. (2017). Thermal responses of a gas hydrate-bearing sediment to a depressurization operation. *RSC Adv.*, 2017, 7, 5554–5577.
- Yang, M., Song, Y., Liu, Y., Chen, Y., and Li, Q. (2010). Influence of pore size, salinity and gas composition upon the hydrate formation conditions. *Chinese Journal of Chemical Engineering*, 18(2), 292–296.

- Yang, X., Sun, C. Y., Su, K. H., Yuan, Q., Li, Q. P., and Chen, G. J. (2012). A three-dimensional study on the formation and dissociation of methane hydrate in porous sediment by depressurization. *Energy Conversion and Management*, 56, 1–7.
- Yang, S., Lang, X., Wang, Y., Wen, Y., and Fan, S. (2014). Numerical simulation of Class 3 hydrate reservoirs exploiting using horizontal well by depressurization and thermal co-stimulation. *Energy Conversion and Management*, 77, 298–305.
- Yang, M., Fu, Z., Zhao, Y., Jiang, L., Zhao, J., and Song, Y. (2015). Effect of depressurization pressure on methane recovery from hydrate–gas–water bearing sediments. *Fuel*, 166, 419–426.
- Yang, M., Zheng, J., Liu, W., Liu, Y., and Song, Y. (2015b). Effects of  $C_3H_8$  on hydrate formation and dissociation for integrated  $CO_2$  capture and desalination technology. *Energy*, 93, 1971–1979.
- Ye Y., Liu C., (2013). *Natural Gas Hydrates, Experimental Techniques*. Springer Geophysics, New York.
- Yefremova, A. G., and Zhizchenko, B. P., (1974), Occurrence of crystal hydrates of gases in the sediments of modern marine basins: *Doklady Akademii Nauk SSSR*, v. 214, p. 1179–1181.
- Yousif, M. H., Abass, H. H., Selim, M. S., and Sloan, E. D. (1991). Experimental and Theoretical Investigation of Methane-Gas-Hydrate Dissociation in Porous Media. *SPE Reservoir Engineering*, 6(1), 69–76.
- Yuan, Q., Sun, C. Y., Yang, X., Ma, P. C., Ma, Z. W., Liu, B., Maa, Q.L., Yang, L.Y., Chen, G. J. (2012). Recovery of methane from hydrate reservoir with gaseous carbon dioxide using a three-dimensional middle-size reactor. *Energy*, 40(1), 47–58.
- Yuan, Q., Sun, C., Wang, X., Zeng, X., Yang, X., Liu, B., and Ma, Z. (2013). Experimental study of gas production from hydrate dissociation with continuous injection mode using a three-dimensional quiescent reactor. *Fuel*, 106, 417–424.
- Yücesoy, F, Ergin, M. (1992). Heavy-metal geochemistry of surface sediments from the southern Black Sea shelf and upper slope. *Chemical Geology*, 99 (1992) 265-287.

- Zander, T., Vanneste, M., Berndt, C. (2016). Potential Impacts of Gas Hydrate Exploitation on Slope Stability - A Study from the Danube Fan, Black Sea. Near Surface Geoscience, 4-8 September 2016, Barcelona, Spain.
- Zander, T., Haeckel, M., Berndt, C., Chi, W.C., Klaucke, I., Bialas, J., Klaeschen, D., Koch, S., Atgin, O. (2017). On the origin of multiple BSRs in the Danube deep-sea fan, Black Sea. *Earth and Planetary Science Letters* 462 (2017) 15–25.
- Zang X Y, Liang D Q, Wu N Y. (2013) Gas hydrate formation in fine sand. *Science China: Earth Sciences*, 2013, 56: 549–556.
- Zanjani, N.G., Nazari, K., Moghaddam, A.Z., Taheri, M.M., Sina, M. (2011). Methane Purification by Sequential Gas Hydrate Formation in Porous Media. *Proceedings of the 7<sup>th</sup> International Conference on Gas Hydrates (ICGH 2011)*, Edinburgh, Scotland, United Kingdom, July 17-21, 2011.
- Zhang, P., Wu, Q., Pu, Y., and Deng, Y. (2011). Water Transfer Characteristics during Methane Hydrate Formation Processes in Layered Media. *Energies*, 4(12), 1129–1137.
- Zhang, X. H., Lu, X. B., Shi, Y. H., Xia, Z., and Liu, W. T. (2015). Centrifuge experimental study on instability of seabed stratum caused by gas hydrate dissociation. *Ocean Engineering*, 105(April), 1–9.
- Zhao, J., Cheng, C., Song, Y., Liu, W., Liu, Y., Xue, K., Zhu, Z., Yang, Z., Wang, D., Yang, M. (2012). Heat Transfer Analysis of Methane Hydrate Sediment Dissociation in a Closed Reactor by a Thermal Method, *Energies* 2012, 5, 1292-1308.
- Zhao J., Xu K., Song, Y., Liu, Weiguo., Lam W., Liu Y., Xue K., Zhu Y., Yu X., Li Q., (2012b) A review on research on replacement of CH<sub>4</sub> in Natural Gas Hydrates by use of CO<sub>2</sub>. 2012., *Energies*, 5, 399-419.
- Zhao, J., Ye, C., Song, Y., Liu, W., Cheng, C., Liu, Y, Zhang, Y., Wang, D.Y., Ruan, X. (2012c). Numerical Simulation and Analysis of Water Phase Effect on Methane Hydrate Dissociation by Depressurization. *Ind. Eng. Chem. Res.*, 2012, 51 (7), 3108–3118.
- Zhao, J., Zhu, Z., Song, Y., Liu, W., Zhang, Y., and Wang, D. (2015). Analyzing the process of gas production for natural gas hydrate using depressurization. *Applied Energy*, 142, 125–134.

- Zhao, J., Zhang, L., Chen, X., Zhang, Y., Liu, Y., and Song, Y. (2016). Combined replacement and depressurization methane hydrate recovery method. *Energy Exploration and Exploitation*, 34, 1, 129-139.
- Zhao, Y., Zhao, J., Shi, D., Feng, Z., Liang, W., and Yang, D. (2016b). Micro-CT analysis of structural characteristics of natural gas hydrate in porous media during decomposition. *Journal of Natural Gas Science and Engineering*, 31, 139–148.
- Zheng, J., Babu, P., Linga, P. (2015). Thermodynamics and applications of CO<sub>2</sub> hydrates. In book: *Reaction Mechanisms in Carbon Dioxide Conversion*, Chapter:10, pp 373-402, Springer, New York.
- Zhou, Y., Castaldi, M. J., and Yegulalp, T. M. (2009). Experimental Investigation of Methane Gas Production from Methane Hydrate. *Industrial and Engineering Chemistry Research*, 48, 3142–3149.
- Zou, C. (2013). *Unconventional Petroleum Geology: Chapter 10-Natural Gas Hydrate*. Pp 337-354. Elsevier, USA. ISBN: 978-0-12-397162-3



## CURRICULUM VITAE

**Name** Şükrü MEREY  
**Email** sukrumerey@gmail.com  
**Nationality** Turkish

### EDUCATION

#### B.Sc.

2004– 2009 Middle East Technical University (METU), Ankara  
Department of Petroleum and Natural Gas Engineering  
Cumulative GPA: 3.81 out of 4.00 (High Honor)

#### M.Sc.

October 2011– August 2013  
Middle East Technical University (METU), Ankara  
Department of Petroleum and Natural Gas Engineering  
Cumulative GPA: 3.79 out of 4.00

#### Ph.D.

September 2013– March 2017  
Middle East Technical University (METU), Ankara  
Department of Petroleum and Natural Gas Engineering  
Cumulative GPA: 3.93 out of 4.00

**Languages** Turkish- Native  
English- Good command of written and spoken  
Spanish- Beginner

## Computer Skills

*Operating System:* MS Windows

*Language:* C, C++, Matlab, Octave, Fortran, Python

*Software:* MS Office Applications (Word, Excel, PowerPoint, Access), Internet, Risk, Keycreator, Surfer, RTA, Sapphire, Topaze, Well Test, CMG, OptiCem, Simply Fortran, Minitab, HydrateResSim, Tough+Hydrate, Mathematica, Peridigm

## Experience

06/2007 – 07/2007	Summer practice at Turkish Petroleum Corporation (TPAO), Lüleburgaz (Drilling Department)
07/2008 –08/2008	Summer practice at N.V. Turkse Perenco, Diyarbakir (Production and Well Completion Departments)
01/2010-03/2010	Petroleum and Natural Gas Engineer General Directorate of Petroleum Affairs of Turkey, Ankara
03/2010-05/2011	Well Completion Engineer Turkish Petroleum Corporation (TPAO), Adiyaman
08/2011-Present	Research Assistant Middle East Technical University, Department of Petroleum and Natural Gas Engineering, Ankara

### **International Congresses Attended**

The 65<sup>th</sup> Chemical Engineering Conference, October 4-7, 2015, Calgary, Canada.

6<sup>th</sup> CGS Europe Knowledge Sharing Workshop, September 16-17, 2013, Bratislava, Slovakia.

### **Awards**

SPE Turkey Section Award of Appreciation May 2009.

Performance Award in 2013-2014 academic year, Graduate School of Natural and Applied Sciences, METU

Certificate of Outstanding Contribution in Reviewing, Journal of Natural Gas Science and Engineering, Elsevier, 2016

Certificate of Reviewing, Applied Energy, Elsevier, 2016

Certificate of Reviewing, Journal of Natural Gas Science and Engineering, Elsevier, 2016

Certificate of Reviewing, Journal of Petroleum Science and Engineering, Elsevier, 2016

### **Presentations**

- 1) Merey, Ş., Kaddoura, A. (2009). “Hydrate Inhibition with PEO”, 17<sup>th</sup> International Petroleum and Natural Gas Congress and Exhibition, May 13-15, 2009, Ankara, Turkey.
- 2) Merey, Ş., Sınoy, Ç. (2013). “Experimental Analysis of Adsorption Capacities and Behaviors of Shale Samples” 19<sup>th</sup> International Petroleum and Natural Gas Congress and Exhibition, May 15-17, 2013, Ankara, Turkey.
- 3) Merey, Ş., Sınoy, Ç. (2013). “Unconventional shale gas resources are going to provide new CO<sub>2</sub> storage mediums: an experimental study” 6<sup>th</sup> CGS Europe Knowledge Sharing Workshop, September 16-17, 2013, Bratislava, Slovakia.
- 4) Küçük, H.M., Dondurur, D., Özel, Ö., Parlaktuna, M., Sınoy, Ç., Çiftçi, G., Merey, Ş., Darılmaz, E. (2013). “Gas Hydrate Potential Offshore Amasra-

- Zonguldak and Possible Reasons for Multiple BSR Reflection Occurrence”, 20<sup>th</sup> International Geophysical Congress and Exhibition, November 25-27, 2013, Antalya, Turkey.
- 5) Merey, Ş., Sınyuç, Ç. (2015). “Simulation of Gas Production from Hydrate Reservoirs by using HydrateResSim Numerical Simulator”. 20<sup>th</sup> International Petroleum and Natural Gas Congress and Exhibition, May 29, 2015, Ankara, Turkey.
  - 6) Küçük, H.M., Dondurur, D., Özel, Ö., Sınyuç, Ç., Merey, Ş., Parlaktuna, M., Çifçi, G. and the SeisLab Team, (2015). “Gas and Gas Hydrate Potential Offshore Amasra, Bartın and Zonguldak and Possible Agent for Multiple BSR Occurrence”. Vol. 17, EGU2015-10310-1, 2015.
  - 7) Merey, Ş., Sınyuç, Ç. (2015).” Analysis of Carbon Dioxide Sequestration in Shale Gas Reservoirs by Using Experimental Adsorption Data and Adsorption Models.”. The 65<sup>th</sup> Chemical Engineering Conference, October 4-7, 2015, Calgary, Canada.
  - 8) Merey, Ş., Sınyuç, Ç. (2015).” Investigation of Gas Hydrate Potential and Modelling of Gas Production from Hydrate Reservoirs in the Black Sea.” The 65<sup>th</sup> Canadian Chemical Engineering Conference, October 4-7, 2015, Calgary, Canada.
  - 9) Küçük, H.M., Dondurur, D., Özel, Ö., Sınyuç, Ç., Merey, Ş., Parlaktuna, M., Çifçi, G. (2015). “Acoustic Investigations of Gas and Gas Hydrate Formations, offshore southwestern Black Sea.” American Geophysical Union-Fall Meeting, December 14-18, 2015, San Francisco, USA.
  - 10) Merey, Ş., Öney, M., Sınyuç, Ç. (2016). Characterization of the Potential Black Sea Gas Hydrates. Turkish Marine Sciences Conference, May 31-June 3, 2016, Ankara, Turkey.

## **Publications**

- 1) Merey, Ş. (2013). “Experimental Analysis of Adsorption Capacities and Behaviors of Shale Samples”. M.S. Thesis, METU Petroleum and Natural Gas Engineering Department, August 2013. Supervisor: Asst.Prof.Dr.Çağlar Sınyuç.

- 2) Kök, M.V., Merey, Ş. (2014). Shale Gas: Current Perspectives and Future Prospects in Turkey and the World, *Energy Sources, Part A: Recovery, Utilization, and Environmental Effects*, 36:22, 2492-2501.
- 3) Bülbül, S., Kadoura, A.S., Merey, Ş., Parlaktuna, M. (2014). Hydrate Inhibition with PEO (Poly 2-ethyl-2-oxazoline), *Energy Sources, Part A: Recovery, Utilization, and Environmental Effects*, 36:23, 2613-2620.
- 4) Merey, Ş., Sinayuç, Ç. (2015). “Natural gas hydrate: a potential future energy resource”. Issue N° 31 The Newsletter of the ENeRG Network June 2015.
- 5) Merey, Ş., Sinayuç, Ç. (2016). Investigation of Gas Hydrate Potential of the Black Sea and Modelling of Gas Production from a Hypothetical Class 1 Methane Hydrate Reservoir in the Black Sea Conditions, *Journal of Natural Gas Science and Engineering* 29 (2016) 66-79.
- 6) Merey, Ş., Sinayuç, Ç. (2016). Analysis of Carbon Dioxide Sequestration in Shale Gas Reservoirs by using Experimental Adsorption Data and Adsorption Models. *Journal of Natural Gas Science and Engineering*, 36 (2016) 1087-1105.
- 7) Merey, Ş., Sinayuç, Ç. (2016). Gas-in Place Calculations in Shale Gas Reservoirs using Experimental Adsorption Data with Adsorption Models. *The Canadian Journal of Chemical Engineering*, 94:1683-1692.
- 8) Merey, S., Sinayuc, Ç. (2016), Experimental set-up design for gas production from the Black Sea gas hydrate reservoirs, *Journal of Natural Gas Science and Engineering*, 33 (2016) 162-185.
- 9) Merey, Ş., Sinayuç, Ç. (2016). New Software That Predicts Hydrate Properties and Its Use in Gas Hydrate Studies. *Journal of Chemical and Engineering Data*, 61 (5), pp 1930–1951.
- 10) Merey, S., Sinayuc, C. (2016). Analysis of the Black Sea Gas Hydrates. *World Academy of Science, Engineering and Technology, International Science Index* 116, *International Journal of Chemical, Molecular, Nuclear, Materials and Metallurgical Engineering*, 10(8), 886 - 894.
- 11) Abbasov, A., Merey, S., Parlaktuna, M. (2016). Experimental Investigation of Carbon Dioxide Injection Effects on Methane-Propane-Carbon Dioxide Mixture Hydrates. *Journal of Natural Gas Science and Engineering* 34 (2016) 1148-1158.

- 12) Merey, S., Sinayuc, C. (2016). Analysis of the Black Sea sediments by evaluating DSDP Leg 42B drilling data for gas hydrate potential. *Marine and Petroleum Geology*, 78: 151–167.
- 13) Merey, S. (2016). Drilling of Gas Hydrate Reservoirs. *Journal of Natural Gas Science and Engineering*, 35, 1167-1179.
- 14) Merey, S., Sinayuc, C. (2017). Adsorption Behaviors of Shale Gas Reservoirs. *International Journal of Oil, Gas and Coal Technology*. (In Press)

### **Reviewer**

2015-present	Journal of Natural Gas Science and Engineering
2016-present	Journal of Chemical and Engineering Data
2016-present	Journal of Petroleum Science and Engineering
2016-present	Energy Sources, Part A: Recovery, Utilization, And Environmental Effects
2016-present	Applied Energy
2016-present	Arabian Journal of Geosciences
2016-present	Nature
2016-present	Environmental Geotechnics
2017-present	AAPG Bulletin
2017-present	Open Geosciences

### **Interests**

Sports, History, Space, Reading, Travelling

### **Membership**

2013- present	Chamber of Petroleum Engineers, Turkey
2006- present	Society of Petroleum Engineers (SPE)